FUNDAMENTALS OF SMART GRID SYSTEMS

MUHAMMAD KAMRAN

FUNDAMENTALS OF SMART GRID SYSTEMS

This page intentionally left blank

FUNDAMENTALS OF SMART GRID SYSTEMS

MUHAMMAD KAMRAN
Department of Electrical Engineering and Technology, Riphah International University, Islamabad, Pakistan

ACADEMIC PRESS
An imprint of Elsevier

Academic Press is an imprint of Elsevier
125 London Wall, London EC2Y 5AS, United Kingdom
525 B Street, Suite 1650, San Diego, CA 92101, United States
50 Hampshire Street, 5th Floor, Cambridge, MA 02139, United States
The Boulevard, Langford Lane, Kidlington, Oxford OX5 1GB, United Kingdom

Notices
Knowledge and best practice in this field are constantly changing. As new research and experience broaden our understanding, changes in research methods, professional practices, or medical treatment may become necessary.

Practitioners and researchers must always rely on their own experience and knowledge in evaluating and using any information, methods, compounds, or experiments described herein. In using such information or methods they should be mindful of their own safety and the safety of others, including parties for whom they have a professional responsibility.

To the fullest extent of the law, neither the Publisher nor the authors, contributors, or editors, assume any liability for any injury and/or damage to persons or property as a matter of products liability, negligence or otherwise, or from any use or operation of any methods, products, instructions, or ideas contained in the material herein.

ISBN 978-0-323-99560-3

Publisher: Joseph P. Hayton
Acquisitions Editor: Rachel E. Pomery
Editorial Project Manager: Ali Afzal-Khan
Production Project Manager: Prem Kumar Kaliamoorthi
Cover Designer: Matthew Limbert

Typeset by STRAIVE, India

Dedication

To my parents Muhammad Ramzan (Late) and Naziran BiBi, my brother Muhammad Imran, and my sisters for their support and love.

To my beloved wife Badar Un Nisa and my son M. Sarim Kamran for their inspiration, support, and love.

This page intentionally left blank

Contents

10. Electric vehicles and smart grids

11. Global status of smart grids

This page intentionally left blank

Preface

Conventional grids throughout the world are being changed by the inventions of various technologies. With the increased maturity of renewable energy technologies, the distributed generation concept has evolved as a readily available source of energy for the areas where the sources are abundantly available. These distributed generation technologies need to be integrated into the existing grid. To record the transactions of electricity between these microgrids and the main grid, a communication network and an advanced metering infrastructure are required. These concepts are merged in the smart grid.

The smart grid is not a limited field that confines itself to limited concepts. It is a vast field integrating smart metering, communication technologies, renewable energy sources, power grids, forecasting techniques, power electronics, thermodynamics, electric vehicles, and energy storage systems. The smart grid will support the improvement of energy efficiency and the utilization of renewable energy sources. The energy management system integrated into the smart grid will optimize energy sources and harnessing techniques. This book gives an insight into all the above-stated fields of the smart grid with its associated key features. It also describes the key enabling technologies and thus permits the reader to engage with the immediate development of the power system and take part in the debate over the future of the smart grid.

Chapter 1 gives the introduction to the smart grid and discusses the communication technologies that are used in it. Chapter 2 gives an insight into the conventional and renewable energy technologies that are integrated into the smart grid. Chapter 3 gives a detailed overview of the power grids and their key parts and concepts. Chapter 4 describes the power electronics-based solid-state switches and the power electronics converters that are used in the smart grid for the transformation of voltage from one form to another. This chapter also presents the MATLAB® simulation of rectifiers, converters, inverters, and cycloconverters. Chapters 5 and 6 discuss the planning and modeling of solar photovoltaics and wind energy systems, respectively. Chapter 7 describes the microgrids and topologies of hybrid energy systems, and introduces the energy optimizing software HOMER and RETScreen, which are used for microgrids and hybrid energy systems. Chapter 8 describes energy forecasting techniques, which use the data collected from smart sensors and smart meters. This unstructured data is used to forecast future energy generation and consumption patterns. Chapter 9 presents energy storage technologies that can be integrated into distributed generation and the smart grid, and discusses the

ancillary services that these storage systems provide to the smart grid. Chapter 10 describes the topologies of electric vehicles and their integration into the smart grid. Chapter 11 concludes by discussing the current global status of the smart grid. The technical contents of the book include specialized topics that will appeal to engineers from various disciplines looking to enhance their knowledge of technologies that are making an increasing contribution to the realization of the smart grid.

Muhammad Kamran
Riphah International University,
Islamabad, Pakistan

Acknowledgments

I would like to acknowledge my colleagues and individuals without whom this project would not have succeeded. Particular thanks are due to **Mr. Muhammad Arshad Rasheed** (Research Associate, Department of Electrical Engineering and Technology, Riphah International University, Faisalabad Campus, Pakistan), who helped me in the simulation of a grid-connected solar PV system in the microgrid. I would also like to acknowledge **Muhammad Zunair Zamir** (Lecturer, Department of Electrical Engineering and Technology, Riphah International University, Faisalabad Campus, Pakistan) for reviewing some of the chapters of this book.

This page intentionally left blank

List of abbreviations

AC	alternating current
ACSR	aluminum conductor steel reinforced
AE	autoencoder
AMI	advanced metering infrastructure
ANSI	American National Standards Institute
ARIMA	autoregressive integrated moving average
ARMA	autoregressive moving average
BAN	building area network
BB-PLC	broadband-programmable logic controller
BEV	battery electric vehicle
BDC	bottom dead center
BNN	Bayesian neural network
BoS	balance of system
BPNN	back-propagation neural network
CAE	convolutional autoencoder
CAES	compressed air energy storage
CB	circuit breaker
CE	Coulomb efficiency
CF	capacity factor
CGT	combustion gas turbine
CHP	combined heat and power
CNN	convolutional neural network
COE	cost of energy
DC	direct current
DES	data encryption standard
DFIG	doubly fed induction generator
DG	distributed generation
DIAC	diode for alternating current
DMFC	direct methanol fuel cell
DNN	deep neural network
DOD	depth of discharge
DoS	denial of the service
DR	demand response
EM	energy management system
EMF	electromotive force
ESS	energy storage system
EV	electric vehicle
FC	flying capacitor
FC	fuel cell
FCEV	fuel cell electric vehicle
FES	flywheel energy storage
FFNN	feedforward neural network
FiT	feed-in tariff
FLC	fuzzy logic control

FL	fuzzy logic
GHG	greenhouse gas
GPRS	general packet for radio service
GSM	global system for mobile communication
GTO	gate turn-off
HAN	home area network
HAWT	horizontal axis wind turbine
HEMS	home energy management system
HES	hybrid energy system(s)
HEV	hybrid electric vehicle
HOMER	hybrid optimization model for electric renewables
HRSG	heat recovery steam generator
IAN	industry area network
ICE	internal combustion engine
ICT	information and communication technologies
IEA	International Energy Agency
IEC	International Electrotechnical Commission
IEEE	Institute of Electrical and Electronics Engineering
IG	induction generator
IGBT	insulated gate bipolar transistor
IGCT	Integrated gate-commutated thyristor
INC	incremental conductance
IoT	Internet of things
IRENA	International Renewable Energy Agency
IRR	internal rate of return
ISO	International Organization for Standardization
KCL	Kirchhoff's current law
KVL	Kirchhoff's voltage law
LA	lightning arrester
LCOE	levelized cost of energy
LCS	load commutation switch
LOA	level of autonomy
LOLE	loss of load expected
LPSP	loss of power supply probability
LSTM	long short-term memory
LTE	long-term evolution
LTE-A	long-term evolution-advanced
LTF	long-term forecasting
MAC	media access control
MAE	mean absolute error
MAPE	mean absolute percentage error
MCFC	molten carbonate fuel cell
MIMO	multiple input multiple output
MLI	multilevel inverter
MOV	metal oxide varistor
MPPT	maximum power point tracker
MSC	mobile switching center
MTF	medium-term forecasting
NAN	neighborhood area network
NB-PLC	narrow band-programmable logic controller
NEM	net energy metering
NPV	net present value
NREL	National Renewable Energy Laboratory
NWP	numerical weather prediction
OFDMA	orthogonal frequency-division multiple access

OC	open circuit
P&O	perturb and observe
PAFC	phosphoric acid fuel cell
PCA	principal component analysis
PCC	point of common coupling
PEM	proton exchange membrane
PEMFC	proton exchange membrane fuel cell
PHEV	parallel hybrid electric vehicle
PHEV	plug-in hybrid electric vehicle
PID	proportional integral derivative
PLC	power line communication
PMSG	permanent magnet synchronous generator
PSCAD	Power Systems Computer Aided Design
PSO	particle swarm optimization
PV	photovoltaic
PWM	pulse width modulation
QoS	quality of service
Re-LU	rectified linear unit
RES	renewable energy system
RF	random forest
RMS	root mean square
RMSE	root mean square error
RNN	recurrent neural network
ROI	return on investment
RPM	rounds per minute
RPS	renewable portfolio standard(s)
SCADA	supervisory control and data acquisition
SCR	silicon-controlled rectifier
SCS	silicon-controlled switch
SG	synchronous generator
SHEV	series hybrid electric vehicle
SMES	superconducting magnetic energy storage
SOC	state of charge
SPDT	single pole double throw
SPST	single pole single throw switch
SRF-PLL	synchronous reference frame-phase locked loop
SSCB	solid-state circuit breaker
STCs	standard test conditions
STF	short-term forecasting
SVD	singular value decomposition
SVM	support vector machine
SVR	support vector regression
TDC	top dead center
TEL	total energy loss
THD	total harmonic distortion
TRIAC	triode for alternating current
UMTS	universal mobile telecommunication system
V2G	vehicle to grid
VAR	vector autoregression
VAWT	vertical axis wind turbine
VSTF	very short-term forecasting
VSC	voltage source converter
VSI	voltage source inverter
WAN	wide area network
WPD	wind power density

This page intentionally left blank

CHAPTER

1

Introduction to smart grids

1.1 Introduction

Innovations in renewable energy sources, varying energy demand patterns, and energy-saving policies have rendered obsolete the concept of the conventional power grid. A new concept of an intelligent power grid consisting of flexible functionality and reliable information and communication technologies (ICT) has replaced the conventional power grid and is termed a smart grid. Conventional power grids contain all the components at the power generation station to ensure power transmission, power distribution, and power consumption. Power-generating units are the bulk ones like coal, oil, and gas-based steam power plants, gas power plants, hydropower plants, nuclear power plants, and combined heat and power plants. Bulk power stations may also include wind power plants and solar photovoltaic (PV) systems. The smart grid infrastructure consists of thousands of smart sensors, smart meters, advanced metering infrastructure (AMI), distributed generation sources, communication technologies, demand-side management, energy management systems, energy storage systems, and electric vehicles. All these technologies and instruments communicate with each other intelligently to make the grid smart.

All renewable energy-based production can be connected to the smart grid. Since renewable energy sources are intermittent, if one source is not available the other source will balance the load. Since the smart grid is connected to the Internet for communication purposes, the privacy and security of customers are challenges in the advancement of the smart grid. Hackers may attack the network and identify whether a customer is at home by their energy consumption pattern, and use this information to burgle a house. Hackers may also steal the credit information of a customer.

1.2 Conventional grid

The conventional grid refers to the electricity grid, which consists of power generation facilities, transmission lines, substations distribution lines, and the consumer load. Currently, we plug into a switch and power on electrical appliances. One thing worth mentioning here

https://doi.org/10.1016/B978-0-323-99560-3.00008-9

about the conventional power grid is that it contains unidirectional grids in which electricity flows from the power generation facility to the substation and the end user. The existing conventional power grid was established in the 1890s, and over time advancements were accepted and adopted in delivering the power from generation to the end user.

1.3 Problems with conventional grid

The installation of the conventional grid started in 1870s and the equipment used in conventional grids involves old technology that requires continuous maintenance to ensure uninterrupted flow of electricity from generation to the consumer. With advancements in power grid equipment and the introduction of distributed generation, smart metering, energy storage systems, and the smart grid concept, the challanges in the adoption of the smart grid have been increased. Following are the challanges in the development of the smart grid.

- Conventional power plants, especially fossil fuel-based power plants, were built near localities without keeping in mind the community of remote areas that generate the concept of off-grid energy systems. The energy needs of the growing population and the newly constructed localities are not connected to the conventional power grid, and are out of the main progressive stream of their country.
- Conventional grids are unable to incorporate energy demands during peak hours, which creates the problem of load shedding.
- In conventional grids, if consumers are producing their own electricity through renewable energy sources such as wind turbines, solar PV systems, or biogas power plants, they are not able to sell their surplus energy to the grid.
- The power flow and communication in the conventional grid are unidirectional, i.e., from power generation to the consumer. This system is incapable of estimating the situation of power shortage on the generation side and the requirement of power on the consumer side.
- The power grid is at the risk of collapse because of the load imbalance. When the load demand exceeds the power generation, the system collapses and a complete shutdown may occur.
- Electricity meters in the conventional power grid system are obsolete, providing information only in terms of total energy consumed. They do not record the exact time of the energy consumed, which would indicate whether it was consumed during peak or off-peak hours.

1.4 What is a smart grid?

A smart grid is the electric power grid, which establishes a communication network between the power supplier and the power consumer with the help of smart sensors, smart meters, electric vehicles, and power-generating utilities. The smart grid introduces an energy management system that helps in balancing the energy demand and supply to produce and consume electricity efficiently at a lower cost. A comparison between the conventional power grid and the smart grid is shown in Table 1.1. The Energy independence and security Act (EISA 2007) has indicated the following features of a smart grid.

TABLE 1.1 A comparison between the conventional grid and the smart grid.

Characteristics	Conventional grid	Smart grid
Power generation	**Centralized** With conventional grid infrastructure, the power is generated at the conventional central power station, removing the possibility of integrating renewable energy sources.	**Distributed generation** In smart grid architecture, multiple power sources like wind and solar can be integrated into the grid, balancing out the load during the peak hours and eliminating the possibility of a complete blackout.
Communication	**One-way** In conventional grids, there is no communication from the devices to the grid. Limited one-way communication occurs from the grid to the customer.	**Two-way** The basic feature of the smart grid is communication between smart devices. Signals from all the sensors, and smart meters to the grid and from grid to the smart meters is a two way communication which makes the grid smart.
Metering	**Electromechanical** In conventional grids, electromechanical meters are used with no smart sensors and no communication instruments.	**Smart digital** In smart grids, smart digital meters are used which have the capability of two-way communication, indicating the peak hours and billing information.
Monitoring	**Manual** Because of the limitations of conventional grids, monitoring is done manually.	**Self-monitoring** The deployment of digital technology in smart grids makes them self-monitoring, load balancing, and energy managing.
Power flow	**One-way** In conventional grid infrastructure, power flows from the grid to the load.	**Two-way** In a smart grid, architecture power flows from the grid to the load, and the renewable energy generators can feed the power to the grid at the same time.
Architecture	**Radial** In a conventional grid, bulk generation is transmitted and distributed to the end users. The system is controlled by the central control supervisory control and data acquisition (SCADA) system.	**Network** Power generated by distributed sources is fed to the grid; power can also be sold to the grid, controlled by the two-way communication system. The architecture of the smart grid consists of different layers like the application layer, communication layer, and the power system layer.
Restoration	**Manual** In case of failure in the grid architecture, a technician has to visit the grid to detect the fault and manually repair it, which increases the blackout time.	**Self-healing** In smart grid architecture, smart sensors detect the fault and clear the fault. In case of serious damage, sensors signal the technician about the exact location of the fault.
Controlling	**Limited** In conventional grids, power companies have no control over transmission and distribution; these aspects can only be controlled in the generation plant and the substation.	**Pervasive** The use of smart sensors, smart devices, and two-way communication in the smart grid makes it easy to control the power distribution and flow of power between consumers and the grid.

Continued

TABLE 1.1 A comparison between the conventional grid and the smart grid—cont'd

Characteristics	Conventional grid	Smart grid
Customers	**Fewer** The customers cannot choose to use most of the smart technologies like net metering facilities and integration of renewable energy sources to the grid.	**Many** The use of smart sensors, smart meters, and net metering in the smart grid attracts more customers to purchase from the power utility.

- The efficiency, security, and reliability of the smart grid are increased by the advancement of control technology and communication technology.
- The resources and operation of the smart grid are optimized and secured.
- Renewable energy resources and the distributed generation are integrated.
- Demand-side management is developed in the smart grid.
- The consumer can control the energy consumption pattern and can communicate with the grid in real time.
- Energy storage systems are developed and ancillary services are obtained through hybrid and plug-in hybrid electric vehicles.
- Smart appliances, devices, smart meters, and smart sensors used by the consumer can be integrated into the system.

1.5 Overview of the smart grid

This section details the infrastructure of the smart grid which includes the architecture of the smart grid, distributed generation, electric vehicles, energy storage systems, smart and fast measuring, sensing instruments, integrated communication between all elements of the smart grid, etc. Fig. 1.1 provides an overview of the smart grid.

1.5.1 Smart grid architecture

The difference between the conventional power grid and the smart grid is their architecture. The architecture of the smart grid consists of different layers like the application layer, communication layer, and the power system layer. The infrastructure of the smart grid is shown in Fig. 1.2.

1.5.1.1 Application layer

The application layer enables customer applications, smart meter applications, and power grid applications. In customer applications, it enables home automation, real-time pricing, and demand management. In smart meter applications, it enables auto meter reading, and communication between the consumer and the power company about billing and energy demand in real-time.

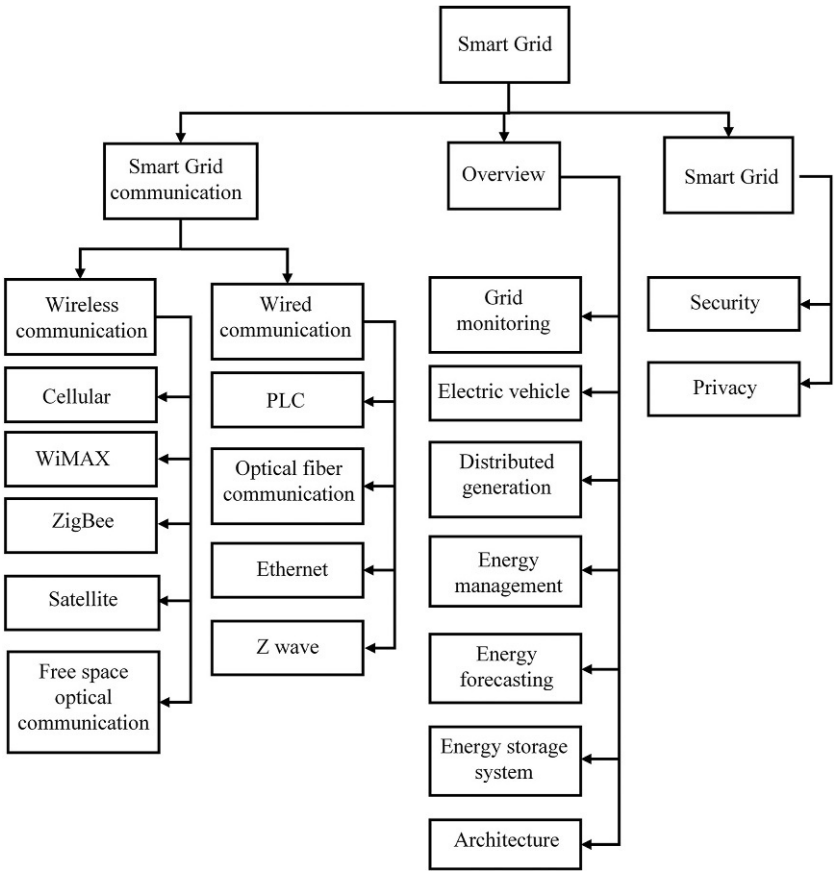

FIG. 1.1 Overview of the smart grid.

1.5.1.2 Communication layer

The architecture of the communication layer is the major difference between the conventional and the smart grid. All the communication between the consumer, smart meter, and the power utility is done through the communication layer. The signals from all the sensors used in the smart grid and in response the signals from the controller to take action are transmitted in the communication layer. A communication network based on geography is divided into the following categories, and a comparison between them is given in Table 1.2.

- **Home area network (HAN):** also known as the customer area network, this enables smart home devices and appliances, and connects them to the smart meter. The range of the HAN is short and the communication reliability with a low data rate is high. Implementation costs and the energy consumption of HAN are lower than the other types of the area networks.
- **Building area network (BAN):** this is a local area network (LAN) similar to the HAN and covers a whole building. If a floor of a building is considered a LAN, then the combination of the LANs of all the floors is considered the BAN.

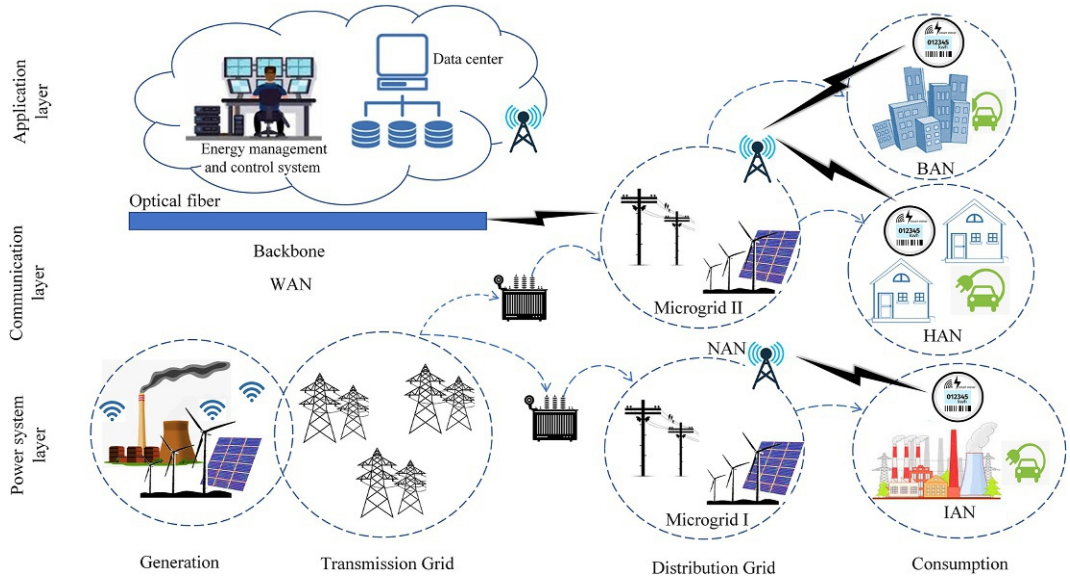

FIG. 1.2 Comprehensive infrastructure and architecture of the smart grid consisting of generation, transmission, distribution, and consumption.

TABLE 1.2 A comparison of different area networks.

Network	Data rate	Coverage	Alternative technology
WAN	10 Mbps–1 Gbps	10–100 km	WiMAX, 3G, 4G, 5G, Ethernet, optical fiber
NAN	100 kbps–10 Mbps	10 m–10 km	ZigBee, Wi-Fi, WiMAX, cellular, power line communication
HAN/BAN/IAN	10–100 kbps	1–100 m	ZigBee, Z-wave, Wi-Fi, Ethernet

- **Industry area network (IAN):** this is a more complex network covering a whole factory or an industry.
- **Neighborhood area network (NAN):** this is responsible for connecting a HAN, BAN, and IAN to a WAN. A NAN allows users to connect to the Internet quickly at a very low cost. Since the range of the NAN is high, its data rate is also high. In the smart grid, a NAN connects thousands of smart meters to the database.
- **Wide area network (WAN):** this is a large area network that enables communication over a large geographic area. In the smart grid, a WAN is used by a NAN to send and receive data from thousands of microgrids, smart meters, and other components of the smart grid. Since a large volume of information is carried by a WAN, a high data rate is required for communication, and optical fiber is commonly used for WAN communication.

1.5.1.3 Power system layer

The power system layer works like the conventional power grid, and handles the generation, transmission, and distribution of power in the smart grid.

1.5.2 Grid monitoring

The reliability and the power quality of the smart grid are ensured by continuous monitoring of the system. If the voltage, current, frequency, and/or power of the grid are beyond the permissible limits, the performance of smart devices and sensors is degraded. Smart sensors, advanced metering infrastructure, and the SCADA system are used to implement smart grid monitoring.

1.5.3 Electric vehicles

Another technology that is part of the smart grid is the electrification of a vehicle, termed the electric vehicle (EV). Different configurations are adopted in EVs. Battery electric vehicles (BEVs) use only battery storage that is externally charged from the grid; no other source of energy like an internal combustion engine is integrated. Hybrid electric vehicles (HEVs) include parallel hybrid electric vehicles, series hybrid electric vehicles, and series-parallel hybrid energy systems. HEVs use two sources of energy: an internal combustion engine and a battery pack. If the state of charge (SOC) of the battery is high, the electric motor uses the battery for transmission. If the SOC of the battery is low, the engine works and provides the transmission. Plug-in hybrid electric vehicles (PHEVs) are the same HEVs with an additional feature of external charging from the grid. Fuel cell EVs use a compressed hydrogen fuel tank and a fuel cell stack. These EVs also provide various ancillary services to the grid. In cases where a grid is not available in a remote area, an EV can be a source of backup power.

1.5.4 Distributed generation

Distributed generation (DG) is defined as the generation of electricity using conventional or the renewable energy sources to feed the load connected to the distribution network. If the distribution network is connected to the transmission network, it may sell and purchase electricity for the grid. Depending upon the location of the DG, the range is defined as a few kilowatts to 400 MW. However, renewable energy sources are abundant but intermittent. The availability of the energy sources and the efficiency of the related energy-harnessing technology decide the efficiency of the DG. The various energy technologies that are considered part of DG are conventional technologies, renewable energy technologies, and mixture of both conventional and renewable energy technologies.

DG technologies are categorized as follows based on the energy source:

(1) DG sources based on conventional fossil fuel-based power plants (microturbine, reciprocating engine, Stirling engine, combined cycle gas turbine, combustion gas turbine, etc.);
(2) DG sources based on renewable energy sources like solar PV systems, wind, biogas, geothermal, micro-hydro, and fuel cell; and.

(3) mixed DG energy sources where conventional and renewable energy sources in combination form a microgrid.

DG technologies like solar PV arrays, wind turbines, solar thermal, micro-hydro, diesel engines, fuel cells, and storage systems are modular and available in smaller units that can be installed in the system and removed from the system in a very short time. Other DG technologies are reciprocating engines, combined cycle gas turbines, microturbines, combustion gas turbines, and Stirling engines.

1.5.5 Smart metering

In conventional meters, recording done manually by a meter reader could be erroneously recorded, and the intervention of the consumer also makes the system unreliable. Fig. 1.3 shows the infrastructure of a conventional meter in which all the communication and the power flow are unidirectional from power generation to the end user, and all is done manually. Smart metering is the key concept in implementing the smart grid concept. The smart meter's various functions include net metering. This is the billing mechanism in which the consumer can dispatch their generated electricity from the renewable energy sources to the grid when they are generating energy that is surplus to their requirements. They can later import electricity from the grid when their production is lower than the energy they need. At the end of the month, a net bill is sent by the company to the consumer. Depending on the net metering policy of the country or province, the consumer receives a retail price per unit of electricity sold to the grid, which encourages people to invest in renewable energy power generation.

A smart meter, in addition to recording the energy imported from the grid and exported to the grid, records the power factor, current, and voltage level. For clarity in billing, smart meters specify for consumers the energy consumed in peak hours and off-peak hours. The infrastructure of smart metering is shown in Fig. 1.4, in which the communication between

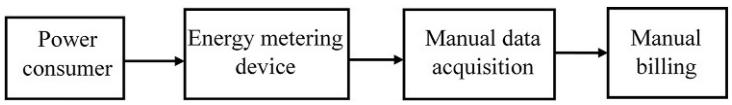

FIG. 1.3 Infrastructure of conventional meter showing unidirectional communication and power flow.

FIG. 1.4 Infrastructure of smart meter showing bidirectional communication and power flow.

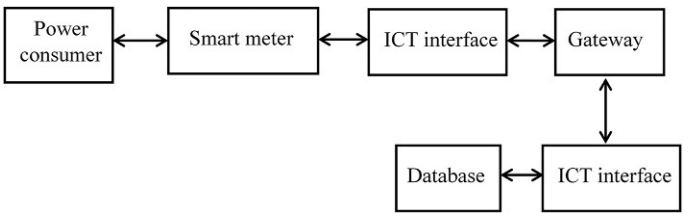

the database and the power consumption is bidirectional through information and communication technology (ICT) and the smart meter. The advanced metering infrastructure (AMI) provides the following advanced functions in the smart meter:

- statistics on power usage;
- prepayments and postpayments;
- electricity theft prevention;
- different events like power off;
- peak hours and off-peak hours;
- meter cover opening; and

The smart meter also monitors the overvoltage, undervoltage, voltage and current imbalance, power factor, voltage, and current.

1.5.6 Energy management

People's lifestyles are reflected in their per capita energy consumption. With an increase in energy demand, the production of energy should also be increased to balance demand and supply. The unpredictable load and intermittent renewable energy sources require either a larger network or an energy management system (EMS) for the smooth operation of the system. The basic components of an EMS are a communication system, renewable energy sources, smart meter, power utility, hybrid electric vehicles, and load. All these components are connected with a bidirectional power flow and two-way communication, as shown in Fig. 1.5. An EMS is the main feature of a smart grid because it:

- is a digitalized automatic system free from human intervention, which reduces errors in load and resource prediction;
- helps in balancing the energy production and consumption, which optimizes the system and reduces the cost of energy; and
- helps in implementing the demand response.

An EMS is applied to the following three main actors of the smart grid.

- Electricity producers use the EMS to optimize the power production, keeping in view the energy demand. For example, if energy demands fluctuate at a specific time, the power producer may shut down some of the generators that generate expensive units of electricity. Similarly, on a cloudy day, the power producer may shift the load to other renewable energy sources like wind, biomass, biogas, etc.
- System operators use the EMS to regulate the power flow in the transmission and distribution system, reducing the line losses and increasing the penetration of the renewable energy-based electricity.
- Power consumers use the EMS to minimize power consumption during peak hours by scheduling the load.

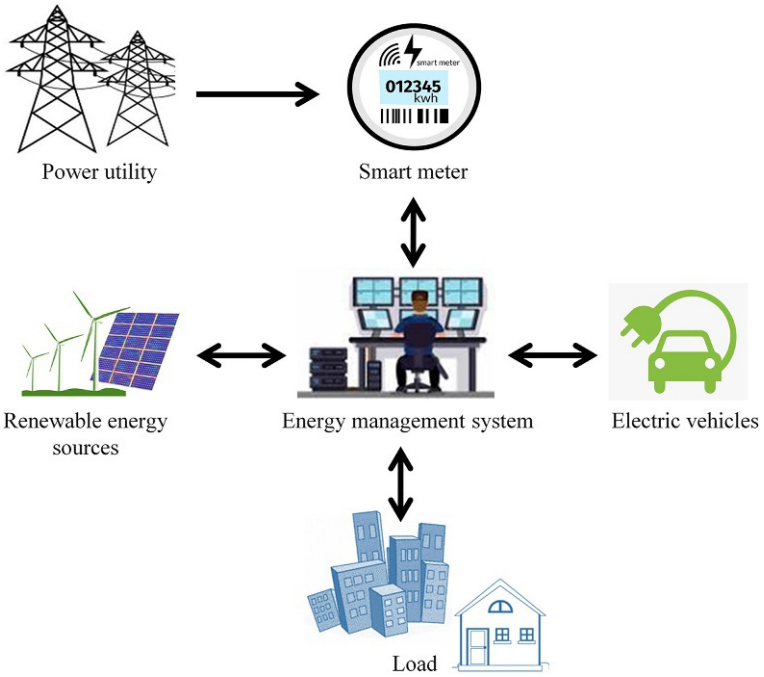

FIG. 1.5 Energy management system in a smart grid.

1.5.7 Energy forecasting

In addition to the smart meter and the network of sensors, forecasting is another key feature of the smart grid. In a smart grid, three types of forecasting are performed: energy demand forecasting, energy production forecasting, and price forecasting. The consumption of energy is estimated by considering the energy demand by residential, commercial, and industrial energy consumers. Energy production forecasting is performed considering the availability of renewable energy sources like wind speed, solar irradiance, biomass, and geothermal energy. Price forecasting depends on the time of energy production and the source of energy from which electricity is being generated. Which technology for a single energy source is being used to harness the energy also impacts the price of the end product, i.e., electricity. Concerning the time horizon, the following types of forecasting are performed:

- very short-term forecasting (VSTF);
- short-term forecasting (STF);
- medium-term forecasting (MTF); and
- long-term forecasting (LTF).

The following methods are used for the above-stated time horizon types of forecasting:

- statistical
- machine learning
- deep learning

- probabilistic
- probabilistic deep learning
- hybrid
- preprocessing.

1.5.8 Demand response

The ability provided by the smart grid to consumers to alter their pattern of energy consumption by decreasing or shifting their electricity usage in response to peak hours for the sake of incentives is termed demand response (DR). Advanced metering infrastructure (AMI) and communication between the power-producing company and the end user let them decide when to produce and when to consume electricity, respectively. DR programs are used to balance the demand and supply of electricity. Customers are engaged in DR by being offered different incentives like time of use pricing, variable peak pricing, critical peak pricing, critical peak rebates, and real-time pricing. DR can also be part of the home energy management system (HEMS), where a consumer can switch off appliances that require heavy loads during peak hours, such as air conditioners and air and water heaters, and switch them on only during off-peak hours.

1.5.9 Energy storage system

Another key component of the smart grid is the energy storage system (ESS). In a conventional grid, the integration of the ESS is not feasible, but the smart grid and distributed energy sources make it possible to incorporate the ESS. With advancements and innovations in renewable energy sources and their harnessing techniques, distributed generation has become a novel concept, and the ESS is an essential component of the hybrid energy system and the smart grid. It helps to bridge the gap between energy production and energy demand. Because of the intermittent and unpredictable nature of renewable energy sources like solar and wind, grid ancillary services are not easy to obtain. The ESS is the best solution to incorporate these services. Ancillary services include grid stabilization, renewable energy integration, power quality, frequency regulation, load following, peak shaving, spinning reserve, time-shifting, and transient stability. Energy is stored in three different forms: electromagnetic, mechanical, and chemical. Technologies that are used to store energy in an electromagnetic form are capacitors, supercapacitors, and superconductors. Mechanical technologies to store the energy are pumped hydro energy storage systems, compressed air energy storage systems, and flywheel energy storage systems. Chemical energy is stored in the form of conventional batteries, flow batteries, and regenerative fuel cells.

1.6 Smart grid communication

1.6.1 Wireless communication

1.6.1.1 Cellular communication

Cellular communication is the most feasible option for the placement of communication infrastructure, since this system already exists in the telecommunication framework. Cellular

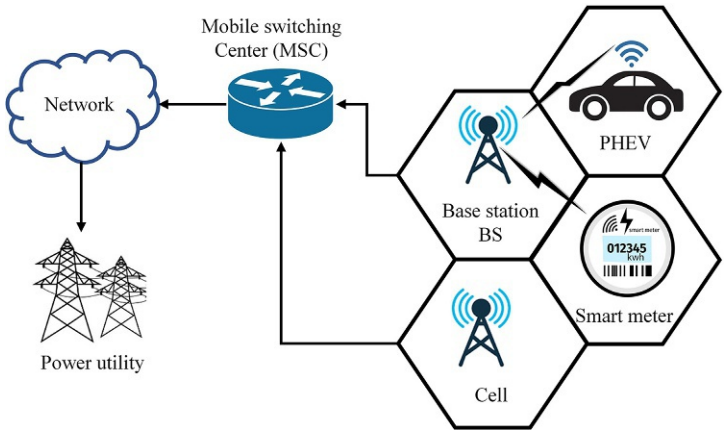

FIG. 1.6 Cellular communication in a smart grid.

technology is a reliable, high-quality, and high data rate network. Technology is still in development stages. Different technologies for cellular communication are the global system for mobile communication (GSM), general packet for radio service (GPRS), enhanced data rate for GSM evaluation (EDGE), the universal mobile telecommunication system (UMTS), high-speed packet access (HSPA), and long-term evolution-advanced (LTE-A) [1,2]. These cellular technologies are being used for electric vehicle communication, wide area networks (WANs), advanced metering infrastructure (AMI), and house area networks (HANs). The land area is divided into small areas called cells; multiple frequencies are assigned to a cell, and that cell contains the corresponding radio base station, as shown in Fig. 1.6. These frequencies can be reused in other cells, but not in adjacent cells, to avoid signal interference. Smart devices in the cells are connected to the base station, which is connected to the rest of the network through the mobile switching center (MSC) [3,4]. The power utility is also connected to the network. The application of cellular communication in the smart grid is shown in Fig. 1.6.

1.6.1.2 WiMAX

Worldwide interoperability for microwave access (WiMAX) is a wireless communication technology based on the set of IEEE 802.16 standards. WiMAX is similar to LTE and competes with it. It works within a range of 50 km with a 70 Mbps data rate. WiMAX works in two frequency bands. The frequency band of the line of sight communication is 11–66 GHz and for nonline of sight communication, it is 2–11 GHz [5]. WiMAX can also work as a network by scaling it to the local and regional levels. The IEEE 802.16 standard defines the physical and MAC layers. Multiple input multiple output (MIMO) and orthogonal frequency division multiple access (OFDMA) antennas are provided by the physical layer, which increases the nonline of sight capabilities. Secure and reliable communication is ensured by the media access control (MAC) layer by enabling data encryption standards (DES) and advanced encryption standards (AES). Because of the signal loss or attenuation, coverage of WiMAX becomes limited, which is its only drawback [6,7].

1.6.1.3 ZigBee

ZigBee is a wireless communication network based on the IEEE 802.15.4 standards. The key characteristics of this energy-efficient technology are the low data rate and short-range communication. ZigBee works on 2.4 GHz, 915 MHz, and 868 MHz frequency bands [8,9]. It has mesh capabilities that have the ability to self-manage and self-connect to any node when required. For this, ZigBee can be used in HANs for remote monitoring, consumer electronics control, home automation, and smart meter reading [10]. The disadvantage of ZigBee is that it can interfere with nearby USB, Wi-Fi, Bluetooth, and microwave since they operate on the same frequency as ZigBee [10].

1.6.1.4 Z-wave

Z-Wave is a wireless communication standard mostly used for home automation in residential and commercial areas and is based on the IEEE 802.15.4 standard. Z-wave is a low-cost, low data rate, and short-range technology that has a 30 m indoor communication range and a 100 m outdoor communication range.

1.6.1.5 Satellite communication

Conventionally, satellites are used for planes, TV, radio broadcasting, military purposes, navigation, weather forecasting, and communication in vehicles. The advanced key feature of superior performance and reliability of satellite communication makes it favorable for the smart grid communication. Since the satellite is above the earth's surface, in space, it is invulnerable to natural disasters. Communication between all components of the smart grid is carried through the satellite. Satellite communication consists of two parts: a satellite in space and the primary control center on the ground [11]. Smart meters, power-generating facilities, and energy storage devices communicate through the satellite. Delay in data transfer is the major drawback of satellite communication. This technology is not feasible for real-time communication, since the data travels over a large distance from one device to the other [12]. Satellite communication in a smart grid is shown in Fig. 1.7.

1.6.1.6 Free space optical communication

Free space optical communication is a wireless communication and optical communication technology in which the signal is transmitted through the space in the form of light. No physical connection like an optical fiber cable is required to transmit the data. Table 1.3 compares different wireless communication technologies.

1.6.2 Wired communication

1.6.2.1 Power line communication (PLC)

Power line communication (PLC) refers to communication through existing power lines. PLC works on a physical medium and requires no intervention from communication companies. Since all the devices in the smart grid are connected to the power line, which is also used to receive and transmit the signals, no further communication medium is required. For this reason, PLC is considered an important part of future smart grids [13]. PLC is categorized as

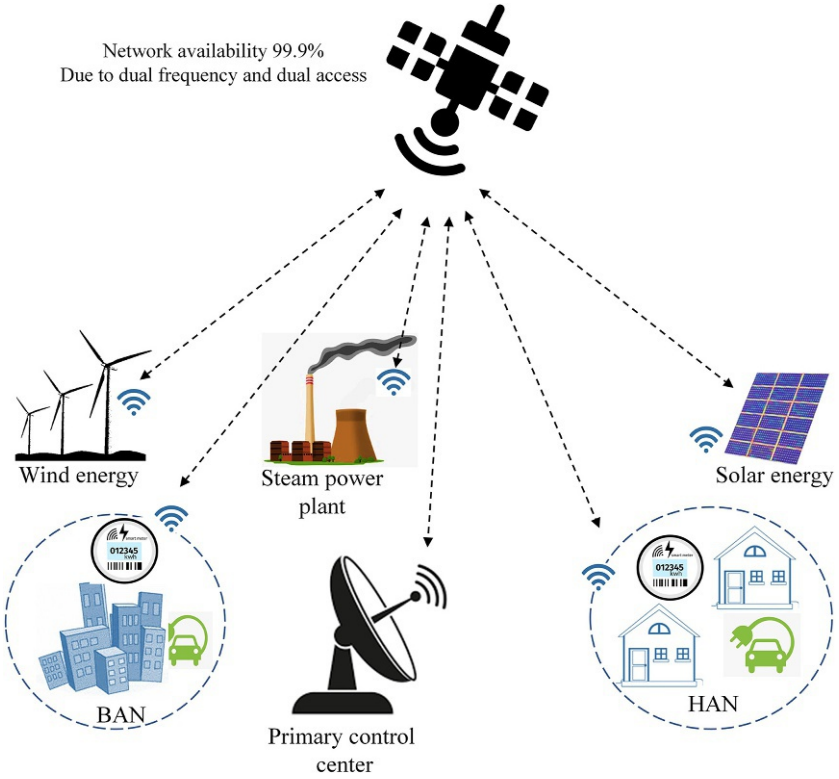

FIG. 1.7 Satellite communication in a smart grid.

TABLE 1.3 Comparison of wireless communication technologies.

Technology	Standard	Advantages	Disadvantages
WiMAX	• IEEE 802.16 • IEEE 802.16j • IEEE 802.16m	• Covers more distance than Wi-Fi • A connection-oriented control of the channel bandwidth	• Complex network management • Licensed spectrum is required • Terminal equipment are expensive
GSM	• 2G TDM, IS95 • 2.5G HSCSD, GPRS • 3G UMTS • 3.5G HSPA, CDMA EVDO • LTE, LTE-A	• Supports millions of devices • High flexibility • Low power consumption of terminal equipment	• Expensive service provider networks • Expensive licensed spectrum

TABLE 1.3 Comparison of wireless communication technologies—cont'd

Technology	Standard	Advantages	Disadvantages
Satellite	• LEO • MEO • GEO	• High reliability • Long distance	• High latency • High cost of terminal equipment
WPAN	• IEEE 802.15.4 • ZigBee, ZigBee Pro • ISA 100.11a	• Low cost deployment • Very low power consumption • Compatible with IPv6	• Limitations to build large networks • Low bandwidth
Wi-Fi	• IEEE 802.11e • IEEE 802.11n • IEEE 802.11s • IEEE 802.11p (WAVE)	• Network deployment cost is low • High flexibility • Less expensive equipment	• Spectrum interference is high • Too much power consumption

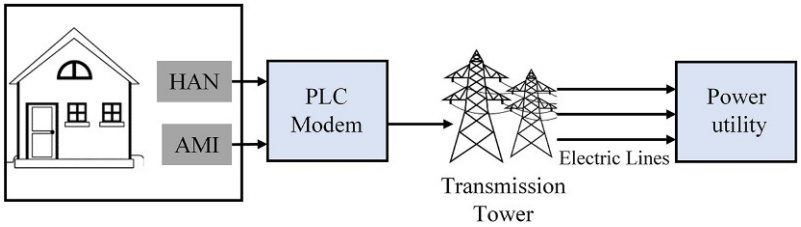

FIG. 1.8 Power line communication in smart grid.

narrowband PLC (NB-PLC) and broadband PLC (BB-PLC). The PLC communication architecture in the smart grid is shown in Fig. 1.8.

1.6.2.2 Fiber optical communication

Fiber optical communication technology is expensive but has various advantages over other communication methods, including high data rate, high bandwidth, and long range. There are also no chances of electromagnetic interference with the optical fiber. It is used for communication between substations and utility companies [14,15].

1.6.2.3 Ethernet

Ethernet is the most commonly available wired communication technology, and is best suited for WANs between substations and control centers. For smart grid applications, Ethernet is used in HANs for smart meter communications.

1.7 Advantages of smart grid

1.7.1 Energy conservation

Renewable energy sources like solar, wind, biogas, biomass, fuel cell, and geothermal are continuous sources of energy, but they are intermittent. This intermittency can be overcome by integrating energy storage systems. With the advancements in energy harnessing technologies from renewable energy sources, conventional energy sources are being replaced. In addition, the use of energy forecasting techniques, smart metering, and energy management systems has proved to be more energy conserving. Customers can save energy by rescheduling their use of energy from peak to off-peak hours.

1.7.2 Reliability

The use of communication technologies and smart meters makes the smart grid more reliable. Communication technologies keep the power producers, power operators, and power consumers in touch and update the status of the grid continuously. Smart meters enable consumers to be aware of peak hours and the related pricing policy. Distributed generation is another key element that ensures the reliability of the smart grid. At times when the source of energy is not available, another source of energy keeps feeding the load.

1.7.3 Advancement in electric vehicles

Electric vehicles are another part of the smart grid, and act as energy storage devices. Smart charging stations use solar energy to charge electric vehicles. In hybrid electric vehicles, vehicles are recharged with the regenerative braking process. If the SOC of the battery of the vehicle is 100%, this electricity can be sold to the grid in peak hours at a competitive high price, and in off-peak hours the battery can be recharged from the grid at lower rates. Hence, the smart grid creates oppertunities for the innovative research in the field of the electric vehicles.

1.7.4 Reduction in carbon footprint

The basic ideas behind the smart grid are to reduce reliance on conventional fossil fuels and to promote renewable and alternative energy sources. Every effort in the smart grid is focused on reducing the emissions from the generation of electricity.

1.7.5 Competitive price of energy

In smart grids, the flow of energy and the communication is bidirectional; consumers can limit their energy consumption during peak and off-peak hours. They can either sell their energy to the grid or purchase it from the grid at a relatively low price. If a consumer purchases electricity from the renewable energy-based microgrid during off-peak hours, they will be charged less, while if they purchase conventional fuel-based electricity during peak hours, they will be charged more.

1.7.6 Smart devices and smart homes/smart buildings

The intelligence of the smart grid lies in the smartness of smart meters, smart devices, smart home appliances, smart buildings, and smart cities. Smart devices and smart home appliances can be accessed and operated from anywhere with the help of the Internet. Smart homes, smart buildings, and smart cities help in promoting a smart grid.

1.8 Issues and challenges relating to smart grids

Fig. 1.9 illustrates all the issues and challenges faced by the smart grid. These issues and challenges are discussed in the following subsections.

1.8.1 Communication challenges

1.8.1.1 Lack of standards

Different components in the smart grid communicate with each other in a framework that requires standards. To tackle the advancement in communication technologies, advanced communication standards are required. Some communication standards have been formulated by the Institute of Electrical and Electronics Engineering (IEEE), International Organization for Standardization (ISO), International Electrotechnical Commission (IEC), and American National Standard Institute (ANSI). Some of these standards cover communication over electrical lines (IEEE 1901), smart grid interoperability (IEEE 2030), electrical power

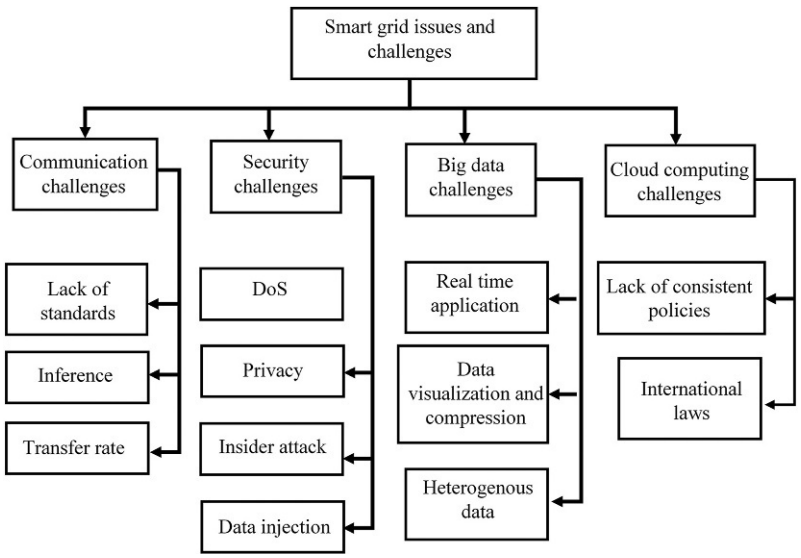

FIG. 1.9 Issues and challenges in a smart grid.

system communication distributed network protocol (IEEE 1815–2012), synchro phasor data transfer (IEEE C37.118.2–2011), advanced metering infrastructure, and cyber security (IEC 62351).

1.8.1.2 Interference

Interference is the wireless communication challenge in which the interfering signal from other devices may distort the original information. The interfering signal has its own frequency characteristics. Channel switching techniques can be used to avoid interference from other devices or the grid itself.

1.8.1.3 Transfer rate

As thousands of devices are connected in the smart grid, ensuring a high data transfer rate without compromising quality of service (QoS) is a challenge.

1.8.2 Security challenges

Because of the presence of various sensors, communications, and the Internet, a smart grid is always vulnerable to security threats. Microgrids, smart sensors, distributed generations, electric vehicles, and the grid are interconnected, which increases the vulnerability of the smart grid. Hackers may illegally access software and database management systems, and may steal and alter the data of the consumers as well as the power utility. If a hacker disconnects the communication between the power consumer and the power producer, the smart meter might be tampered with to alter the billing information and the money credits. The following points are instances where the security of the smart grid could be threatened.

1.8.2.1 Denial of service (DoS) attack

Denial of service (DoS) attacks refer to the prevention of services to consumers which can be obtained by multiple attacks on a system, causing it to become overwhelmed. The attacker thus stops the services to the customer and sends false messages to the control. The control messages in response might face a delay and the complete system may face the failure of the system. Advanced DoS attacks are modified to be very difficult to detect, because they pretend to be from a trustworthy source and may appear legitimate.

1.8.2.2 Privacy

Smart meters in the smart grid acquire various information about the customers like identity card number, location, mode of payment, credit card information, and load preferences. Attackers may hack a user's smart meter, and look at the energy usage pattern to guess when the residents are at home and when they leave the house. Advertisers may steal the contact numbers for customers and send them ad messages. Therefore, the privacy of the customers' information must be secured.

1.8.2.3 Insider attack

Insiders are entities who are authorized in the smart grid to perform a function and have information legally. They include power producers, power consumers, third parties

providing any service, operators, and employees. If an insider steals information and performs illegal activity in the smart grid, this is termed an insider attack. These attacks are serious threats to the smart grid since legal authority is in place to use the passwords, and the firewall cannot easily detect fraudulent activities. Such activities can be spotted by checking for irregular behaviors in the system.

1.8.2.4 Data injection

System operators can send false information to the central controlling entities to mislead them regarding the information related to the power generation side or the power user end. The operator may send false data regarding a specific customer to change their energy usage hours. The customer can change his peak hours to off-peak hours and will be charged less during peak hours.

1.8.3 Big data challenges

1.8.3.1 Real-time application

Smart grids are meant to survey the energy consumption pattern of thousands of customers and get real-time data from the smart meters. The smart grid must be able to handle the data from thousands of connected devices in real-time to ensure the grid's accurate operation. Internet of Things (IoT)-based applications can be adapted to handle the issue by analyzing the required data rate for a smart device and allocating a dedicated band for that device for a specific time.

1.8.3.2 Data visualization and compression

Data from thousands of sensors, smart meters, and smart devices is stored for further record processing and analysis. Real-time data compression is a necessity to maintain the real-time operation of the system. The data can presented in a visual way to be used for further research such as energy forecasting, demand response, and load forecasting.

1.8.3.3 Heterogeneous data

The heterogeneity of the data refers to the different types of data from different sources. The smart grid receives data from smart sensors, smart meters, smart home devices and appliances, stations, actuators, software, and mobile applications. These devices receive and send authentication messages, error messages, messages indicating peak hours, messages indicating off-peak hours, etc. This is called the heterogeneity of the data. In this way, the grid has to tackle and process structured, semistructured, and unstructured data.

1.8.4 Cloud computing challenges

Cloud computing is defined as the model for enabling on-demand network access to a shared pool of configurable computing resources (servers, networks, services, storage, and applications) that can easily be released with minimum interaction of the Internet service provider and minimal management efforts. The basic purpose of cloud computing is to distribute resources to multiple computers. The application of cloud computing in the smart grid is

considered a challenge since smart grid users have concerns over the authenticity of cloud computing [16,17]. Hence, the following challenges must be considered when designing cloud computing for smart grid systems.

- lack of consistent policies;
- inefficient cloud security policy;
- location of data;
- mixing of data; and
- international laws.

1.9 Conclusion

The smart grid is an efficient electrical power system with better performance than the conventional grid. Continuous monitoring in the smart grid increases its reliability and safety. Electric vehicles can act as energy storage systems, providing all ESS applications and ancillary services. EVs can be charged from the grid during off-peak hours and discharged to the grid during peak hours. All the distributed generation that makes a microgrid can form a smart grid. Conventional electricity meters have been replaced with advanced metering infrastructure (AMI), which carries the bidirectional power flow and the communication system. Various energy storage systems can be integrated to the smart grid. In short, all the features of the smart grid and the energy forecasting methods provide an efficient energy management system for the smart grid.

Problems

Problems 1–7 contain four answer options: A, B, C, and D. Choose the correct answer.

1. Which of the following is a key feature of the smart grid?
   A. The consumer can control and communicate in real-time.
   B. The renewable energy resources and the distributed generation are integrated.
   C. The resources and the operation of the smart grid are optimized and secured.
   D. All of the above.

2. The architecture of the smart grid consists of which layer(s)?
   A. Application layer
   B. Communication layer
   C. Power system layer
   D. All of the above

3. Which of the following are parts of the communication layer?
   A. Home area network, building area network
   B. Home area network, building area network, industry area network
   C. Home area network, building area network, industry area network, neighborhood area network
   D. Home area network, building area network, industry area network, neighborhood area network, wide area network

4. Which of the following is a time horizon-based type of the energy forecasting technique?
   A. Very short-term forecasting method
   B. Short-term forecasting method
   C. Medium-term forecasting method
   D. Long-term forecasting method
5. What is demand response?
   A. The ability of a consumer to change their electricity usage pattern in response to peak hours.
   B. The ability of a generating station to change its generation pattern in response to demand.
   C. The ability of an energy storage system to provide electricity during peak hours.
   D. The ability of a transmission system to enhance the current carrying capacity during peak hours.
6. What wireless communication technologies are used in smart grids?
   A. Cellular communication, WiMAX
   B. Cellular communication, WiMAX, ZigBee, Z-wave
   C. Cellular communication, WiMAX, ZigBee, Z-wave, satellite communication
   D. Cellular communication, WiMAX, ZigBee, Z-wave, satellite communication, free space optical communication
7. What wired communication technologies are used in smart grids?
   A. Power line communication
   B. Fiber optical communication
   C. Ethernet
   D. All of the above

Answer the following short questions

1. How would you define the conventional power grid, and which sources are used in the conventional grid?
2. What problems arose from the conventional grid that demanded the smart grid?
3. List the key features of a smart grid indicated by the Energy Independence and Security Act (EISA).
4. Give a detailed comparison of the smart grid and the conventional grid.
5. Give an overview of the smart grid.
6. Present the architecture of the smart grid.
7. Which networks are involved in the communication layer of the smart grid architecture?
8. Which wireless communication technologies are used in the smart grid?
9. Which wired communication technologies are used in the smart grid?
10. What is the role of smart metering in the smart grid?
11. Differentiate between electromechanical and smart digital meters.
12. Why is the energy management system considered the main feature of the smart grid?
13. Which actors are involved in the energy management system of the smart grid?
14. Which three elements of the smart grid are forecasted?
15. In terms of time duration, what types of forecasting are there?
16. Which energy forecasting techniques are used in the smart grid?
17. Define demand response in the smart grid.

18. List the different technologies of the energy storage systems.
19. Which ancillary services are provided by the energy storage system?
20. What types of challenges are involved in the advancement of the smart grid?
21. What security challenges are involved in the smart grid?
22. What communication challenges are involved in the smart grid?
23. What big data challenges are involved in the smart grid?
24. What cloud computing challenges are involved in the smart grid?

References

[1] H. Hui, Y. Ding, Q. Shi, F. Li, Y. Song, J. Yan, 5G network-based internet of things for demand response in smart grid: a survey on application potential, Appl. Energy 257 (2020) 113972, https://doi.org/10.1016/J.APENERGY.2019.113972.
[2] M. Garau, E. Ghiani, G. Celli, F. Pilo, S. Corti, Co-simulation of smart distribution network fault management and reconfiguration with LTE communication, Energies 11 (6) (2018) 1332, https://doi.org/10.3390/EN11061332.
[3] G. Karagiannis, G.T. Pham, A.D. Nguyen, G.J. Heijenk, B.R. Haverkort, F. Campfens, Performance of LTE for smart grid communications, in: Lect. Notes Comput. Sci. (including Subser. Lect. Notes Artif. Intell. Lect. Notes Bioinformatics), vol. 8376, 2014, pp. 225–239, https://doi.org/10.1007/978-3-319-05359-2_16.
[4] S. Ahmadzadeh, G. Parr, W. Zhao, A review on communication aspects of demand response management for future 5G IoT- based smart grids, IEEE Access 9 (2021) 77555–77571, https://doi.org/10.1109/ACCESS.2021.3082430.
[5] A. Usman, S.H. Shami, Evolution of communication technologies for smart grid applications, Renew. Sustain. Energy Rev. 19 (2013) 191–199, https://doi.org/10.1016/J.RSER.2012.11.002.
[6] F.E. Abrahamsen, Y. Ai, M. Cheffena, Communication technologies for smart grid: a comprehensive survey, Sensors 21 (23) (2021) 8087, https://doi.org/10.3390/S21238087.
[7] P. Rengaraju, C.H. Lung, A. Srinivasan, Communication requirements and analysis of distribution networks using WiMAX technology for smart grids, in: IWCMC 2012—8th Int. Wirel. Commun. Mob. Comput. Conf, 2012, pp. 666–670, https://doi.org/10.1109/IWCMC.2012.6314284.
[8] A. Mahmood, N. Javaid, S. Razzaq, A review of wireless communications for smart grid, Renew. Sustain. Energy Rev. 41 (2015) 248–260, https://doi.org/10.1016/J.RSER.2014.08.036.
[9] R. Zafar, A. Mahmood, S. Razzaq, W. Ali, U. Naeem, K. Shehzad, Prosumer based energy management and sharing in smart grid, Renew. Sustain. Energy Rev. 82 (2018) 1675–1684, https://doi.org/10.1016/J.RSER.2017.07.018.
[10] Y. Ai, M. Cheffena, Q. Li, Radio frequency measurements and capacity analysis for industrial indoor environments, in: 2015 9th European Conference on Antennas and Propagation (EuCAP), IEEE Conference Publication | IEEE Xplore, 2015.
[11] M. De Sanctis, E. Cianca, G. Araniti, I. Bisio, R. Prasad, Satellite communications supporting internet of remote things, IEEE Internet Things J. 3 (1) (2016) 113–123, https://doi.org/10.1109/JIOT.2015.2487046.
[12] A. Meloni, L. Atzori, The role of satellite communications in the smart grid, IEEE Wirel. Commun. 24 (2) (2017) 50–56, https://doi.org/10.1109/MWC.2017.1600251.
[13] M. Emmanuel, R. Rayudu, Communication technologies for smart grid applications: a survey, J. Netw. Comput. Appl. 74 (2016) 133–148, https://doi.org/10.1016/J.JNCA.2016.08.012.
[14] M. Faheem, et al., Smart grid communication and information technologies in the perspective of industry 4.0: opportunities and challenges, Comput. Sci. Rev. 30 (2018) 1–30, https://doi.org/10.1016/J.COSREV.2018.08.001.
[15] N.A. Qarabsh, S.S. Sabry, H.A. Qarabash, Smart grid in the context of industry 4.0: an overview of communications technologies and challenges, Indones. J. Electr. Eng. Comput. Sci. 18 (2) (2020) 656–665, https://doi.org/10.11591/IJEECS.V18.I2.PP656-665.
[16] W. Deng, F. Liu, H. Jin, B. Li, D. Li, Harnessing renewable energy in cloud datacenters: opportunities and challenges, IEEE Netw. 28 (1) (2014) 48–55. Network, and undefined 2014.
[17] M. Ward, R. Schmieder, G. Highnam, D. Mittelman, Big data challenges and opportunities in high-throughput sequencing, Syst. Biomed. 1 (1) (2013) 29–34, https://doi.org/10.4161/sysb.24470. Taylor Fr.

CHAPTER

2

Energy sources and technologies

2.1 Introduction

The consumption of energy is the best measuring tool for the progress of any country. The prosperity of a nation is measured by the per capita energy consumption since it relates to the industrial development of that country. Electricity is one of the forms of energy that has a major share in global energy consumption. Various energy sources are available that can be used to generate electricity. Energy is present in the form of conventional energy sources like oil, coal, and gas, and alternative renewable energy sources like wind, solar, biomass, biogas, geothermal, and hydro. Conventional sources of energy are not renewable, since once they are consumed they will not be replenished. The reserves of oil, coal, and gas are vanishing, and their prices are rising. Conventional energy harnessing technologies like steam power plants, gas power plants, combined cycle power plants, and diesel power plants are matured and efficient technologies.

Renewable energy sources are those energy sources that, once used, replenish themselves. The sun is an eternal source of energy irrespective of the amount we use. Similarly, the wind also blows because of the density difference of the air in different regions of the earth. The sun is again behind this phenomenon. Renewable energy sources are abundantly available on the earth and are being harnessed successfully. The technologies to harness energy from renewable energy sources are still in development and are less efficient than conventional technologies. The energy from the sun is exploited in three different ways. One is solar thermal technologies such as solar parabolic troughs, solar dishes, solar water heaters, solar cookers, solar towers, and solar dryers in which the thermal effect of the sunlight is used to raise the temperature of the working medium. In some technologies, steam is produced to run steam turbines. The second technology of solar energy is the solar photovoltaic cell. Photovoltaic materials take the energy from the sun's photons to raise the electrons from the valence band to the conduction band. In the conduction band, electrons move to the external circuit, which is termed direct current (DC). The third technology of exploiting the solar energy is indoor lighting systems like the Himawari indoor lighting system, in which sunlight is focused on a point by using Fresnel lenses. At the focal point of the Fresnel lenses, optical fibers are placed that take the sunlight inside a room and lighten the room naturally.

https://doi.org/10.1016/B978-0-323-99560-3.00010-7

Wind turbines are used to harness the energy from the kinetic energy of the blowing winds. They consist of blades that use aerodynamic effects to rotate and run a coupled electrical generator that converts the rotational mechanical energy into electrical energy. Different types of wind turbines are used to exploit wind energy. Steam turbine technologies are used to harness energy from geo heat. Biomass, biogas, and biodiesel are used to generate electricity using different technologies. For example, fuel cells are used to generate electricity using hydrogen gas as fuel. This chapter discusses all the renewable energy sources and the conventional energy sources along with their harnessing technologies. All these distributed generation sources are the main constituents of a smart grid system.

2.2 Solar thermal energy

Solar thermal power plants work on the principle that the sunlight is collected through the collectors and focused on the receiver to generate steam. The solar collectors are the mirrors that can concentrate the solar irradiance on its focal point. In most solar thermal systems, a working fluid is circulated through the receiver that is a heat exchanger and produces steam. This steam is then used to generate electricity using steam turbines. Parabolic troughs, solar towers, parabolic dishes, solar cookers, solar dryers, and solar water heaters are some of the technologies to harness the sun's energy and either use it to generate electricity or use its heat for space heating, water heating, and process heating. Each of these technologies is discussed in detail. The classification of energy harnessing techniques from the sun is shown in Fig. 2.1.

2.2.1 Parabolic trough

A parabolic trough is a type of solar thermal energy and is the most developed solar energy technology. It consists of a parabolic trough of a polished mirror of metal, an absorber tube located at the focal length of the metal mirror, and solar field piping. Parabolic troughs are mounted on a solar tracker. Solar irradiance falling on the parabolic trough is reflected and focused on an absorber tube. This tube contains a heat-absorbing, fluid-like molten salt mixture or synthetic oil. Heat exchangers are used to transfer the heat from the molten salt to the working fluid, converting it into steam and operating a steam turbine for power generation. Fig. 2.2 shows a schematic diagram of a solar parabolic trough.

The thermodynamics of the solar parabolic trough power system are shown in Fig. 2.3. Steam generated by the solar trough system is passed through the Rankine cycle. This cycle consists of the following four processes:

$1 \rightarrow 2$ Isentropic or adiabatic compression in the pump by external work, as shown in Eq. (2.1).

$2 \rightarrow 3$ Constant pressure or isobaric-heat addition in evaporator from the solar collector, as shown in Eq. (2.2).

$3 \rightarrow 4$ Isentropic or adiabatic-expansion in the turbine doing output work, as shown in Eq. (2.3).

$4 \rightarrow 1$ Constant pressure or isobaric-heat rejection in the condenser to the cooling tower, as shown in Eq. (2.4).

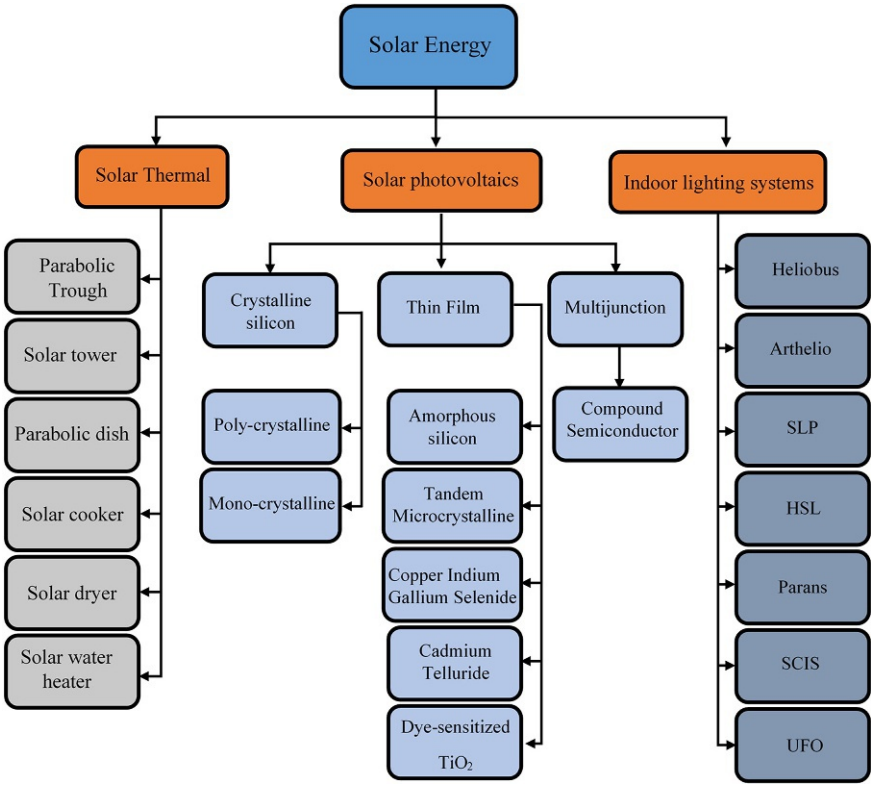

FIG. 2.1 Classification of solar energy harnessing techniques.

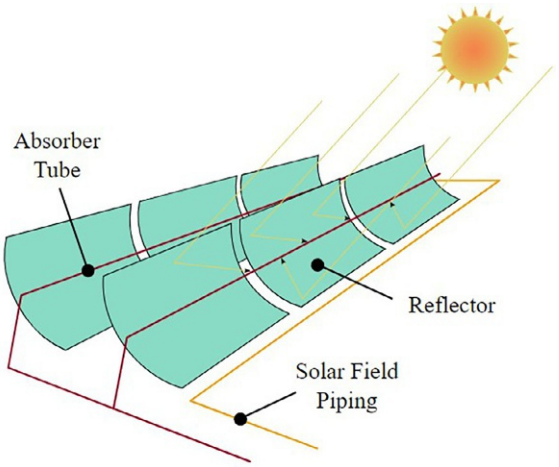

FIG. 2.2 Solar parabolic trough. *Source: Wikipedia.*

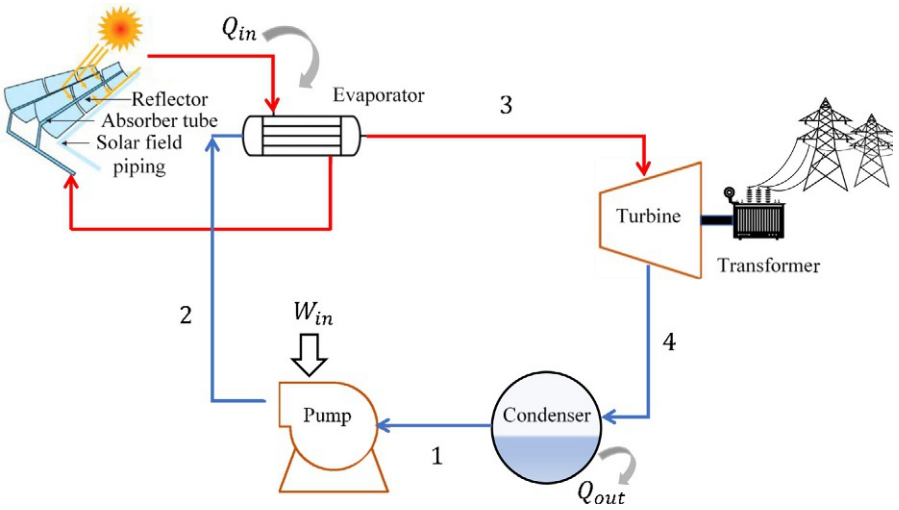

FIG. 2.3 Rankine cycle working on the solar parabolic trough.

$$W_{in} = h_2 - h_1 \tag{2.1}$$

$$Q_{in} = h_3 - h_2 \tag{2.2}$$

$$W_{out} = -(h_4 - h_3) \tag{2.3}$$

$$Q_{out} = -(h_1 - h_4) \tag{2.4}$$

The efficiency of the Rankine cycle is determined by the output energy to input energy ratio. The simplified formula of the efficiency is given in Eq. (2.5).

$$\eta = \frac{output\ energy}{Input\ energy}$$

$$\eta = \frac{W_{out} - W_{in}}{Q_{in}} = \frac{Q_{in} - Q_{out}}{Q_{in}}$$

$$\eta = \left(1 - \frac{Q_{out}}{Q_{in}}\right)100\% \tag{2.5}$$

2.2.2 Solar tower

The solar tower is another technology of concentrated solar thermal energy. It consists of multiple heliostats located at different locations in the field, thermal storage, and the power generating unit. The heliostats are of polished metal surfaces. The sunlight is reflected from the heliostats and focused on the solar receivers. The heliostats are mounted on the solar tracker, which is necessary to keep the heliostats directed toward the sun for maximum concentration on the solar receiver. The working fluid in the piping is the water, molten salt, or

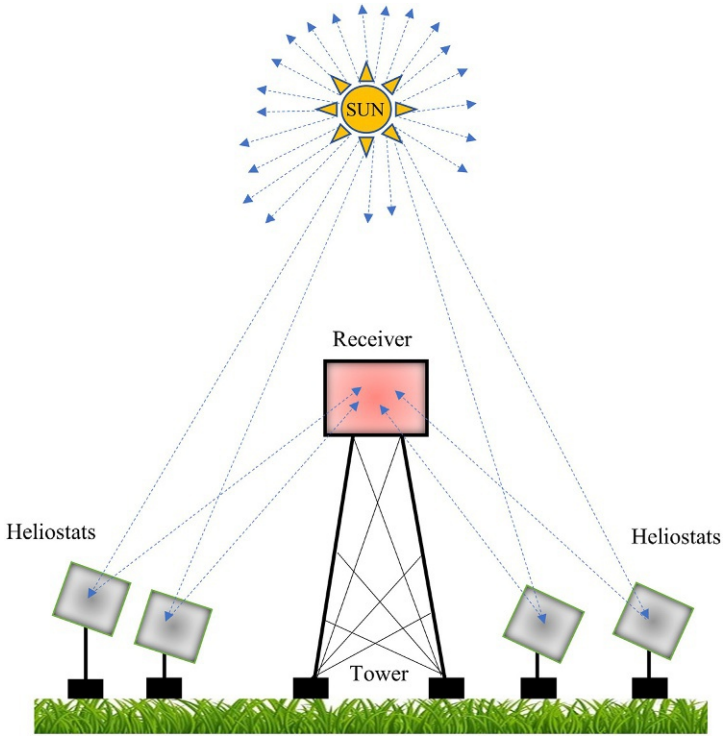

FIG. 2.4 Solar tower.

air. The heat from the solar receiver is absorbed by the working fluid and the heat is transferred through the heat exchanger to generate steam and operate the generator-coupled steam turbine. A schematic diagram of a solar tower is shown in Fig. 2.4.

2.2.3 Parabolic dish

A parabolic dish system is composed of a large solar light reflector, a parabolic receiver and a Stirling engine, and a power generator. The sunlight is collected and reflected by the large parabolic dish. The reflected solar irradiance is concentrated at the solar receiver placed at the focal length of the mirror. The solar dish is mounted on the dual-axis solar tracker to keep the solar collector directed to the sun for the maximum concentration of the solar irradiance on the solar receiver. The conversion efficiency of the Stirling engine from solar energy to electricity is reported at 30%, which is higher than for other solar thermal conversion technologies. A general setup of a parabolic dish is shown in Fig. 2.5.

2.2.4 Solar water heater

The solar water heater is the simplest application of solar thermal energy. The solar water heating system consists of the water storage tank, piping system, and solar collector. Solar

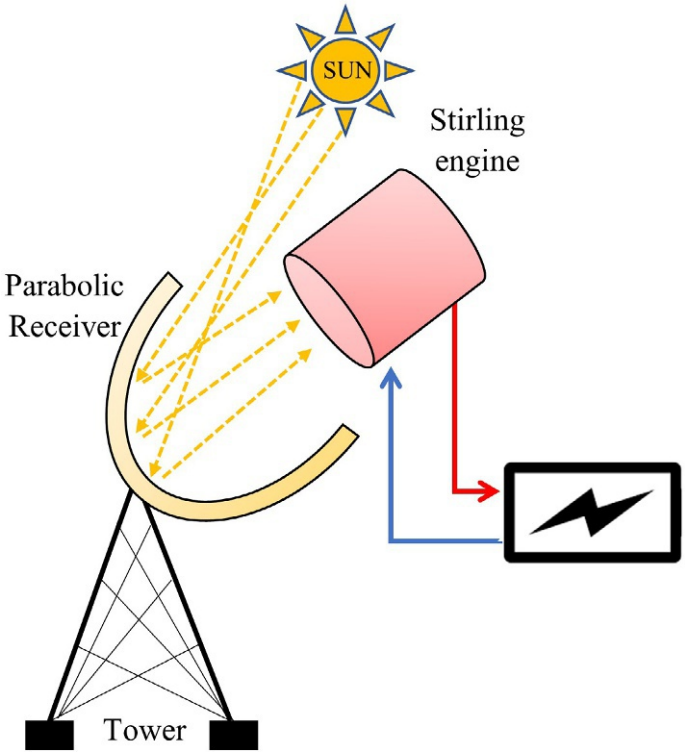

FIG. 2.5 Solar parabolic dish [1].

water heaters are classified as active and solar water heaters and direct and indirect solar water heaters. Active and passive classification is based on the requirement of the pumping for the solar water heater. In passive solar water heaters, heat is transferred from the collector to the water tank located at the top of the collector by the process of natural circulation. In active solar water heaters, the water is circulated from the solar collector to the water storage by using a water pump.

Solar water heaters in which heat is transferred from the working fluid to the water with the help of the heat exchanger are called indirect solar water heaters and solar water heaters in which no heat exchanger is used for the transference of heat are called direct solar water heaters. Fig. 2.6 provides a general diagram of a solar water heater.

2.2.5 Solar dryer

A solar dryer is another technology to harness the solar energy that is used to dry fruits, vegetables, and crops for preservation. Solar dryers are of two types: direct and indirect. In direct solar dryers, the substance that is to be dehydrated is exposed to the sunlight in a vast field. Indirect solar dryers consist of an insulated box coated inside with a black absorption surface, an air inlet and an air outlet, and a single- or double-glazed glass. A solar dryer works on the principle of the density differential. The inlet air hole is at the lower side for the

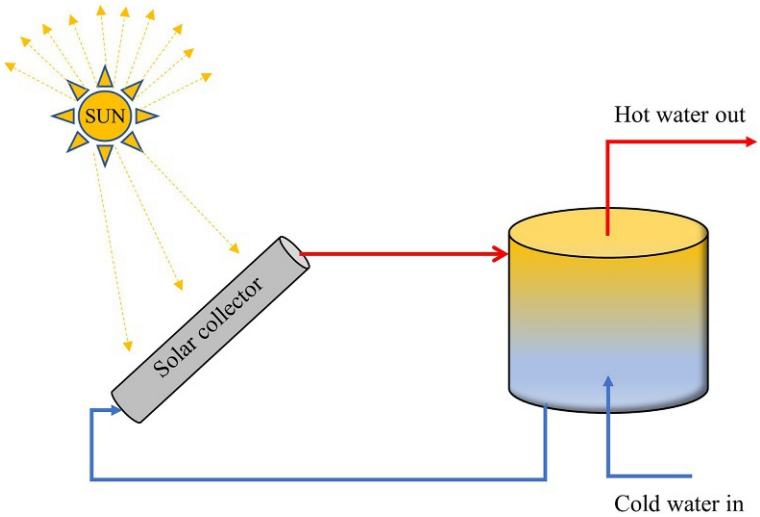

FIG. 2.6 Solar water heater [2].

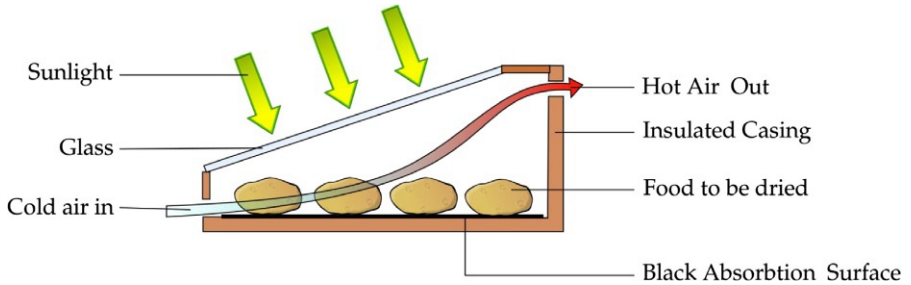

FIG. 2.7 Solar dryer. *Source: Wikipedia.*

entrance of the cold air and the outlet air is at the upper side of the opposite wall. The sunlight coming through the glazing keeps the inner environment warm, which dehydrates the substance. The cold air takes the hot air enriched with moisture content from the box and, because of the difference in the density, the air is ventilated through the hot air outlet. Fig. 2.7 illustrates the working principle of a solar dryer.

2.2.6 Solar cooker

In operation, a solar cooker is similar to a solar parabolic dish, in that the sunlight is reflected by a mirror-shaped parabolic trough. The light is reflected and concentrated on a small cooking area where a cooking pot is placed. For a wide range of temperatures, mirrors can be arranged and placed in diverse orders. Solar cookers can achieve a temperature to melt metals and salts, but such a high temperature is not desired for household kitchen needs. The pot is placed at the focal point of the parabolic dish reflectors. A diagram of a solar cooker is shown in Fig. 2.8.

FIG. 2.8 Solar cooker [3].

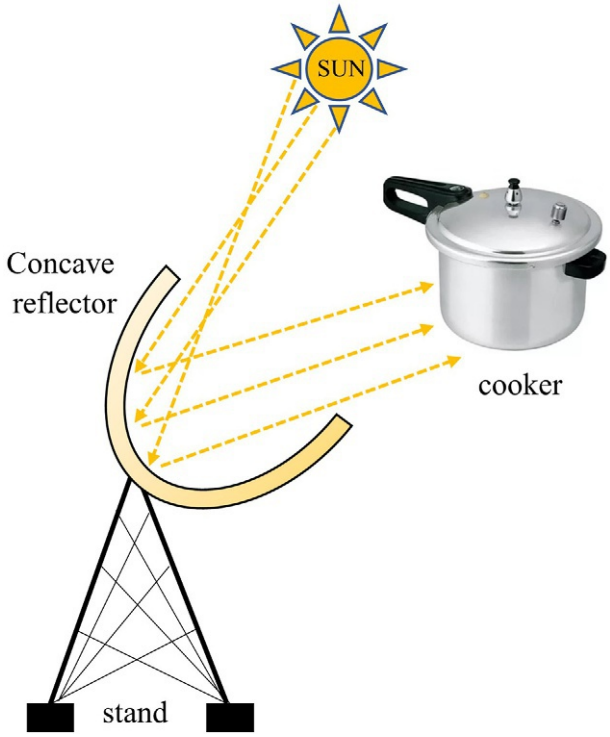

2.3 Solar photovoltaics

Solar photovoltaics (PV) is another technology to harness energy from the sun. This method of energy extraction uses semiconductor materials. The sunlight falls on the photovoltaic material, and the energy of the photons is transferred to the electrons in the valence shell. If the energy of the photon is greater than the bandgap energy, the electron will move from the valence band to the conduction band, from where it moves to the external circuit, named direct current (DC). The bandgap energy is the amount of energy required by an electron to move from the valence band to the conduction band. This energy depends upon the type of semiconductor material. Silicon is the most commonly used photovoltaic material. Based on the materials used in solar cells, they are categorized into crystalline silicon, thin-film, and multijunction [4–6].

Crystalline silicon solar cells are globally the most commonly used solar cell with a laboratory efficiency of 25% for a single solar cell and 20% for multiple cells. The efficiency of the cells available in the market under standard test conditions (STC) is 18%–22%. Crystalline solar cells can be monocrystalline or polycrystalline [7].

Thin-film solar cells are second-generation solar cells in which thin layers of photovoltaic materials are deposited on a substrate. This substrate may be of plastic, glass, or metal. The various technologies of thin-film solar cells are amorphous silicon, tandem microcrystalline,

copper indium gallium selenide, cadmium telluride, and dye-sensitized TiO_2. Solar photovoltaic systems, DC-DC converters, PV cell models, the impact of temperature and irradiance, and maximum power point tracker (MPPT) algorithms are discussed in Chapter 5.

2.4 Wind energy

The energy stored in the blowing wind is harnessed using wind turbines. The kinetic energy of the wind is used to rotate the blades of the turbine. The blades are connected to a shaft connected to the rotor of the generator. Based on the locations of wind turbines, they are classified as offshore or onshore. Offshore wind turbines are installed in the sea [8], while onshore wind turbines are installed on land. Offshore wind turbines are shown in Fig. 2.9. Wind speed offshore is greater than that onshore, meaning that more electricity is produced from offshore wind turbines. The fundamental equation of wind power, types of turbines, power conversion systems, and frequency control methods are described in Chapter 6.

FIG. 2.9 Offshore wind power plants.

2.5 Hydro energy

Hydropower is the most mature technology to extract energy from water at high altitudes. Water from a river or a canal in the case of a micro-hydro where the water falls from high potential to low potential is diverted toward a turbine and passed through it; the potential energy is converted into the rotational energy of the turbine and a coupled generator converts the rotational energy into electrical energy.

2.5.1 Fundamental equation of hydropower

The energy that is contained in water at a height can be calculated by the hydropower equation. The power is defined as the time rate of change of energy, as given in Eq. (2.6).

$$P = \frac{dE}{dt} \tag{2.6}$$

The energy that the water contains at a specific head is the potential energy given by Eq. (2.7).

$$P.E. = mgh \tag{2.7}$$

Putting the value of potential energy in Eq. (2.6) and simplifying, we obtain Eq. (2.8).

$$P = \frac{d(mgh)}{dt}$$

$$P = gh\frac{dm}{dt} \tag{2.8}$$

The mass of the wind which will interact with the wind turbine is calculated by the density equation shown in Eq. (2.9).

$$\rho = \frac{m}{V} \longrightarrow m = \rho V \tag{2.9}$$

We put the value of mass of water in Eq. (2.8).

$$P = gh\frac{d(\rho V)}{dt}$$

$$P = \rho gh\frac{d(V)}{dt}$$

The time rate of change of volume is termed the flow rate.

$$Q = \frac{d(V)}{dt}$$

$$P = \rho ghQ \tag{2.10}$$

Thus Eq. (2.10) gives the potential available at the head. The actual power that is obtained to be fed to the grid is calculated by incorporating the efficiency of the turbine and generator, as given in Eq. (2.11).

$$P = \rho g h Q \eta \tag{2.11}$$

This is the fundamental equation of hydropower, showing that the power has a direct relation to the height, flow rate, and the efficiency of the turbine and generator. The head is almost constant for a given specific location, and the efficiency of the turbine and generator decreases with time. The flow rate of water is a parameter that is vulnerable to variations linked with the seasonal pattern and some technical issues. Flow rate is a major factor that influences power. To get a clear idea of the flow rate at a proposed location, we draw flow duration curves.

2.5.2 Components of a hydropower plant

2.5.2.1 Forebay

A forebay is the artificial water storage at upstream. It is used to direct water from the mainstream to the penstock (see Section 2.5.2.3). The storage in the forebay depends upon the required supply for that area. A forebay could be natural storage, taking water from the mainstream to the penstock.

2.5.2.2 Intake structure

Designs of the intake structures vary from location to location, depending upon the local conditions. The intake structure transfers the water from the forebay to the penstock. The intake structure contains various other components like a trash rack. Trash racks are used to rid the water of the debris, unwanted plants, and trees that may block the penstock gates or damage the turbine blades. Trash racks are installed at the gates of the penstock. They are made up of steel rods inclined at an angle of 60–80° with the horizontal axis of the trash rack frame and the spacing between the rods depends upon the type of the turbine. In areas with cold weather conditions, ice is produced in the water. The trash rack is connected to an electricity supply to heat and melt this ice before it enters the penstock. The intake structure also includes a rack and trolley arrangement to clean the trash racks and penstock gates. A weir is another part of the intake structure which is used to alter the flow characteristics of the water.

2.5.2.3 Penstock

A penstock is a passage of pipe that transfers water from the intake structure to a hydro turbine. The potential energy in the water is converted into kinetic energy as the water moves down the penstock. Designing of the penstock includes various parameters such as diameter, thickness, and losses [9]. Each of these is calculated individually. The diameter of the penstock is determined using Eq. (2.12).

$$D = 2.69 \times \left(n^2 \times Q^2 \times \frac{L}{H_g} \right)^{0.1875} \tag{2.12}$$

where:

D is the internal diameter of the penstock;
n is the Manning coarseness coefficient changes with the penstock material;
Q is the design flow;
L is the penstock length; and
H_g is the gross head.

The penstock thickness is calculated using Eq. (2.13).

$$t = \frac{D + 508}{400} + 1.2 \tag{2.13}$$

where D is the penstock diameter and t is the thickness of penstock wall.

The cross-sectional area of the penstock is determined using Eq. (2.14).

$$A = \frac{\pi D^2}{4} = \pi r^2 \tag{2.14}$$

where:

D is the penstock diameter;
A is the penstock cross-sectional area; and
r is the penstock radius.

The velocity of water through the penstock is determined by considering the fact that as the water moves down the penstock, kinetic energy is increased and the potential energy is decreased. Eq. (2.15) is used to determine the velocity of water through the penstock.

$$\textit{Gain in kinetic energy} = \textit{Loss in potential energy}$$

$$\frac{1}{2}mv^2 = mgh$$

$$v = \sqrt{2gh} \tag{2.15}$$

where:

g is the gravitational acceleration;
v is the velocity of the water;
h is the height of the falling water; and
m is the mass of falling water.

As the water enters the penstock, moves down its length, and passes through a valve, it experiences hindrance that causes a decrease in the gross head. These losses are called head friction losses, entrance losses, and valve losses, and are given in Eqs. (2.16), (2.18), and (2.19), respectively.

$$h_f = f \times (L/D) \times \frac{v^2}{2g} \tag{2.16}$$

$$f = 124.5 \times \frac{n^2}{D^{1/3}} \tag{2.17}$$

$$h_e = f_e \times \frac{v^2}{2g} \tag{2.18}$$

$$h_v = f_v \times \frac{v^2}{2g} \tag{2.19}$$

where f is the friction factor given by Eq. (2.17), f_e is the entrance coefficient which is taken as 0.5 for micro-hydro, and f_v is the valve coefficient depending upon the type of the valve. All the losses are aggregated and subtracted from the gross head to get the net head, given by Eq. (2.20).

$$Head\ Losses = h_f + h_i + h_v$$

$$Net\ Head = Gross\ Head - Head\ losses \tag{2.20}$$

2.5.2.4 Surge chamber

A surge chamber is also known as the surge tank and it is a cylindrical type reservoir connected to the penstock and the upper side is open. As we have seen, the power generated from the wind turbine is directly proportional to the flow rate. If the power requirement is decreased, the supply of water to the turbine will have to be decreased by closing the valves. As the valves are closed, high pressure is developed between the reservoir and the turbine, which is called water hammering. To control this, a storage tank known as a surge chamber is connected to the penstock. When a huge amount of water is required by the turbine, the surge chamber releases the water to the penstock and the water level in the surge chamber goes down.

2.5.2.5 Hydraulic turbine

Hydraulic turbines are devices that convert the translational kinetic energy of water into the rotational kinetic energy of a turbine; this energy is then converted to electrical energy using a generator coupled to the turbine. Hydropower plants use either impulse turbines or reaction turbines.

In impulse turbines, water is ejected through a nozzle-type opening and is thrown over the buckets of the turbine. The nozzle converts all the energy of the water into kinetic energy. The buckets are located at the circumference of the turbine. Pelton, Turgo, and crossflow turbines are examples of impulse turbines.

Reaction turbines are placed in the water and use both the velocity of the moving water and the pressure of water to rotate the turbine. The water enters the turbine along the tangent direction and rotates it. Francis and propeller are types of reaction turbines [10].

2.5.2.6 Power house

The powerhouse consists of a turbine area, an electrical generator, and the service area. The powerhouse protects the turbine and the generator. Generators are the power generating equipment that converts the rotational kinetic energy of the shaft coupled to the turbine into electrical energy. The service area consists of the offices, controlling and testing rooms, maintenance shop, storage rooms, and auxiliary equipment rooms.

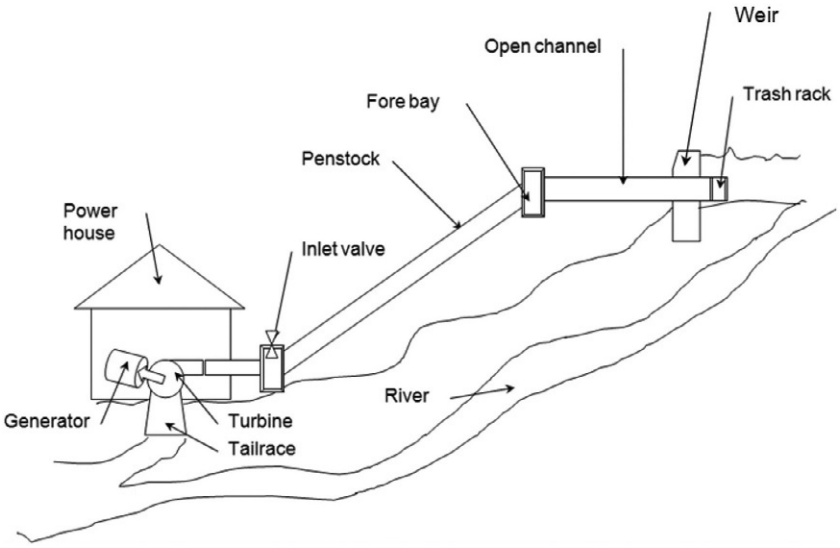

FIG. 2.10 Schematic diagram of a micro hydropower system. *Source: Wikipedia.*

2.5.2.7 Draft tube

In cases where reaction turbines are used in the hydropower plant, a draft tube is connected to the outer side of the turbine and the inlet of the tailrace (see Section 2.5.2.8). The diameter of the draft tube gradually increases so that the water is drained out to the tailrace with safe velocity and pressure limits. For repair and maintenance purposes, the draft tube is provided with gates.

2.5.2.8 Tailrace

The channel that takes the water from the turbine to the mainstream is called the tailrace. If the mainstream is away from the turbine, a channel is made that directs the water after passing through the turbine to the mainstream. This channel is termed the tailrace. All the above-illustrated components of the hydropower plant are shown in Fig. 2.10.

2.5.3 Flow duration curves

The design of a hydropower plant starts from the flow duration curves. The design considerations of the hydropower plant are randomly changing with advances in technology and with increasing requirements. The flow duration curve is a plot of the flow rate on the y-axis against the percentage exceedance on the x-axis. To draw the flow duration curves, the flow rate data is determined for each month of the year. This data is arranged in descending order in tabular form, as shown in Table 2.1, which shows the flow rate for each month arranged in descending order and the percentage exceedance of each month. The graph between flow rate on the y-axis and percentage exceedance on the x-axis is shown in Fig. 2.11. The percentage exceedance is obtained by dividing 100% by the number of data points. In our case, we have data points of 12 months; therefore, by dividing, we get $\frac{100}{12} = 8.33$, which is the first value of the percentage exceedance column. The next value is obtained by adding the 8.33 in the previous value and so on.

TABLE 2.1 Flow rate and percentage exceedance of a year.

Sr. no.	Month	Flow rate (m^3/s)	Percentage exceedance (%)
1	June	4.75	8.33
2	July	4.25	16.66
3	August	3.49	24.99
4	September	3.10	33.32
5	October	2.14	41.65
6	November	2.01	49.98
7	December	1.82	58.31
8	January	1.49	66.64
9	February	1.29	74.97
10	March	1.10	83.30
11	April	1.02	91.63
12	May	1.00	100.00

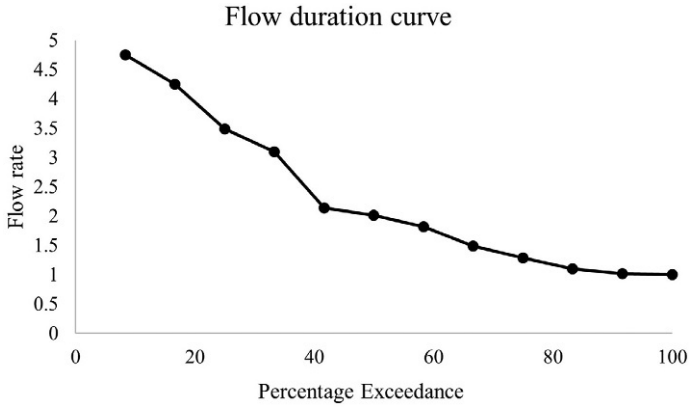

FIG. 2.11 Flow duration curve.

2.6 Bioenergy

2.6.1 Biomass

Biomass is an organic material received from living organisms like animals and plants. Biomass is categorized into four types: vegetable oils, sugar and starch, lignocellulosic material, and wet biomass. Different technologies are used to convert these types of biomass into biofuels, chemicals, heat, and electricity, which are directly used for various purposes. Transesterification is used to convert vegetable oil into bio diesel. Sugar and starch and

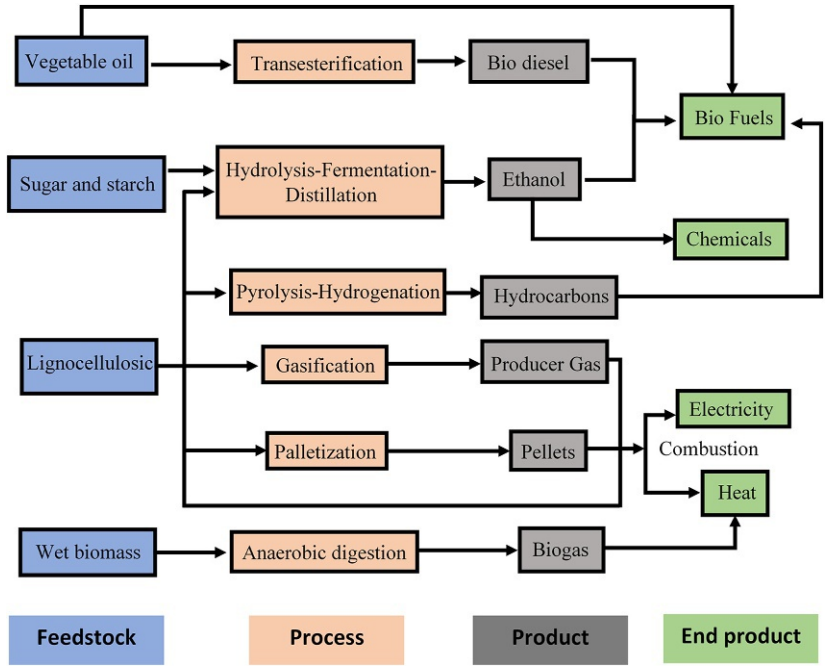

FIG. 2.12 Conversion process from feedstock biomass material to the end product.

lignocellulosic material are converted into ethanol through the hydrolysis-fermentation distillation process. Lignocellulosic material is converted into hydrocarbons and biofuels through pyrolysis-hydrogenation. It is also converted into producer gas through the gasification process. In addition, lignocellulosic material can be palletized and then combusted to produce heat and electricity. Biogas is produced through anaerobic digestion of wet biomass. All the above-stated technologies are discussed further in this chapter. Fig. 2.12 shows the conversion of different types of biomass into various types of energy.

Biomass is collected from agricultural waste, municipal solid waste and industrial waste, and forest residues. Agricultural waste and processing residues include sugar cane trash, sugar cane top, bagasse, cotton stalks, cotton shells, rice husk, wheat straw, animal manure, and animal dung [11].

2.6.1.1 Proximate analysis

Proximate analysis indicates the composition of the biomass regarding the moisture content, volatile matters, ash content, and fixed carbon. The type of biomass regarding storage capacity, energy contents, and biomass is graded based on this proximate analysis.

Moisture content: This is defined as the percentage of moisture in a biomass sample under examination when it is heated just over the boiling point of water (105°C). The heat given at this temperature evaporates the water from the sample of the biomass, which changes the original weight of the biomass. At the point that it stops changing, the difference between

the initial weight and the final weight expresses the moisture content that is the weight loss. It is expressed as a percentage of biomass material.

Volatile matter: When the biomass is burnt, volatile matter is easily burnt out in the presence of oxygen and is determined as the mass loss. A high quantity of volatile matter in the biomass is undesirable because it produces tar in the internal combustion engine (ICE), creating serious problems. A gasifier is designed by considering the amount of tar in the fuel and the continuous removal of the tar from the cooling and cleaning system is managed. Biomass contains more volatile matter than coal does, which makes the ignition of biomass easier.

Ash content: When the biomass is incinerated, the moisture content is evaporated, and the volatile matter is burnt out, the remaining material is known as the ash of the biomass. This remaining material has no energy value. Ash content is made up of inorganic matters. If the value of ash content in biomass is beyond the acceptable limits, it causes problems in thermochemical processes such as pyrolysis, combustion, and gasification. Since the ash is alkaline, the increased amount of ash tends to decrease the fusion point, which may cause slagging and fouling.

Fixed carbon: This is defined as the combustible remaining solid residue when a sample of the biomass is burnt at a temperature of 750°C for 7 min. When the moisture content, ash content, and volatile matter are removed from the biomass, the remaining is the fixed carbon, as shown in Eq. (2.21).

$$Fixed\ carbon = 100 - (\%H_2O + \%Ash + \%VM) \tag{2.21}$$

2.6.1.2 *Ultimate analysis*

The ultimate analysis determines the % wt of carbon, hydrogen, oxygen, sulfur, and nitrogen in liquid and both inorganic and organic solid samples. Ultimate analysis is also known as the elemental composition of the coal or biomass.

2.6.2 Biogas/anaerobic digestion process

Biogas is a clean and renewable source of energy that is produced by the anaerobic digestion process of biodegradable materials like animal dung, animal dung, agricultural waste and residues, and human excretion. Biogas is a mixture of methane gas (CH_4), carbon dioxide (CO_2), and traces of other gases. The methane accounts for 50%–75% and carbon dioxide for 25%–50%. In the anaerobic digestion process, the complex biodegradable materials like carbohydrates, fats, and proteins are decomposed by the methane and acidic bacteria into simpler molecules like sugar, amino acids, and fatty acids. Anaerobic digestion includes four steps: hydrolysis, acidogenesis, acetogenesis, and methanogenesis. These steps and the flow of the process of anaerobic digestion are shown in Fig. 2.13.

2.6.2.1 *Hydrolysis*

The first step of the anaerobic digestion process is hydrolysis, where complex polymers of organic matters (polysaccharides, proteins, and lipids) are decomposed into lower simple fatty acids, sugar, and amino acids by fermentative bacteria. The biochemistry of the

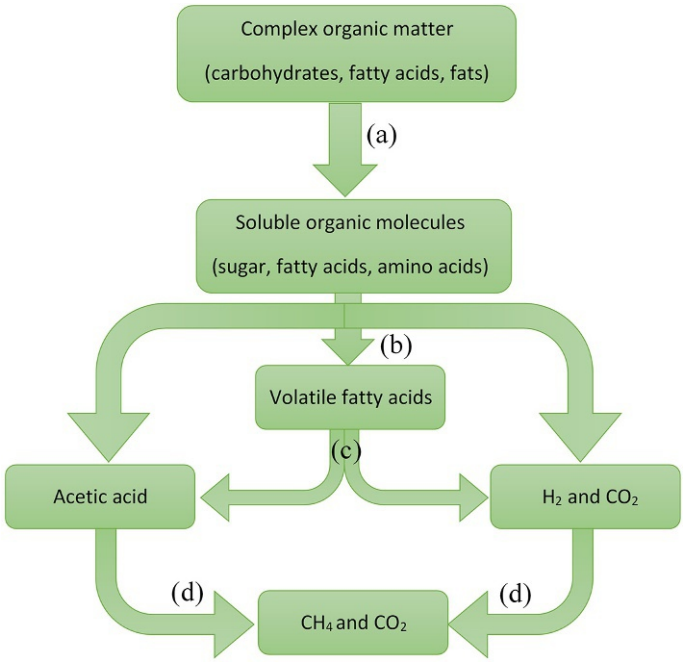

FIG. 2.13 Anaerobic digestion process [11].

hydrolysis is shown in the following equation, which states that the mixture of the biomass material with the water produces monomers and hydrogen.

$$Biomass + water \longrightarrow monomers + H_2$$

$$C_6H_{10}O_5 + H_2O \longrightarrow C_6H_{12}O_6 + H_2$$

2.6.2.2 *Acidogenesis*

The product of the hydrolysis process (sugar, fatty acids, and amino acids) is further decomposed into volatile fatty acids, ammonia, hydrogen sulfide, and carbon dioxide by fermentative bacteria. The biochemistry of the acidogenesis process is shown in Eqs. (2.22)–(2.24).

$$C_6H_{12}O_6 \longrightarrow 2C_2H_5\,OH + 2CO_2 \tag{2.22}$$

$$C_6H_{12}O_6 + 2H_2 \leftrightarrow C_2H_5\,COOH + 2H_2O \tag{2.23}$$

$$C_6H_{12}O_6 \leftrightarrow 3CH_3COOH \tag{2.24}$$

2.6.2.3 *Acetogenesis*

Acetic acids, carbon dioxide, and hydrogen are further produced by the degradation of the products of the acidogenesis by acetic bacteria. The biochemistry of acetogenesis is shown in Eqs. (2.25)–(2.27).

$$C_2H_5\,COO^- + 3H_2O \leftrightarrow CH_3COO^- + H^+HCO_3^- + 3H_2 \quad (2.25)$$

$$C_6H_{12}O_6 + 2H_2O \leftrightarrow 2CH_3COOH + 2CO_2 + 4H_2 \quad (2.26)$$

$$C_2H_5OH + 2H_2O \leftrightarrow CH_3COO^- + 3H_2 + H^+ \quad (2.27)$$

2.6.2.4 Methanogenesis

In methanogenesis, the last process of anaerobic digestion, acetic acids, carbon dioxide, and hydrogen are further decomposed into methane and carbon dioxide. The biochemistry of methanogenesis is shown in Eqs. (2.28)–(2.30).

$$3CH_3COOH \longrightarrow CH_4 + CO_2 \quad (2.28)$$

$$CO_2 + 4H_2 \longrightarrow CH_4 + 2H_2O \quad (2.29)$$

$$2C_2H_5OH + CO_2 \longrightarrow CH_4 + 2CH_3COOH \quad (2.30)$$

The end product of the anaerobic digestion process contains 50%–75% methane, which is used as natural gas for burning. The percentage of methane may vary depending on the type of feedstock for the anaerobic digestion. The percentages of methane in various feedstocks are as follow:

- poultry waste 68%
- cattle manure 50–60%
- beet leaves 84.8%
- horse dung 66%
- corn silage 54.5%
- dried leaves 58%
- barley straw 77%
- wheat straw 78.5%
- grass 84%
- sheep dung 65%
- pig manure 60%.

2.6.3 Biodiesel

2.6.3.1 Transesterification

Esterification is defined as a chemical reaction of two chemical reactants, usually acid and alcohol, to form esters. An alcohol like methanol with a catalyst is mixed with oils and fats to perform the esterification process, as shown in Fig. 2.14. Sodium hydroxide and potassium hydroxide can be used as catalysts. The oils and fats are collected from plants, vegetable oil, recycled grease, animal fats, and other triglyceride materials. These materials are not pure and contain some impurities; therefore, they cannot be used as they are in the production of biodiesel. The impurities are free fatty acids, odorants, water vapors, phosphor-lipids, and

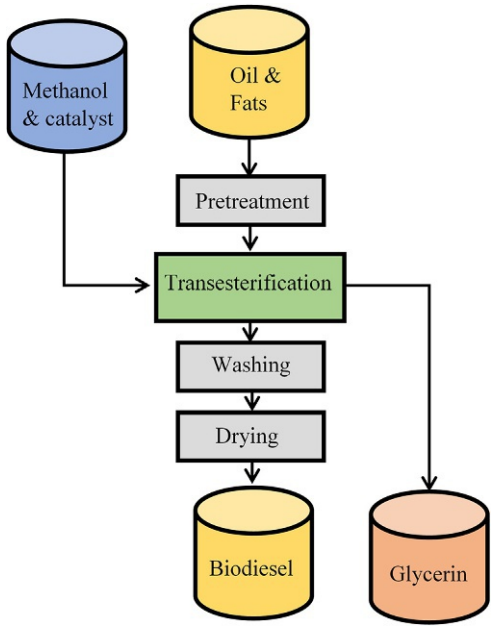

FIG. 2.14 Transesterification process.

sterols. They are first passed through a pretreatment process. The products of the transesterification process are biodiesel and glycerine. The biodiesel is first passed through a washing and drying process.

The overall process of transesterification is shown in Fig. 2.15. Triglyceride as oil and fat is reacted with methanol in the presence of sodium hydroxide as a catalyst. The by-product of the reaction is glycerine. The main product is biodiesel, which is a mixture of fatty esters. Biodiesels are categorized based on their properties like flash point, boiling point, freezing point, cloud point, pour point, and calorific value; these are discussed in detail in the following subsections. Fig. 2.15 shows the mathematical equation of the transesterification chemical reaction.

2.6.3.2 Flash point

The flash point of biodiesel is not an operation-related property, but it governs the storage and handling of the fuel. It is defined as the temperature of the liquid fuel at which the surface of the liquid fuel produces adequate vapors to ignite. The flash point of the biodiesel is higher (average 150°C) than that of fossil diesel (average range 55–66°C). The biodiesel flash point is measured by the closed cup method, in which the sample is heated at a constant rate in a closed cup and the temperature is regularly measured at intervals of 1°C or 2°C. At each interval, the cup is opened and brought close to the ignition source. If the vapors over the surface of the biodiesel sample achieve ignition, this temperature is termed the flash point of the fuel. Fuels with low flash points are carefully stored and handled, as they achieve ignition at a lower temperature.

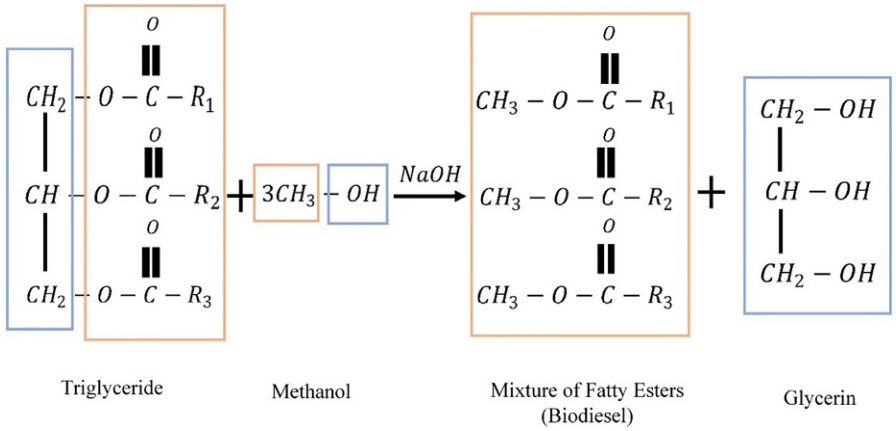

FIG. 2.15 Chemical reaction of biodiesel formation.

2.6.3.3 Boiling point

To define the boiling point of biodiesel, two pressures are required: the vapor pressure of the biodiesel and the atmospheric pressure near the surface of the biodiesel. The temperature at which these two pressures become equal is called the boiling point. When this temperature is achieved, vapors are created near the surface. For different values of atmospheric pressure, the boiling point will change.

2.6.3.4 Cloud point

The temperature of biodiesel is decreased until it starts converting into crystals; this temperature is called the cloud point. The temperature is reduced by 3°C in each step and is noted down when crystals are observed. This property becomes significant in cold climates since it relates to the storage of biodiesel.

2.6.3.5 Pour point

While measuring the cloud point of the sample, the sample temperature is further diminished even after achieving the cloud point. The temperature is decreased in steps of 1°C until the sample loses its flowing characteristics and reaches a standstill. This temperature at which this occurs is called the pour point. Both the pour point and cloud point are cold temperature properties of the fuel and become substantial in cold weather situations.

2.6.3.6 Calorific value

Calorific value is defined as the amount of heat energy generated by burning 1 kg of fuel in the presence of oxygen measured as kJ/kg. Mathematically, it can be written as the following equation.

$$Calorific\ value = \frac{heat\ produced}{amount\ of\ fuel}$$

The numerator of this equation is the heat liberated on burning, and it is determined by using the following thermodynamic equation.

$$Q = nC_P\Delta T$$

where Q is the heat produced, n is the no. of moles of fuel, C_P is the heat capacity at constant pressure (1 bar), and ΔT is the difference between the initial and final temperatures.

2.6.4 Hydrogen production

With the potential extinction of conventional energy sources, the utilization of renewable energy sources by diverse technologies has become a very popular field of research. Hydrogen is a clean source of energy and is the best fuel for fuel cells. Biomass is a major source of hydrogen production by various processes. These include biological, thermochemical, and water-splitting processes. Each of these hydrogen production processes is discussed in the following subsections. The methods of hydrogen production are set out in Fig. 2.16.

2.6.4.1 Biological processes

(a) Dark fermentation

Among the biological process of hydrogen production, dark fermentation is the most common process. This process is carried in the dark in the presence of facultative and obligate anaerobes and the absence of oxygen. Lignocellulosic and carbohydrate materials like municipal solid waste, crop residues, and industrial wastewater are used as substrates on which bacteria act and generate hydrogen. A process flow diagram of dark fermentation is shown in Fig. 2.17. Before the fermentation process, the biomass undergoes pretreatment processes for preparation to be a substrate. The chemical equation of the dark fermentation process is shown in Eq. (2.31). It can be seen that organic acid and hydrogen are key products of this reaction.

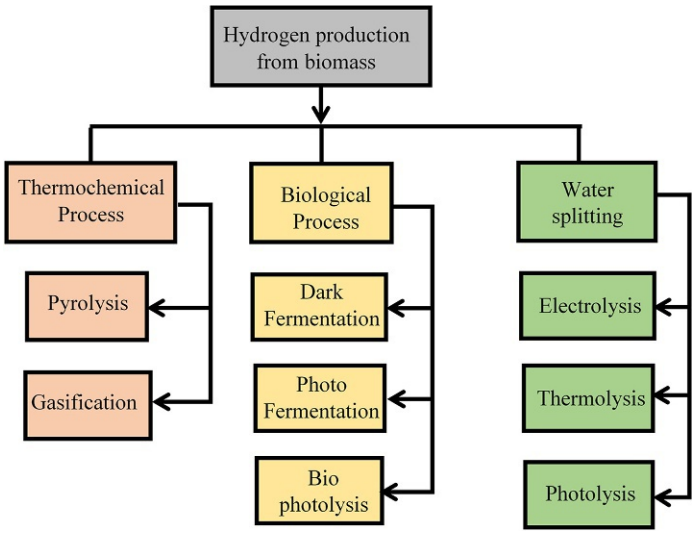

FIG. 2.16 Hydrogen production methods.

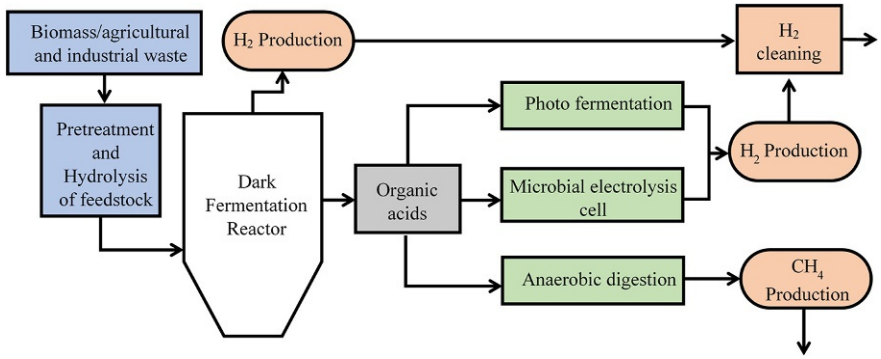

FIG. 2.17 Dark fermentation process of hydrogen production.

$$C_6H_{12}O_6 + 2H_2O \longrightarrow 2CH_3COOH + 2CO_2 + 4H_2 \tag{2.31}$$

$$CH_3COOH + 2H_2O \xrightarrow{\text{sun light}} 4H_2 + 2CO_2 \tag{2.32}$$

The organic acid produced as a result of the dark fermentation is further passed through photo-fermentation, microbial electrolysis cells, and anaerobic digestion. Photo-fermentation and microbial electrolysis cells produce hydrogen from the organic acid and the anaerobic digestion process generates methane gas. Eq. (2.32) shows the photo-fermentation process.

(b) Photo-fermentation

The photo-fermentation process involves the generation of hydrogen from biomass in the presence of sunlight by photosynthesis bacteria. The chemical process of photo-fermentation is shown in Eq. (2.33); the efficiency of this process depends upon the type of the substrate and the growth rate of the bacteria. The growth rate of the photosynthesis bacteria is lower than that of the dark fermentation bacteria meaning that the efficiency of the photo-fermentation process is less than that of dark fermentation.

$$CH_3COOH + 2H_2O \xrightarrow{\text{sun light}} 4H_2 + 2CO_2 \tag{2.33}$$

(c) Bio-photolysis

Splitting process of water into molecular oxygen and hydrogen in the presence of sunlight and biological organisms is called the bio-photolysis process. The photosynthesis process is carried out by biological organisms. Microalgae bacteria and cyanobacteria are biological organisms, also called autotrophs. They take water from the earth and carbon dioxide from the environment in the presence of light to form biomass, as shown in Eq. (2.34).

$$6H_2O + 6CO_2 + \text{light} \longrightarrow C_6H_{12}O_6 + 6O_2 \tag{2.34}$$

In a subsequent process, the biomass is passed through the dark fermentation process to generate hydrogen and organic acid like methanoic acid, as shown in Eq. (2.35).

$$C_6H_{12}O_6 + 2H_2O \longrightarrow 4H_2 + 2CH_3COOH + 2CO_2 \tag{2.35}$$

The organic acid produced from dark fermentation is passed through the photo-fermentation process in the presence of light and water to form hydrogen and carbon dioxide, as shown in Eq. (2.36).

$$2CH_3COOH + 4H_2O + light \longrightarrow 8H_2 + 4CO_2 \quad (2.36)$$

The complete reaction of the bio-photolysis is shown in Eq. (2.37).

$$12H_2O + light \longrightarrow 12H_2 + 6O_2 \quad (2.37)$$

2.6.4.2 *Thermochemical processes*

(a) Pyrolysis

At a high temperature of 625–800 K, biomass is decomposed by heating in the absence of oxygen and air. Since biomass is organic matter, it is decomposed into gas, liquid fuel, and charcoal. This is one of the fundamental reactions of hydrogen production and is known as pyrolysis. The process of pyrolysis is shown in Fig. 2.18. Before performing the pyrolysis reaction of biomass, it is passed through a pretreatment process in which it is dried by removing the moisture content using heat generated from the burning of the gas in this process, as shown in Fig. 2.18. After removing the moisture content, solid biomass is pulverized and fed to the pyrolysis reactor. The pulverized biomass ensures the complete combustion of the biomass. The chemical reaction of the pyrolysis process is shown in Eqs. (2.38)–(2.40). The heat for the process is obtained by burning the gas and charcoal, which are the products of this reaction. The products of the pyrolysis reactions are passed through a cyclone where the char is removed from the bottom by a circular movement. The gas and biodiesel are separated by a cooling process.

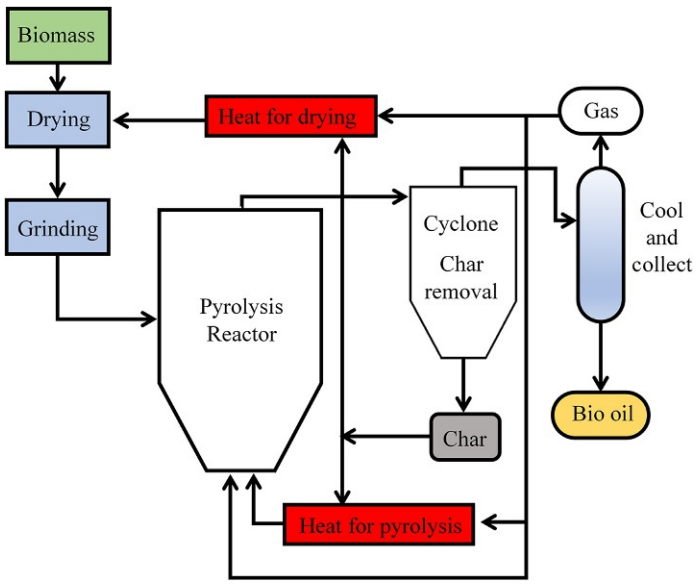

FIG. 2.18 Pyrolysis process of hydrogen production.

The products of the main pyrolysis reaction are methane gas, carbon monoxide, and hydrogen. Among other products, charcoal is obtained. Methane gas and carbon dioxide are further reacted with water to produce hydrogen. The process is clearly defined in Eqs. (2.38)–(2.40).

$$Heat + Biomass \xrightarrow{pyrolysis} CH_4 + CO + H_2 + other\ products \tag{2.38}$$

$$CH_4 + H_2O \longrightarrow 3H_2 + CO \tag{2.39}$$

$$CO + H_2O \longrightarrow CO_2 + H_2 \tag{2.40}$$

(b) Gasification

High polymers of the biomass are degraded into lower polymers by the incomplete combustion of the biomass in the existence of an oxidizing agent; this is called biomass gasification. The products of the gasification process are hydrogen, methane gas, carbon dioxide, and carbon monoxide. The oxidizing agents used in this process are air and steam. The gasification process reaction is shown in Eq. (2.41) and a process flow diagram is shown in Fig. 2.19. Before the gasification process, biomass is first made moisture-free and pulverized. The steam enters the gasifier from the top, and the air and biomass material enter from the side. Ash is collected at the bottom and the gas is passed to a gas scrubber and a gas filter that remove the harmful particulates from the gas.

$$Biomass + O_2 + H_2O\,(steam) \xrightarrow{gasification} CH_4 + CO_2 + CO + H_2 + other\ products \tag{2.41}$$

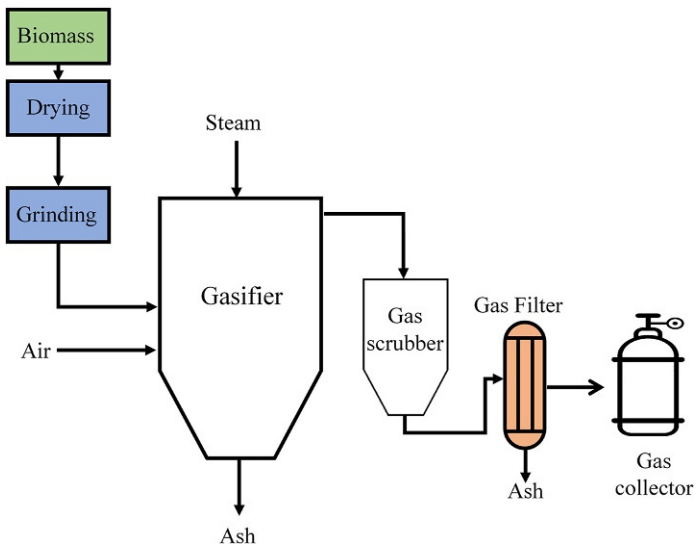

FIG. 2.19 Gasification process of hydrogen production

2.6.4.3 Water splitting

(a) Electrolysis

The dissociation of water into hydrogen and oxygen by passing electricity through an electrolysis cell is called electrolysis. For dissociation of water, a potential of 1.22 V is connected across the anode and cathode of the electrolytic cell. Eq. (2.42) is associated with the electrolysis chemical reaction. The voltage required for the electrolysis of water is determined by calculating the change in enthalpy, change in entropy, and the Gibbs free energy.

$$H_2O + \textit{electrical energy} \Longrightarrow H_2 + \frac{1}{2}O_2 \tag{2.42}$$

The change in enthalpy of the water-splitting process is shown in Eq. (2.43).

$$\Delta H = (h_f)_{H_2} + \frac{1}{2}(h_f)_{O_2} - (h_f)_{H_2O} \tag{2.43}$$

$$\Delta H = 0 + 0 - (-286)$$

$$\Delta H = 286\frac{\text{kJ}}{\text{mol}}$$

Similarly, the change in entropy of the water-splitting reaction is determined using Eq. (2.44).

$$\Delta S = (S_f)_{H_2} + \frac{1}{2}(S_f)_{O_2} - (S_f)_{H_2O} \tag{2.44}$$

$$\Delta S = 0.13066 + \frac{1}{2}(0.20517) - 0.06996$$

$$\Delta S = 0.163\frac{\text{kJ}}{\text{mol}}$$

The Gibbs free energy is determined by using Eq. (2.45) at standard temperature.

$$\Delta G = \Delta H - T.\Delta S \tag{2.45}$$

$$\Delta G = 286\frac{\text{kJ}}{\text{mol}} - 298\left(0.163\frac{\text{kJ}}{\text{mol.}}\right)$$

$$\Delta G = 237.4\ \frac{\text{kJ}}{\text{mol}}$$

The electrical energy that is required to carry out the water-splitting reaction is determined using Eq. (2.46).

$$V_{rev} = \frac{\Delta G}{nF} \tag{2.46}$$

where:

ΔG is the Gibbs free energy;

F is the Faraday's number ($96485\,\frac{C}{mol}$);
V_{rev} is the reversible potential; and
n is the number of electrons involved in the reaction.

$$V_{rev} = \frac{237.4\ \frac{kJ}{mol}}{2\left(96485\,\frac{C}{mol}\right)}$$

$$V_{rev} = 1.229\ V$$

(b) Thermolysis

The dissociation of a molecule by using heat is known as the thermolysis process. This heat can be obtained either directly from a source like the sun or from a chemical reaction. The process of thermolysis can be written as Eq. (2.47).

$$H_2O + \textit{thermal energy energy} \Longrightarrow H_2 + \frac{1}{2}O_2 \tag{2.47}$$

The heat from the sun is collected using solar towers, solar parabolic troughs, and solar dishes.

(c) Photolysis

Photolysis is also known as photo-dissociation, photo-fragmentation, and photo-decomposition. It is the chemical reaction of breaking the molecules by the photons of sunlight. The chemical reaction for it is shown in Eq. (2.48).

$$H_2O + \textit{light energy} \Longrightarrow H_2 + \frac{1}{2}O_2 \tag{2.48}$$

The production of hydrogen for fuel cells from the dissociation of water by sunlight is a renewable source of energy.

2.7 Geothermal energy

2.7.1 Dry steam power plant

Dry steam power plants were the earliest type of geothermal power plant; the first dry steam power plant was built at Lardarello in Italy in 1904. Dry steam power plants use 99.99% dry steam at a temperature greater than 150°C. These power plants are rare because of the unavailability of dry steam. Steam from underground sources is directed through a pipe on a turbine/generator set. Since steam is directly used to run a steam turbine, it eliminates the need for burning of coal or other fossil fuels to generate electricity. Fig. 2.20 shows a schematic diagram of a dry steam power plant.

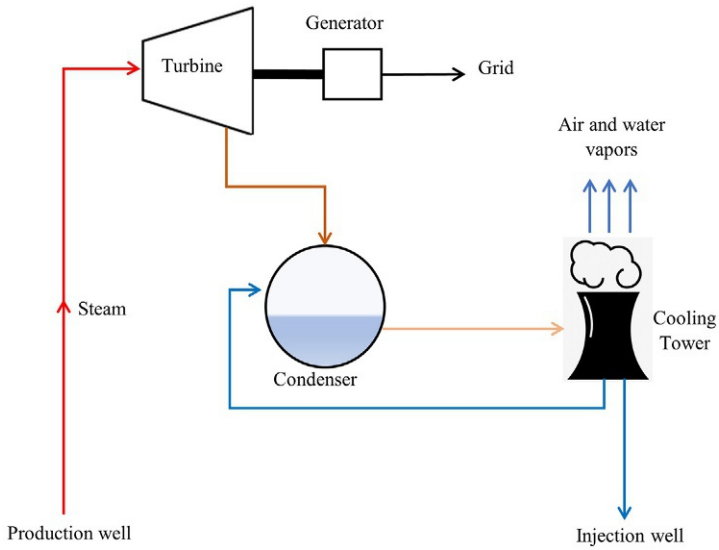

FIG. 2.20 Schematic diagram of a dry steam power plant.

2.7.2 Flash steam power plant

The most common type of geothermal power plant is the flash steam power plant. These plants are installed where the temperature is not enough to produce dry steam; instead, the steam and water are found mixed at a temperature of 182°C. The hot water in the liquid form is under high pressure beneath the earth. When it moves upward, it loses pressure and gets converted into steam. Hence, the steam that is formed from the hot condensate when the pressure is reduced is called flash steam. Above the earth, steam and water are passed through a steam separator. This separates the steam from the liquid water and throws it on a high-pressure steam turbine that is coupled to an electrical generator. The remaining hot water still contains some steam; it is therefore passed through another separator and the steam is passed through the low-pressure turbine. Fig. 2.21 shows a process diagram of a flash steam power plant

2.7.3 Binary cycle power plant

Flash steam and dry steam power plants are high-temperature thermal power plants. For low-temperature applications of geothermal energy, the binary cycle power plant is used. It uses recent advanced technology of energy harnessing from geothermal resources of temperatures lower than 100°C. The operation of a binary cycle power plant is very similar to that of conventional fossil fuel-based and nuclear-based power plants. It employs a low boiling point working fluid that takes the heat from the hot medium coming from the underground hot reservoir. The working fluid is chosen due to having certain thermodynamic properties. This working fluid extracts the energy from the geofluid in a heat exchanger and evaporates. The geofluid is the fluid beneath the earth which is collected from the production well in the form of steam and sent back to the injection well in the form of hot water after extracting energy from it.The organic compound being used as the working fluid evaporates and runs the

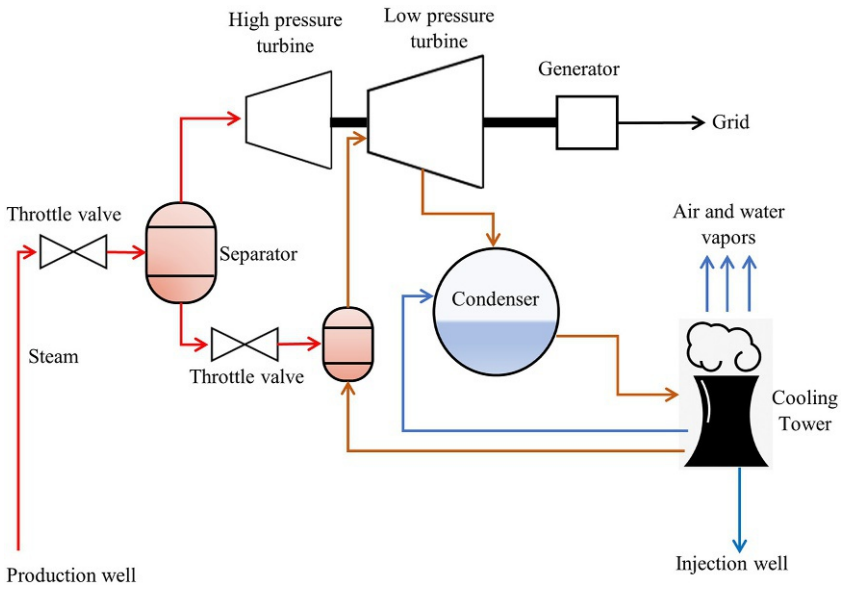

FIG. 2.21 Schematic diagram of a flash steam power plant.

turbine, generating electricity. The working fluid, after expanding at the turbine, is sent to the condenser and then back to the heat exchanger, working as the evaporator. A schematic diagram of a binary cycle power plant is shown in Fig. 2.22. This plant takes advantage of using two separate working fluids and geofluid to generate electricity at a relatively low temperature [12].

2.7.4 Combined cycle power plant

Combined cycle power plants are a combination of gas and steam turbines. The result is that the generation of electricity is increased almost by 50%. The steam from the production well is used to run the steam turbine, and the steam after expansion still has heat content, which is recaptured in the heat exchanger. This captured heat is used to run the organic Rankine cycle. The process of the combined cycle power plant is shown in Fig. 2.23. The geofluid, after losing waste heat into the heat exchanger, is sent back to the injection well [13].

2.8 Fuel cells

A fuel cell is an electrochemical device that converts the chemical energy from the various types of chemicals like hydrogen, methanol, phosphoric acid, molten carbonate, etc. into DC electrical energy. Fuel cells are environmentally friendly since no nitrogen oxide (NO_x) is produced, and because there are no moving parts, no noise or wear and tear are involved in the cells' operation. Fuel cells work on the principle of oxidation and reduction reactions. The chemical reactions and the working principle of each type of fuel cell are discussed in the following subsections.

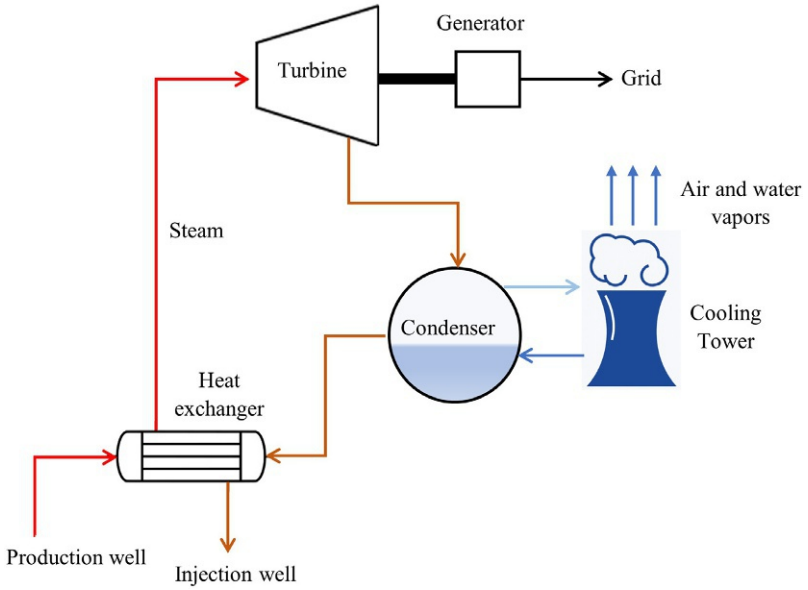

FIG. 2.22 Schematic diagram of a binary cycle power plant.

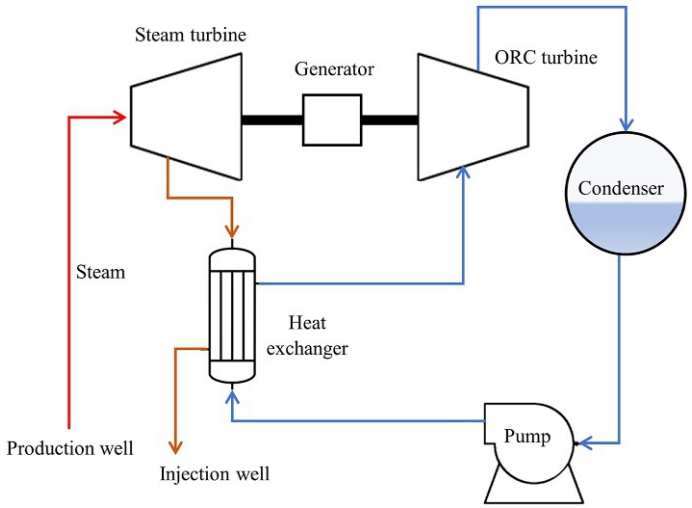

FIG. 2.23 Schematic diagram of a combined cycle power plant.

2.8.1 Proton exchange membrane fuel cell

A proton exchange membrane fuel cell (PEMFC) consists of two gas diffusion layers named the cathode and anode, a permeable membrane (also called the proton exchange membrane, or PEM) which acts as a separation wall between anode and cathode, an anode catalyst layer, and a cathode catalyst layer. The working principle of the proton exchange membrane

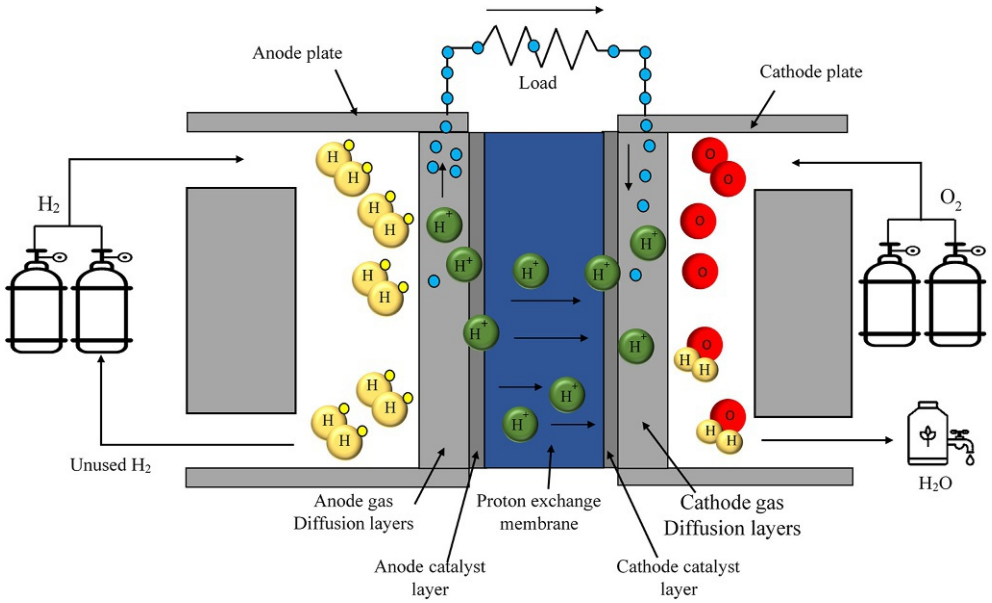

FIG. 2.24 Schematic diagram of a proton exchange membrane fuel cell.

fuel cell is set out in Fig. 2.24. Hydrogen gas enters the anode from the hydrogen fuel tank. The hydrogen is split into electrons and protons by the platinum catalyst. The electrons are diffused on the anode gas diffusion layer, from where they travel outside the circuit toward the load. The protons pass through the PEM and enter the cathode gas diffusion layer. At the cathode, protons collect the electrons coming from the outside, making hydrogen gas and reacting it with the oxygen to produce water [14]. The electrons moving from the anode to the cathode through the external circuit are termed the DC. Eq. (2.49) shows the oxidation reaction at the anode where the hydrogen loses an electron and Eq. (2.50) shows the reduction reaction at the cathode where the proton receives electrons. The overall reaction of the PEMFC is given in Eq. (2.51).

Oxidation at anode:

$$2H_2 \longrightarrow 4H^+ + 4e^- \tag{2.49}$$

Reduction at cathode:

$$O_2 + 4H^+ + 4e^- \longrightarrow 2H_2O \tag{2.50}$$

Overall reaction:

$$2H_2 + O_2 \longrightarrow 2H_2O \tag{2.51}$$

2.8.2 Alkaline fuel cell

The name of the alkaline fuel cell is based on potassium hydro oxide (KOH), which is an electrolyte. Oxygen enters the cell from the cathode side and hydrogen enters from the anode side. Oxygen receives the electrons coming through the external circuit, forming hydro oxide ions in the electrolyte. The hydro oxide ions move from the electrolyte to the anode where

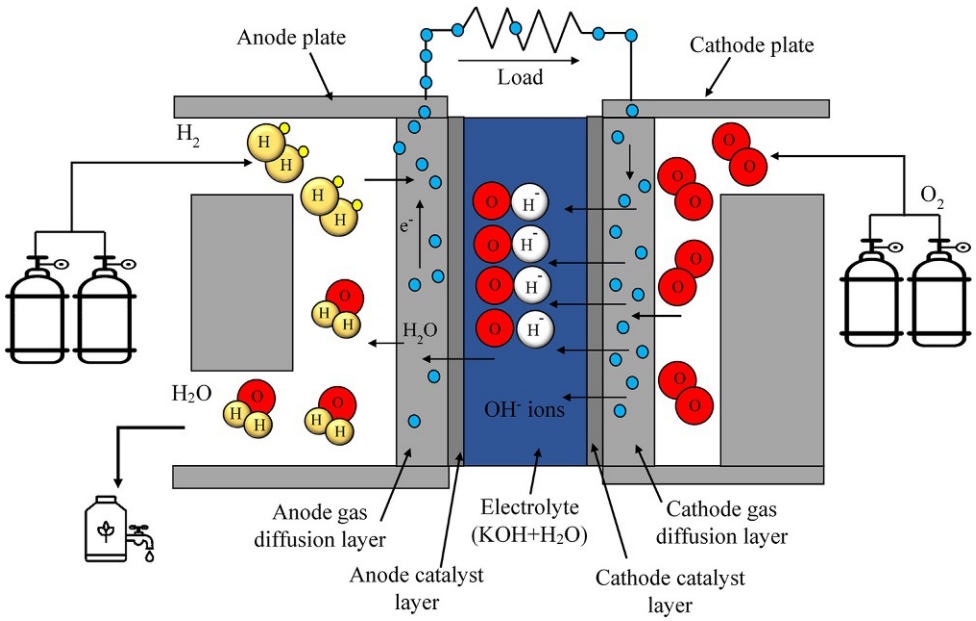

FIG. 2.25 Schematic diagram of an alkaline fuel cell.

they react with hydrogen, generating free electrons and water. The electrons move from the anode to the external circuit, making DC. The oxidation at the anode and the reduction at the cathode are given in Eqs. (2.52), (2.53). The working principle of the alkaline fuel cell is explained in Fig. 2.25.

Oxidation at anode:

$$\text{Anode} : 2H_2 + 4OH^- \longrightarrow 4H_2O + 4e^- \tag{2.52}$$

Reduction at cathode:

$$\text{Cathode} : O_2 + 4e^- + 2H_2O \longrightarrow 4OH^- \tag{2.53}$$

2.8.3 Direct methanol fuel cell

In direct methanol fuel cells (DMFCs), the chemical energy stored in the methanol-water is converted into electricity. The construction of the DMFC is similar to that of the PEMFC. Methanol water enters the anode where it is oxidized, liberating protons and electrons along with carbon dioxide. Electrons move the external circuit and the protons pass through the proton exchange membrane. At the cathode, protons absorb electrons from the external circuit and oxygen from the environment to form water. The oxidation at the anode, the reduction at the cathode, and the overall reaction are shown in Eqs. (2.54), (2.55), and (2.56), respectively. The energy conversion process of the DMFC is described in Fig. 2.26.

Oxidation at anode:

$$\text{Anode} : CH_3OH + H_2O \longrightarrow 6H^+ + 6e^- + CO_2 \tag{2.54}$$

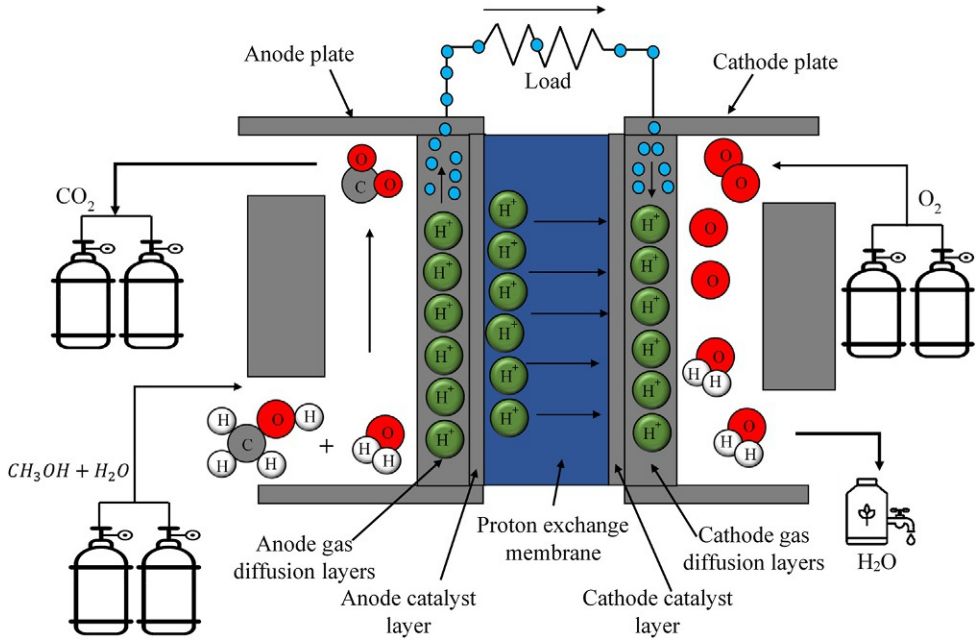

FIG. 2.26 Schematic diagram of a direct methanol fuel cell.

Reduction at cathode:

$$\text{Cathode} : \frac{3}{2}O_2 + 6H^+ + 6e^- \longrightarrow 3H_2O \tag{2.55}$$

$$\text{Overall} : CH_3OH + \frac{3}{2}O_2 \longrightarrow 2H_2O + \frac{1}{2}CO_2 \tag{2.56}$$

2.8.4 Molten carbonate fuel cell

In molten carbonate fuel cells (MCFSs), alkaline carbonate is used as an electrolyte. Like other types of fuel cells, an MCFS consists of an anode, cathode, anode gas diffusion layer, cathode gas diffusion layer, electrolyte, and catalyst layers. The working principle of the MCFS is shown in Fig. 2.27. Carbon dioxide, a product of the reduction reaction, reacts with the oxygen and free electrons to form carbonate ions. These carbonate ions are oxidized at the anode to water, carbon dioxide, and free electrons. The electrons move through the external circuit, water is collected as a by-product, and carbon dioxide is used in the reduction reaction at the cathode. The oxidation and reduction reactions are shown in Eqs. (2.57), (2.58), respectively.

Oxidation at anode:

$$\text{Anode} : H_2 + CO_3^{-2} \rightarrow H_2O + CO_2 + 2e^- \tag{2.57}$$

Reduction at cathode**:**

$$\text{Cathode} : O_2 + 2CO_2 + 4e^- \rightarrow 2CO_3^{-2} \tag{2.58}$$

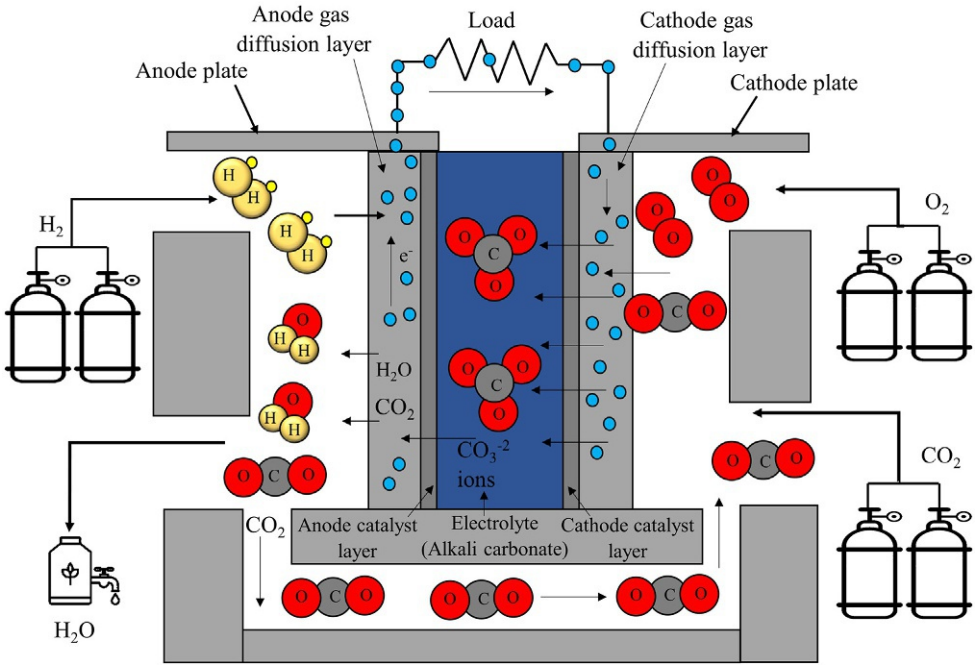

FIG. 2.27 Schematic diagram of a molten carbonate fuel cell.

2.8.5 Phosphoric acid fuel cell

The phosphoric acid fuel cell (PAFC) is named for the catalyst that is used in it. The working principle of the PAFC is similar to that of the PEMFC. Hydrogen is used as a fuel and is oxidized at the anode, generating free electrons moving toward the external circuit and the protons moving through the selectively permeable membrane toward the cathode. At the cathode, a reduction reaction takes place where the oxygen reacts with the protons and electrons. The oxidation and reduction reactions are shown in Eqs. (2.59), (2.60), respectively. Fig. 2.28 shows the conversion process of the phosphoric acid fuel cell.

Oxidation at anode:

$$\text{Anode} : 2H_2 \longrightarrow 4H^+ + 4e^- \tag{2.59}$$

Reduction at cathode:

$$\text{Cathode} : O_2 + 4H^+ + 4e^- \longrightarrow 2H_2O \tag{2.60}$$

2.8.6 Solid oxide fuel cell

The construction of the solid oxide fuel cell is similar to that of the PEMFC except for the electrolyte. Oxygen is transferred to the cathode where it is oxidized by the electrons coming through the cathodic electrode from the external circuit to form oxygen ions. These oxygen ions move through the ceramic/solid oxide electrolyte toward the anode, where they oxidize the hydrogen gas to form water and free electrons. Free electrons move from the anode to the cathode through the external circuit. The oxidation and reduction reactions at the anode and

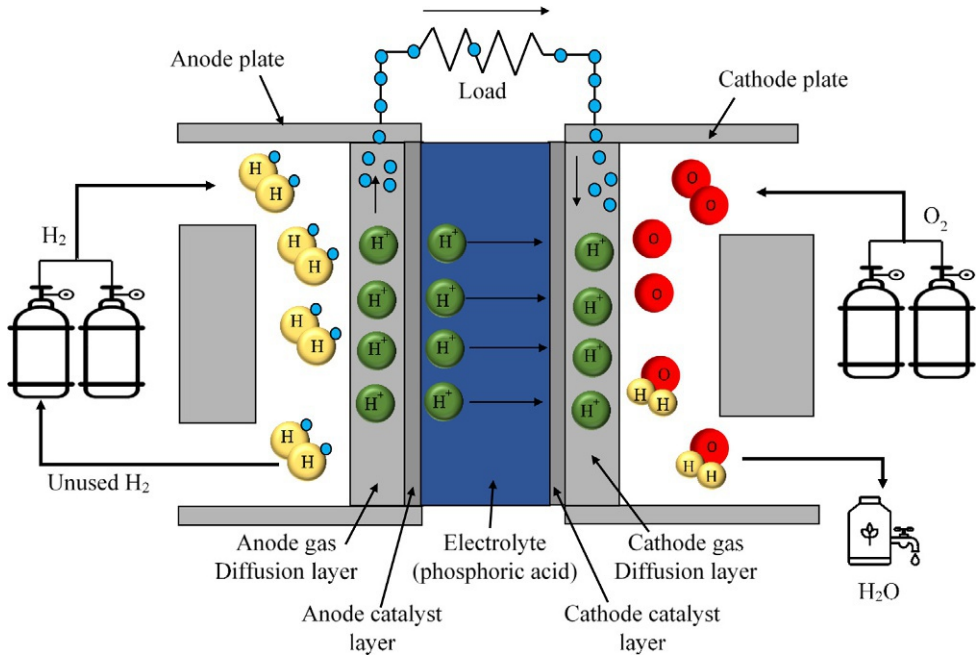

FIG. 2.28 Schematic diagram of a phosphoric acid fuel cell.

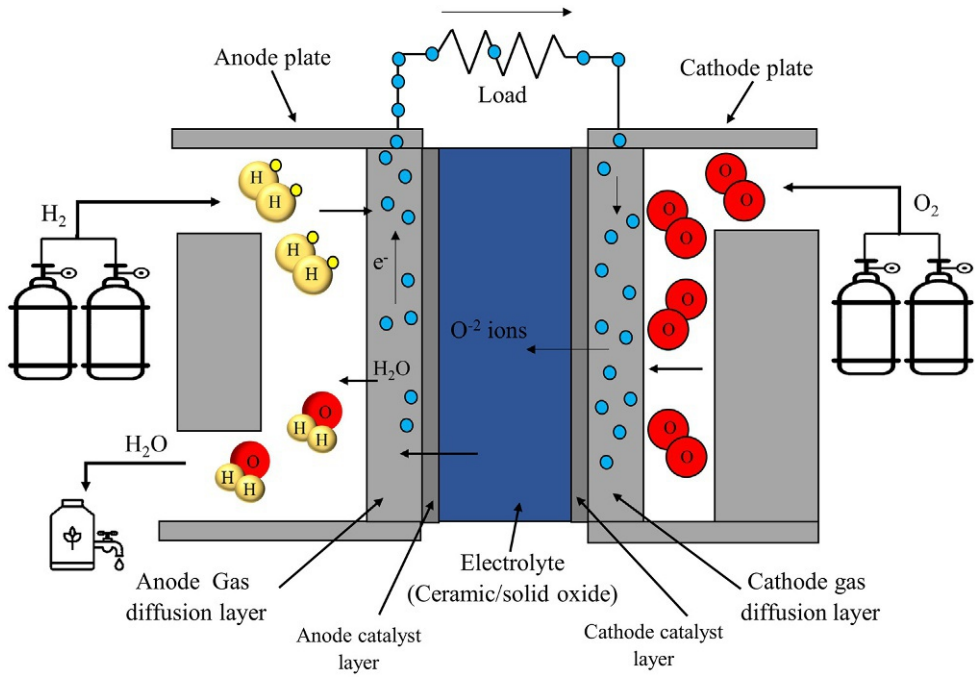

FIG. 2.29 Schematic diagram of a solid oxide fuel cell.

cathode are given in Eqs. (2.61), (2.62). Fig. 2.29 presents a schematic diagram of the energy conversion process of a solid oxide fuel cell.

Oxidation at anode:

$$\text{Anode} : H_2 + O^{-2} \longrightarrow H_2O + 2e^- \tag{2.61}$$

Reduction at cathode:

$$\text{Cathode} : O_2 + 4e^- \longrightarrow 2O^{-2} \tag{2.62}$$

2.9 Steam turbine power plants

A steam turbine power plant converts the heat energy of the feedstock into electrical energy. The feedstock could be coal or biomass. The steam generated in the boiler by burning the coal is used to turn the steam turbine. The coupled generator generates electrical energy. A practical model of the complete power station consists of various other components discussed in detail in Fig. 2.30. This section briefly describes all these components. A Rankine cycle is run on the steam turbine, which will be discussed in detail later in this section.

2.9.1 Components of a steam turbine power plant

2.9.1.1 Boiler

A boiler is used to generate steam by taking heat from burning feedstock. Steam from the boiler is passed to the turbine and the flue gases are passed through the superheater, economizer, and air preheater before being released into the atmosphere through chimneys.

2.9.1.2 Superheater

Steam generated in the boiler is wet; therefore, before it is sent to the turbine, it is first dried by passing through the superheater. A superheater is also used to convert saturated steam into superheated steam. Superheaters take the heat from the flue gases of the boiler and transfer this heat to generate superheated steam or to dry the steam. The purpose of avoiding wet steam in the turbine is to protect the turbine from corrosion.

2.9.1.3 Economizer

In a boiler, water is used as a working medium which is converted into steam. Before this water is sent as feed water to the boiler, it is first passed through the economizer. The flue gases coming from the superheater still have energy that can be extracted. The economizer uses these flue gases to preheat the feed water.

2.9.1.4 Air preheater

The flue gases coming from the superheater and the economizer still contain energy, which is used to preheat the air before sending it to the boiler. A forced draught fan is used to send the air from the atmosphere to the air preheater and then send it to the boiler. The process of preheating the feed water and air increases the thermal efficiency of the overall process.

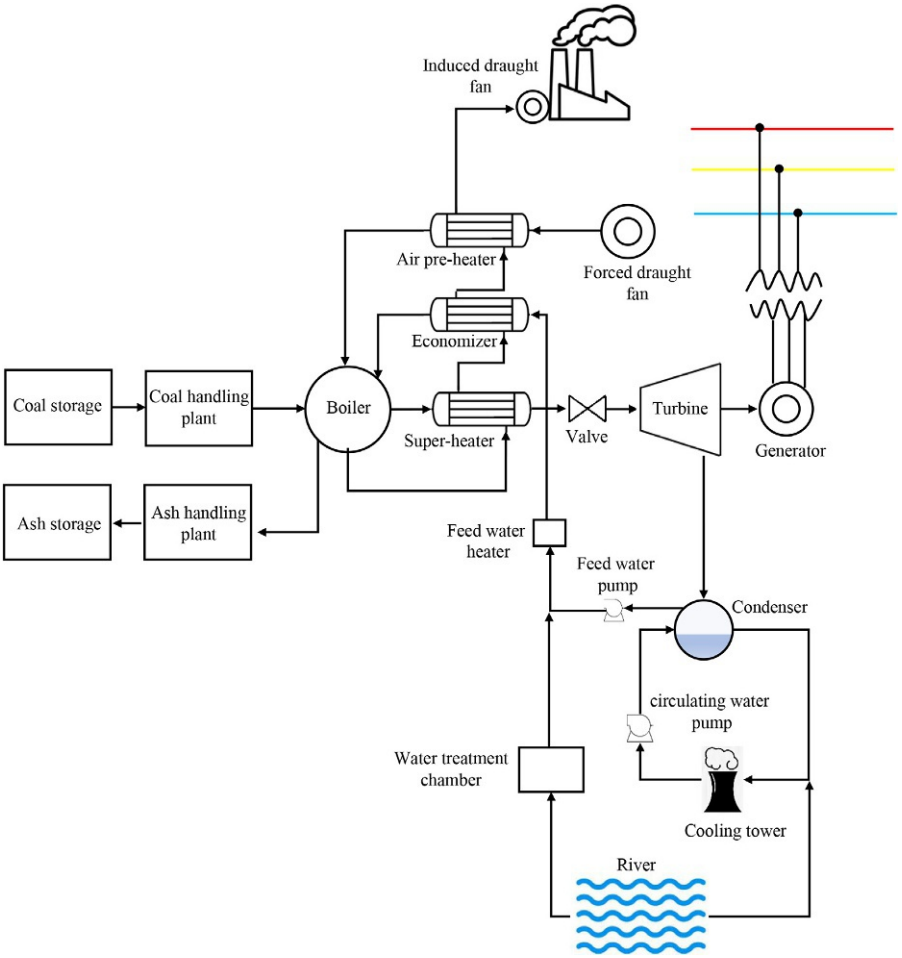

FIG. 2.30 Schematic diagram of a steam turbine power plant.

The general process of the steam turbine power plant can be explained as follows. The inputs to the boiler are the energy source, which could be coal or biomass, air, and water. Coal is first stored and pretreatment is performed before it is sent to the boiler. The generated steam is wet and it is passed through the superheater to get superheated steam. The flue gas is further passed through the economizer and air preheater, where energy is extracted to preheat the water and air, respectively. Finally, the flue gases are emitted to the atmosphere through a chimney, where a forced draught fan is used. The superheated steam is passed through a turbine where it rotates the turbine and a coupled generator. After passing through the turbine, the steam expands and is sent to the condenser. In the condenser, the steam condenses by the cooling process and the water is sent to the cooling tower for further processing.

2.9.2 Steam turbine Rankine cycle

The ideal cycle for steam or vapor is called the Rankine cycle; this uses superheated steam in a turbine and condenses it completely in the condenser. The ideal Rankine cycle consists of the following four thermodynamic processes:

- Stage 1–2 isentropic compression in the pump;
- Stage 2–3 isobaric heat addition in the boiler;
- Stage 3–4 isentropic expansion in the turbine; and
- Stage 4–1 isobaric heat rejection in the condenser.

The process of the Rankine cycle starts from stage 1, at which the water enters the pump that increases the pressure of the water, keeping the entropy constant. In stage 2, when the water enters the boiler, it is at the pressure of the boiler; in the boiler, it gets the heat energy and is converted into steam. The energy is obtained by burning oil, coal, gas, nuclear reactor, or biomass. In stage 3, the output from the boiler is superheated steam that is expanded over the turbine, and the steam turbine rotates and the steam loses its pressure in stage 4. The turbine is connected to a generator through a common shaft that converts the heat energy of the steam into electrical energy. The working fluid at stage 4 is the saturated liquid–vapor mixture that enters the condenser. The condenser is a large heat exchanger that emits the heat to a nearby cooling tower or any other technology like an air preheater, economizer, or superheater. The pressure in this stage is kept constant. Fig. 2.31 indicates that from stage 1 to stage 2, electric work is done on the system, from stage 2 to stage 3, heat is added to the system, from stage 3 to stage 4, work is done by the system by generating electric power, and at stage 4 to stage 1, heat is rejected from the system. No work is done that involves the boiler and the condenser, and no heat exchange is involved at the compressor and the turbine. The energy conservation equations for each of the devices can be expressed by Eqs. (2.63)–(2.66).

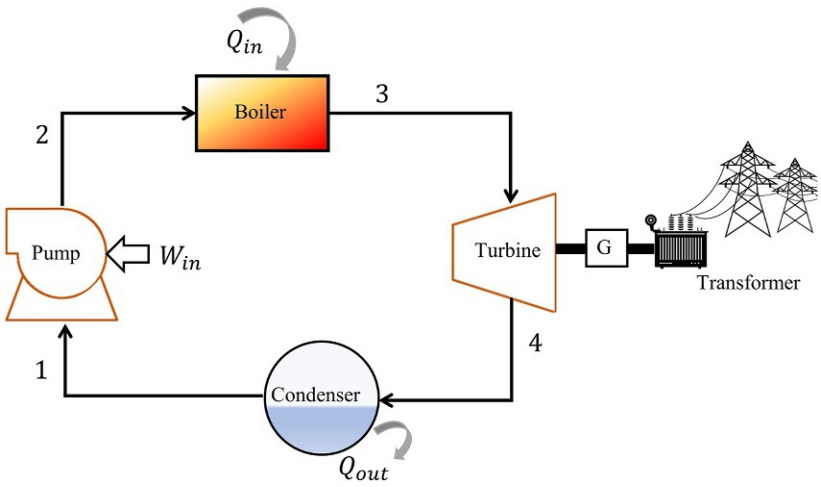

FIG. 2.31 Rankine cycle working on a steam turbine.

$$\text{At pump} : W_{in} = h_2 - h_1 \tag{2.63}$$

$$\text{At boiler} : Q_{in} = h_3 - h_2 \tag{2.64}$$

$$\text{At turbine} : W_{out} = -(h_4 - h_3) \tag{2.65}$$

$$\text{At condenser} : Q_{out} = -(h_1 - h_4) \tag{2.66}$$

The efficiency of a system is defined as the ratio of the obtained energy to the consumed energy, as given in the following relation which is further simplified in Eq. (2.67).

$$\eta = \frac{output\ energy}{Input\ energy}$$

$$\eta = \frac{W_{out} - W_{in}}{Q_{in}} = \frac{Q_{in} - Q_{out}}{Q_{in}}$$

$$\eta = \left(1 - \frac{Q_{out}}{Q_{in}}\right)100\% \tag{2.67}$$

The efficiency of the Rankine cycle can be improved by lowering the pressure of the condenser, superheating the steam at high temperature, i.e., by increasing the temperature of the boiler, and by increasing the pressure of the boiler.

2.10 Gas turbine power plants

A power station that uses hot and high-pressure gas to run a gas turbine and generate electricity is called a gas turbine power plant. The air is taken from the atmosphere and passed through a compressor, which raises the pressure of the air. The high pressure is passed through the combustion chamber where the air is heated. In the combustion chamber, heat is added from burning the coal, oil, or gas. The hot and high-pressure gases from the combustion chamber are passed through the turbine. This turbine, coupled to an electrical generator, converts this heat energy into electrical energy. To increase the efficiency of the gas turbine power plant, a regenerator is associated with it. This is a device that consists of tubes in which the air moves. In the outer chamber, hot flue gases coming from the turbine are passed. The heat exchanging process takes place and the air in the tubes takes the wasted heat from the flue gases and is preheated before going into the combustion chamber. Fig. 2.32 shows a process flow diagram of a gas turbine power plant. Gas turbine power plants work on the Bryton cycle, which consists of four thermodynamic cycles:

- isentropic compression in the compressor;
- isobaric heat addition through the heat exchanger;
- isentropic expansion in the turbine; and
- isobaric heat rejection through the heat exchanger.

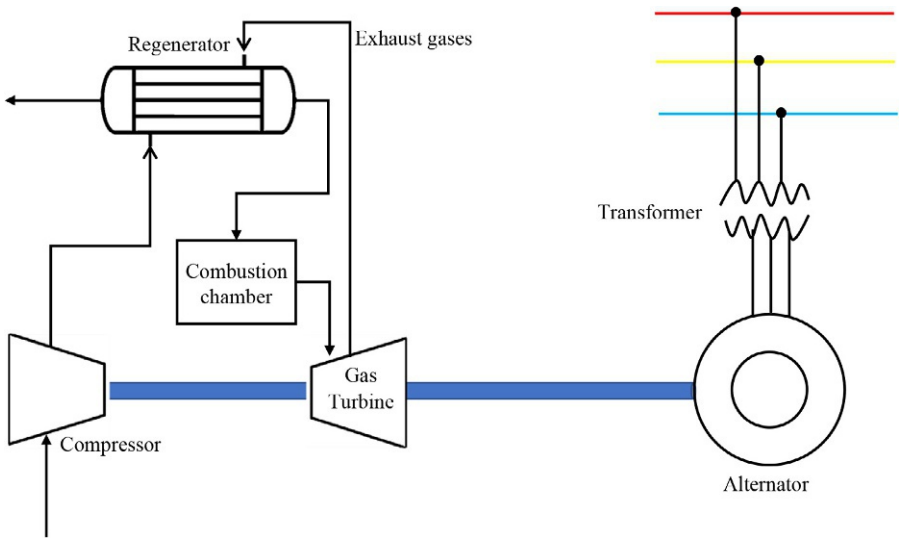

FIG. 2.32 Schematic diagram of a gas turbine power plant.

2.11 Nuclear power plants

A power plant that converts nuclear energy into electrical energy is called a nuclear power plant. In nuclear power plants, nuclear fission reaction is performed in a nuclear reactor, which produces a huge amount of heat energy that is used to generate steam. A nuclear fission reaction is the split of U-235 (Uranium-235) by the bombardment of a neutron on the nucleus. The uranium nucleus split into barium and krypton with three further neutrons and a huge amount of heat. The nuclear fission reaction is given in the following equation.

$$U_{92}^{235} + n_0^1 \longrightarrow Ba_{56}^{144} + Kr_{36}^{89} + 3n_0^1 + 210\ \text{MeV}$$

A huge amount of heat energy is used to raise the temperature of water, generating steam and running the steam turbine to generate electricity through the turbine coupled with a generator. A small amount of uranium can generate a huge amount of electricity. The amount of heat that is generated by burning high-quality 4500-ton coal is same that is generated by a fission reaction of 1 kg uranium.

As a result of the fission reaction, three neutrons are generated, which are further absorbed by three other nuclei of uranium; they also split, carrying out the same fission reaction. If the reaction is not controlled, a chain reaction starts and the uncontrolled fission reaction becomes catastrophic. Nuclear reactors control the fission reaction by absorbing the newly generated neutrons with cadmium rods. Fig. 2.33 shows a process flow diagram of a nuclear power plant. The rest of the process is the same as that for a steam turbine power plant.

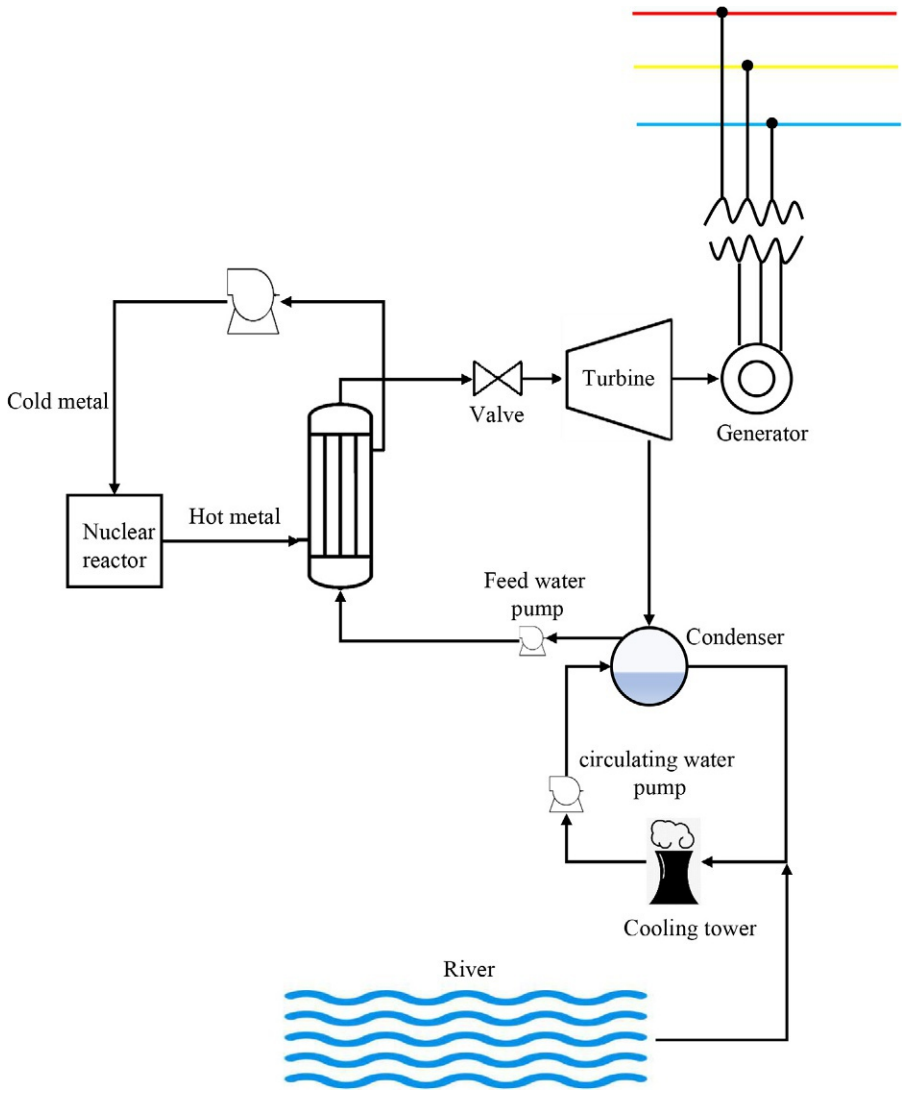

FIG. 2.33 Schematic diagram of a nuclear power plant.

2.12 Conclusion

Distributed generation (DG) is the fundamental concept of smart grid systems. Any of the conventional source-based or the renewable energy-based power plants located on the distribution level to meet the local load demand is called the distributed generation. A well-effective control system and communication between these DG sources make the microgrid a smart grid. Conventional energy sources are coal, gas, and oil. These sources are used to run

steam turbine power plants, gas turbine power plants, and diesel-based power plants. Renewable energy sources and technologies include solar thermal energy, solar photovoltaics, and solar indoor lighting systems. Other renewable energy sources like wind energy, fuel cell, biomass, hydrogen production, and geothermal energy were discussed in detail along with their energy harvesting technologies.

Problems

Problems 1–33 contain three/four answer options A, B, C, and D. Choose the correct answer.

1. What energy conversion takes place in a hydropower plant?
   - **A.** The ionization energy of water is used to generate steam and run the steam turbine.
   - **B.** The kinetic energy of water is converted into mechanical energy of the turbine.
   - **C.** The rotational kinetic energy of the turbine is converted into electrical energy of the turbine.
   - **D.** The steam energy of the steam is converted into mechanical energy of the turbine.
2. Which of the following is a type of reaction turbine?
   - **A.** Turgo
   - **B.** Pelton
   - **C.** Cross flow
   - **D.** Francis
3. Which of the following is a type of impulse turbine?
   - **A.** Pump as a turbine
   - **B.** Pelton
   - **C.** Propeller
   - **D.** Francis
4. What head(s) are reaction turbines are used at?
   - **A.** Low head
   - **B.** Medium head
   - **C.** High head
   - **D.** Low head and medium head
5. In a hydro plant, if the discharge is $200\,m^3/s$ and the head of the water is 100 m, and the efficiency of the turbine alternator is set to 0.85, find the power developed.
   - **A.** 177 MW
   - **B.** 150.7 MW
   - **C.** 66.67 MW
   - **D.** 166.6 MW
6. In which order is the flow rate arranged to draw flow duration curves?
   - **A.** Ascending order
   - **B.** Descending order
   - **C.** Apple pie order
   - **D.** First in first out order

7. In flow duration curves, data is arranged in what way against the flow rate?
   A. Percentage exceedance
   B. Incremental order
   C. Decremental order
   D. Ascending order
8. Which is the correct formula for a bottom line slope?
   A. $S = \left(\frac{Q \times h}{A \times R^{2/3}}\right)^2$
   B. $S = \left(\frac{Q \times n}{A \times R^{2/3}}\right)^2$
   C. $S = \left(\frac{Q \times P}{A \times R^{2/3}}\right)^2$
   D. $S = \left(\frac{Q \times P \times h}{A \times R^{2/3}}\right)^2$
9. Determine the penstock thickness if the penstock diameter is 5 m.
   A. 3.01 m
   B. 2.60 m
   C. 2.01 m
   D. 2.48 m
10. What does the process of anaerobic digestion yield?
    A. CO_2 and CH_4
    B. CO_2 and H_2O
    C. CH_4 and H_2O
    D. All of the above
11. What is the conversion process of vegetable oil into biodiesel known as?
    A. Pyrolysis
    B. Photosynthesis
    C. Fermentation
    D. Transesterification
12. Which of the following is a substrate for biogas production?
    A. Metallic waste
    B. Municipal solid waste and residential waste
    C. Gaseous waste
    D. All of the above
13. Lignocellulosic biomass can be converted into ethanol through what process?
    A. Gasification
    B. Hydrolysis-fermentation
    C. Palletization
    D. Pyrolysis
14. Biodiesel is produced by what chemical reaction?
    A. Transesterification
    B. Fermentation
    C. Pyrolysis
    D. Photosynthesis
15. Which of the following processes is not part of anaerobic digestion?
    A. Acetogenesis
    B. Biogenesis

C. Methanogenesis
D. Acidogenesis

16. Photosynthesis can be represented by what chemical reaction?
A. $6CO_2 + 6H_2O \longrightarrow 2C_6H_{12}O_6 + 6O_2$
B. $C_6H_{10}O_5 + H_2O \longrightarrow C_6H_{12}O_6 + H_2$
C. $C_6H_{12}O_6 \longrightarrow 2C_2H_5\,OH + 2CO_2$
D. $C_6H_{12}O_6 + 2H_2 \leftrightarrow C_2H_5\,COOH + 2H_2O$

17. Which of the following elements are found in proximate analysis?
A. Moisture content and volatile matter
B. Fixed carbon and ash content
C. Oxygen, hydrogen, and carbon
D. Moisture content, volatile matter, fixed carbon, and ash content

18. Which of the following best indicates the steps of anaerobic digestion?
A. Generator → waste water feed → digester → biogas → biogas storage
B. Waste water feed → biogas storage → generator → biogas
C. Waste water feed → biogas → digester → biogas storage → generator
D. Waste water feed → digester → biogas → biogas storage → generator

19. Which of the following is not a thermochemical process used to produce hydrogen?
A. Photo-fermentation
B. Dark fermentation
C. Bio-photolysis
D. Pyrolysis

20. What is incomplete combustion of biomass in the presence of an oxidizing agent called?
A. Fermentation
B. Bio-photosynthesis
C. Gasification
D. Pyrolysis

21. What is the product of the acetogenesis reaction?
A. Ketone
B. Acetone
C. Ethanol
D. Acetate

22. Hydrogen can be produced by what process?
A. Biological
B. Thermochemical
C. Water splitting
D. All of the above

23. Which of the following is a cold weather characteristic of a fuel?
A. Melting point
B. Flash point
C. Cloud point
D. Boiling point

24. What is the entropy of the formation of water?
A. $-0.183\frac{\text{kJ}}{\text{mol}}$

B. $-0.173\frac{\text{kJ}}{\text{mol}}$

C. $-0.153\,\frac{kJ}{mol}$

D. $-0.163\,\frac{kJ}{mol}$

25. What is the enthalpy change of the formation of water?

A. $-288\,\frac{kJ}{mol}$

B. $-287\,\frac{kJ}{mol}$

C. $-286\,\frac{kJ}{mol}$

D. $-285\,\frac{kJ}{mol}$

26. What is the correct relation for the Gibbs free energy?

A. $\Delta G = \Delta T - T.\ \Delta S$

B. $\Delta G = \Delta H - T.\ \Delta H$

C. $\Delta G = \Delta H + T.\ \Delta S$

D. $\Delta G = \Delta H - T.\ \Delta S$

27. What is the Gibbs free energy for the formation of water?

A. $-257\,\frac{kJ}{mol}$

B. $-247\,\frac{kJ}{mol}$

C. $-227\,\frac{kJ}{mol}$

D. $-237\,\frac{kJ}{mol}$

28. Which of the following represents terminal voltage of the stack of a fuel cell?

A. $V_T = N(E_T - L)$

B. $V_T = N(E_T + L)$

C. $V_T = (E_T - L)$

D. $V_T = N(E_T - \eta_{ohmic})$

29. What is the efficiency of a direct methanol fuel cell?

A. 95.7%

B. 98.7%

C. 96.7%

D. 97.7%

30. What is the anode reaction of a direct methanol fuel cell?

A. $CH_3OH + H_2 \longrightarrow 6H^+ + 6e^- + CO_2$

B. $H_2 + CO_3^{-2} \longrightarrow H_2O + CO_2 + 2e^-$

C. $\frac{3}{2}O_2 + 6H^+ + 6e^- \longrightarrow 3H_2O$

D. None of the above

31. What is the enthalpy of formation of methanol?

A. $+736\,\frac{kJ}{mol}$

B. $-736\,\frac{kJ}{mol}$

C. $-726\,\frac{kJ}{mol}$

D. $+726\,\frac{kJ}{mol}$

32. Which of the following statements about fuel cells is incorrect?

A. The emissions from the fuel cells are quite low.

B. The operation of the fuel cell is quite noisy.

C. Fuel cells are modular.

D. The efficiency of the fuel cell is high.

33. Which of the following is not an example of a fuel cell?
- **A.** Phosphoric acid fuel cell
- **B.** Hydrogen-oxygen fuel cell
- **C.** Hexanone-oxygen fuel cell
- **D.** Direct methanol fuel cell

Give brief answers to the following short questions

1. Differentiate between solar thermal energy and solar photovoltaics.
2. Which technologies are used to harness the thermal energy from the sun?
3. Differentiate between two types of hydro turbines.
4. You are a hydrologist and have been instructed to install a micro-hydropower project on a hill. Measure the flow rates of water for 12 days and sketch the flow duration curves.
5. The water enters an open channel with a radius of 300 cm and an area of cross-section is 14.1 m^2. Determine the section factor of this open channel.
6. How would you differentiate between the net head and the gross head? Explain your answer mathematically.
7. What kind of losses occur in the penstock as the water moves from high head to low head?
8. In a micro-hydropower plant, the water flow rate is 20 m^3/s, and the losses in the penstocks are 5.6 m. The gross head is 30 m, and the turbine and coupled generator are 95% efficient. Determine the power that would be available from the turbine.
9. Perform SWOT analyses of the following renewable energy sources:
- **(a)** Hydropower
- **(b)** Solar energy
- **(c)** Wind energy
- **(d)** Fuel cell
- **(e)** Bioenergy

10. Define the term biogas digester substrate and list which materials can be used as substrates.
11. Define the term producer gas and explain how it is obtained.
12. Which biological techniques are used to generate hydrogen gas?
13. What is the difference between fermentation and pyrolysis? Give the chemical reactions of each.
14. Define proximate analysis and explain what is determined in this analysis.
15. How are pellets formed and why are they a preferred energy source?
16. Define ultimate analysis and explain what is determined in this analysis.
17. How is hydrolysis used to generate hydrogen? Determine the cell potential that is required for the hydrolysis process.
18. State a difference between a fuel cell and a solar PV cell.
19. What losses are incurred in a fuel cell?
20. Determine the Gibbs free energy of the following reaction.

$$CH_3OH + \frac{3}{2}O_2 \longrightarrow 2H_2O + CO_2$$

21. Briefly describe the hydrogen production process.
22. State the working principle of a proton exchange membrane fuel cell.

References

[1] M.I. Soomro, A. Mengal, Y.A. Memon, M.W.A. Khan, Q.N. Shafiq, N.H. Mirjat, Performance and economic analysis of concentrated solar power generation for Pakistan, Process 7 (9) (2019) 575, https://doi.org/10.3390/PR7090575.

[2] C. Te Lee, P.T. Ho, Y.Y. Lee, L.B. Chen, A research on the 4th generation intelligent energy-saving solar water heating tank, Electron 9 (11) (2020) 1941, https://doi.org/10.3390/ELECTRONICS9111941.

[3] M. Mofijur, et al., Phase change materials (PCM) for solar energy usages and storage: an overview, Energies 12 (16) (2019) 3167, https://doi.org/10.3390/EN12163167.

[4] M. Kamran, M. Mudassar, M.R. Fazal, M.U. Asghar, M. Bilal, R. Asghar, Implementation of improved Perturb & Observe MPPT technique with confined search space for standalone photovoltaic system, J. King Saudi Univ. Eng. Sci. 32 (7) (2020) 432–441, https://doi.org/10.1016/J.JKSUES.2018.04.006.

[5] M. Kamran, et al., Solar photovoltaic grid parity: a review of issues and challenges and status of different PV markets, Int. J. Renew. Energy Res. 9 (1) (2019) 244–260, https://doi.org/10.20508/IJRER.V9I1.8933.G7580.

[6] H. Shahid, M. Kamran, Z. Mehmood, M.Y. Saleem, M. Mudassar, K. Haider, Implementation of the novel temperature controller and incremental conductance MPPT algorithm for indoor photovoltaic system, Sol. Energy 163 (2018) 235–242, https://doi.org/10.1016/J.SOLENER.2018.02.018.

[7] A. Goetzberger, V. Hoffmann, Photovoltaic solar energy generation, Springer Ser. Opt. Sci. 112 (2005) 1–229, https://doi.org/10.1007/B137803.

[8] G.M. Joselin Herbert, S. Iniyan, E. Sreevalsan, S. Rajapandian, A review of wind energy technologies, Renew. Sustain. Energy Rev. 11 (6) (2007) 1117–1145, https://doi.org/10.1016/J.RSER.2005.08.004.

[9] M. Kamran, R. Asghar, M. Mudassar, M.I. Abid, Designing and economic aspects of run-of-canal based micro-hydro system on Balloki-Sulaimanki link canal-I for remote villages in Punjab, Pakistan, Renew. Energy 141 (2019) 76–87, https://doi.org/10.1016/J.RENENE.2019.03.126.

[10] M. Kamran, Hydro energy, in: Renewable Energy Conversion Systems, Academic Press, 2021, pp. 193–219.

[11] M. Kamran, Bioenergy, in: Renewable Energy Conversion Systems, Academic Press, 2021, pp. 243–264.

[12] O.A. Povarov, V.A. Saakyan, A.I. Nikol'skij, V.E. Luzin, V.M. Morgun, M.B. Sapozhnikov, Binary cycle power plants, in: Tyazheloe Mashinostr, 2005, pp. 163–196, https://doi.org/10.1016/B978-185617474-9/50040-6. no. 8.

[13] M.R. Fazal, M. Kamran, Geothermal energy, in: Renewable Energy Conversion Systems, Academic Press, 2021, pp. 265–281.

[14] M. Kamran, Fuel cell, in: Renewable Energy Conversion Systems, Academic Press, 2021, pp. 221–242.

This page intentionally left blank

CHAPTER

3

Power grids

3.1 Introduction

An electric power grid is an interrelated electrical network consisting of an electrical power generating station, electrical power transmission system, electrical power distribution system, and the end consumer. Electrical power generation is of two types. Direct current or DC flows because of the potential difference between two lines of a circuit. Alternating current or AC is very different and complicated; it is produced by Faraday's law of electromagnetic induction, which states that the time rate of change of flux through a coil induces a voltage in it. Today it may be asked why our electrical power system is AC. There is an interesting story behind this, which is known as the war of currents between Edison and Tesla.

This chapter discusses the complete electric power system from generation to distribution. The difference between AC and DC circuit breakers (CBs) based on the quenching of the arc is discussed. The types of AC and DC CBs are discussed in detail. AC CBs include oil CBs, vacuum CBs, air blast CBs, and SF_6 CBs. DC CBs are divided into mechanical DC breakers, solid-state DC breakers, and hybrid DC breakers. Substation bus bars and their types are also described in this chapter. Bus bars include single bus bars, sectionalized bus bars, single breaker double bus bar configurations, double breaker double bus configurations, main and transfer bus bar configurations, breaker and a half configurations, and ring bus configurations. The advantages and disadvantages of each type of bus bar configuration are identified.

Power factor with the help of the power triangle is explained. Causes of low power factor, impact of low power factor on transmission, and power factor improvement methods are explained in detail. Conductors and insulators in the transmission line and their types are also explored in detail. Other concepts like the resistance of the transmission line, skin effects, proximity effect, and spirality effects are also discussed briefly. Formation of corona effect, its causes and advantages, and corona effect reduction methods are also given. The types of faults in the transmission line are also discussed. The distribution system with all its components like feeder, distributor, and service main are considered. Connection schemes, configurations, and types of AC and DC distribution systems are explained. Single-phase transformers and the connections of three-phase transformers are discussed in detail.

https://doi.org/10.1016/B978-0-323-99560-3.00005-3

3.2 Electrical power stations

Electricity is produced at an electrical power station through either conventional fossil fuels (oil, coal, and gas) or renewable energy sources. In conventional sources, electromechanical generators are driven by either gas turbines or steam turbines. From renewables, wind energy is used to drive a wind turbine coupled with an electrical generator, while solar irradiance is used to generate DC electricity through solar photovoltaics, to drive a steam turbine using solar concentrated technology and geothermal energy. A biogas power plant generates electricity by driving a steam turbine or gas turbine. DC electricity is produced by fuel cells using hydrogen as fuel. These electric power stations are near available energy sources and away from populated, congested areas. The types of conventional and renewable electric power stations were discussed in detail in Chapter 2.

3.3 Electrical substations

From generation to the end consumer, the transmission line may pass through numerous substations consisting of transforms to transform the voltages at different levels. Electric substations perform the function of stepping up and down the voltages and transform the AC voltages into DC voltages or DC to AC voltages many times between the power station and the load. The transition between transmission and distribution occurs through the substation. Substations are divided into three types, based on their functioning, as follows.

3.3.1 Step-up substation

In step-up substations, the voltages of the generators at the generation power plant are increased for efficient transmission. The increase in the transmission voltage at a step-up substation decreases the current in the transmission, keeping the power constant. The decrease in current reduces the heat losses in the resistance of transmission conductors.

3.3.2 Step-down substation

In a step-down substation, the transmission voltages are lowered to subtransmission voltages for industrial applications. The output of the step-down substation is directed to the input of the distribution substation.

3.3.3 Distribution substation

A distribution substation delivers electricity to industrial and residential users. Apart from the transformers, a distribution substation may include CBs, lightning arresters (LAs), switches, isolators, and busbars, as discussed below (Fig. 3.1).

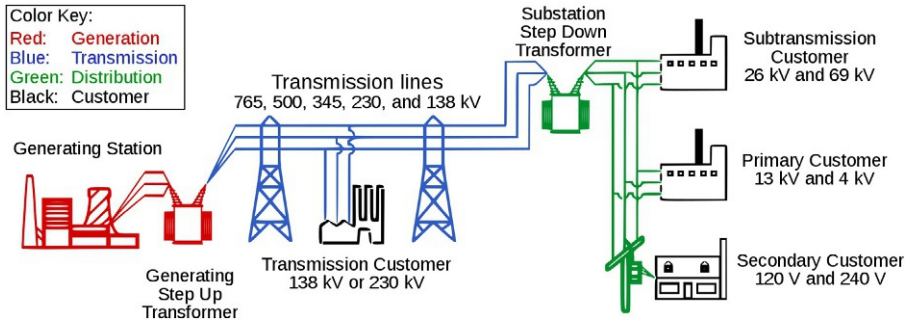

FIG. 3.1 Electrical power transmission and distribution system. *Source: Wikipedia.*

3.4 AC circuit breakers

A CB is an automatically operated electrical switch that operates in case of a fault in the circuit to interrupt the inrush current. It isolates the rest of the circuit from the faulty equipment. After the removal of the fault, the CB is reclosed to recommence the normal operation. The first duty of the CB is to detect the fault. For low current and low voltage applications, this duty of detecting the fault is performed by the breaker itself through a heating or magnetic effect, whereas in large current and high voltage applications, CB is provided with a protective relay and a separate power source to detect the fault and perform the opening function. On the detection of the fault, the contacts of the CB are opened using the mechanical energy stored in the spring in the CB or solenoid that becomes magnetized when a high current passes through it, and it attracts the contacts to open the CB.

During the opening of the contacts of the CB, an arc is produced because of the high fault current. The arc produces heat, which must be endured by the metal contacts. The arc must also be quenched as it is produced to increase the service life of the contacts. The following methods of introducing high resistance in the path of the arc are used to extinguish the arc.

- **Quenching the arc in zero-crossing**: In AC, the waveform is sinusoidal, containing zero-crossing twice the frequency of the AC signal. In a 50 Hz system, an AC signal passes the zero-crossing 100 times per second. The arc is quenched during the zero-crossing that hampers the restricking of the arc.
- **Exhaustive cooling**: An intensive cooling effect is produced to reduce the heat produced during the formation of the arc.
- **Lengthening the arc**: The resistance of the arc is directly proportional to its length, which can be increased by increasing the distance between the contacts.
- **Splitting the arc**: This is another way of increasing the resistance of the arc. The arc is divided into partial arcs by inserting some conducting plates between the contact, which increases the resistance in the path of the arc and helps in quenching the arc.

The most commonly used thermal-magnetic miniature CB is shown in Fig. 3.2. The components labeled are (1) actuator lever, (2) actuator mechanism, (3) contacts, (4) terminals, (5) bimetallic strip, (6) calibration screw, (7) solenoid, and (8) arc quencher.

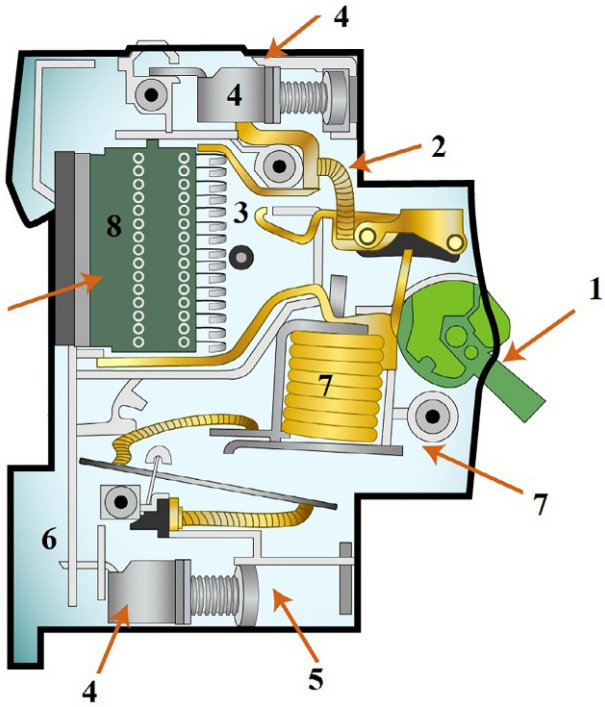

FIG. 3.2 Internal structure of thermal-magnetic miniature circuit breaker. *Source: Wikipedia.*

Based on the arc extinguishing medium, CB is classified into an oil CB, air blast CB, vacuum CB, and sulfur hexafluoride CB. All these types of AC CBs are discussed in the following subsections.

3.4.1 Oil circuit breaker

In oil CB, oil is used as an arc extinguishing medium. As the arc is produced, the oil around the arc is evaporated generating hydrogen gas around the arc. The oil is pushed away from the arc, the hydrogen gas helps in cooling down the arc, and the fault current is interrupted. Oil CB has two types: (1) bulk oil CB, in which oil in bulk is used that performs the arc extinguishing as well as the insulation of the current-conducting parts and (2) low oil CB in which minimum oil is used only to quench the arch whereas the insulation is provided by the air or the organic insulating materials.

3.4.2 Vacuum circuit breaker

From a capacitor point of view, the properties of vacuum as a dielectric are well-known. A vacuum has the highest insulating properties. During a fault, when the contacts are opened in a vacuum, the forming arc has to face insulation that the first zero-crossing uses to quench the arc quickly. Vacuum CB has a higher arc quenching property than any other material.

3.4.3 Air blast circuit breaker

Air blast CB is a type of CB that employs an air blast to quench the arc. On detection of the falling current, the breaker contacts are opened and the blast valve is also opened. The air blast increases the length of the arc and quenches it. If the blast valve is opened at the zero-crossing, the chances of the restriking of the arc have vanished. The three types of air blast CB are axial blast type, cross blast type, and radial blast type.

3.4.4 SF_6 circuit breaker

In SF_6 CB, sulfur hexafluoride gas (SF_6) is used as an arc quenching medium. The property of absorbing free electrons makes it electronegative gas. As the CB contacts are opened, a blast of SF_6 gas is released, which absorbs the free electrons in the arc and the arc is quenched. SF_6 gas quickly absorbs the free electrons, which makes it most suitable for use in high voltage and high current applications.

3.5 DC circuit breakers

In DC substations or DC microgrids, direct current circuit breakers (DCCBs) are used. DCCBs, as the name suggests, are used for the protection of electrical devices that operate on direct current. The main difference between direct current and alternating current is that in DC the voltage output is constant, while in AC it cycles several times per second. For a 60 Hz frequency system, an AC signal changes its polarity 120 times and 120 times the signal passes through the zero-crossing. As there is no zero-crossing in the DC signal, arc quenching in the DCCB is a hurdle. Because of the absence of the arc quenching methods in DCCB, DC grids did not develop as the AC grids developed after the war of currents between Nikola Tesla and Thomas Edison.. The main three types of DC breakers are mechanical DC breakers, solid-state DC breakers, and hybrid DC breakers.

3.5.1 Mechanical DC breaker

A mechanical DC breaker is the simplest and most conventional DCCB. It consists of three parallel paths: nominal current path, commutation path, and energy absorption path, as shown in Fig. 3.3. During the normal operation of the system, the CB is closed in the nominal current path, giving a low resistive path to the current to pass through. On the occurrence of a fault, contacts in the nominal current path are opened that produce an arc. The arc produced is quenched either by introducing an artificial resonance circuit for zero-crossing interruption of the fault current or by lengthening the arc and cooling.

3.5.2 Solid-state DC breaker

With the advancement in power electronics, various semiconductor power switches have been introduced that could be used as current commutation devices in solid-state DC CBs. These power electronics devices include insulated gate bipolar transistors (IGBTs), IGCTs,

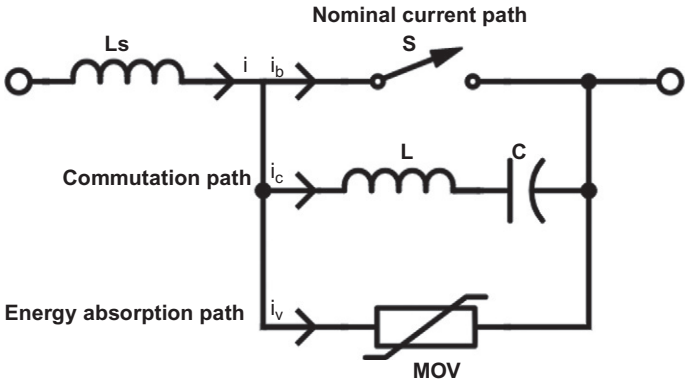

FIG. 3.3 Mechanical DC circuit breaker.

thyristors, and gate turn-offs (GTOs) that are suggested for the DCCB. However, IGBTs and IGCTs are preferred for solid-state DC CBs [1–3]. Fig. 3.4 shows the typical configuration of a bidirectional solid-state circuit breaker (SSCB) consisting of a nominal current branch that contains IGBT switches in parallel to the diode and an energy absorption path that contains a metal oxide varistor (MOV) [3]. Fig. 3.5 shows an IGCT-based SSCB. During normal operation, semiconductor switches are in conduction mode. During a fault, a series inductor limits the di/dt. A control circuit detects the fault and turns the semiconducting devices OFF, and the voltage across the switches is limited by the parallel energy absorption branch. As the IGBT and the diode have high on-state resistance, they are subject to high conduction losses [4].

Shen et al. [5] reviewed the state-of-the-art self-powered solid-state DC CBs. This novel concept of SSCB uses normally ON semiconductor static switches to interrupt the fault current. During a fault, the rising terminal voltage is detected and the switches are turned OFF, diverting the fault current to the energy absorption path.

Magnusson et al. [6] investigated the overvoltage transients across the semiconductor switch because of the speedily diminishing current through the stray inductance during the turn-off of the power electronics static switch. They proposed the separation of the energy

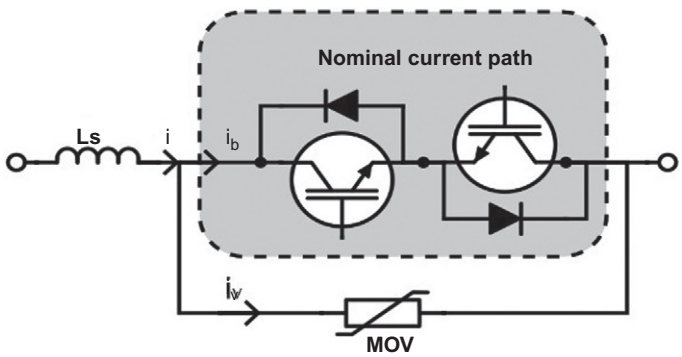

FIG. 3.4 IGBT-based solid-state DC circuit breaker.

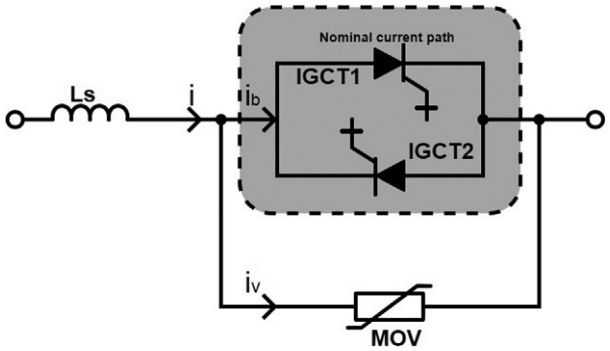

FIG. 3.5 IGCT-based solid-state DC circuit breaker.

absorption and the overvoltage protection by inserting a snubber consisting of an extra MOV_{ov} of high voltage ratings in parallel to the energy-absorbing branch (MOV_E) close to the power electronics switch (IGBT). As the MOV_{ov} is placed close to the switch, the lower value of the stray inductance will cause a higher voltage drop across the MOV_{ov}, which will commutate the current to the MOV_E. The proposed SSCB has been simulated in PSCAD and experimentally verified on a small-scale setup.

Shen et al. [7] proposed a self-powered wide band gap (WBG) semiconductor switch-based SSCB. Instead of sensing the current through the switch, it detects the fault by detecting the voltage rise across the drain and source of the switch. During normal conduction, it does not require any external power supply for the control circuit, and during the fault condition, it turns it off and holds using the fault current until the fault is cleared. Shen et al. implemented the proposed SSCB by using a SiC JFET of 1200 V rating to interrupt and switch off the fault current of 125 A in 1 μs without the need of any external power source.

Vemulapati et al. [8] improved the IGCT for DC SSCB by optimizing the on-state conduction losses and the turn-off current capability. During the normal operation, the proposed design of the IGCT has a blocking capability of 2.5 kV with 0.9 V voltage drop at 1 kA that amounts to almost less than 1 kW conduction losses. Under a fault condition, it has a current capacity of 6.8 kA at 1.6 kV.

Liu et al. [9] stated that the safety of the semiconductor switch against the overvoltage depends upon its snubber circuit. They proposed three types of snubbers consisting of a resistor, capacitor, and diode such as charge-discharge type, discharge suppressing type I, and discharge suppressing type II. Comparison of the various indicators like peak voltage and peak current of the proposed snubbers revealed that the discharge suppressing type I is the most applicable one.

3.5.3 Hybrid DC breaker

The generic structure of a hybrid DCCB is shown in Fig. 3.6, consisting of three parallel branches: a nominal current path consisting of a combination of commutating element and an isolating switch. A secondary branch contains semiconductor switches. On a fault in the circuit, semiconductor switches in the secondary branch are on and provide a bypass to the fault current. The third branch is the energy absorption branch consisting of a MOV.

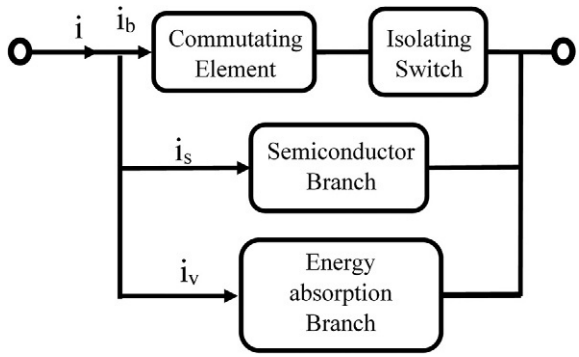

FIG. 3.6 Configuration of a hybrid DC circuit breaker.

Callavik et al. [10] developed a hybrid DC CB with ultrafast current interrupting capabilities and negligible conduction losses. The developed DC breaker, presented in Fig. 3.7, consists of two branches: the main breaker consisting of various IGBT switches with parallel surge arrestors and a bypass branch formed by a load commutation switch (LCS) in series with an ultra-fast mechanical disconnector (UFD). Under normal conditions, the main breaker remains off and the current passes through the bypass branch that reduces the conduction losses since no current passes through the IGBTs. In SSCB, normal current passes through the solid state switches which causes conduction losses. . Under a fault, the LCS switches off and the UFD opens, commutating the fault current to the main breaker. The presented structure of the bypass branch reduces the voltage ratings of the LCS. Callavik et al. demonstrated the proposed hybrid DCCB in ABB facilities and verified the expected results. A fault current of 9 kA was interrupted with less than 5 ms delay of the UFD. An interrupting capacity of 9 kA was limited by the existing semiconductor devices which would be increased to 16 kA in second-generation semiconductor devices.

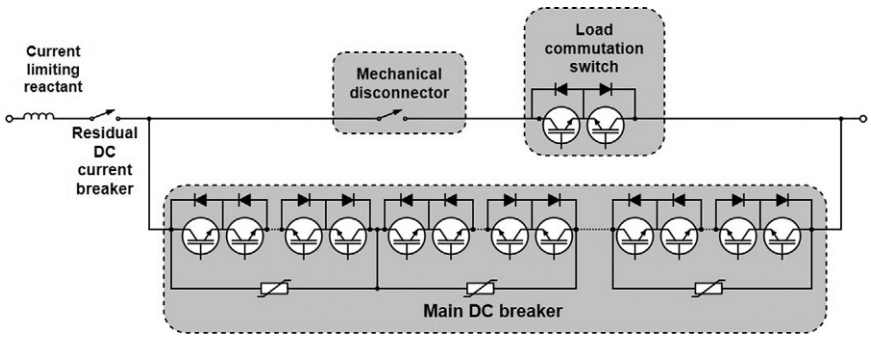

FIG. 3.7 Hybrid DC circuit breaker developed by ABB.

3.6 Substation bus bars

The electrical substation bus bar is the interconnection point of incoming and outgoing transmission lines, and transformers. They are generally placed at the substations where the incoming and outgoing conductors carry the same voltage. They are generally uninsulated, supported by the insulated pillars, and hard enough to withstand their own weight and environmental forces like air pressure and earthquakes.

3.6.1 Single bus bar

In a single bus bar configuration, all the inward and outward power lines are connected to the same bus bar, as depicted in Fig. 3.8. We can see that the incoming line of 11 kV is connected to the bus bar through the CB and the isolator, whereas the three-phase 400 V and single-phase 220 V lines are connected to the bus bar through the isolator, CB, and step-down transformer. The major drawback of this configuration is that the fault at any point

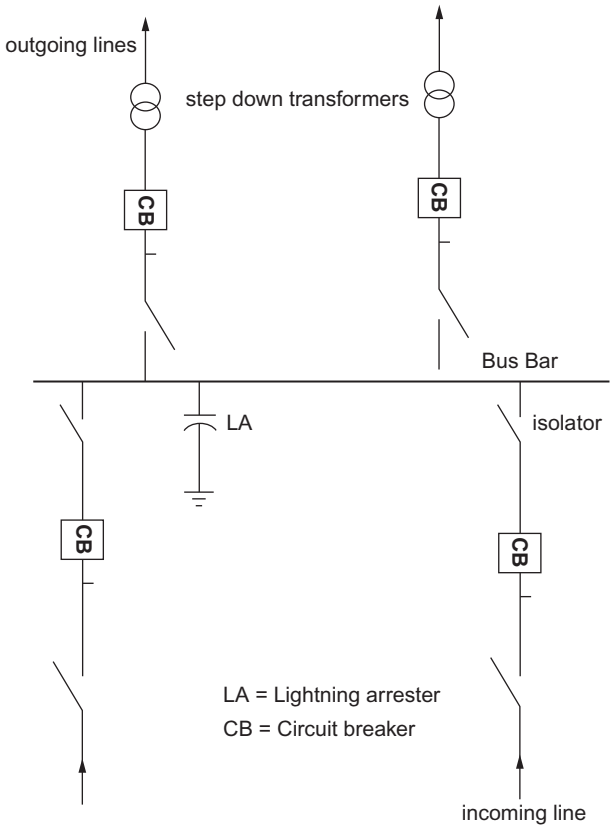

FIG. 3.8 Configuration of single bus bar.

of the bus leads to complete shutdown, and the substation cannot be expanded without complete power shutdown. This configuration is cost-effective as only one CB is required for the outgoing lines.

3.6.1.1 Advantages

- Small area is required.
- Cost-effective.
- Simple operation.
- Can easily be expanded.
- The failure of a single breaker in a line does not interrupt the whole system; only that feeder is interrupted.

3.6.1.2 Disadvantages

- Without interrupting the feeder, maintenance cannot be performed.
- Less reliable.

3.6.2 Sectionalized single bus bar

In this configuration, a single bus bar is sectionalized with the help of a CB. This bus bar can be operated in a way in case of emergency or for maintenance purposes, whereby when some of the feeders are disconnected from the bus, the rest of the feeders are kept feeding. The bus bar can be sectionalized into two or three dividing the bus bar into two or three sections, respectively. In cases where a section of the bus bar is de-energized, the feeders connected to this section of the bus bar may be connected to the other healthy section of the bus bar through a CB. Like the single bus bar configuration, it is cost-effective and simple in its operation. In the case of a fault, there is no blackout of the whole system; only the faulty section is shut down. The disadvantage of this type of configuration is that when there is a fault, or during maintenance, half of the bus bar is out of operation from the substation. In cases of maintenance of a CB in any feeder, that feeder is disconnected from the bus bar. The configuration is shown in Fig. 3.9.

3.6.2.1 Advantages

- More reliable than the single bus bar.
- More flexible operation than the single bus bar.
- For maintenance or failure of the circuit, the complete substation does not need to be shut down. Only half of the bus bar is de-energized through a breaker.

3.6.2.2 Disadvantages

- Relative to the single bus bar, sectionalized bus bar is expensive since an additional breaker is required for sectionalizing.
- For maintenance, half of the bus bar is de-energized.

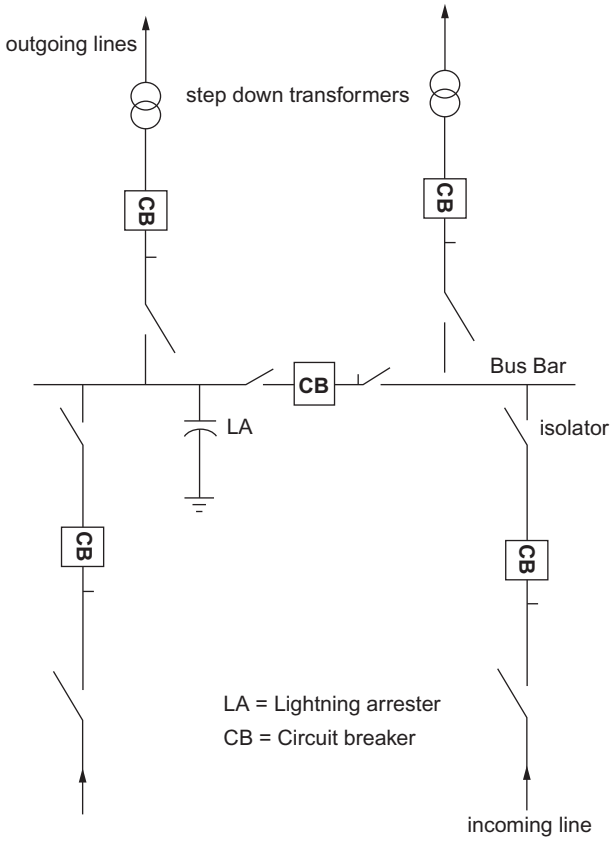

FIG. 3.9 Configuration of sectionalized single bus bar.

3.6.3 Single breaker double bus bar configuration

This type of configuration consists of two identical bus bars, bus-I and bus-II, named as the main bus and the main-cum-transfer bus bar. Both bus bars are connected with each other through a bus coupler breaker. The load can be connected to either of the bus bars, meaning that both bus bars have the capability of serving the entire substation load. Fig. 3.10 shows the configuration of a single breaker double bus bar. Under normal operation, the bus coupler breaker remains closed, and some of the feeders are connected to bus-I while others are connected to bus-II.

3.6.3.1 Advantages

- Two bus bars increase the operational flexibility.
- The circuit can easily be removed from the faulty bus bar and connected to the healthy bus bar through a bus coupler.
- Any of the buses can be interrupted for maintenance.

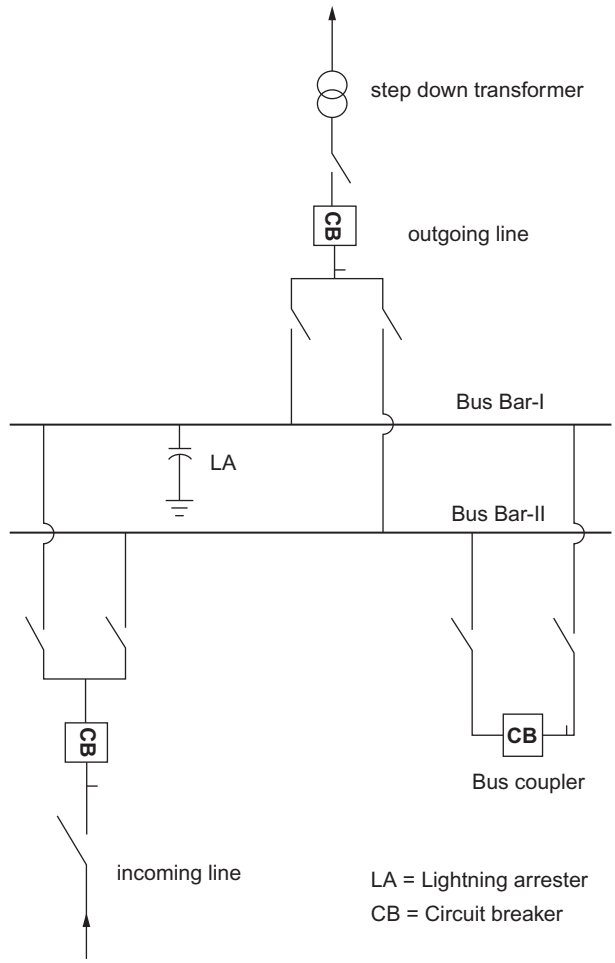

FIG. 3.10 Configuration of a single breaker double bus bar.

3.6.3.2 Disadvantages

- An extra CB is required for bus coupling
- Extra isolators are required for each bay.

3.6.4 Double breaker double bus bar configuration

A double breaker double bus bar configuration is shown in Fig. 3.11. It consists of two main buses, named bus bar-I and bus bar-II. Since this configuration is very expensive, it is used only for large generating stations with high security concerns. Since each circuit consists of two CBs, the feeder can be fed from any of the bus bars through the breaker. In case of maintenance of the CB or a fault occurring, the feeder is powered up through the other breaker connected to the other bus bar.

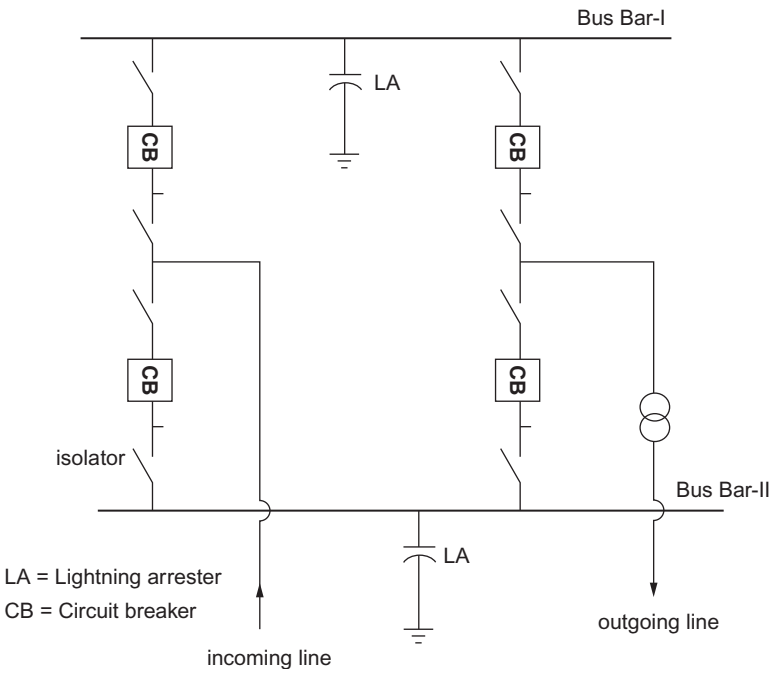

FIG. 3.11 Double breaker double bus bar configuration.

3.6.4.1 Advantages

- Each feeder is connected between two CBs, giving the flexibility of being fed from any of the bus bar.
- It is highly reliable because during maintenance any breaker can be taken out of the circuit, continuing the operation through other breaker and bus bar.
- No interruption to any feeder during a bus fault.
- Each feeder can be connected to any bus bar through the CB.

3.6.4.2 Disadvantages

- This configuration is very expensive.
- In the case of failure of both breakers, the feeder is shut down.
- Each circuit requires a double CB.

3.6.5 Main and transfer bus bar configuration

The configuration of a main and transfer bus is shown in Fig. 3.12. It consists of two bus bars named the main bus and the transfer bus. Both buses are connected with each other through a bus coupler breaker. Under normal operation, the main bus bar is energized and all the incoming and outgoing lines are connected to the main bus through the CBs and the isolators. While transferring the feeder from the main bus to the transfer bus during

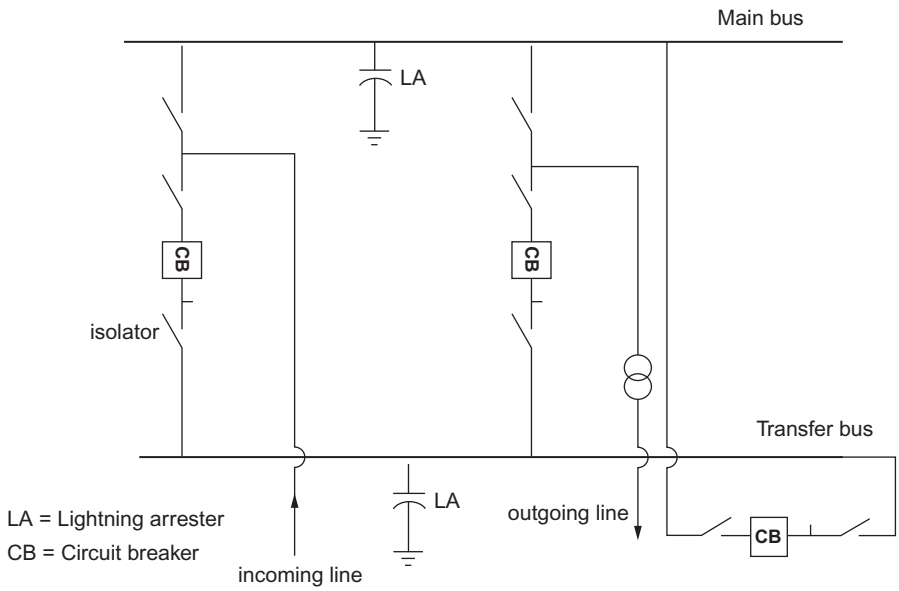

FIG. 3.12 Main and transfer bus bar configuration.

maintenance at the breaker, the isolator of the CB which is to be isolated is first closed, the bus coupler breaker and its isolators are closed to couple the main bus and the transfer bus, the CB and its isolators are opened, and the breaker is taken out of the circuit for maintenance. The feeder is then being fed from the transfer bus instead of the main bus.

3.6.5.1 Advantages

- In the case of faults on any bus or the breaker, the feeder can be entertained from the other bus.
- The transfer of the circuit from the main bus to the transfer function is easy.
- Less expensive.

3.6.5.2 Disadvantages

- An extra bus coupler breaker is required to transfer from the main bus to the transfer bus.
- Failure of a bus or a breaker causes the blackout of the substation.
- Switching of isolators while transferring from main bus to the transfer bus is complex.

3.6.6 Breaker and a half configuration

A breaker and a half bus bar configuration is shown in Fig. 3.13. This configuration also consists of two bus bars. Each bus bar is connected through three CBs and their associated isolators. The incoming and outgoing lines are connected between any two CBs. In this way, one CB is left spare. The name "breaker and a half" is derived from the fact that among three CBs, each line shares one CB and the half central CB. A fault on any of the bus bars does

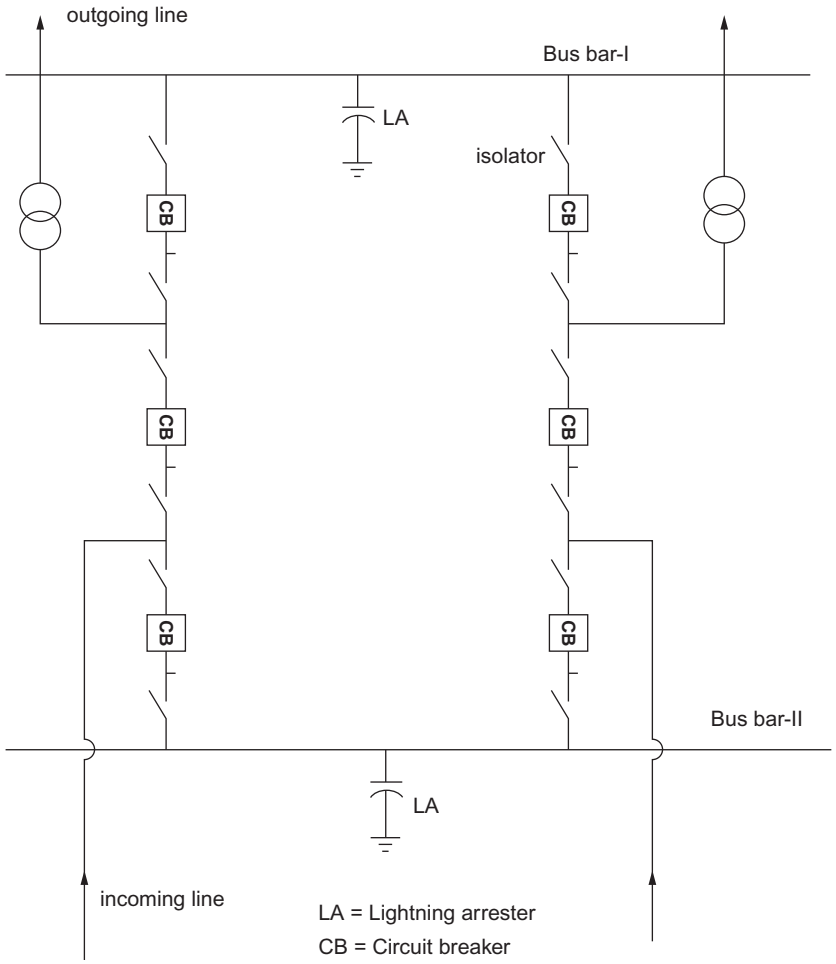

FIG. 3.13 Breaker and a half configuration.

not interrupt the circuit. However, the failure of the central breaker causes the failure of two circuits, and one circuit fails if the outer breaker fails.

3.6.6.1 Advantages

- This configuration is more cost-effective than the double breaker double bus bar configuration.
- Highly reliable.
- In the case of failure of one breaker, the feeder is connected to the other bus through the two remaining breakers.
- A fault on any bus bar does not interrupt the feeder operation.
- Maintenance of the breaker does not interrupt the feeder operation.

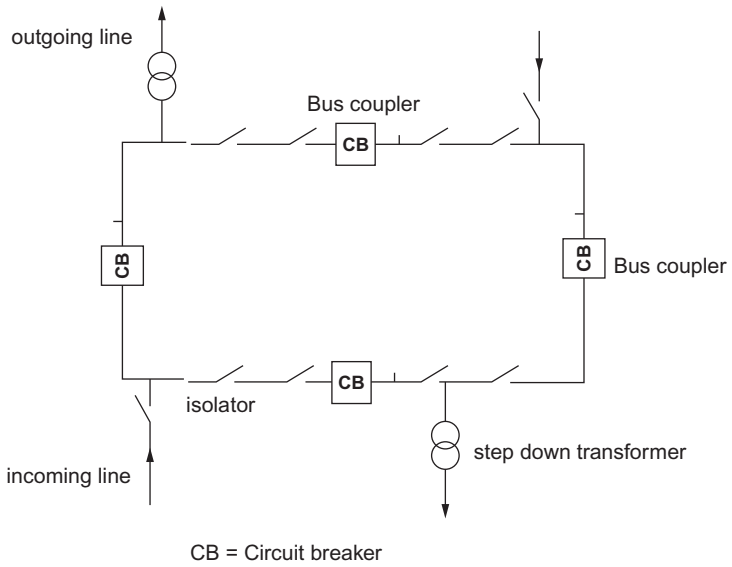

FIG. 3.14 Ring bus configuration.

3.6.6.2 Disadvantages

- Each circuit requires one and a half CB.
- A fault on either of the circuits needs to be responded to by the central CB.

3.6.7 Ring bus configuration

The ring bus configuration is obtained by the interconnection of the open ends of the same bus that makes a ring. This configuration is the extension of the sectionalized bus bar configuration. In a ring configuration, sections are made at multiple locations through bus coupler breakers. The incoming and outgoing lines can be connected in any of the sections. The supply of only one circuit in a section increases reliability and flexibility. A ring bus configuration is shown in Fig. 3.14.

3.6.7.1 Advantages

- Cost-effective.
- Reliable.
- Flexible.
- Each circuit is fed by a double line.
- Only one breaker to each section is required.
- No concept of a main bus.

3.6.7.2 Disadvantages

- Relaying of each circuit requires its own potential source.
- A fault in two circuits makes the relaying complex.

3.7 Lightning arresters

LAs are protective equipment used to protect the transmission line from lightning strikes and traveling waves. LAs divert the surge toward the ground. These protective devices are mounted on the poles, transmission lines, or even on the building, providing a secure path to the surge currents. An LA consists of two terminals. A high voltage terminal picks the lightning surge from the transmission line, the insulation between the LA and the earth breaks, and the surge current is directed to the earth. Different types of LA are as follows; they are the same in working principle but different in construction:

(i) horn gap arresters
(ii) multigap arresters
(iii) valve type arresters
(iv) pellet type arresters.

3.7.1 Advantages

- Equipment in a substation and in its premises can be protected.
- Transmission line are protected against lightning damage.
- Protection against electromagnetic interference.
- Easy operation.
- Protection of buildings against lightning.

3.7.2 Disadvantages

- Occupies more space.
- Expensive installation.

3.8 Power factor

The quality of the power generated, transmitted, and distributed to consumers depends upon the load power factor and the transmission line parameters. In a power system, all the loads are inductive in which current lags the voltage that deteriorate the power factor. A power factor close to unity or 1 is preferred in which current and the voltage are in phase.

Power factor is defined as the cos of the angle between active and apparent power, as shown in Eq. (3.1). Fig. 3.15 shows the power triangle which defines the active power, reactive power, apparent power, and power factor.

$$Power\ factor = \cos\theta = \frac{P}{S} = \frac{Active\ power}{Apparent\ power} \tag{3.1}$$

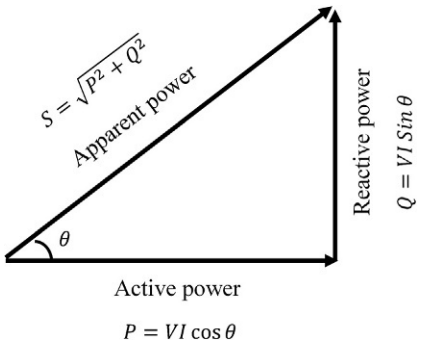

FIG. 3.15 Power triangle.

3.8.1 Causes of low power factor

- Most of the motors in the industry are single-phase and three-phase induction motors. In induction motors current lags behind the voltage, making the motor a lagging load. When the load on the motor is small, its power factor reduces to 0.2–0.3 and it increases to 0.8–0.9 at full load.
- Transformers are a lagging load since they draw the magnetizing current. Hence, transformers cause the power factor to be low.
- The load in the industry is not constant. It varies over time, which causes the low power factor. This is because the supply voltage is increased at low loads and the motor draws more magnetizing current.
- The heating furnace in the industry is the inductive load that operates at low lagging power factor.

3.8.2 Disadvantages of low power factor

For a three-phase supply, load current is given by Eq. (3.2).

$$I_L = \frac{P}{\sqrt{3}V_L \cos\theta} \tag{3.2}$$

This relation clearly indicates that the power factor and the load current are inversely proportional to each other. Based on this concept, the following are disadvantages of low power factor.

- **Effect on the transmission conductors**: In a transmission line, to transmit a fixed power at constant voltage, at low power factor, a large amount of current will flow that will require a conductor of a large cross-sectional area. The increased cross-sectional area will increase the conductor volume for the same length of the transmission line. This will increase the capital cost for the transmission line.
- **Large kVA rating of the equipment**: On rearranging the power equation, we have the following relation shown in Eq. (3.3) giving the kVA ratings.

$$VI = \frac{P}{\cos\theta}$$

$$kVA = \frac{kW}{\cos\theta} \tag{3.3}$$

This equation shows the kVA rating of the equipment which is inversely proportional to the power factor. If the power factor is low, we will need the equipment of large kVA ratings, which will increase the cost of the equipment.

- **Copper losses**: Another disadvantage of the low power factor is the copper losses. If the power factor is low, the increased current will increase the copper losses (I^2R) in the transformer, transmission line, and load.
- **Poor voltage regulation**: If the power factor is low, large line current is drawn, which causes a voltage drop in the generator, transformer, and transmission line. To compensate the voltage regulation, extra cost is incurred on the voltage regulators.

3.8.3 Power factor improvement

The basic cause of poor power factor is the presence of the inductive load, which draws lagging current from the source. To improve the power factor, a device should be connected in parallel that provides the leading current. One such device is the capacitor, which is a leading load since in a capacitor, current leads the voltage. The methods used to improve the power factor are:

(i) static capacitors
(ii) synchronous condensers
(iii) phase advancers.

3.8.3.1 Static capacitors

Power factor is improved by connecting capacitors in parallel to the main at the load end. Capacitors draw leading current, which neutralizes the lagging current and takes the power factor toward unity. The arrangements of capacitors in star and delta format to the three phase are shown in Fig. 3.16.

Advantages

- Losses are less.
- Since they do not have any rotating parts, no maintenance is required.
- Not vulnerable to the atmospheric changes.
- Easy installation, no extra arrangement is required to install.

Disadvantages

- Limited service life of 8–10 years.
- Does not contain any over voltage protection.
- If the capacitor is damaged, it is expensive to replace.
- Complex switching while adding or removing the capacitor from the capacitor bank.

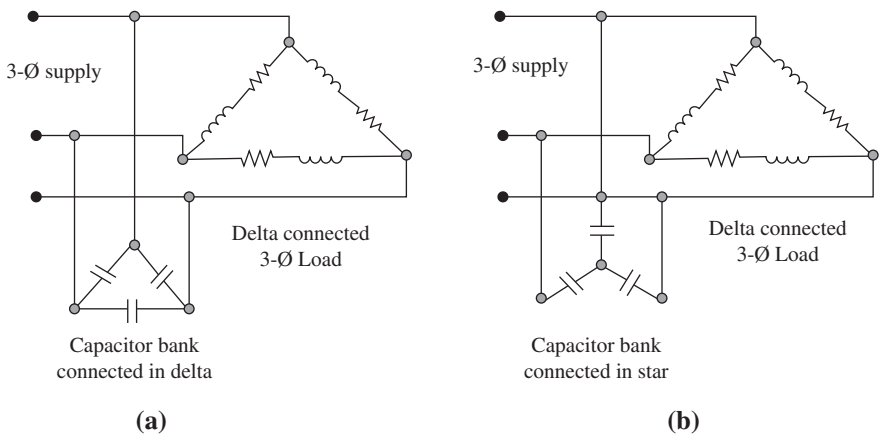

FIG. 3.16 Power factor improvement: (A) static capacitors in delta format and (B) static capacitors in star format.

3.8.3.2 Synchronous condensers

When a synchronous motor is overexcited at no load, it behaves like a capacitor because it starts taking leading current at no load. Hence a synchronous motor when overexcited at no load is termed as a synchronous condenser. To improve the power factor, a synchronous condenser is connected in parallel to the load. It provides leading current that partially neutralizes the reactive power and improves the power factor. Fig. 3.17 provides a diagram of a synchronous condenser.

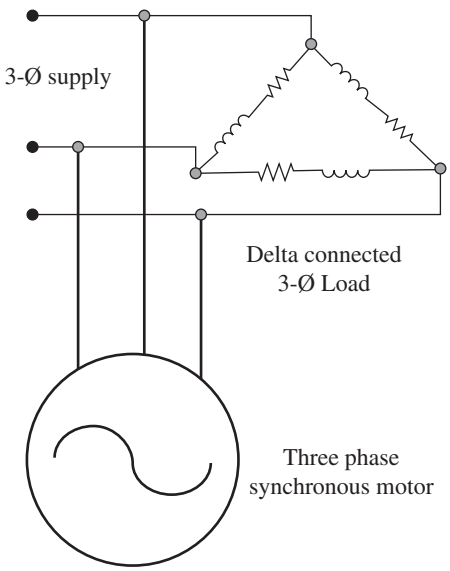

FIG. 3.17 Power factor improvement by synchronous condenser.

Advantages

- Easy to control the power factor because the current drawn by the synchronous condenser can be changed by changing the field excitation.
- It can absorb and supply reactive power that controls the power factor smoothly.
- The synchronous condenser improves the system stability since the effect of sudden variation in the load is compensated by the high inertia of the synchronous condenser.

Disadvantages

- The losses in the motor are increased.
- Since it contains moving parts, it causes noise, and the wear and tear requires regular maintenance.
- For low ratings, its cost is increased as compared to the static capacitors.
- Like static capacitors, its rating cannot be altered by adding and removing the units in the system already installed.
- Extra equipment is required for providing self-starting torque.

3.8.3.3 Phase advancers

An induction motor lowers the power factor because its stator behaves as an inductive load in which the current lags behind the voltage. The impact factor can be improved by providing excitation to the stator from an external AC source which is mounted on the same shaft. Hence, a phase advancer is simply an AC exciter mounted on the rotor shaft.

3.9 Transmission line

3.9.1 Conductors

The electric current from the power station to the consumer is carried through the conductor. The conductors being used for the transmission must have the following characteristics.

- The material must have high conductivity and minimum resistance.
- The tensile strength of the material must be high to resist the mechanical stresses.
- The material must have the ability to resist the corrosion in all meteorological conditions.
- The material must be lightweight and have low specific gravity to bear its own weight.
- The coefficient of thermal expansion and thermal stability should be high to avoid deformation in all unfavorable conditions.

3.9.1.1 Types of conductor materials

Previously, copper was used for overhead transmission lines. Aluminum, because of its light weight and lower cost for the same resistance, has now replaced copper. Other materials such as cadmium, galvanized steel, bronze, and phosphor are also used for transmission lines. The following are some materials that are used as materials for transmission line conductors.

Copper

- Highly conductive, because it has very low resistance to the flow of current.
- High current density, allows more current to flow from small cross-sectional area.
- Robust and has high scrap value.
- High cost and rare availability.
- Higher tensile strength than that of the aluminum.

Aluminum

- Conductivity of aluminum is 60% of copper.
- For same resistance, aluminum conductor has 1.26 times diameter that of a copper conductor.
- Aluminum conductor has lower tensile strength than that of copper.
- Almost half the weight of a copper conductor.
- Preferred for overhead transmission lines to copper based on cost, weight, strength, and conductivity.

Cadmium copper

- Cadmium copper is an alloy of 98%–99% copper and 1%–2% cadmium.
- The addition of 1% impurity of cadmium increases the tensile strength of copper by 50% and reduces the conductivity by 15%.
- Because of high cost of cadmium, cadmium copper may be uneconomic for transmission lines.

Aluminum conductor steel reinforced (ACSR)

- ACSR conductors are made by surrounding a central galvanized steel core with a stranded aluminum conductor, as shown in Fig. 3.18.

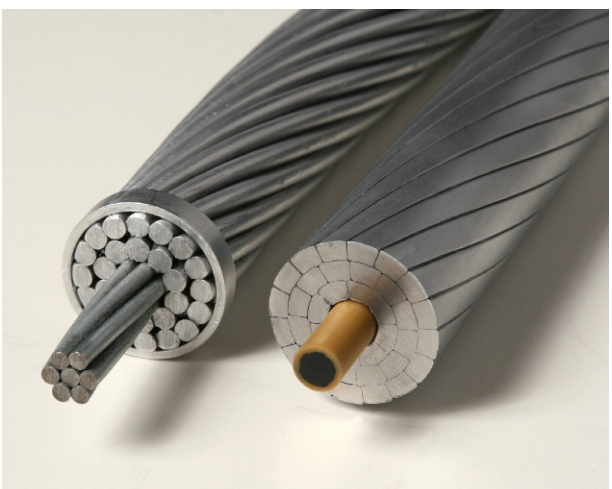

FIG. 3.18 Aluminum conductor steel reinforced and stranded conductors. *Source: Wikipedia.*

- Steel stranded conductors have increased tensile strength.
- The use of ACSR decreases the sag, increases the span, and also reduces the tower height. The overall cost of the transmission line is reduced.
- ACSR is preferred for high voltage and long transmission lines.

3.9.1.2 Types of conductors

The construction and shape of the conductors can be divided into four types:

(i) solid conductors
(ii) stranded conductors
(iii) hollow conductors
(iv) bundled conductors.

Solid conductors

A solid conductor is also termed a single strand wire of a single metal wire. Solid conductors are difficult to handle because of their limited flexibility. In transmission lines where a long span is required, single wire-based solid conductors are not used. Instead, multiple wires in a stranded form are used for transmission lines.

Stranded conductors

Stranded conductors are composed of multiple single metal conductors wrapped or stranded to give increased tensile strength. Multiple solid conductors are wrapped around a core conductor in opposite directions, as shown in Fig. 3.18. When comparing a stranded conductor to a single solid conductor of the same cross-sectional area, the stranded conductor is highly flexible, ensuring a significant span in the transmission line.

At higher frequencies, the current concentrates on the outer surface of the conductor and the central layers are depleted of electrons. This effect is called skin effect. Stranded conductors show less skin effect than solid conductors since the total surface area of the strands is greater than the surface area of the equivalent solid conductor.

Hollow conductors

A hollow conductor is a type of the conductor in which the conductors are stranded on the surface and the central part is a hollow one. This is to increase the diameter of the conductor. Corona effect and the skin effect are reduced in the hollow conductor compared to stranded and solid conductors. The inside, being hollow, does not contain any charge and has no electrostatic forces. Compared to solid conductors, hollow conductors have less internal inductance and a low voltage gradient. With a large diameter, the area exposed to the air pressure is increased and the amount of ice accumulating over the surface of the conductor is also increased. Hence, the weight of the transmission line is increased. Fig. 3.19 shows a hollow conductor with a central hollow part, and stranded conductors form the surface of the conductor.

Bundled conductors

For long transmission lines, high voltages are employed. At higher voltages, the electrostatic stress on the atmospheric neutral molecules and the ions becomes significant, generating the phenomenon of corona effect. This effect for such high voltage and long transmission

FIG. 3.19 Hollow conductor. *Source: Wikipedia.*

lines causes significant power loss and creates interference with other communication equipment. In a bundle conductor, two or more conductors are placed at specific distances forming a single phase. This is done for each phase. The space between the conductors also behaves as a conductor. The corona effect is reduced in the bundled conductors since the voltage gradient and hence the electrostatic stress is reduced. However, in extra high voltage transmission lines, potential gradient becomes significant to create the corona effect. Fig. 3.20 shows a transmission line consisting of four conductors in a phase forming a bundled conductor. Some key advantages of the bundled conductors are as follows:

- Skin effect and corona effect are reduced in bundled conductor.
- Reactance of the transmission line is reduced.
- Ability to cool themselves is high since a large area is exposed to air.
- Bundled conductor lines have high capacitance with respect to neutral and high charging current that improves the power factor.

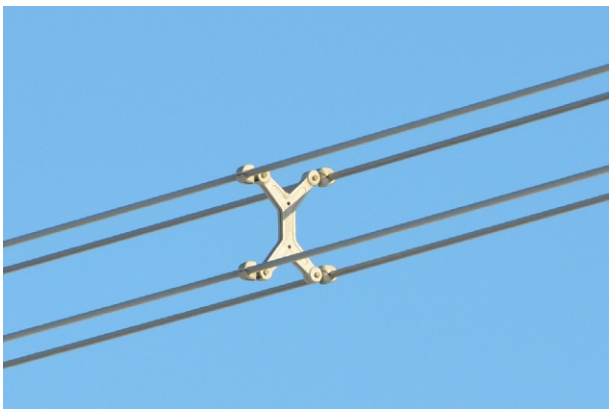

FIG. 3.20 Bundled conductor. *Source: Wikipedia.*

3.9.2 Insulators

In transmission and distribution lines, the overhead conductors are supported on the poles with the help of insulators avoiding a connection between the conductor and the ground. Depending upon the voltage level, insulators are classified into four types:

(i) pin type
(ii) suspension type
(iii) strain
(iv) shackle.

The insulators must carry the following properties for being used as the insulator in the transmission and distribution lines.

- The insulator must have high electrical resistance so that there is no chance of connection between the conductor and the earth or the pole.
- The insulator must have the ability to carry the weight of the conductors and the wind stress.
- The dielectric strength of the insulator must be high so the insulating material must have a high relative permittivity.

3.9.2.1 Pin type insulator

PA pin type insulator consisting of a single piece is used for 25 kV. For higher voltages, multiple pieces of pin type insulators are used. However, with the increase in number of pieces, the weight of the insulator becomes significant in the sense that the bending moment on the pin mounted on the cross arm is increased, which may damage the insulator and the conductor mounted on it. For this reason, pin type insulators with multiple rings are allowed up to 33 kV. Beyond this they become expensive compared to suspension insulators. The pin type insulator is pinned on the cross arm of the pole with the help of nuts and bolts. The top of the insulator contains a groove where the conductor is placed and tied there with the same material of the conductor. The pin type insulator is a suspensionless insulator.

To ensure the successful operation of the insulators, they must endure mechanical and electrical stress. The failure of an insulator due to electrical stress may be because of high voltage, which may collapse the insulator. Flashover occurs between the conductor and the insulator pin through the air gap consisting of ions. The current completes its path through the air, which produces an arc. Another reason for the collapse of an insulator is a puncture. This happens when a path of current occurs from the conductor to the insulator pin through the upper skin of the insulator. This produces excessive heat, which permanently damages the insulator. When the insulator becomes wet, its upper surface starts conducting. To avoid a puncture, the insulator is made in an umbrella shape. This protects the pin of the insulator from rainwater. Fig. 3.21 shows the installation of a pin type insulator on the cross arm of the pole.

3.9.2.2 Suspension type insulator

Pin type insulators are recommended for transmission lines up to 33 kV; beyond this, suspension type insulators are used. Suspension type insulators consist of multiple discs of

FIG. 3.21 Pin type insulator. *Source: Wikipedia.*

porcelain connected in series to each other with the help of metal links. A string is secured to the cross arm of the transmission tower. The conductor is suspended at the bottom of the suspension insulator. By counting the number of strings in the suspension string, the voltage of the transmission line can be measured as one disc is used for a minimum voltage level of 11 kV—e.g., for a transmission line of 66 kV, six discs will be connected in series to make a suspension insulator string. A suspension type insulator in a transmission line is shown in Fig. 3.22.

The voltage across the suspension insulator is not evenly distributed. Maximum voltage is dropped across the uppermost disc, which is close to the conductor. This happens because of the concept of mutual capacitance. Since the insulator disc is connected to the other disc

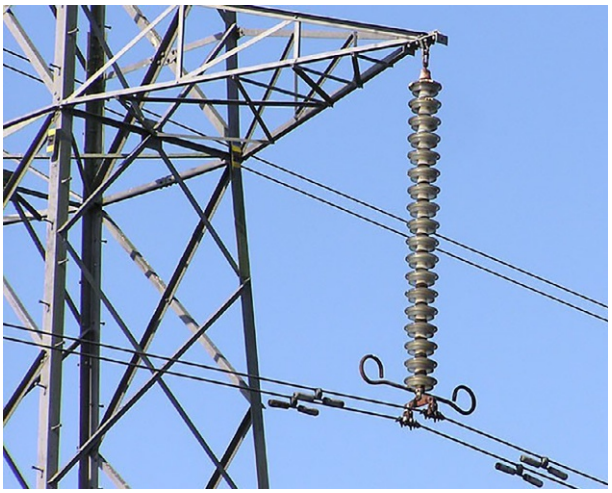

FIG. 3.22 Suspension insulator. *Source: Wikipedia.*

through the metal contact and a porcelain insulator is placed between them acting as a dielectric, forming the concept of mutual capacitance. The efficiency of the string is calculated by Eq. (3.4).

$$\eta_{string} = \frac{voltage\ across\ the\ sring}{total\ number\ of\ discs \times no.of\ discs\ in\ the\ string} \tag{3.4}$$

Advantages

- Depending upon the transmission voltage, the required number of discs in the insulator can be connected in series. One disc is required for an 11 kV transmission line.
- For transmission voltages greater than 33 kV, suspension type insulators are cheaper than the pin type insulators.
- In case of any fault, the whole insulator need not to be replaced. Instead, only the damaged discs should be replaced.
- A suspension insulator, as its name suggests, has the capability to bear environmental stresses and can swing in the air, bearing the air stress.
- In case of increased demand of the transmission voltage, the whole insulator is not replaced; instead the required numbers of discs are added to the string already installed.

3.9.2.3 Strain insulator

The transmission line faces high stress when it reaches a dead end, or passes through a corner or a curved path. At a dead end or a corner, the transmission line is disconnected electrically but connected to the other side of the corner mechanically; the electrical connection is made by another small conductor as shown in Fig. 3.23. The term "dead end" is used for the ending or starting of the transmission line. At both ends, strain insulators are used at the cross arms. If the tension is high, two or more strain insulators can be connected in parallel to distribute the tension evenly in the line. Fig. 3.23 shows the use of a strain insulator at the curved path.

FIG. 3.23 Strain insulator. *Source: Wikipedia.*

FIG. 3.24 Shackle type insulator. *Source: Wikipedia.*

3.9.2.4 *Shackle type insulator*

Previously, shackle insulators were used as the strain insulators. Now they are used as the strain insulator for low voltage applications in the distribution networks. They can be mounted directly on the cross arm or the pole using nuts and bolts. They can be placed horizontally and vertically. The conductor is fastened to the insulator with a soft metal conductor. A shackle type insulator is shown in Fig. 3.24.

3.9.3 Resistance

Resistance is defined as hindrance to the flow of electrons. This is not a constant parameter since the temperature affects the resistance of a material. When the temperature is increased, the vibratory motion of the atoms is also increased. The increased vibratory motion presents an obstacle to the flow of electrons, increasing the resistance. The resistance of a conductor can be calculated by the formulas given in Eqs. (3.5)–(3.7). The unit for resistance is ohms, represented by Ω.

$$R = \frac{V}{I} \tag{3.5}$$

$$R = \frac{P}{I^2} \tag{3.6}$$

$$R = \frac{V^2}{P} \tag{3.7}$$

The resistance of the conductor of specific length (L), material, and cross-sectional area (A) is calculated by Eq. (3.8).

$$R = \frac{\rho L}{A} \tag{3.8}$$

where ρ is the resistivity and it is different for different materials.

In a DC conductor, DC uses the whole cross-sectional area of the conductor to flow, but this is not true for AC, which is not uniformly distributed across the cross-sectional area

of the conductor. This is due to skin effect, proximity effect, and spirality effect. These effects become significant only at higher frequencies.

3.9.3.1 Skin effect

The inclination of the alternating current to concentrate and flow along the surface of the conductor is termed the skin effect. The consequences of this effect are that the effective useful area of the conductor is reduced and more conductors are required to carry the maximum current. The skin effect of the conductor depends upon the nature of the material of the conductor, the cross-sectional area of the conductor, the frequency of the supply, the resistivity and permeability of the conductor material, and the distance between two conductors.

3.9.3.2 Proximity effect

The proximity effect is observed when the current carrying conductor is within the effect of flux of another current carrying conductor. When a current carrying conductor is within the vicinity of another conductor, its resistance is effectively increased because of the effect of flux from the other conductor. The proximity effect also depends upon the nature of the material of the conductor, the cross-sectional area of the conductor, the frequency of the supply, the resistivity and permeability of the conductor material, and the distance between two conductors.

3.9.3.3 Spirality effect

The spirality effect increases not only the resistance but also the internal reactance of the conductor. The effect is different for hollow, solid, and stranded conductors. In transmission lines, mostly ACSR is used in which conductors are spiraled in opposition direction to hold the strands together. This increases the effect of the inductor and causes additional internal reactance of the conductor.

3.9.4 Corona

The ionization of the air around the conductor is termed corona. The formation of corona can be easily understood by applying a low voltage across two conductors placed at a distance larger than their diameter; no variation in the surrounding atmosphere is noticed. When the applied voltage is increased and it reaches a critical disruptive voltage, a hissing sound is produced and in a dark environment, an indistinct violet spark is seen across the conductor, as shown in Fig. 3.25. This phenomenon is called corona.

3.9.4.1 Formation of corona effect

Because of the presence of ultraviolet radiation in the atmosphere, the air around the conductors is ionized, i.e., neutral molecules, positive ions, and free electrons are present under normal conditions. When a potential difference is applied between two conductors, a potential gradient is set up and provides velocity to the free electrons in the atmosphere around the conductor. At a potential gradient of 30 kV/cm, the potential gradient is enough to strike the neutral molecule and remove electrons from it. The process of removing electrons from the neutral molecule continues until a spark is produced with a hissing sound, and the production of ozone makes the concept of corona.

FIG. 3.25 Corona effect. *Source: Wikipedia.*

3.9.4.2 Causes of corona effect

- **Spacing between conductors**: If the space between the conductors is much larger than their diameters, the corona effect may not be seen. This is because conductors further apart will have no electrostatic stress for free electrons around the conductors and corona will not be formed.
- **Size of the conductor**: The formation of corona effect also depends upon the shape and structure of the conductor. If the surface of the conductor is smooth and regular, the corona effect will not be visible since the chances of electric breakdown of the conductor are reduced. The corona effect in stranded conductors is greater than in solid conductors because the structure of stranded conductors is irregular.
- **Atmosphere**: Corona occurs due to the ionization of atmospheric neutral molecules around a conductor. In stormy and foggy weather, the number of ions in the atmosphere is greater than in other weather.
- **Line voltage**: As discussed earlier, at low potential difference, the low potential gradient is not enough to create the electrostatic stress on the surface of the conductor. At a higher line voltage, the electrostatic stress causes the air to conduct around the conductor.

3.9.4.3 Advantages of the corona effect

- Corona effectively increases the diameter of the conductor, and the effective capacitance of the conductors, which reduces the surge current transients.
- The presence of the ions around the conductor increases the virtual diameter of the conductor, which diminishes the electrostatic forces between the conductors.

3.9.4.4 Disadvantages of the corona effect

- Corona causes energy losses, leading to inefficient transmission of electricity.
- The production of ozone by corona effect may cause corrosion on the surface of a conductor.

3.9.4.5 *Reduction of the corona effect*

The corona effect is observed beyond 33 kV transmission line. If the design of the substations is not carefully planned, serious impacts from the corona effect may be faced. To avoid the corona effect, the following parameters must be selected carefully.

- **Size of the conductors**: Corona effects may be reduced by increasing the size of the conductor. By increasing the size, electric breakdown occurs at a relatively high voltage.
- **Distance between the conductors**: If the distance between the conductors is increased, the electrostatic forces between the conductor and the ionized atmosphere around the conductor are not enough to create the hissing sound, showing a glow and producing ozone gas. Hence the corona effect may be avoided.
- **Hollow conductors**: In hollow conductors, the effective cross-sectional area and the diameter are larger than in a normal solid conductor. From Eq. (3.9), we can estimate that the corona effect is inversely proportional to the conductor's diameter. In hollow conductors, the increased diameter reduces the corona effect.

$$power\ losses \propto \sqrt{\frac{r}{D}} \tag{3.9}$$

- **Bundled conductor**: In bundled conductors, two or more conductors are placed at a distance for each phase to avoid the skin effect losses. In bundled conductors, the diameter of the conductor is increased, which reduces the corona effect.

3.9.5 Ferranti effect

The Ferranti effect is the phenomenon of a transmission line at light load or no load in which the load at the receiving end is more than the sending voltage. This phenomenon was first observed by the engineer Ziani de Ferranti in 1887. He concluded that this effect is due to the interaction of the capacitance and inductance of the transmission line. Capacitance and inductance are the two main parameters of a transmission line of 240 km or longer. On such a transmission line, capacitance is not concentrated at definite points; instead it is uniformly distributed over than transmission line. When the sending voltage is applied at no load or light load, the capacitance draws more current than the current associated to the load. This charging current through the capacitance of the line causes a voltage drop across the inductance of the line which is in phase to the sending voltages. This voltage drop increases from the sending end to the receiving end. Hence, the receiving end voltage is higher than the constant sending end voltage.

The Ferranti effect can be reduced by connecting a shunt compensation device at the receiving end. A shunt compensation device is a shunt reactor connected in parallel to the transmission line which absorbs the reactive power at the receiving end.

3.10 Transmission line faults

3.10.1 Open circuit faults

Open circuit faults occur because of the failure of one of the conductors. This may be because of the failure of an overhead line, the melting of a fuse in one or more lines, or the failure of a breaker in one or more lines. These faults are categorized as follows:

- single-phase open conductor;
- two-phase open conductor; and
- three-phase open conductor.

Fig. 3.26 illustrates each type of open circuit faults. These faults are also called series faults.

Before the occurrence of the fault, a transmission line is working with a balanced load. In cases where an open circuit fault occurs on a single line, actual loading on the alternator is reduced and the acceleration is increased, which increases the speed of the alternator to be slightly greater than the synchronous speed. This higher speed generates higher voltages in the transmission line. Thus, single-phase and two-phase open conductors cause the system to be unbalanced, which causes serious damage to equipment.

3.10.2 Short circuit faults

Short circuit faults are the most severe faults in the transmission line and account for 5% of the total faults in the transmission line. The causes of the short circuit faults are as follows.

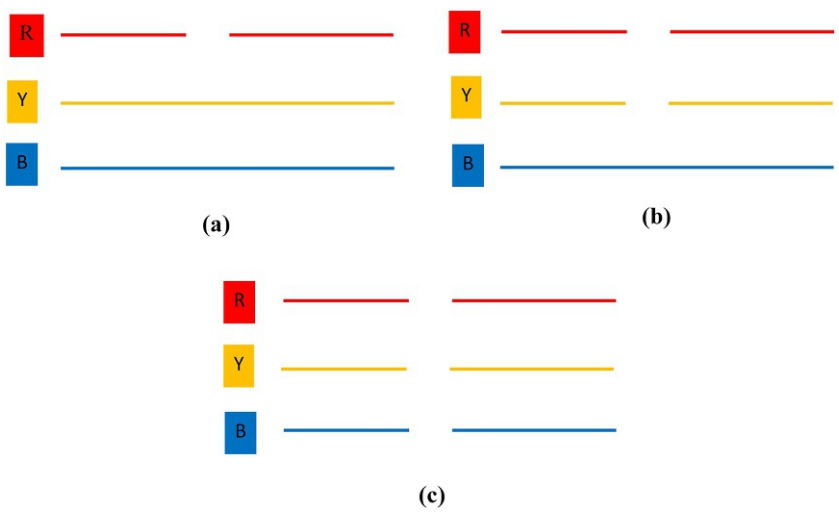

FIG. 3.26 (A) Single-phase open conductor, (B) two-phase open conductor, and (C) three-phase open conductor.

3.10.2.1 *Symmetrical faults*

(a) Line-line-line fault (L-L-L)

In three-phase line faults, all the phases are short and the fault is called symmetrical but such faults are severe. The L-L-L fault is shown in Fig. 3.27A. Zero sequence, positive sequence, and negative sequence currents are equal. The fault current determines the breaking capacity of the breaker before which the breaker must operate without damaging itself.

(b) Line-line-line-ground fault (L-L-L-G)

The L-L-L-G fault occurs between the three phases and the ground. All the phases and the ground are involved in an L-L-L-G fault, as shown in Fig. 3.27B.

3.10.2.2 *Unsymmetrical faults*

Unsymmetrical faults give rise to unsymmetrical currents and phases in the transmission lines. These are faults that include one or two phases. The types of the unsymmetrical faults are as follows.

(a) Single line-to-ground fault (L-G)

This type of fault occurs when a conductor falls on the ground or the neutral conductor. Of the faults in a power system, 70%–80% are L-G faults. The fault can be detected by the presence of the zero sequence. Only zero sequence is presence in L-G fault. L-G fault is shown in Fig. 3.28A.

(b) Line-to-line fault (L-L)

When two conductors are short circuited, a line-line (L-L) fault occurs. This fault is mostly caused by heavy winds. The winds swing the line conductors, which may touch each other and cause a short circuit. This type of fault accounts for approximately 15%–20% of faults. Fig. 3.28B shows the L-L fault. This type of fault is detected by the absence of the zero sequence component.

(c) Double line-to-ground fault (L-L-G)

In double line-to-ground faults, two of the conductors touch each other along with the ground. These faults occur in 10% of faults in a power system. This type of fault is detected

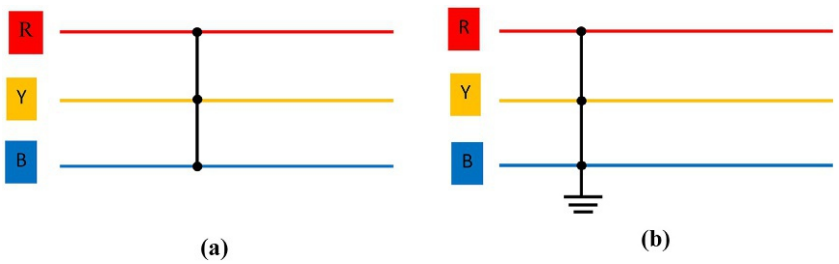

FIG. 3.27 Symmetrical faults in transmission line: (A) line-line-line fault (L-L-L) and (B) line-line-line-ground fault (L-L-L-G).

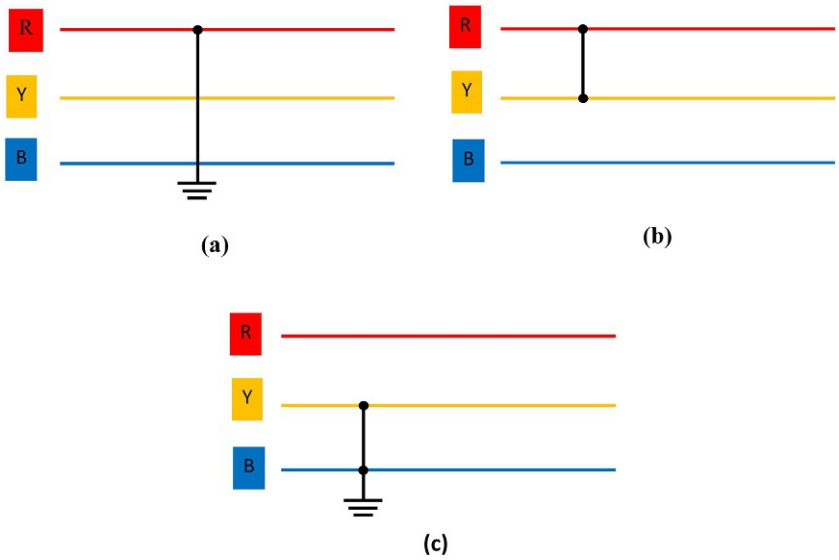

FIG. 3.28 (A) Single line-to-ground fault, (B) line-to-line fault, and (C) double line-to-ground fault.

by Eq. (3.10), which shows that the sum of the zero sequence current and negative sequence current is equal to the positive sequence current. Fig. 3.28C shows the L-L-G fault.

$$I_1 = I_0 + I_2 \tag{3.10}$$

3.11 Distribution system

The part of the electrical power system that distributes electric power to local users is called the distribution system. It is an electrical power system between the substation and the end users. The substation is fed by the power transmission line. A distribution system is generally comprised of feeders, distributors, and service mains. Fig. 3.29 shows a distribution system consisting of substation, feeder, distributor, and service main.

(a) A **feeder** is a conductor that connects the substation to the power distribution area. It operates at primary distribution voltages and distribute power through the main service area. A feeder is designed for the current carrying capacity and no tapping is made in the feeder to keep the current constant. The design consideration of a feeder is its current carrying capacity.

(b) A **distributor** is a conductor from the feeder to the service main from where the tapping occurs to supply the consumers. Distributors are indicated by "A" and "B" in Fig. 3.29. The current is not same throughout the distributors since tapping occurs. The main design consideration is the voltage drop along the length. The design consideration of the distributor is the voltage drop.

(c) A **service main** is a small cable connecting the distributor to the consumer's terminal.

Distribution systems are classified on the basis of nature of current, type of construction and the scheme of connection. Based on the nature of the current, it is classified as the AC

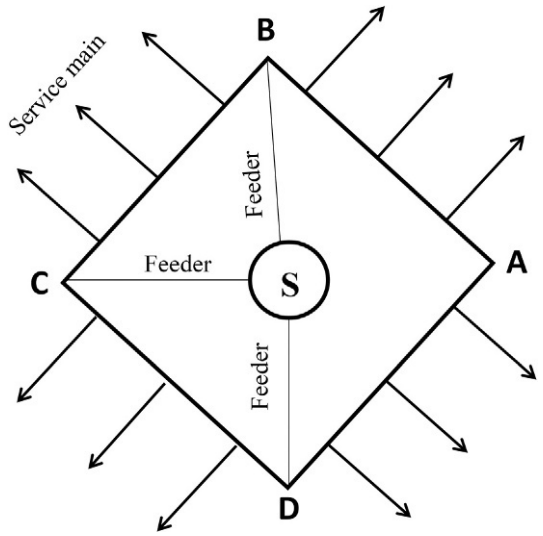

FIG. 3.29 Power distribution system from a substation to a service main.

distribution system and DC distribution system. Based on the construction of the distribution system, it is classified as an overhead distribution system and underground distribution system. Based on connection schemes, the distribution system is classified as a radial system, ring main system, and interconnected system.

3.11.1 AC distribution systems

In 1882, Thomas Edison introduced the DC system and in 1886, George Westinghouse introduced the AC distribution system. Because of the availability of the transformers at that time, this war of currents was won by Westinghouse. The other reason for the implementation of the AC transmission system was the availability of AC breakers, which work on the natural zero-crossing, which was not available in DC. Nowadays, electricity is generated, transmitted, and distributed in AC form. Transformers are used to increase transmission voltages, which greatly reduce the current in the transmission line, mitigating transmission losses. Based on the voltage of the distribution line, it is classified into a primary distribution system and secondary distribution system.

3.11.1.1 Primary distribution system

A primary distribution system operates at higher voltages such as 3.3, 6.6, and 11 kV. Primary distribution is usually a three-phase and three-wire system. The power from the power generating station is transmitted at a higher voltage of 33–765 kV through extra high tension transmission lines. At the receiving substation, the power is stepped down to 11, 6.6, or 3.3 kV using step-down power transformers. A primary distribution system from the transmission voltage of 33 kV to a distribution voltage of 11 kV is shown in Fig. 3.30.

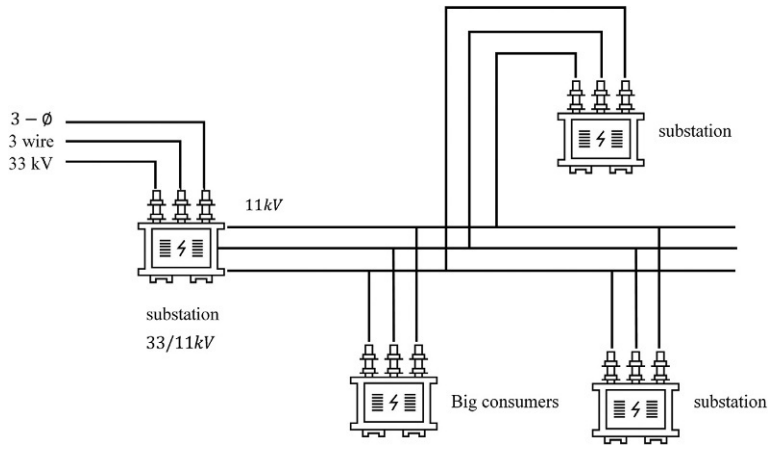

FIG. 3.30 Primary distribution system.

3.11.1.2 Secondary distribution system

The part of the AC distribution system in which the voltages are lowered to the level of the consumer's utility is called a secondary distribution system. The voltages are stepped down at the substation using a delta-star transformer converting the voltages from 11 kV to 400/230 V, using a four-wire system. The power coming from the primary distribution system is delivered to various substations. These substations are called distribution substations, having a step-down transformer, and step down the voltages from 11 kV to 400/230 V. The secondary distribution system is shown in Fig. 3.31. In a four-wire AC system, voltage between two phases is 400 V and voltage between a phase and a neutral is 230 V. The single-phase utilities are connected between a phase and a neutral, and a three-phase load is connected across three phases directly.

3.11.2 DC distribution systems

As discussed in the previous section, power generation, transmission, and distribution are inherently AC. However, for certain applications, power distribution is DC. The generation from solar photovoltaics and from fuel cells is inherently DC, and for microgrid applications a battery storage system is necessary. For these areas, a DC distribution system is required. From the substation, DC supply is obtained as either a two-wire system or a three-wire system, as discussed in the following subsections.

3.11.2.1 Two-wire DC system

A two-wire DC distribution system consists of a positive or an incoming wire and a negative or the return wire. The DC loads like DC fan and DC lights are connected in parallel between the two wires.

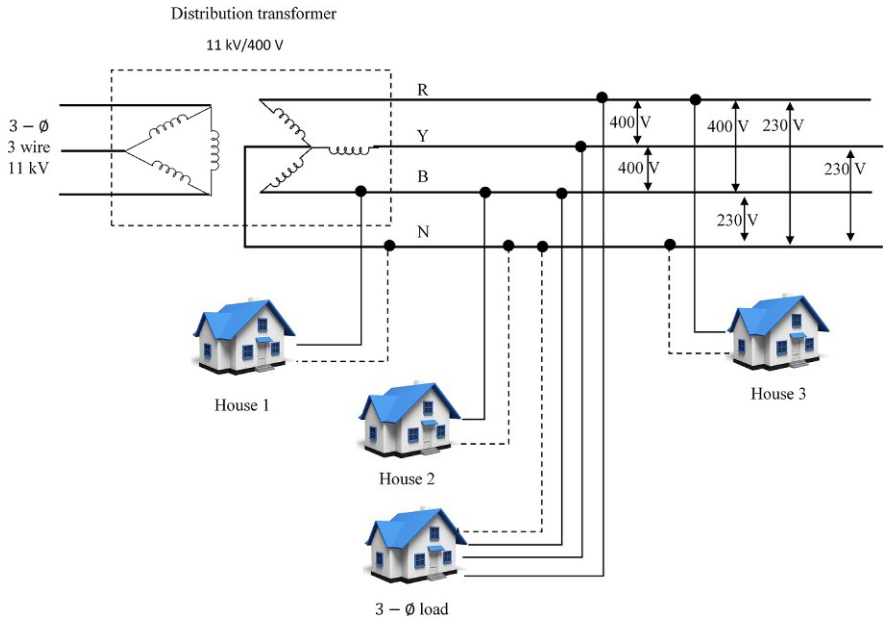

FIG. 3.31 Secondary distribution system.

3.11.2.2 Three-wire DC system

A three-wire DC system consists of two outer wires and a middle or neutral wire which is earthed at the substation. The voltage between the outer and neutral wire is half of the voltage between two outer wires. The major advantage of this type of distribution system is the availability of two voltage levels: "V" voltage between the outer and neutral wire and "2V" voltage between two outer wires.

3.11.3 Overhead versus underground distribution system

The power distribution system can be an overhead distribution system or underground distribution system. In the overhead distribution system, power lines or conductors are mounted to the poles. These poles could be wooden, steel, or concrete. They are arranged to carry both the conductors and the distribution transformers. In an underground distribution system, power lines are beneath the surfaces of streets and footpaths. The selection of an overhead distribution system or underground distribution system is based on:

- public safety;
- capital cost;
- maintenance cost;
- flexibility;
- faults;
- appearance;
- fault location and repair;

- voltage drop and current carrying capacity;
- useful life; and
- interference with communication circuits.

3.11.4 Connection schemes of a distribution system

3.11.4.1 Radial system

In a radial distribution system, various feeders are originated from the substation. Each feeder feeds the distributor at only one point. Fig. 3.32 shows a single line diagram of a DC radial system. A feeder OC originates from the substation and a distributor is taken only from a single point A. Distributor is shown by AB, from which the consumers are supplied. A single line diagram of the AC radial system is shown in Fig. 3.33. In an AC radial system, voltages are stepped down before the distributor. The radial system is the simplest circuit which is mostly used where generation is at the center of the load. The drawbacks of the radial system are as follows.

- The end of the distributor close to the feeder is heavily loaded.
- The consumers are supplied from a single feeder and the associated distributor. In the case of a fault in the feeder, the consumers connected to the distributor will go offline. In the case of a fault at the distributor, the consumers located at the other side away from the feeder will be cut off.
- In the case of variation in load at the distributor, the users at the far end of the distributor will observe voltage fluctuations.

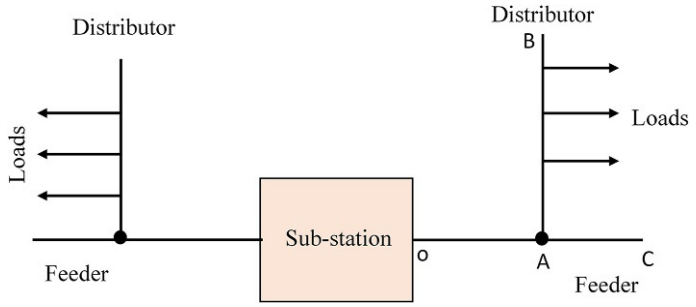

FIG. 3.32 DC radial distribution system.

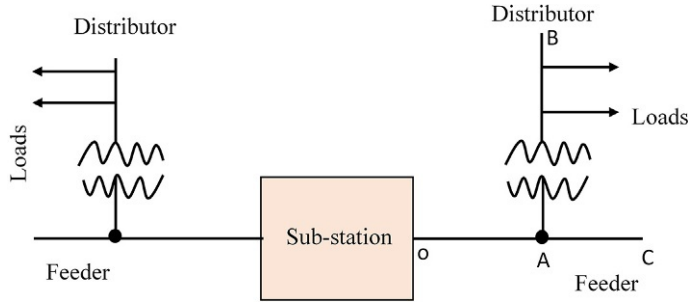

FIG. 3.33 AC radial distribution system.

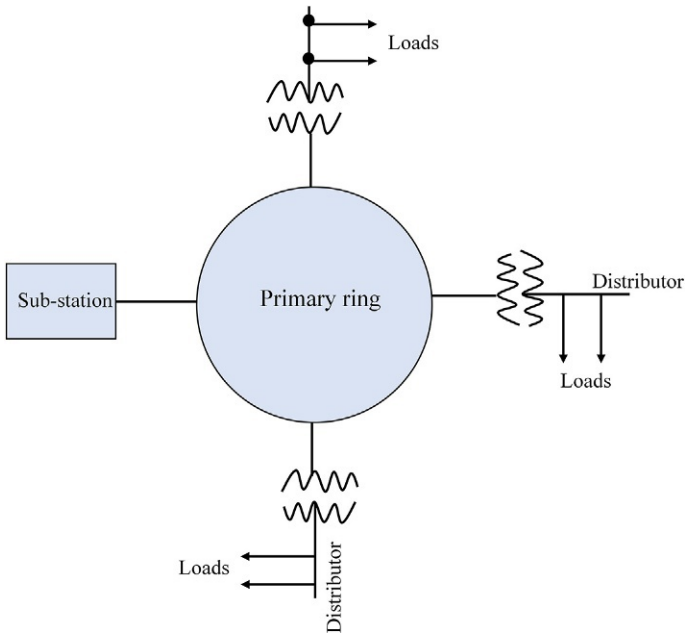

FIG. 3.34 Ring main system.

3.11.4.2 Ring main system

In a ring main system, a loop is designed by connecting the primary of each distribution transformer. The input to the ring main is from the substation. Distributors are attached to the ring main through the step-down transformer. A single line diagram of the ring main system for AC distribution is shown in Fig. 3.34. The distributor is tapped from the ring at different points. The advantages of the ring main distribution system are as follows.

- Voltage fluctuations at the consumers' terminals are lower.
- Each distributor is fed by two feeders, which increases the reliability of the system to feed the load. In the case of a fault occurring in the feeder, the distributor is isolated from that feeder for maintenance and repair. In the meantime, the distributor is fed from the other feeder.

3.11.4.3 Interconnected system

A system is called an interconnected system if the ring is energized by two or more substations. Fig. 3.35 shows an interconnected system in which the ring is energized by two substations, S1 and S2. Distributors are connected to the feeders in the ring through the distribution transformers. The advantages of the interconnected system are as follows.

- The system is reliable since the fault in the one substation does not affect the supply to the feeders and distributor.
- During peak hours, an area can be fed from the other substation to meet the load demand (Fig. 3.36).

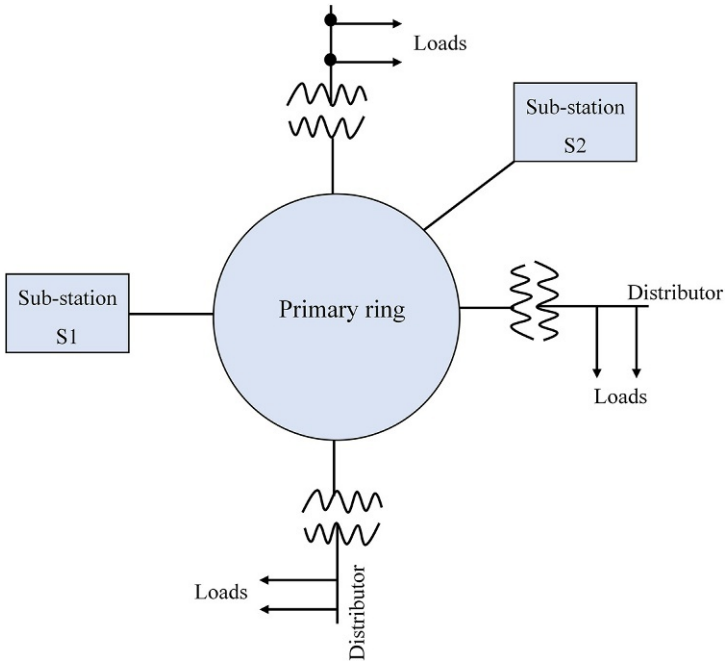

FIG. 3.35 Interconnected distributed system.

3.12 Transformers in electric power grids

A transformer is a device that at a constant frequency changes the voltage from one level to another. The transformed voltage could be higher or lower. It consists of two electrically insulated and magnetically coupled windings wrapped on the two legs of a same ferromagnetic core. One of the windings is called the primary winding, which takes the input from the voltage source which is to be transformed; the other winding is called the secondary winding, which gives the output transformed voltage. Based on the voltage level, transformers are classified into step-up transformers and step-down transformers. A step-up transformer raises the voltage at the primary to a higher level at the secondary. Similarly, a step-down transformer changes the voltage at the primary side to a lower level at the secondary side. In a power system, the voltage at the generation site is stepped up for the efficient transmission purposes. At the consumer side, voltage is reduced to a lower suitable voltage level for utilization. Fig. 3.37 shows a labeled diagram of an ideal transformer.

3.12.1 Electromotive force equation of a transformer

When alternating voltage is fed to the primary winding of the transformer containing N1 turns, it produces alternating flux in the primary winding that induces voltage E1 in the primary winding. The flux is also linked to the secondary winding containing N2 turns through the ferromagnetic core inducing voltage $E2$ at the secondary windings. The average

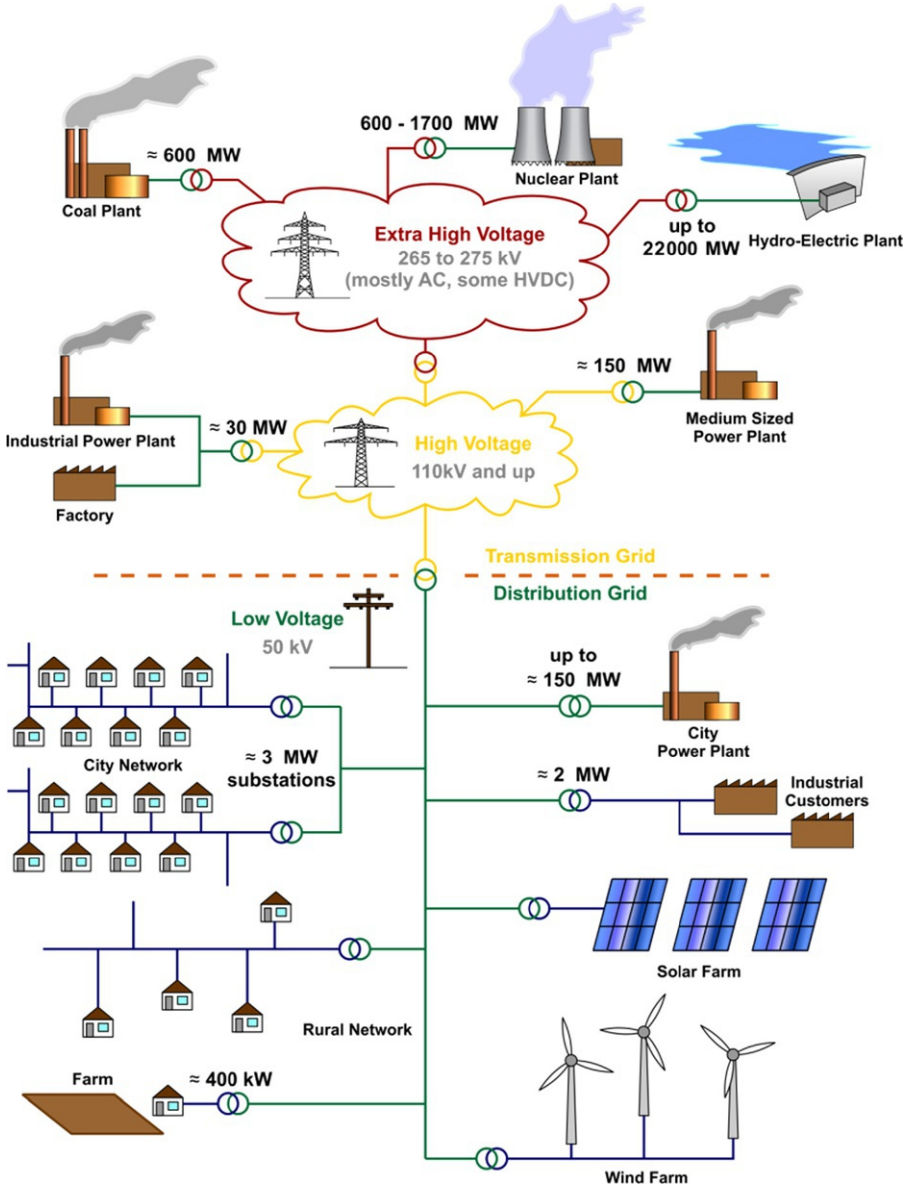

FIG. 3.36 A complete power system consisting of generation, transmission, distribution, and distributed generation system. *Source: Wikipedia.*

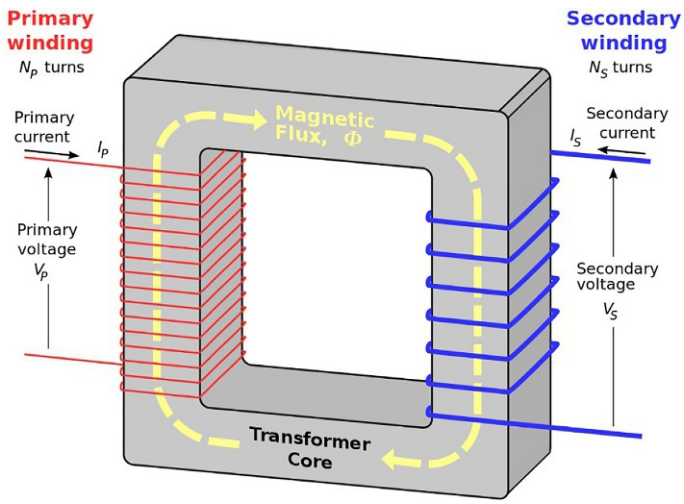

FIG. 3.37 An ideal transformer. *Source: Wikipedia.*

electromotive force (EMF) induced per N turns can be defined as the rate of change of flux per unit time. Mathematically, it can be written as Faraday's law of electromagnetic induction.

$$average\ EMF = N \cdot \frac{d\phi}{dt}$$

$$average\ EMF = N \cdot \frac{\phi_m - 0}{1/4f}$$

$$average\ EMF = 4f \cdot N \cdot \phi_m$$

The average EMF can be converted into a root mean square (RMS) value using the form factor formula given in Eq. (3.11).

$$Form\ factor = 1.11 = \frac{RMS\ value}{average\ value} \tag{3.11}$$

$$RMS\ value\ of\ induced\ EMF = 4.44\, f \cdot N \cdot \phi_m.$$

Hence the EMF equation for the primary and secondary induced EMF can be written in Eqs. (3.12), (3.13), respectively.

$$E_1 = 4.44\, f \cdot N_1 \cdot \phi_m \tag{3.12}$$

$$E_2 = 4.44\, f \cdot N_2 \cdot \phi_m \tag{3.13}$$

3.12.2 Voltage ratio of a transformer

The induced voltages and the number of turns in the transformer can be related in the following way. The ratio can be obtained by dividing the EMF equations derived above.

$$\frac{E_2}{E_1} = \frac{4.44 f \cdot N_2 \cdot \phi_m}{4.44 f \cdot N_1 \cdot \phi_m}$$

$$\frac{E_2}{E_1} = \frac{N_2}{N_1} = K \tag{3.14}$$

This secondary to primary turn ratio is also called the voltage ratio of the transformer and is denoted by K. This equation gives important information about the type of the transformer, i.e., step-up or step-down transformer.

If $E_2 > E_1$, or $N_2 > N_1$, this means that the transformer is a step-up transformer. If $E_2 < E_1$, or $N_2 < N_1$, this means that the transformer is a step-down transformer.

3.12.3 Current ratio of a transformer

The input and the output power of the transformer are calculated by the following two equations. For an ideal transformer we can assume that $E_1 = V_1$, and $E_2 = V_2$.

$$P_1 = E_1 I_1$$

$$P_2 = E_2 I_2$$

For an ideal transformer having no conversion losses, we can say that the input power is equal to the output power. Thus,

$$E_2 I_2 = E_1 I_1$$

$$\frac{E_2}{E_1} = \frac{I_1}{I_2} = K \tag{3.15}$$

By comparing Eqs. (3.14), (3.15), we can deduct a generalized formula relating voltage, current, and turns, as given in Eq. (3.16).

$$\frac{E_2}{E_1} = \frac{N_2}{N_1} = \frac{I_1}{I_2} = K \tag{3.16}$$

3.12.4 Equivalent circuit of a transformer

A transformer with no core losses, zero winding resistance, no leakage flux, and high permeability of the core is known as an ideal transformer. As the ideal transformer does not practically exist, we discuss here the practical transformer. This has core losses such as hysteresis losses and eddy current losses, winding resistance causing copper losses, and leakage flux. When a practical transformer is given a supply at its primary without connecting any load at the secondary, it draws a no load current from the primary denoted as I_o. The no load current I_o consists of active and reactive components.

(i) **Active component**: this is also called the core loss component and is responsible for producing all the core losses. It is represented by I_w, by the name wattful component.

(ii) **Reactive component**: this is also called the magnetization component and is responsible for producing flux in the core. It is represented by I_μ.

$$\overline{I_o} = \overline{I_\mu} + \overline{I_w} \tag{3.17}$$

These two components of the no load current are added by vector methods, as shown in Fig. 3.38 and Eq. (3.17). On connecting load to the secondary side, the load draws current I_2 which in primary is denoted by I_2'. Hence in primary side, the total current is the sum of I_o, and I_2', which is collectively denoted by I_1, shown in Eq. (3.18).

$$\overline{I_1} = \overline{I_o} + \overline{I_2'} \tag{3.18}$$

For ease of understanding and analysis purposes, the winding resistance of the primary R_1 and secondary winding R_2, and leakage flux of the primary X_1 and secondary X_2 side are shown external to the transformer, as illustrated in Fig. 3.39. The complete equivalent circuit of a single-phase transformer consisting of primary and secondary winding resistance, primary and secondary leakage flux, magnetizing and core current components, and winding turn ratio is shown in Fig. 3.39.

Equivalent resistance: the resistance in the primary and secondary windings R_1 and R_2, respectively, cause copper losses that can be calculated by Eq. (3.19).

$$Total\ copper\ losses = I_1^2 R_1 + I_2^2 R_2 \tag{3.19}$$

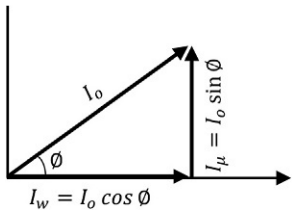

FIG. 3.38 Active and reactive components of no load current of a transformer.

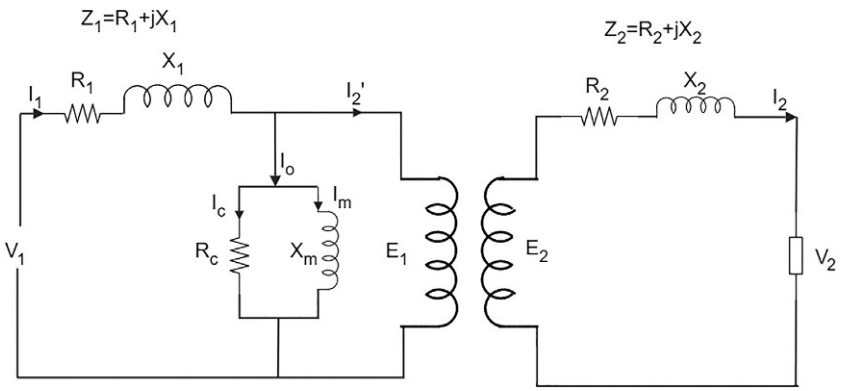

FIG. 3.39 Equivalent circuit of a transformer.

Taking I_1^2 common from the above equation:

$$Total\ copper\ losses = I_1^2\left[R_1 + \left(\frac{I_2}{I_1}\right)^2 R_2\right]$$

$$Total\ copper\ losses = I_1^2\left[R_1 + \left(\frac{1}{K}\right)^2 R_2\right]$$

$$Total\ copper\ losses = I_1^2\left[R_1 + \frac{R_2}{K^2}\right]$$

This equation indicates that $\frac{R_2}{K^2}$ is the effective value of the secondary winding resistance when it is referred to the primary side. Hence we can deduct a relation given in Eq. (3.20).

$$R_2' = \frac{R_2}{K^2} \tag{3.20}$$

Hence the equivalent resistance referred to primary ($R_{e,\,p}$) as shown in Fig. 3.40 can be calculated using Eq. (3.21).

$$R_{e,p} = R_1 + R_2'$$

$$R_{e,p} = R_1 + \frac{R_2}{K^2} \tag{3.21}$$

Similarly, using Eq. (3.19), a relation can be derived for the resistance of the primary windings as referred to the secondary. Taking I_2^2 common from Eq. (3.19),

$$Total\ copper\ losses = I_2^2\left[\left(\frac{I_1}{I_2}\right)^2 R_1 + R_2\right]$$

$$Total\ copper\ losses = I_2^2\left[(K)^2 R_1 + R_2\right]$$

$$Total\ copper\ losses = I_2^2\left[R_1 K^2 + R_2\right]$$

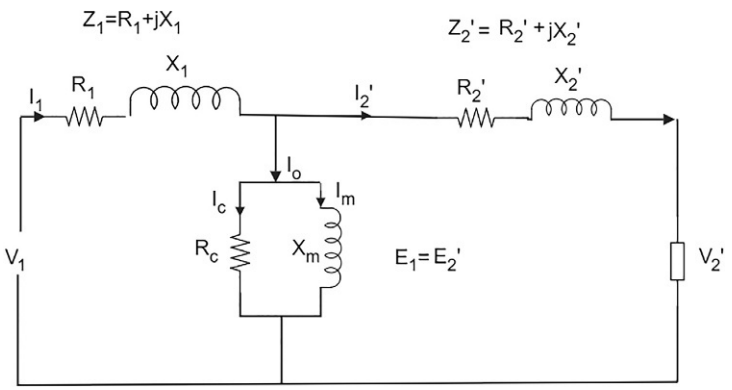

FIG. 3.40 Equivalent circuit of a transformer as referred to primary.

This equation indicates that R_1K^2 is the effective value of the primary winding resistance when it is referred to the secondary side. Hence we can deduct a relation given in Eq. (3.22).

$$R_1' = R_1K^2 \tag{3.22}$$

Hence the equivalent resistance referred to secondary ($R_{e,\,s}$) as shown in Fig. 3.41 can be calculated using Eq. (3.23).

$$R_{e,s} = R_1' + R_2$$

$$R_{e,s} = R_1K^2 + R_2 \tag{3.23}$$

Equivalent leakage reactance: the leakage reactances in the primary and secondary windings are represented by X_1 and X_2, respectively

$$X_2' = \frac{X_2}{K^2}$$

Hence the equivalent leakage reactance referred to primary ($X_{e,\,p}$) shown in Fig. 3.40 can be calculated using Eq. (3.24).

$$X_{e,p} = X_1 + X_2'$$

$$X_{e,p} = X_1 + \frac{X_2}{K^2} \tag{3.24}$$

Similarly:

$$X_1' = X_1K^2$$

Hence the equivalent leakage reactance referred to secondary ($X_{e,\,s}$) as shown in Fig. 3.41 can be calculated using Eq. (3.25).

$$X_{e,s} = X_1' + X_2$$

$$X_{e,s} = X_1K^2 + X_2 \tag{3.25}$$

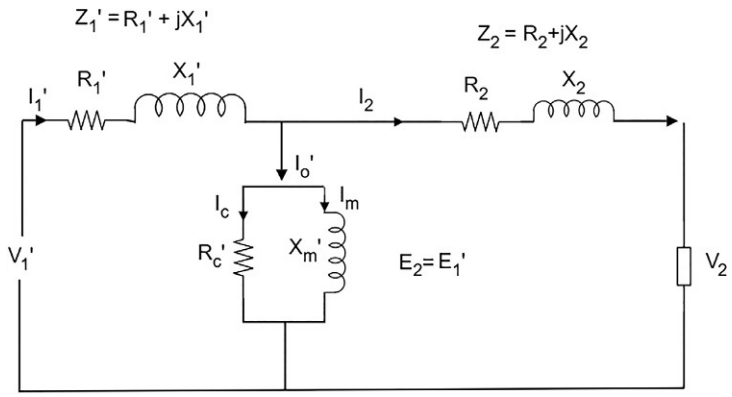

FIG. 3.41 Equivalent circuit of a transformer as referred to secondary.

Equivalent impedance: the impedance of the transformer at primary and secondary windings can be calculated using Eqs. (3.26), (3.27), respectively.

$$Z_1 = R_1 + jX_1 \tag{3.26}$$

$$Z_2 = R_2 + jX_2 \tag{3.27}$$

Eqs. (3.28), (3.29) can be used to calculate the equivalent impedance referred to primary and equivalent impedance referred to secondary, respectively.

$$Z_{e,p} = R_{e,p} + jX_{e,p} \tag{3.28}$$

$$Z_{e,s} = R_{e,s} + jX_{e,s} \tag{3.29}$$

3.12.5 Voltage regulation of transformer

Voltage regulation of the transformer is the percentage drop in the secondary winding voltages from no load to load. As the load is increased, the load current increases that drops the voltage at the load. The percentage voltage of the transformer is expressed using the relation given in Eq. (3.30).

$$\%\ voltage\ regulation = \frac{E_2 - V_2}{E_2} = \left(1 - \frac{V_2}{E_2}\right)100 \tag{3.30}$$

where E_2 is the no load voltage and V_2 is the load voltage.

3.12.6 Losses in a transformer

Two types of losses occur in the core and the windings of the transformer.

(i) Core losses (iron losses): the alternating flux passes through the core that causes the core losses which are of two further types: eddy current losses and hysteresis losses. Core losses are calculated by the open circuit test, since at no load, only the no load current passes through the core, which causes magnetization and core losses.

Eddy current: when the input supply is connected to the primary winding, an alternating flux is produced in the core because of Faraday's law of electromagnetic induction. The induced voltage builds up a current in the core that circulates in the core and causes heat losses in the core. Eddy current losses can be calculated by Eq. (3.31).

$$I_{eddy} = K_e B_m^t f^2 t^2 \tag{3.31}$$

where

K_e is the eddy current constant;
f is the frequency of the input supply;
t is the core thickness; and
B_m is the maximum flux density.

Hysteresis losses: the hysteresis losses are given by Eq. (3.32).

$$h_{Losses} = K_h f.V.B_m^{1.67} \tag{3.32}$$

where

K_h is the hysteresis constant that depends upon the type of the core material;
f is the frequency of the input supply;
V is the core volume; and
B_m is the maximum flux density.

(ii) Copper losses: since the winding of the transformer carries the resistance, when the load is connected to the secondary, current passes through the windings causing the copper losses. Copper losses occur in the primary and secondary windings, and are calculated as follows.

$$Copper\ losses = primary\ copper\ losses + secondary\ copper\ losses$$

$$Total\ copper\ losses = I_1^2 R_1 + I_2^2 R_2$$

$$Total\ copper\ losses = I_1^2 \left(R_1 + \frac{I_2^2}{I_1^2} R_2 \right)$$

$$Total\ copper\ losses = I_1^2 \left[R_1 + \left(\frac{1}{K} \right)^2 R_2 \right]$$

$$Total\ copper\ losses = I_1^2 \left[R_1 + \frac{R_2}{K^2} \right]$$

$$Total\ copper\ losses = I_1^2 \left[R_1 + R_2' \right]$$

To practically measure the copper losses in the windings of the transformer, a short circuit test is conducted.

3.12.7 Efficiency of a transformer

The efficiency of the transformer is the ratio of the output power to the input power, as shown in Eq. (3.33). From Fig. 3.39, we can conclude that the output power is the difference between the input power and the losses, or we can say that some part of the input power appears at the output and the rest is lost in the core and copper of the transformer. This can be written in Eqs. (3.34), (3.35).

$$\eta = \frac{P_{out}}{P_{in}} \tag{3.33}$$

$$P_{in} = P_{out} + P_{losses} \tag{3.34}$$

$$P_{out} = P_{in} - P_{losses} \tag{3.35}$$

Putting the values of input power and output powers from Eqs. (3.34), (3.35) into Eq. (3.33):

$$\eta = \frac{P_{out}}{P_{out} + P_{losses}} \tag{3.36}$$

P_{losses} are the sum of copper losses and the core losses, i.e., $P_{copper} + P_{core}$. In addition, the output power can be written as $P_{out} = V_2 I_2 \cos \text{Ø}$. Thus, Eq. (3.36) becomes

$$\eta = \frac{V_2 I_2 \cos \text{Ø}}{V_2 I_2 \cos \text{Ø} + P_{copper} + P_{core}} \tag{3.37}$$

3.12.8 Condition for maximum efficiency

The efficiency of a transformer varies with the load when the input voltage and the frequency are kept constant. By increasing load, efficiency of the transformer also increases until a point reaches where the efficiency becomes maximum and if the load is further increased, the efficiency starts decreasing. We can find a condition for the maximum efficiency of the transformer. Fig. 3.42 shows the graph between the load current and the efficiency. Condition for maximum efficiency can be found by differentiating the slope of the graph at the maximum efficiency point.

The slope of the maximum efficiency point can be written as Eq. (3.38).

$$\frac{dy}{dx} = \frac{d\eta}{dI_2} = 0 \tag{3.38}$$

$$\frac{d}{dI_2}\left(\frac{V_2 I_2 \cos \varnothing}{V_2 I_2 \cos \varnothing + I_2^2 R_{2,eq} + P_{core}}\right) = 0$$

By applying the quotient rule,

$$\left(V_2 I_2 \cos \varnothing + I_2^2 R_{2,eq} + P_{core}\right)\left(V_2 \cos \varnothing\right) - \left(V_2 I_2 \cos \varnothing\right)\left(\left(V_2 \cos \varnothing + 2 I_2 R_{2,eq}\right) = 0\right.$$

$$\left(V_2 I_2 \cos \varnothing + I_2^2 R_{2,eq} + P_{core}\right)\frac{d}{dI_2} V_2 I_2 \cos \varnothing = 0$$

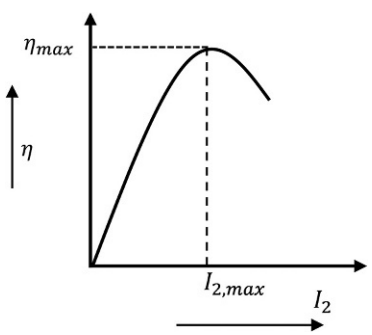

FIG. 3.42 Graph of load current and efficiency of a transformer.

$$P_{core} = P_{copper}$$

$$Copper\ losses = core\ losses \tag{3.39}$$

Hence, Eq. (3.39) indicates that the transformer will be maximally efficient if its copper losses are equal to its core or iron losses.

3.13 Three-phase transformer

A three-phase transformer consists of either three single-phase transformers or three windings on three cores or on a single core. The primary and secondary windings of a three-phase transformer can be connected in the following combinations of star and delta connections:

- star-star (Y-Y)
- star-delta (Y-Δ)
- delta-star (Δ-Y)
- delta-delta (Δ-Δ).

3.13.1 Star-star (Y-Y)

Figs. 3.43 and 3.44 show the star-star (Y-Y) connection of the three-phase transformer. Fig. 3.43 shows the Y-Y connection of three single-phase transformers, whereas Fig. 3.44 shows the alternative connections of three phase windings of primary and secondary. The current from the primary and the secondary windings will be equal to the lines to which they are connected. Eqs. (3.40), (3.41) show the phase voltage and line voltage at each primary of the three phase transformer, respectively.

$$V_{\phi,P} = \frac{1}{\sqrt{3}} V_{L,P} \tag{3.40}$$

$$V_{L,P} = \sqrt{3} V_{\phi,P} \tag{3.41}$$

Similarly, Eqs. (3.42), (3.43) show the phase voltage and line voltage at each secondary of the three-phase transformer, respectively.

$$V_{\phi,S} = \frac{1}{\sqrt{3}} V_{L,S} \tag{3.42}$$

$$V_{L,S} = \sqrt{3} V_{\phi,S} \tag{3.43}$$

Hence, the voltage ratio of the three-phase transformer can be calculated using Eq. (3.44).

$$\frac{V_{L,P}}{V_{L,S}} = \frac{\sqrt{3} V_{\phi,P}}{\sqrt{3} V_{\phi,S}} = K \tag{3.44}$$

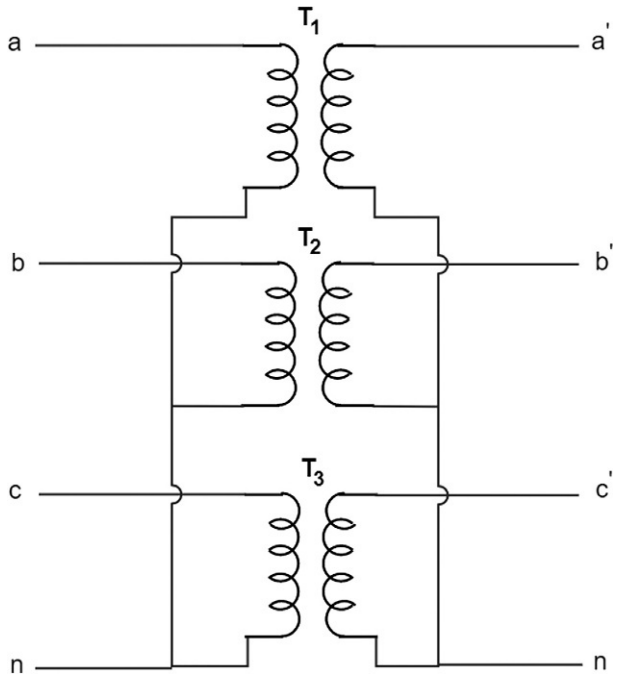

FIG. 3.43 Star-star connection of three single-phase transformers.

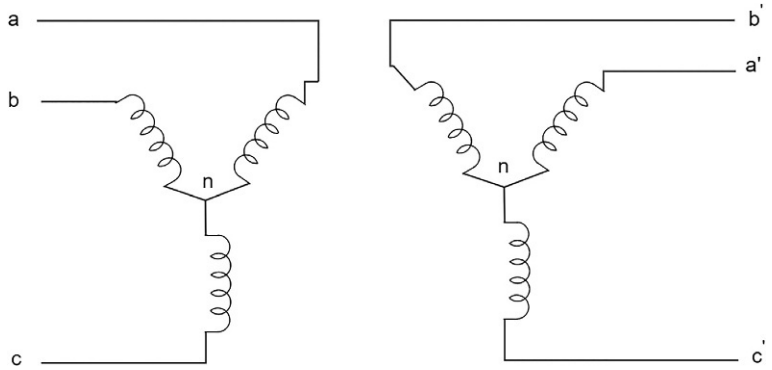

FIG. 3.44 Star-star connections of a three-phase transformer.

3.13.1.1 Advantages

- In a star connection, the phase voltage is $1/\sqrt{3}$ times the line voltage. Thus, the required turn per phase is reduced, as is the required insulation.
- Between primary and secondary voltages, there is no phase displacement.
- A neutral point is available at both the primary and secondary side because of the star connection.

3.13.1.2 Disadvantages

- The phase voltage of the transformer becomes unbalanced in a case where the load is unbalanced; this can be balanced by earthing the neutral point of the load side.
- Third harmonic voltages may be large but can be avoided by connecting the primary side neutral to the neutral of the generator. The neutral path provides a path to the third harmonic current and the return path for the unbalanced conditions.

3.13.2 Star-delta (Y-Δ)

The star-delta connection of a transformer is used to step down the voltage at the substation end of the transmission line. Fig. 3.45 shows connections of three single-phase transformers. The primary winding is connected in star with a neutral. The secondary windings are connected in delta with no neutral. The alternative diagram of star-delta winding of a three phase transformer is shown in Fig. 3.46. The relation between the primary line and phase voltage is shown in Eq. (3.45).

$$V_{L,P} = \sqrt{3} V_{\phi,P} \tag{3.45}$$

The line and phase voltages at the secondary side is the same since the windings are connected in delta, as shown in Eq. (3.46).

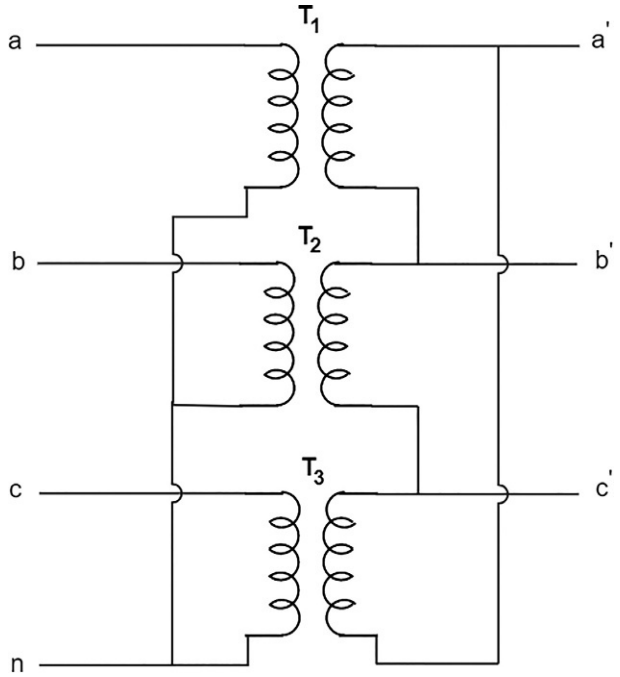

FIG. 3.45 Star-delta connections of three single-phase transformers.

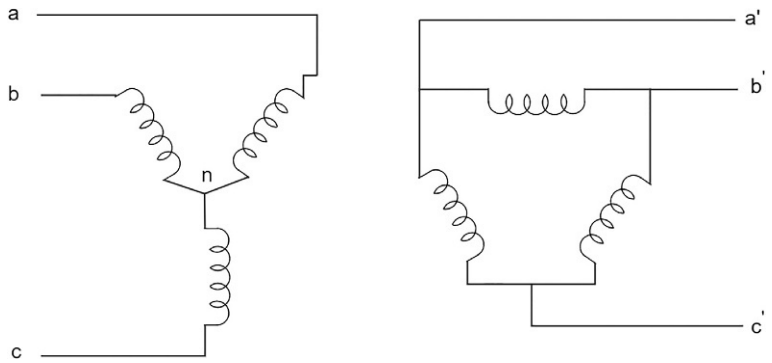

FIG. 3.46 Star-delta connections of three-phase transformer.

$$V_{L,s} = V_{\phi,s} \tag{3.46}$$

The primary to secondary voltage ratio at each phase is given by Eq. (3.47).

$$\frac{V_{\phi,P}}{V_{\phi,s}} = K \tag{3.47}$$

Similarly, the line voltage ratio from primary to secondary is determined by dividing Eq. (3.45) to Eq. (3.46), as shown in Eq. (3.48). The line voltage ratio from primary to secondary is shown in Eq. (3.49).

$$\frac{V_{L,P}}{V_{L,s}} = \frac{\sqrt{3}V_{\phi,P}}{V_{\phi,s}} \tag{3.48}$$

$$\frac{V_{L,P}}{V_{L,s}} = \sqrt{3}\,K \tag{3.49}$$

No third harmonics are present since the third harmonic currents flow through the neutral of the delta winding. When the load is unbalanced, the neutral point redistributes the imbalance condition.

3.13.3 Delta-star (Δ-Y)

A delta-star connected transformer is used at the start of a high tension transmission line, where the voltage is to be stepped up for transmission purposes. Fig. 3.47 shows a connection diagram of three single-phase transformers. The primary windings are connected in delta and the secondary windings are connected in star with a neutral grounded providing a three-phase, four-wire system. The alternative winding diagram of a three-phase transformer connected in delta-star is shown in Fig. 3.48. The relation between the primary line and phase voltage is shown in Eq. (3.50).

$$V_{L,P} = V_{\phi,P} \tag{3.50}$$

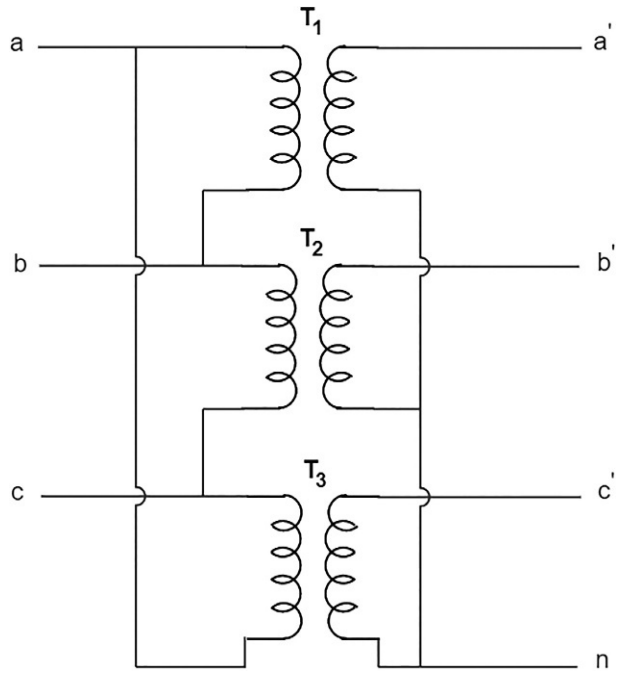

FIG. 3.47 Delta-star connections of three single-phase transformers.

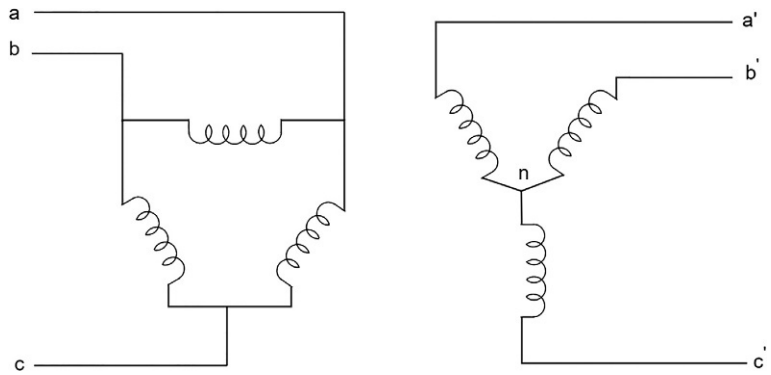

FIG. 3.48 Delta-star connections of three-phase transformer.

The line and phase voltages at the secondary side are given by Eq. (3.51).

$$V_{L,s} = \sqrt{3} V_{\phi,s} \tag{3.51}$$

The primary to secondary voltage ratio at each phase is given by Eq. (3.52).

$$\frac{V_{L,P}}{V_{L,s}} = K \tag{3.52}$$

Similarly, the line voltage ratio from primary to secondary is determined by dividing Eq. (3.50) to Eq. (3.51), as shown in Eqs. (3.53), (3.54).

$$\frac{V_{L,P}}{V_{L,s}} = \frac{V_{\phi,P}}{\sqrt{3}V_{\phi,s}} \tag{3.53}$$

$$\frac{V_{L,P}}{V_{L,s}} = \frac{K}{\sqrt{3}} \tag{3.54}$$

The advantage of the delta-star connections is the same as that of the star-delta connection.

3.13.4 Delta–delta (Δ-Δ)

The delta-delta connection of the three single-phase transformers is shown in Fig. 3.49, in which the primary and the secondary windings are both connected in delta. Fig. 3.50 shows the alternative winding diagram of the delta-delta connection of a three-phase transformer. The relation between the primary line and phase voltage is shown in Eq. (3.55).

$$V_{L,P} = V_{\phi,P} \tag{3.55}$$

The line and phase voltages at the secondary side are the same as shown in Eq. (3.56), since the windings are also connected in delta.

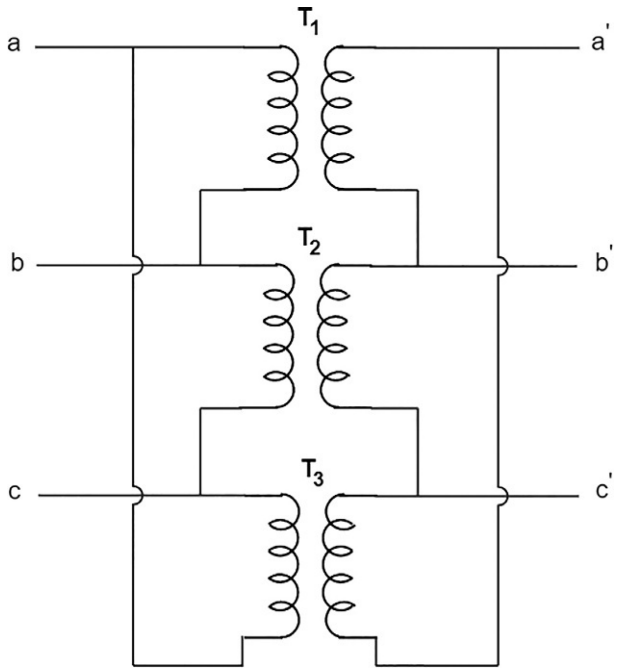

FIG. 3.49 Delta-delta connections of three single-phase transformers.

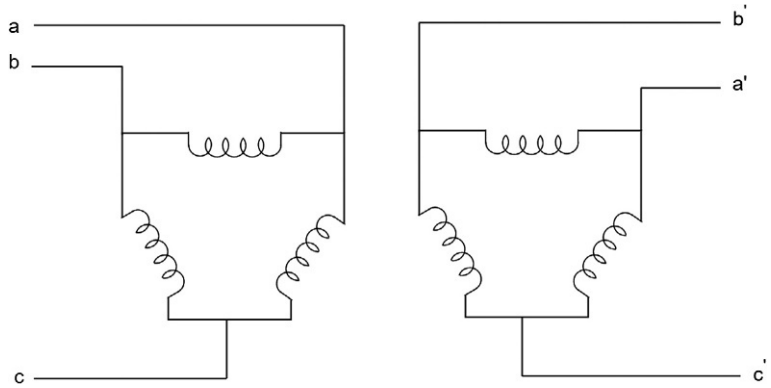

FIG. 3.50 Delta-delta connections of three-phase transformer.

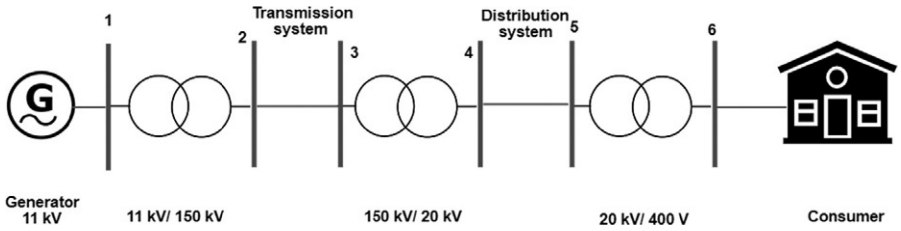

FIG. 3.51 Application of a transformer in an electric power system.

$$V_{L,s} = V_{\phi,s} \tag{3.56}$$

The line voltage ratio from primary to secondary is determined by dividing Eq. (3.55) to Eq. (3.56), as given by Eq. (3.57).

$$\frac{V_{L,P}}{V_{L,s}} = \frac{V_{\phi,P}}{V_{\phi,s}} = K \tag{3.57}$$

In a delta-delta connection, there is no problem of third harmonics and the unbalanced load.

Fig. 3.51 shows a complete electric power grid consisting of an electrical power generating station of 11 kV, a transmission system, a distribution system, and the end user. The electricity from generation to the end user is transformed over time. At the start, a step-up transformer is used to increase the voltage for transmission purposes. The reason behind this is transmission at low current to avoid various transmission losses. At the end of the transmission line, the voltage is reduced again by the step-down transformer for distribution purposes.

3.14 Conclusion

To understand the functioning of the smart grid, knowledge of the complete electric power grid is necessary. This chapter has highlighted all the parts of the electric grid and present details where necessary. AC CBs and DC CBs are used to interrupt the fault current in the

case of a fault in the AC or DC transmission lines, respectively. Different bus bar configurations were described. Causes of low power factors, disadvantages of low power factor, and methods to improve the power factor were discussed in detail. The chapter also described the types of faults in single-phase and three-phase lines. Distribution systems and the types of transformers in distribution and transmission systems were also discussed in detail.

Problems

Problems 1–21 contain four answer options, A, B, C, and D. Choose the correct answer.

1. Which of the following is part of an electrical power system?
   A. Generation
   B. Transmission
   C. Distribution
   D. All of the above
2. Which of the following is a type of electric substation?
   A. Step-up substation
   B. Step-down substation
   C. Distribution substation
   D. All of the above
3. What increases the resistance of the arc?
   A. Quenching the arc in zero-crossing
   B. Exhaustive cooling
   C. Lengthening the arc
   D. Splitting the arc
   E. All of the above
4. In a 50 Hz system, what will the number of zero-crossings be?
   A. 100
   B. 120
   C. 140
   D. 150
5. Which of the following is a type of AC circuit breaker?
   A. Oil circuit breaker
   B. Vacuum circuit breaker
   C. Solid-state circuit breaker
   D. Oil circuit breaker and vacuum circuit breaker
6. Which of the following is a type of DC circuit breaker?
   A. Mechanical circuit breaker
   B. Solid-state circuit breaker
   C. Hybrid circuit breaker
   D. All of the above
7. What produces zero-crossing in the DC circuit break?
   A. Natural zero-crossing
   B. Artificial resonance
   C. Metal oxide varistor
   D. All of the above

8. All the inward and the outward power lines are connected to the same bus bar in what configuration?
   A. Single bus bar
   B. Sectionalized single bus bar
   C. Single breaker double bus bar
   D. Double breaker double bus bar
9. Which of the following is a type of lightning arresters?
   A. Horn gap
   B. Multigap
   C. Valve type
   D. All of the above
10. Which of the following defines power factor?
   A. $\frac{Active\ power}{Apparent\ power}$
   B. $\frac{Active\ power}{Real\ power}$
   C. $\frac{Real\ power}{Apparent\ power}$
   D. $\frac{Real\ power}{Active\ power}$
11. Which of the following methods is used to improve the power factor?
   A. Static capacitor
   B. Synchronous condenser
   C. Phase advancers
   D. All of the above
12. Which of the following is a type of insulator?
   A. Strain insulator
   B. Stranded insulator
   C. Hollow insulator
   D. Horn gap insulator
13. Which of the following is a type of open circuit fault?
   A. Single phase open conductor
   B. Two phase open circuit
   C. Three phase open conductor
   D. All of the above
14. Which of the following is a type of symmetrical fault?
   A. Line-line-line
   B. Line-line-ground
   C. Line-line
   D. Line-line-line and line-line-ground
15. Which of the following is a type of unsymmetrical fault?
   A. Single line-to-ground
   B. Line-to-line
   C. Double line-to-ground
   D. All of the above

16. Which of the following is a part of a distribution system from the substation to the consumer?
    A. Feeder
    B. Distributor
    C. Service main
    D. All of the above
17. Which of the following is a type of AC distribution system?
    A. Primary distribution system
    B. Secondary distribution system
    C. Tertiary distribution system
    D. Primary and secondary systems
18. Which of the following is a connection scheme of a distribution system?
    A. Radial system
    B. Ring main system
    C. Interconnected system
    D. All of the above
19. What is the form factor of an AC signal?
    A. 1.11
    B. 1.22
    C. 1.12
    D. 1.21
20. How is the form factor of a signal defined?
    A. $\frac{Average\ value}{RMS\ value}$
    B. $\frac{RMS\ value}{Average\ value}$
    C. $\frac{Average\ value}{Peak\ value}$
    D. $\frac{Peak\ value}{Average\ value}$
21. What is the condition for maximum efficiency of a transformer?
    A. Copper losses > core losses
    B. Copper losses < core losses
    C. Copper losses = core losses
    D. Copper losses = 0

Give brief answers to the following short questions

1. What are the different types of electrical substation?
2. Give a brief comparison of a conventional grid and a smart grid.
3. How is a high resistance inserted in the path of an arc to quench it?
4. What are the types of AC circuit breakers?
5. What is zero-crossing and how is it used in AC circuit breakers?
6. What is the difference between AC and DC circuit breakers?
7. How is zero-crossing created in the DC circuit breakers?

8. What are the types of DC circuit breakers?
9. What are the different types of substation bus bars?
10. Define the power factor and describe the causes of low power factor.
11. What are the different methods of power factor improvement?
12. Illustrate the effect of low power factor on transmission line conductors.
13. List the different causes of corona effects.
14. How many methods are used to reduce the corona effect?
15. List the characteristics of a good transmission line conductor.
16. State some key advantageous properties of a bundled conductor.
17. Based on their construction and shape, how are conductors classified?
18. Illustrate the following effects in a power transmission line:
    (a) Skin effect
    (b) Proximity effect
    (c) Spirality effect
    (d) Ferranti effect
19. List the different types of open circuit faults.
20. What are the different types of short circuit faults?
21. Differentiate between symmetrical and unsymmetrical faults.
22. Differentiate between AC and DC distribution systems.
23. Give a brief comparison between primary and secondary distribution systems.
24. Explain the differences between feeder, distributor, and service mains.
25. Compare overhead and underground distribution systems.
26. Briefly describe the radial system, ring main system, and interconnected system.
27. What tests are conducted on a transformer to measure copper losses and iron losses?
28. What is the significance of form factor in electrical systems?
29. In what combinations can the primary and secondary windings of a three-phase transformer be connected?
30. Illustrate the eddy current losses and hysteresis losses of a transformer.
31. Draw the equivalent circuit diagram of a transformer.

References

[1] C.M. Franck, HVDC circuit breakers: a review identifying future research needs, IEEE Trans. Power Deliv. 26 (2) (2011) 998–1007, https://doi.org/10.1109/TPWRD.2010.2095889.
[2] M. Hajian, D. Jovcic, B. Wu, Evaluation of semiconductor based methods for fault isolation on high voltage DC grids, IEEE Trans. Smart Grid 4 (2) (2013) 1171–1179, https://doi.org/10.1109/TSG.2013.2238260.
[3] R. Schmerda, R. Cuzner, R. Clark, D. Nowak, S. Bunzel, Shipboard solid-state protection: overview and applications, IEEE Electrif. Mag. 1 (1) (2013) 32–39, https://doi.org/10.1109/MELE.2013.2273395.
[4] M. Mobarrez, M.G. Kashani, S. Bhattacharya, R. Adapa, Comparative study of DC circuit breakers using realtime simulations, in: IECON Proc. (Industrial Electron. Conf.), Feb. 2014, pp. 3736–3742, https://doi.org/10.1109/IECON.2014.7049056.
[5] Z.J. Shen, Z. Miao, A.M. Roshandeh, Solid state circuit breakers for DC micrgrids: current status and future trends, in: 2015 IEEE 1st Int. Conf. Direct Curr. Microgrids, ICDCM 2015, 2015, pp. 228–233, https://doi.org/10.1109/ICDCM.2015.7152044.
[6] J. Magnusson, R. Saers, L. Liljestrand, G. Engdahl, Separation of the energy absorption and overvoltage protection in solid-state breakers by the use of parallel varistors, IEEE Trans. Power Electron. 29 (6) (2014) 2715–2722, https://doi.org/10.1109/TPEL.2013.2272857.

[7] Z.J. Shen, G. Sabui, Z. Miao, Z. Shuai, Wide-bandgap solid-state circuit breakers for DC power systems: device and circuit considerations, IEEE Trans. Electron Devices 62 (2) (2015) 294–300, https://doi.org/10.1109/TED.2014.2384204.

[8] U. Vemulapati, M. Arnold, M. Rahimo, A. Antoniazzi, D. Pessina, Reverse blocking IGCT optimised for 1 kV DC bi-directional solid state circuit breaker, IET Power Electron. 8 (12) (2015) 2308–2314, https://doi.org/10.1049/IET-PEL.2015.0028/CITE/REFWORKS.

[9] F. Liu, W. Liu, X. Zha, H. Yang, K. Feng, Solid-state circuit breaker snubber design for transient overvoltage suppression at bus fault interruption in low-voltage DC microgrid, IEEE Trans. Power Electron. 32 (4) (2017) 3007–3021, https://doi.org/10.1109/TPEL.2016.2574751.

[10] M. Callavik, A. Blomberg, J. Häfner, B. Jacobson, The Hybrid HVDC Breaker an Innovation Breakthrough Enabling Reliable HVDC Grids, 2012.

This page intentionally left blank

CHAPTER

4

Power electronics for smart grids

4.1 Introduction

Power electronics is the application of electronic circuits in controlling and conversion of electrical energy. For example, in a solar photovoltaic (PV) system, DC power generated by the solar panels is first converted into AC using power electronics inverters to feed the grid and entertain the AC load. The power electronic converter needs a control circuit like a maximum power point tracking algorithm, fuzzy logic-based controller, neural network-based controller, and proportional integral derivative (PID) controller. The block diagram defining the power electronics and their application in different areas is shown in Fig. 4.1. Raw input is taken from any of the sources like solar PV, wind turbine, battery, fuel cell, utility, or any other source of AC or DC electricity, and is given to the power electronic processing circuit. The power electronic circuit could be a rectifier, converter, inverter, or cycloconverter. These power electronic circuits are controlled by one of the controllers like fuzzy logic-based controller, neural network-based controller, perturb and observe algorithms, incremental conductance algorithm, and PID controller. At the output, the desired voltage, current, power, and frequency are obtained.

Fig. 4.2 shows the conversions between AC and DC, AC and AC, and DC and DC using different power electronic converters. For AC to DC conversion, rectifiers are used. For DC to AC conversion, inverters are used. For AC to AC conversion with variable frequency, cycloconverters are employed. For DC to DC conversion with voltage step-up and step-down, converters are used. Following is the list of each type of converter with its function in the smart grid systems.

- AC-DC converters (rectifiers);
- AC-AC converters (step-up and step-down cycloconverters);
- DC-DC converters (buck converters, boost converters, buck-boost converters, Cuk, and flyback converters); and
- DC-AC converters (H-bridge inverters, multilevel inverters).

This chapter deals with the basics of power electronics which is a fundamental part of smart grid systems. The applications of power electronics components and devices are discussed briefly. Solid-state switches are fundamental components of power electronics

https://doi.org/10.1016/B978-0-323-99560-3.00009-0

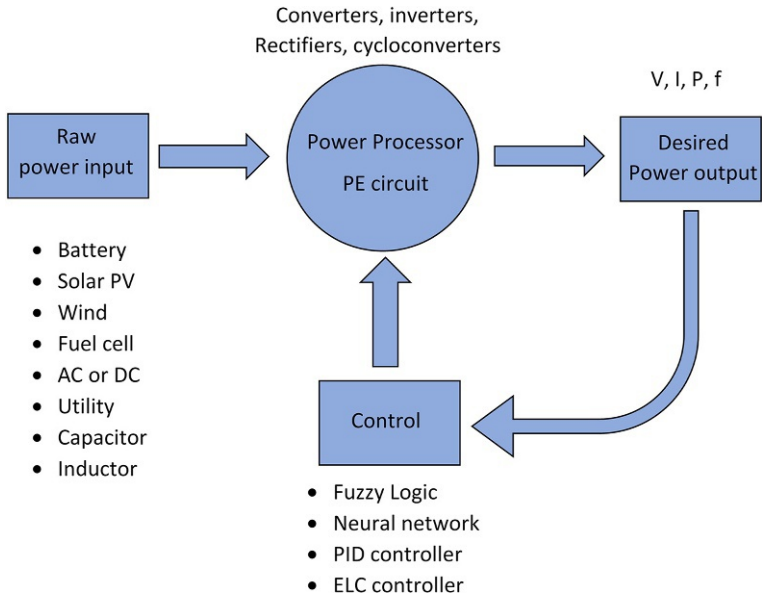

FIG. 4.1 Application of power electronics converters in various renewable energy systems with control system.

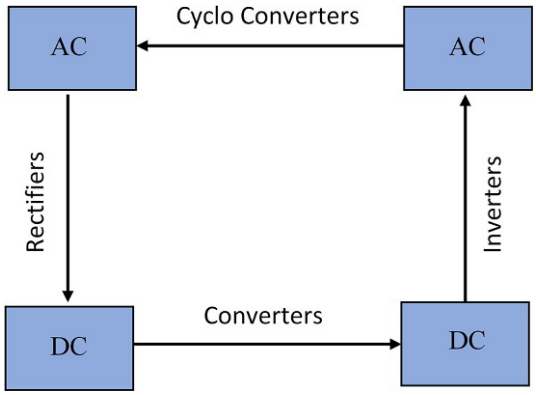

FIG. 4.2 Conversion between AC and DC using power electronics converters.

converters. The construction, working principles, and turn-on and turn-off methods are described in detail. Power electronics rectifiers are categorized into controlled and uncontrolled rectifiers with resistive, inductive, and inductive loads with freewheeling diodes. Mathematical relations of average voltage, current, and power for each of the above are derived. The circuit diagram of each rectifier is simulated in MATLAB, whose waveforms verify their functioning. Step-up and step-down DC-DC converters are described with their mathematical modeling for different switching states, and their generalized relations between inputs and outputs based on duty cycle are derived. The MATLAB simulation circuits also verify the validity of the mathematical model. The functioning and the switching schemes of

inverters are elaborated theoretically and the single-phase and three-phase inverters are also implemented in MATLAB. The output waveforms verify the validity of the model. Different multilevel inverters are also described and simulated in MATLAB. To step up or step down the frequency of the AC signals, cycloconverters are discussed and simulated in MATLAB. The waveforms of both types of cycloconverters describe the frequency of the input and output voltages.

4.2 Applications of power electronics

4.2.1 Solar photovoltaic system

A solar photovoltaic system consists of various energy conversion stages in which the DC-generated electricity is first converted to the desired DC voltage incorporating the maximum power point tracker. Depending upon the requirements, the voltage is either boosted up or bucked down using one of the DC choppers like a step-down buck converter, step-up boost converter, buck-boost converter, single-ended primary inductor converter (SEPIC converter), flyback converter, and Cuk converter. The other conversion is DC to AC conversion to feed the AC load or the grid. The inverter is used to convert DC from the solar panels to AC. Both these conversions contain power electronic converters and inverters. Fig. 4.3 is a block diagram of a solar photovoltaic system, indicating the application of converter and inverter in a solar energy system [1].

4.2.2 Solar photovoltaic hybrid energy system

In hybrid solar photovoltaic (PV) energy systems, solar PV is integrated with some of the other conventional or renewable energy sources as shown in Fig. 4.4. Either the energy from all the energy sources is dumped on a common DC link, or both the AC and DC; power electronic converters play a role here. Fig. 4.4 shows the configuration of a hybrid energy system in which wind, biogas, and Genset are generating AC feeding the AC bus. On the other hand, solar PV, fuel cells, and the battery are giving DC to the DC bus. The power generated from solar PV and fuel cells is first converted into the required voltage of the DC bus. In between AC and DC buses, there exists a bidirectional inverter that is used to perform both AC-DC and DC-AC conversion.

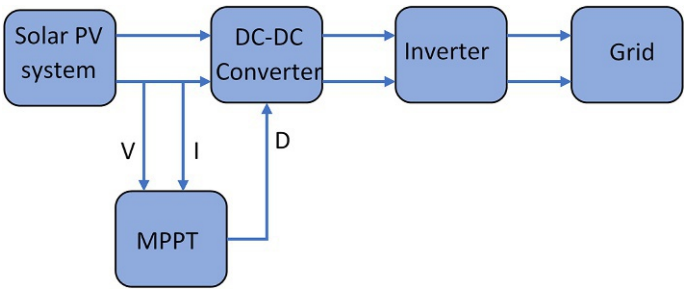

FIG. 4.3 Application of power electronics in a solar photovoltaic system.

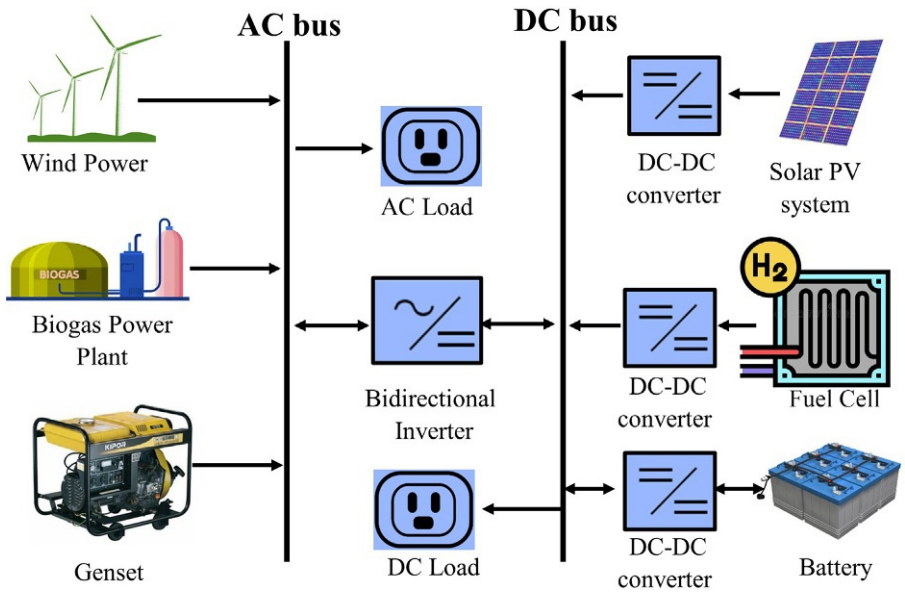

FIG. 4.4 Application of power electronics in hybrid renewable energy systems.

4.2.3 Wind energy system

The operation of the synchronous generators with the wind turbine becomes challenging with varying wind speed. When the wind speed varies, the turbine rotation speed and the rotation speed of the rotor also vary. The variable output is achieved at the terminals of the synchronous generator. A schematic diagram of a synchronous generator under variable wind speed is shown in Fig. 4.5. The three-phase output of the synchronous generator is first passed through the power electronics converters. The converter consists of two back-to-back rectifiers and an inverter in series. The rectifier converts the variable AC into constant DC and the inverter inverts the constant DC into constant AC. Diodes and thyristors in the rectifier and inverter generate harmonic and generate fluctuations through the DC link [2]. A DC link capacitor is used at the output of the rectifier and acts as a buffer between the rectifier and inverter.

The frequency of the generator varies with variations in the wind speed. Whatever the frequency of the generator is, its AC output is first rectified into DC and then, by using an inverter, this DC is converted into AC of a constantly desired frequency. The use of a power electronic rectifier and inverter with the doubly fed induction generator and wind turbine is shown in Fig. 4.6.

4.2.4 Electric and hybrid vehicles

Power electronics have revolutionized the electric vehicle application. Fig. 4.7 shows the architecture of an electric vehicle. This electric vehicle consists of a fuel cell as the energy source consuming hydrogen. The output voltage of the fuel cell is first conditioned using a DC-DC boost chopper and fed to the common DC link [3]. The energy storage system

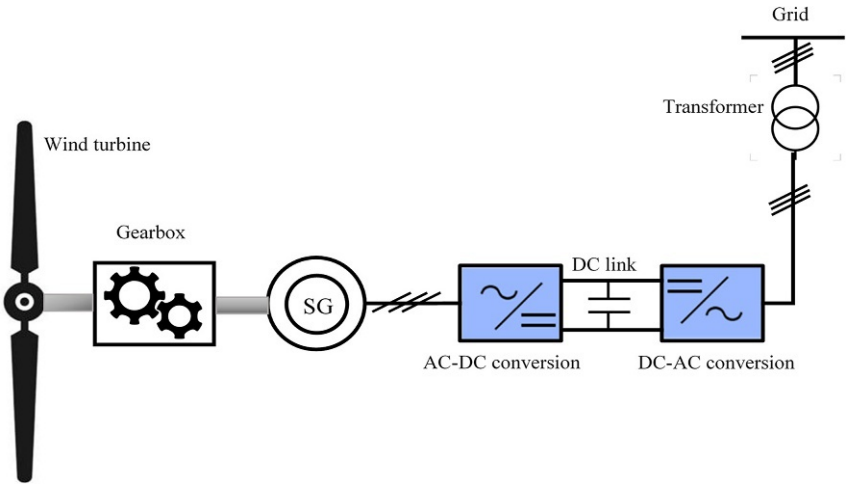

FIG. 4.5 Application of power electronics converters in the synchronous generator-based wind energy system.

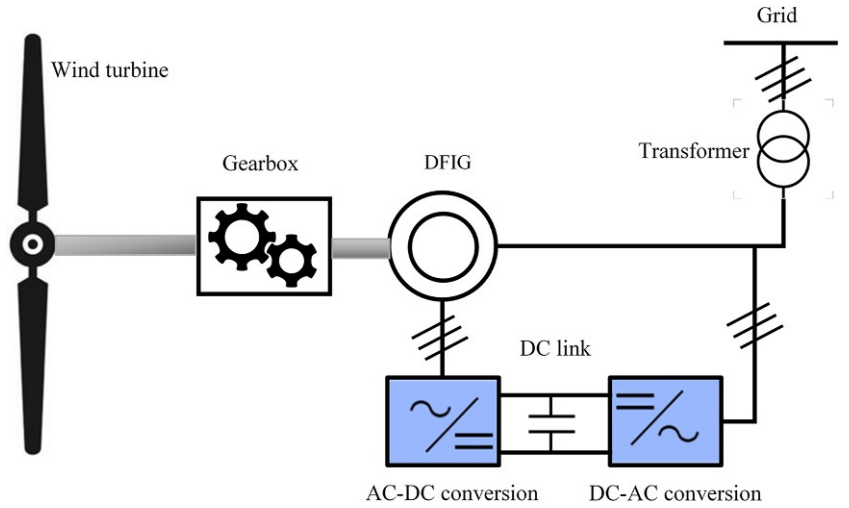

FIG. 4.6 Application of power electronics in double-fed induction generator-based wind energy system.

consists of a supercapacitor and batteries. Both the supercapacitor and the batteries are connected to the DC link through bidirectional converters. The electric motor is integrated into the DC link through the DC-AC inverter to operate the electric motor.

4.2.5 Fuel cell

The application of the power electronics devices and converters is significant in low voltage, low current densities, and unstable production of power from fuel cells for standalone or portable applications. For practical application of the fuel cell, a power conditioning unit is

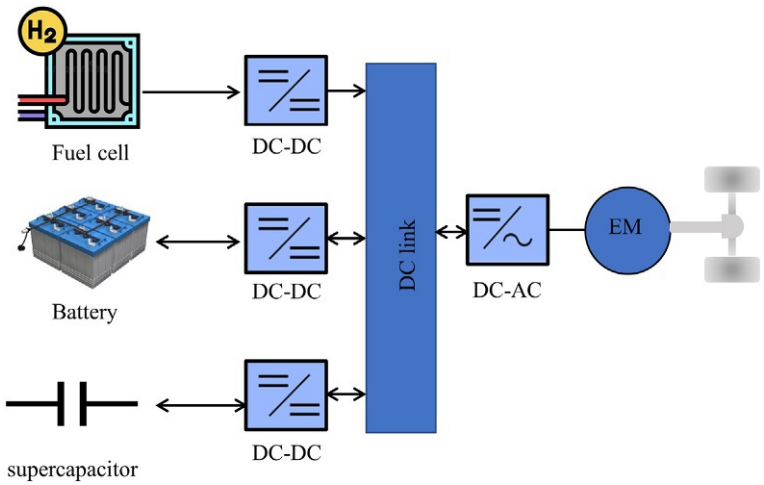

FIG. 4.7 Application of power electronics in electric vehicles and hybrid electric vehicles.

required to maintain the output voltage to a level that can be fed to the load. These power conditioning units may include any type of converters. The most used converters are buck converters and boost converters. Depending upon the nature of the load, the fuel cell is integrated with the DC-DC converter if the load is DC. If the load is AC, an inverter is integrated with the fuel cell. Two topologies are used in fuel cells: single-stage topology and multistage topology. In a single-stage topology, the output voltage from the fuel cell is either directly converted to DC for DC applications or into AC for AC applications, as shown in Fig. 4.8.

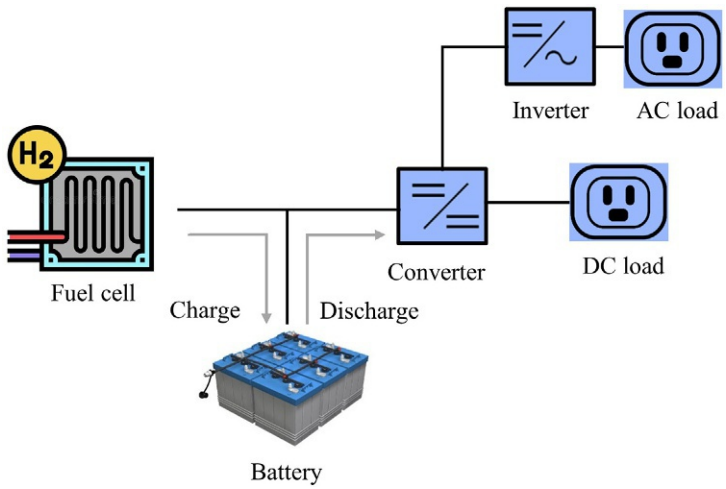

FIG. 4.8 Application of power electronics in fuel cell energy system.

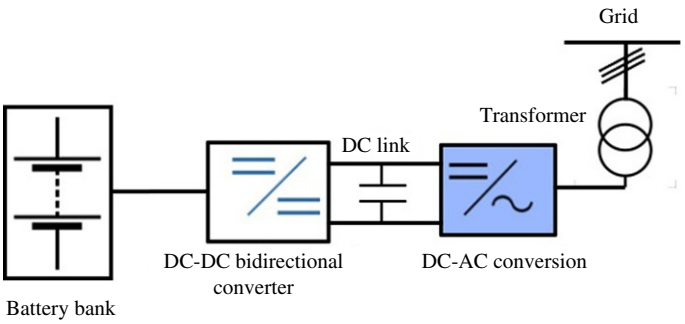

FIG. 4.9 Application of power electronics in a battery energy storage system.

4.2.6 Power electronics in the battery storage system

Fig. 4.9 shows the application of the power electronics converters and inverters in battery energy storage systems. The battery is directly connected to the bidirectional DC-DC converter to step up or step down the DC voltages. When the battery is in the discharging mode, the DC-DC converter works in the step-up mode to boost the battery voltages to the grid voltage. The inverter then converts the DC into AC and feeds the grid through the passive filter.

4.2.7 Electric drives

In industrial and domestic applications, speed controls of the motors is a major requirement of the various processes like pumps, machine tools, robots, washing machine, milling machine, transport, fans, etc. Fig. 4.10 shows the block diagram of the general electric drive system consisting of the following elements.

(a) Power source

For low voltage applications single-phase drives are used and for high voltage applications, three-phase drives are preferred.

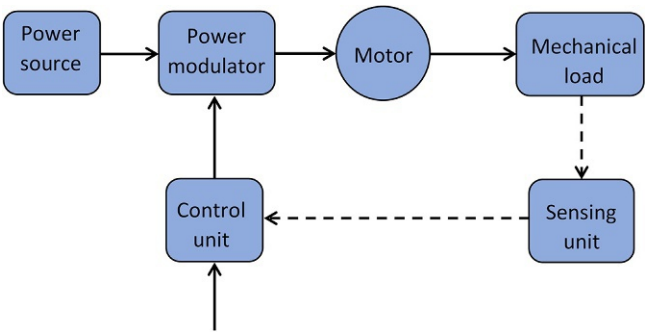

FIG. 4.10 Application of power electronics in electric drives.

(b) Power modulator

Power modulators are used to control the power from the source to the load in a way that the torque-speed characteristics of the motor are observed. When the motor is started, or braking, or when the rotation of the motor is reversed, there are transients in the system which limit the motor and source voltages within the allowed permissible range. The mode of the operation of the motor like starting, braking, and reverse rotation is performed with the help of power modulators. Power modulators also conditioned the electrical energy to the form required by the motor. Any one of the following power electronic components could be a power modulator:

i. controlled rectifiers for AC to DC conversion;
ii. inverters for DC to AC conversion;
iii. DC-DC converters for stepping up or stepping down the DC voltage level; or
iv. cycloconverters for changing frequency from AC power to AC.

(c) Electrical motors

DC motors, AC motors, and some special motors are used for speed controlling mechanisms. DC motors include shunt motors, series motors, compound motors, long shunt motors, short shunt motors, and separately excited DC motors. AC motors include induction motors, synchronous motors, and wound rotor motors. Special motors include brushless DC motors, servo motors, and stepper motors.

(d) Sensing unit

The sensing unit consists of one of the following sensors taking the reading from the motor and giving feedback to the control circuit:

i. temperature sensing;
ii. speed-sensing;
iii. position sensing;
iv. torque-sensing; and
v. voltage and current sensing.

(e) Control unit

The control unit contains the implementation of the control circuit for the power modulator. The control unit takes the feedback from the sensing unit and implements the power conditioning to give signal to the power modulator, which consists of the power electronics components.

4.3 Solid-state devices

4.3.1 Construction of SCR

Thyristors are also known as silicon-controlled rectifiers (SCRs). These consist of three junctions (J_1, J_2, J_3), four layers (P-N-P-N), and three terminals. The terminals are called the

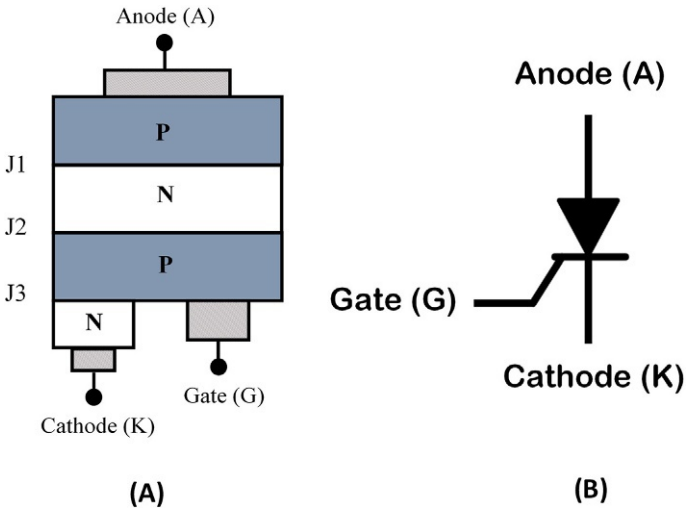

FIG. 4.11 (A) Construction diagram of the thyristor and (B) symbolic representation of thyristor.

anode (A), cathode (K), and gate (G). SCRs are extensively used in power electronics inverters, converters, rectifiers, cycloconverters, energy storage systems, and hybrid energy systems. In power electronics, SCRs are used as fast switching devices. An SCR can operate in three different modes: forward conduction mode, forward blocking mode, and regenerative mode. An SCR works in a forward blocking mode when the anode terminal is at positive potential and the cathode is at negative potential and there is no signal on the gate terminal. If the SCR is in forward blocking mode and a gate signal is provided at the gate, the SCR goes into forward conduction mode. A symbol and layer diagram of the SCR with its terminals, junctions, and layers is shown in Fig. 4.11. The layered diagram shows that SCR is a P-N-P-N device whose upper P-layer is connected to the anode terminal, the lower P layer is connected to the gate terminal, and the lower N layer is connected to the cathode terminal [4].

4.3.2 Two transistor model of SCR

A two transistor model of SCR is shown in Fig. 4.12. which describes the complete interpretation of the SCR working. Two transistors are coupled in a way that the p terminal of Q_1 is coupled to the p-terminal of Q_2. The base of Q_1 (n-terminal) is coupled to the collector of Q_2 (n-terminal). Similarly the base of Q_2 (p-terminal) is coupled to the collector of Q_1 (p-terminal). The junction of both p-terminals is called the gate terminal of the SCR through which its switching is controlled. Briefly, the base of each transistor is coupled to the collector of the other transistor. One leftover p-terminal which is an emitter of Q_1 is deemed as the anode and the one leftover n-terminal which is an emitter of Q_2 is deemed as the cathode.

4.3.3 Turning SCR ON

To understand the turn-on and turn-off process of the SCR, it is inevitable to have a detailed knowledge of the holding current and the latching current. Holding current is defined

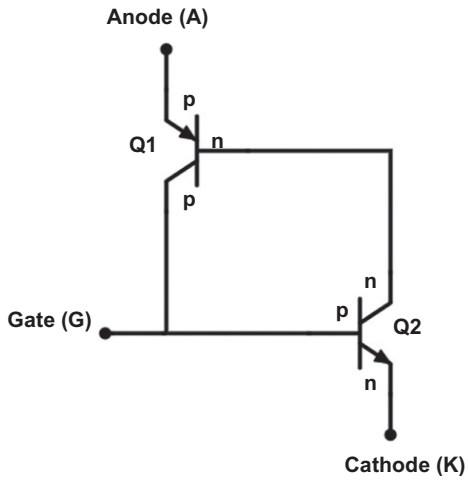

FIG. 4.12 Two transistor model of thyristor (SCR).

as the minimum value of the anode current which is necessary to be present to keep the thyristor in forward conduction mode. If the anode current reduces and becomes less than the holding current, the thyristor will go into forward blocking mode.

Latching current is identified as the lowest possible value of the anode current which is necessary to pass through the thyristor to turn it on even after the gate signal is eliminated. If the value of the current passing through the anode is greater than the latching current, the thyristor will remain in conduction regardless of the existence of the controlling signal at the gate. If the anode current is below the latching current, the removal of the gate signal will stop conduction through the thyristor. Table 4.1 shows a brief comparison of the holding and latching current.

(a) Turning the SCR on by light

The thyristor can be turned on by allowing the light to fall on the junction of the thyristor since it increases the electron-hole pairs in the junction.

TABLE 4.1 Comparison between latching current and holding current.

Sr. no.	Latching current	Holding current
1	Minimum values of the anode current below which thyristor is turned off on the removal of the gate signal.	The minimum value of the anode current below which thyristor goes into forward blocking mode.
2	It is associated with the turn-on process of the SCR thyristor.	It is associated with the turn-off process of the SCR thyristor.
3	The value of the latching current is greater than the holding current.	The value of the holding current is smaller than the latching current.

(b) Turning the SCR on by thermal energy

The electron-hole pairs in the wafer or the substrate (a thin slice of semiconductor) of the thyristor material can be increased by increasing the temperature of the material. The increased temperature increases the leakage current through the SCR, which could be enough to initiate the regenerative process and turn on the thyristor. This method of turning on the thyristor is normally avoided, since it may damage the thyristor due to excessive heat.

(c) Turning the SCR on by high $\frac{dV}{dt}$

When the thyristor is in forward blocking mode, the junction J_1 and J_3 are forward biased and junction J_2 is reverse biased. Hence the wafer behaves as a capacitor with J_1 and J_3 as conducting plates and the junction J_2 as the dielectric. Instead of increasing the forward voltage across the SCR, it can be turned on just by increasing the rate of change of applied voltage. However, this method of turning on the thyristor is also avoided because it creates large voltage spikes across the thyristor, which may damage the SCR.

(d) Turning the SCR on by increasing forward voltage

In this method of turning the SCR ON by increasing the forward biasing voltage, the gate terminal is kept open and no signal at the gate is applied to take it to the forward conduction mode due to which neither Q_1 nor Q_2 are ON. Emitter-base junction and the collector-base junction of both of the transistors Q_1 and Q_2 are forward biased and reverse biased, respectively, by applying a voltage of high polarity at the anode and relatively less polarity at the cathode. In this condition, both transistors Q_1 and Q_2 are in the forward blocking mode and no current passes through the SCR since there are not enough charges to jump the depletion regions of the junction J_2. Leakage current of minute value passes through the reverse-biased junctions (collector-base junction) of both the transistors Q_1 and Q_2, and this small amount of current cannot take the transistors from forward blocking mode to the forward conduction mode. The total current that passes through the SCR is the sum of the base and collector current of the transistor Q_2given as ($I_{E2} = I_{B2} + I_{C2}$). The conduction of the full current from the anode to the cathode is stuck by the depletion region of the junction J_2, since it is still reverse biased, though the junction J_1 and J_3 are forward biased.

After applying the forward-biasing voltage at the anode and cathode, the voltage at the anode is increased, which increases the number of charge carriers at the junction J_2 and increases the collector current of Q_1 (leakage current), which is also the same current passing through the base of Q_2. If the leakage current through the collector of Q_1 is made large enough, a significant amount of current passes through the base of Q_2. The increased base current of Q_2 increases the collector current of Q_1, which is also the base current of Q_1. To make this process happen, we need to increase the forward voltages at the anode. This is the point where the regenerative process starts in which the transistor Q_1 helps the conduction through transistor Q_2, and conduction through transistor Q_2 helps the conduction through transistor Q_1. This helping process is called the regenerative switching process. The voltage at which the regenerative process of transistors starts is called the forward break over voltage (V_{BR}). Once the break over voltage is applied across the thyristor, the junction J_2 breaks, conduction starts through the SCR from the anode to the cathode, and the voltages across the thyristor drop. The whole process and the forward blocking region, forward conduction region, and regenerative regions are shown in Fig. 4.13. The conduction through the SCR is maintained until the

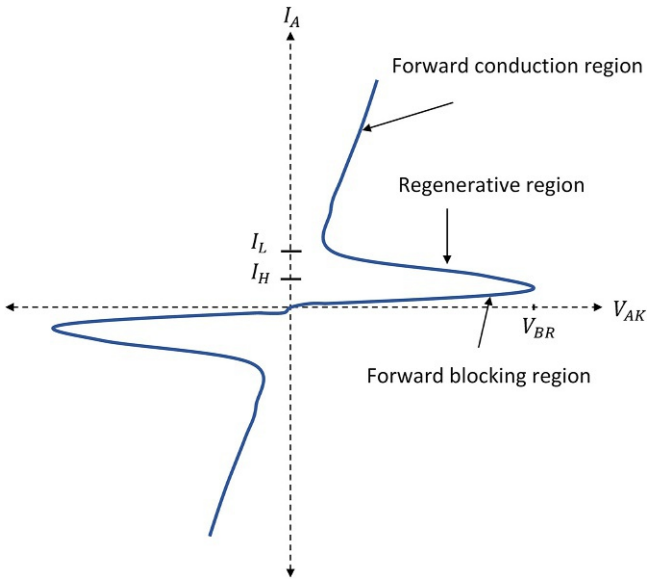

FIG. 4.13 Characteristic curve of the thyristor (SCR) showing working regions and holding and latching current.

current passing through it is greater than the holding current. If the anode current is reduced below the holding current as shown in Fig. 4.13, the SCR will somehow come to the forward blocking mode where the conduction stops and the device is OFF.

(e) Turning the SCR on by triggering

The other way of turning the SCR ON is using the gate terminal. Instead of increasing the anode voltage across the SCR, a short pulse is applied at the gate terminal which increases the number of charge carriers at the depletion region of the junction J_2. The instant gate signal is applied, J_2 breaks, and the conduction starts without the application of break over voltage. The device goes into the forward conduction mode from the forward blocking mode. Once the current through the SCR is greater than the latching current, the device is called latched and it stays in the forward conduction mode. There is no need to maintain the signal at the gate. After latching, the gate signal is removed. The relation between the gate current (I_G) and break over (V_{BR}) voltage is shown in Fig. 4.14. If the amount of gate current is further increased, conduction starts earlier and fewer voltages appear across the SCR.

4.3.4 Turning the SCR off or the SCR commutation circuit

(a) Line commutation

Line commutation is also termed natural commutation, and involves commutation being done by the AC source itself. It is known that in an AC signal, because of the nature of the AC signal, the current becomes zero once in every cycle. During the negative cycle of the input supply, the SCR goes into reverse mode regardless of the existence of the gate signal. Fig. 4.15A shows the line commutation circuit and the waveforms are shown in Fig. 4.15B. The turn-off time of the SCR is given in its datasheet. If the time of application of the AC source

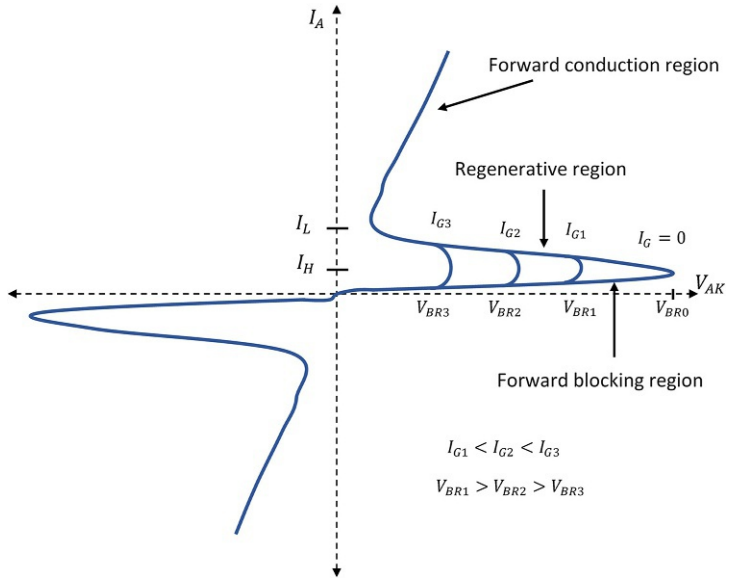

FIG. 4.14 SCR triggering curves showing the relation between break over voltage and gate current.

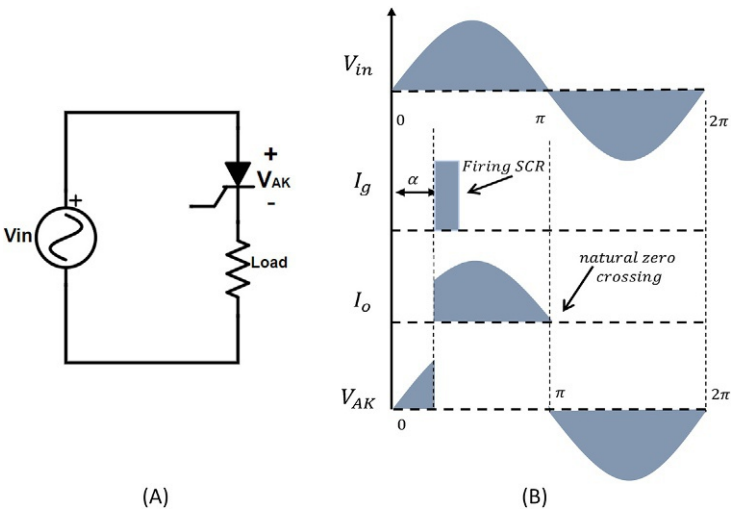

FIG. 4.15 (A) Line commutation circuit of SCR and (B) graphical representation of line commutation.

during the negative half cycle is greater than the SCR turn-off time, the SCR will turn off. Line commutation is used in controlled rectifiers, cycloconverters, and inverters. The following information can be deducted from the waveform shown in Fig. 4.15B.

- **i.** A thyristor is fired at an angle α of the input supply.
- **ii.** Since the nature of the load is resistive, the load current or the SCR current follows the input current waveform, following the turn-on and turn-off of the thyristor.

iii. When the first zero crossing of the input AC signal is reached, the polarity of the voltage across the thyristor is reversed, which reverse biases the thyristor, and the load current or the SCR current becomes zero.

iv. If the time of the reverse biasing of the SCR is greater than the turn-off time of the SCR, the current through the SCR will be smaller than the holding current and the SCR will be turned off.

(b) Forced commutation

Forced commutation is implemented when the input voltage is a DC and there is no natural zero crossing. In forced commutation, an external auxiliary circuit is required to bring the SCR current below the holding current and keep it in the reverse biasing mode for some time greater than the SCR turn-off time. The following techniques of forced commutation are used.

(i) Class A—self or load commutation

Load commutation or self-commutation is also known as the class A commutation of the thyristor. If the SCR is connected in a forward mode, it would not conduct since the gate signal is absent. To turn off the SCR, its anode current must fall below the holding current and sustain its reverse blocking state for sufficient time so that SCR gets its blocking state. The circuit diagram of the load commutation is shown in Fig. 4.16. On the application of the gate signal, the SCR starts conducting and the capacitor starts charging. When the capacitor is fully charged to its peak or equal to the input voltage, the polarity of the inductor is reversed. The reverse polarity decreases the flow of current and as soon as the current falls below the holding current, the thyristor is turned off. The energy stored in the capacitor is dissipated through the load.

(ii) Class B—resonant pulse commutation

The class B commutation circuit is also termed resonant pulse commutation and differs slightly from class A. In class A commutation, inductor capacitor (LC) resonant circuit is connected in series to the thyristor, whereas in class B commutation circuit, an LC resonant circuit is connected in parallel to the thyristor. The full load current does not flow through the SCR. The circuit diagram of the class B resonant pulse commutation is shown in Fig. 4.17.

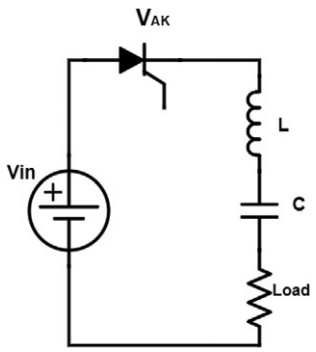

FIG. 4.16 Class A—self or load commutation circuit.

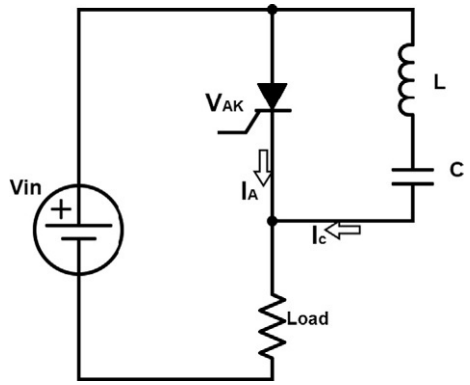

FIG. 4.17 Class B—resonant pulse commutation circuit.

When the input voltage is applied across the SCR, it remains in forward blocking mode unless the gate signal is applied. As the gate signal is applied, SCR comes in forward conduction mode and the current is divided into two parts. Now a constant current flows through the load and a sinusoidal resonant current passes through the LC circuit that charges the capacitor with the reverse polarity of the voltage. This reverse voltage also appears across the thyristor, bringing the thyristor into reverse mode, and the anode current though the thyristor falls below the holding current, turning the thyristor off.

(iii) Class C—complementary commutation

Class C commutation, also known as complementary commutation, is shown in Fig. 4.18. The circuit consists of two thyristors. One is the main thyristor and the other is the auxiliary thyristor. Thyristor T_1 is used to turn off the thyristor T_2 and T_2 is used to turn off the thyristor T_1; that is why this is called a complementary commutation circuit. Initially, when the gate signal is not provided, both thyristors are in reverse blocking mode and the voltage across

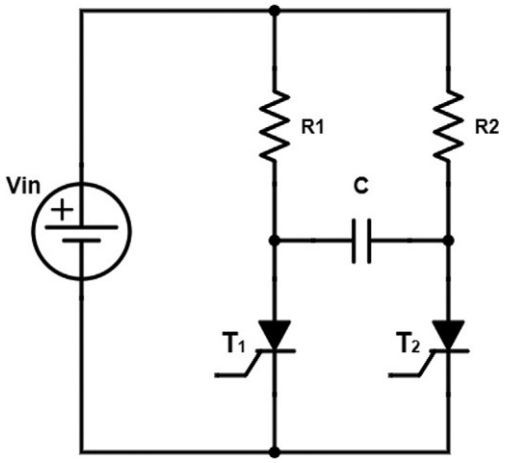

FIG. 4.18 Class C—complementary commutation circuit.

the capacitor is zero. On application of the gate signal to the main thyristor T_1, the current starts flowing through the two paths. One path is through R_1 and T_1 and the other path is through R_2, C, and T_1. The load current passes through the first path and then through the second path capacitor starts charging with a positive polarity on the right side plate and negative polarity on the left side plate.

To turn off the main thyristor, the auxiliary thyristor needs to be on. When the auxiliary thyristor T_2 is turned on by applying a gate signal, the current starts flowing through R_1, C, and thyristor T_2; as a result, the reverse polarity of the current through the thyristor T_1 turns it off. The switching on and switching off the process of T_1 and T_2 repeats.

(iv) Class D—impulse commutation

Like the class C commutation circuit, the class D commutation circuit also known as the impulse commutation consists of two thyristors. The circuit of the impulse commutation is shown in Fig. 4.19. Thyristor T_1 is the main thyristor and the close-loop consisting of the thyristor T_2, a diode, and the inductor make a commutation circuit. Initially, both the thyristors are off and the voltage across the capacitor is initially zero, which can be understood by the application of the gate signal to the T_2. When the gate signal is applied to T_2, it starts conducting the current to the load, and the capacitor gets charged with a positive polarity on the upper plate and negative polarity on the lower plate. The reverse polarity of the voltage across the capacitor will turn off the thyristor T_2.

Now the gate signal is applied to the gate of the thyristor T_1 and a current follows the path V_{in}, T_1, load, V_{in}. On the other hand, a current flows in the commutating loop in a path C+, T_1, L, D, C−. In this loop, the capacitor is fully discharged and starts charging again in the reverse direction such that the upper plate is negatively charged and the lower plate is positively charged. Now, the capacitor does not discharge again in this loop because of the reverse biasing of the diode. Now the SCR T_2 is turned on by a gate signal and the capacitor discharges through C+, T_2, T_1, and C−. When the discharging current of the capacitor increases the load current, SCR T_1 is off. The capacitor again starts charging and the process repeats itself.

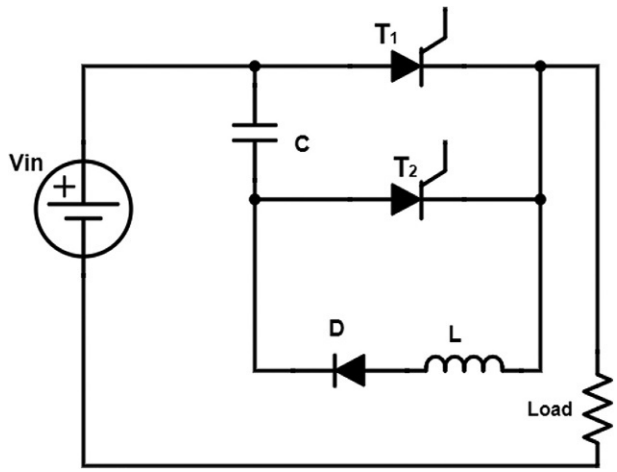

FIG. 4.19 Class D—impulse commutation circuit.

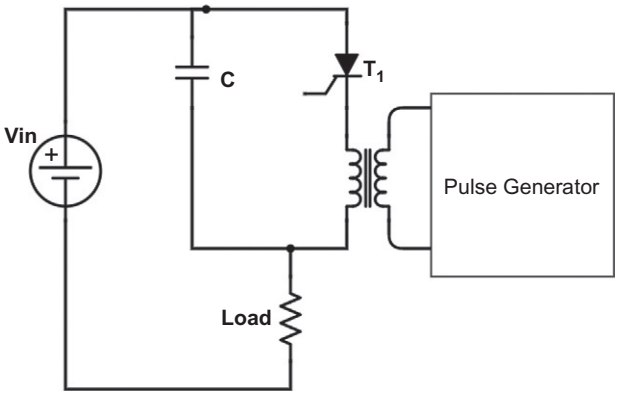

FIG. 4.20 Class E—external impulse commutation circuit.

(v) Class E—external impulse commutation

Fig. 4.20 shows the circuit diagram of the class E commutation circuit, also known as external impulse commutation. In this method of commutation, a pulse from an external source is applied to reverse bias the thyristor. For this reason, this method is also known as the external pulse commutation. To commutate the thyristor T_1, a pulse through a pulse transformer is applied for a duration equal to or slightly greater than the turn-off time of the thyristor. The pulse transformer is designed in such a way that the primary and secondary windings are tightly coupled, and there is a small air gap between both the windings to avoid the saturation on the application of the pulse during commutation. The complete operation of the commutation circuit can be understood in the following two modes.

- **Mode 1:** when the input voltage is applied, the thyristor is in forward blocking mode unless the gate signal is applied. When the gate signal is applied, T_1 goes into forward conduction mode and the current follows the path $V_{in}+$, T_1, primary of the pulse transformer, load, and $V_{in}-$.
- **Mode 2:** when the thyristor is to off, a pulse to the primary of the pulse transformer is applied that induces a pulse in the secondary of the transformer. The induced voltage in the secondary appears as a reverse polarity across the thyristor, which reduces the current through the thyristor below the holding current.

4.3.5 Gate turn-off (GTO) thyristor

Another type of solid-state switch is the gate turn-off (GTO) thyristor. Like the SCR, the device consists of three terminals named anode, gate, and cathode. The extra feature of the device is controlling it through the gate terminal. It can be switched ON and OFF through the gate terminal. This extra feature of turning-off GTO is obtained by heavily doping the gate terminal with p material. A positive pulse is used at the gate terminal to turn on the GTO thyristor and a negative pulse is applied at the gate to turn it off. A symbol diagram and a layer diagram of the GTO thyristor are shown in Fig. 4.21.

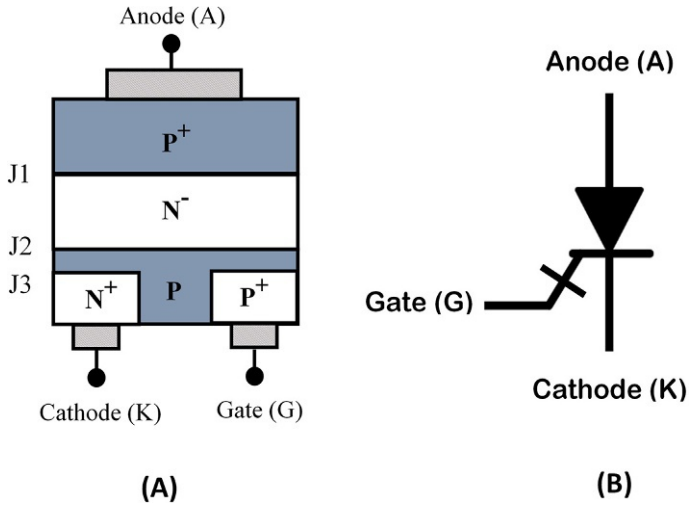

FIG. 4.21 (A) Construction and (B) symbolic representation of GTO thyristor.

4.3.6 Silicon-controlled switch (SCS)

The construction of a silicon-controlled switch (SCS) is the same as that of an SCR. The turn-on process of the SCS is the same as that of the SCR in that it can be turned on either by increasing the forward anode voltage or by applying a gate signal. It has an additional feature of turning the SCS on and off by the additional gate terminal. The SCS carries two gate terminals. One is the primary gate terminal, also known as the cathode gate since its location is close to the cathode terminal. The other gate terminal is known as the secondary gate terminal or the anode gate terminal since it is located close to the anode of the SCS. The cathode gate is the common point of the p-type collector of Q_1 and p-type base of Q_2, and the anode gate terminal is the common point of the n-type base of Q_1 and n-type collector of Q_2. Briefly stated, the cathode gate is p-type, and the anode gate is n-type. A structural diagram and the symbol of the SCS are shown in Fig. 4.22. and a two transistor equivalent model of the SCS is shown in Fig. 4.23.

An SCS can be turned on and turned off by both the primary gate and the secondary gate. It can be turned on by the cathode gate by applying a positive pulse since it is a p-type. An SCS can also be turned on by the anode gate by applying a negative pulse since it is an n-type. It can be turned off by the cathode gate by applying a negative pulse and can also be turned off by the anode gate by applying a positive pulse.

4.3.7 Diode for alternating current (DIAC)

A diode for alternating current (DIAC) consists of four layers, four junctions (J_1, J_2, J_3, and J_4), and two terminals (anode 1 and anode 2). A DIAC is a gateless device and has only two terminals, named anode 1 and anode 2. The p and n layers are stacked in such a way that there are two structures. One is the *pnpn* structure and the other is the *npnp* structure. The *pnpn* structure is like the structure of a gateless SCR and the *npnp* structure is like an inverted gateless thyristor. Both these structures are stacked together, making anode 1 and anode 2

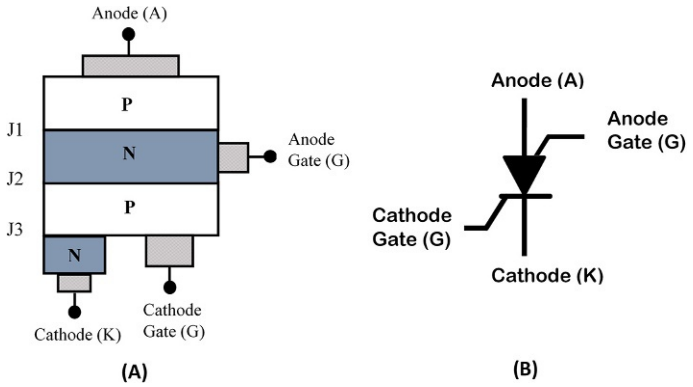

FIG. 4.22 (A) Construction and (B) symbolic representation of an SCS.

with no gate. In the layer diagram and symbol shown in Fig. 4.24, anodes are represented by A_1 and A_2.

A four transistor equivalent model of DIAC is shown in Fig. 4.25. It consists of four transistors named Q_1, Q_2, Q_3, and Q_4. The combination of Q_1 and Q_2 makes the SCR with no gate terminal and the combination of Q_3 and Q_4 makes an inverted SCR with no gate terminal. The positive emitter of Q_1 and the negative emitter of Q_3 are connected and this terminal is called anode 1. Similarly the negative emitter of Q_2 and the positive emitter of Q_4 are coupled and the terminal is called anode 2. The availability of both p-type and n-type at the two anodes makes the DIAC a bidirectional device. The polarity of the voltage at the anodes decides the direction of the flow of current. If the polarity of the voltage at anode 1 (A_1) is greater than the voltage at anode 2 (A_2), Q_1 and Q_2 are forward biased and the conduction starts from A_1 to A_2 through Q_1 and Q_2. Similarly, if the polarity at anode 2 is higher than at anode 1, the conduction starts from A_2 to A_1 through Q_4 and Q_3.

The characteristic curve between anode voltage and the current of a DIAC is depicted in Fig. 4.26. The first quadrant shows the conduction from A_1 to A_2 through Q_1 and Q_2. Similarly the third quadrant shows the conduction from A_2 to A_1 through Q_4 and Q_3.

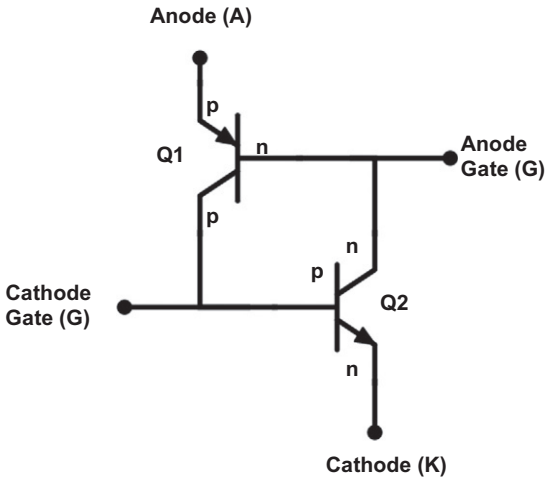

FIG. 4.23 Two transistor equivalent model of an SCS.

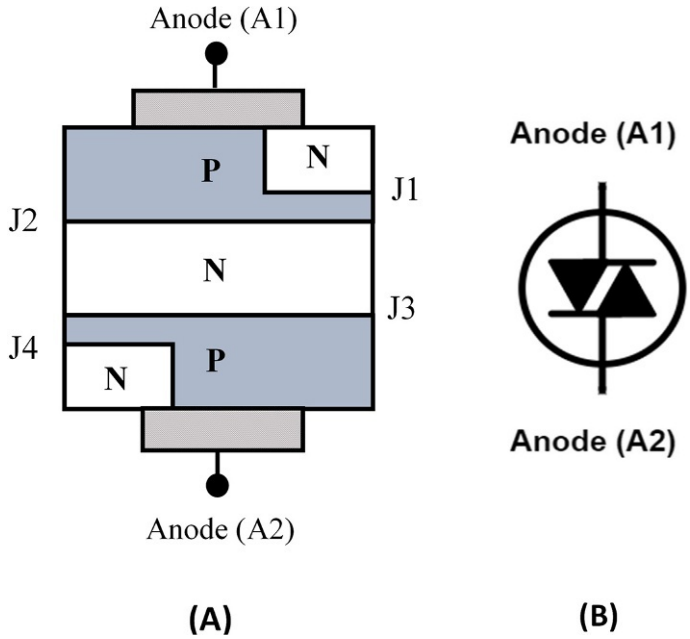

FIG. 4.24 (A) Structural diagram and (B) symbolic representation of DIAC.

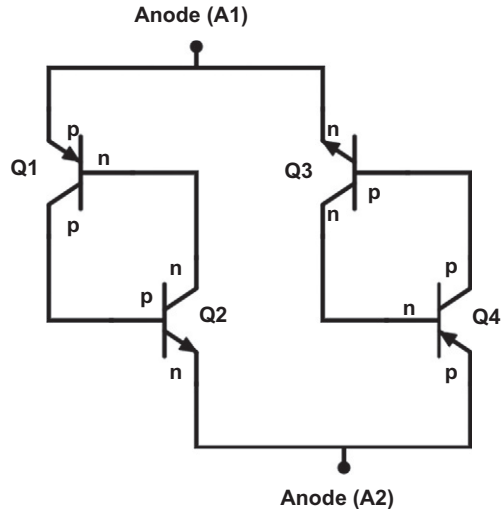

FIG. 4.25 Transistors-based equivalent model of DIAC.

4.3.8 Triode for alternating current (TRIAC)

The structural diagram of a triode for alternating current (TRIAC) is the same as that of a DIAC with an extra feature of the gate terminal. A layered diagram and the symbol of TRIAC are shown in Fig. 4.27. A transistor-based equivalent diagram of a TRIAC is shown in Fig. 4.28. Transistors Q_2 and Q_3 are the *npn* transistors with base p-type. The p-type base of both

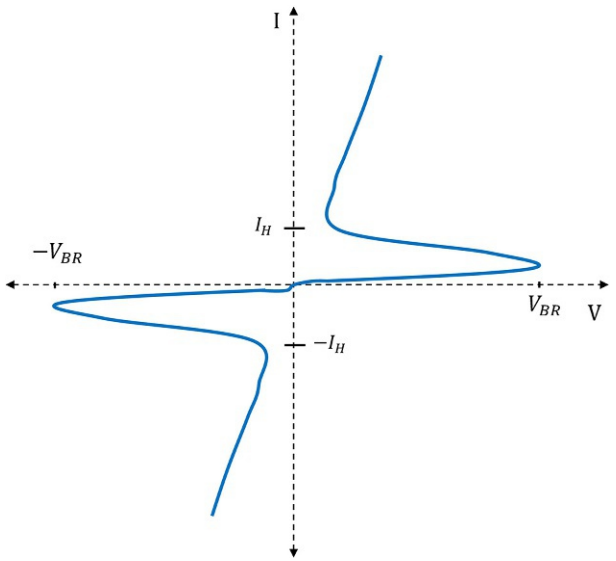

FIG. 4.26 Characteristic curve of a DIAC.

these transistors is connected, making the gate terminal. The direction of conduction is decided by the polarity of the gate with respect to the anodes. To start the conduction from A_1 to A_2, the first condition is to keep the polarity of anode 1 higher than anode 2. The second condition is to keep the polarity of the gate current higher than anode 2. Similarly, for the reverse conduction of current from anode 2 to anode 1, the polarity of anode 2 must be higher than anode 1. The second condition is to keep the polarity of the gate current higher than anode 1.

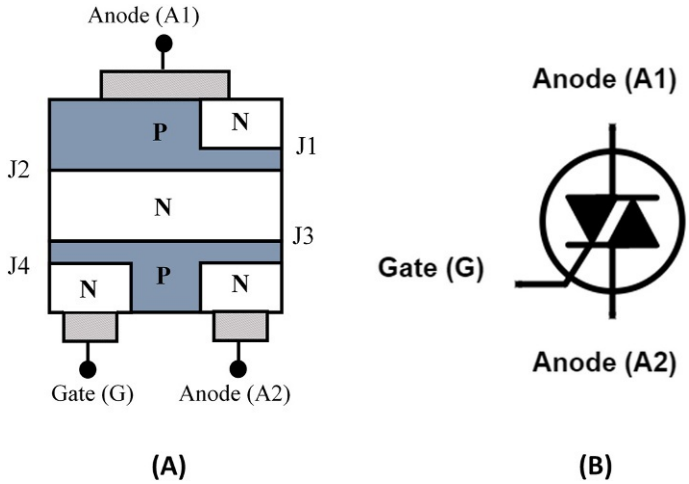

FIG. 4.27 (A) Construction and (B) symbolic diagram of TRIAC.

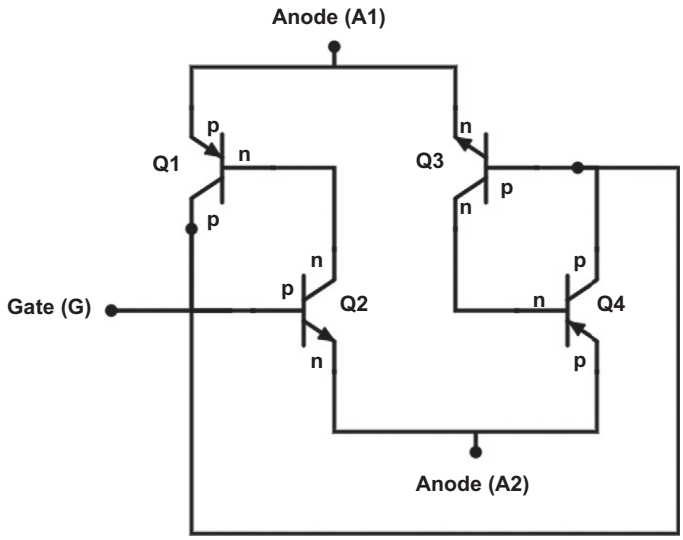

FIG. 4.28 Transistors-based equivalent model of a TRIAC.

A characteristics graph of a TRIAC is shown in Fig. 4.29. The first quadrant shows the conduction from A_1 to A_2 through Q_1 and Q_2. Similarly the third quadrant shows the conduction from A_2 to A_1 through Q_4 and Q_3.

4.4 Rectifiers (AC-DC converters)

Rectifiers are one of the major components or devices of the power electronics family performing the function of converting AC into DC. With respect to control, rectifiers are categorized as controlled or uncontrolled. In controlled rectifiers, a semiconductor-based solid-state device is used as the switching element, whereas in uncontrolled rectifiers, a simple diode is used to perform the rectification. The rectification process depends upon the polarity of the voltage across the switching element (thyristor or a diode).

4.4.1 Single-phase half-wave uncontrolled rectifier with resistive load

Rectifiers that use a diode as a switching element are termed uncontrolled rectifiers. The rectifier depicted in Fig. 4.30 has the diode as a switching element that does not has any gate terminal to control the switching period. The switching of this rectifier depends only upon the biasing of the diode. The diode is forward biased during the positive cycle of the input signal, and the device conducts and is reverse biased during the negative cycle of the input, blocking all the input voltage across itself.

The voltage of the input is shown in Eq. (4.1). The diode is forward biased when the voltage at the anode of the diode is positive in the first half cycle $(0-\pi)$. In this period, the diode conducts and all the input voltage appears across the load and no voltage (except the forward breakdown voltage, 0.7 V for silicon) appears across the diode as shown in Fig. 4.31. Similarly,

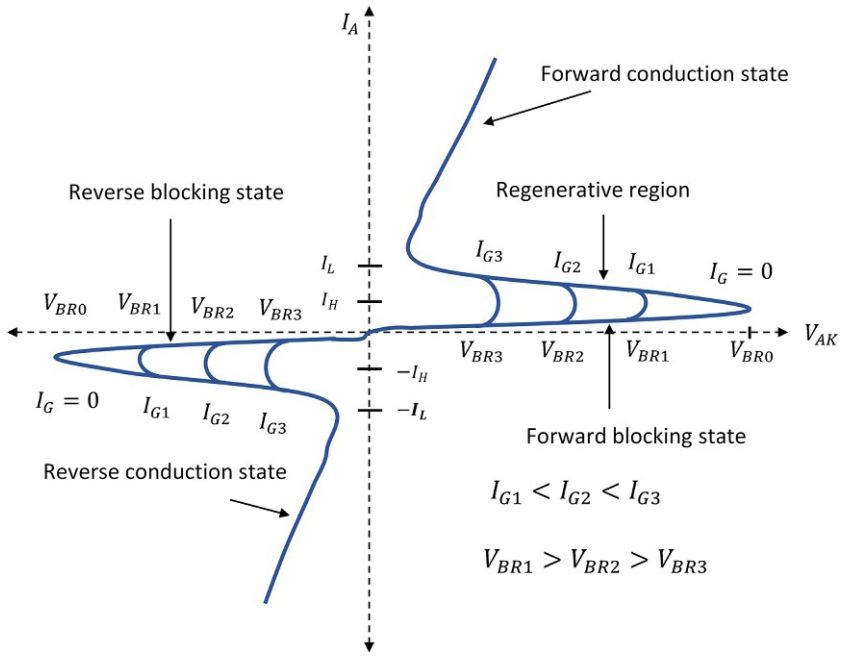

FIG. 4.29 Characteristic curves of a TRIAC showing triggering mechanism.

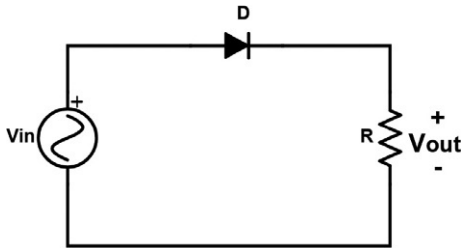

FIG. 4.30 Circuit of single-phase half-wave uncontrolled rectifier with resistive load.

the diode is reverse biased during the negative cycle of the input signal ($\pi - 2\pi$) and all the input voltage appears across the diode and no voltage appears across the load as shown in Fig. 4.31. The process remains the same for the next cycle. Eq. (4.1) shows the magnitude of the input voltage [5].

$$V_{in} = V_m \sin(\omega t) \tag{4.1}$$

The average output voltage is determined by using following equation, which states that the average output voltage of the single-phase rectifier is the division of the area under the curve of a complete cycle to the time period for that cycle.

$$V_{O(avg)} = \frac{Area\ under\ the\ curve}{T}$$

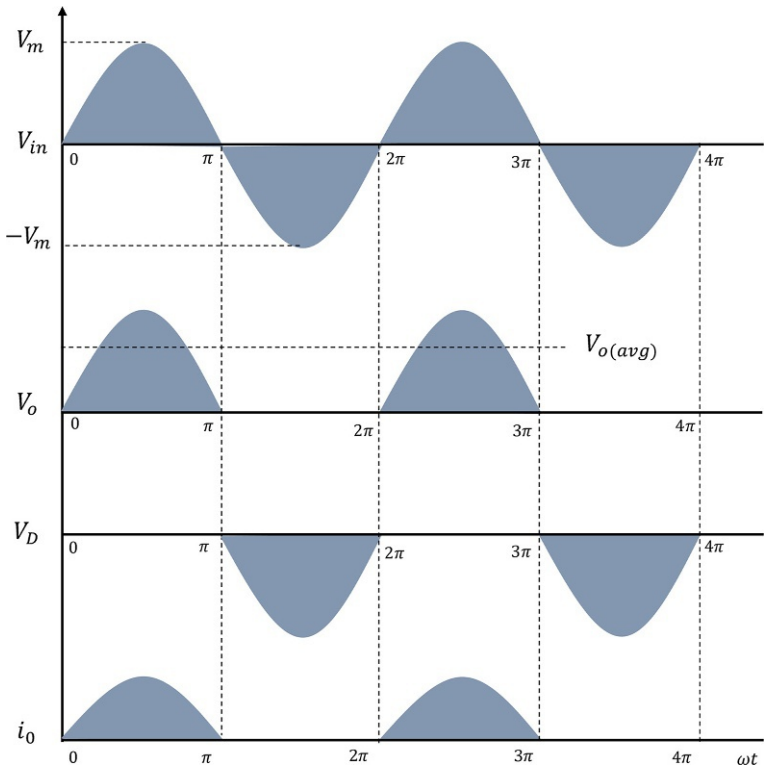

FIG. 4.31 Graphs of a single-phase half-wave uncontrolled rectifier (resistive load).

The other way of calculating the average output voltage is by integrating the one complete cycle of the output graph using Eq. (4.2). The output graph consists of a positive half cycle from ($0-\pi$), and no output from ($\pi-2\pi$). 2π is the time period of one complete cycle.

$$V_{O(avg)} = \frac{1}{2\pi}\int_0^{2\pi} V_{out}.d(\omega t) \tag{4.2}$$

$$V_{O(avg)} = \frac{1}{2\pi}\left[\int_0^{\pi} V_m \sin(\omega t).d(\omega t) + \int_{\pi}^{2\pi} 0.d(\omega t)\right]$$

$$V_{O(avg)} = \frac{V_m}{\pi} \tag{4.3}$$

Eq. (4.3) is used to determine the average output voltage of a half-wave uncontrolled rectifier. This average voltage is used to calculate the average current at the output by using Ohm's law and is given in Eq. (4.4).

$$I_{O(avg)} = \frac{V_{O(avg)}}{R}$$

$$I_{O(avg)} = \frac{V_m}{\pi R} \tag{4.4}$$

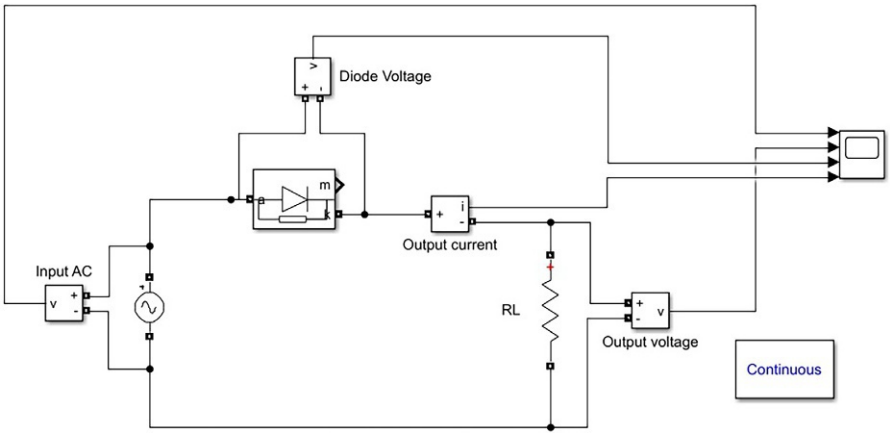

FIG. 4.32 MATLAB simulation circuit of single-phase uncontrolled half-wave rectifier with resistive load.

After getting the average value of voltage and current at the output of a half-wave rectifier, the output power can be determined by their multiplication, as shown in Eq. (4.5) for the resistive load.

$$P_{O\ (avg)} = V_{O(avg)} \times I_{O(avg)}$$

$$P_{O\ (avg)} = \left(\frac{V_m}{\pi}\right)^2 \cdot \frac{1}{R} \tag{4.5}$$

Fig. 4.32 is the MATLAB simulation circuit diagram of the single-phase uncontrolled half-wave rectifier connected to the resistive load. The outputs of the simulation shown in Fig. 4.33 can be compared to the outputs shown in Fig. 4.31.

4.4.2 Single-phase half-wave uncontrolled rectifier with inductive load

An inductive load-based half-wave uncontrolled rectifier is depicted in Fig. 4.34. Again the uncontrolled term is used because of the diode which is being used as a switching device and the load, in this case, is inductive. Since the load is an energy storing element, its graph will be different from the resistive load graph for both positive and negative input cycles. The diode is forward biased during the positive cycle of the input signal $(0-\pi)$, and the device conducts and is reverse biased during the negative cycle of the input $(\pi-2\pi)$, blocking all the input voltage across itself. During the positive half cycle, the inductor stores energy in the magnetic field in five time constants. As soon as the polarity of the input voltage is changed, the inductor takes some time to reverse the polarity across it and continues charging in the same direction until the angle ϕ even the negative half cycle of the input starts. The diode in the negative half cycle is reverse biased and it blocks all the input voltage at the output, we have only inductor stored energy as shown in Fig. 4.35, which explains the input AC voltage, the inductive behavior at the output, the voltage across the diode, and the output current.

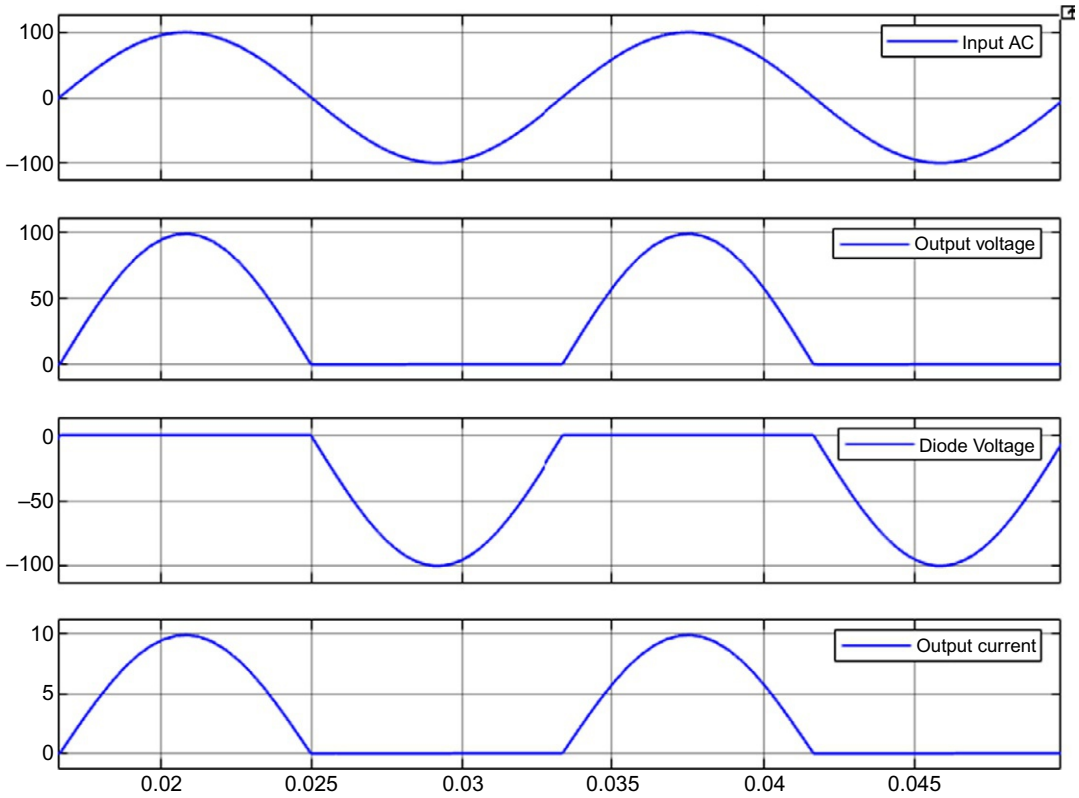

FIG. 4.33 Simulated outputs curves of single-phase half-wave uncontrolled rectifier with resistive load.

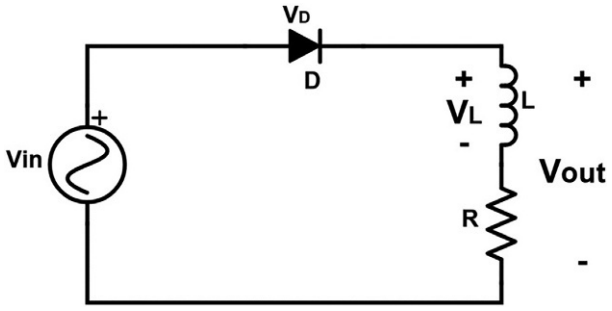

FIG. 4.34 Circuit of uncontrolled single-phase and half-wave rectifier (inductive load).

$$V_{in} = V_m \sin(\omega t)$$

The average output voltage is determined by using Eq. (4.6), which states that the average output voltage of the single-phase rectifier is the division of the area under the curve of a complete cycle to the time period for that cycle.

$$V_{O(avg)} = \frac{Area\ under\ the\ curve}{T} \tag{4.6}$$

The other way of calculating the average output voltage is by integrating the one complete cycle of the output graph using Eq. (4.7). The output graph is from $(0-\theta,$ and $\theta-2\pi)$ where $\theta=\pi+\phi$, and there is no output signal from $(\theta-2\pi)$. 2π is the time period of one complete cycle.

$$V_{O(avg)} = \frac{1}{2\pi}\int_0^{2\pi} V_{out}.d(\omega t) \tag{4.7}$$

$$V_{O(avg)} = \frac{1}{2\pi}\int_0^{\theta} V_m \sin(\omega t).d(\omega t) + \int_{\theta}^{2\pi} 0.d(\omega t)$$

$$V_{O(avg)} = \frac{V_m}{\pi}\left(\frac{1-\cos\theta}{2}\right) \tag{4.8}$$

The average voltage is given in Eq. (4.8) is used to calculate the average current at the output by using Ohm's law, and is given by Eq. (4.9).

$$I_{O(avg)} = \frac{V_{O(avg)}}{R}$$

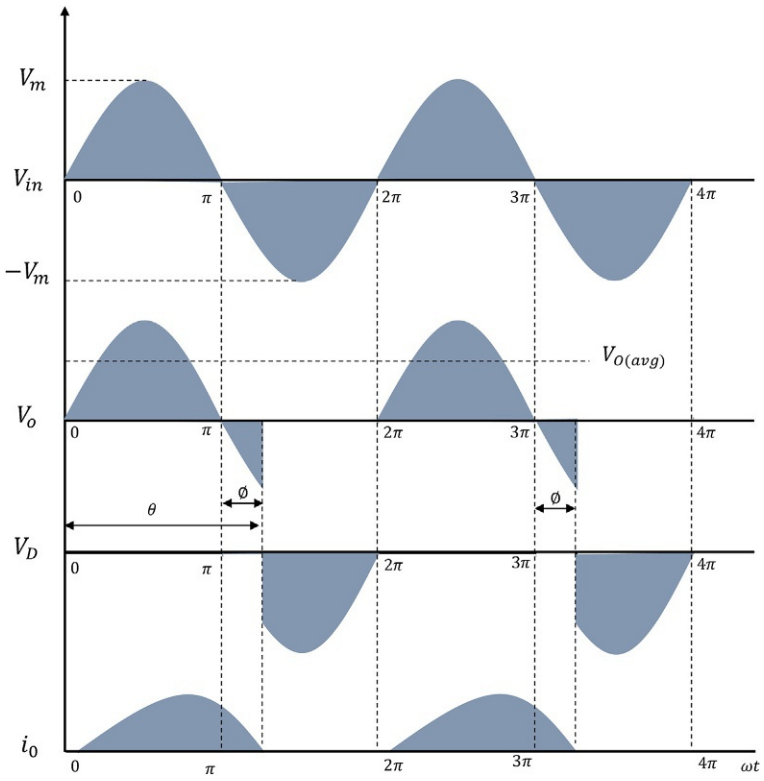

FIG. 4.35 Waveforms of uncontrolled single-phase and half-wave rectifier (inductive load).

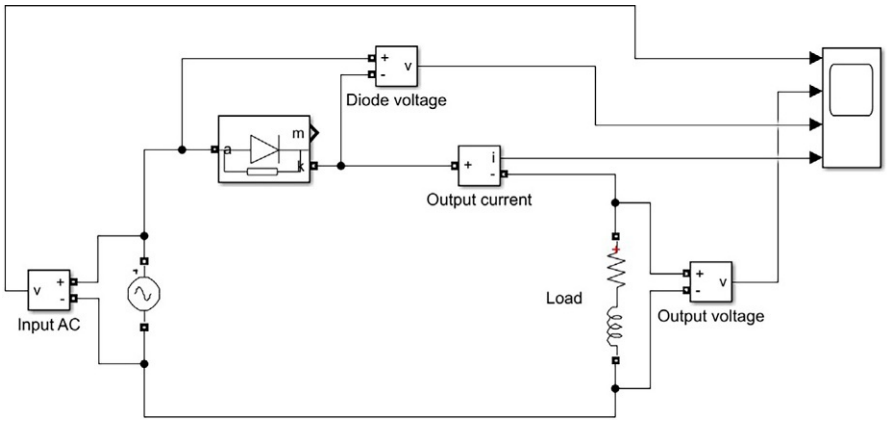

FIG. 4.36 MATLAB simulation circuit of uncontrolled single-phase half-wave rectifier (inductive load).

$$I_{O(avg)} = \frac{V_m}{\pi R}\left(\frac{1-\cos\theta}{2}\right) \tag{4.9}$$

After obtaining the average value of voltage and current at the output of a half-wave rectifier, the output power can be determined by their multiplication, as shown in Eq. (4.10) for the inductive load.

$$P_{O\ (avg)} = V_{O(avg)} \times I_{O(avg)}$$

$$P_{O\ (avg)} = \frac{{V_m}^2}{\pi^2 R}\left(\frac{1-\cos\theta}{2}\right)^2 \tag{4.10}$$

Fig. 4.36 shows the MATLAB simulation circuit diagram of the single-phase uncontrolled half-wave rectifier connected to the resistive load. The outputs of the simulation shown in Fig. 4.37 can be compared to the outputs shown in Fig. 4.35.

4.4.3 Single-phase uncontrolled half-wave rectifier with inductive load and freewheeling diode

The energy stored in the inductive load in the negative half cycle of the input voltage appears across the load even though the polarity of the input voltage has been changed. With the change in polarity of the input voltage, the diode must be reverse biased, but it continues conducting until the angle ϕ. This undesired behavior of the inductor in the rectifier is overcome by introducing a parallel diode known as the freewheeling diode [6,7]. A freewheeling diode is connected in parallel to the inductive load, as shown in Fig. 4.38.

The waveforms of the rectifier after the application of the freewheeling diode are shown in Fig. 4.39, and it is evident that after using the freewheeling diode, the rectifier behaves like the one for the resistive load. The complete input cycle is conducted through the diode and the negative cycle is dropped across the diode. The current at the output is the sum of two currents, i_{d1} and i_{d2}. The current passing through the diode during the positive half cycle when it is forward biased is termed as i_{d1} and when the diode becomes reverse biased and the energy stored in the inductor dissipates through the freewheeling diode. The current that passes through the freewheeling diode in the negative cycle is called i_{d2} or i_{FWD}.

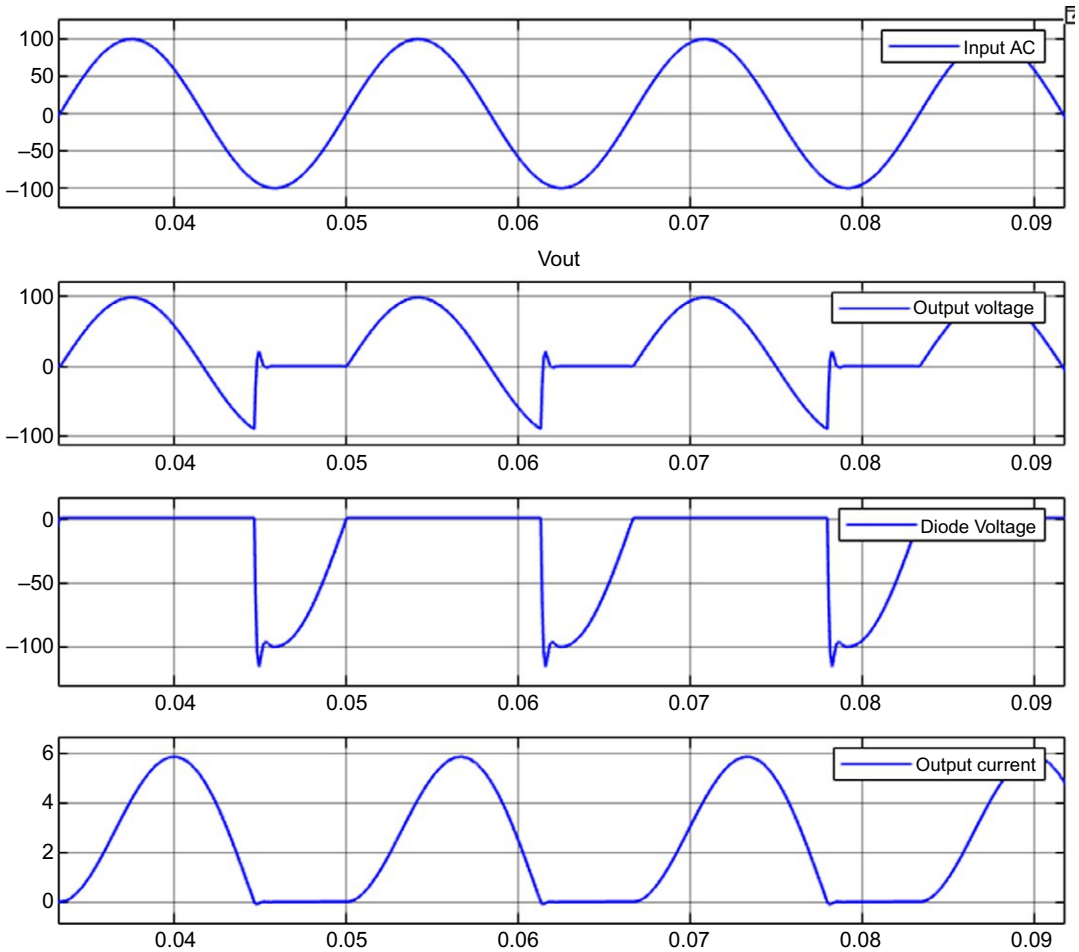

FIG. 4.37 MATLAB simulation waveforms of uncontrolled single-phase half-wave rectifier (inductive load).

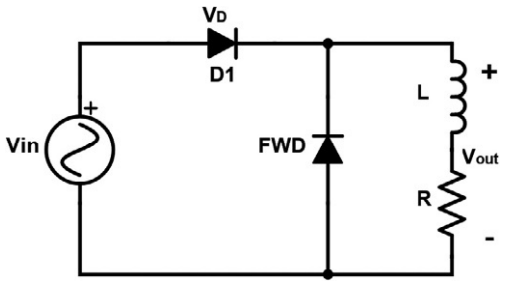

FIG. 4.38 Circuit of uncontrolled single-phase half-wave rectifier (inductive load and freewheeling diode).

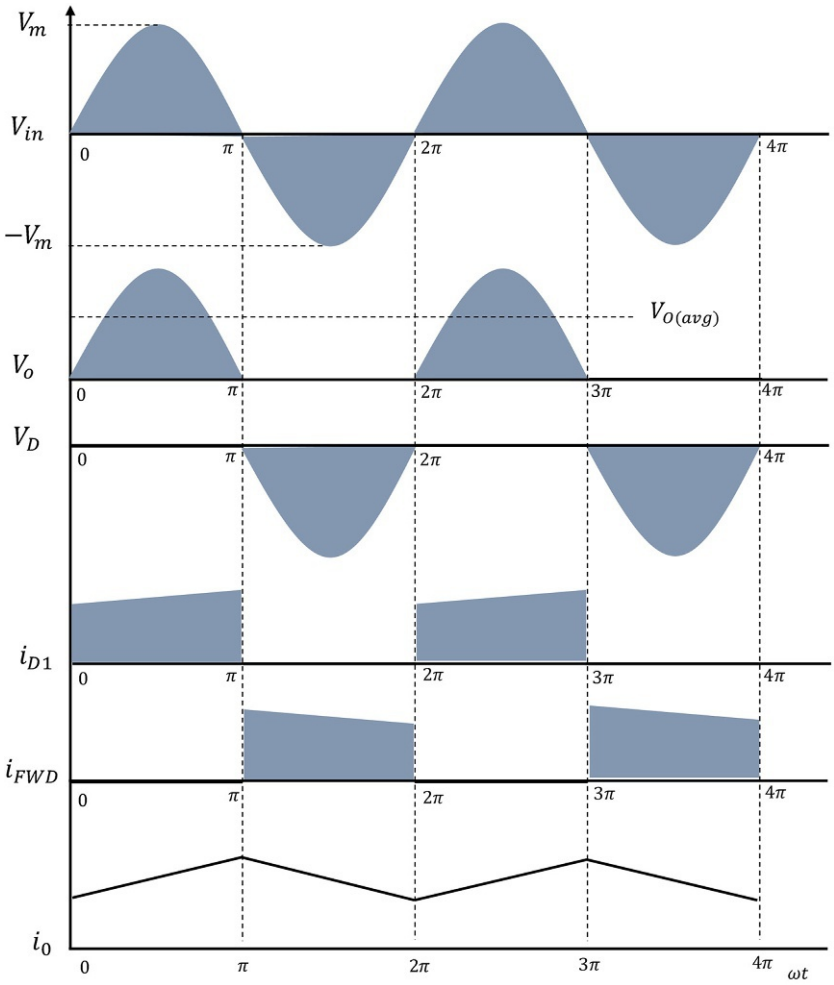

FIG. 4.39 Waveforms of uncontrolled single-phase half-wave rectifier (inductive load and freewheeling diode).

Since the output graphs of the rectifier with freewheeling diodes are like the graphs of resistive load, the same equations are used to determine the average output voltage, current, and power. Fig. 4.40 shows the simulation circuit diagram of the single phase half wave uncontrolled rectifier with inductive load and freewheeling diode in MATLAB. The resultant waveforms of the above stated simulation are shown in Fig. 4.41.

4.4.4 Single-phase half-wave controlled rectifier with resistive load

The controlled rectifier is a converter from AC to DC with a controlled power fed to the load. The circuit diagram of the controlled half-wave rectifier is similar to the uncontrolled rectifier except for the fact that the uncontrolled diode is replaced by a controlled SCR. Fig. 4.42 shows the circuit of the controlled half-wave rectifier. The load at the output is

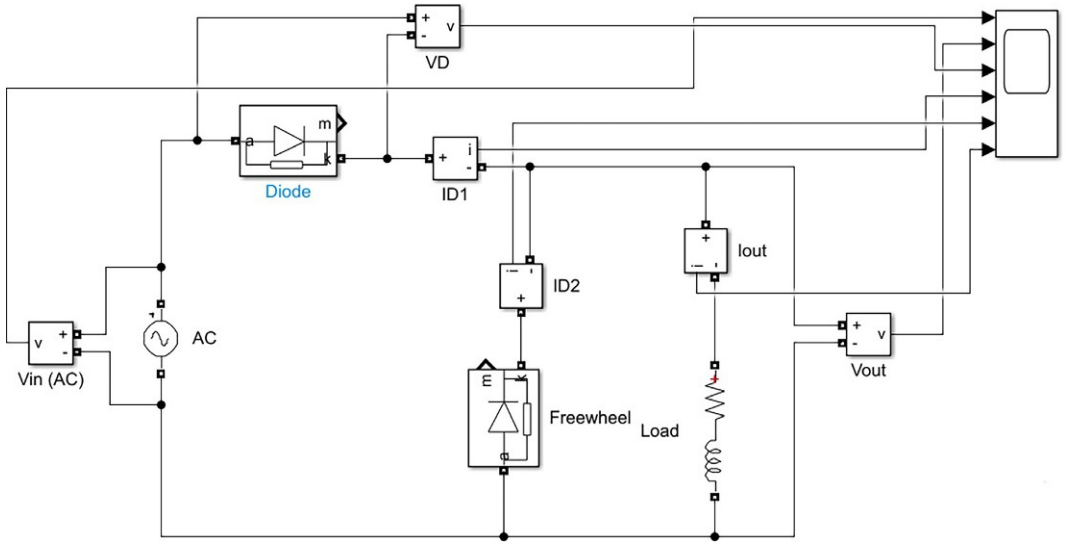

FIG. 4.40 MATLAB simulation circuit of uncontrolled single-phase half-wave rectifier (inductive load and freewheeling diode).

resistive. When the input voltage is applied to the circuit, the polarity across the SCR is such that the SCR is forward biased. The SCR is in the forward blocking mode since the control terminal of the SCR is still unbiased. In the first positive half cycle, the gate signal is applied at the gate at an angle α. The instant gate signal is applied, the thyristor goes into forward conduction mode and the SCR starts conducting. The waveforms shown in Fig. 4.43 indicates that the voltage at the load is available only when the SCR is in forward mode and the gate signal is also present. The input voltage drops across the SCR when it is in a reverse biasing state as in the second half cycle or when the gate signal is also not present. The voltage V_{AK} is the voltage across the thyristor.

The average output voltage is determined by using Eq. (4.11), which states that the average output voltage of the single-phase rectifier is the division of the area under the curve of a complete cycle to the time period for that cycle.

$$V_{in} = V_m \sin(\omega t)$$

$$V_{O(avg)} = \frac{Area\ under\ the\ curve}{T} \tag{4.11}$$

The other way of calculating the average output voltage is by integrating the one complete cycle of the output graph using Eq. (4.12). The output graph consists of a positive half cycle from $(\alpha - \pi)$, and no output from $(0 - \alpha)$ and $(\pi - 2\pi)$. 2π is the time period of one complete cycle.

$$V_{O(avg)} = \frac{1}{2\pi}\int_0^{2\pi} V_{out}.d(\omega t) \tag{4.12}$$

Based on the switching-on and switching-off of the SCR, we divide the above area into three regions: $(0 - \alpha)$, $(\alpha - \pi)$, and $(\pi - 2\pi)$.

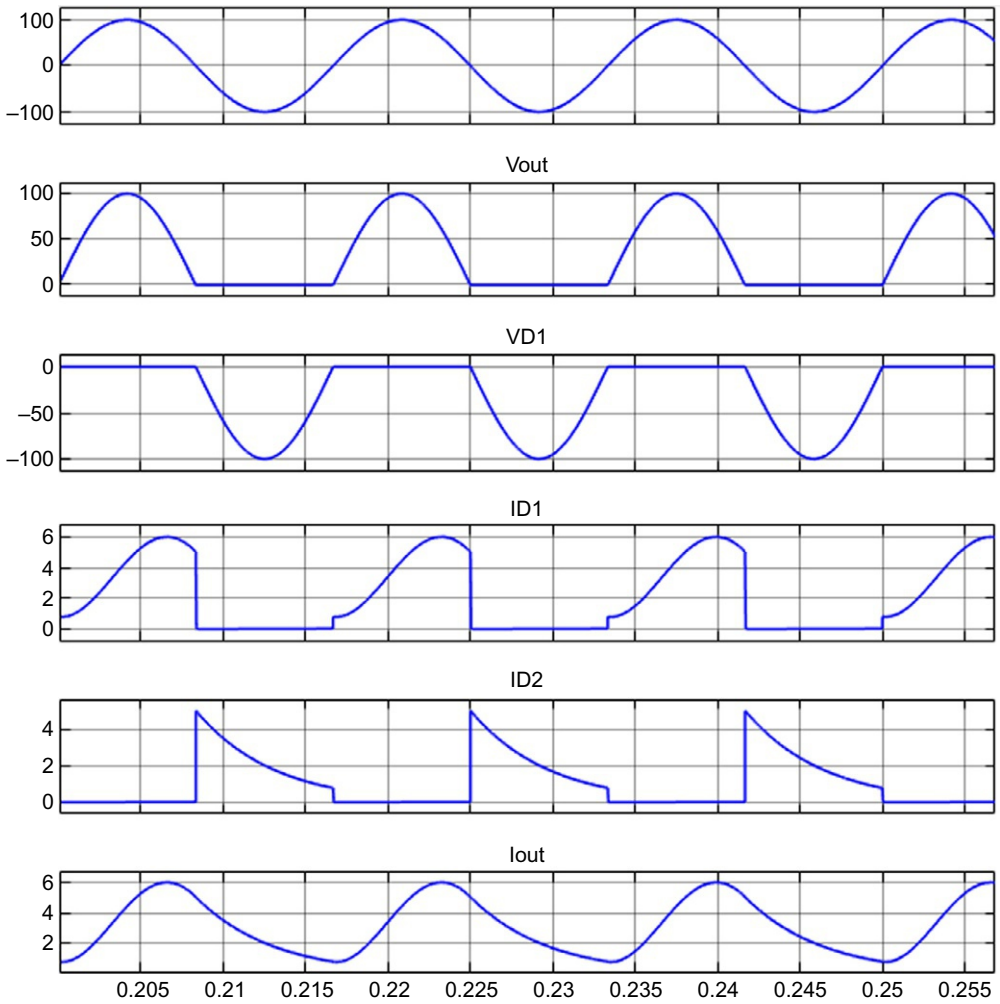

FIG. 4.41 MATLAB simulation waveforms of uncontrolled single-phase half-wave rectifier (inductive load and freewheeling diode).

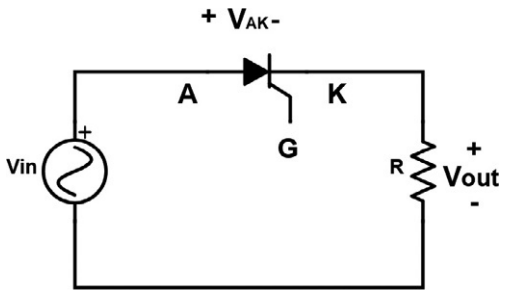

FIG. 4.42 Circuit of controlled single-phase half-wave rectifier (resistive load).

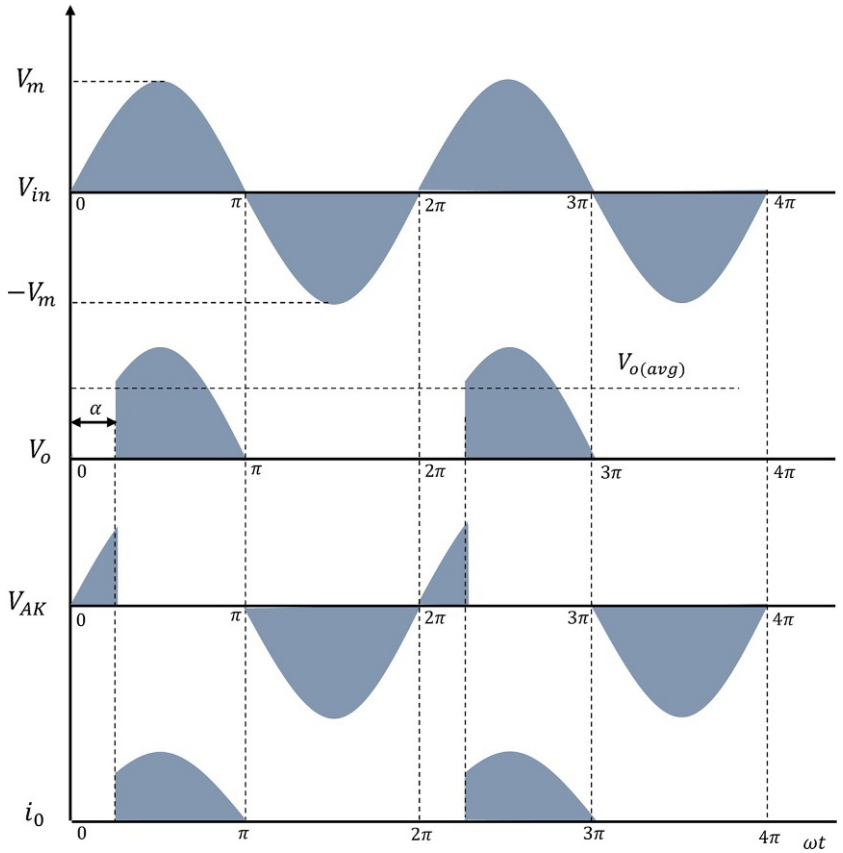

FIG. 4.43 Waveforms of controlled single-phase half-wave rectifier (resistive load).

$$V_{O(avg)} = \frac{1}{2\pi}\left[\int_0^{\alpha} 0 + \int_{\alpha}^{\pi} V_m \sin(\omega t) + \int_{\pi}^{2\pi} 0\right].d(\omega t)$$

As $V_{Out}=0$ for the intervals ($0 \le \omega t \le \alpha$, $\pi \le \omega t \le 2\pi$), so the above equation becomes the following:

$$V_{O(avg)} = \frac{1}{2\pi}\int_{\alpha}^{\pi} V_m \sin(\omega t).d(\omega t)$$

$$V_{O(avg)} = \frac{V_m}{\pi}\left(\frac{1+\cos\alpha}{2}\right) \tag{4.13}$$

After calculating the average of the output voltage using Eq. (4.13), we can determine the average output current using Ohm's law, which is given in Eq. (4.14).

$$I_{O(avg)} = \frac{V_{O(avg)}}{R}$$

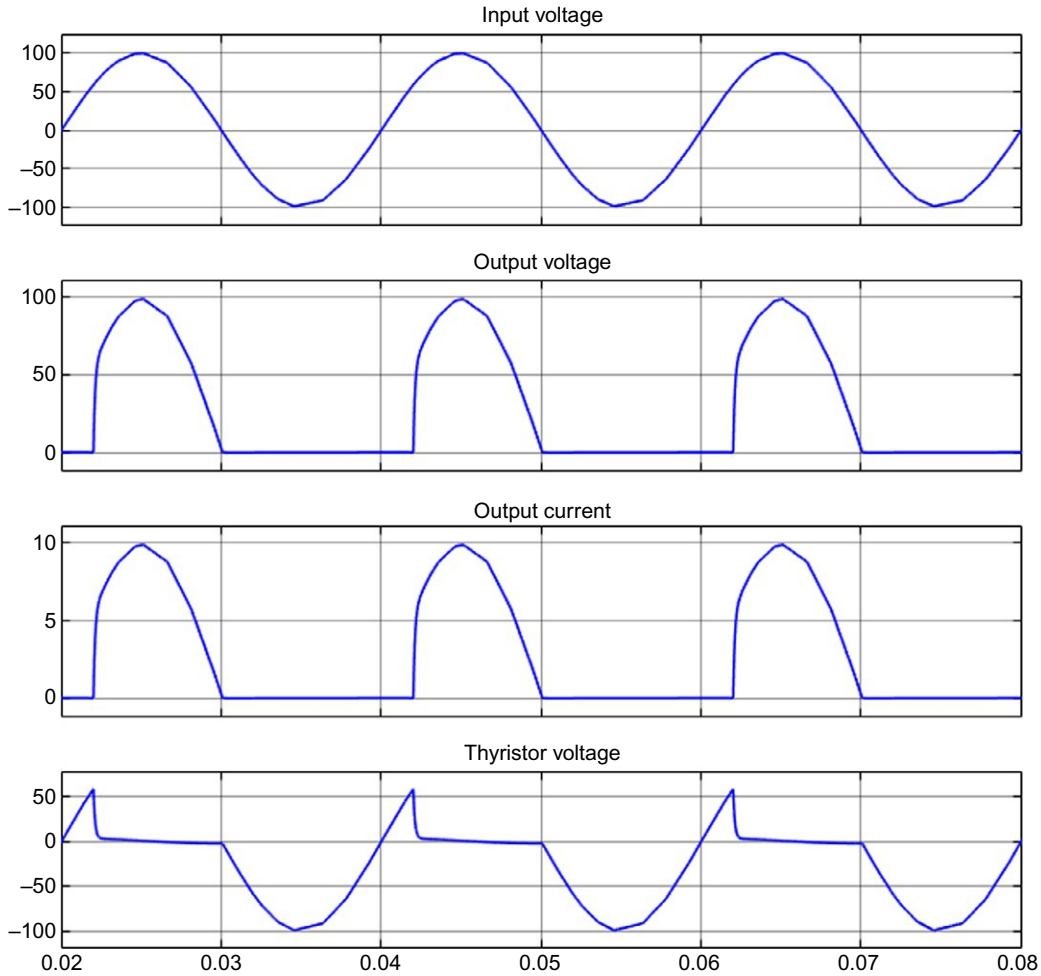

FIG. 4.44 MATLAB simulation waveforms of controlled single-phase half-wave rectifier (resistive load).

$$I_{O(avg)} = \frac{V_m}{\pi R}\left(\frac{1 + \cos\alpha}{2}\right) \tag{4.14}$$

After getting the average value of voltage and current at the output of a half-wave rectifier, the output power can be determined by their multiplication, as shown in Eq. (4.15) for the resistive load. The waveforms of the MATLAB simulation of single phase half wave controlled rectifier with resistive load is shown in Fig. 4.44.

$$P_{O\ (avg)} = V_{O(avg)} \times I_{O(avg)}$$

$$P_{O\ (avg)} = \frac{{V_m}^2}{\pi^2 R}\left(\frac{1 + \cos\alpha}{2}\right)^2 \tag{4.15}$$

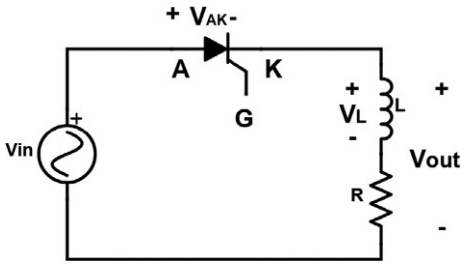

FIG. 4.45 Circuit of controlled single-phase half-wave rectifier (inductive load).

4.4.5 Single-phase controlled half-wave rectifier (inductive load)

The circuit of the controlled rectifier with inductive load is the same as we studied in the uncontrolled rectifier. The difference is the replacement of the uncontrolled diode with the controlled SCR. Fig. 4.45 shows the circuit of the single-phase controlled half-wave rectifier with an inductor at the output. The conduction from the SCR requires the correct polarity across the SCR and the gate signal at the gate. In the first half cycle, the SCR is in the forward blocking mode until the angle α since the firing angle of the SCR is α. At firing angle α, both the conditions of forward conduction mode are fulfilled and the SCR conducts the input positive cycle to the load. As soon as the polarity of the input voltage is changed the inductor takes some time to reverse the polarity across it and continues charging in the same direction until the angle ϕ even the negative half cycle of the input starts. The effect of the inductive nature of the load can be described as the inductor stores energy in its magnetic field in five-time constants. During the positive half cycle, the inductor stores energy in the magnetic field. The thyristor in the negative half cycle is reverse biased and it blocks all the input voltage and at the output; we have only inductor stored energy as shown in Fig. 4.46 which explains the input AC voltage, the inductive behavior at the output, the voltage across the SCR, and the output current.

The average value of the output is determined by dividing the area under the curve for one complete cycle by the time for that cycle, as given in Eq. (4.16).

$$V_{O(avg)} = \frac{Area\ under\ the\ curve}{T} \tag{4.16}$$

The above formula for the calculation of the average voltage at the load can be implemented by integrating the complete cycle.

$$V_{O(avg)} = \frac{1}{2\pi}\int_0^{2\pi} V_{out}.d(\omega t)$$

$$V_{O(avg)} = \frac{1}{2\pi}\int_0^{2\pi} V_m \sin(\omega t).d(\omega t)$$

Based on the switching-on and switching-off of the SCR, we divide the above area into three regions: $(0-\alpha)$, $(\alpha-\theta)$, and $(\theta-2\pi)$.

$$V_{O(avg)} = \frac{1}{2\pi}\left[\int_0^{\alpha} 0 + \int_{\alpha}^{\theta} V_m \sin(\omega t) + \int_{\theta}^{2\pi} 0\right].d(\omega t)$$

As $V_{Out}=0$ for the intervals ($0\leq\omega t\leq\alpha$, $\theta\leq\omega t\leq 2\pi$), so the above equation becomes the following:

$$V_{O(avg)}=\frac{1}{2\pi}\int_{\alpha}^{\theta}V_m\sin(\omega t).d(\omega t)$$

$$V_{O(avg)}=\frac{V_m}{\pi}\left(\frac{\cos\alpha-\cos\theta}{2}\right) \tag{4.17}$$

After calculating the average of the output voltage given in Eq. (4.17), we can determine the average output current using Ohm's law, which is given in Eq. (4.18).

$$I_{O(avg)}=\frac{V_{O(avg)}}{R}$$

$$I_{O(avg)}=\frac{V_m}{\pi R}\left(\frac{\cos\alpha-\cos\theta}{2}\right) \tag{4.18}$$

After getting the average value of voltage and current at the output of a half-wave rectifier, the output power can be determined by their multiplication, as shown in Eq. (4.19) for the inductive load. Fig. 4.47 shows the MATLAB simulation diagram of the single phase half wave controlled rectifier with inductive load and the resulting waveforms are shown in Fig. 4.48.

$$P_{O\ (avg)}=V_{O(avg)}\times I_{O(avg)}$$

$$P_{O\ (avg)}=\frac{{V_m}^2}{\pi^2 R}\left(\frac{\cos\alpha-\cos\theta}{2}\right)^2 \tag{4.19}$$

4.4.6 Single-phase controlled half-wave rectifier with inductive load and freewheeling diode

The waveforms of the controlled rectifier after the application of the freewheeling diode with inductive load are shown in Fig. 4.49, and it is evident that after using the freewheeling diode the rectifier behaves like the one for the resistive load. The input cycle is conducted through the diode and the negative cycle is dropped across the diode. The current at the output is the sum of two currents, i_{d1} and i_{d2}. The current passing through the diode during the positive half cycle when it is forward biased is termed as i_{d1} and when the diode becomes reverse biased and the energy stored in the inductor dissipates through the freewheeling diode. The current that passes through the freewheeling diode in the negative cycle is called i_{d2} or i_{FWD}. Since the output graphs of the rectifier with freewheeling diodes are like the graphs of resistive load, the same equations are used to determine the average output voltage, current, and power. Fig. 4.50 shows the simulation circuit diagrm of the single phase half wave controlled rectifier with inductive load and freewheeling diode in MATLAB and the resulting waveforms of the above stated simulation are shown in Fig. 4.51.

4.5 Converters (DC-DC converters)

Converters of power electronics are applied for the DC-DC conversion either from low to high DC voltage or from low to high DC voltage. The basic operating rule of the DC-DC

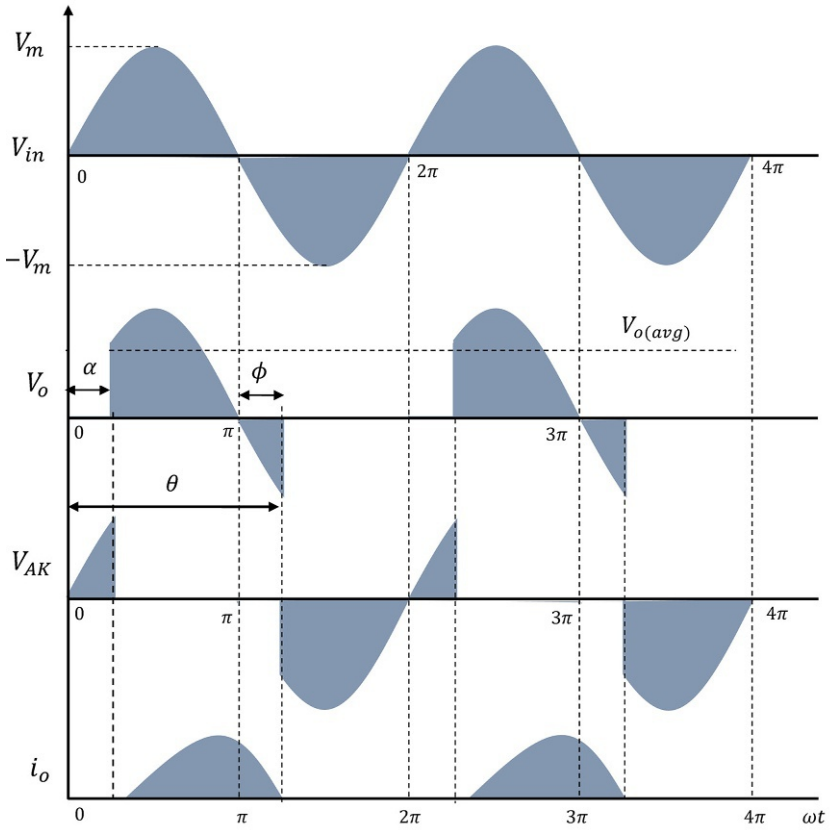

FIG. 4.46 Waveforms of controlled single-phase half-wave rectifier (inductive load).

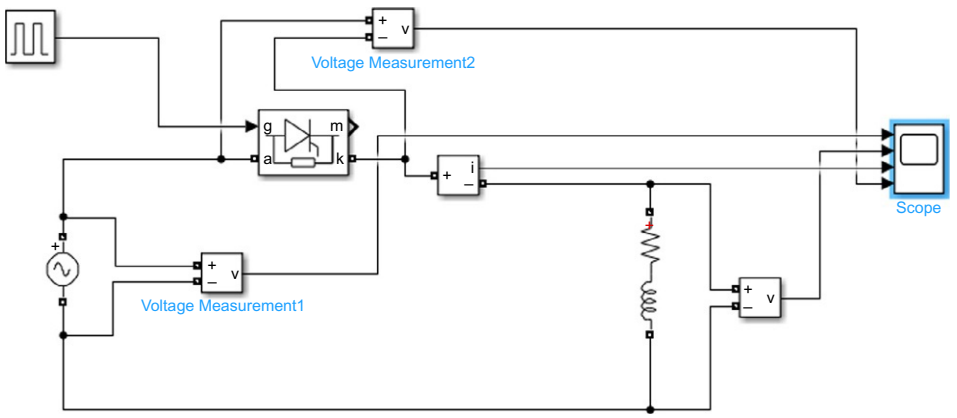

FIG. 4.47 MATLAB simulation circuit of controlled single-phase half-wave rectifier (inductive load).

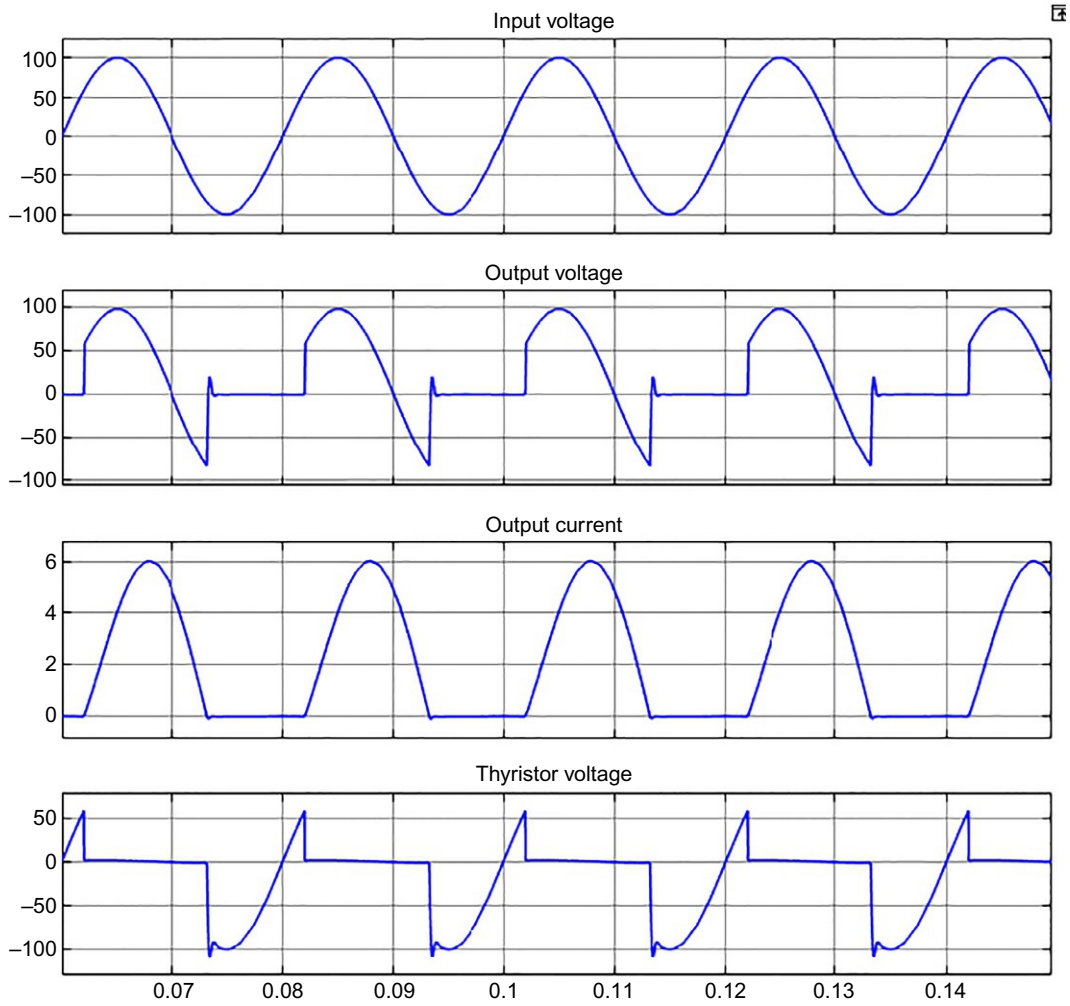

FIG. 4.48 MATLAB simulation waveforms of controlled single-phase half-wave rectifier (inductive load).

choppers can be understood in Fig. 4.52A. The switch in this circuit is repeatedly ON and OFF for a time period DT and $D'T$, respectively. The time period of the circuit becomes $T = DT + D'T$ and the frequency is $\frac{1}{T}$. The average voltage at the output of the circuit can be calculated using Eq. (4.20).

$$V_{out} = \frac{1}{T}\left[\int_0^{DT} V_{in}dt + \int_{DT}^{D'T} 0.dt\right]$$

$$V_{out} = \frac{V_{in}}{T}\,DT \tag{4.20}$$

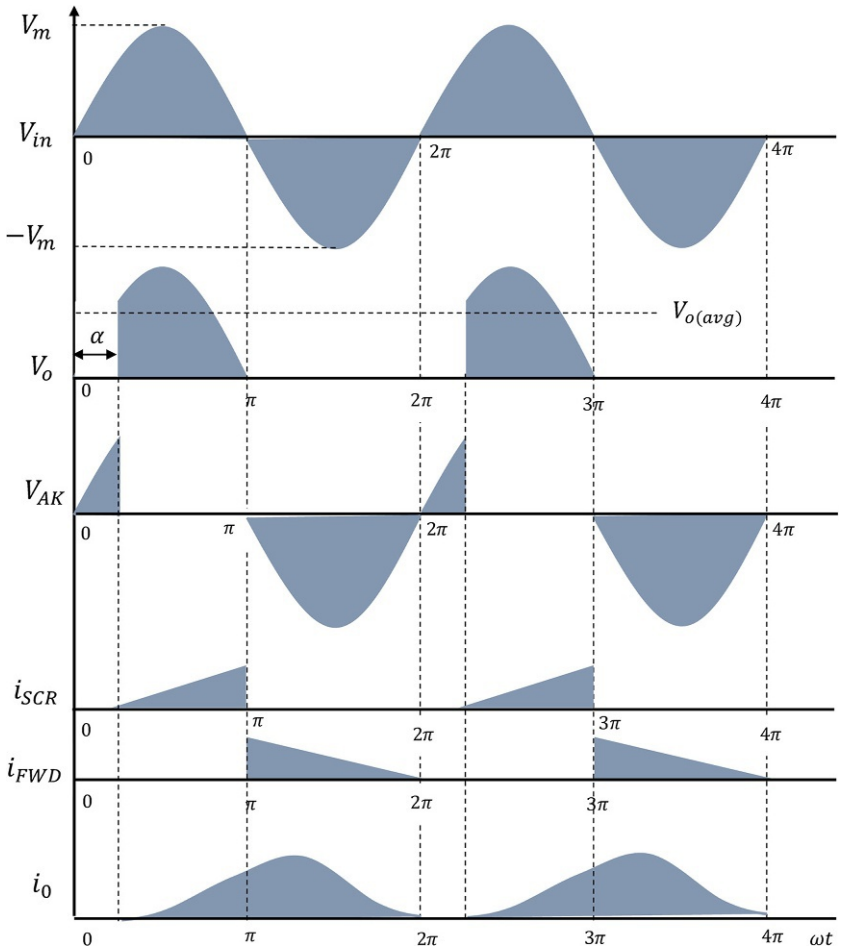

FIG. 4.49 Waveforms of controlled single-phase half-wave rectifier (inductive load and freewheeling diode).

The single pole single through (SPST) switch is replaced by a power electronics solid-state device like an SCR, GTO, transistor, etc. By fixing the time period (T) of the circuit, the voltage at the load can be varied between 0 and V_{in} by varying the switching ON time (DT) of the switch. Fig. 4.52A is the simplest circuit to understand the working of a chopper. In practical DC choppers, SPST is replaced by a thyristor and, extra energy storing elements like inductor and capacitor and the commutation circuit are inserted in the circuit [8,9].

The switching of the SPST switch consists of both on and off times. DT is considered as the time for which the switch is closed and $D'T$ is the time for which the switch is opened. D and D' are the duty cycles during on and off time, respectively, explained in Fig. 4.52B.

$$T = T_{ON} + T_{OFF}$$

$$T = DT + D'T$$

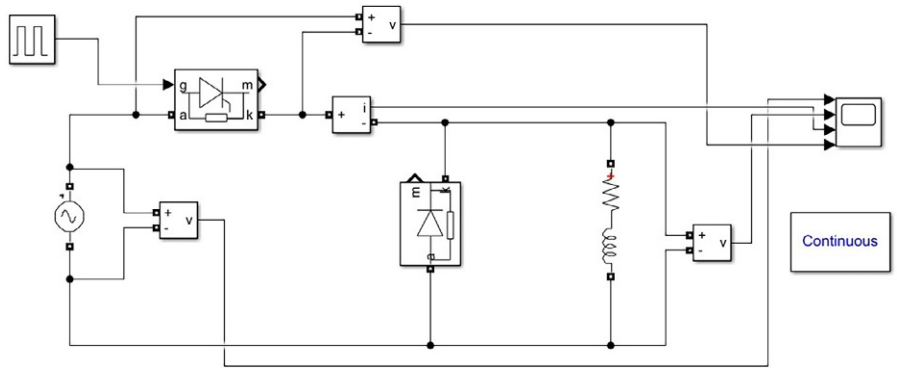

FIG. 4.50 MATLAB simulation circuit of controlled single-phase half-wave rectifier (inductive load and free-wheeling diode).

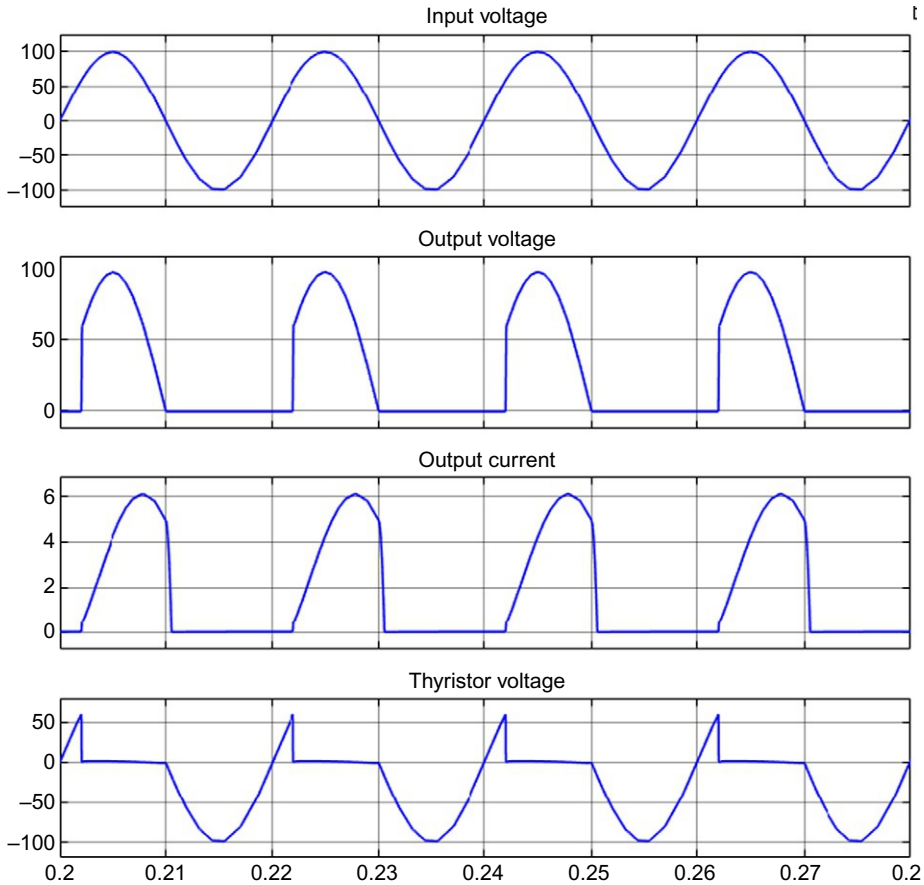

FIG. 4.51 MATLAB simulation waveforms of controlled single-phase half-wave rectifier (inductive load and free-wheeling diode).

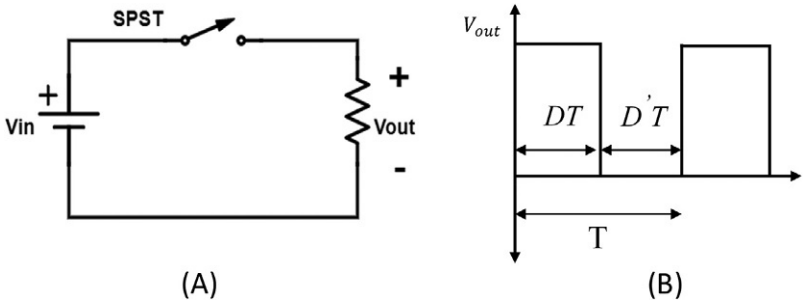

FIG. 4.52 (A) Simple circuit to understand the basic operation of converters and (B) understanding the turn-on and turn-off time.

$$T = T\,(D + D')$$

$$D + D' = 1$$

4.5.1 Buck converters

Buck converters are the power electronics chopper circuits that are used to step down the DC voltages. Fig. 4.53 shows the mechanical switch-based circuit of a DC-DC buck converter.

For the practical derivation of the DC-DC buck converter circuit shown in Fig. 4.53, two single pole single throw switches (SPST) are replaced by a single pole double throw switch (SPDT) , and a low pass filter at the load side is connected. When the switch is connected to pole 1, the input is connected and when the switch is connected to pole 2, the input is disconnected. To get the above-stated operation with the power electronic circuit independent of the mechanical switch, SPDT is replaced by an active and a passive switch as shown in Fig. 4.54. The active switch could be a thyristor, GTO, transistor, etc., and the passive switch is a diode that acts as a freewheeling diode.

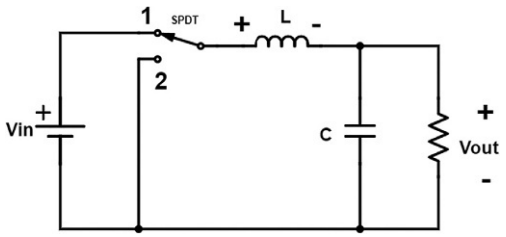

FIG. 4.53 Mechanical switch (single pole double throw)-based diagram of DC-DC buck converter.

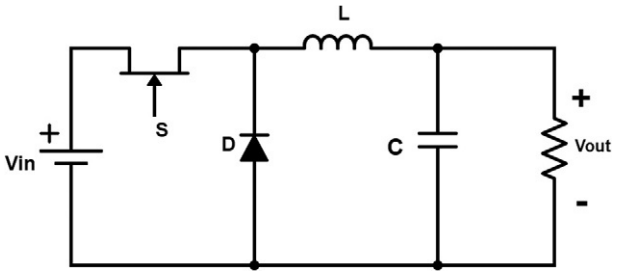

FIG. 4.54 Solid-state switch-based diagram of DC-DC buck converter.

The switch in Fig. 4.54 can be operated by a gate signal. The time during which the switch is ON is termed as DT and the time during which it is OFF is termed as $D'T$. The biasing of the diode depends upon the switching state of the switch S. The on-state of the switch takes the diode into a reverse biasing state, and during OFF time, it acts as a freewheeling diode. The switching time period is represented by Eq. (4.21).

$$T = DT + D'T \tag{4.21}$$

Case 1, when the solid-state switch is on: In case 1, the switch is kept ON behaving like a short circuit and the polarity of the voltage across the diode makes it reverse biased acting as an open circuit as shown in Fig. 4.55. The input supply is directly charging the inductor and supplying the load. By applying Kirchhoff's voltage law (KVL) on the input side loop of the circuit shown in Fig. 4.55, we get the voltage across the inductor during the turn-on time given by Eq. (4.22).

$$V_{in} - V_L - V_{out} = 0$$

$$V_L = V_{in} - V_{out} \tag{4.22}$$

Case 2, when the solid-state switch is off: In case 2, the switch S is kept OFF and it behaves like an open circuit disconnecting the input supply from the rest of the circuit as shown in Fig. 4.56. As the input supply is disconnected the inductor starts discharging and a reverse polarity voltage is induced across the inductor. The reverse polarity across the inductor forward biases the diode, which behaves like a short circuit. By applying KVL on the input side loop of the circuit shown in Fig. 4.56, we get the voltage across the inductor during the turn-off time given by Eq. (4.23).

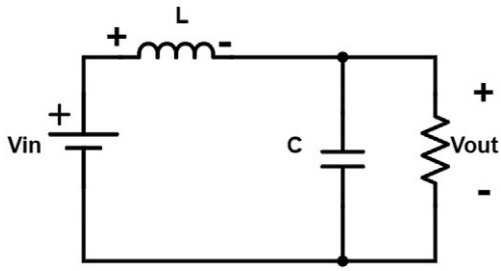

FIG. 4.55 DC-DC buck converter circuit during the turn-on duty cycle.

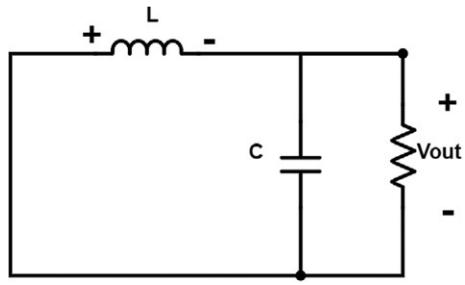

FIG. 4.56 DC-DC buck converter circuit during the turn-off duty cycle.

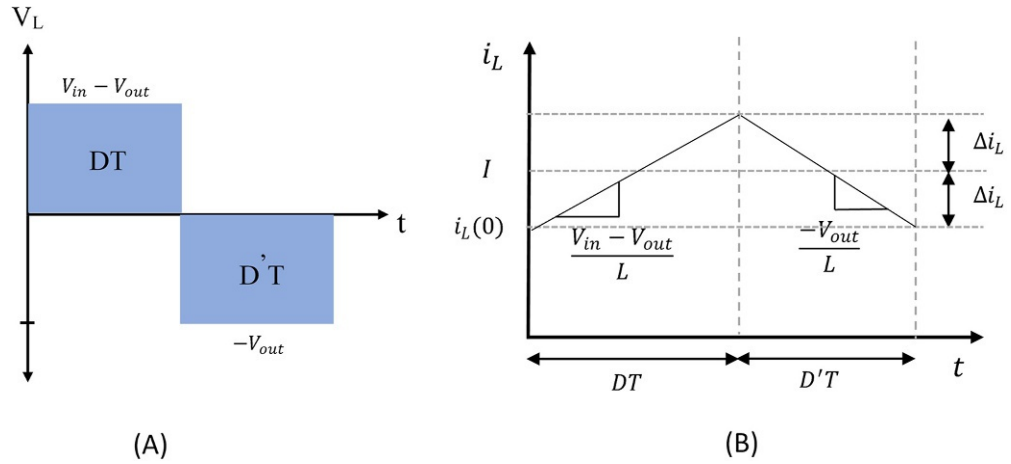

FIG. 4.57 (A) Voltage across inductor during turn-on and turn-off time and (B) inductor current during turn-on and turn-off time

$$-V_L - V_{out} = 0$$

$$V_L = -V_{out} \tag{4.23}$$

Fig. 4.57A shows the voltage across the inductor during turn-on and turn-off time. The average voltage across the inductor can be calculated by finding the area of the shaded region and dividing by the complete time period as follows.

$$\langle V_L \rangle = \frac{(V_{in} - V_{out})(DT) + (-V_{out})(D'T)}{T}$$

Since the inductor stores energy in the positive half cycle and discharges the energy in the negative half cycle irrespective of the presence of the source, the average voltage across the inductor is zero.

$$0 = \frac{T[D(V_{in} - V_{out}) - D'V_{out}]}{T}$$

$$0 = DV_{in} - DV_{out} - D'V_{out}$$

$$0 = DV_{in} - V_{out}(D + D')$$

$$V_{out} = DV_{in} \tag{4.24}$$

In the above equation, duty cycle D can be varied between 0 and 1, in return varying the output voltage. Hence the output voltage will be duty cycle times the fraction of input voltage.

Inductor design for buck converter: the above-derived Eqs. (4.22), (4.23) are used to find out the relation for the rate of change of current through the inductor. Eqs. (4.25), (4.26) are the general relations for the inductor voltage during turn-on and turn-off time.

$$V_L = L.\frac{di}{dt_{(DT)}} \tag{4.25}$$

$$V_L = L.\frac{di}{dt_{(D'T)}} \tag{4.26}$$

By comparing Eqs. (4.22), (4.25), we get Eq. (4.27), which is the rate of change of current through the inductor during turn-on time.

$$L\frac{di}{dt_{(DT)}} = V_{in} - V_{out}$$

$$\frac{di}{dt_{(DT)}} = \frac{V_{in} - V_{out}}{L} \tag{4.27}$$

Eqs. (4.23), (4.26) are compared to determine the relation for the current change through the inductor during the turn-off time of the switch given in Eq. (4.28).

$$L\frac{di}{dt_{(D'T)}} = -V_{out}$$

$$\frac{di}{dt_{(D'T)}} = \frac{-V_{out}}{L} \tag{4.28}$$

Eqs. (4.27), (4.28) determined for DT and $D'T$ are applied to sketch the graph of the inductor current for a complete cycle plotted in Fig. 4.57B. During the turn-on time, the inductor current starts increasing gradually from zero given as $i_L(0)$ in the graph at a rate $\frac{di}{dt_{(DT)}} = \frac{V_{in}-V_{out}}{L}$ given in Eq. (4.27) and $\frac{di}{dt_{(D'T)}} = \frac{-V_{out}}{L}$ given in Eq. (4.28) indicate the slope of the inductor current during on and off periods. Fig. 4.57B is used to derive a relation for the value of the inductor to be used in the buck converter. The graph of the inductor current says that the current change through the inductor is the product of the slope of the current in a positive cycle and the time period for that interval, as given in Eq. (4.29).

$$change\ in\ i_L = (slope)(length\ of\ sub - interval) \tag{4.29}$$

$$2\Delta i_L = \frac{V_{in} - V_{out}}{L}.DT$$

$$L = \frac{V_{in} - V_{out}}{2\Delta i_L}.DT \tag{4.30}$$

The converters also follow the first law of thermodynamics, which states that energy cannot be generated nor destroyed, but can be converted from one form to another. The input power given to the inductor is equal to the output power. Using Fig. 4.55, we can say that the inductor current is the input current $\langle i_{in}\rangle = \langle i_L\rangle$, which can be averaged as follows.

$$P_{in} = P_{out}$$

$$V_{in}.\langle i_{in}\rangle = \frac{\langle V_{out}\rangle^2}{R}$$

$$\langle i_{in}\rangle = \langle i_L\rangle = \frac{\langle V_{out}\rangle^2}{V_{in}.R}$$

So by putting the value of inductor current in Eq. (4.30) it takes the form of Eq. (4.31).

$$L = \frac{V_{in}(V_{in} - V_{out}).R}{2\langle V_{out}\rangle^2}.DT \tag{4.31}$$

Example 4.1

For a DC-DC buck converter, the input voltage is 12 V.

(a) Find the output voltage by adjusting the duty cycle to 30%, 50%, and 80%, and elaborate on the results.

(b) Simulate the above-given example in MATLAB Simulink by setting the switching time period to 50% and find out the output voltage.

Solution:

(a) For the switching period 30%:

$$V_{in} = 12\,V$$

Eq. (4.24) is used to find out the output voltage of the buck converter.

$$V_{out} = 3.6\,V$$

For the switching period 50%:
Similarly, Eq. (4.24) is used to find out the output voltage of the buck converter.

$$V_{out} = 6\,V$$

For the switching period 80%:
Eq. (4.24) is used to find out the output voltage of the buck converter.

$$V_{out} = 9.6\,V$$

It can be noted from the above results that by increasing the duty cycle, the output voltages also increase, but the value of the output voltage cannot exceed the input voltage. The output voltage will always be less than the input voltage whatever the value of the duty cycle is.

(b) The circuit of the buck converter shown in Fig. 4.58 is the circuit of the boost converter simulated in MATLAB/Simulink. An inductor of 1 mH and a capacitor of 220 μF were used. The input voltage was set at 12 V and the switching period is 50%. The output voltage is 5.571 V, as shown in Fig. 4.58.

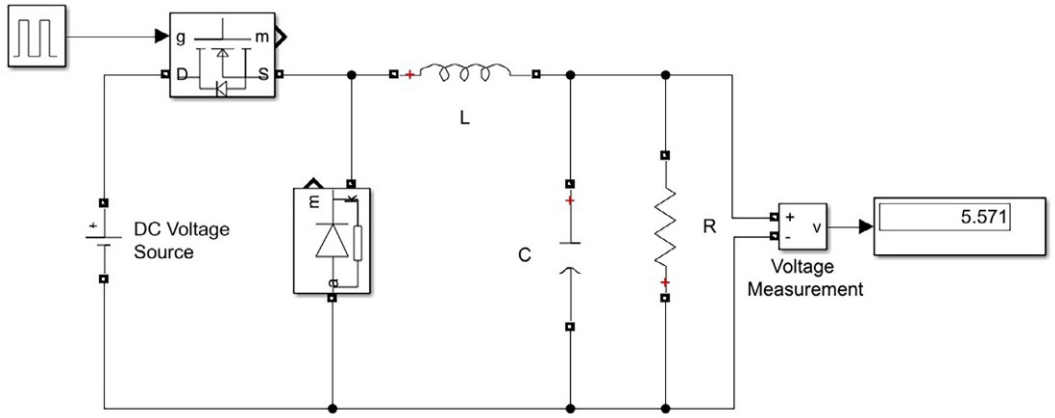

FIG. 4.58 MATLAB simulation circuit diagram of DC-DC buck converter.

4.5.2 Boost converters

Contrary to the buck converter, the boost converter, also known as the step-up chopper, is used to increase the voltage level of the DC voltage. Fig. 4.59 shows the basic circuit of a DC-DC boost converter having a mechanical SPDT switch to understand the switching mechanism of the boost converter. In Fig. 4.60, the SPDT switch is replaced by an active and a passive switch [10]. The active switch could be a thyristor, GTO, transistor, etc. and the passive switch is a diode that connects and disconnects the input supply from the input during turn-off time and turn-on time of the switch, respectively. Fig. 4.60 shows the solid-state switch-based boost converter circuit.

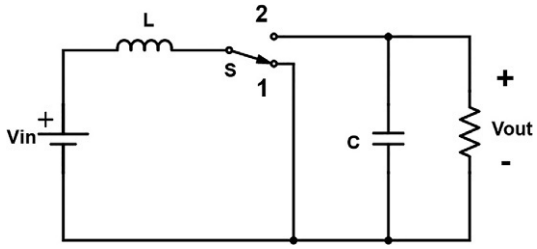

FIG. 4.59 Mechanical switch-based D-DC boost converter.

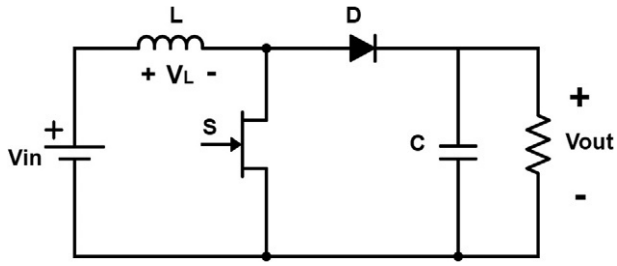

FIG. 4.60 Power electronics switch-based DC-DC boost converter.

Case 1, when the solid-state switch is on: In case 1, the switch is on behaving like a short circuit and the polarity of the voltage across the diode reverse biases it and the circuit becomes open disconnecting the output from the input and the inductor. Now in this case the current linearly increases through the inductor, since it is directly connected to the input supply. The inductor is charged during the turn-on time of the switch. During the turn-on time, the resultant circuit is as shown in Fig. 4.61. We apply KVL on this circuit and determine the relation for inductor voltage. Eq. (4.32) shows that all the input voltage is developed across the inductor.

$$V_{in} - V_L = 0$$
$$V_L = V_{in} \tag{4.32}$$

Case 2, when the solid-state switch is off: During the negative duty cycle the switch is off, behaving as a short circuit. Now the inductor and the input supply are connected to the load. The energy stored in the inductor now dissipates and the reverse polarity of the voltage across the inductor forward biases the diode that behaves like a short circuit. By applying KVL on the circuit shown in Fig. 4.62, we determine the equation of the inductor voltage. The resultant inductor voltage is given in Eq. (4.33).

$$V_{in} - V_L - V_{out} = 0$$
$$V_L = V_{in} - V_{out} \tag{4.33}$$

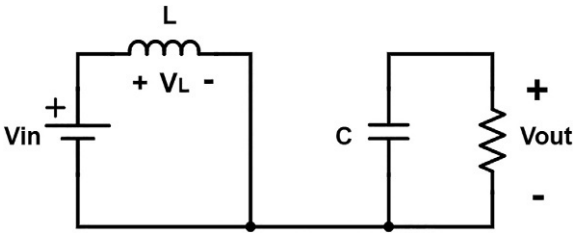

FIG. 4.61 DC-DC boost converter circuit during the turn-on duty cycle.

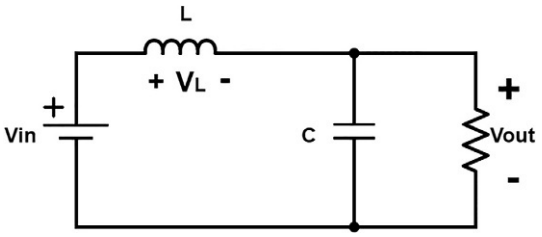

FIG. 4.62 DC-DC boost converter circuit during the turn-off duty cycle.

Fig. 4.64A shows the duty cycle given to the switch of the boost converter and the voltage across the inductor in turn-on and off time. The average voltage of the inductor is calculated by integrating the area under the curve over the complete time period shown in Fig. 4.64A and given in Eq. (4.34).

$$\langle V_L \rangle = \frac{(V_{in})(DT) + (V_{in} - V_{out})(D'T)}{T} \tag{4.34}$$

Since the inductor stores energy in the positive half cycle and discharges the energy in the negative half cycle, irrespective of the presence of the source, the average voltage across the inductor is zero.

$$0 = DV_{in} + D'V_{in} - D'V_{out}$$

$$0 = V_{in}(D + D') - D'V_{out}$$

$$V_{out} = \frac{V_{in}}{1 - D} \tag{4.35}$$

Eq. (4.35) is the generalized relationship between the input and output voltage of the boost converter based on the duty cycle of the solid-state switch.

Example 4.2

For a DC-DC boost converter, the input voltage is 24 V.

(a) Find the output voltage by adjusting the duty cycle to 30%, 50%, and 70% and elaborate on the results.

(b) Simulate the above-given example in MATLAB Simulink by setting the switching time period to 70% and find out the output voltage.

Solution:

(a) For the switching period 30%:

$$V_{in} = 24\ V$$

Eq. (4.35) is used to find out the output voltage of the boost converter.

$$V_{out} = 34.28\ V$$

For the switching period 50%:
Similarly, Eq. (4.35) is used to find out the output voltage of the boost converter.

$$V_{out} = 48\ V$$

For the switching period 70%:
Eq. (4.35) is used to find out the output voltage of the boost converter.

$$V_{out} = 80\ V$$

It can be noted from the above results that by increasing the duty cycle, the output voltages also increase, but the value of output voltage cannot be lower than the input voltage. The output voltage will always be greater than the input voltage whatever the value of the duty cycle is.

(b) The circuit of the boost converter shown in Fig. 4.63 is simulated in MATLAB/Simulink. An inductor of 1 mH and a capacitor of 33 μF were used. The input voltage was set at 24 V and the switching period is 70%. The output voltage is 78.88 V, as shown in Fig. 4.63.

Inductor design for buck converter: To determine the value of the inductor to be used in the boost converter, we first need to determine the rate of change of current using the inductor voltages derived for the on and off time of the active switch of the boost converter. The voltage across the inductor during turn-on time is given by Eq. (4.36).

$$V_L = L.\frac{di}{dt_{(DT)}} \tag{4.36}$$

Eqs. (4.32), (4.36) are compared to find the relation for the rate of change of current through the inductor.

$$L\frac{di}{dt_{(DT)}} = V_{in}$$

$$\frac{di}{dt_{(DT)}} = \frac{V_{in}}{L} \tag{4.37}$$

Eq. (4.37) is used to determine the change in current through the inductor during the turn-off time of the switch. Similarly during T_{OFF}, rate of change of current through the inductor is given by Eq. (4.38).

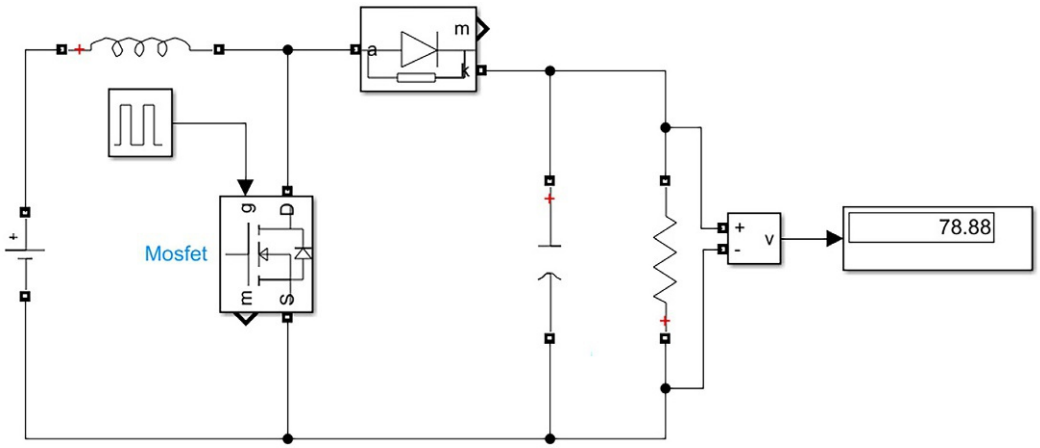

FIG. 4.63 MATLAB simulation diagram of DC-DC boost converter.

$$V_L = L.\frac{di}{dt_{(D'T)}} \tag{4.38}$$

By comparing Eqs. (4.33), (4.38), we simplify the relation and get Eq. (4.39), which gives the rate of change of current through the inductor during switching off time.

$$L\frac{di}{dt_{(D'T)}} = V_{in} - V_{out}$$

$$\frac{di}{dt_{(D'T)}} = \frac{V_{in} - V_{out}}{L} \tag{4.39}$$

The graph of the inductor current can be drawn by using equations determined for DT and $D'T$, as shown in Fig. 4.64B. During the turn-on time, the inductor current starts increasing gradually from zero given as $i_L(0)$ in the graph at a rate $\frac{di}{dt_{(DT)}} = \frac{V_{in}}{L}$ given by Eq. (4.37), and $\frac{di}{dt_{(D'T)}} = \frac{V_{in}-V_{out}}{L}$ given by Eq. (4.39) represent the slope of the inductor current that can be used to find out the value of the inductor to be used in the boost converter by multiplying the slope of the inductor current by the turn-on time as shown below.

$$change\ in\ i_L = (slope\ of\ inductor\ charging\ current)(length\ of\ sub-interval\ DT)$$

$$2\Delta i_L = \frac{V_{in}}{L}.DT$$

$$L = \frac{V_{in}}{2\Delta i_L}.DT \tag{4.40}$$

The converters also follow the first law of thermodynamics, which states that energy cannot be created nor destroyed, but can be transformed from one form to another. The input power given to the inductor is equal to the output power. As shown in Fig. 4.61, we can say that the inductor current is the input current $\langle i_{in}\rangle = \langle i_L\rangle$, which can be averaged as follows.

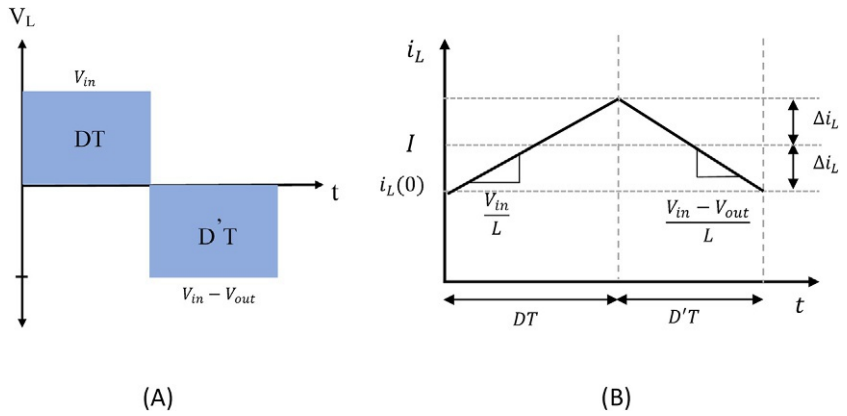

FIG. 4.64 (A) Voltage across inductor during turn-on and turn-off time and (B) inductor current during turn-on and turn-off time.

$$P_{in} = P_{out}$$

$$V_{in}.\langle i_{in}\rangle = \frac{\langle V_{out}\rangle^2}{R}$$

$$\langle i_{in}\rangle = \langle i_L\rangle = \frac{\langle V_{out}\rangle^2}{V_{in}.R}$$

Thus by putting the value of inductor current in Eq. (4.40), it takes the form of Eq. (4.41).

$$L = \frac{(V_{in})^2.R}{2\langle V_{out}\rangle^2}.DT \tag{4.41}$$

4.5.3 Buck-boost converters

The mechanical switch-based circuit of the DC-DC buck-boost converter is shown in Fig. 4.65. The mechanical switch is a single pole double throw switch with two positions. In position 1, it helps in connecting the input DC supply to the inductor, and the inductor is charged in this position. When it is in position 2, it connects the inductor to the load. The inductor gets energy from the input when the switch is in position 1 and discharges this energy to the load when the switch is in position 2. For practical application of the buck-boost converter, the mechanical switch is replaced by the solid-state switch. To get the same impact as the SPDT switch, the switch realization is done by replacing the mechanical switch with an active and a passive switch. The active switch is the controlled switch like the SCR, GTO, and IGBT, and the passive switch is the uncontrolled switch like a diode. The power electronics-based circuit of the DC-DC buck-boost converter is shown in Fig. 4.66. The active switch is intentionally controlled by the gate signal and the passive switch is controlled by the polarity

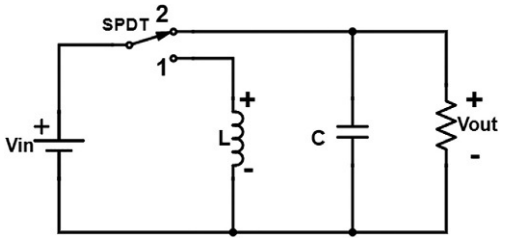

FIG. 4.65 Mechanical switch-based DC-DC buck-boost converter.

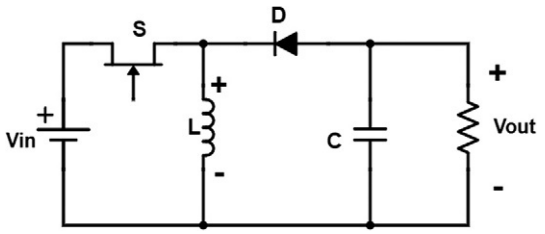

FIG. 4.66 Power electronics switch-based DC-DC buck-boost converter.

of the voltage across it, which is determined by the charging and discharging of the inductor [11].

Case 1, when the switch S is on: When the solid-state switch is on for DT time period, the switch acts as a short circuit and the inductor is directly connected to the input. The inductor is linearly charged to the full value of the input. During the charging process, the polarity that appears across the passive switch reverse biases the diode, and the resultant circuit during DT is shown in Fig. 4.67. The voltage across the inductor is determined by applying KVL in the input loop. The inductor voltage during the switching on time is given in Eq. (4.42).

$$V_{in} - V_L = 0$$
$$V_L = V_{in} \tag{4.42}$$

Case 2, when the switch S is OFF: When the solid-state switch is OFF in the $D'T$ time period, the switch acts as an open circuit and the input supply is disconnected from the inductor and the load. The inductor starts discharging which reverses the polarity of the induced voltage across it. The polarity of the inductor forward biases the diode and it also acts as a short circuit. The inductor is now directly connected to the load. The inductor dissipates its stored energy to the load. In short, the inductor is charged from the DC source in the DT time and discharges to the load in time period $D'T$. The resultant circuit during the $D'T$ is shown in Fig. 4.68. The voltage across the load is determined by applying the KVL to the output loop. Eq. (4.43) indicates that the load voltage is equal to the inductor voltage.

$$V_L - V_{out} = 0$$
$$V_L = V_{out} \tag{4.43}$$

Fig. 4.69A shows the duty cycle given to the switch of the boost converter consisting of DT and $D'T$ and the voltage developed across the inductor during these time periods. The

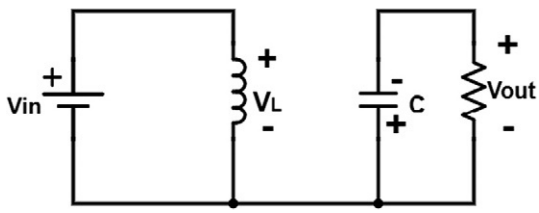

FIG. 4.67 DC-DC buck-boost converter circuit during the turn-on duty cycle.

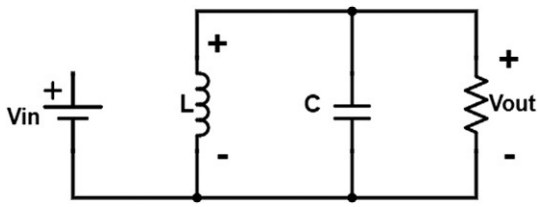

FIG. 4.68 DC-DC buck-boost converter circuit during the turn-off duty cycle.

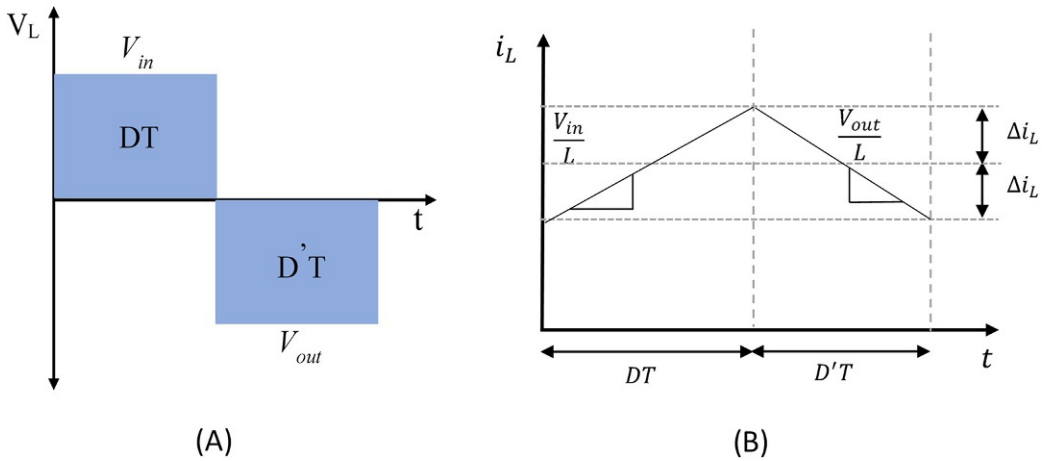

FIG. 4.69 (A) Voltage across inductor during turn-on and turn-off time and (B) inductor current during turn-on and turn-off time.

inductor average voltage is determined by dividing the area under the curve for one complete cycle by the time taken for that cycle as shown in Eq. (4.44).

$$\langle V_L \rangle = \frac{V_{in}(DT) + V_{out}(D'T)}{T} \tag{4.44}$$

As the average voltage across the inductor is zero, so

$$0 = \frac{T(DV_{in} + D'V_{out})}{T}$$

$$V_{out} = -\frac{D}{D'}V_{in}$$

$$V_{out} = -\left(\frac{D}{1-D}\right)V_{in} \tag{4.45}$$

Eq. (4.45) is the general equation to determine the output voltage of the buck-boost converter relating the input voltage and output voltages based on the duty cycle.

$$V_L = L.\frac{di}{dt_{(DT)}} \tag{4.46}$$

By comparing Eqs. (4.42), (4.46), we get the relation for the rate of charging current through the inductor during turn on time (DT).

$$L.\frac{di}{dt_{(DT)}} = V_{in}$$

$$\frac{di}{dt_{(DT)}} = \frac{V_{in}}{L} \tag{4.47}$$

Eq. (4.47) describes the rate of change of charging current through the inductor during DT. Similarly, for $D'T$,

$$V_L = L.\frac{di}{dt_{(D'T)}} \tag{4.48}$$

$$L.\frac{di}{dt_{(D'T)}} = V_{out}$$

By comparing Eqs. (4.43), (4.48), we get the rate of the discharging current through the inductor.

$$\frac{di}{dt_{(D'T)}} = \frac{V_{out}}{L} \tag{4.49}$$

Eq. (4.49) gives the time rate of change of discharging current through the inductor during $D'T$. The inductor current is plotted during DT and $D'T$, as shown in Fig. 4.69B. The slope of the graph for DT and $D'T$ gives the rate of charging and discharging current through the inductor, respectively. The relation for the inductor of the buck-boost converter is determined by multiplying the slope of the charging current by the time interval. Eq. (4.50) is the relation for the inductor of the buck-boost converter.

$$change\ in\ i_L = (slope)(length\ of\ sub-interval)$$

$$2\Delta i_L = \frac{V_{in}}{L}.DT$$

$$L = \frac{V_{in}}{2\Delta i_L}.DT \tag{4.50}$$

A DC-DC buck-boost converter is simulated in MATLAB. Fig. 4.70 shows the circuit simulated without any feedback. The output voltage depends upon the value of the duty cycle. The input voltage is 100 V and the duty cycle is 30%. The simulated circuit gives −42.05 V at

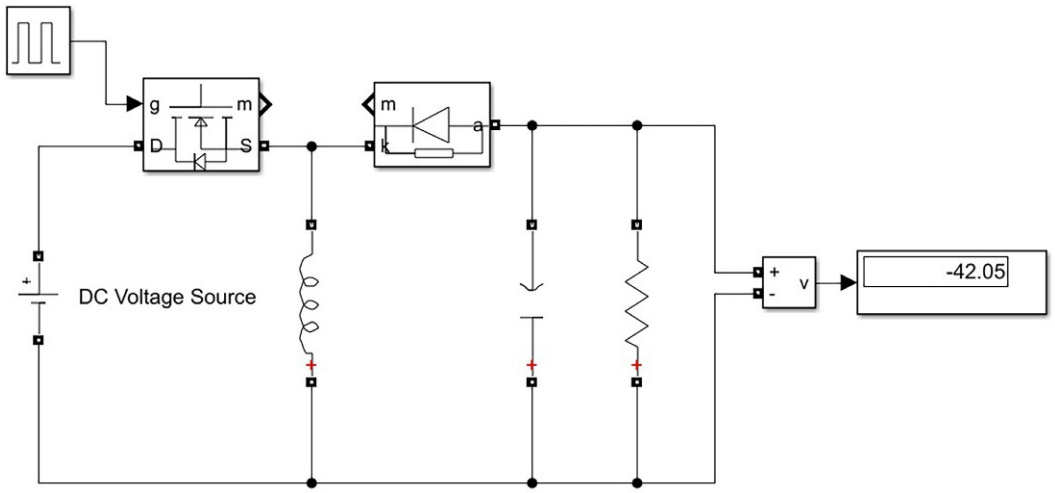

FIG. 4.70 MATLAB simulation diagram of DC-DC buck-boost converter.

the output. It is noticed that by changing the duty cycle, the output voltage also varies. The results of this circuit verify Eq. (4.45). Fig. 4.71 shows a simulated circuit diagram of a buck-boost converter with a feedback control circuit. The control circuit shown in Fig. 4.72 observes the reference voltage, which is set at 100 V in this case, and the voltages obtained at the output. If the output voltage deviates from the reference voltage, the feedback circuit adjusts the duty cycle in a way that we obtain the output voltage equal to the reference voltage [12].

4.5.4 Cuk converters

The Cuk converter is a type of DC-DC buck-boost converter having a mutual capacitor to transfer energy. The circuit of the Cuk converter is obtained by combining a boost converter with a buck converter as presented in Fig. 4.73. The circuit contains two SPDT switches arranged in a way that if one switch is ON, the other switch will be OFF.

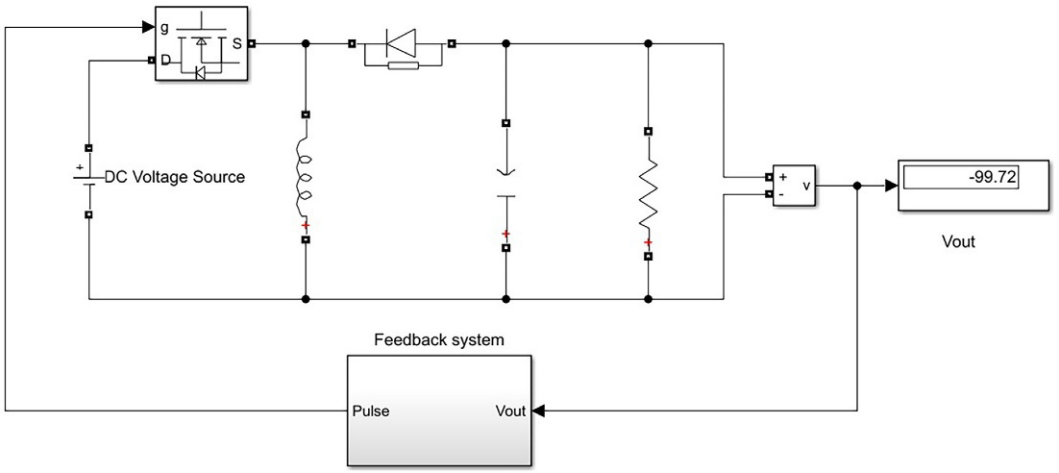

FIG. 4.71 MATLAB simulation diagram of DC-DC buck-boost converter with feedback control system.

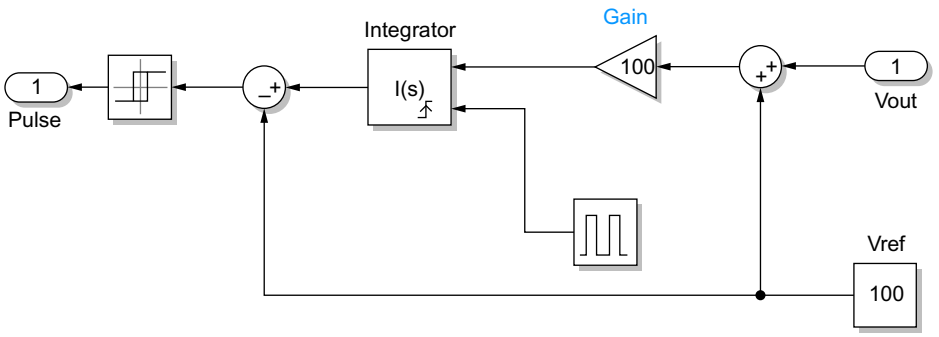

FIG. 4.72 Feedback control system of DC-DC buck-boost converter.

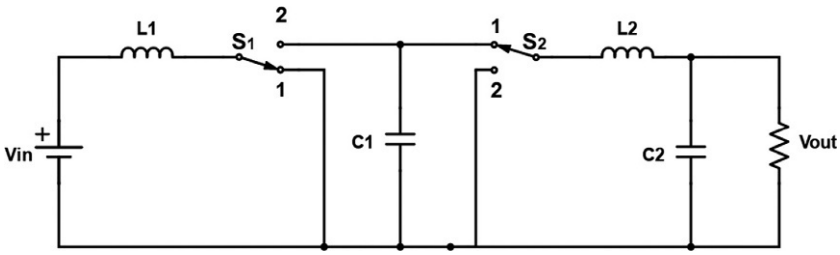

FIG. 4.73 DC-DC Cuk converter.

Case 1, when switch 1 and switch 2 are in position 1: In the first case the switch S_1 and switch S_2 both are kept in position 1. The inductor L_1 is directly coupled to the input DC supply and is disconnected from the rest of the circuit. The position of the switch S_2 connects the load to the capacitor that was previously charged when the switches were in position 2. We apply KVL at the input loop and output loop to determine the relation for the inductors' voltage V_{L1}, and V_{L2}. Eq. (4.51) gives the voltage across the inductor L_1 when both the switches are in position 1.

$$V_{in} - V_{L1} = 0$$

$$V_{L1} = V_{in} \tag{4.51}$$

Likewise, the voltage across the inductor L_2 is determined by applying KVL at the output loop and the voltage is given in Eq. (4.52). The input and the output loops are shown in Fig. 4.74.

$$-V_1 - V_{L2} - V_2 = 0$$

$$V_{L2} = -V_1 - V_2 \tag{4.52}$$

Case 2, when switch 1 and switch 2 are in position 2: in this case, the capacitor is coupled to the input and the rest of the output circuit is disconnected from the input supply and the capacitor. The input supply charges the capacitor in this case. In short, in the second case, the capacitor is charged by the input supply and in the first case, the capacitor is connected to the output and is discharged through the load. The voltage across the inductors L_1 and L_2 is determined by applying KVL at the input and output loop and the voltage across L_1 is given in Eq. (4.53).

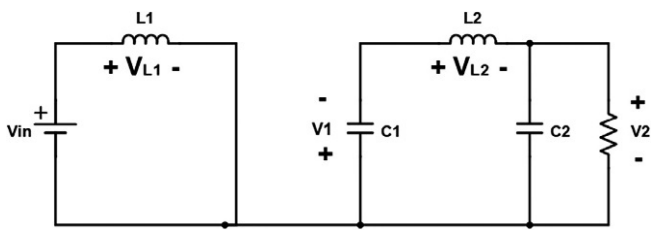

FIG. 4.74 DC-DC Cuk converter when the switch S_1 and S_2 are in position 1.

$$V_{in} - V_{L1} - V_1 = 0$$

$$V_{L1} = V_{in} - V_1 \tag{4.53}$$

Similarly the voltage across the inductor L_2 is determined by the KVL at the output loop and voltage is given in Eq. (4.54). The input and output loops are shown in Fig. 4.75.

$$-V_{L2} - V_2 = 0$$

$$V_{L2} = -V_2 \tag{4.54}$$

The average voltage of the inductor V_{L1} is determined using Fig. 4.76A for DT and $D'T$. The area under the graph is divided by the one complete cycle as shown in Eq. (4.55).

$$\langle V_{L1} \rangle = \frac{(V_{in})(DT) + (V_{in} - V_1)(D'T)}{T} \tag{4.55}$$

The average voltage across the inductor for one complete cycle is zero.

$$0 = V_{in}D + V_{in}D' - V_1D'$$

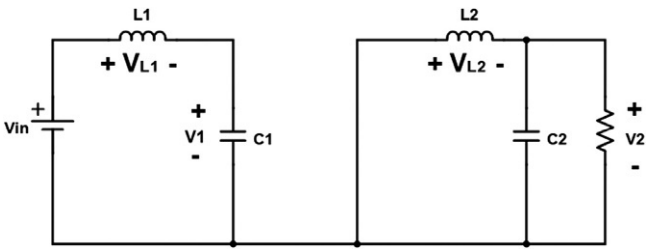

FIG. 4.75 DC-DC Cuk converter when switches S_1 and S_2 are in position 2.

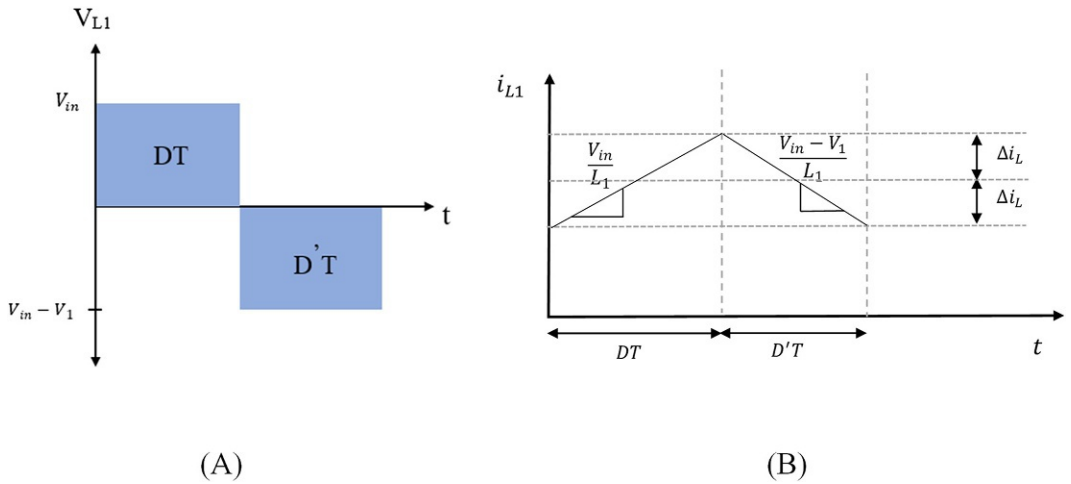

FIG. 4.76 DC-DC Cuk converter: (A) inductor voltage V_{L1} and (B) charging and discharging current of the inductor L_1 during DT and $D'T$.

$$0 = V_{in}(D + D') - V_1 D'$$

$$V_1 = \frac{V_{in}}{D'} \tag{4.56}$$

where V_1 is the voltage at the capacitor given in Eq. (4.56). Similarly, the average voltage of the inductor V_{L2} is determined using Fig. 4.77A for DT and $D'T$. The area under the graph is divided by the one complete cycle, as shown in Eq. (4.57).

$$\langle V_{L2} \rangle = \frac{(-V_1 - V_2)(DT) + (-V_2)(D'T)}{T} \tag{4.57}$$

$$0 = -V_1 D - V_2 D - V_2 D'$$

$$0 = -V_2(D + D') - V_1 D$$

$$V_2 = -V_1 D$$

By taking V_1 from Eq. (4.56),

$$V_2 = -\frac{V_{in}}{D'} D$$

$$V_2 = -\left(\frac{D}{1 - D}\right) V_{in} \tag{4.58}$$

Inductor (L_1) design for Cuk converter: To determine the relation for the inductor L_1, we need to calculate the rate of change of current through the inductor L_1 during T_{ON} and T_{OFF}, as shown in Fig. 4.77A. The voltage across the inductor L_1 is given by Eq. (4.59).

$$V_{L1} = L_1 . \frac{di_{L1}}{dt}_{(DT)} \tag{4.59}$$

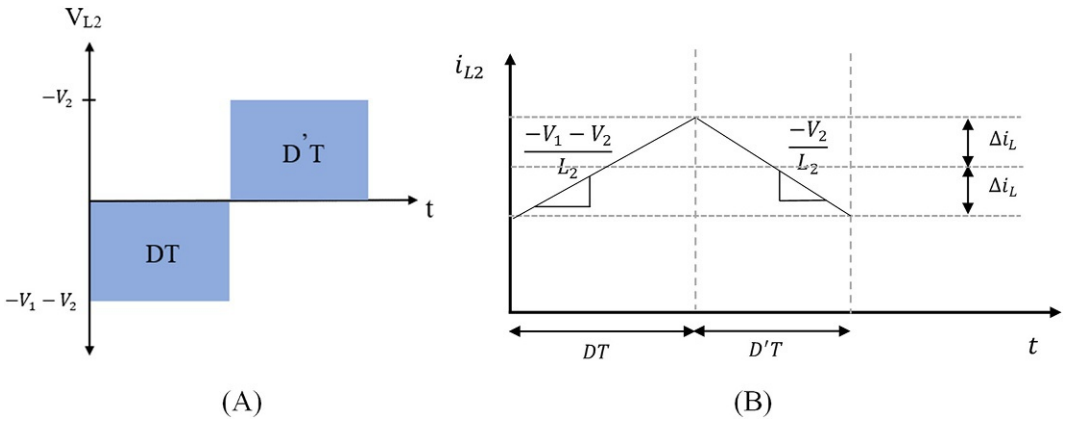

FIG. 4.77 DC-DC Cuk converter: (A) inductor voltage V_{L2} and (B) charging and discharging current of inductor L_1 during DT and $D'T$

By comparing Eqs. (4.51), (4.59),

$$L_1.\frac{di_{L1}}{dt}_{(DT)} = V_{in}$$

$$\frac{di_{L1}}{dt}_{(DT)} = \frac{V_{in}}{L_1} \tag{4.60}$$

Eq. (4.60) gives the charging current through the inductor L_1 when both the switches are in position 1. The relation of the inductor voltage during turn off time is given in Eq. (4.61).

$$V_{L1} = L_1.\frac{di_{L1}}{dt}_{(D'T)} \tag{4.61}$$

By Eq. (4.53), $V_{L1} = V_{in} - V_1$, So by comparing Eqs. (4.53), (4.61), we can conclude as follows:

$$L_1.\frac{di_{L1}}{dt}_{(D'T)} = V_{in} - V_1$$

$$\frac{di_{L1}}{dt}_{(D'T)} = \frac{V_{in} - V_1}{L_1} \tag{4.62}$$

Eq. (4.62) is the current change through the inductor L_1 when the switches are in position 2.

$$change\ in\ i_L = (slope)(length\ of\ sub - interval)$$

$$2\Delta i_{L1} = \frac{V_{in}}{L_1}.DT$$

$$L_1 = \frac{V_{in}}{2\Delta i_{L1}}.DT \tag{4.63}$$

Inductor (L_2) design for Cuk converter: To determine the relation for the inductor L_2, we need to calculate the rate of change of current through the inductor L_2 during T_{ON} and T_{OFF} as shown in Fig. 4.77. The voltage across the inductor L_2 is given by Eq. (4.64).

$$V_{L2} = L_2.\frac{di_{L2}}{dt}_{(DT)} \tag{4.64}$$

By Eq. (4.52), $V_{L2} = -V_1 - V_2$, thus the above equation can be written as follows:

$$L_2.\frac{di_{L2}}{dt}_{(DT)} = -V_1 - V_2$$

$$\frac{di_{L2}}{dt}_{(DT)} = \frac{-V_1 - V_2}{L_2} \tag{4.65}$$

Eq. (4.65) is the current change through the inductor L_2 when the switches are in position 1. For turn-off time, the voltage across the inductor is written as Eq. (4.66).

$$V_{L2} = L_2.\frac{di_{L2}}{dt}_{(D'T)} \tag{4.66}$$

By Eq. (4.54), $V_{L2} = -V_2$, By comparing Eqs. (4.54), (4.66), we get the rate of charge of current through the inductor L_2.

$$L_2 . \frac{di_{L2}}{dt}_{(D'T)} = -V_2$$

$$\frac{di_{L2}}{dt}_{(D'T)} = \frac{-V_2}{L_2} \tag{4.67}$$

Eq. (4.67) is the current change through the inductor L_2 when the switches are in position 2.

$$change\ in\ i_{L2} = (slope)(length\ of\ sub - interval)$$

$$2\Delta i_{L2} = \frac{-V_1 - V_2}{L_2} . DT$$

$$L_2 = \frac{-V_1 - V_2}{2\Delta i_{L2}} . DT \tag{4.68}$$

4.6 Inverters (DC-AC inverters)

4.6.1 Single-phase full bridge inverter

In a solar photovoltaic system, the DC output needs to be converted into AC to entertain the AC load or to feed the grid. Inverters are used to convert the DC voltage into AC. A single-phase full-wave bridge inverter which is also called an H-bridge inverter is presented in Fig. 4.78. The switches S_1 and S_2 are the single pole double through switches. When switch S_1 is connected to pole 1, the positive terminal of V_{dc} is tied to the load and when switch S_2 is connected to pole 1, the negative terminal of V_{dc} is tied to the load. Similarly, When switch S_1 is tied to pole 2, the negative terminal of V_{dc} is tied to the load and when switch S_2 is tied to pole 2, the positive terminal of V_{dc} is tied to the load. In this way, different switching sequence generates positive and negative polarity signals.

For practical applications, the realization of the mechanical SPDT switches is performed by substituting one SPDT switch with two active switches. In Fig. 4.79, switch S_1 is replaced by Q_1 and Q_2 controlled switches and switch S_2 is replaced by Q_3 and Q_4 controlled switches. The load is connected between the center of the left and right legs A and B. When switches Q_1 and Q_2 are on and Q_3 and Q_4 are off, the current follows the path $V_{dc}^{+} - Q_1 - A - V_{out} - B - Q_2 - V_{dc}^{-}$.

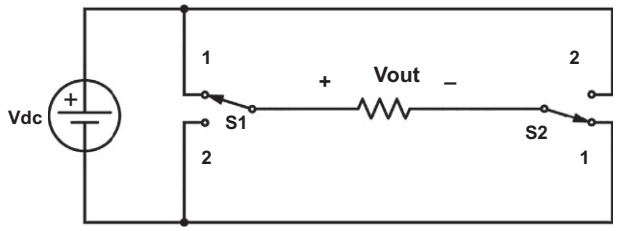

FIG. 4.78 Mechanical switches-based H-bridge inverter.

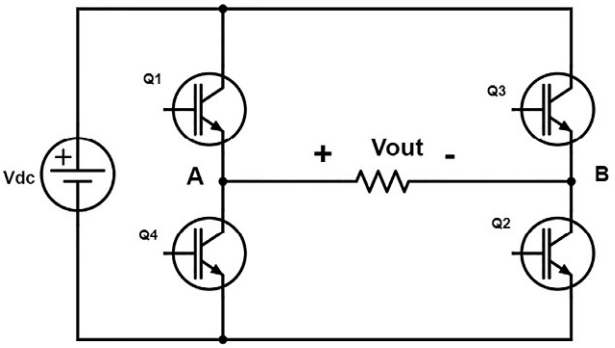

FIG. 4.79 Solid-state switches-based on H-bridge inverter.

Similarly, when switches Q_3 and Q_4 are on and Q_1 and Q_2 are off, the current follows the path $V_{dc}^{+} - Q_3 - B - V_{out} - A - Q_4 - V_{dc}^{-}$. In short, for the first switching period, the current follows the path from A to B, and in the second switching period, the current follows the path from B to A, generating an AC voltage waveform.

The full-bridge inverter or the H-bridge inverter was also simulated in MATLAB/Simulink. Fig. 4.80 shows a circuit diagram simulated in MATLAB consisting of four controlled switches Q_1– Q_4. It can be noted that Q_1 and Q_2 are triggered from the same pulse generator and Q_3 and Q4 are triggered from another pulse generated. The input voltage V_{dc} is 100 V. The waveform at the output can be visualized at two different points. One right after the conversion circuit and the other after the LC filter circuit. Fig. 4.81 shows the output of the inverter before the filtering circuit which is a square wave of positive and negative periods. Fig. 4.82 demonstrates the output voltage waveform after the filtering circuit. The input voltage was 100 V DC and Figs. 4.81 and 4.82 show the output AC voltage waveform of 100 V, confirming the conversion of DC into AC with the help of an inverter.

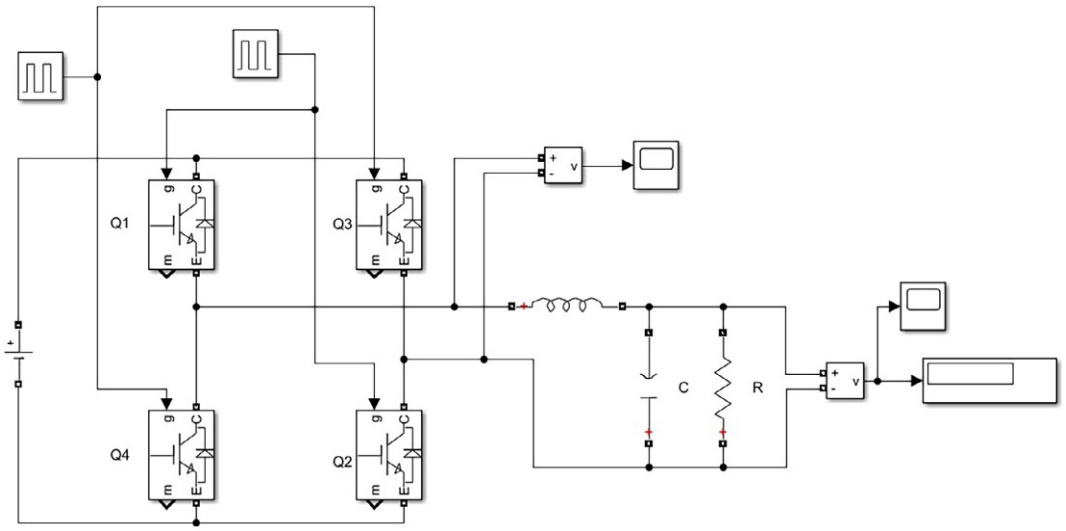

FIG. 4.80 MATLAB simulation diagram of an H-bridge inverter.

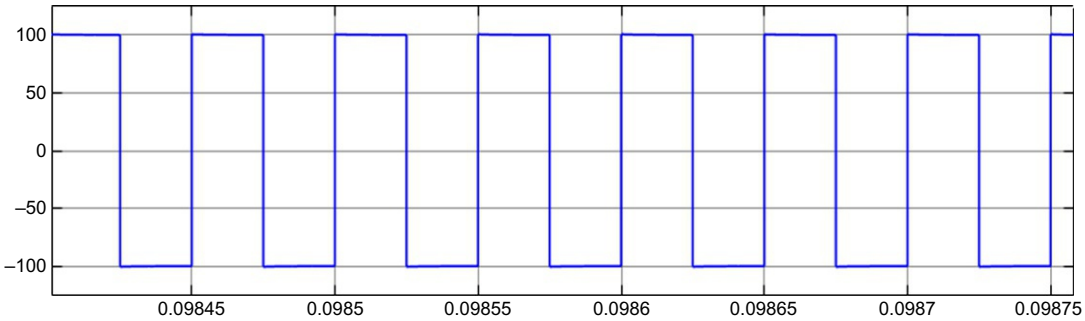

FIG. 4.81 Output waveform of MATLAB simulated inverter without filter.

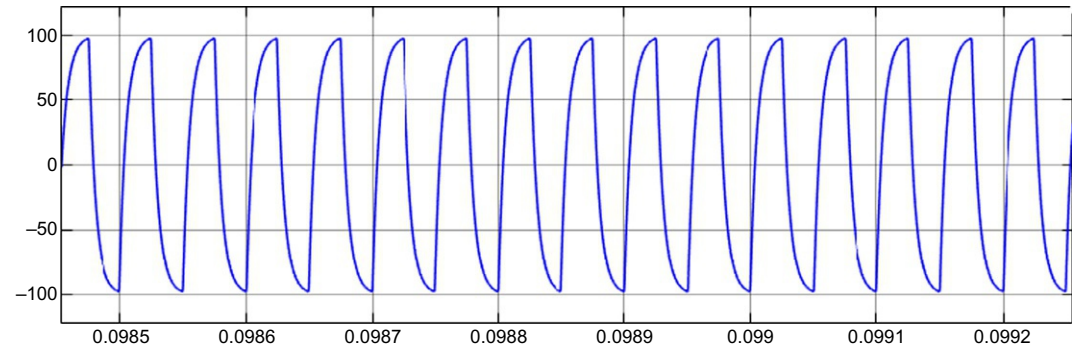

FIG. 4.82 Output waveform of MATLAB simulated inverter with filter at the output.

4.6.2 Three-phase full bridge inverter

A three-phase inverter consists of three legs and each leg contains two switches. The output is taken from each leg between the two switches as shown in Fig. 4.83. The first leg contains Q_1 and Q_4, leg 2 contain Q_3 and Q_6, and leg 3 contain Q_5 and Q_2. At any time, both of the switches in a single leg cannot be on. The switching scheme of the switches Q_1–Q_6 is discussed below.

In three-phase AC voltages, each phase remains in positive polarity for 120°. We assume the conduction time is 180° for each switch. We start from the switch Q_1 and keep it on until 180° as shown in Fig. 4.84, but after 120° of phase A, phase B also becomes positive so switch Q_3 is turned on after 120° for a period of 180 (120°–300) as shown in Fig. 4.85. Similarly after 120° of phase B, Phase C also becomes positive for 180° (240–60). Concluding we can say that each switch remains closed for 180° and opened for other 180°. It must also be kept in mind that in each leg one switch will remain closed for 180° and the other switch will be opened for that 180°. Both switches in each leg cannot be closed or open for the same time period.

To satisfy the above-stated condition, we turn off Q_1, Q_3, and Q_5 in the predetermined order. This means that when Q_1 is on, Q_4 will be off. When Q_3 is on, Q_6 will be off. When Q_5 is on, Q_2 will be off, as shown in Fig. 4.86. After completion of the conduction period of Q_1, we will have to turn on Q_4. After completion of the conduction period of Q_3, we will have to turn on

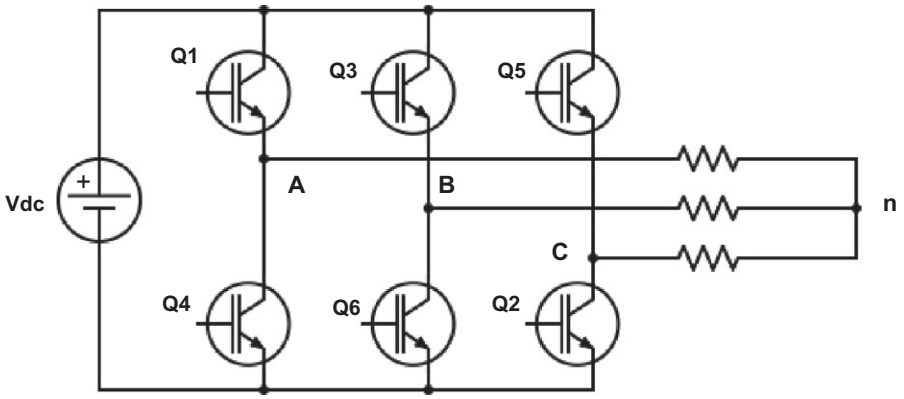

FIG. 4.83 Circuit diagram of three-phase inverter.

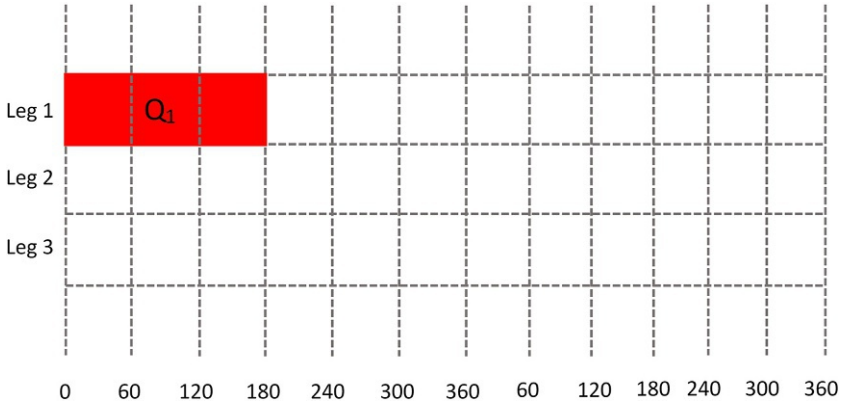

FIG. 4.84 Switching states of Q_1 in leg 1.

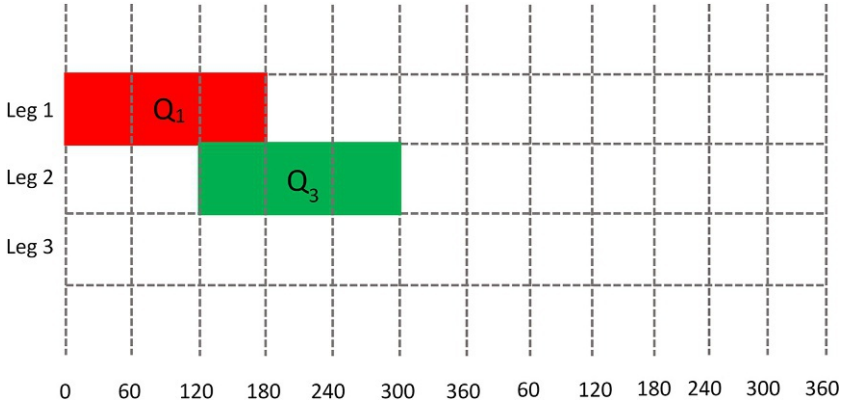

FIG. 4.85 Switching states of Q_3 in leg 2.

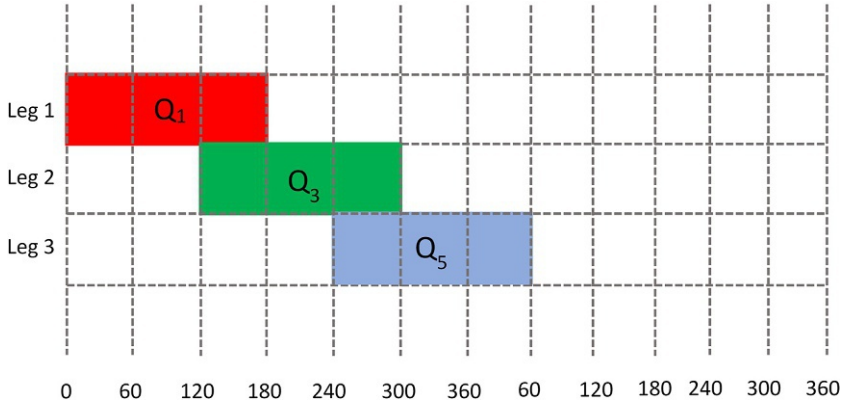

FIG. 4.86 Switching states of Q_5 in leg 3.

Q_6we will have to on Q_6. After completion of the conduction period of Q_5, we will have to turn on Q_2. Following the same symmetry, as discussed above, we can fill the unfilled time periods in Fig. 4.87. The resulting complete switching scheme is shown in Fig. 4.88, which can be elaborated as follows.

i. From 0°–60°; Q_1, Q_6, and Q_5 will be on and Q_2, Q_3, and Q_4 will be off.
ii. From 60°–120°; Q_1, Q_6, and Q_2 will be on and Q_3, Q_4, and Q_5 will be off.
iii. From 120°–180°; Q_1, Q_3, and Q_2 will be on and Q_4, Q_5, and Q_6 will be off.
iv. From 180°–240°; Q_4, Q_3, and Q_2 will be on and Q_1, Q_5, and Q_6 will be off.
v. From 240°–300°; Q_4, Q_3, andQ_5 will be on and Q_1, Q_2, and Q_6 will be off.
vi. From 300°–360°; Q_4, Q_6, and Q_5 will be on and Q_1, Q_2, and Q_3 will be off.

The switching pattern continues in the same way as described above.

The above-described inverter is also simulated in MATLAB/Simulink. Fig. 4.89 shows a simulation diagram of a three-phase inverter consisting of switches ($Q_1 - Q_6$) in three legs.

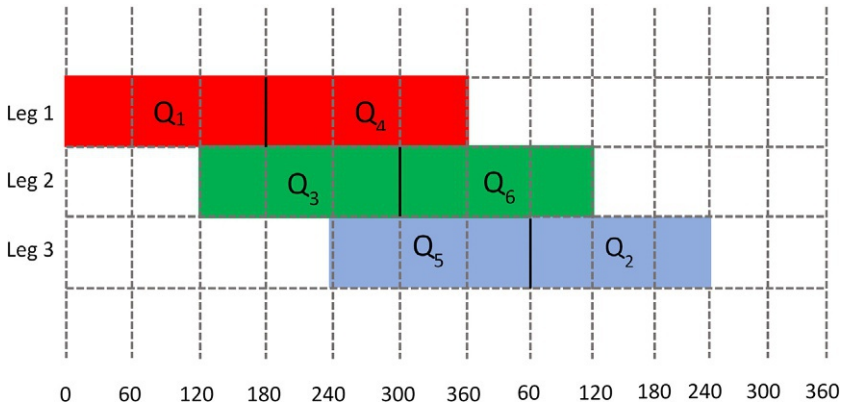

FIG. 4.87 Switching states of Q_4, Q_6, and Q_2 in leg 1, leg 2, and leg 3, respectively.

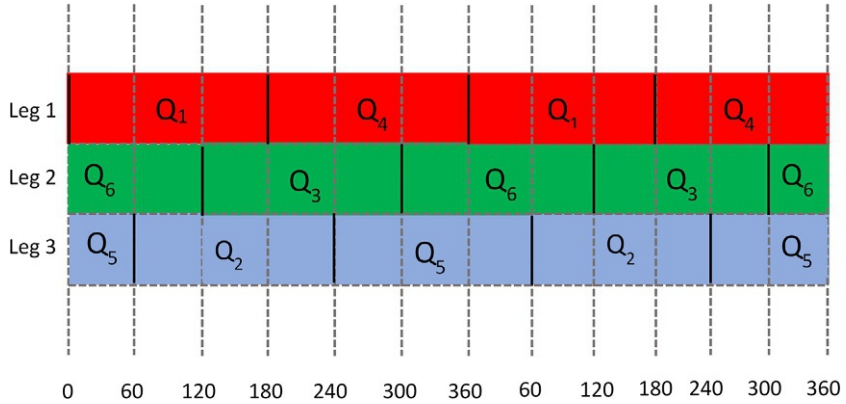

FIG. 4.88 Switching states of all the switches from 0° to 360°.

Q_1 and Q_4 are in the first leg, Q_3 and Q_6 are in the second leg, and Q_5 and Q_2 are in the third leg. The output of three-phase inverter is taken from the central point of each leg. Fig. 4.90 shows the output voltage of all three phases—phase A, phase B, and phase C—without using any filter. It can be seen that there is a phase shift of 120°. We use an LC filter at the output, and the output voltage and output current of a three-phase inverter are shown in Figs. 4.91 and 4.92, respectively.

4.6.3 Multilevel inverters

4.6.3.1 Diode clamped MLI

Diode clamped multilevel inverters (MLIs) are also identified as neutral point clamped inverters. A circuit diagram of a three-level DC-MLI is shown in Fig. 4.93. The DC-MLI contains two pairs of series switches and the output is taken from the midpoint of these pairs of series switches [13].

The number of the circuit components that are required to develop the DC-MLI are calculated by the equations. For an MLI of n levels, Eq. (4.69) is used to determine the number of voltage sources (N_{dc}), Eq. (4.70) is used to determine the number of DC bus capacitors (N_C), Eq. (4.72) is used to determine the number of switches (N_Q), and Eq. (4.71) is used to determine the number of clamping diodes (N_D).

$$N_{dc} = (n-1) \tag{4.69}$$

$$N_C = (n-1) \tag{4.70}$$

$$N_D = (n-1)(n-2) \tag{4.71}$$

$$N_Q = 2(n-1) \tag{4.72}$$

To implement a three-level DC-MLI, we found that two diodes, two capacitors, and four switches are required. A circuit diagram of a three-level inverter is provided in Fig. 4.93. Two capacitors, C_1 and C_2, connected in series, divide V_{dc} in three levels: $V_{dc}/2$, 0, and $-V_{dc}/2$. The

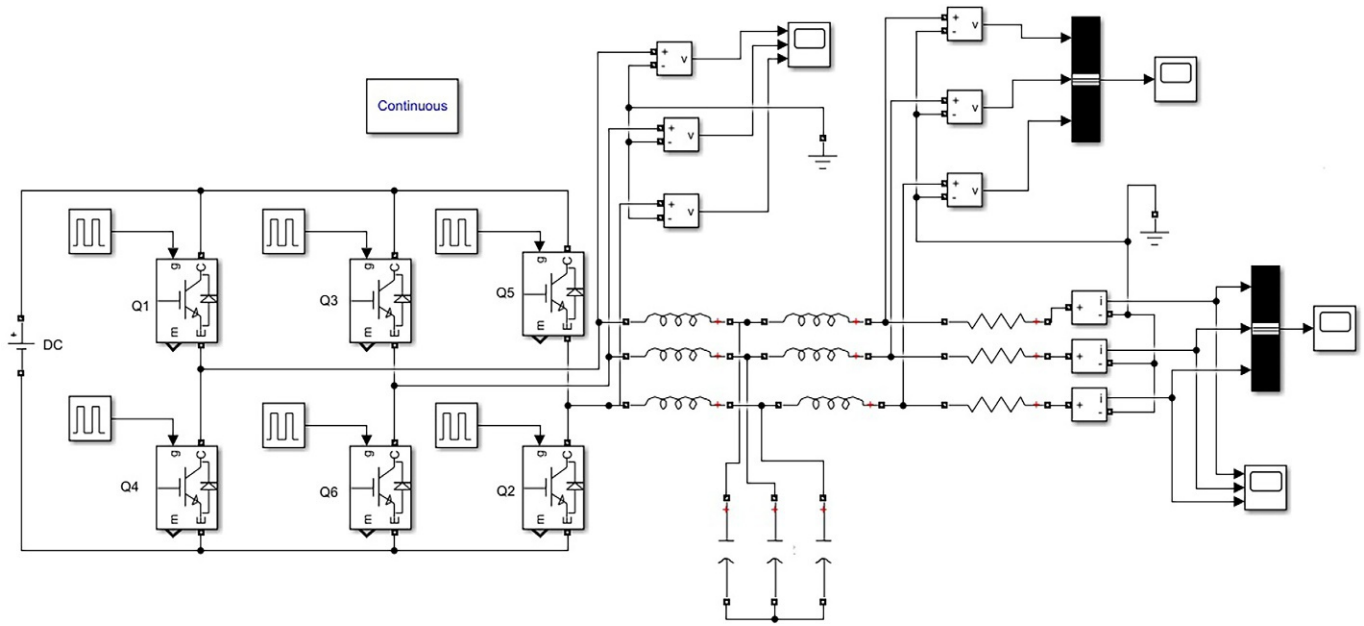

FIG. 4.89 MATLAB simulation diagram of three-phase inverter.

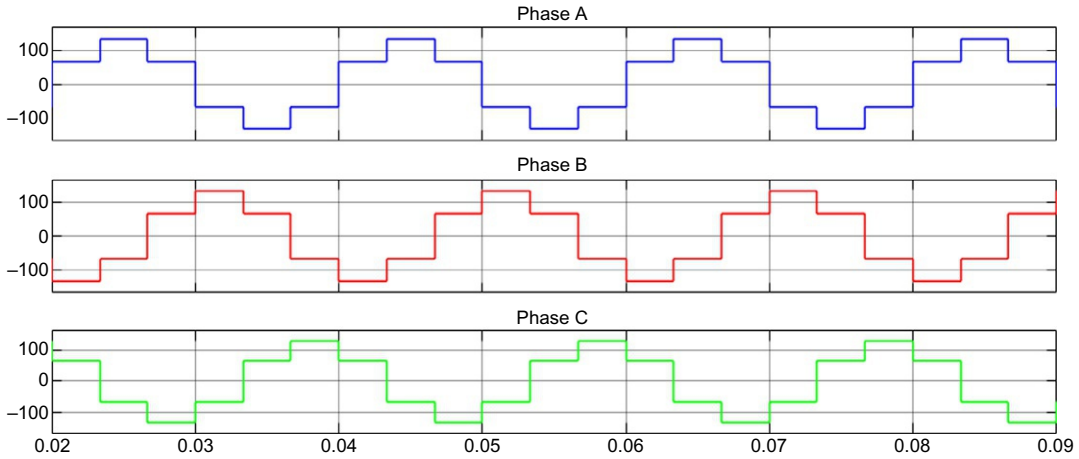

FIG. 4.90 Output voltage waveforms of MATLAB simulation of three-phase inverter without output filter.

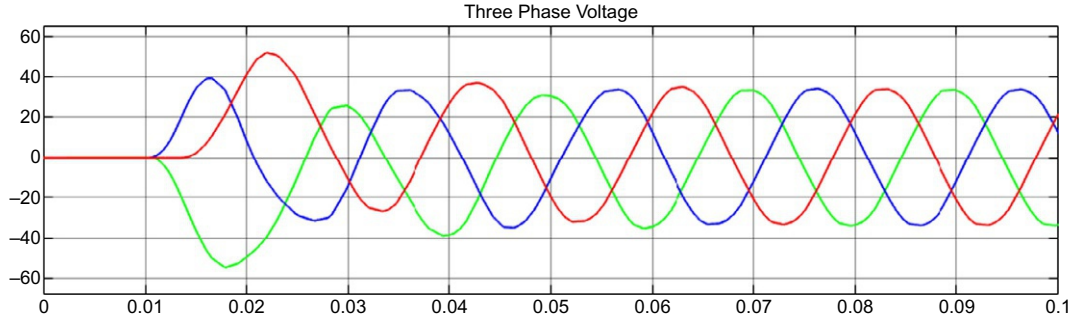

FIG. 4.91 Output voltage waveforms of MATLAB simulation of three-phase inverter without output filter.

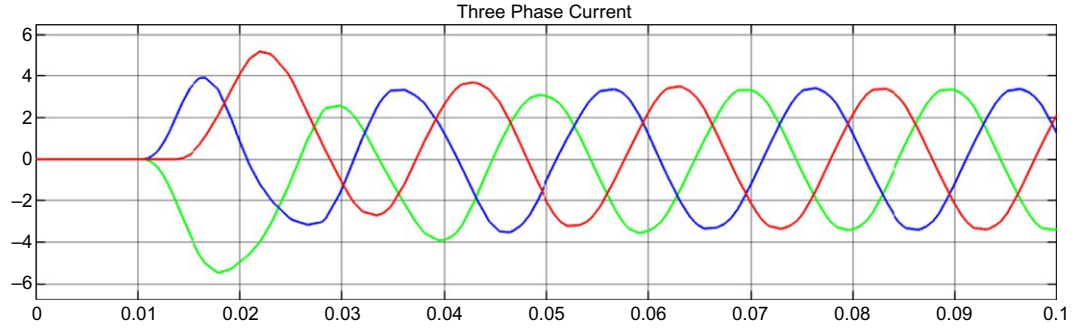

FIG. 4.92 Output current waveforms of MATLAB simulation of three-phase inverter with an output filter.

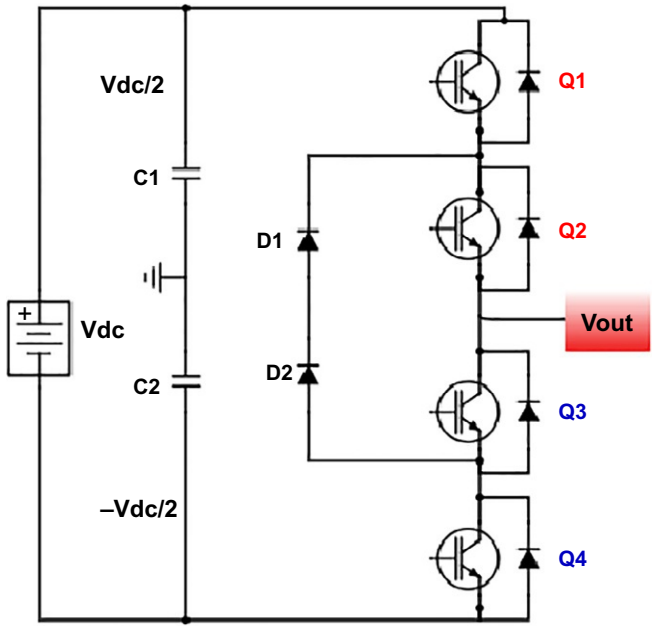

FIG. 4.93 Circuit diagram of diode clamped three-level multilevel inverter.

switching states for each voltage level are depicted in Fig. 4.94. The switches Q_1 and Q_2 are triggered for voltage level $V_{dc}/2$, Q_3 and Q_4 are triggered for voltage level $-V_{dc}/2$, and Q_2 and Q_3 are triggered for 0 voltage levels.

For a five-level DC-MLI, n will be taken as five in the equations. To implement a five-level DC-MLI we need four capacitors, 12 diodes, and eight switches. The circuit diagram of a five-level DC-MLI is shown in Fig. 4.95. The voltage across each capacitor is $\frac{V_{dc}}{4}$, hence, the voltage levels for a five-level DC-MLI are $\frac{V_{dc}}{2}$, $\frac{V_{dc}}{4}$, 0, $\left(\frac{-V_{dc}}{4}\right)$, and $\left(\frac{-V_{dc}}{2}\right)$. The switching states of all the switches (Q_1 *to* Q_8) for given five levels of voltage are shown in Fig. 4.96.

For voltage level $\frac{V_{dc}}{2}$, switches (Q_1, Q_2, Q_3, and Q_4) are triggered whereas remaining (Q_5, Q_6, Q_7, and Q_8) are OFF. The source voltage V_{dc} is connected to the load through the capacitors C_1 and C_2, and switches Q_1, Q_2, Q_3, and Q_4. For voltage level $\frac{V_{dc}}{4}$, switches (Q_2, Q_3, Q_4, and Q_5) are triggered whereas the remaining (Q_1, Q_6, Q_7, and Q_8) are OFF. The source voltage V_{dc} is connected to the load through the capacitors C_2, diode D1 and switches, Q_2, Q_3, Q_4, and Q_5. As only C_2 is connected, the voltage level is $\frac{V_{dc}}{4}$. For zero voltage level, switches (Q_3, Q_4, Q_5, and Q_6) are triggered whereas the remaining (Q_1, Q_2, Q_7, and Q_8) are OFF. Therefore, no capacitor is connected, and both sides of the switches are directly connected to the ground, maintaining a zero voltage level across the load. For voltage level $-\frac{V_{dc}}{4}$, switches (Q_4, Q_5, Q_6, and Q_7) are triggered whereas the remaining (Q_1, Q_2, Q_3, and Q_8) are OFF. Capacitor C_3 is connected to the load and ground through the switches Q_4, Q_5, Q_6, and Q_7. The polarity of the voltage is negative as the current flows from the ground to the load. For voltage level $-\frac{V_{dc}}{2}$, switches (Q_5, Q_6, Q_7, and Q_8) are triggered whereas remaining Q_1, Q_2, Q_3, and Q_4

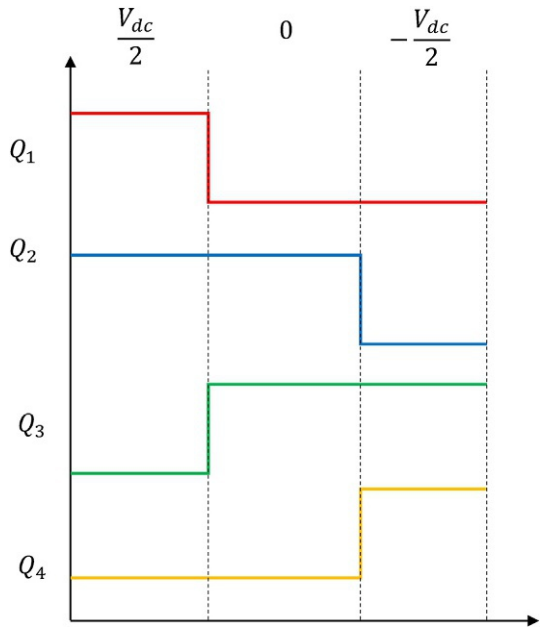

FIG. 4.94 Voltage levels for different switching states of three-level diode clamped multilevel inverter.

are OFF. Capacitor C_3 and C_4 are connected to the load and ground through the switches Q_5, Q_6, Q_7, and Q_8. Again, the polarity of the voltage is negative as the current flows from the ground to the load. The voltage levels for different switching states of the solid-state switches are shown in Fig. 4.96. A circuit diagram of a three-phase diode clamped multilevel inverter is shown in Fig. 4.97. Table 4.2 shows the number of components in different levels of DC-MLI.

4.6.3.2 Flying capacitor MLI

Compared to the diode clamped multilevel inverter in which diodes are used as a voltage clamping device, a new topology of MLI in which capacitors are used as the voltage clamping device. This topology is termed flying capacitor multilevel inverter. The number of components depends upon the level of the inverter. For n levels of FC-MLI, Eq. (4.74) is used to determine the number of DC bus capacitors (N_C), Eq. (4.73) is used to determine the number of voltage sources (N_{dc}), Eq. (4.76) is used to determine the number of switches (N_Q), and Eq. (4.75) is used to determine the number of balancing capacitors (N_{BC}).

$$N_{dc} = (n-1) \tag{4.73}$$

$$N_C = (n-1) \tag{4.74}$$

$$N_{BC} = {}^{(n-1)(n-2)}/_{2} \tag{4.75}$$

$$N_Q = 2(n-1) \tag{4.76}$$

Using the above-stated equations, we can find out the required number of components for any level of the inverter. For a three-level MLI, two DC-bus capacitors, four solid-state

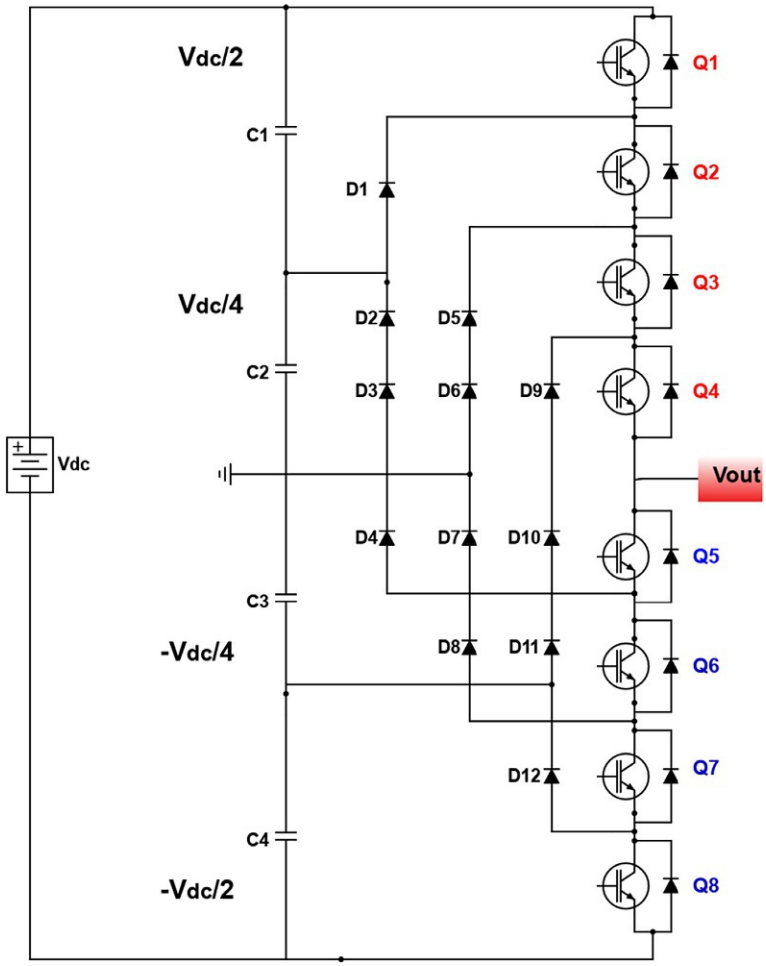

FIG. 4.95 Circuit diagram of diode clamped five-level multilevel inverter.

switches, and one balancing capacitor are used. The number of voltage sources depends upon the number of DC-bus capacitors and the equations of both are also the same. The circuit diagram of a FC-MLI of three levels is depicted in Fig. 4.98 [14].

The capacitors C_1 and C_2 are connected in series to split the V_{dc} in following voltage levels: $V_{dc}/2$, 0, and, $-V_{dc}/2$. Because of the series connection of C_1 and C_2, V_{dc} equally charges both capacitors and an equal voltage appears across them. The switching scheme of the three-level FC-MLI is shown in Fig. 4.99. To obtain the voltage level $V_{dc}/2$ at the output, Q_1 and Q_2 are in the conduction mode and Q_3 and Q_4 are off. For 0 voltage level, Q_1 and Q_3 are conducting and Q_2 and Q_4 are in the off state. To obtain the voltage level $-V_{dc}/2$ at the output, Q_3 and Q_4 are conducting and Q_1 and Q_2 are in the off state.

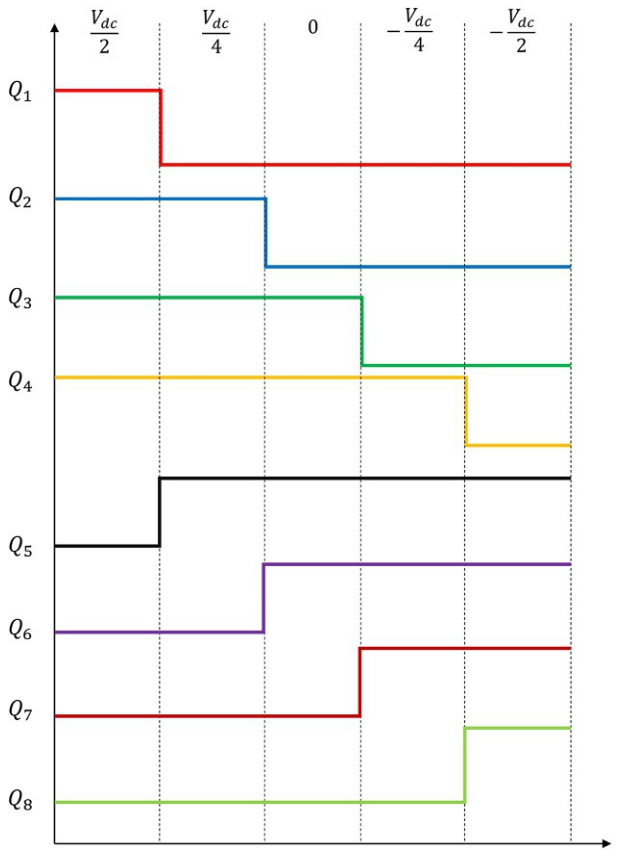

FIG. 4.96 Voltage levels for different switching states of five-level diode clamped multilevel inverter.

To implement a five-level inverter, all the required number of components are determined using Eqs. (4.73)–(4.76). For a five-level inverter, four DC-bus capacitors, eight solid-state switches, and six balancing capacitors are used. A circuit diagram of A five-level FC-MLI is depicted in Fig. 4.100. Fig. 4.101 indicates the switching states and associated voltage levels of a five-level inverter. Each capacitor voltage is $\frac{V_{dc}}{4}$, hence, the voltage levels for a five-level FC-MLI are $\frac{V_{dc}}{2}$, $\frac{V_{dc}}{4}$, 0, $(\frac{-V_{dc}}{4})$, and $\frac{-V_{dc}}{2}$. Each voltage level is associated with a specific switching state of the solid-state switches (Q_1 to Q_8) as shown in Fig. 4.101. For voltage level $\frac{V_{dc}}{2}$, switches (Q_1 to Q_4) are triggered whereas remaining switches (Q_5 to Q_8) are off. For voltage level $\frac{V_{dc}}{4}$, switches Q_1, Q_2, Q_3, and Q_5 are ON whereas the remaining (Q_4, Q_6, Q_7, and Q_8) are OFF. For zero voltage level, switches Q_1, Q_2, Q_5, and Q_6 are ON whereas the remaining Q_3, Q_4, Q_7, and Q_8 are OFF. For voltage level $-\frac{V_{dc}}{4}$, switches Q_1, Q_5, Q_6, and Q_7 are ON whereas the remaining Q_2, Q_3, Q_4, and Q_8 are OFF. For voltage level $-\frac{V_{dc}}{2}$, switches Q_5, Q_6, Q_7, and Q_8 are ON whereas remaining Q_1, Q_2, Q_3, and Q_4 are OFF. The switching states for different voltage levels in five-level FC-MLI are summarized in Fig. 4.101.

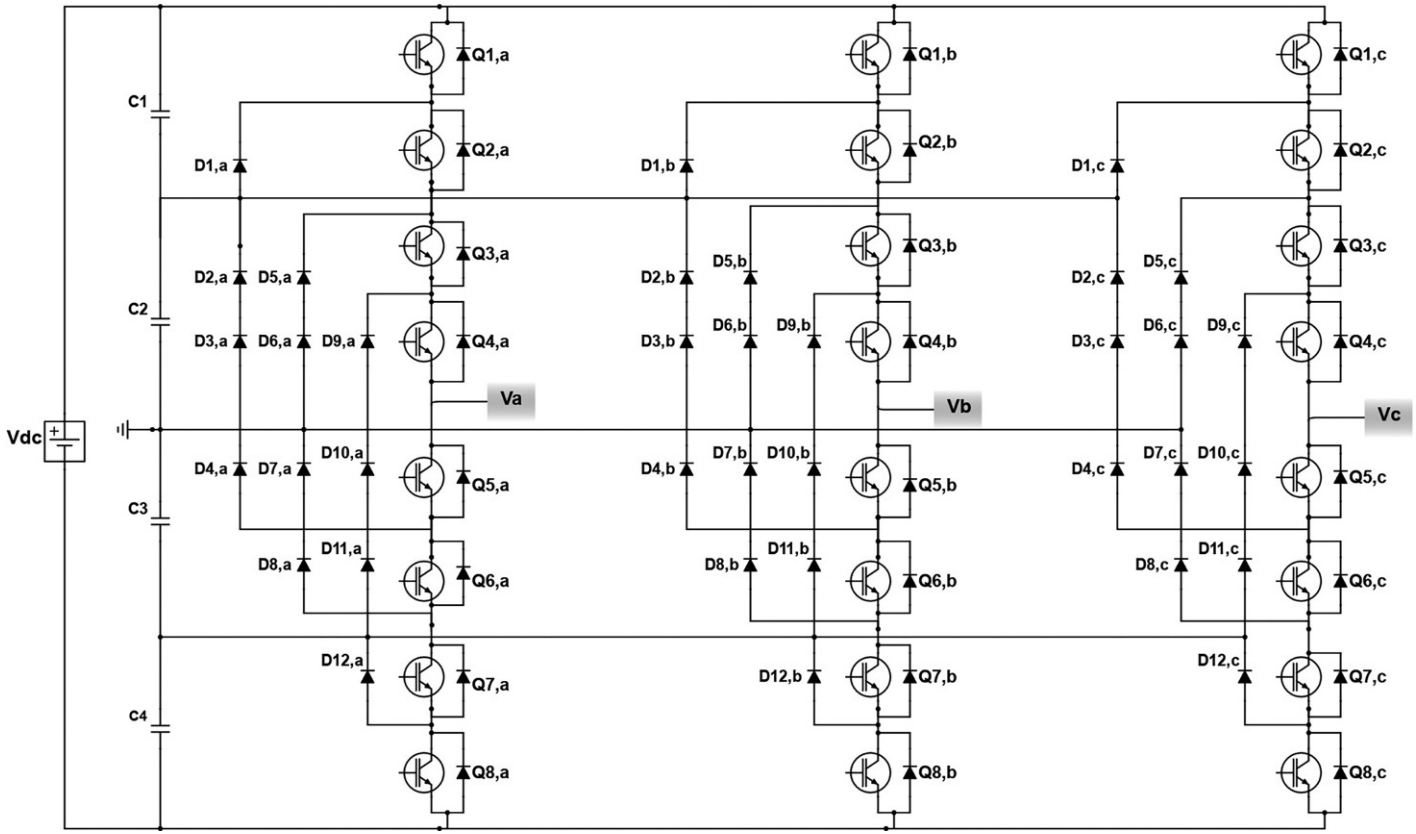

FIG. 4.97 Circuit diagram of diode clamped three-phase multilevel inverter.

TABLE 4.2 Various elements for various voltage levels of diode clamped multilevel inverter (DC-MLI).

Level "n"	Capacitors (N_C)	Diodes (N_D)	Switches (N_Q)
3	2	2	4
5	4	12	8
7	6	30	12
9	8	56	16
11	10	90	20
13	12	132	24

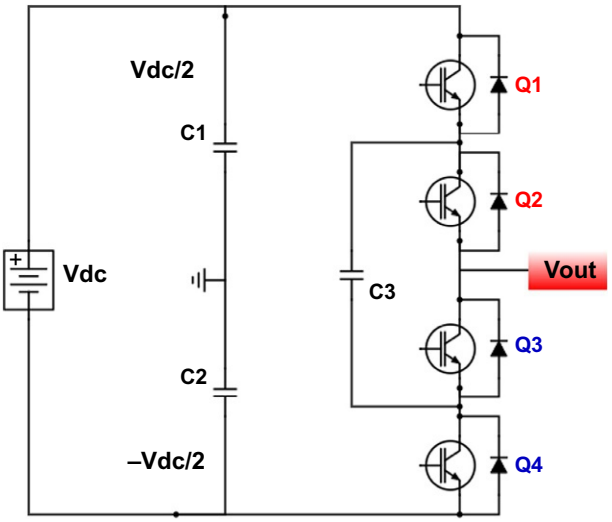

FIG. 4.98 Circuit diagram of flying capacitor three-level multilevel inverter.

4.6.3.3 Cascaded H-bridge multilevel inverter

Cascaded H-bridge inverters are considered a cost-effective MLI since they require fewer components to implement than other types of MLIs. H-bridge MLI is the series combination of H-bridge inverters. Each H-bridge inverter has its voltage source. Since the voltage sources for each inverter are isolated from the others, they can easily be used with different DC sources like fuel cells and solar photovoltaics. The lower and upper limits of the voltage levels are determined by using Eqs. (4.77), (4.78); the other components like the number of solid-state switches and the number of capacitors are determined using Eqs. (4.79), (4.80).

$$V_{min} = (-V_{dc})\frac{n-1}{2} \tag{4.77}$$

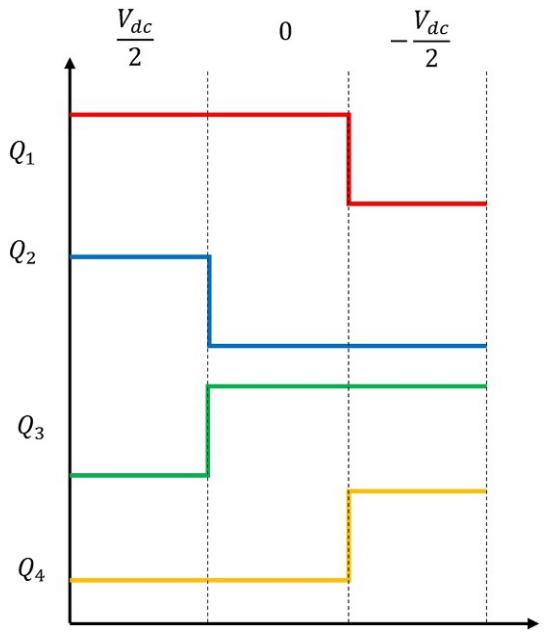

FIG. 4.99 Voltage levels for different switching states of three-level flying capacitor multilevel inverter.

$$V_{max} = (V_{dc})\frac{n-1}{2} \tag{4.78}$$

$$N_Q = 2\,(n-1) \tag{4.79}$$

$$N_C = \frac{n-1}{2} \tag{4.80}$$

A three-level cascaded H-bridge inverter is the same as discussed in Section 4.6.1. A five-level inverter is obtained by connecting two H-bridge inverters in series for $2V_{dc}$, V_{dc}, 0, $-V_{dc}$, and $-2V_{dc}$ voltage levels. The required number of components for any level of CHB-MLI is found by using the abovementioned equations. For five-level inverter, two capacitors and eight solid-state switches are used. A circuit diagram of a five-level CHB-MLI is shown in Fig. 4.102. Voltage levels and the corresponding switching states of the solid-state switches are shown in Fig. 4.103.

Voltage level $2V_{dc}$: switches Q_1, Q_2, Q_5, and Q_6 must be ON while switches Q_3, Q_4, Q_7, and Q_8 must be OFF. To obtain this voltage level, the current follows the track V_{dc1}, Q_1, *load*, Q_6, V_{dc2}, Q_5, Q_2, and V_{dc1}. Since both the sources are in the track of the current, the sum of both of them is obtained at the output.

Voltage level V_{dc}: switches Q_1, Q_2, Q_6, and Q_8 must be ON while switches Q_3, Q_4, Q_5, and Q_7 should be OFF. The adopted track for this level is V_{dc1}, Q_1, *load*, Q_6, Q_8, Q_2, and V_{dc1}. Since the second voltage source is sidestepped, only V_{dc} is obtained at the output.

Zero voltage level: switches Q_2, Q_4, Q_6, and Q_8 must be ON while switches Q_1, Q_3, Q_5, and Q_7 must be OFF. No voltage source is present in the path described above.

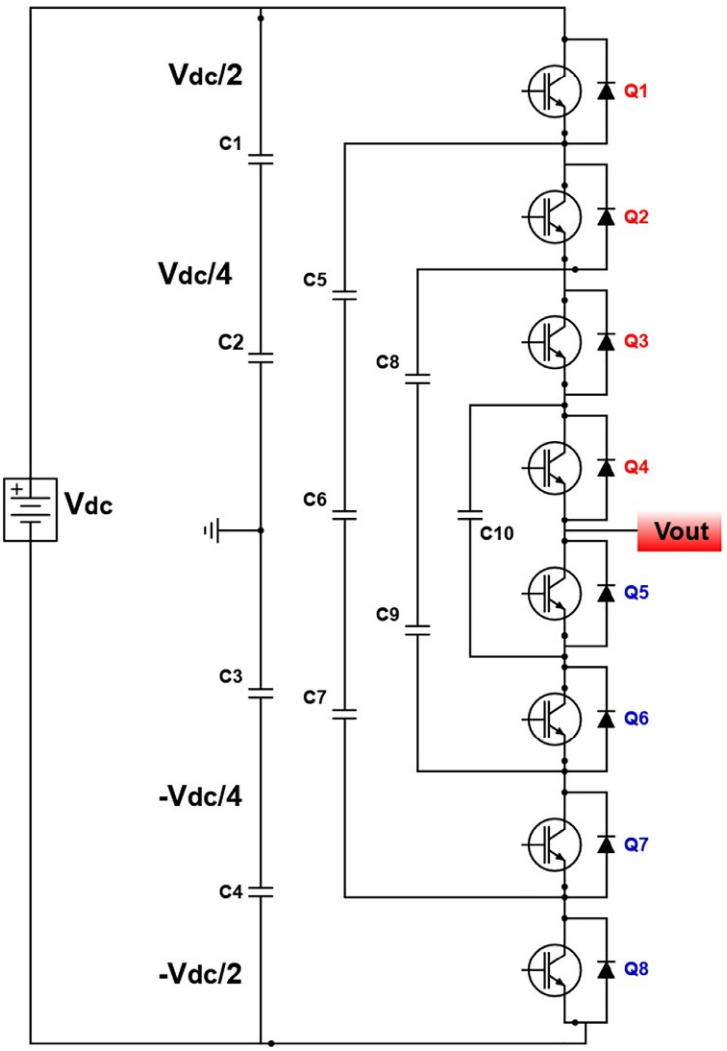

FIG. 4.100 Circuit diagram of flying capacitor five-level multilevel inverter.

Voltage level $-V_{dc}$: switches Q_3, Q_4, Q_6, *and* Q_8 must be ON while switches Q_1, Q_2, Q_5, *and* Q_7 must be OFF. The path V_{dc1}, Q_3, Q_8, Q_6, *load* Q_4, *and* V_{dc1} is followed for the output voltage $-V_{dc1}$. Since the second voltage source is sidestepped, only $-V_{dc}$ is the output. The minus sign shows the reverse direction of the current.

Voltage level $-2V_{dc}$: switches Q_3, Q_4, Q_7, and Q_8 must be ON while switches Q_1, Q_2, Q_5, and Q_6 must be OFF. The path V_{dc1}, Q_3, Q_8, V_{dc2}, Q_7 *load*, and Q_4 is followed by the current for the voltage level $-2V_{dc}$. Since both the sources are in the track of the current, the sum of both of them is obtained at the output. The minus sign shows the reverse direction of the current. Fig. 4.104 represent the MATLAB simulation waveform of a five level multilevel inverter.

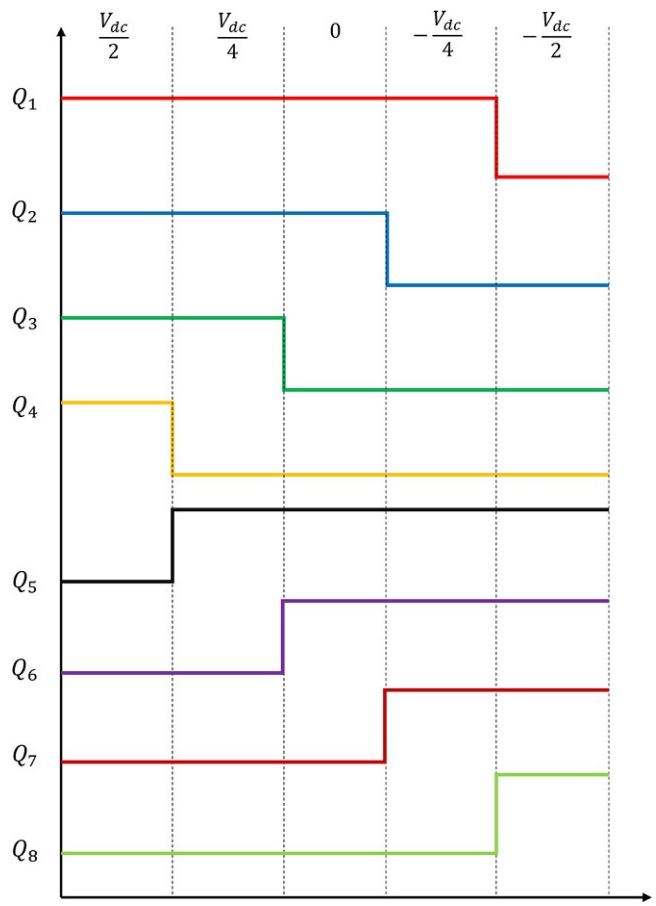

FIG. 4.101 Voltage levels for different switching states of five-level flying capacitor multilevel inverter.

Fig. 4.105 represent the MATLAB simulation waveform of a seven level multilevel inverter. Fig. 4.106 represent the MATLAB simulation waveform of an eleven level multilevel inverter.

4.7 Cycloconverters (AC-AC converters)

Conventionally, there are two ways of converting AC into AC to get different voltage levels. One is a two-stage conversion in which AC is first rectified and then DC is converted into AC by using an inverter, as in a DC-link converter. The other is a single-stage cycloconverter, also known as a frequency shifter, which is used to change the frequency of the input voltage. Cycloconverters are mainly used in driving synchronous and induction motors in ship propulsion drives, rolling mill drives, mine winders, cement mill drives, and ore grinding mills. A circuit diagram of a cycloconverter is shown in Fig. 4.107. A cycloconverter consists of two back-to-back controlled rectifiers. The left converter consists

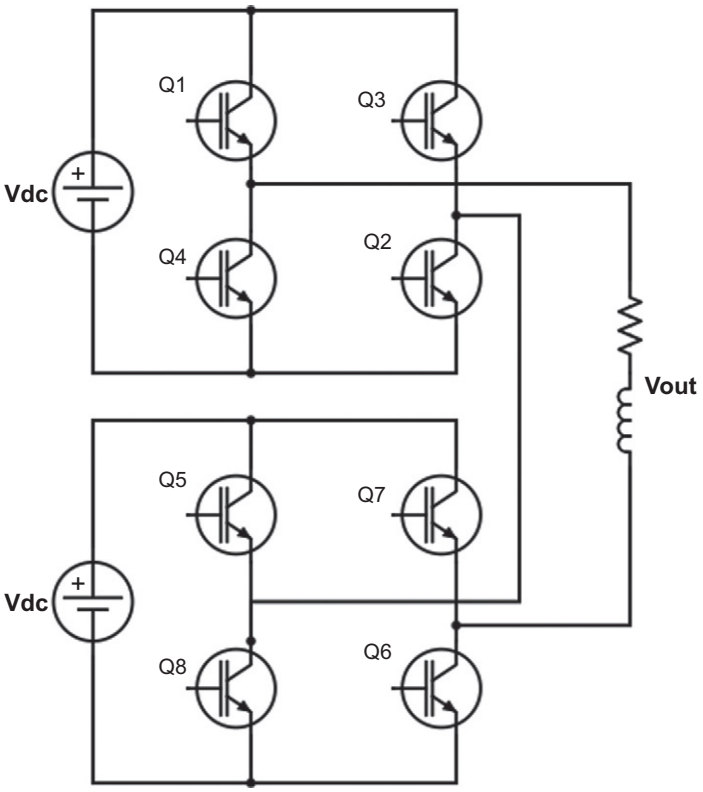

FIG. 4.102 Circuit diagram of cascaded H-bridge five-level multilevel inverter.

of four SCRs named P_1, P_2, P_3, and P_4, and is termed as the positive converter; the right-hand side converter consists of four SCRs, N_1, N_2, N_3, and N_4, and is termed as negative converter. The load is connected between the positive and negative converters as shown in Fig. 4.107.

The output frequency determines the type of cycloconverter. If the output frequency is higher than the input frequency, it is called a step-up frequency shifter. If the output frequency is lower than the input frequency, it is called a step-down frequency shifter.

4.7.1 Step-up cycloconverter

In a step-up cycloconverter, one pair of switches from the positive converter and one pair from the negative converter are alternative triggered. During the positive half cycle, P_1 and P_2 from the positive converter and N_3 and N_4 from the negative converter are alternatively triggered to conduct. The path for the P_1 and P_2 is $V^+ - P_1 - V_{out} - P_2 - V^-$. Similarly path for N_3 and N_4 is $V^+ - N_4 - V_{out} - N_3 - V^-$. Similarly, during the negative half cycle, P_3 and P_4 from the positive converter and N_1 and N_2 from the negative converter are alternatively triggered to conduct. The path for the P_3 and P_4 is $V^+ - P_3 - V_{out} - P_4 - V^-$. Similarly path for N_1 and N_2

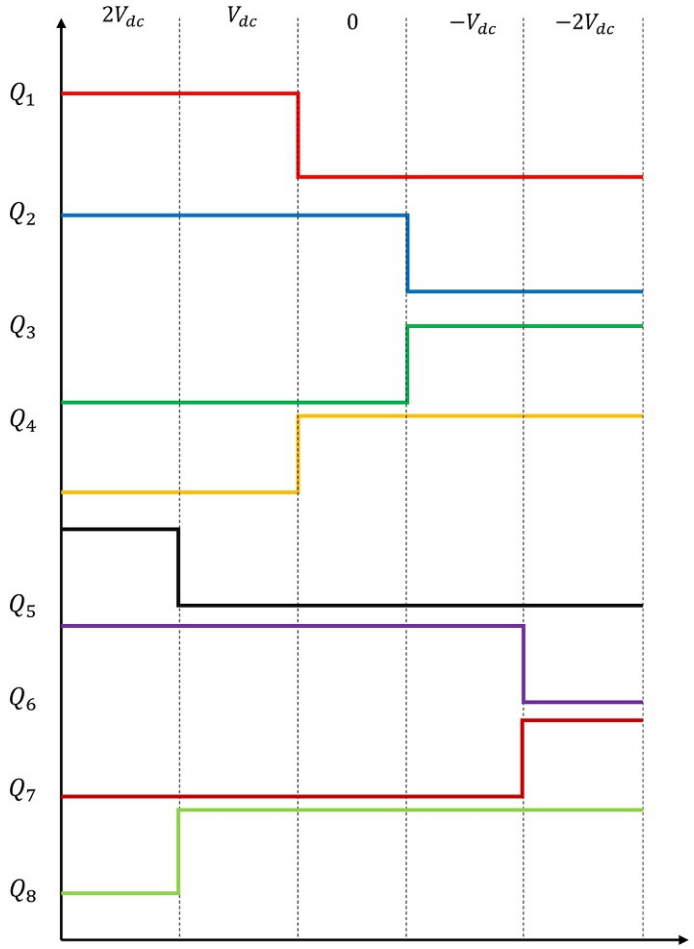

FIG. 4.103 Voltage levels for different switching states of five-level cascaded H-bridge multilevel inverter.

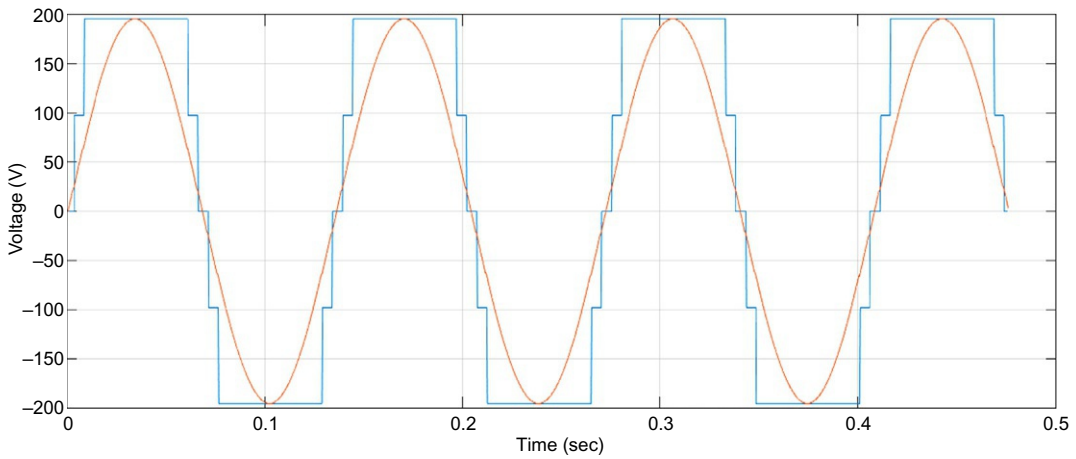

FIG. 4.104 MATLAB simulation output waveform of a five-level multilevel inverter.

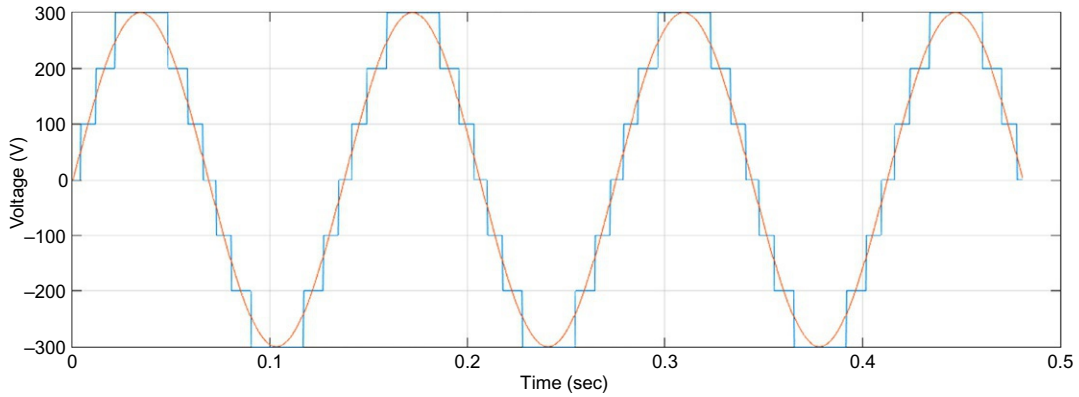

FIG. 4.105 MATLAB simulation output waveform of a seven-level multilevel inverter.

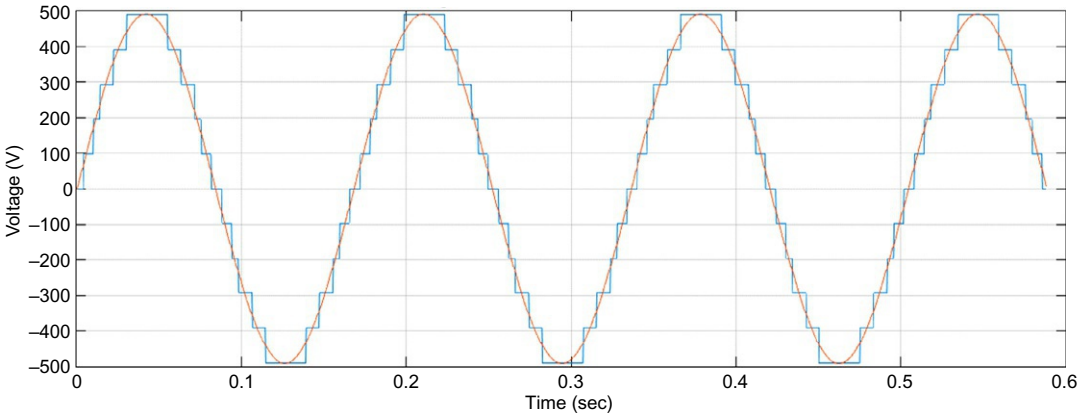

FIG. 4.106 MATLAB simulation output waveform of an 11-level multilevel inverter.

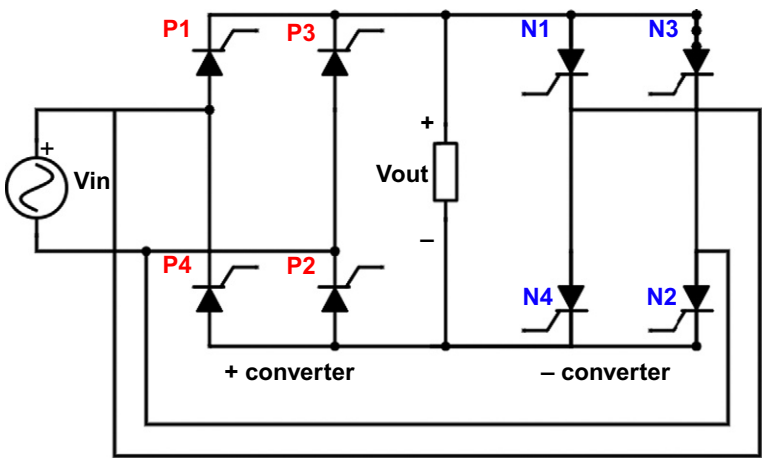

FIG. 4.107 Circuit diagram of AC-AC cycloconverter.

is $V^+ - N_1 - V_{out} - N_2 - V^-$. Fig. 4.108 shows the input AC voltage and the output voltage with increased frequency. The switching sequence is also shown in Fig. 4.108. The frequency of the output voltage is four times the frequency of the input voltage, so this is a step-up boost converter.

4.7.2 Step-down cycloconverter

In a step-down cycloconverter, to reduce the frequency of the output voltage, one pair of switches from the positive converter is triggered in the positive half cycle and the other pair of switches from the positive converter is triggered in the negative half cycle. In the next cycle of the input voltage, one pair of switches from the negative converter is triggered in the positive half cycle and the other pair of switches from the negative converter is triggered in the negative half cycle. Fig. 4.109 shows an output voltage with a frequency of half of the input frequency and Fig. 4.110 shows an output voltage with a frequency of one-third of the input frequency.

Fig. 4.111 shows a simulation circuit diagram of a cycloconverter. The green blocks present the switching scheme of the positive converter and the blue blocks present the switching scheme of the negative converter. The switching scheme decides whether the cycloconverter will be a step-up or step-down cycloconverter. In both cases, the input voltage is 220 V and 50 Hz. Fig. 4.112 shows the output voltage of a step-down cycloconverter with a frequency half of the input frequency, i.e., 25 Hz in this case. Similarly, Fig. 4.113 shows the output voltage of a step-up cycloconverter. The frequency of the output voltage is six times the frequency of the input voltage, i.e., 300 Hz in this case.

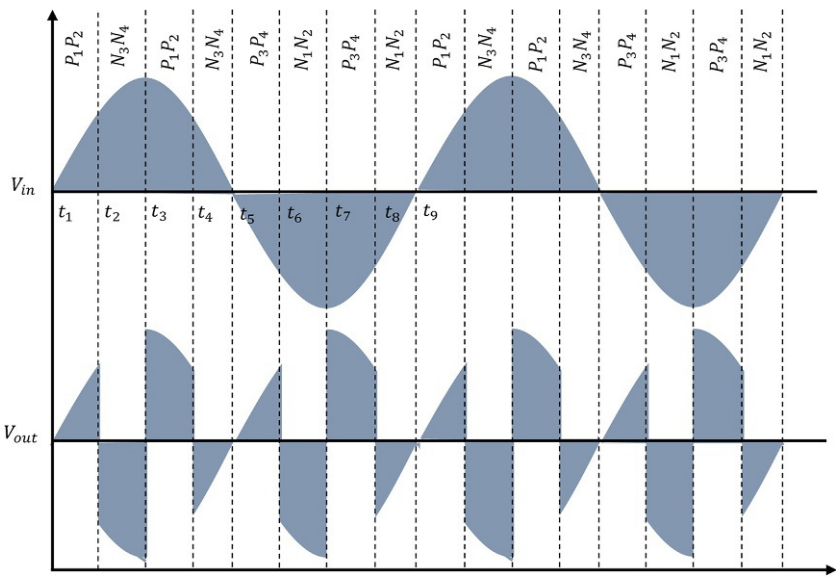

FIG. 4.108 Input and output waveforms of a step-up cycloconverter with output frequency four times the input frequency.

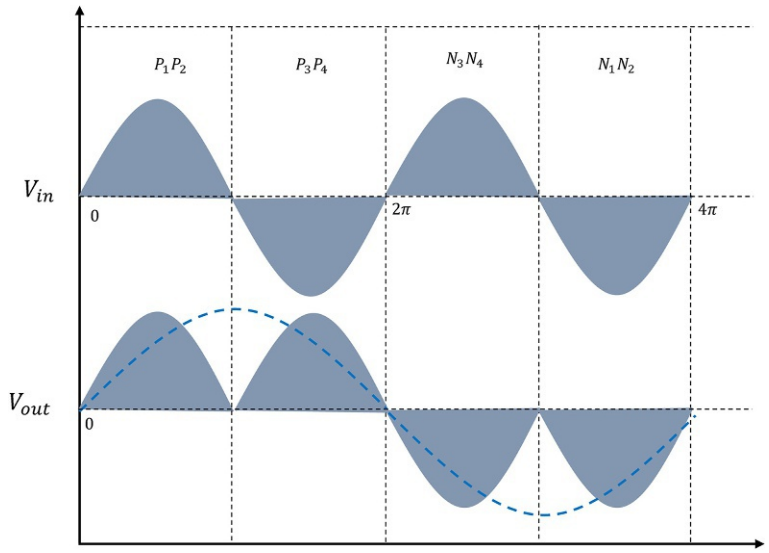

FIG. 4.109 Input and output waveforms of a step-down cycloconverter with output frequency half of the input frequency.

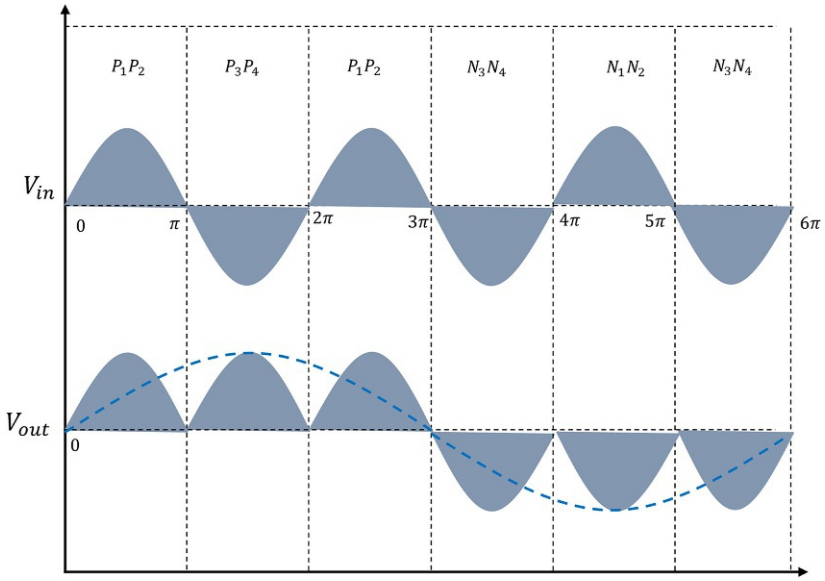

FIG. 4.110 Input and output waveforms of a step-down cycloconverter with output frequency one-third of the input frequency.

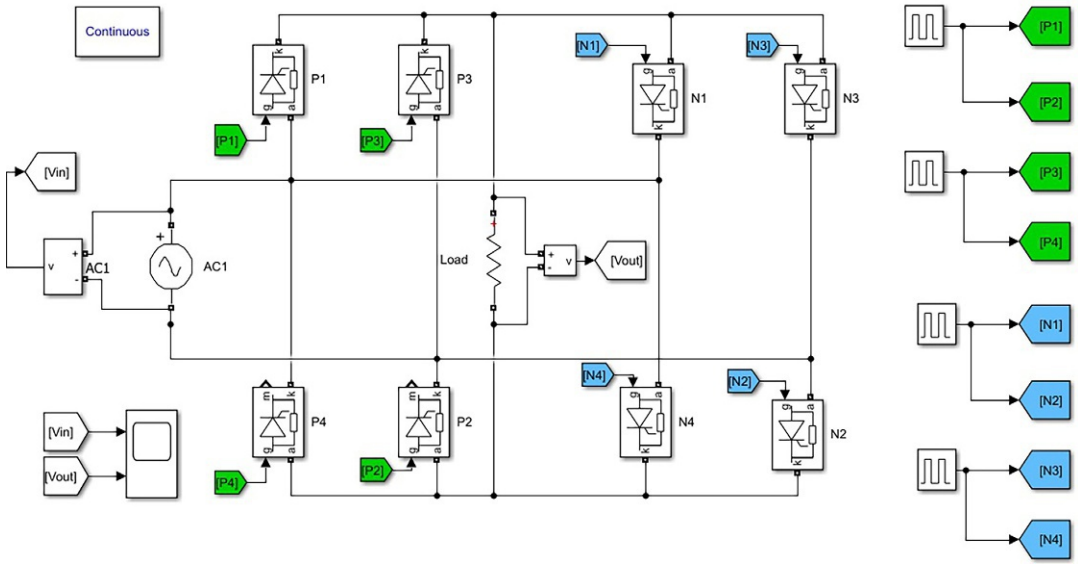

FIG. 4.111 MATLAB simulation diagram of AC-AC cycloconverter.

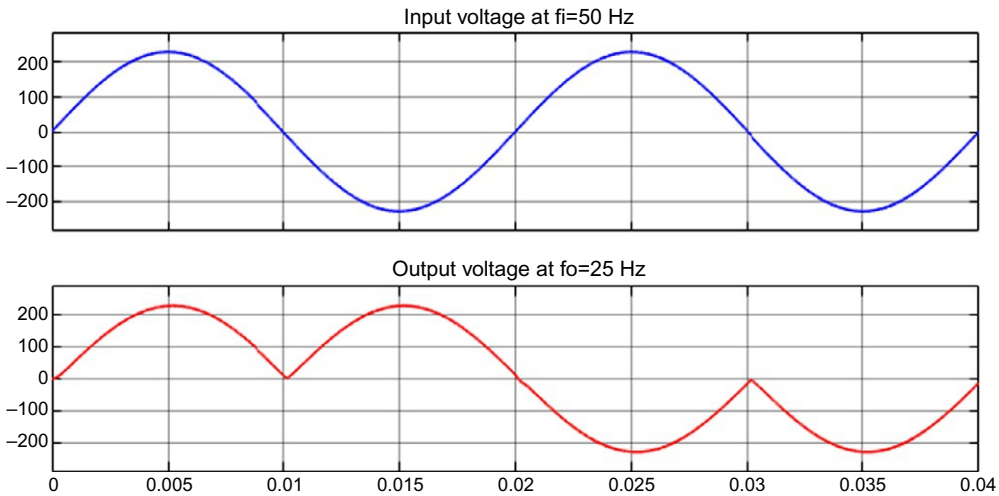

FIG. 4.112 Input and output waveforms of a step-down cycloconverter simulated in MATLAB with output frequency half of the input frequency.

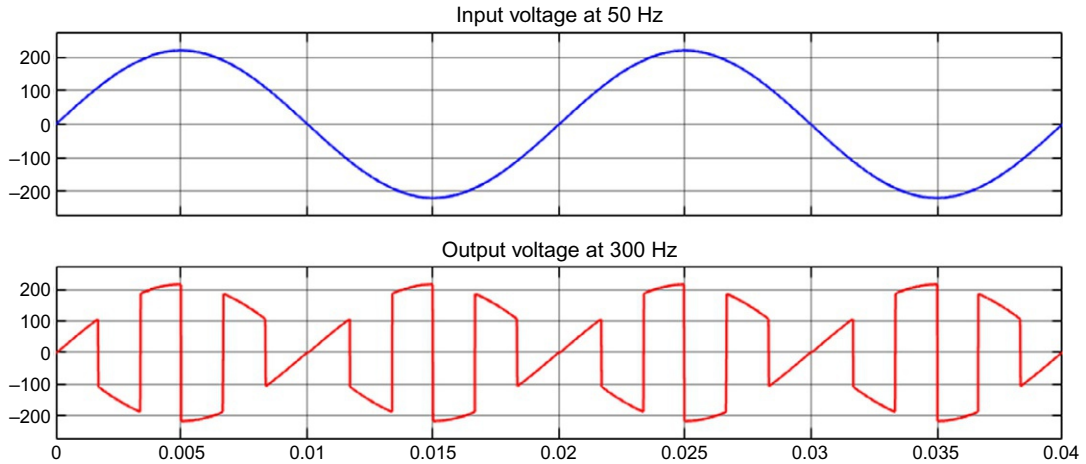

FIG. 4.113 Input and output waveforms of a step-up cycloconverter simulated in MATLAB with output frequency six times the input frequency.

4.8 Conclusion

Power electronics finds its applications in the field of integration of renewable energy sources like wind and solar energy, fuel cells, battery storage systems, electric drives, electric vehicles, and hybrid energy systems. With the invention of solid-state devices, like silicon-controlled rectifiers, gate turn-off thyristors, silicon-controlled switches, TRIAC, and DIAC, the conventional grid has been introduced as a smart grid. Power electronics finds applications in smart grid systems. The conversion of DC into DC such as in solar cells and fuel cells is possible due to the development of DC-DC converters. Integration of solar photovoltaic systems to the grid is possible due to the development of inverters. Rectifiers are also based on solid-state switches; they are used for AC to DC conversion and find their applications with battery energy storage systems integrated into solar photovoltaic systems. Cycloconverters are used for AC to AC conversion with variable frequency. This chapter discussed all the above-stated components and devices, and also implemented their simulations in MATLAB.

Problems

Problems 1–10 contain four answer options A, B, C, and D. Choose the correct answer.

1. What are some of the applications of solid-state switches?
- **A.** DC-DC choppers
- **B.** AC-DC rectifiers
- **C.** DC-AC inverters
- **D.** All of the above

2. Where can power electronics be applied?
   A. Hybrid energy systems
   B. Electric vehicles
   C. Battery energy storage systems
   D. All of the above
3. Which of the following can be turned on by the gate terminal but cannot be turned off by it?
   A. Silicon-controlled rectifier
   B. Silicon-controlled switch
   C. Gate turn-off thyristor
   D. TRIAC
4. Among the following solid-state switches, which one is turned on and turned off by the gate terminal?
   A. Silicon-controlled rectifier
   B. Silicon-controlled switch
   C. Gate turn-off thyristor
   D. TRIAC
5. Which solid-state switch contains two gates?
   A. Silicon-controlled rectifier
   B. Silicon-controlled switch
   C. Gate turn-off thyristor
   D. TRIAC
6. Which solid-state switch is a device with no gate terminal?
   A. Silicon-controlled rectifier
   B. TRIAC
   C. Silicon-controlled switch
   D. DIAC
7. Which power electronics switch is a bidirectional device?
   A. Silicon-controlled rectifier
   B. TRIAC
   C. Silicon-controlled switch
   D. DIAC
8. Which of the following are solid-state switches?
   A. Voltage-controlled devices
   B. Uncontrolled devices
   C. Current-controlled devices
   D. None of the above
9. In DC choppers, a single pole double throw (SPDT) switch is accomplished by what?
   A. A passive switch
   B. An active switch
   C. An active and a passive switch
   D. A diode
10. What can an SCR be turned on by?
    A. Light
    B. Thermal energy
    C. High $\frac{dV}{dt}$
    D. All of the above

11. What can an SCR be turned off by?
- **A.** Self-commutation or load commutation
- **B.** Resonant pulse commutation
- **C.** Complementary commutation
- **D.** All of the above

12. How many switches does a five-level DC-MLI contain?
- **A.** 10
- **B.** 20
- **C.** 25
- **D.** 90

13. A solar photovoltaic system is to provide the load during peak hours. Which power electronics converter will be used to integrate the PV system into the grid?
- **A.** Rectifier
- **B.** SCR
- **C.** chopper
- **D.** inverter

14. A converter is connected to a solar PV system of 24 V. If the MPPT is giving a 0.6 duty cycle to the switching elements of the converter, what will be the output voltage?
- **A.** 10 V
- **B.** 36 V
- **C.** −36 V
- **D.** −10 V

Give brief answers to the following short questions.

1. List some of the applications of power electronics.
2. Draw a diagram of the application of power electronics in electric drives.
3. Describe the use of power electronics converters and inverters in solar and wind energy.
4. Explain the working of an SCR with the help of two-transistor model.
5. Discuss the turn-on methods of an SCR.
6. How is an SCR turned on with the help of a gate? Give a graphical representation.
7. Discuss the commutation methods of an SCR.
8. Define line commutation and forced commutation.
9. Define self or load commutation.
10. What is the resonant pulse commutation method?
11. Explain the complementary commutation method.
12. Discuss the impulse commutation and external pulse commutation methods.
13. Give a brief comparison between holding current and latching current with the help of the characteristic curve of an SCR.
14. Why is a freewheeling diode in a phase-controlled half-wave rectifier with inductive load used?
15. A step-up boost converter is taking 12 V from the solar PV system and is connected to a battery storage system of 24 V. The switching time of the converter is 2.5 ms with a duty cycle of 0.5. What will be the average voltage across the inductor?

16. Which DC choppers are used to step up and step down DC voltages? Give a mathematical equation of each that relates the input voltage, output voltage, and the duty cycle.
17. Differentiate a transformer from a cycloconverter.

References

[1] M. Kamran, Solar energy, in: Renewable Energy Conversion Systems, 2021, pp. 109–152, https://doi.org/10.1016/B978-0-12-823538-6.00008-7.
[2] M. Rayyan Fazal, M. Kamran, Wind energy, in: Renewable Energy Conversion Systems, 2021, pp. 153–192, https://doi.org/10.1016/B978-0-12-823538-6.00003-8.
[3] P.K. Maroti, S. Padmanaban, M.S. Bhaskar, V.K. Ramachandaramurthy, F. Blaabjerg, The state-of-the-art of power electronics converters configurations in electric vehicle technologies, Electr. Power Compon. Syst. 1 (2022), 100001, https://doi.org/10.1016/J.PEDC.2021.100001.
[4] M. Kamran, Power electronics for renewable energy systems, in: Renewable Energy Conversion Systems, Academic Press, 2021, pp. 53–108.
[5] F.G. Turnbull, O. Pauk, Power electronics—rectifiers, filters, and power supplies, in: Ref. Data Eng, 2002, p. 14. 1 https://doi.org/10.1016/B978-075067291-7/50016-9.
[6] B. Singh, B.N. Singh, A. Chandra, K. Al-Haddad, A. Pandey, D.P. Kothari, A review of single-phase improved power quality AC-DC converters, IEEE Trans. Ind. Electron. 50 (5) (2003) 962–981, https://doi.org/10.1109/TIE.2003.817609.
[7] J.L. Afonso, et al., A review on power electronics technologies for power quality improvement, Energies 14 (2021) 8585, https://doi.org/10.3390/EN14248585.
[8] D. Czarkowski, DC–DC converters, in: Power Electronics Handbook, 2011, pp. 249–263, https://doi.org/10.1016/B978-0-12-382036-5.00013-6.
[9] DC-DC converters, Electron. Des. 50 (1) (2018) 275–288, https://doi.org/10.1016/B978-0-12-811407-0.00010-6.
[10] K.S. Rathore, U.K. Kalla, D.K. Palwalia, B. Singh, A.K. Mishra, Voltage-controlled power factor corrected CSC derived DC–DC converter for PMBLDC driven home appliances, IET Power Electron. 13 (15) (2020) 3407–3418, https://doi.org/10.1049/IET-PEL.2020.0004.
[11] V. Bist, B. Singh, An adjustable-speed PFC bridgeless buck-boost converter-fed BLDC motor drive, IEEE Trans. Ind. Electron. 61 (6) (2014) 2665–2677, https://doi.org/10.1109/TIE.2013.2274424.
[12] L. Ashok Kumar, S. Albert Alexander, M. Rajendran, Control of DC–DC converters, in: Power Electron. Convert. Sol. Photovolt. Syst, 2021, pp. 235–288, https://doi.org/10.1016/B978-0-12-822730-5.00006-4.
[13] S.P. Sunddararaj, S.S. Rangarajan, N. Subashini, An extensive review of multilevel inverters based on their multifaceted structural configuration, triggering methods and applications, Electronics 9 (2020) 433, https://doi.org/10.3390/ELECTRONICS9030433.
[14] A. Bughneda, M. Salem, A. Richelli, D. Ishak, S. Alatai, Review of multilevel inverters for PV energy system applications, Energies 14 (2021) 1585, https://doi.org/10.3390/EN14061585.

CHAPTER

5

Planning and modeling of solar energy systems

5.1 Introduction

The progress in industry of a country is linked with per capita energy consumption. Conventional energy sources are becoming extinct because of their exhaustive use and causing serious environmental damage. Renewable energy sources are replacing existing conventional power plants operated on fossil fuels. Solar energy is a renewable energy source that has various advantages over other conventional and renewable energy sources. The source of solar energy is free and unexhausted. Solar energy can be extracted in different forms: solar thermal, solar photovoltaic, and solar lighting. This chapter discusses the planning and modeling of photovoltaic-based solar energy systems. Solar PV systems consist of solar PV modules as a source of energy, DC-DC power converters to boost up or buck down the voltages, and inverters to convert the DC power of PV modules into AC power to manage the load or feed the grid. The performance of the solar cells depends upon environmental parameters like solar irradiance and cell temperature. These parameters are not constant; they vary with the change in sun position and the cloudy seasons. The solar irradiance determines the short circuit current of the solar cell and the cell temperature determines the open-circuit voltage. The change in any of these parameters causes a change in power.

The sun continuously changes its position in the sky during the day. To get the maximum solar insolation on the panel, the panel must track the sun. Solar trackers are discussed in this chapter. Maximum power point trackers (MPPTs) are used to let the solar cell operate at its maximum power. Various algorithms have been developed that make sure the maximum power from the solar cell in fluctuating atmospheric environments. Incremental conductance (INC) and perturb and observe (P&O) algorithms are the most commonly used MPPT algorithms. This chapter gives a comprehensive knowledge of the P&O algorithm and its implementation with the solar PV system in MATLAB. The defects of the P&O algorithm are the oscillations at the maximum power point (MPP) and poor response time. This chapter also optimizes the P&O algorithm using fuzzy logic (FL). A Sun Power A-300 solar cell is simulated in LabVIEW and the parameters in the datasheet and the results confirmed the validity of the model. INC is also simulated in LabVIEW.

https://doi.org/10.1016/B978-0-323-99560-3.00004-1

In 2018, the global cumulative installed capacity of the solar photovoltaic systems was 480 GW, which is 2% of the world's electricity production. It is forecasted that the capacity will reach 2840 GW by 2030 and 8500 GW by 2050. The installed global capacity of cumulative solar PV in 2021 was 843 GW [1]. In various PV markets, solar PV has achieved grid parity and since it is location-dependent, in most PV markets it is still more expansive than grid electricity [2].

Various researchers have proposed optimized versions of the MPP tracking algorithms. Hifsa et al. [3] suggested an algorithm based on the instantaneous conductance and INC for an indoor photovoltaic system incorporated with the optical temperature controller. They optimized the algorithm by controlling the temperature of the solar panel optically for the indoor PV systems. Kamran et al. [4] proposed an enhanced edition of the P&O MPPT algorithm. They confined the search space of the MPP on the *P-V* curve of the solar panel and cope with the poor response time and oscillations at the MPP of the conventional P&O algorithm.

5.2 Solar photovoltaics

Photovoltaics is the direct conversion of sunlight into electricity. The photovoltaic effect was first detected by Henri Becquerel in 1839 and is defined as the appearance of voltage across the terminals of a liquid or solid PV material upon falling of the light. The device which is formulated to observe the photovoltaic effect is called a solar cell, and is a combination of p and n material. A material that absorbs the sunlight and generates free electrons is called a semiconductor material. Materials are classified into conductors, insulators, and semiconductors based on their conductivity, as follows [5].

- If conductivity is $\sigma > 10^4$ $(\Omega\ \text{cm})^{-1}$, the material is called a conductor.
- If conductivity is $\sigma < 10^{-8}$ $(\Omega\ \text{cm})^{-1}$, the material is called a semiconductor.
- If conductivity is $10^4 > \sigma > 10^{-8}$ $(\Omega\ \text{cm})^{-1}$, the material is called an insulator.

When sunlight falls on a semiconductor material, the energy in the light is absorbed by the electrons and they travel from the valence band to the conduction band. If the energy immersed by the electrons is larger than the bandgap energy of the photovoltaic material, they travel to the conduction band and move in the external circuit, making a current. If the energy absorbed is less than the bandgap energy of the material, the electrons travel from the conduction band to the forbidden energy band and move back to the valence band and recombination of the electron-hole occurs. For an energy level within the forbidden band, four fundamental processes are possible:

- An electron is knocked down from the occupied energy band to the conduction band.
- An electron is collected by an unoccupied energy level.
- A hole is created in the valence band.
- A hole is captured by an occupied energy level.

The recombination of electrons and holes increases the losses in the PV cell, which decreases the efficiency. The relation between bandgap energy and the efficiency of the PV cell is shown in Fig. 5.1.

Photovoltaic technology is preferred over other renewable and conventional energy sources because:

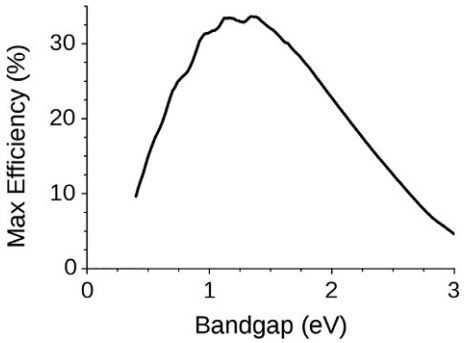

FIG. 5.1 Relation between bandgap energy and efficiency. *Source: wikipedia.*

- it converts solar irradiance directly into electricity;
- high temperatures are not required;
- it is environmentally friendly;
- it causes no noise, since no moving parts are involved, and no wear and tear maintenance;
- PV modules have long lifetimes;
- the source of energy is inexhaustible; and
- PV modules are flexible, ranging from microwatts to megawatts.

Solar photovoltaics is categorized based on the types of materials (see Fig. 5.2). Amorphous silicon is an alloy of silicon and hydrogen. The bandgap energy of the A-Si is smaller than the bandgap energy of the sunlight. The boundaries of the conduction band and valence bands are not well defined and overlap; because of this, the mobility of electrons is low and the support of an internal electrical field is thus required. A comparison between different PV material-based solar cells is given in Table 5.1.

5.3 Modeling of photovoltaic cell

A single diode model of the solar photovoltaic cell consisting of a current source, a shunt diode, a shunt resistor, and a series resistor is shown in Fig. 5.3. When a photon from the sunlight hits the semiconductor material it can be passed through the material if does not contain enough energy to knock off the electrons from the valence band, or it can be reflected from the panel surface, or it can be absorbed by the semiconductor material if its energy is higher than the bandgap energy of the semiconductor material. In the single diode model, the current source represents the generation of electrons from the semiconductor material as the solar irradiance with energy greater than the bandgap energy of the semiconductor material falls on it. This current is termed the photocurrent being generated by the sunlight. The semiconductor material takes the energy from the sunlight to knock down the electrons from the valence band to the conduction band. In the conduction band, these electrons are free to move in the external circuit through the metal contacts.

As the current passes through the semiconductor may face resistance, the interfacing between the semiconductor material and the metal contact also acts as a resistance, and the metal contacts additionally have their resistance. All these resistances faced by the

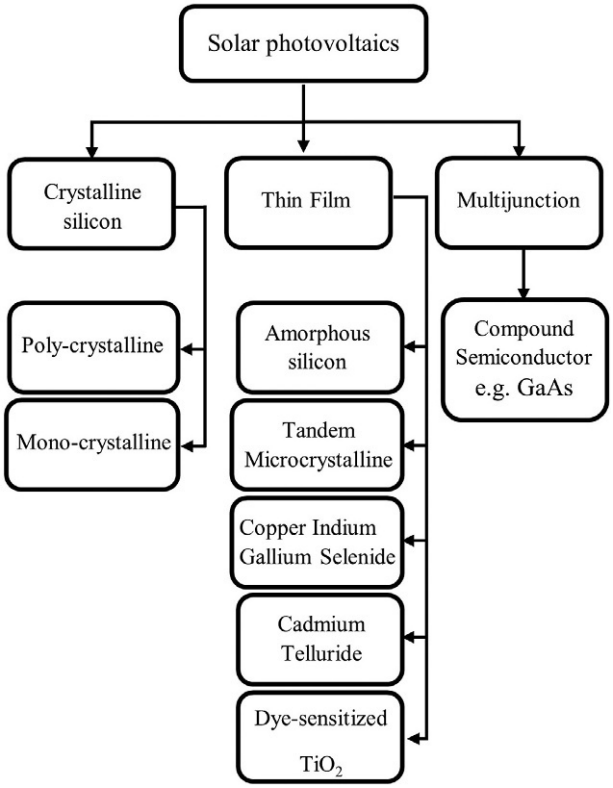

FIG. 5.2 Classification of solar photovoltaic technologies.

TABLE 5.1 Characteristics of different PV material-based solar cells.

Category	Brand	V_{oc} (mV)	J_{sc} (mA/cm^2)	FF (%)	Efficiency
Crystalline silicon					
Monocrystalline Si	m-Si	696	42.0	83.60	0.244
Multicrystalline Si	p-Si	650	37.4	76.20	0.185
Thin film transfer Si	t-Si	650	37.8	77.60	0.191
III–V-cell					
GaAs	GaAs	1122	29.7	86.50	0.288
Thin film					
CIGS	CIGS	705	35.5	77.90	0.195
Cadmium telluride	CdTe	845	25.9	75.50	0.165
Amorphous silicon	a-Si	859	17.5	63.00	0.95
Dye sensitized solar cell	DSSC	736	20.9	72.20	0.111
Organic solar cell					
DTDCTP:C70	Org.	950	12.1	56.00	0.64

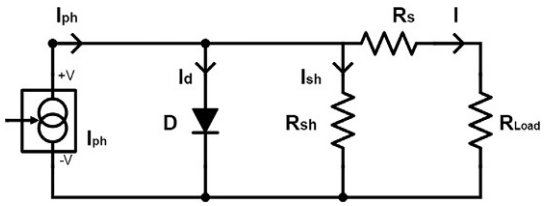

FIG. 5.3 Single diode model of a solar cell.

photogenerated current as it passes from the semiconductor material to the external circuit are expressed as the series resistance. An ideal solar cell is expressed as the current source in parallel to the diode. In the single diode equivalent model of the solar cell shown in Fig. 5.3, series resistance expressed as R_s is connected in series to both the current source and the diode. The impact of the series resistance is that on the generation of the current by the solar cell, it will lose voltages at the series resistance. The greater the series resistance, the larger the voltage drop. Thus, the series resistance must be as low as possible.

Another resistance in the solar cell is the macroscopic defect in the manufacturing of the solar cell that gives an alternative path to the flow of the photogenerated current. This impact is represented as the shunt or a parallel resistance to the current source and the diode in the single diode model of the solar cell is denoted as R_{sh}. In case of a crack through the solar cell, a parallel path will be formed for the current or if a current passes through the edge of the solar cell will also give an alternative path to the current. All these alternative paths will be considered as shunt resistance. A larger shunt means the less photogenerated current is lost in the shunt. Thus, the shunt resistance must be as high as possible [6].

Applying Kirchhoff's current law (KCL) on the circuit given in Fig. 5.3, photogenerated current can be expressed as Eq. (5.1).

$$I = I_{Ph} - I_D - I_{sh} \tag{5.1}$$

where

I_D is the current through parallel diode D;
I_{Ph} is the photonic current;
I is the current through the series resistance R_s; and
I_{sh} is the current through the shunt resistance R_{sh}.

The current passing through the diode is given by the Shockley diode equation shown in Eq. (5.2).

$$I_D = I_0\left[\left(e^{\frac{V_{sh}\cdot q}{n\cdot k\cdot T}}\right) - 1\right] \tag{5.2}$$

where

I_0 is the saturation current;
q is the charge on an electron (1.602×10^{-19} C);
V_{sh} is the voltage across the shunt resistance;
k is the Boltzmann's constant (1.381×10^{-23} J/K);
n is the ideality factor of solar material; and
T is the cell temperature (K).

The current passing through the shunt can be determined by Ohm's law, as given in Eq. (5.3).

$$I_{sh} = \frac{V_{sh}}{R_{sh}} = \frac{V + IR_s}{R_{sh}} \tag{5.3}$$

Eq. (5.1) can be rewritten as Eq. (5.4), which is also termed the short circuit current I_{sc}.

$$I = I_{Ph} - I_0\left[\left(e^{\frac{V_{sh}}{n \cdot V_T}}\right) - 1\right] - \frac{V + IR_s}{R_{sh}} \tag{5.4}$$

$$I_{sc} = I_{Ph} - I_0\left[\left(e^{\frac{V_{sh}}{n \cdot V_T}}\right) - 1\right] - \frac{V + IR_s}{R_{sh}} \tag{5.5}$$

When the load is connected to the output, Eq. (5.5) gives the short circuit current. If the circuit is open at the output, no current passes through the load, i.e., $I = 0$. As no current passes at the output side, hence no voltage is dropped across the series resistance, i.e., $IR_s = 0$. As the output circuit is open, we can denote the output voltage V as V_{oc}. Eq. (5.5) can be rewritten as Eq. (5.6).

$$0 = I_{Ph} - I_0\left[\left(e^{\frac{V_{oc}}{n \cdot V_T}}\right) - 1\right] - \frac{V_{oc}}{R_{sh}} \tag{5.6}$$

The value of the term $\left(\frac{V_{oc}}{R_{sh}}\right)$ is so small as the value of the shunt resistor is always intended to be high. Thus we neglect the last factor of Eq. (5.6).

$$0 = I_{Ph} - I_0\left[\left(e^{\frac{V_{oc}}{n \cdot V_T}}\right) - 1\right]$$

$$\frac{I_{Ph}}{I_0} = \left(e^{\frac{V_{oc}}{n \cdot V_T}}\right) - 1$$

$$V_{oc} = \ln\left(\frac{I_{Ph}}{I_0} + 1\right)\left(\frac{n \cdot k \cdot T}{q}\right)$$

Fig. 5.4 shows the double diode model of the solar cell. The double diode model is a more accurate model of a solar cell, but requires more parameters than the single diode model, which increases the complexity and implementation of the equivalent two diode model of the solar cell.

Applying KCL on the circuit of the double diode model of the solar cell given in Fig. 5.4, photogenerated current can be expressed as follows.

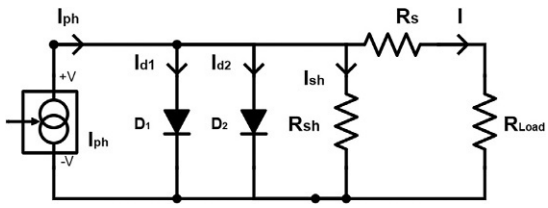

FIG. 5.4 Two diode model of a solar cell.

$$I_{Ph} = I + I_{D1} + I_{D2} + I_{sh}$$

$$I = I_{Ph} - I_{D1} - I_{D2} - I_{sh}$$

The current through both shunt diodes D_1 and D_2 are expressed using the Shockley diode current equations as follows:

$$I_{D1} = I_{01}\left[\left(e^{\frac{V_{sh}\cdot q}{n\cdot k\cdot T}}\right) - 1\right]$$

$$I_{D2} = I_{02}\left[\left(e^{\frac{V_{sh}\cdot q}{n\cdot k\cdot T}}\right) - 1\right]$$

Following the same approach as was used in the single diode model, the values of the I_{Ph}, I_{D1}, I_{D2}, and I_{sh} are put in the equation of photogenerated current that gives the value of the short circuit current in a double diode model of the solar cell shown in Eq. (5.7).

$$I = I_{Ph} - I_{01}\left[\left(e^{\frac{V_{sh}}{n\cdot V_T}}\right) - 1\right] - I_{02}\left[\left(e^{\frac{V_{sh}\cdot q}{n\cdot k\cdot T}}\right) - 1\right] - \frac{V + IR_s}{R_{sh}} \tag{5.7}$$

The *I-V* and *P-V* characteristics curves of the solar cell are shown in Figs. 5.5 and 5.6, respectively. When the output of the solar cell is not connected to any load (open circuit), there is no current at the output, and the voltages that appear at the output are termed the open-circuit voltages, this is the maximum voltage of the solar cell. This point is located at the *X*-axis as V_{oc}. On the other hand, if the solar cell is short-circuited, no voltage drop, but the current is flowing through the solar cell is maximum, this is known as the short circuit current (I_{sc}). This point is located on the *Y*-axis as I_{sc}. An *I-V* curve is drawn between these two extreme points by increasing the load from no load to full load and drawing the point on the *I-V* graph. The resultant *I-V* characteristic curve is shown in Fig. 5.5.

For each point of the *I-V* curve, voltage and current are multiplied to get the power at that point. The power of each point is plotted against the voltage on the *P-V* graph to obtain the *P-V* characteristic curve of a solar cell, as shown in Fig. 5.6. On the *P-V* curve, there is only one point at which the solar cell gives maximum power and this point is termed the MPP.

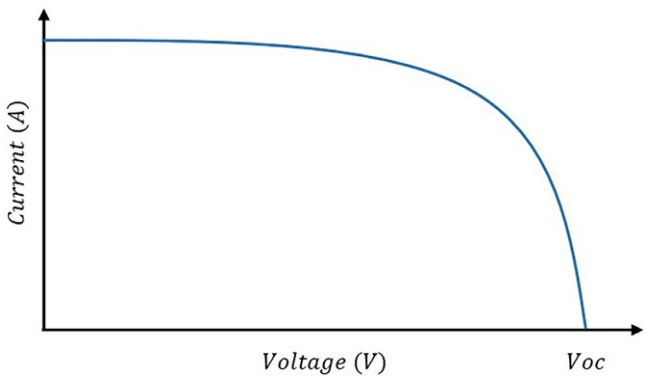

FIG. 5.5 *I-V* curve of a single solar cell.

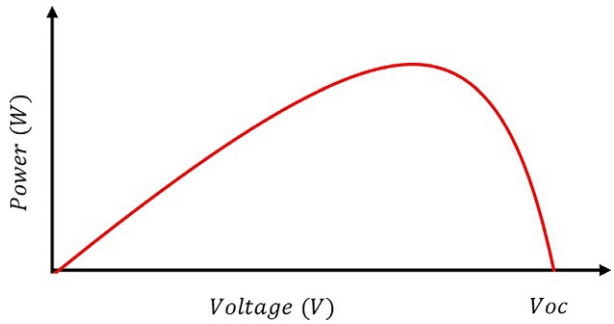

FIG. 5.6 *P-V* curve of a single solar cell.

5.4 Effect of series resistance on the *I-V* curve of a solar cell

As has been observed, the series resistance causes the voltage to drop across it that leading to the loss of power from the solar cell. Fig. 5.7 shows the impact of series resistance on the *I-V* curve of a solar cell. At the open circuit, the value of the series resistance does not have any impact on the *I-V* curve. This is because, in an open circuit, no current passes through the load and the series resistance, and hence no voltage drops across it. As we move from open-circuit voltage to the short circuit current through the *I-V* curve, a significant impact can be seen on the *I-V* curve. There is slight variation in the series resistance, but the short circuit current is not much affected. However, with a significant increase in the series resistance, the short circuit current significantly decreases. There comes a sag in the graph, moving from maximum value to the origin. The solar cells start behaving like a resistor at $R_s = 20\ \Omega\ \text{cm}^2$. The series resistance losses are determined by Eq. (5.8).

$$P_{loss} = V_{R_s} \times I = I^2 \times R_s \tag{5.8}$$

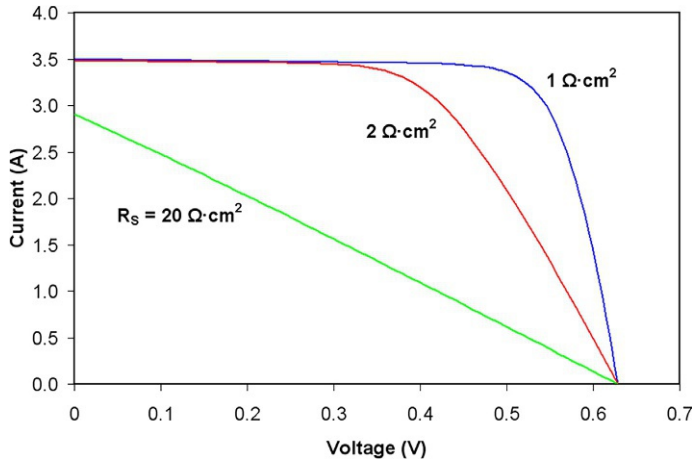

FIG. 5.7 Effect of series resistance on the *I-V* curve of a solar cell.

The losses at the series resistance become significant at the high photo intensity or the high photogenerated current, as can be seen from Eq. (5.8).

5.5 Effect of parallel resistance on the *I-V* curve of a solar cell

Fig. 5.8 shows the impact of shunt resistance on the *I-V* curve of a solar cell. As the shunt resistance is increased, the current diverted to the shunt path is reduced and the current at the output goes near to the short circuit current. If the shunt resistance is decreased, a very small current will pass through it and there will be no significant impact on the short circuit current. On a significant decrease in the shunt resistance, a large current passes through it, which increases the voltage drop in the cell voltage that reduces the open-circuit voltage of the cell at $R_{sh} = 20\ \Omega\ \text{cm}^2$.

5.6 Effect of temperature on the *I-V* and *P-V* curves of a solar cell

The parameter that affects the performance of the solar panel is the solar panel temperature. At higher temperatures, the electrons in the semiconductor material start vibrating. The vibration of the electrons causes the bonding of the electrons in the valence band week and hence the increasing temperature reduces the bandgap energy of the material. The increased vibrations of the electrons create a hindrance to the flow of current, which increases the resistance to the flow of current causing a voltage drop and reducing the open-circuit voltage. The impact of the cell temperature on the open-circuit voltage is shown in Fig. 5.9.

The effect of the temperature on the solar photovoltaic cell can be comprehended by the *I-V* and *P-V* curves. Fig. 5.9 shows the *I-V* curves of the PV cell under varying temperatures. As we increase the temperature from 25°C to 35°C, 45°C, and 55°C, the open-circuit voltage of the solar panel decreases and there is no change in the short circuit current of the solar panel.

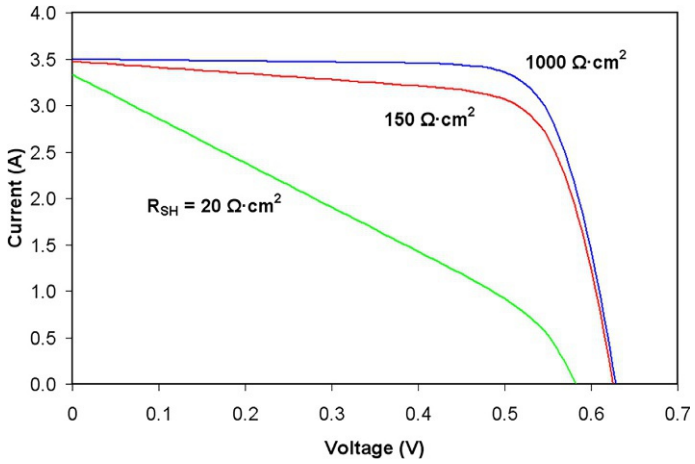

FIG. 5.8 Effect of parallel resistance on the *I-V* curve of a solar cell.

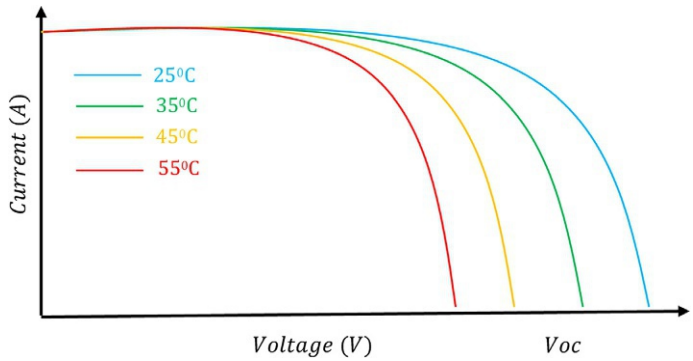

FIG. 5.9 Effect of temperature on the *I-V* curve of a solar cell.

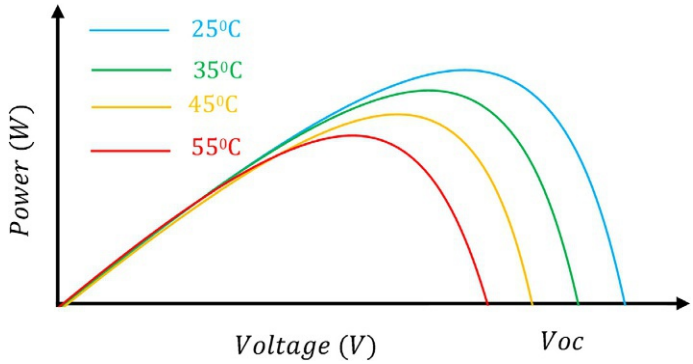

FIG. 5.10 Effect of temperature on the *P-V* curve of a solar cell.

The impact of temperature can also be seen in the *P-V* curve shown in Fig. 5.10. The *P-V* curve also indicates that because of the decrease in voltage with increasing temperature, the maximum power delivered by the solar panel also decreases.

5.7 Effect of irradiance on the *I-V* and *P-V* curves of a solar cell

Solar energy is intermittent as it is always vulnerable to varying atmospheric conditions. The solar irradiance received by the location where the solar photovoltaic system is to install is subject to variation because of the scattering elements like clouds, season, time of the day, and latitude. In cloudy weather, lower-intensity irradiance reaches the earth and at this intensity, sunlight does not have enough energy to excite the electrons from the valence band to the conduction band by overcoming the bandgap energy of the solar material. The bandgap energy of the photon must be higher than the bandgap energy of the PV material so that it can excite the electrons from the valence band and pass it through the forbidden energy gap to the conduction band. If the bandgap energy of the photon is lower than the bandgap energy of the PV material, the electrons are not excited and effectively the photogenerated current is reduced.

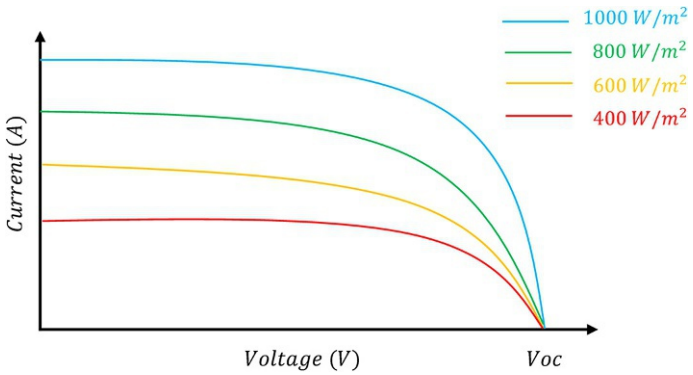

FIG. 5.11 Effect of solar irradiance on the *I-V* curves of a solar cell.

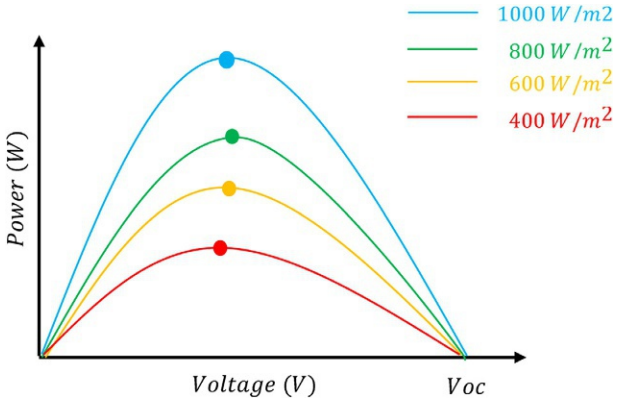

FIG. 5.12 Effect of solar irradiance on the *P-V* curves of a solar cell.

The effect of the irradiance on the solar photovoltaic cell can be comprehended by the *I-V* and *P-V* curves. Fig. 5.11 shows the *I-V* curves of the PV cell under varying solar irradiance. As we decrease the solar irradiance from 1000 to 800, 600, 400, and 200 W/m^2, the current generated by the solar panel decreases and there is no change in the open-circuit voltage of the solar panel. The impact of solar irradiance can also be seen in the *P-V* curve shown in Fig. 5.12. The *P-V* curve also indicates that there is no change in the open-circuit voltage, but because of the decrease in current with diminishing irradiance, the maximum power delivered by the solar panel also decreases.

5.8 Fill factor

The fill factor of a PV cell can be defined and calculated using the *I-V* curve of a solar cell. FF is the measure of the efficiency of a solar cell. Fig. 5.13 shows the *I-V* characteristic curve of a

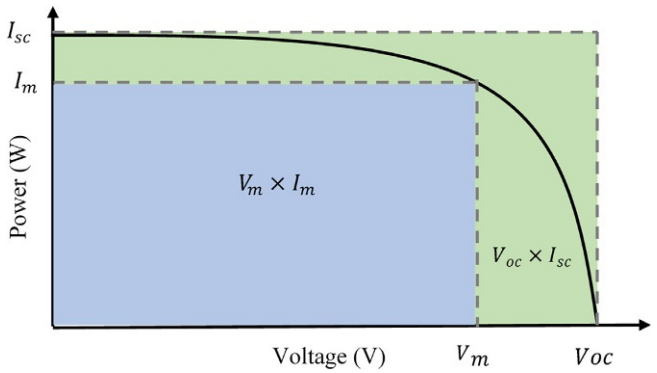

FIG. 5.13 Fill factor calculation of a solar cell.

solar cell labeled maximum voltage and maximum current at the MPP and the open-circuit voltage and the short circuit current. In this way, we get two triangle areas: one in blue and the other in green. The blue shows the maximum power that is being provided by the solar cell. The green represents the power obtained by the product of short circuit current and open-circuit voltage. The fill factor is defined as the ratio of the maximum power that can be obtained from the solar cell to the product of short circuit current and open-circuit voltage, as shown in Eq. (5.9).

$$FF = \frac{I_{\max} \times V_{\max}}{I_{sc} \times V_{oc}} \tag{5.9}$$

Example 5.1

A silicon solar cell is operating at 25°C and 1000 W/m^2 is generating a short circuit current of 3.1 A and the open-circuit voltage is 0.47 V. The area of the solar cell is 110 cm^2. Assume the fill factor of the solar cell is 70%. You are required to calculate:

(a) the input power to the solar cells;
(b) the efficiency of the solar cell; and
(c) the peak power of the solar cell.

Solution

(a) The input power to the solar cell can be calculated by multiplying the solar irradiance coming from the sun to the solar cell and the area of the solar cell.

$$P_{in} = 1000 \frac{\text{W}}{\text{m}^2} \left(90\ \text{cm}^2\right).$$

$$P_{in} = 9.0\ \text{W}$$

(b) The efficiency of the solar cell is calculated using Eq. (5.10).

$$\eta = V_{oc}\, I_{sc}\, \frac{FF}{P_{in}} \tag{5.10}$$

$$\eta = 0.47\ V(3.1\ \text{A})\frac{0.70}{9}(100)$$

$$\eta = 11.33\%$$

(c) The maximum power of the solar cell can be calculated using the fill factor formula.

$$FF = \frac{I_{\max} \times V_{\max}}{I_{sc} \times V_{oc}}$$

$$FF = \frac{P_{\max}}{I_{sc} \times V_{oc}}$$

$$P_{\max} = I_{sc} \times V_{oc} \times FF$$

$$P_{\max} = (3.1\ A)(0.47\ V)(0.70)$$

$$P_{\max} = 1.02\ W$$

5.9 Simulation of single diode model of a solar cell in LabVIEW for *I-V* and *P-V* curves under varying temperature and irradiance

Fig. 5.14 provides a datasheet of the Sun Power A-300 monocrystalline silicon solar cell. The datasheet gives the following dimensions of the solar cell:

- open circuit voltage;
- short circuit current;
- maximum power;
- the voltage at maximum power;
- current at maximum power; and
- efficiency of the solar cell.

The datasheet also gives the *I-V* characteristics of the solar cell. We implement the single diode model of the solar cell in LabVIEW by equations determined in Section 5.3 for the Sun Power A-300 solar cell using characteristics from the datasheet. We also verify the effect of solar irradiance and temperature on the characteristics of the solar cell.

In LabVIEW, mathematical equations can be implemented in two ways: by using simulated blocks and by using a calculator. Using a calculator, the equation of the unknown parameters that need to be calculated is saved by specifying the input and output parameters We use the calculator provided in the MathScript RT module to calculate the value of

A-300 SOLAR CELL
MONO CRYSTALLINE SILICON

Physical Characteristics

Construction:	All-back contact
Dimensions:	125 mm x 125 mm - nominal
Thickness:	270 μm ± 40 μm

ELECTRICAL CHARACTERISTICS OF TYPICAL CELL AT STANDARD TEST CONDITIONS (STC)

STC is defined as: irradiance of 1000W/m^2, spectrum AM 1.5g and cell temperature of 25°C

Open Circuit Voltage:	0.670 V
Short Circuit Current:	5.9 A
Maximum Power Voltage:	0.560 V
Maximum Power Current:	5.54 A
Rated Power:	3.1 W
Efficiency:	Up to 21.5 %

Temperature Coefficients

Voltage:	–1.9 mV / °C
Power:	–0.38 % / °C

ATTRIBUTES

- High efficiency reduces module assembly and system installation costs
- Uniform front appearance - no contact grid
- Back contact design simplifies circuit assembly
- Lower temperature coefficient improves energy delivery

PACKAGING

- Cells are packed in boxes of 1000 each; grouped in shrink-wrapped stacks of 50 with interleaving
- Twelve boxes are packed in a water-resistant “Master Carton” containing 12,000 cells suitable for air transportation

FIG. 5.14 Datasheet of Sun Power A-300 solar cell.

open-circuit voltage, short circuit current, maximum power, voltage at maximum power, current at maximum power, fill factor, and efficiency of the solar cell.

Fig. 5.15 shows the complete simulation of the single diode model of the solar cell. The inputs that were used in the simulation are reference open-circuit voltage, reverse short circuit current, solar irradiance, cell temperature, ideality factor (n), series resistance, shunt resistance, load resistance, and cell area. The output parameters are the open-circuit voltage, short circuit current, saturation current, reverse saturation current, voltage at maximum power, current at maximum power, maximum rated power, fill factor, and efficiency of the solar cell. All the input and output parameters are shown in Fig. 5.16.

Using the output parameters, we draw the *I-V* and *P-V* characteristic curves and the MPPT at standard test conditions (STCs). Fig. 5.17A shows the *P-V* characteristic curve and Fig. 5.17B shows the *I-V* characteristic curve of a solar cell. Comparing the simulated *I-V* curve with the *I-V* curve given in the datasheet, we can see that the curves are identical in all aspects.

Now we determine the impact of varying atmospheric conditions by changing the value of solar irradiance and the temperature. First, we reduce the solar irradiance from 1000 to 800, 600, 400, and 200 W/m^2. It is observed that the decrease in solar irradiance does not have a significant effect on the open-circuit voltage and the short circuit current also decreases with decreasing irradiance. As a result, the rated maximum power delivered by the solar cell is reduced. The impact of decreasing irradiance can be seen in the *P-V* and *I-V* curves of the solar cell shown in Fig. 5.18A and B, respectively. The values of various parameters as mentioned above at varying solar irradiance are given in Table 5.2.

The other parameter that deteriorates the performance of the solar cell is the cell temperature. We increase the temperature of the solar cell from STCs (25°C) to 35°C, 50°C, 65°C, and 75°C. From the *P-V* curve, it is observed that the increase in the cell temperature reduces the open-circuit voltage as depicted in Fig. 5.19A whereas the *I-V* curves reveal that the increasing temperature does not impact the short circuit current, as shown in Fig. 5.19B. Hence the increasing temperature reduces the maximum power delivered by the solar cell. The values of various parameters as mentioned above at varying cell temperatures are given in Table 5.3.

5.10 Series and parallel connections of solar cells

To get the voltage of the solar PV system equal to the input voltage of the inverter, solar panels are connected in series, as shown in Fig. 5.20. Three solar panels of 12 V and 5 A each are connected in series giving 36 V and 5 A to the inverter. In series, the voltage of each panel adds up and the current remains equal to the single solar panel. The series connection is made by connecting the positive terminal of the first solar panel to the negative terminal of the second solar panel. Similarly, all the solar panels are connected for a series connection. The inverter is connected by connecting its negative terminal to the negative terminal

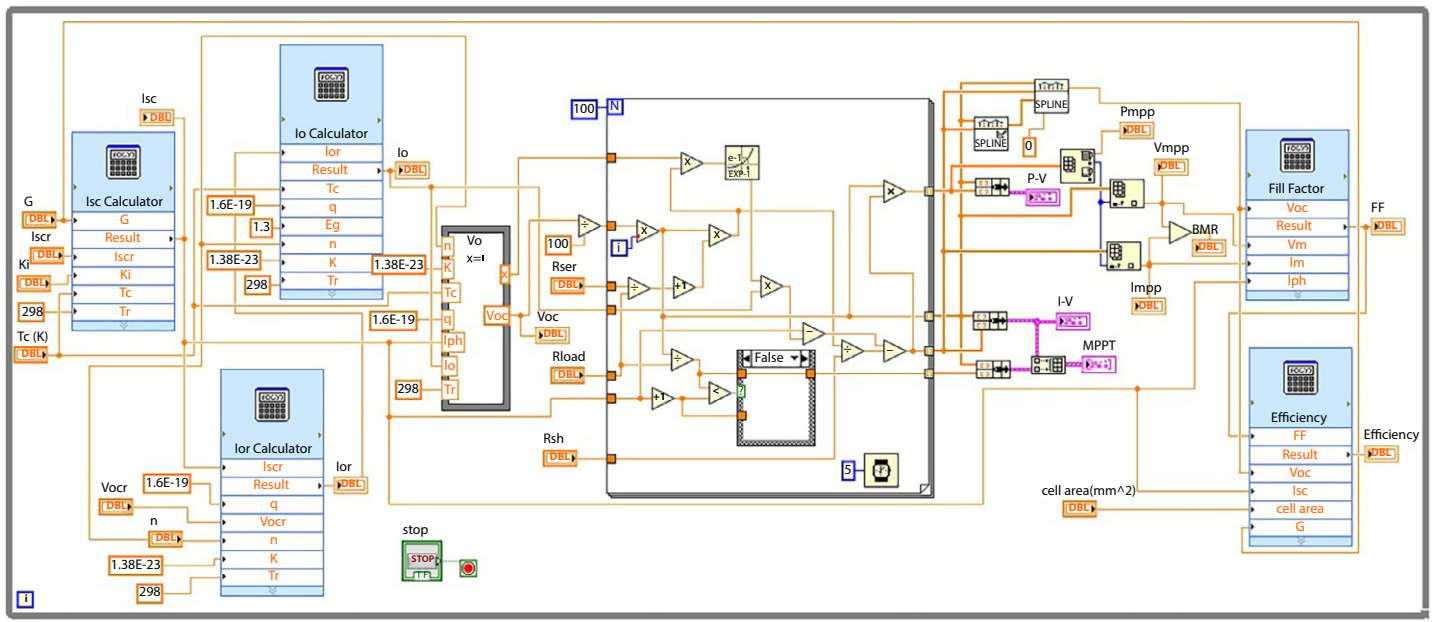

FIG. 5.15 LabVIEW-based simulation of a solar cell.

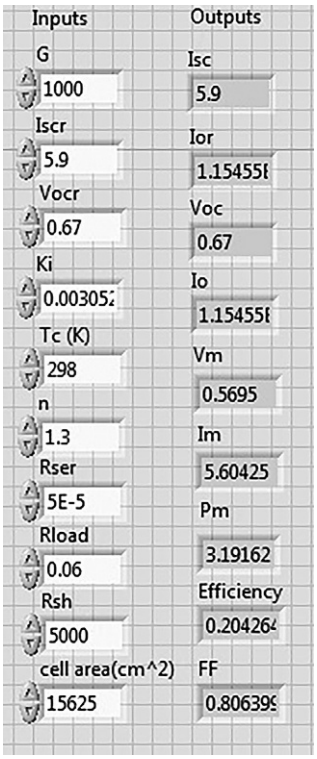

FIG. 5.16 Input and output parameters of Sun Power A-300 solar cell simulated in LabVIEW.

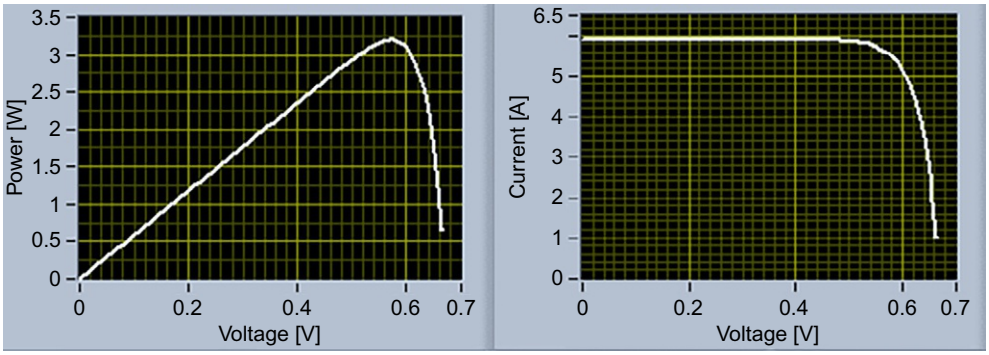

FIG. 5.17 (A) *P-V* curve and (B) *I-V* curve of Sun Power A-300 solar cell simulated in LabVIEW.

of the first solar panel and the positive terminal to the positive terminal of the last solar panel.

The *I-V* curve of the series of solar panels is shown in Fig. 5.21. The red *I-V* curve is of a single solar panel of 5 A and 12 V. The blue *I-V* curve is of two series solar cells in which voltage is added up to 24 V, keeping the current at 5 A. The green *I-V* curve is of three series solar cells in which voltage is added up to 36 V, keeping the current at 5 A.

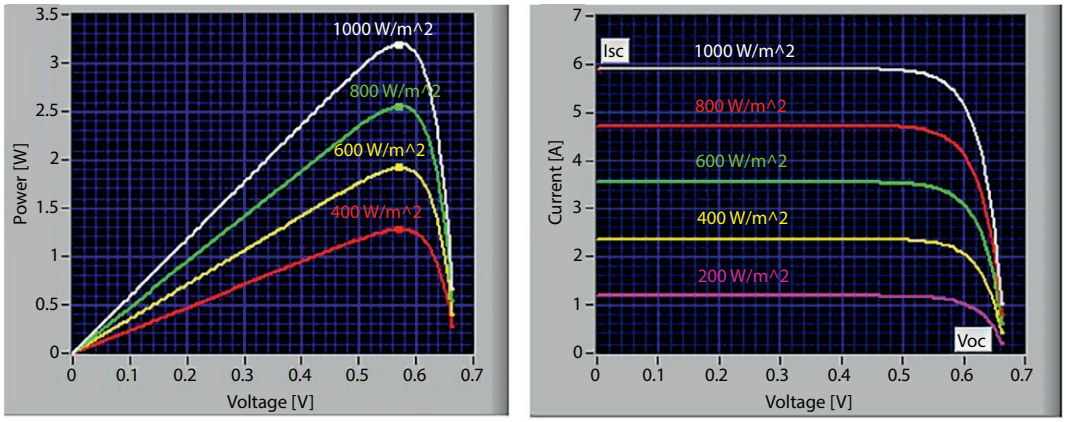

FIG. 5.18 Effect of solar irradiance on (A) *P-V* curves and (B) *I-V* curves of Sun Power A-300 solar cell.

TABLE 5.2 Characteristics of Sun Power A-300 solar cell under varying solar irradiance.

G (W/m^2)	I_o (A)	V_{oc} (V)	I_{sc} (A)	I_{or} (A)	I_{mpp} (A)	V_{mpp} (V)	P_m (W)	FF	η (%)
1000	1.15E-8	0.67	5.90	1.154E-8	5.60	0.56	3.19	0.806	20.4
800	4.53E-8	0.64	5.93	1.160E-8	5.56	0.54	3.05	0.796	19.5
600	3.02E-7	0.60	5.97	1.169E-8	5.564	0.51	2.84	0.781	18.2
400	1.71E-6	0.57	6.02	1.178E-8	5.552	0.47	2.62	0.764	16.8
200	5.05E-6	0.54	6.05	1.184E-8	5.560	0.44	2.49	0.752	15.9

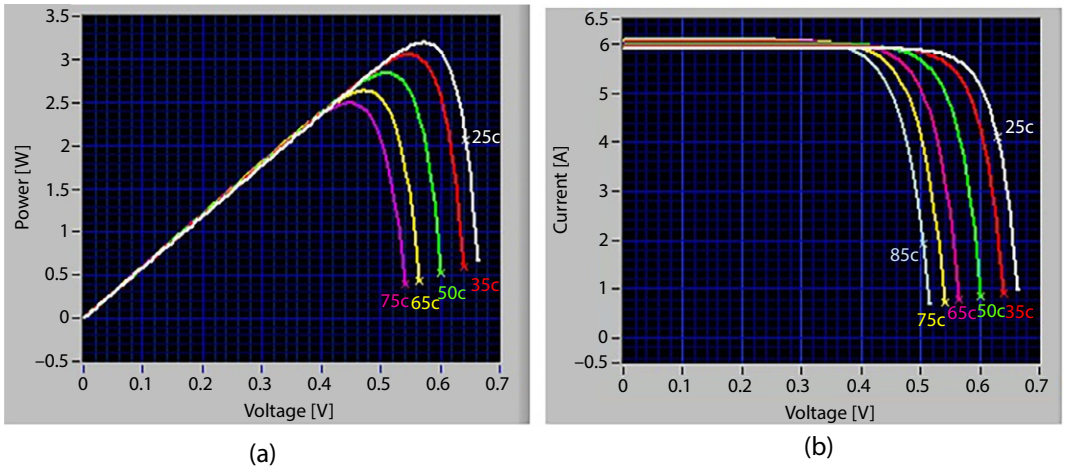

FIG. 5.19 Effect of temperature on (A) *P-V* curves and (B) *I-V* curves of Sun Power A-300 solar cell.

TABLE 5.3 Characteristics of Sun Power A-300 solar cell under varying temperature.

T_c (C°)	I_o (A)	V_{oc} (V)	I_{sc} (A)	I_{or} (A)	I_{mpp} (A)	V_{mpp} (V)	P_m (W)	FF	η (%)
25	1.15E-8	0.67	5.90	1.154E-8	5.60	0.56	3.19	0.806	20.4
35	4.53E-8	0.64	5.93	1.160E-8	5.56	0.54	3.05	0.796	19.5
50	3.02E-7	0.60	5.97	1.169E-8	5.564	0.51	2.84	0.781	18.2
65	1.71E-6	0.57	6.02	1.178E-8	5.552	0.47	2.62	0.764	16.8
75	5.05E-6	0.54	6.05	1.184E-8	5.560	0.44	2.49	0.752	15.9
85	1.40E-5	0.52	6.08	1.190E-8	5.562	0.42	2.34	0.740	15.0

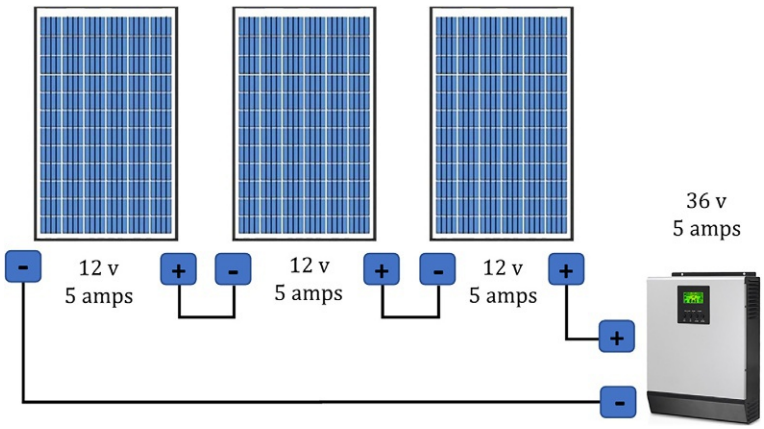

FIG. 5.20 Three solar panels connected in series.

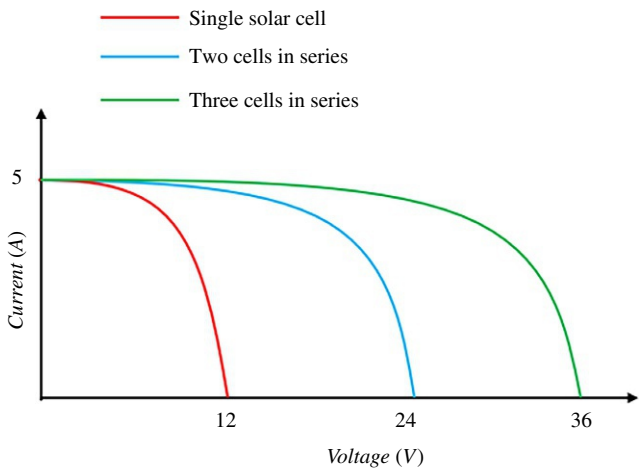

FIG. 5.21 *I-V* curves of three solar panels connected in series.

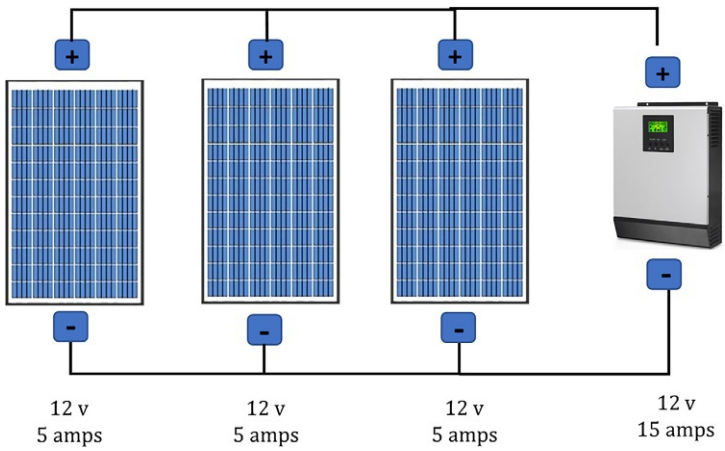

FIG. 5.22 Three solar panels connected in parallel.

To get the current of the solar PV system within the amperage limits of the inverter, solar panels are connected in parallel, as shown in Fig. 5.22. Three solar panels of 12 V and 5 A each are connected in parallel, giving 12 V and 15 A to the inverter. In a parallel connection, the current generated by each panel adds up and the voltage across each parallel component is the same. The parallel connection is made by connecting the positive terminal of all the solar panels to the positive terminal of the inverter and the negative terminal of all the solar panels to the negative terminal of the inverter.

The *I-V* curve of the parallel solar panels is shown in Fig. 5.23. The red *I-V* curve is of a single solar panel of 5 A and 12 V. The blue *I-V* curve is of two parallel solar cells, in which the current is added up to 10 A, keeping the voltage at 12 V. The green *I-V* curve is of three parallel solar cells in which current is added up to 15 A, keeping the voltage at 12 V.

To meet the both voltage and current limitations of the inverter in a solar photovoltaic system, different combinations of series and parallel connections of the solar cells are made. The

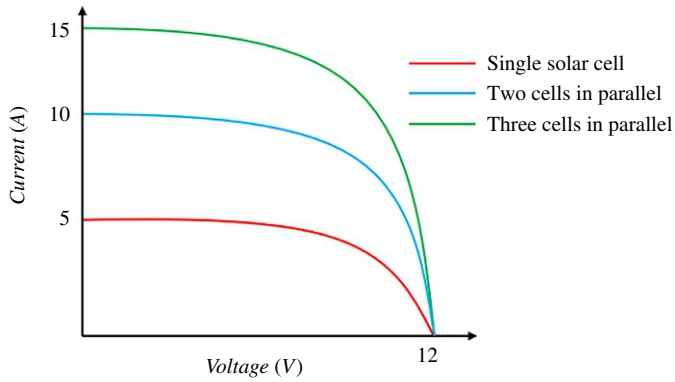

FIG. 5.23 *I-V* curves of three solar panels connected in parallel.

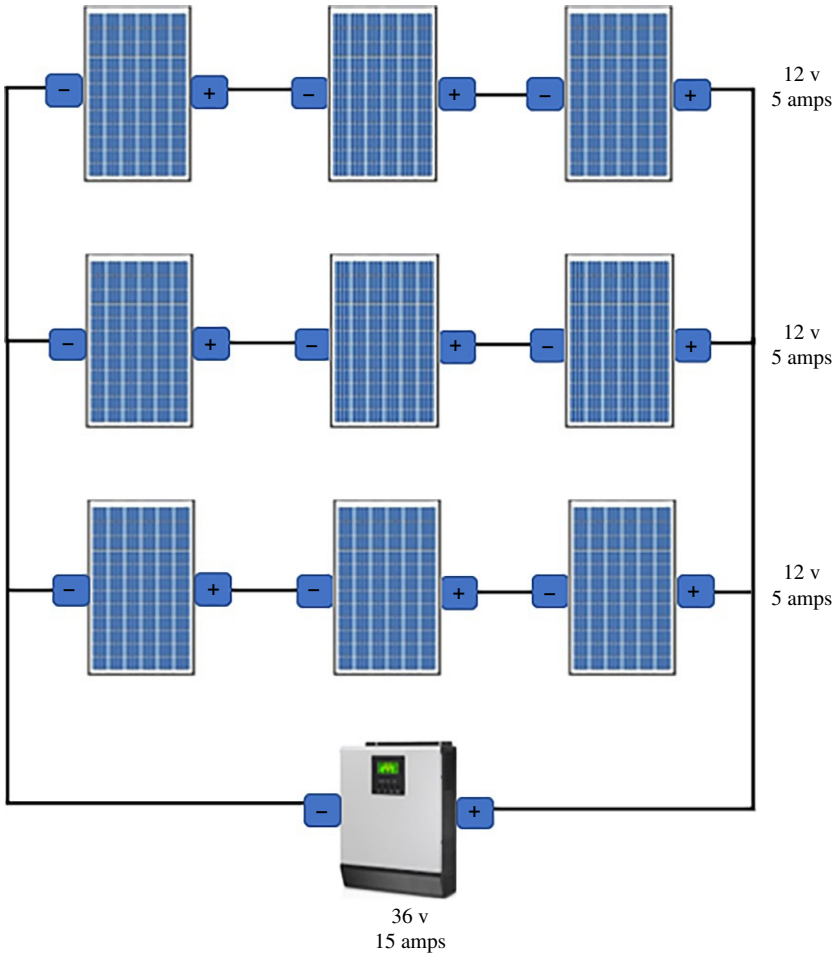

FIG. 5.24 Series and parallel connections of solar panels.

series combination increases the voltage and the parallel combinations increase the current of the solar photovoltaic system. Fig. 5.24 shows the series and parallel connections of the solar panels of a solar PV system. A branch of three solar cells is connected in series. These three branches are connected in parallel, increasing both current and voltages. These series and parallel connections increase the voltage to 36 V and increase the current to 15 A. The *I-V* curves of series-parallel connections of the solar cells to increase both voltage and current are shown in Fig. 5.25. The *I-V* curve in red is of a single solar cell. The blue *I-V* curve is of two series solar panels in parallel to two other series solar panels giving 24 V and 10 A. The *I-V* curve in green represents the three series solar panels in parallel to the other three series solar panels that give 36 V and 15 A to the inverter.

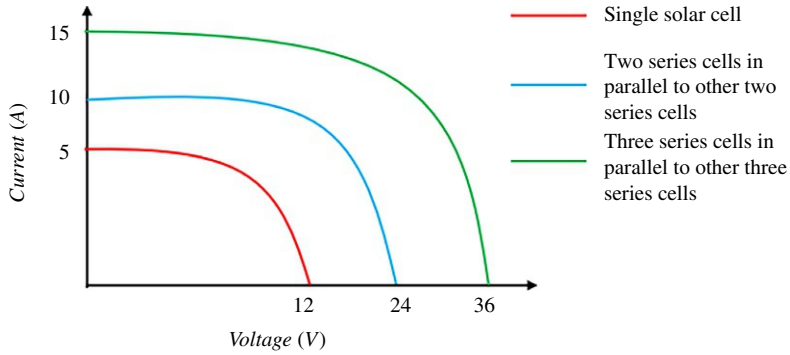

FIG. 5.25 *I-V* curves of different solar panels connected in series and parallel.

5.11 Hot spot due to partial shading

In a solar photovoltaic module, if a solar cell in series is defective or shaded, the power of all other cells is dumped on that defective cell, generating heat and causing a failure of the solar panel. Fig. 5.26 shows six solar cells connected in series; five cells are unshaded and one cell is shaded. A shaded solar cell causes the reduction of current through the good solar cells stopping the current through the load, hence the good cells produce a high voltage, which reverse biases the bad cell. The power of all the cells is dissipated in the bad cell.

The hot spot damage can be avoided by connecting a reverse-biased diode across each cell, which will increase the cost of the panel. Nowadays, each solar panel comes with three bypass diodes. If a cell is shaded, the bypass diode will bypass the current, leaving out the shaded part from the circuit. In this way, the shading on a few cells or panels will not disturb the generation of electricity from the solar PV system.

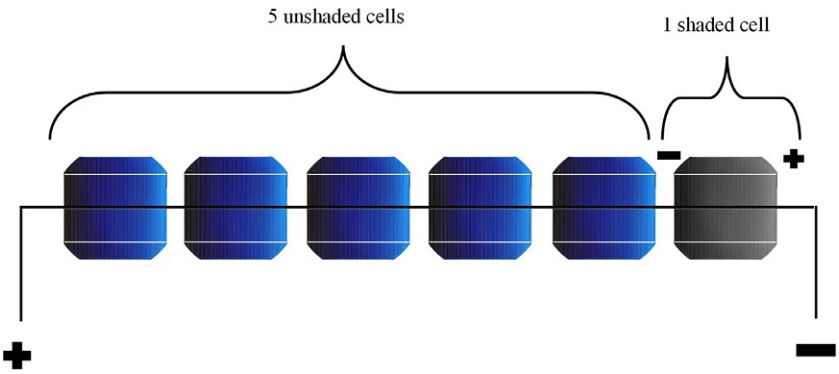

FIG. 5.26 Solar cell under shading.

5.12 Design considerations of a solar photovoltaic system

5.12.1 Load

For standalone systems, the load is defined as the amount of energy required at a specific location. While designing a solar PV system for building a house or an office, the first step is to calculate the load demand that a PV system is to fulfill. Load is measured in terms of the energy consumed by the appliances by multiplying the wattage of the appliance to the daily hourly use, as shown in Eq. (5.11).

$$E_t = \sum_{i=1}^{n} (P_i \times T_i) \tag{5.11}$$

where

E_t is the total energy demand per day by all appliances in watt-hour (Wh);
P_i is the rating of an individual appliance in watts;
T_i is the time of use of an individual appliance in a day; and
n is the total number of appliances.

While designing the system, we must have a worksheet listing the appliances, number of appliances, their wattage, their operation hours, and the daily energy consumption. The load data calculation for a specific house is determined in Table 5.4. The energy demand calculated in this table is 13,633 Wh/day and the power is 1353 W.

5.12.2 Inverter

The DC power produced by the solar panel is first converted into AC power to manage the AC loads. The ratings of the inverter should never be lower than the total watts of the load calculated in this section. The nominal voltages of the inverter must be the same as that of the battery system. For a stand-alone solar PV system, the wattage of the inverter must be large enough to handle the total wattage of the load at one time. Generally, the wattage of the inverter is kept 25%–30% greater than the watts of the loads. If the load is a compressor or a motor, the inverter capacity must be three times greater than the rating of such load. The nominal voltage of the inverter is 24 V.

TABLE 5.4 Load calculation.

Sr. no.	Load	No. of appliances	Power rating (W)	Hourly daily use	Total energy use (Wh)
1	Lights	6	18	6	648
2	Fan	6	45	12	2160
3	Television	1	75	3	225
5	Freezer	1	400	24	9600
6	Water pump	1	500	2	1000
	Total				**13,633**

$$Total\ watts\ of\ the\ load = 18 \times 6 + 6 \times 45 + 75 + 400 + 500 = 1353\ \mathrm{W}$$

As discussed above the wattage of the inverter should be 25–30% higher than the load. Thus the inverter size should be 1759 W. If we consider the inverter to be 90% efficient, the input energy to the inverter should be as follows:

$$input\ energy\ to\ the\ inverter = \frac{13{,}633\ \mathrm{Wh/day}}{0.90}$$

$$input\ energy\ to\ the\ inverter = 15{,}148\ \mathrm{Wh/day}$$

5.12.3 Battery

Deep cycle batteries are recommended for solar PV system applications. The design of the deep cycle batteries is dedicated to being deeply discharged and recharged for years. The size of the battery should be large enough to manage the load on cloudy days.

The battery rating is determined by the following:

$$battery\ rating = \frac{15{,}148\ \mathrm{Wh/day}}{12\ \mathrm{V}}$$

$$battery\ rating = 1262\ \mathrm{Ah/day}$$

Depth of discharge (DoD) is also incorporated by dividing the above-calculated battery ratings to the DoD as follows. For lithium-ion batteries, DoD is kept at 80%.

$$battery\ rating = \frac{1262\ \mathrm{Ah/day}}{0.80}$$

$$battery\ rating = 1578\ \mathrm{Ah/day}$$

Solar energy is intermittent and there may be no sunny days. In such a case, the battery system should be large enough to manage the load. This is incorporated by the autonomy of the system defined as the number of days the system should supply load without sunlight. If the autonomy is kept 1 day, it means 1 day plus today. Two days of autonomy mean 2 days plus today, as shown in Eq. (5.12).

$$Autonomy = 2\ days + today = 3\ days \tag{5.12}$$

$$battery\ rating = 1578\ \mathrm{Ah/day} \times 3$$

$$battery\ rating = 4734\ \mathrm{Ah}$$

In the present case, we keep the autonomy of 1 day and the battery rating is calculated as follows.

$$battery\ rating = 1578\ \mathrm{Ah/day} \times 1$$

$$battery\ rating = 1578\ \mathrm{Ah/day}$$

In the market, we have selected a battery of 12 V and 180 Ah. In our case, the number of batteries that would be required is as follows:

$$No.\ of\ batteries = \frac{1578\ \text{Ah/day}}{180}$$

$$No.\ of\ batteries = 9$$

The system voltage is 24 V. To get 24 V from the battery, we will have to connect two batteries in series. To connect two batteries in series we will have to include one more battery, i.e., 10 batteries.

If the battery system is assumed to be 80% efficient, the input energy to the batteries should be as follows.

$$input\ energy\ to\ the\ batteries = \frac{15{,}148\ \text{Wh/day}}{0.85}$$

$$input\ energy\ to\ the\ batteries = 17{,}821\ \text{Wh/day}$$

Hence the PV modules should supply 17,821 Wh/day which is location-dependent.

5.12.4 PV panels

The location where the solar PV system is to be installed receives 6 kWh/m^2 in a day, but at the STCs solar irradiance is 1000 W/m^2. The input energy to the batteries will be delivered by the solar panels and it would be the output energy from the solar panel.

$$output\ energy\ from\ the\ PV\ modules = 17{,}821\ \text{Wh/day}$$

$$output\ power\ from\ the\ PV\ modules = \frac{17{,}821\ \text{Wh/day}}{6\ \text{h/day}}$$

$$output\ power\ from\ the\ PV\ modules = 2970\ \text{W}$$

We purchase solar panels from the market of 150 W and 12 V.

$$No.\ of\ PV\ modules\ required = \frac{2970}{150} = 19.8 \cong 20$$

5.13 Solar tracker

From dawn to dusk, the sun rises in the east and sets in the west continuously changing its position in the sky. The devices that use sunlight for their operation require to track the sun continuously to be always directed to the sun. Solar towers, solar parabolic troughs, solar dishes, solar cookers and stoves, solar photovoltaics, and indoor lighting systems require the function of a solar tracking system for efficient operation [7].

The sun position in the sky is explained by the three angles. The **solar altitude angle**, also called the **elevation angle**, is defined as the angle of the sun relative to the earth's horizon. It is

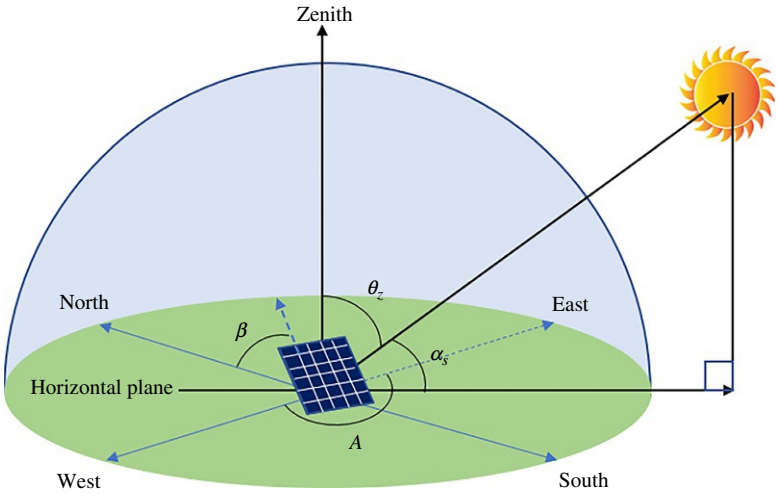

FIG. 5.27 Solar altitude angle.

measured from the horizontal to the line from the horizon to the sun and is denoted as α_s as shown in Fig. 5.27. The range of the solar altitude angle is $0 \leq \alpha_s \leq 90$. The altitude angle is the complement of the zenith angle.

The angle between the vertical line and the line from the earth's horizon to the sun is termed the **zenith angle** and it is the complement of the solar altitude angle. The range of the zenith angle is also $0 \leq \theta_z \leq 90$.

Another angle that is used to locate the position of the sun in the sky in the east–west direction is the **azimuthal angle**, denoted by A. It is the angle between a line parallel to the south to the projection of beam radiation on the horizontal plane. If the projection of beam radiation is east of south, the angle will be positive and if the projection of beam radiation is west of south, the angle will be negative. For example, if the projection is due east, the angle will be 90° and if the projection is due south, the angle will be −90°. If the projection is due south, it means the azimuthal angle is zero and the solar panel is directed toward the sun. another angle related to the positioning of the solar panel is the angle of inclination, denoted as β [8].

As stated above, the two angles—solar altitude angle and azimuthal angle—change continuously because of seasonal patterns or weather conditions, and the solar insolation reaching the solar panel is not maximum. At noon, the angle between the incident light of the sun and the normal to the solar panel is minimum, so the solar panel collects maximum solar irradiance. In the morning and the afternoon, the azimuthal angles are greater and the light reaching the solar panel is oblique. To maximize the collection of the solar irradiance by the solar panel, mechanisms have been developed to keep the direction of the solar panel toward the sun. Solar trackers have been introduced to achieve this. They are of two types: single-axis solar trackers and dual-axis solar trackers.

In a single-axis solar tracker, the tilted solar panel is mounted on the structure that uses a motor and a controller that rotates to the trajectory of the sun. A single-axis solar tracker tracks the sun in the east-west direction following the azimuthal angle. In single-axis solar trackers, north-south tilt is not tracked because it does not contribute significantly to energy production compared to the cost incurred on the north-south tracking [9,10].

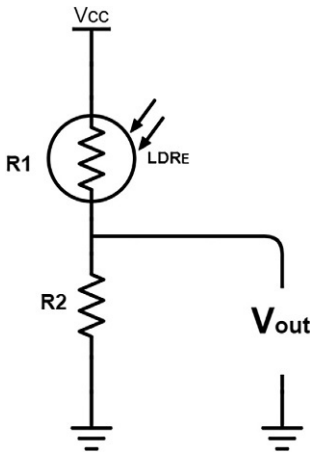

FIG. 5.28 Implementation of LDR in solar tracker.

Solar trackers are implemented by using light-dependent resistors (LDRs), motors, and the mounting structure. LDRs, also called photoresistors, are passive components whose resistance varies as the light falls on the sensitive surface of the component. In solar trackers, an LDR is used in series with another resistor making a voltage dividing circuit. As the solar irradiance falling on the LDR varies, its resistance also changes, and the output voltage of the voltage dividing circuit is changed. In short, the change in irradiance is translated in terms of a change in voltage. The change in voltage across both such circuits of east and west are compared, and the decision is made to move the solar panel toward east or west. The voltage dividing circuit consisting of resistance and an LDR is shown in Fig. 5.28.

In a dual-axis solar tracker, both the east-west trajectory and north-south tilt are tracked, which maximizes the collection of solar irradiance by the solar panels. Dual-axis solar tracking is best suitable for the indoor lighting system where the sunlight is to be concentrated on a single point of collection by the optical fiber. Another application of the dual-axis solar tracker is solar thermal technologies such as solar towers, solar parabolic troughs, solar dishes, and solar cookers. In a dual-axis solar tracker, four LDR circuits are used for east, west, north, and south detection of solar irradiance. Fig. 5.29 shows a flowchart of a dual-axis solar tracker.

5.14 Perturb and observe (P&O) maximum power point tracker (MPPT) algorithm

The performance and the efficiency of the solar photovoltaic system are always vulnerable to the varying solar irradiance and the temperature. The varying irradiance throughout the day because of the solar position and the weather conditions do not let the solar cell operate at the MPP. The MPP is the point on the *P-V* curve of a solar cell at which the power is maximum, as shown in Fig. 5.30. A MPPT is adopted to let the solar cell operate at the maximum power. An MPPT consists of an algorithm that tracks the MPP and adjusts the duty cycle of the converter to reach the MPP. The most commonly used MPPT algorithm is the P&O algorithm. This algorithm is the least complex and most easy to implement [11,12].

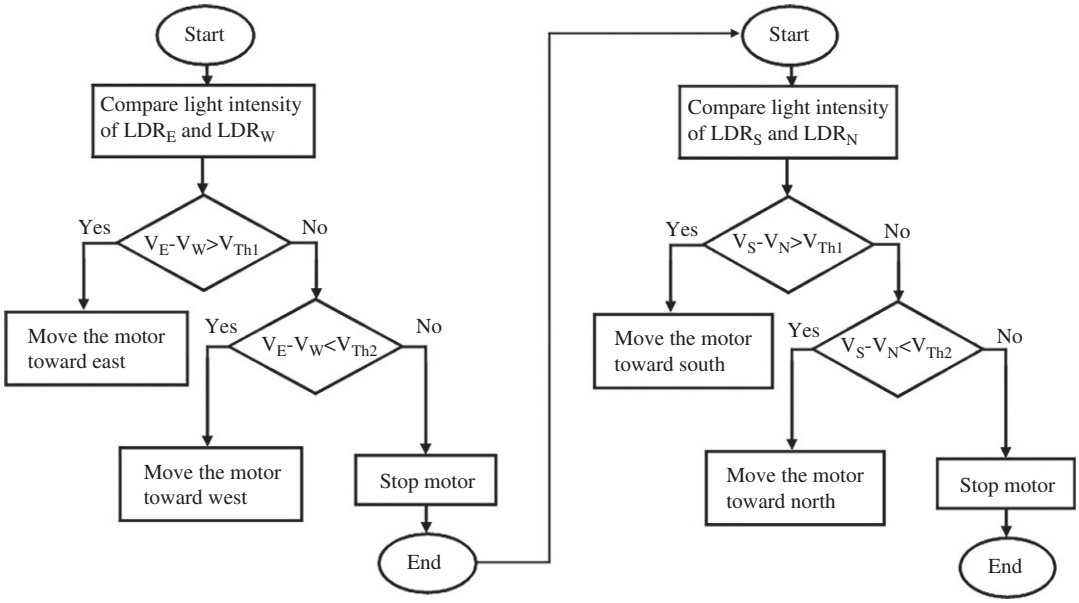

FIG. 5.29 Flowchart of a dual axis solar tracker.

For the derivation of the P&O algorithm, four different cases are considered.

1. In the first case, the operating power point is moving toward the MPP from the right-hand side of the *P-V* curve. $V(k)$ and $P(k)$ are the value of the voltage and power, respectively, at the current time, whereas $V(k-1)$ and $P(k-1)$ are the values of voltage and current, respectively, at the previous time. In this case, the observation is that the change in power (ΔP) is positive and the change in the voltage (ΔV) is negative. The voltage is being reduced and approaching the MPP. To reach the MPP, we have to decrease the voltage further. For that purpose, the perturbation is made by decreasing the duty cycle by an amount of ΔD. ΔD is called a step size, having a very small fixed or variable value. Case 1 is shown in Fig. 5.30.
2. In the second case, the operating power point is moving toward the MPP from the left-hand side of the *P-V* curve, as shown in Fig. 5.31. $V(k)$ and $P(k)$ are the value of the voltage and power, respectively, at the current sample time (k), whereas $V(k-1)$ and $P(k-1)$ are the values of voltage and current, respectively, at the previous sample time ($k-1$). In this case, the observation is that the change in power and the change in voltage are positive. The voltage is being increased and approaching the MPP. To reach the MPP, we have to increase the voltage further. For that purpose, the perturbation is made by increasing the duty cycle by an amount of ΔD. ΔD is a very small fixed value.
3. In the third case, the operating power point is moving away from the MPP on the right-hand side of the *P-V* curve, as shown in Fig. 5.32. $V(k)$ and $P(k)$ are the value of the voltage and power, respectively, at the current sample time (k), whereas $V(k-1)$ and $P(k-1)$ are the values of voltage and current, respectively, at the previous sample time ($k-1$). In this case, the observation is that the change in power is negative and the change in voltage is

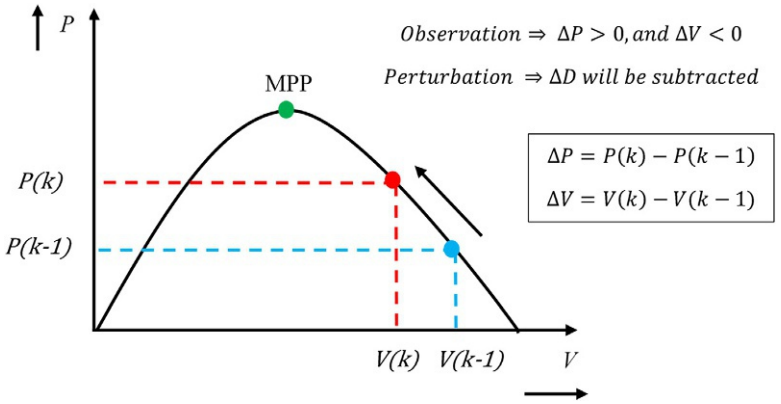

FIG. 5.30 Case 1, when operating point moving toward MPP from right-hand side.

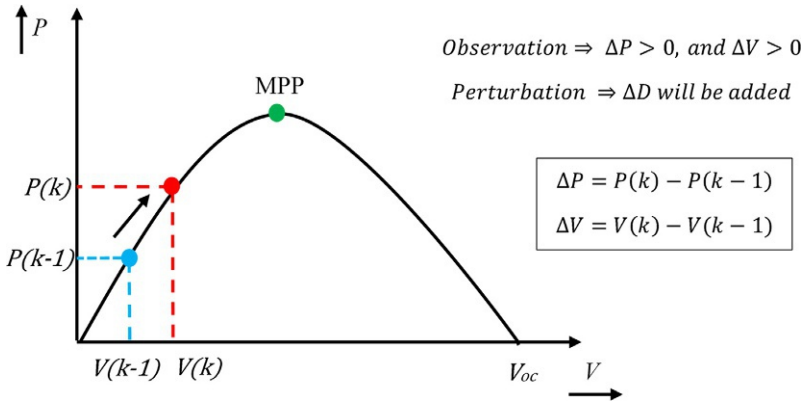

FIG. 5.31 Case 2, when operating point moving toward MPP from left-hand side.

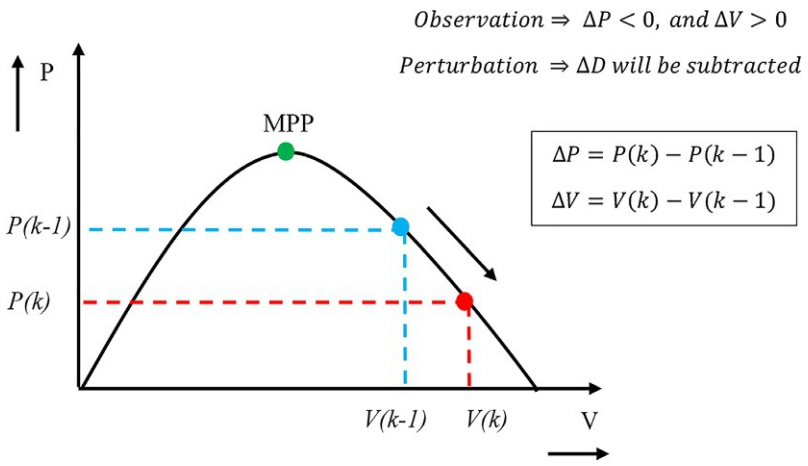

FIG. 5.32 Case 3, when operating point moving away from MPP toward right-hand side.

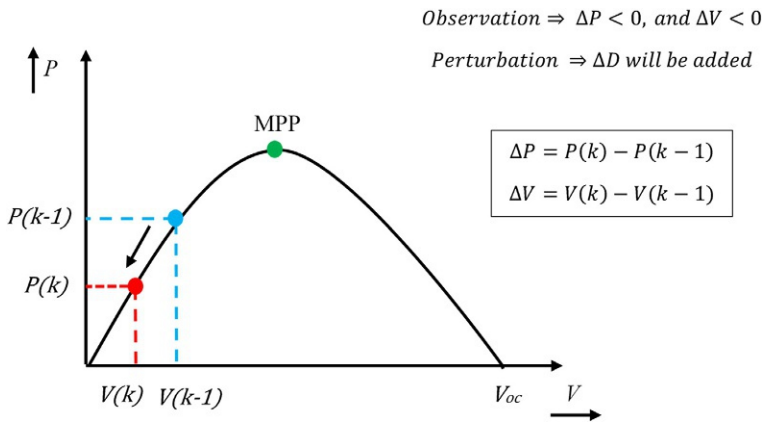

FIG. 5.33 Case 4, when operating point moving away from MPP toward left-hand side.

positive. The voltage is being increased and moving away from the MPP. To reach the MPP, we have to decrease the voltage. For that purpose, the perturbation is made by decreasing the duty cycle by an amount of ΔD. ΔD is a very small fixed value. Case 3 is shown in Fig. 5.32.

4. In the fourth case, the operating power point is moving away from the MPP on the left-hand side of the *P*-*V* curve, as shown in Fig. 5.33. $V(k)$ and $P(k)$ are the value of the voltage and power, respectively, at the current sample time (k), whereas $V(k-1)$ and $P(k-1)$ are the values of voltage and current, respectively, at the previous sample time ($k-1$). In this case, the observation is that the change in power and the change in voltage are negative. The voltage is being decreased and moving away from the MPP. To reach the MPP, we have to increase the voltage. For that purpose, the perturbation is made by increasing the duty cycle by an amount of ΔD. ΔD is a very small fixed value. Case 4 is shown in Fig. 5.33.

Based on the four cases presented above, an algorithm is developed that continuously observe the values of (ΔP) and (ΔV) and decides the perturbation. Perturbation and observation of each case are shown in Figs. 5.30–5.33. A flowchart shown in Fig. 5.34 is developed for the P&O algorithm based on the above discussed four cases. $D(k)$ is the value of the duty cycle in the current sample time which is obtained by perturbing the previous duty cycle $D(k-1)$, whereas $D(k-1)$ is the value of the duty cycle in the previous time before perturbation. The perturbation could be positive or negative based on the observation.

5.14.1 Problems with conventional P&O algorithm

The conventional P&O algorithm is a fixed step-size algorithm that carries the following problems.

1. In tracking the MPP, perturbation is made against each observation. Each time the perturbation is made, the operating point moves toward the MPP. When the operating point is near the MPP, the next perturbation takes the operating point a little ahead of the MPP without guessing that it has moved away from the MPP. In the next perturbation, it

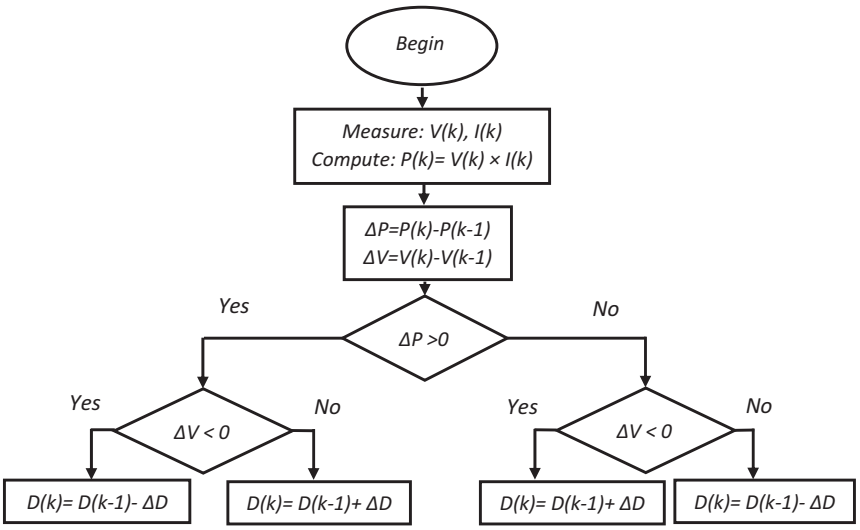

FIG. 5.34 Flowchart of perturb and observe (P&O) algorithm.

tracks the MPP but again it moves away from the MPP to the other side. The conventional P&O is unable to calculate the exact perturbation to reach the MPP. In this way, oscillations are generated at the MPP, showing the poor performance of the algorithm.

2. Multiple perturbations and observations increase the response time of the algorithm in tracking the MPP.

5.15 Simulation of perturb and observe MPPT algorithm in MATLAB

The P&O MPPT algorithm discussed in Section 5.16 is implemented with the solar photovoltaic system in MATLAB Simulink. Fig. 5.35 shows the block diagram of the simulation of a complete solar photovoltaic system. In this diagram, a PV array of 100 kW is simulated with inputs irradiance and temperature. The output of the solar PV is connected to the boost converter whose duty cycle is decided by the MPPT. The MPPT block contains the P&O algorithm. A simulation diagram of the P&O algorithm is shown in Fig. 5.36. The MPPT block as discussed in the flowchart of P&O takes the sample time of the voltage and power at the time (k) and ($k-1$) and calculates the (ΔP) and (ΔV). Based on four cases presented in Section 5.14, the algorithm observes the (ΔP) and (ΔV) and perturbs accordingly. The duty cycle decided by the MPPT block is fed to the boost converter, which is connected to the load.

Fig. 5.37 shows a graph of the panel temperature and solar irradiance. The temperature of the solar cell is kept constant at 25°C and the irradiance is changed after regular intervals. For the first second, the irradiance and temperature are kept at STCs, i.e., 25°C and 1000 W/m^2. For this period, we can see there is no change in the output power, voltage, and duty cycle since the solar panels are already operating at the MPP. After 1 s, the solar irradiance is reduced keeping the temperature constant, during this variation we can observe the decrease

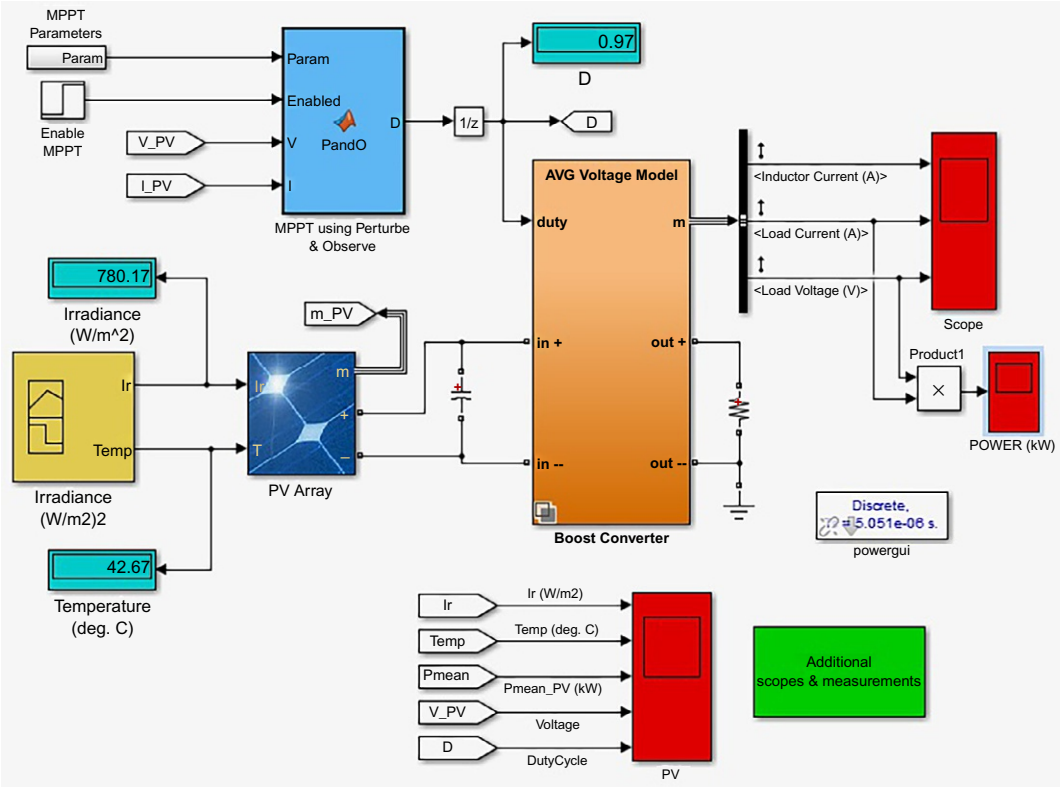

FIG. 5.35 MATLAB simulation of MPPT-based solar PV system.

in the power and the oscillations in the graph. The MPPT algorithm comes into action, which can be seen in the variation in the duty cycle. Accordingly, there is a change in the voltage and power graphs. The power graph shown in Fig. 5.37 again maintains it at the MPP until the variation occurs in the solar irradiance. The complete graphs of the solar irradiance, panel temperature, panel power, output voltage, and duty cycle under varying atmospheric conditions are shown in Fig. 5.37.

Fig. 5.38 shows the output power under different atmospheric conditions. Fig. 5.38A is the power at STCs, i.e., 25°C and 1000 W/m^2. The conventional P&O controller takes 8.6 s to reach the MPP with a large step size. The maximum power tracked is 213.15 W. The efficiency is 98.75%. Fig. 5.38B is the power at 25°C and 900 W/m^2. The conventional P&O controller takes 8.6 s to reach the MPP with a large step size. The maximum power tracked is 191.6 W. The efficiency is 98.70%. Fig. 5.38C is the power at 50°C and 900 W/m^2. The conventional P&O controller takes 8.6 s to reach the MPP with a large step size. The maximum power tracked is 171.6 W. The efficiency is 98.48%. Hence, under varying temperatures and solar irradiance, the conventional P&O algorithm tracked the MPP with an efficiency of almost 98% with a large response time.

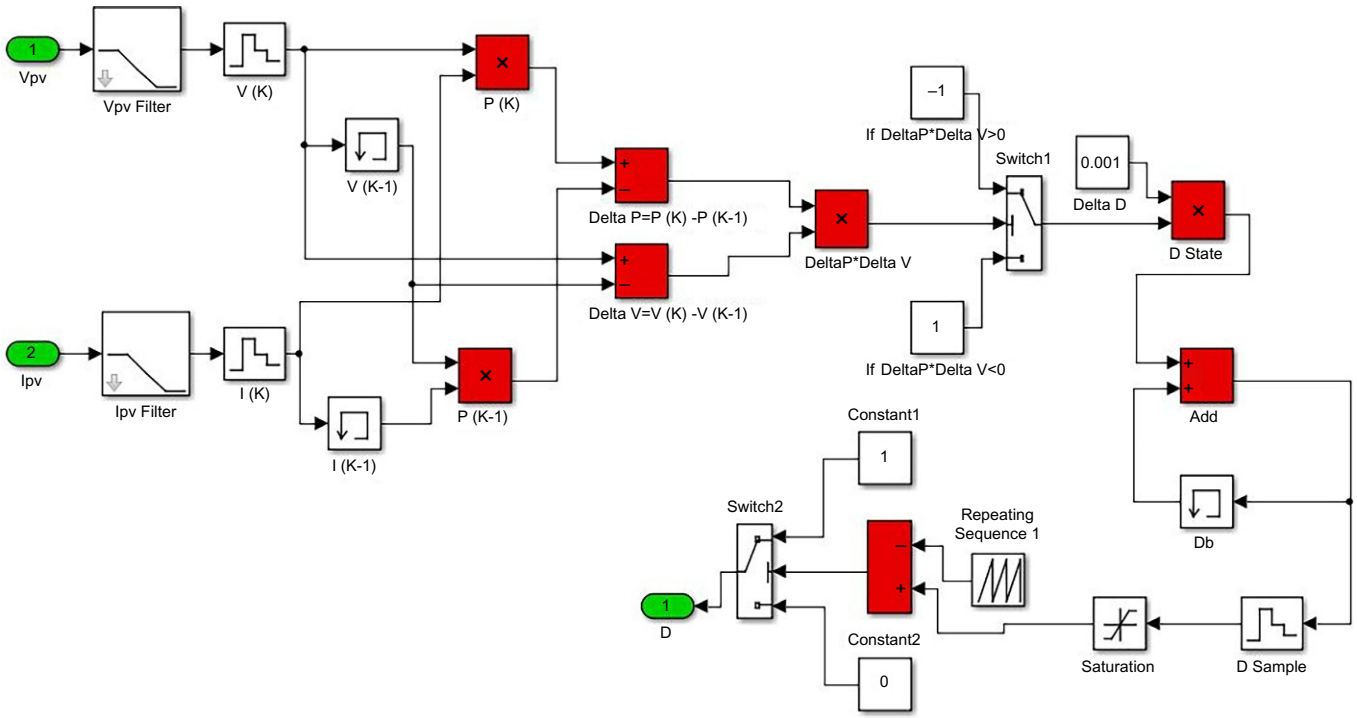

FIG. 5.36 MATLAB simulation of P&O algorithm.

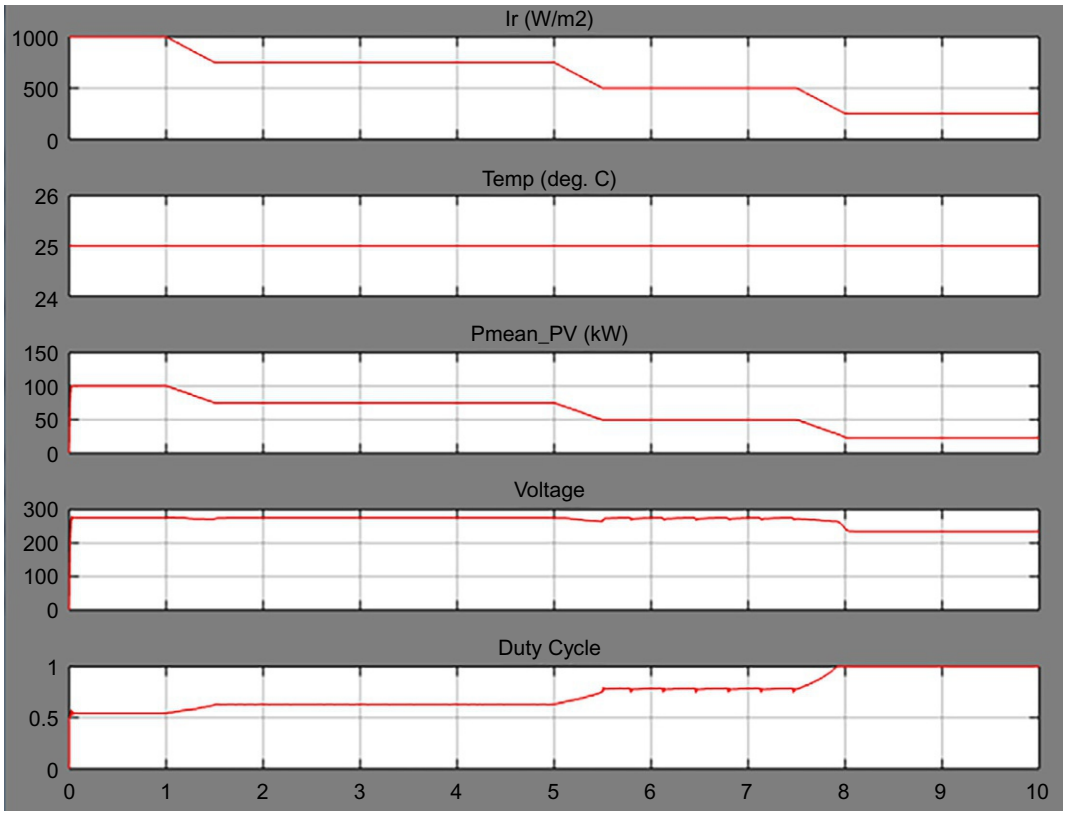

FIG. 5.37 Various outputs of P&O simulation.

5.16 Simulation of fuzzy logic-based perturb and observe MPPT algorithm in MATLAB/Simulink

Section 5.17 presents the simulation of a fixed step-sized P&O MPPT algorithm that carries the problems of oscillations at the MPP and the high response time in tracking the MPP. These problems are overcome by introducing an algorithm that observes the exact variation in the value of (ΔP) and (ΔV) and trains a system that perturbs a variable step size (ΔD) in the duty cycle.

A FL-based P&O algorithm is proposed that is a variable step-sized algorithm. The block diagram of the proposed FLC-based P&O algorithm is shown in Figs. 5.39 and 5.40. The controller takes the sample of voltage and current from the solar panel, defines the input variables (ΔP) and (ΔV) of the FLC, and decides the output (ΔD). FL consists of fuzzification of the input variables, rule-based inference, and defuzzification to give the output variable. In fuzzification, numerical values of variables like (ΔP) and (ΔV) are transformed into linguistic variables using membership functions. Each linguistic variable is assigned a value of a membership function. The linguistic variables are [13]:

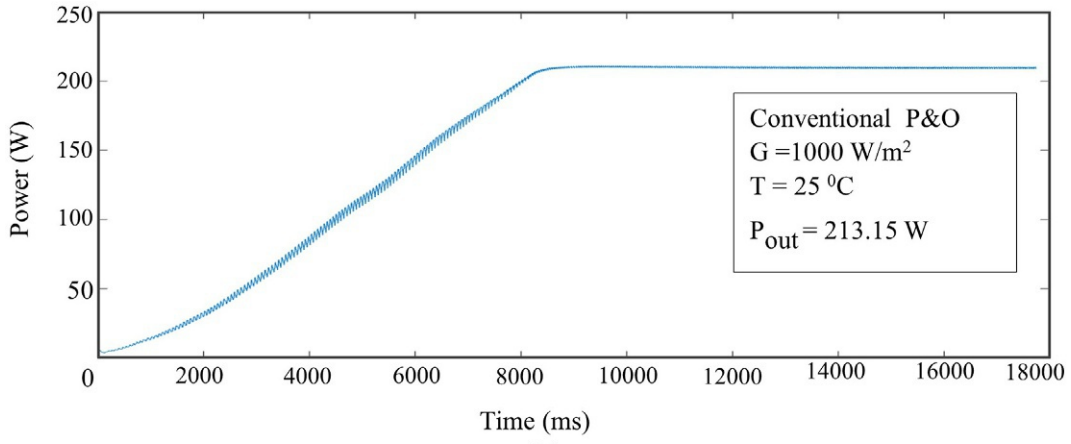

(a)

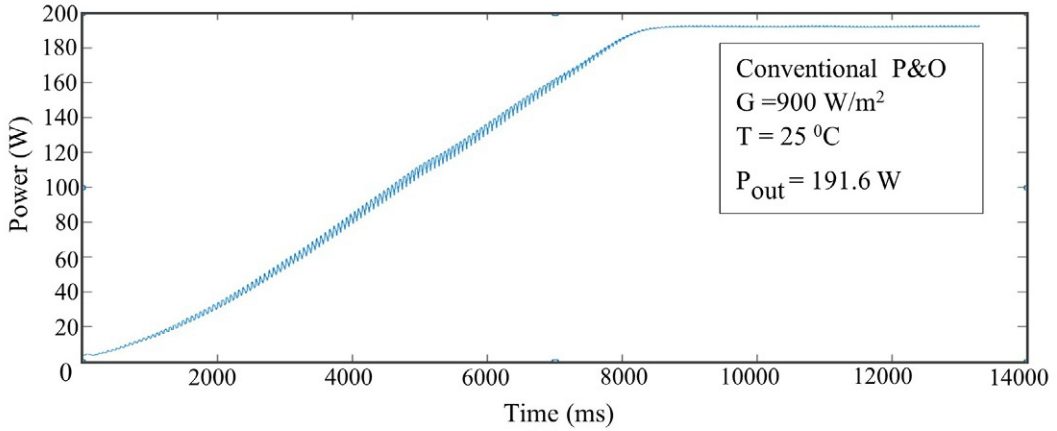

(b)

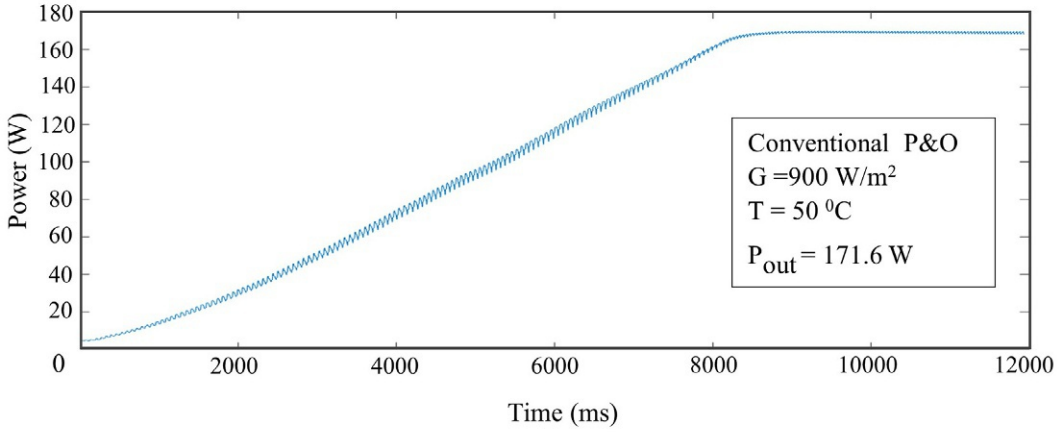

(c)

FIG. 5.38 Output power of P&O-based solar PV at (A) standard test conditions, (B) 900 W/m^2 solar irradiance and 25°C temperature, and (C) 900 W/m^2 solar irradiance and 50°C temperature.

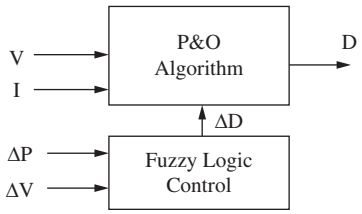

FIG. 5.39 Block diagram of the implementation of fuzzy logic with P&O MPPT algorithm.

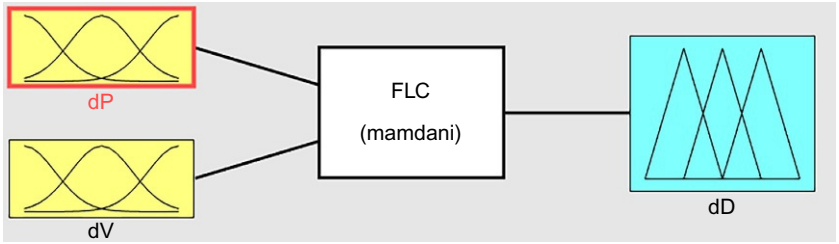

FIG. 5.40 Block diagram of the implementation of fuzzy logic with P&O MPPT algorithm in MATLAB.

- positive small (PS);
- negative small (NS);
- negative big (NB);
- positive big (PB);
- negative medium (NM);
- positive medium (PM); and
- zero (ZE).

The inference rule is the second step in which the fuzzy processor takes the input vectors along with some rules and assigns the value to the output vector. The fuzzy inference involves the membership functions, the if-then rule, and the logic operators. The membership functions defined for the inputs (ΔP) and (ΔV) of the FL-based P&O algorithm are shown in Table 5.5. If-then statements consist of two parts; the "If" part is called the antecedent and the "Then" part is called the consequent. The antecedent defines the fuzzy region of all the input variables separated by the logic operator and the consequent defines the output in the fuzzy region. The logic operator could be an AND operator, OR operator, or a NOT operator. For the proposed P&O FLC, seven membership functions for the input variables are defined in MATLAB, as shown in Fig. 5.41. Membership functions of the input variables and output variables and the rules defined are shown in Table 5.5 [13,14].

FL rules in MATLAB and the rule viewer are shown in Figs. 5.42 and 5.43, respectively, showing the input and output variables. Rule viewer shows the change in input variables and the corresponding output. In Fig. 5.43, it can be seen that if ΔP is 3.67 and ΔV is 2.73, ΔD equal to 0.0405 will be perturbed in the duty cycle. For each value of the input variable, i.e., for each change in voltage or the current, different values of the change in duty cycle will be

TABLE 5.5 Fuzzy rules of input variables.

	ΔV						
ΔP	**NB**	**NM**	**NS**	**ZE**	**PS**	**PM**	**PB**
NB	NB	NM	NM	NS	ZE	ZE	ZE
NM	NB	NM	NM	NS	ZE	PS	PM
NS	NM	NM	NS	ZE	ZE	PS	PM
ZE	NS	ZE	ZE	ZE	PS	PM	PB
PS	ZE	PS	PS	PS	PM	PM	PB
PM	ZE	PS	PS	PM	PM	PM	PB
PB	PM	PM	PM	PB	PB	PB	PB

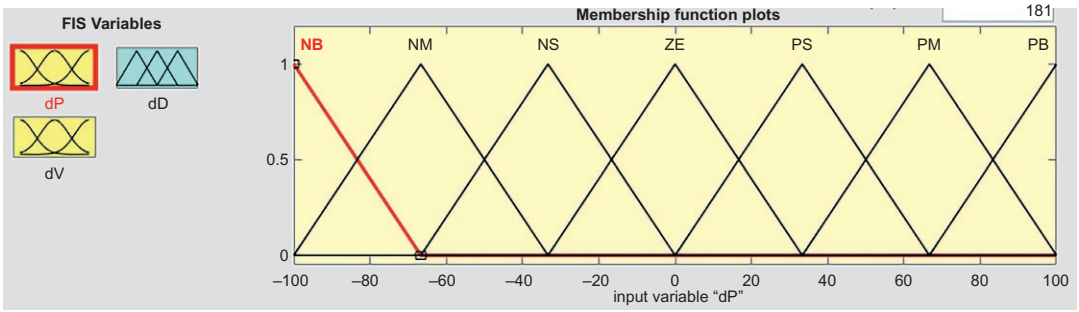

FIG. 5.41 Membership function plots of input and output variables.

perturbed. This type of algorithm is called a variable step-sized FL-based P&O algorithm. In this way, the FLC is ready to be used in the P&O MPPT solar photovoltaic system.

After preparing the FLC in MATLAB, it is embedded in the simulation of the conventional P&O algorithm implemented in Section 5.15. The flowchart of the proposed FL-based P&O MPPT algorithm is shown in Fig. 5.44. At the start, the sample of the voltage and power at the current time (k) and the previous time ($k-1$) are measured and stored to calculate the (ΔP) and (ΔV). The algorithm consists of two parts: the first one is the conventional P&O algorithm that observes the change in voltage and the change in current and decides whether the perturbation will be added or subtracted. The second part of the flowchart is the FL-based calculation of the perturbation in the duty cycle. The flowchart is simulated in the MATLAB Simulink shown in Fig. 5.45, in which it can be seen that both parts of the algorithm are implemented separately.

Fig. 5.46 shows the output power under different atmospheric conditions. Fig. 5.46A is the power at STCs, i.e., 25°C and 1000 W/m^2. The conventional P&O controller takes 2.9 s to reach the MPP with a large step size. The maximum power tracked is 213.15 W. The efficiency is 99.22%. Fig. 5.46B is the power at 25°C and 900 W/m^2. The conventional P&O controller takes 2.9 s to reach the MPP with a large step size. The maximum power tracked is 191.6 W. The

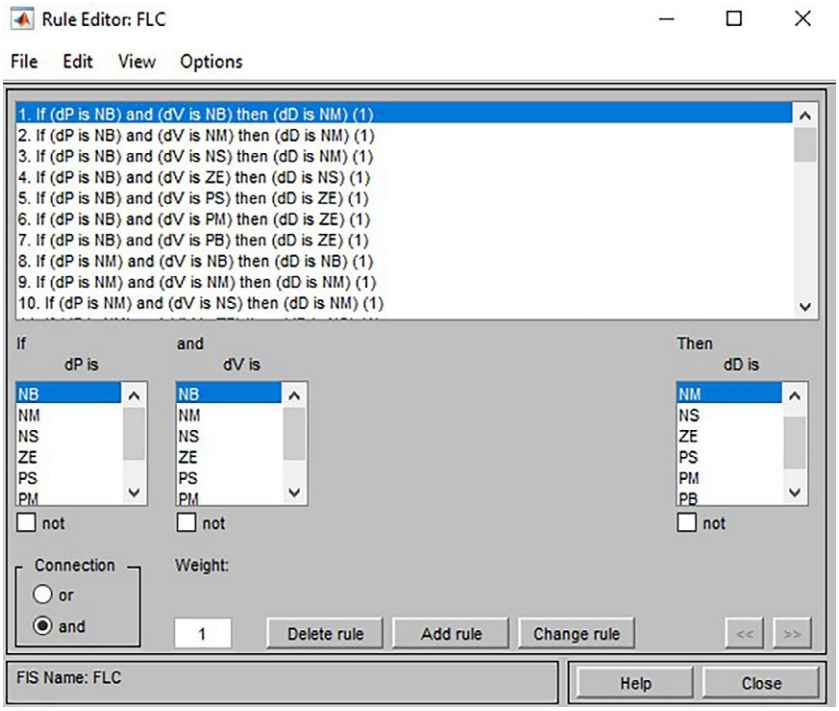

FIG. 5.42 Fuzzy logic rules written in MATLAB.

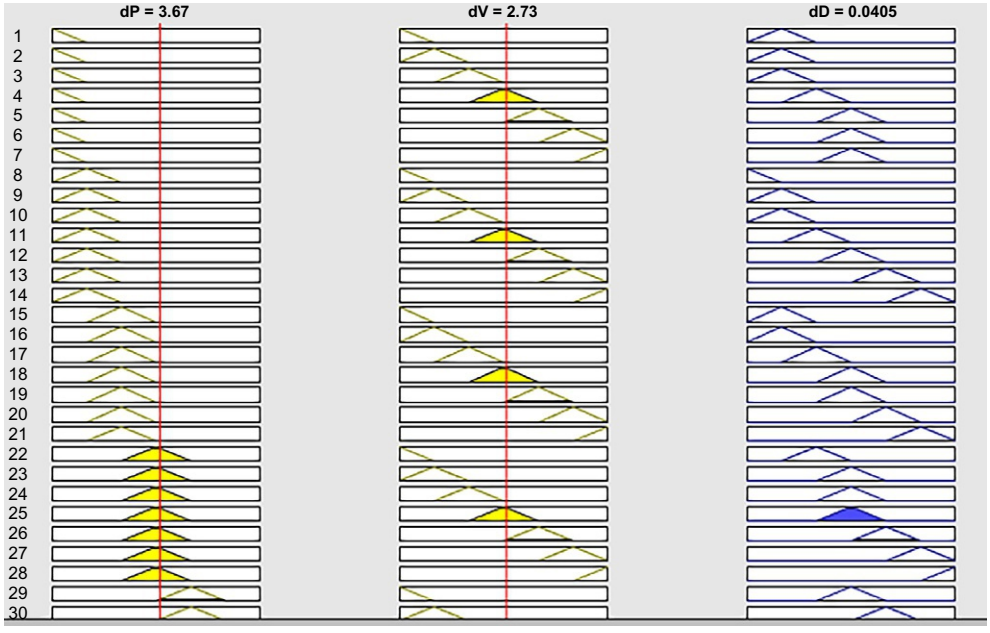

FIG. 5.43 Rules viewer in MATLAB.

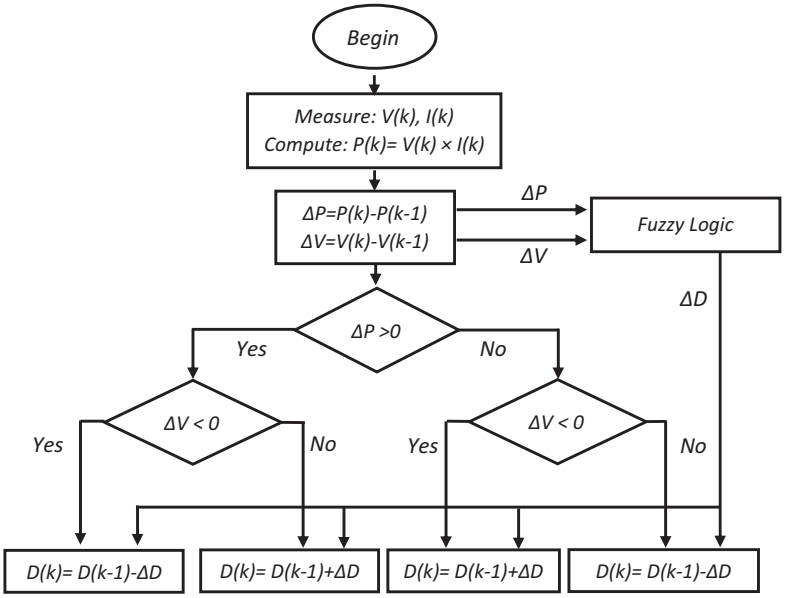

FIG. 5.44 Flowchart of fuzzy logic-based P&O algorithm.

efficiency is 99.12%. Fig. 5.46C is the power at 50°C and 900 W/m^2. The conventional P&O controller takes 2.9 s to reach the MPP with a large step size. The maximum power tracked is 171.6 W. The efficiency is 99.06%. Hence, under varying temperatures and solar irradiance, FL-based P&O algorithm tracked the MPP with an efficiency of almost 99% with a low response time and small step size. Fig. 5.47 shows the output power graphs of both conventional and proposed FL-based P&O algorithms. Table 5.6 also gives a comparison of response time, step size, and efficiency between conventional and FL-based P&O algorithms under varying atmospheric conditions.

5.17 Incremental conductance (INC) MPPT algorithm

The drawbacks of the abovementioned P&O algorithm are overcome by the advanced MPPT algorithms. The INC algorithm is one of the advanced algorithms that calculate the slope of the *P_V* curve of the solar panel and tracks the MPP by tracking the peak point of the *P-V* curve. An INC algorithm is derived by using the power formula of a DC source, as shown in Eq. (5.13).

$$P = VI \tag{5.13}$$

Taking the derivative of both sides of Eq. (5.13) with respect to V:

$$\frac{dP}{dV} = \frac{d(VI)}{dV}$$

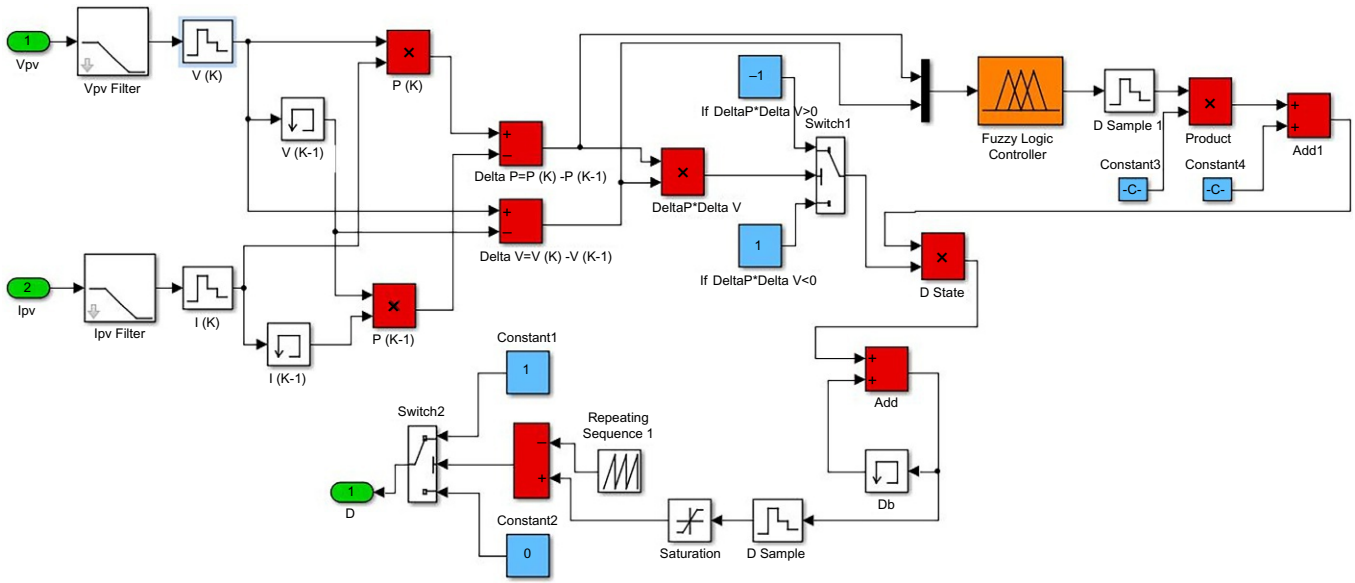

FIG. 5.45 MATLAB simulation of fuzzy logic-based P&O MPPT algorithm.

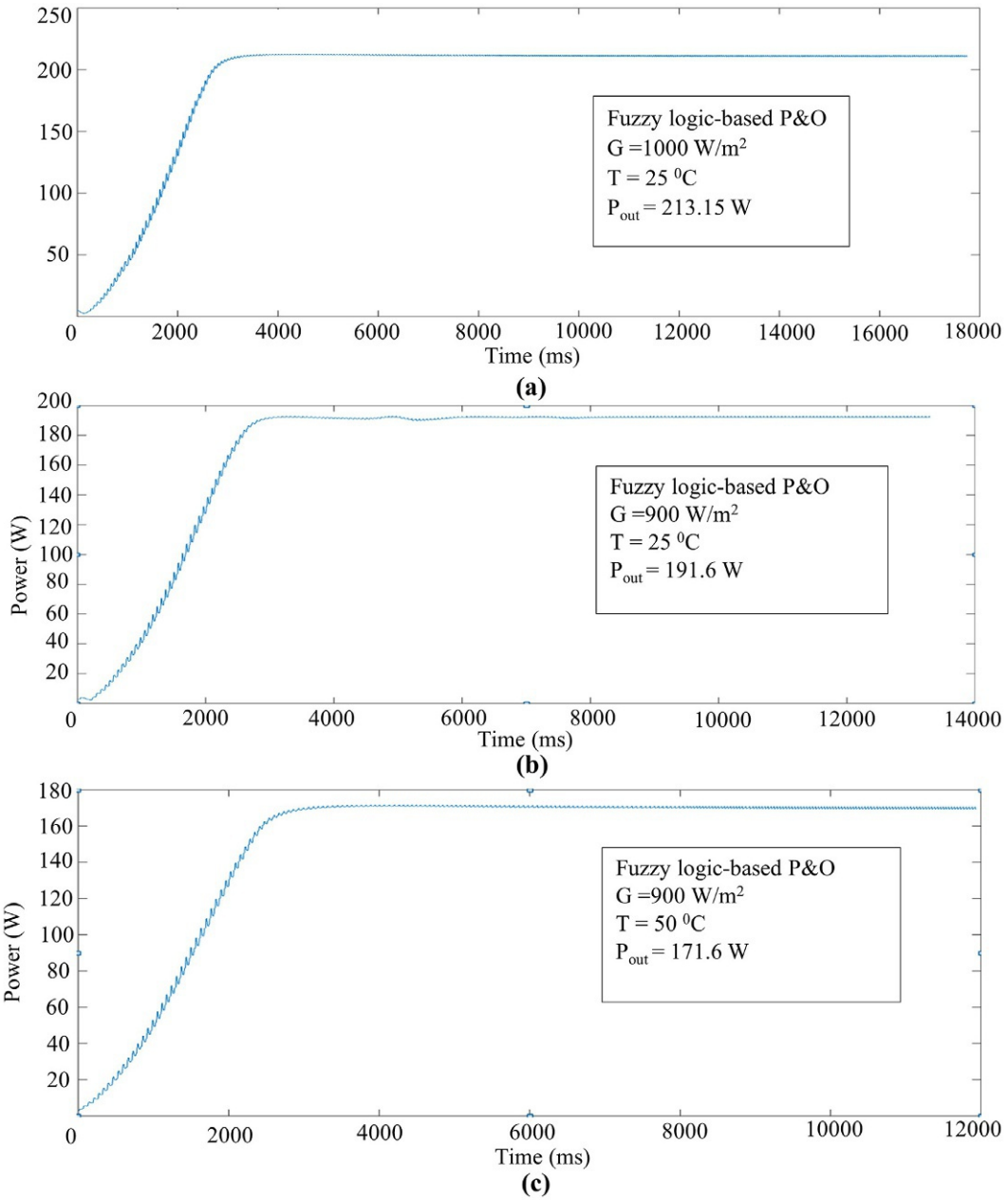

FIG. 5.46 Output power of fuzzy logic-based P&O solar PV at (A) standard test conditions, (B) 900 W/m^2 solar irradiance and 25°C temperature, and (C) 900 W/m^2 solar irradiance and 50°C temperature.

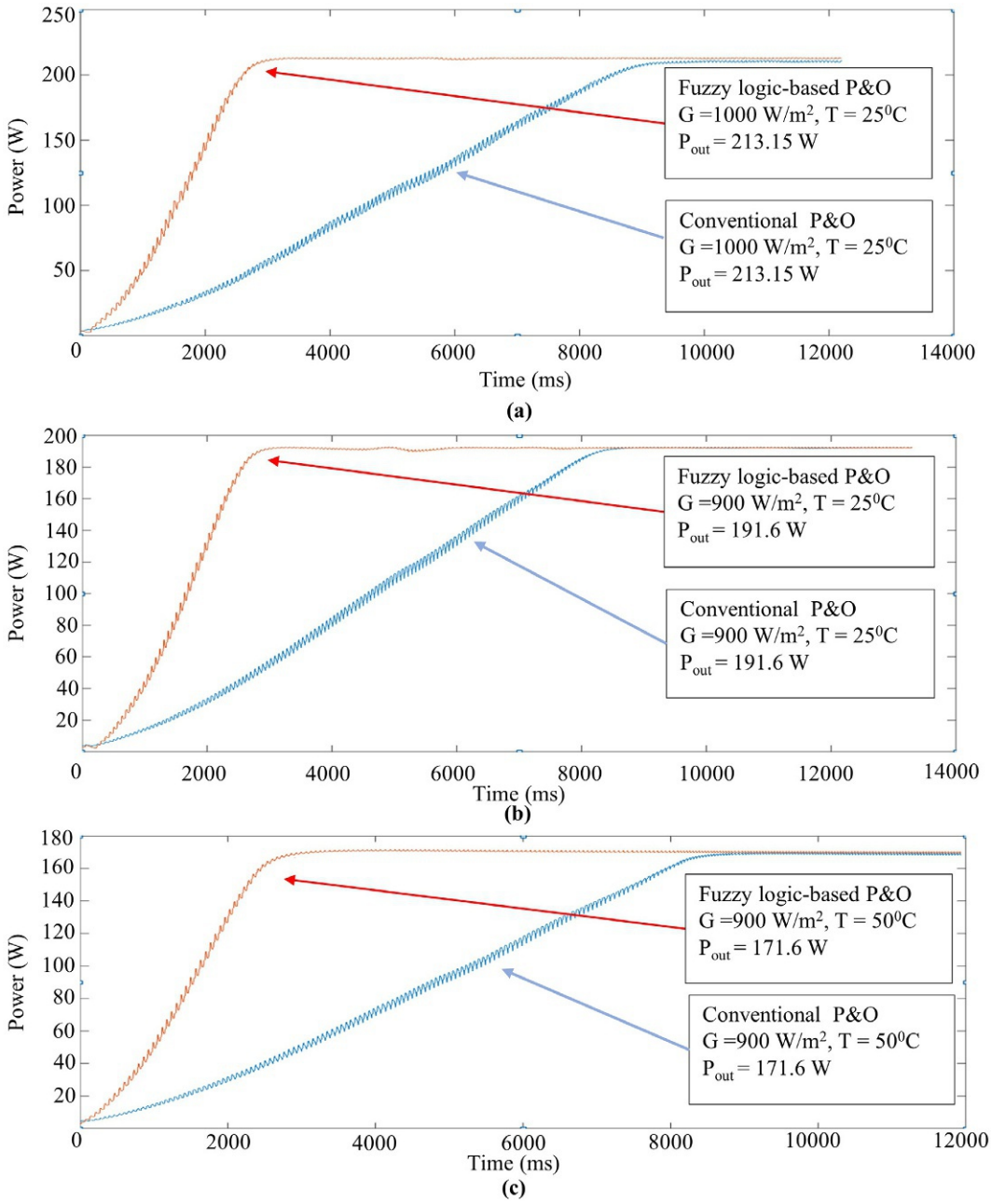

FIG. 5.47 Comparison between conventional P&O algorithm and fuzzy logic-based P&O algorithm: output power of fuzzy logic-based P&O solar PV at (A) standard test conditions, (B) 900 W/m^2 solar irradiance and 25°C temperature, and (C) 900 W/m^2 solar irradiance and 50°C temperature.

TABLE 5.6 Comparison of conventional P&O algorithm and fuzzy logic-based P&O algorithm under varying atmospheric conditions.

Environmental conditions	Response time (s)		Steps to reach steady state		Efficiency (%)	
	Conventional P&O	FLC-based P&O	Conventional P&O	FLC-based P&O	Conventional P&O	FLC-based P&O
$T=25$ (°C) $G=1000$ (W/m^2)	8.6	2.9	Large	Small	98.75	99.22
$T=25$ (°C) $G=900$ (W/m^2)	8.6	2.9	Large	Small	98.70	99.12
$T=50$ (°C) $G=900$ (W/m^2)	8.6	2.9	Large	small	98.48	99.06

$$\frac{dP}{dV} = V \cdot \frac{dI}{dV} + I \tag{5.14}$$

As we move from the zero voltage to the open-circuit voltage on the *P-V* curve of a solar cell, we find that the slope of the curve is increasing in the left-hand region of the *P-V* curve and the slope is decreasing in the right-hand region. Both the regions are separated by a single point named as the MPP at which the slope of the curve is zero. To find the relation at the maximum power, we put the slope of the *P-V* curve equal to zero $\left(\frac{dP}{dV} = 0\right)$ in Eq. (5.14) as the slope of the *P-V* curve at the MPP is zero, also shown in Fig. 5.48. Eq. (5.15) is the relation between conductance and the INC for the MPP saying that at MPP both the INC and conductance of the solar cell are equal. Similarly, by using the slopes of the *P-V* curve at the left of MPP and the right of MPP, we can determine Eqs. (5.16), (5.17). Now, with the help of Eqs. (5.15)–(5.17), we can draw a flowchart of the INC algorithm shown in Fig. 5.49. The INC controller measures the voltage and current at the present time (k) and previous time ($k-1$). Measures the change in voltage (ΔV) and change in current (ΔI). If there is no change in voltage

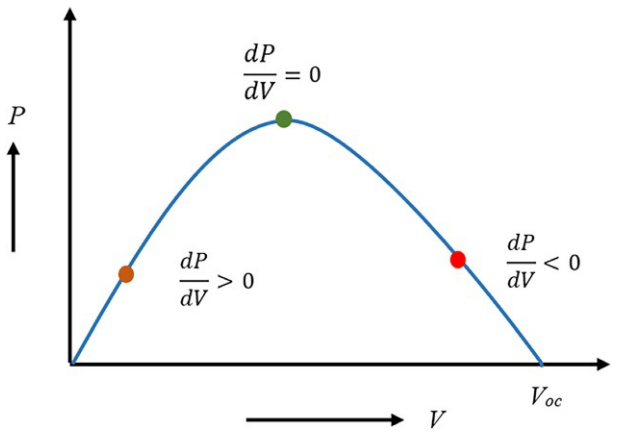

FIG. 5.48 Slopes of *P-V* curve of a solar cell.

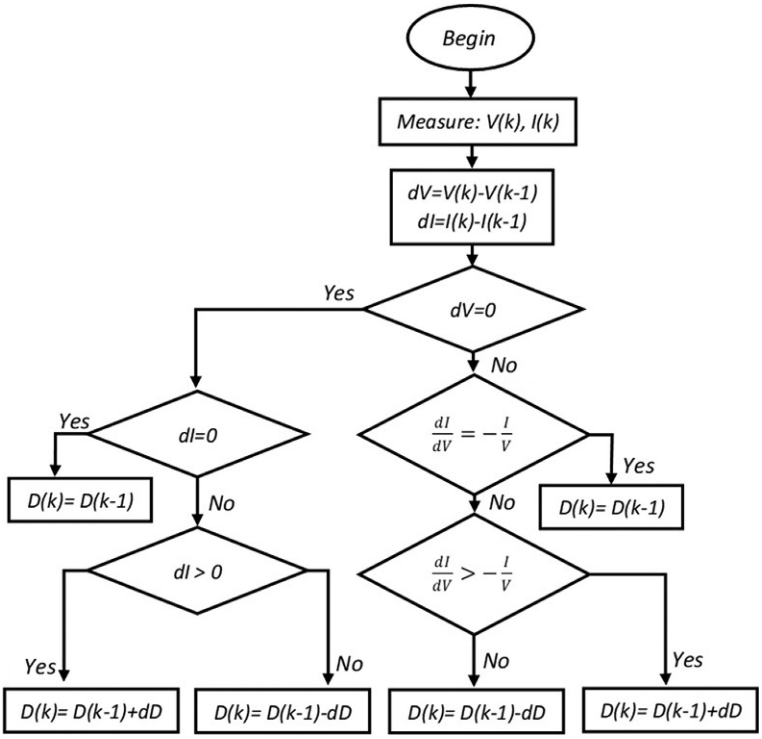

FIG. 5.49 Flowchart of incremental conductance MPPT algorithm.

and current, its mean the solar panel is already operating at the MPP. If the controller finds a change in the voltage, it determines the INC and compares it to the instantaneous conductance. If the INC and the instantaneous conductance are equal it means the solar panel is already operating at the MPP and there is no need to take any action. On the other hand, if the INC is less than the negative of the instantaneous conductance, it means that the operating point of the solar panel is at the right-hand side of the MPP. To track the MPP, we need to decrease the operating voltage and this can be done by decreasing the duty cycle of the DC-DC converter. If the INC is greater than the negative of the instantaneous conductance, it means that the operating point of the solar panel is at the left-hand side of the MPP. To track the MPP, we need to increase the operating voltage; this can be done by increasing the duty cycle of the DC-DC converter.

$$\frac{dP}{dV} = 0 \Rightarrow -\frac{I}{V} = \frac{dI}{dV}; \textit{Maximum Power Point} \tag{5.15}$$

$$\frac{dP}{dV} > 0 \Rightarrow -\frac{I}{V} > \frac{dI}{dV}; \textit{Right side of the Maximum Power Point} \tag{5.16}$$

$$\frac{dP}{dV} < 0 \Rightarrow -\frac{I}{V} < \frac{dI}{dV}; \textit{Left side of the Maximum Power Point} \tag{5.17}$$

5.18 Simulation of incremental conductance (INC) MPPT algorithm in LabVIEW

The INC algorithm shown in Fig. 5.50 is implemented in the LabVIEW MathScript RT module. MathScript RT module is the math-oriented text computing language to address tasks of mathematical calculations and implementation of mathematical equations. To simulate the INC algorithm, we take voltage and currents at the present time (k) and previous time ($k-1$) from the simulation of single diode model of the solar cell performed in Section 5.9. The simulation of a flowchart of the INC algorithm is performed in the LabVIEW MathScript RT module shown in Fig. 5.50. The simulation of the INC algorithm implements the flowchart and decides the duty cycle of the DC-DC boost converter.

Fig. 5.51 shows the output power under constant solar irradiance which indicates that the maximum rated power delivered by the solar cell at STCs, i.e., 25°C and 1000 W/m^2 is 3.1 W. The implemented INC algorithm tracks the MPP successfully. At constant irradiance, no oscillations are there at the MPP. Under varying solar irradiance, the graph of the output power can be seen in Fig. 5.52. As the solar irradiance changes, a new MPP is located and tracked by the INC controller.

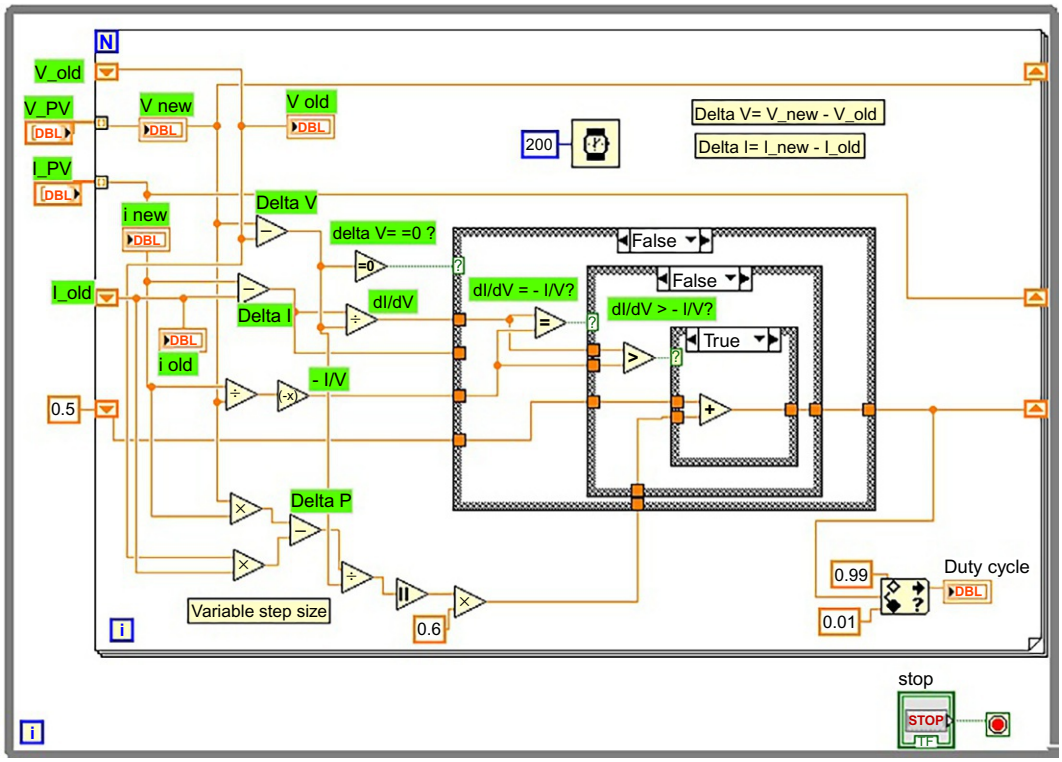

FIG. 5.50 LabVIEW-based simulation of incremental conductance algorithm [15].

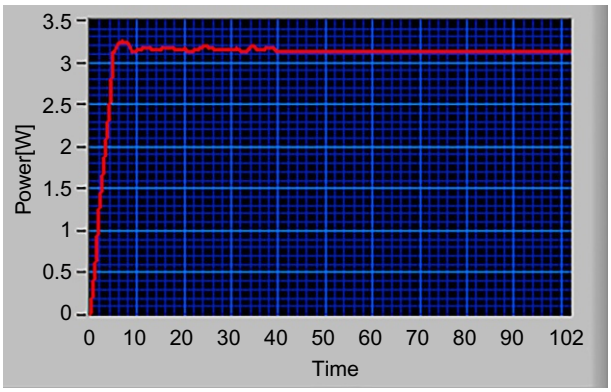

FIG. 5.51 Output power of incremental conductance algorithm at constant solar irradiance [15].

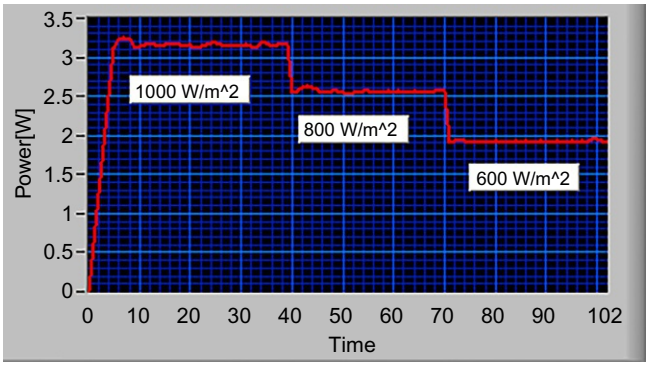

FIG. 5.52 Output power of incremental conductance algorithm under varying solar irradiance [15].

5.19 Solar net metering

The cumulative installed capacity of a rooftop solar PV system has increased because of the reduction in the cost of solar PV systems. Various solar PV markets in the world have introduced net energy metering (NEM) and feed-in tariffs (FiTs) for power producers from solar PV against the power injected to the grid. NEM is the two-way flow of electricity in a distribution system between the energy-producing customer and the distribution system. The consumer generates electricity using renewable energy sources like solar, and wind and fulfills its energy demands, and stores the surplus energy in off-peak hours. In peak hours, after fulfilling its own energy demands rest of the energy is sold out to the grid. During the low accessibility of renewable energy sources, energy demand is fulfilled by purchasing from the grid. At the end of the billing period, the customer pays only for the net electricity purchased from or sold to the grid. Net metering allows customers or power producers to sell their surplus energy at the retail price. Since the retail price of electricity is much higher than the wholesale price, the customers prefer to invest in the grid-connected renewable energy systems with net metering. In the absence of net metering, the customer would sell their excess electricity to the utility grid at wholesale price.

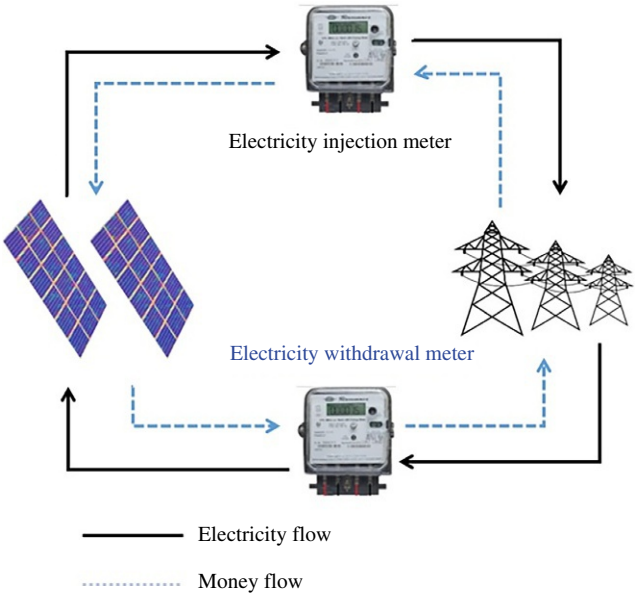

FIG. 5.53 Payment and electricity flow in a net billing method.

TABLE 5.7 Types of tariffs for net metering.

Method	Description	
Time-dependent tariff	Static	A static time of use tariff is determined in advance and is based on historical power system balance. This type of tariff is being practiced in Mexico
	Dynamic	A dynamic time of tariff is determined in real time and is based on actual power system balance or it is linked to the wholesale electricity prices. The tariff varies time to time. For example, it might be changed depending upon the solar irradiance. This type of tariff is being practiced in Finland
Location-dependent tariff	Location-based tariff depends upon various environmental factors varying from location to location. This type of tariff is being practiced in New York	

In the NEM mechanism, consumers are charged for the net energy consumed. Bidirectional energy meters records the energy consumed and injected to the grid. The mechanism of power flow and payments in the NEM is shown in Fig. 5.53, which shows that 2 m are needed to implement the net billing scheme. One meter is used to record the electricity injected to the grid and other meter is used to record the electricity purchased from the grid. Net billing scheme methods for the injection of surplus energy to the grid are given in Table 5.7.

5.20 Conclusion

Solar photovoltaics is a growing technology for harnessing energy from the sun. Various PV materials have been prepared with increased efficiency in converting solar energy into

electrical energy. A solar PV cell is modeled using the various impacts as the current generates and flows to the external circuit. These effects are represented by series resistance, shunt resistance, shunt diode, and current source. By using these impacts, the solar cell is represented by a single diode model or a double diode model. The complete solar PV system consists of a solar panel, DC-DC converter, inverter, and load. The varying impact of solar irradiance and cell temperature degrades the performance of the solar panel so that it does not operate at its maximum power. The impact of varying irradiance and cell temperature is mitigated by using MPPTs. P&O algorithms, FL-based P&O algorithms, and INC algorithms are implemented in MATLAB and LabVIEW. A comparison is given between different MPPT algorithms. The changing position of the sun in the sky is tracked throughout the day using single-axis and dual-axis solar trackers. A case study of a solar PV system determines the ratings and quantity of the components for a specific load.

Problems

Problems 1–21 contain three, four, or five answer options A, B, C, D, and E. Choose the correct answer.

1. In a single diode model of a solar cell, what are losses due to mismatch between bandgap energies of solar irradiance and solar material represented by?
   A. A diode
   B. Shunt resistor
   C. Series resistor
   D. Current source
2. Which cell is used to convert solar energy directly into electrical energy?
   A. Photovoltaic cell
   B. Fuel cell
   C. Dry cell
   D. Thermoelectric cell
3. What does the solar photovoltaic module refer to?
   A. Series combination of cells
   B. Parallel combination of solar cells
   C. Series and parallel combination of solar cells
   D. None of the above
4. Which of the following applications is relevant to solar energy?
   A. Water heating
   B. Space heating
   C. Power generation
   D. All of the above
5. If increased current is required, how should solar panels be connected?
   A. Parallel
   B. Series
   C. Series and parallel
   D. All of the above

6. If a solar cell's temperature is increased, what happens to its open-circuit voltage?
   A. It increases
   B. It decreases
   C. It remains constant
   D. None of the above
7. What is the approximate efficiency of a solar cell?
   A. 15%
   B. 25%
   C. 48%
   D. 63%
8. If the solar irradiance is increased, what happens to the short circuit current of the solar cell?
   A. It decreases
   B. It increases
   C. It remains constant
   D. None of the above
9. What is used to measure solar irradiance?
   A. Pyranometer
   B. Thermometer
   C. Arduino and LM35
   D. All of the above
10. If observations are $\Delta P < 0$ and $\Delta V > 0$, what will the perturbation in the P&O algorithm be?
    A. ΔD will be added
    B. ΔD will be subtracted
    C. No perturbation
    D. None of the above
11. If observations are $\Delta P < 0$ and $\Delta V < 0$, what will the perturbation in the P&O algorithm be?
    A. ΔD will be added
    B. ΔD will be subtracted
    C. No perturbation
    D. None of the above
12. What are the weakness(es) of the conventional P&O algorithm?
    A. Oscillations at the maximum power point
    B. High response time
    C. Both A and B
    D. Computational cost
    E. None of the above
13. Which of the following represents the incremental conductance algorithm?
    A. $-\frac{I}{V} = \frac{dI}{dV}$ *at Maximum Power Point*
    B. $-\frac{I}{V} > \frac{dI}{dV}$ *at Maximum Power Point*
    C. $-\frac{I}{V} < \frac{dI}{dV}$ *at Maximum Power Point*
    D. All of the above

14. What is the slope of the power curve at the MPP?
- **A.** $\frac{dP}{dV} > 0$
- **B.** $\frac{dP}{dV} < 0$
- **C.** $\frac{dP}{dV} = 0$

15. What angle(s) does the azimuthal angle track the sun from?
- **A.** North to south
- **B.** East to west
- **C.** Both A and B

16. What angle(s) does the altitude angle track the sun from?
- **A.** North to south
- **B.** East to west
- **C.** Both A and B

17. What is the zenith angle the complement of?
- **A.** Azimuthal angle
- **B.** Altitude angle
- **C.** Tilt angle
- **D.** None of the above

18. Which of the following is used to measure the intensity of the sun light in solar trackers?
- **A.** Light-emitting diode
- **B.** Thermistor
- **C.** Thermocouple
- **D.** Light-dependent resistor

19. What is the bandgap energy of silicon?
- **A.** 3.7 eV
- **B.** 3.5 eV
- **C.** 2.0 eV
- **D.** 1.12 eV

20. What is the definition of the fill factor of a solar cell?
- **A.** $\frac{\eta \times V_{\max}}{I_{sc} \times V_{oc}}$
- **B.** $\frac{\eta}{I_{sc} \times V_{oc}}$
- **C.** $\frac{1}{I_{sc} \times V_{oc}}$
- **D.** $\frac{I_{\max} \times V_{\max}}{I_{sc} \times V_{oc}}$

21. What does the series resistance in the single diode model of the solar represent?
- **A.** Bandgap energy losses
- **B.** Rare and top contact resistance
- **C.** The resistance of the wire
- **D.** All of the above

Give brief answers to the following short questions.

1. How do solar photovoltaic cells work?
2. What are the applications of solar thermal energy?
3. How does the increased temperature of a solar cell deteriorate its performance?

4. Explain the impact of solar irradiance on the open-circuit voltage and the short circuit current of the solar cell.
5. Define the ideality factor of the solar cell.
6. Explain the relation between the bandgap energy of the photovoltaic material and the bandgap energy of the photons.
7. What are the standard test conditions (STCs) for solar photovoltaic cells?
8. Sketch the impact of series and shunt resistance in the *I-V* curve of a solar cell.
9. You are provided with six solar panels having $I_{Ph} = 2.5\ A$ and $V = 12\ v$ each. To design a solar photovoltaic system your inverter requires 24 V and 8 A. What would be the configuration of the solar panels?
10. What is the role of power inverters and converters in solar photovoltaic systems?
11. How would you derive the relations for the incremental conductance algorithm?
12. How is fuzzy logic used in optimizing the MPPT algorithms?
13. What is the role of the maximum power point tracker in the solar photovoltaic system?
14. List the names of five maximum power point tracking algorithms.
15. How can the steady-state oscillations in tracking the maximum power point be reduced?
16. What is the difference between a solar tracker and a maximum power point tracker?
17. Explain the working principle of a solar water heater, with the help of a diagram.
18. At standard test conditions (STCs), $I_{Ph} = 2.5$ A and $I_0 = 0.2$ A, determine the open-circuit voltage (V_{oc}). If FF is 0.55 and the power coming from the sun is 9 W, find out the efficiency of the solar cell.
19. Define solar photovoltaic grid parity.
20. What is net metering? State the conditions in which energy is sold to the grid and purchased from the grid at peak and off-peak hours.
21. What types of tariffs are offered to solar power producers?

References

[1] Solar Energy, Available from: https://www.irena.org/solar. (Accessed 26 May 2022).
[2] M. Kamran, et al., Solar photovoltaic grid parity: a review of issues and challenges and status of different PV markets, Int. J. Renew. Energy Res. 9 (1) (2019) 244–260, https://doi.org/10.20508/IJRER.V9I1.8933.G7580.
[3] H. Shahid, M. Kamran, Z. Mehmood, M.Y. Saleem, M. Mudassar, K. Haider, Implementation of the novel temperature controller and incremental conductance MPPT algorithm for indoor photovoltaic system, Sol. Energy 163 (2018) 235–242, https://doi.org/10.1016/J.SOLENER.2018.02.018.
[4] M. Kamran, M. Mudassar, M.R. Fazal, M.U. Asghar, M. Bilal, R. Asghar, Implementation of improved Perturb & Observe MPPT technique with confined search space for standalone photovoltaic system, J. King Saud Univ. Eng. Sci. 32 (7) (2020) 432–441, https://doi.org/10.1016/J.JKSUES.2018.04.006.
[5] A. Goetzberger, V. Hoffmann, Photovoltaic solar energy generation, Springer Ser. Opt. Sci. 112 (2005) 1–229, https://doi.org/10.1007/B137803.
[6] P.A. Cotfas, D.T. Cotfas, P.N. Borza, D. Sera, R. Teodorescu, Solar cell capacitance determination based on an RLC resonant circuit, Energies 11 (3) (2018) 672, https://doi.org/10.3390/EN11030672.
[7] N. Kuttybay, et al., Optimized single-axis schedule solar tracker in different weather conditions, Energies 13 (19) (2020) 5226, https://doi.org/10.3390/EN13195226.
[8] M. Božiková, et al., The effect of Azimuth and tilt angle changes on the energy balance of photovoltaic system installed in the Southern Slovakia Region, Appl. Sci. 11 (19) (2021) 8998, https://doi.org/10.3390/APP11198998.

[9] C.S. Chin, A. Babu, W. McBride, Design, modeling and testing of a standalone single axis active solar tracker using MATLAB/Simulink, Renew. Energy 36 (11) (2011) 3075–3090, https://doi.org/10.1016/J.RENENE.2011.03.026.
[10] N. Al-Rousan, N.A.M. Isa, M.K.M. Desa, Advances in solar photovoltaic tracking systems: a review, Renew. Sust. Energ. Rev. 82 (2018) 2548–2569, https://doi.org/10.1016/J.RSER.2017.09.077.
[11] R. Alik, A. Jusoh, Modified Perturb and Observe (P&O) with checking algorithm under various solar irradiation, Sol. Energy 148 (2017) 128–139, https://doi.org/10.1016/J.SOLENER.2017.03.064.
[12] T.H. Kwan, X. Wu, High performance P&O based lock-on mechanism MPPT algorithm with smooth tracking, Sol. Energy 155 (2017) 816–828, https://doi.org/10.1016/J.SOLENER.2017.07.026.
[13] C.R. Algarín, J.T. Giraldo, O.R. Álvarez, Fuzzy logic based MPPT controller for a PV system, Energies 10 (12) (2017) 2036, https://doi.org/10.3390/EN10122036.
[14] T. Ramalu, M.A. Mohd Radzi, M.A. AtiqiMohd Zainuri, N.I. Abdul Wahab, R.Z. Abdul Rahman, A photovoltaic-based SEPIC converter with dual-fuzzy maximum power point tracking for optimal buck and boost operations, Energies 9 (2016) 604, https://doi.org/10.3390/EN9080604.
[15] M. Kamran, M. Bilal, Z.J. Zaib, LabVIEW based simulator for solar cell characteristics and MPPT under varying atmospheric conditions, Mehran Univ. Res. J. Eng. Technol. 37 (3) (2018) 529–538, https://doi.org/10.22581/MUET1982.1803.07.

CHAPTER

6

Planning and modeling of wind energy systems

6.1 Introduction

Wind energy has been a cynosure in recent years because of the advancement in distributed generation and smart grids. Numerous wind energy configurations are used to harness the energy from the wind. This chapter discusses the fundamental equation of wind power having all the parameters affecting the generation of power from the wind. The fundamental equation of wind power also shows the impact of the power coefficient of the turbine. The advantages of wind energy and the challenges in the advancement of wind energy are discussed. Wind turbine components included from the foundation to the hub are discussed in detail, as are wind energy conversion systems consisting of various generators. Since wind speed is always vulnerable to variation, the output frequency does not remain constant. Various frequency controlling methods are described in this chapter.

The first electricity-generating wind turbine was installed in Scotland in 1887 by James Blyth to charge a battery. In wind turbines, the kinetic energy of the wind is used to rotate the wind turbine and the rotor of the electrical generator, which is mechanical energy, and the generator converts this mechanical energy into electrical energy [1]. In America, the first wind turbine was installed in 1888 by Charles F. Brush.

In 2020, the generation of electricity was the highest among all the renewable energy sources. An increase of 11% in generation from wind was recorded in 2020. In 2020, the installation of wind turbine was double than installation in 2019, amounting to 108 GW [2].

6.2 Basic components of a wind turbine

The basic components of a wind turbine are the foundation, tower, rotor, hub, nacelle, and generator. This chapter discusses all of these in detail. A hub of a wind turbine with all inside components labeled is shown in Fig. 6.1.

https://doi.org/10.1016/B978-0-323-99560-3.00003-X

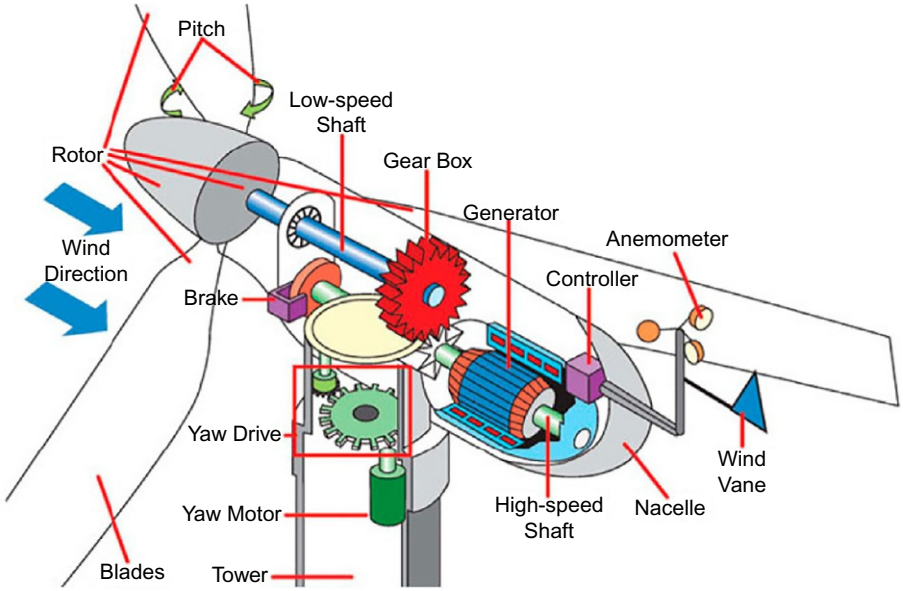

FIG. 6.1 Hub of wind turbine with all inside components mentioned. *Source: Wikipedia.*

6.2.1 Foundation

A foundation is under the earth and is covered by the soil; it gives erection support to the wind tower. Foundation type depends upon the type of the tower, turbine, size of the plant, mechanical, operational, and meteorological stress, and the local soil conditions. A foundation is designed by considering the lowest cost of manufacturing, and installation for the specific soil conditions.

6.2.2 Tower

The basic and key function of the tower is to give height to the wind turbine to maximize the wind interaction with the turbine and maximize the power generation. While designing the tower, the vibrations of the tower itself, rotor, nacelle, and the gearbox are kept in mind. Various parameters and dimensions are considered for transportation, installation, and erection. The height of the tower mainly depends upon the rotor radius and on-site conditions. The advantages and disadvantages of different types of towers are shown in Table 6.1. Types of turbine towers are shown in Fig. 6.2.

6.2.3 Rotor

The rotor is the rotating part of the stator connected to the blades of the turbine through the gearbox. The rotor is rotated by the wind turbine blades and it induces voltages at the stator of the generator. The rotor is attached to the wind turbine blades and the literature indicates that three is the optimum number of blades in a horizontal axis wind turbine. A wind turbine with

TABLE 6.1 Advantages and disadvantages of different types of turbine towers.

Type	Advantages	Disadvantages
Monopole	• Artistically pleasing	• Manufacturing and transportation are expensive • More steel is required
Guyed	• Minimum material is required, cheap • Good grounding for lightning • Guy wire tension can adjust the pole's natural frequency	• Not trespasser-proof • Cannot be used in urban areas
Tubular lattice	• Transportation and assembly are cheap	• Life cycle is short because corrosion can damage the bolts
Sectional lattice	• Life cycle is long • Light and stiff • Manufacturing is cheap	• Less protection for electric wires

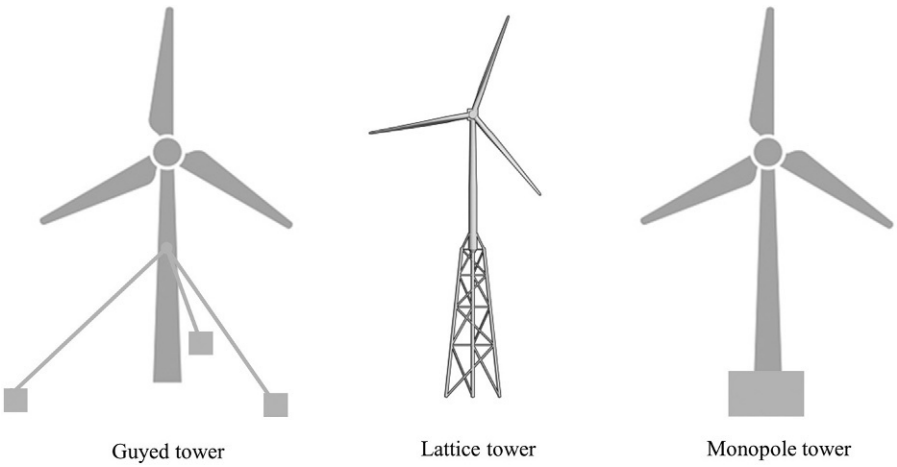

FIG. 6.2 Types of turbine towers. *Source: Wikipedia.*

three blades has fewer vibrations, less noise, fewer dynamic problems, and favorable mass distribution. Generally, the blades are selected based on fatigue strength, admissible stress, specific weight, breaking strength, and modulus of elasticity.

6.2.4 Nacelle

A nacelle is a cover housing containing the power generating components including gearbox, drive train, generator, low-speed shaft, high-speed shaft, and control electronics. It protects all the inside components from environmental hazards.

6.2.5 Gearbox

The gearbox is a part of the power train that connects the turbine shaft to the generator shaft. The gearbox is used to divide the shaft into slow and fast shafts. The gearbox is located in the nacelle and its efficiency is about 98% per gear level.

6.3 Classification of wind turbines

The classification of wind turbines based on the axis is shown in Fig. 6.3. The major types are the vertical axis and horizontal axis wind turbines which are further classified into subtypes as discussed below.

6.3.1 Horizontal axis wind turbines (HAWTs)

Horizontal axis wind turbines are the most commonly used type of wind turbine. They can be defined as the turbine in which the shaft of the rotor is in the direction of the wind as shown in Fig. 6.4. The wind turbine could be single-bladed, double-bladed, or three-bladed. The blades are aerodynamically designed that rotate by the aerodynamic lift of the force. The pressure difference is created between the upward and lower faces of the turbine blades. The speed of air through the front side of the blade is high and a low-pressure area is created there. On the other hand, airspeed is low on the rear side and a high-pressure area is created there. The air from the high-pressure region moves the blades upward giving an aerodynamic lift. This relation is called Bernoulli's relation, which states that where the pressure is high speed will be low for a fluid. The blades of the turbine are connected to the rotor of the electrical generator. HAWT can capture stronger winds and has greater efficiency [3]. Fig. 6.5 shows a Dutch-type horizontal axis wind turbine and Fig. 6.6 shows a multibladed horizontal axis wind turbine. Based on the direction of wind toward the turbine blades, the turbine is classified into upwind and downwind, as shown in Fig. 6.7.

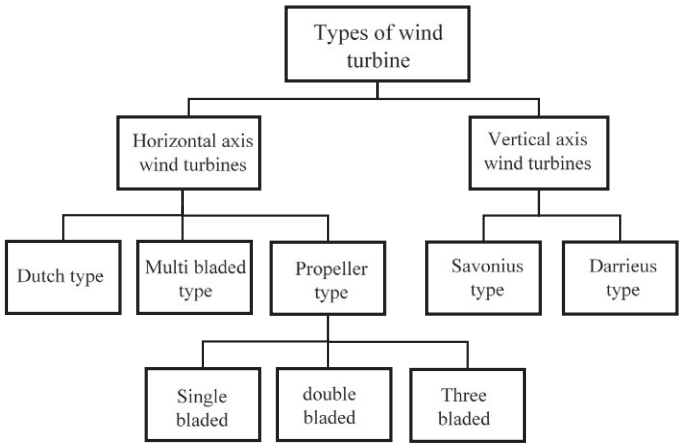

FIG. 6.3 Classification of wind turbines.

(a) (b) (C)

FIG. 6.4 Horizontal axis wind turbines: (A) single-bladed, (B) double-bladed, and (C) three-bladed. *Source: Wikipedia.*

FIG. 6.5 Dutch-type horizontal axis wind turbine. *Source: Wikipedia.*

FIG. 6.6 Multibladed horizontal axis wind turbine. *Source: Wikipedia.*

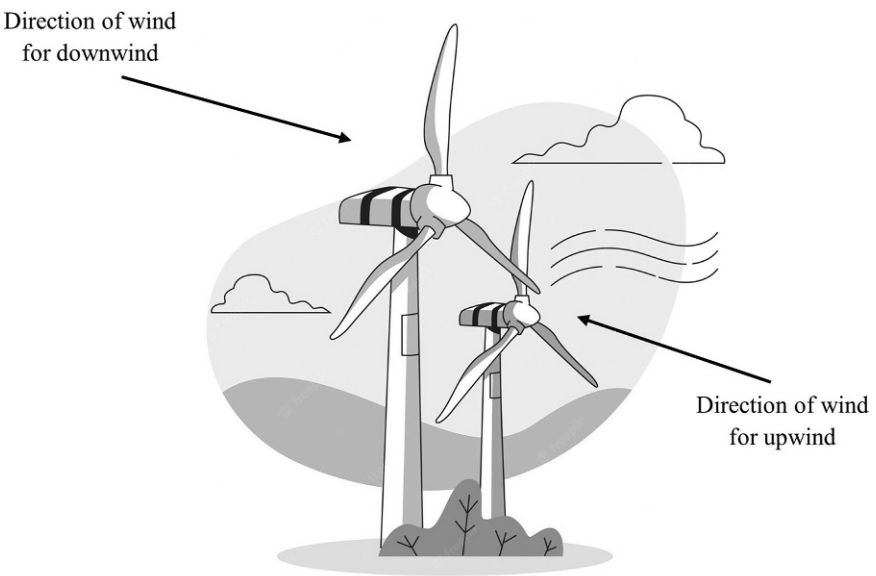

FIG. 6.7 Upwind and downwind HAWTs. *Source: Wikipedia.*

(a) Advantages of HAWT

- The output power is high as compared to the vertical axis wind turbine.
- The efficiency of a HAWT is high.
- It is less expensive than a VAWT (see following section).
- It is more consistent and its rotational speed is high.
- On variation in the wind shear, the tall tower captures more wind.
- Reliability is high.
- The blades of the turbine can be bent using a gearbox to get the best wind attack angle, which results in better performance under stormy conditions.
- The rotor can be tilted by the blades during storms.

(b) Disadvantages of HAWT

- HAWTs are available only in large sizes and are challenging to use in distributed generation.
- As they are of large size and heavyweight, transportation from one place to another is difficult.
- The mounting of a heavy generator and gearbox at the top of the tower requires a stronger structure, which increases the complexity and cost of the structure.
- Installation and maintenance of a HAWT is a difficult process because of the tall tower and heavy turbines.
- Noise from the HAWT is high compared to other wind turbines.
- To design and manufacture a HAWT, heavy machinery is required.

6.3.2 Vertical axis wind turbines (VAWTs)

A vertical axis wind turbine (VAWT) is a type of wind turbine in which the axis of rotation of the rotor is perpendicular to the wind direction. The gearbox and generator are positioned at the base of the turbine, which makes maintenance easy. Since the rotor is perpendicular to the wind speed, no specific aerodynamics are required for the design. The size of the VAWT is smaller than the HAWT which gives them various advantages. There are two types of VAWT: Savonius and Darrieus. Savonius wind turbines have blades built around the vertical shaft in a helix form, which looks like DNA, as shown in Fig. 6.8. Darrieus turbines are like eggbeater shapes whose wings are longer and wider and attached to the upper and lower ends of the rotor shaft, giving a maximum swept area [3]. The shape of the Darrieus turbine is shown in Fig. 6.9.

(a) Advantages of VAWT

- It has fewer vibrations and no noise compared to a HAWT.
- Since the direction of the wings is perpendicular to the wind speed, no specific orientation is required and no yaw control mechanism is necessary.
- It can produce electricity at lower wind speeds.
- Installation and maintenance are very easy since the generator and gearbox are located near the ground.
- It is preferred in the distributed generation since it is usually of smaller size and less noisy.
- VAWTs are visually very attractive [4].

(b) Disadvantages of VAWT

- The efficiency of a VAWT is lower than that of a HAWT.
- Its production of energy is not as much as that of a HAWT of the same height because of the location of the rotor close to the ground, where less air is available due to ground surface drag.

FIG. 6.8 Savonius type vertical axis wind turbine. *Source: Wikipedia.*

- If the structure is not properly designed, replacement and maintenance of parts are difficult since the wings are mounted over the generator and gearbox. Since all the weight of the wings is on the gearbox, a guy wire is used to hold the wings in their place.

6.4 The fundamental equation of wind power

The energy that is contained in the flowing wind can be calculated by the wind power equation, which can be derived as follows; however, first we discuss the concept of power and energy. Power is defined as the rate of change of power concerning time as shown in Eq. (6.1).

$$P = \frac{dE}{dt} \tag{6.1}$$

FIG. 6.9 Darrieus type vertical axis wind turbine. *Source: Wikipedia.*

The energy in the wind is the kinetic energy, which is given by Eq. (6.2).

$$K.E. = \tfrac{1}{2}\, mv^2 \tag{6.2}$$

Putting the value of kinetic energy in Eq. (6.1), simply, we get Eq. (6.3).

$$P = \frac{d\left(\tfrac{1}{2}\, mv^2\right)}{dt}$$

$$P = \frac{1}{2} v^2 \frac{dm}{dt} \tag{6.3}$$

The mass of the wind which will interact with the wind turbine is calculated by the density equation, as shown in Eq. (6.4).

$$\rho = \frac{m}{V} \longrightarrow m = \rho V \tag{6.4}$$

We put the value of the mass of wind in Eq. (6.3).

$$P = \frac{1}{2} v^2 \frac{d(\rho V)}{dt}$$

$$P = \frac{1}{2}\rho v^2 \frac{d(V)}{dt}$$

The volume of the air is taken as the product of length, width, and height. The product of the length and width is taken as the area, as shown in Eq. (6.5).

$$P = \frac{1}{2}\rho v^2 \frac{d(l.w.h)}{dt}$$

$$P = \frac{1}{2}\rho A v^2 \frac{d(h)}{dt} \tag{6.5}$$

$\frac{d(h)}{dt}$ is the time rate of change of displacement which is known as the velocity. Hence we get the final equation which is used to calculate the power in the wind that can be generated from the wind turbine shown in Eq. (6.6).

$$P = \frac{1}{2}\rho A v^3 \tag{6.6}$$

This is the fundamental equation of wind turbine showing a direct relation of the wind power to the sir density, the area covered by the turbine blades, and the wind speed. Eq. (6.6) shows that wind speed has a greater impact on the amount of power from the turbine. Another characteristic can be determined by using Eq. (6.7) as follows.

$$\textit{wind power density } (WPD) = \frac{P}{A} = \frac{1}{2}\rho v^3 \tag{6.7}$$

Eq. (6.7) defines the wind power density, stating the power generated per unit area. This equation gives you the analysis of power independent of the size of the turbine and its quantitative. The National Renewable Energy Laboratory (NREL) has classified wind into different classes based on wind speed and wind power density, as shown in Table 6.2.

Another efficiency measure of the wind turbine is the capacity factor which is a fraction of the actual installed generating capacity of the wind turbine to the power that would be generated under ideal atmospheric conditions and circumstances. The capacity factor can be mathematically defined as Eq. (6.8).

TABLE 6.2 Classification of wind power measured at 50 m above ground according to the NREL.

Wind class	Resource potential	Wind speed (m/s)	WPD in W/m^2
1	Poor	0–5.9	0–200
2	Marginal	5.9–6.7	200–300
3	Fair	6.7–7.4	300–400
4	Good	7.4–7.9	500–600
5	Excellent	7.9–8.4	600–700
6	Outstanding	8.4–9.3	700–800
7	Superb	>9.3	>800

$$\text{capacity factor } (CF) = \frac{E_{actual}}{E_{ideal}} \tag{6.8}$$

6.4.1 Betz limit

Albert Betz, a German scientist, claimed in 1919 that a wind turbine can only convert 59% of the mechanical energy in the wind into electrical energy. This is the maximum wind power that can be converted by the turbine into electrical energy. This is known as the Betz law or the Betz limit and is denoted as C_p, power coefficient. Efficiency of 100% is not possible to achieve because of the mechanical nature of the wind. If it is supposed that 100% kinetic energy of the wind is converted into rotational energy of the turbine, this would mean that the air would come to a standstill and there would be no velocity available to sustain the energy extracting mechanism [5].

$$C_P = 0.59$$

The value of the Betz limit can be determined using Eq. (6.5).

$$P = \frac{1}{2}\rho A v^2 \frac{d(h)}{dt}$$

$\frac{d(h)}{dt}$ is the time rate of change of displacement which is known as the velocity. In this case, we can take the average of the wind speed before and after passing through the wind, i.e., $\frac{d(h)}{dt} = \frac{V_1 + V_2}{2}$, we also take the velocity as the final value minus the initial value, Hence Eq. (6.5) becomes

$$P = \frac{1}{2}\rho A\left(v_2^2 - V_1^2\right)^2\left(\frac{V_1 + V_2}{2}\right)$$

The power coefficient can be defined as the ratio of the extracted power from the wind turbine and the total power in the wind.

$$C = \frac{P_E}{P_T} = \frac{\frac{1}{2}\rho A^2\left(v_2^2 - V_1^2\right)\left(\frac{V_1 + V_2}{2}\right)}{\frac{1}{2}\rho.A.{V_2}^3}$$

$$C = \frac{\left(v_2^2 - V_1^2\right)\left(\frac{V_1 + V_2}{2}\right)}{{V_2}^3}$$

$$C = \frac{1}{2}\frac{\left(v_2^2 - V_1^2\right)(V_1 + V_2)}{{V_2}^3}$$

$$C = \frac{1}{2}\frac{\left(V_1 v_2^2 + v_2^3 - V_1^3 - V_2 v_1^2\right)}{{V_2}^3}$$

$$C = \frac{1}{2}\left[\frac{V_1}{V_2} - \left(\frac{V_1}{V_2}\right)^3 + 1 - \left(\frac{V_1}{V_2}\right)^2\right] \tag{6.9}$$

To get the maximum power from the wind turbine, we take the derivative of Eq. (6.9) with respect to v_1/v_2 and put it equal to zero, as in Eq. (6.10).

$$\frac{d(C)}{d\left(v_1/v_2\right)} = 0, \tag{6.10}$$

$$\frac{d(C)}{d\left(v_1/v_2\right)} = \frac{1}{2}\left[1 - 3\left(\frac{v_1}{v_2}\right)^2 - 2\left(\frac{v_1}{v_2}\right)\right]$$

We put $\frac{d(C)}{d\left(v_1/v_2\right)} = 0$,

$$\frac{1}{2}\left[-3\left(\frac{v_1}{v_2}\right)^2 - 2\left(\frac{v_1}{v_2}\right) + 1\right] = 0$$

$$3\left(\frac{v_1}{v_2}\right)^2 + 2\left(\frac{v_1}{v_2}\right) - 1 = 0$$

Solving the above relation gives us the ratio of v_1 and v_2, $\frac{v_1}{v_2} = \frac{1}{3}$.

We put this ratio in Eq. (6.9) and get the value of C, which is the maximum limit of the wind turbine.

$$C_P = 0.59$$

This value is unique and is a function of the wind speed. To get the extracted power from the wind through a wind turbine, we incorporate the power coefficient in Eq. (6.6) and the resulting Eq. (6.11).

$$P = \frac{1}{2}\rho.A.v^3.C_p \tag{6.11}$$

Example 6.1

A wind turbine is to be installed in a location where the wind speed is 15 m/s. The length of the wind turbine blades is 60 m rotating with 20 rounds per minute (RPM) as shown in Fig. 6.10. After considering the Betz limit and the losses in the bearing box, use the value of the power coefficient 0.4. The air density is a constant and is 1.23 kg/m^3. Calculate:

(a) the actual power of the wind converted to mechanical rotational power in the turbine at given C_p;
(b) the C_p at the given wind speed;
(c) the actual power of the wind converted to mechanical rotational power in the turbine at a newly calculated C_p; and
(d) the wind power density at given C_p.

Solution:

The given data is as follows:

$$v = 15\frac{m}{s}$$

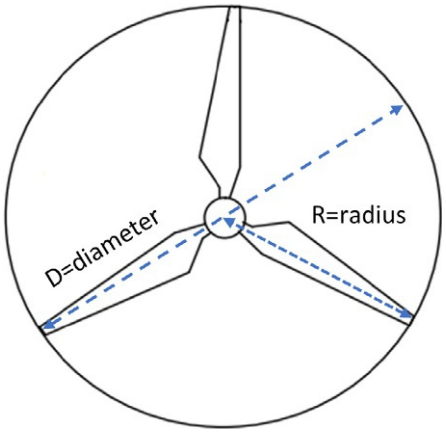

FIG. 6.10 Wind turbine radius and diameter

$$l = r = 60 \text{ m}$$

$$C_P = 0.4$$

$$\rho = 1.23 \text{ kg/m}^3$$

$$\text{rotational speed} = 20 \text{ RPM}$$

(a) The actual power of the wind converted to mechanical rotational power in the turbine at given C_p

All the data which is required for the power calculation using Eq. (6.11) is given except the swept area which can be calculated using the following equation.

$$A = \pi r^2$$

$$= 3.14 \times 60^2$$

$$= 11,304 \text{ m}^2$$

By putting all the given data and the calculated swept area in Eq. (6.11), we can calculate the actual power of the wind converted to the mechanical rotational power of the turbine.

$$P = \frac{1}{2}\rho.A.v^3.C_p$$

$$= \frac{1}{2} \times 1.23 \times 11304 \times 15^3 \times 0.4$$

$$= 9.4 \text{ MW}$$

(b) The C_p at the given wind speed

The power coefficient is defined by the turbine designers. We see the relationship between all the parameters to calculate the power at the actual wind speed rather than the rated wind speed. We calculate the power coefficient for the given wind speed as follows.

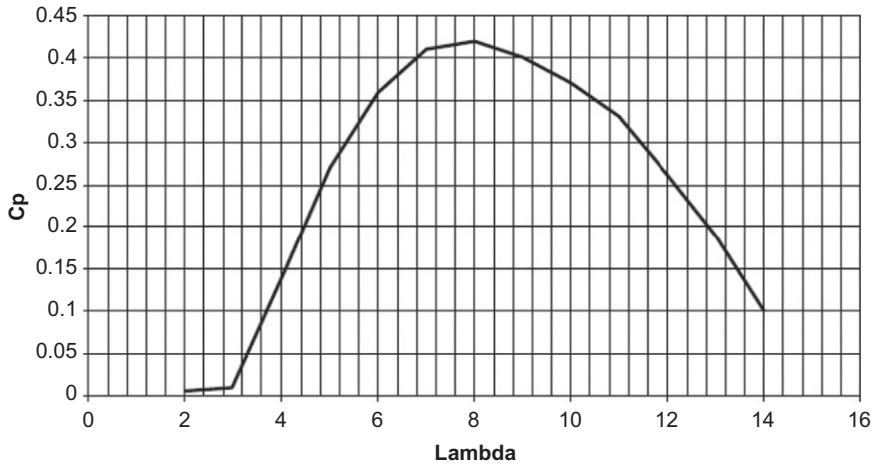

FIG. 6.11 Graph between tip speed ratio and power coefficient

If we know the value of the blade tip speed ratio (λ), we can find the value of Cp from Fig. 6.11. λ is calculated using Eq. (6.12).

$$\lambda = \frac{\textit{blade tip speed}}{\textit{wind speed}} \tag{6.12}$$

We still do not have the value of the blade tip speed, which can be calculated using Eq. (6.13).

$$\textit{blade tip speed} = \frac{\textit{rotational speed} \times \pi \times D}{60} \tag{6.13}$$

$$= \frac{20 \times 3.14 \times 120}{60}$$

$$= 125.6 \text{ m/s}$$

By putting the value of the blade tip speed and wind speed in Eq. (6.12), we can find the λ.

$$\lambda = \frac{125.6 \text{ m/s}}{15 \text{ m/s}}$$

$$= 8.37$$

Now we find the value of the power coefficient on the graph at $\lambda = 8.37$, which is 0.42.

$$C_P = 0.4$$

(c) The actual power of the wind converted to mechanical rotational power in the turbine at a newly calculated C_p

From the above discussion, it is well established that the value of C_P is not a constant, but varies with variation in the wind speed. By using the newly calculated value of C_P, we find the rotational power of the turbine.

$$P = \frac{1}{2}\rho.A.v^3.C_p$$

$$= \frac{1}{2} \times 1.23 \times 11304 \times 15^3 \times 0.42$$

$$= 9.8\,MW$$

(d) The wind power density at given C_p

Wind power density can be calculated using Eq. (6.14).

$$\text{wind power density } (WPD) = \frac{P}{A} = \frac{1}{2}\rho v^3 \tag{6.14}$$

$$= \frac{9.4\,\text{MW}}{11,304\,\text{m}^2}$$

$$WPD = 8.3\ \frac{\text{MW}}{\text{m}^2}$$

6.5 Wind energy conversion systems

The wind energy conversion system starts working by taking the translator kinetic energy from the wind through the turbine in the form of rotational kinetic energy. This rotational kinetic energy is converted into electrical energy in the generator by electromagnetic induction. The generators that are used in the wind turbine are induction generators (IGs), doubly fed induction generators (DFIGs), synchronous generators (SGs), and permanent magnet synchronous generators (PMSGs). The following subsection discusses the mechanism of the wind energy conversion system.

6.5.1 Induction generators

In the case of a synchronous generator, the rotor speed is locked to the synchronous speed and cannot be changed. If a heavy wind hits the turbine, the blades try to speed up but the rotor is locked at the speed of the power grid. Large forces are developed in the hub, gearbox, and generator which cause wear and tear in the system. The solution to this problem is the use of a doubly fed induction generator. A doubly fed induction generator is an AC electrical generator in which both rotor and stator windings are fed with three-phase AC supply. The DFIG

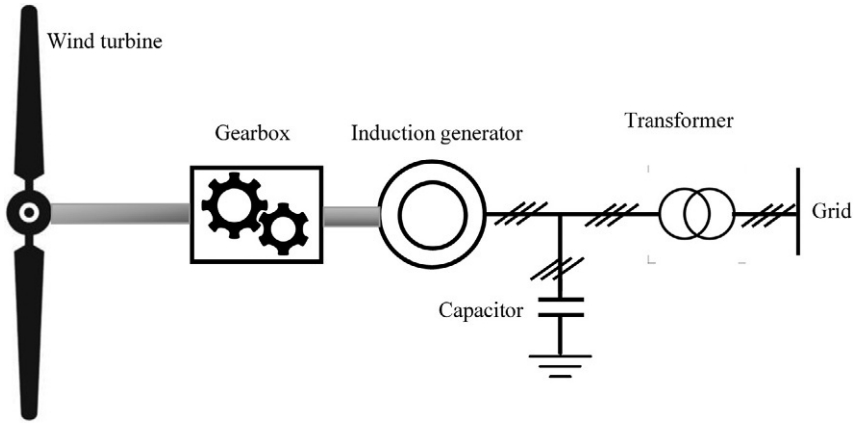

FIG. 6.12 Application of induction generator with wind turbine.

has an additional feature of running at higher than the synchronous speed and lower than the synchronous speed. The working principle of the DFIG is that the stator windings are connected to the grid, and the rotor windings are connected to the back to back connected rectifier and inverter that controls the current of the rotor and the grid. By varying the rotor current through the converters, the active and reactive powers fed to the grid by the stator can be adjusted. The frequency of the generator varies with variations in the wind speed. Whatever the frequency of the generator is, its AC output is first rectified into DC and then by using an inverter, this DC is converted into AC of a constantly desired frequency. The rating of the power electronics converters used in the DFIG is 30% of the ratings of the converters that are used in the synchronous generator. The converters have to provide excitation only in the DFIG, and in a synchronous generator all the power is transmitted through the converters which increase the losses in the power electronic converters, and the overall cost of the control system is also increased. Fig. 6.12 shows the application of an induction generator with a wind turbine, and Fig. 6.13 shows the application of a doubly fed induction generator with a wind turbine.

6.5.2 Synchronous generator

Most of the power generated in the world is supplied by synchronous generators (SGs). SGs operate at a constant speed regardless of the torque at the rotor. Fig. 6.14 shows the wind energy system based on the SG. The blades of the wind turbine are coupled to the rotor of the SG through the gearbox. The basic two components of the SG are the rotor and stator. The windings on the rotor are called field windings or rotor windings. The windings on the stator are called armature windings or stator windings. A rotor magnetic field is produced by applying a DC voltage from the excitation circuit which is a rectifier. The rectifier takes AC supply from the grid, converts it into DC, and supplies it to the rotor windings for excitation. The rotor is then rotated by the wind turbine coupled through the gearbox. The rotating magnetic field of the rotor interacts with the stator windings and produces a set of three-phase AC

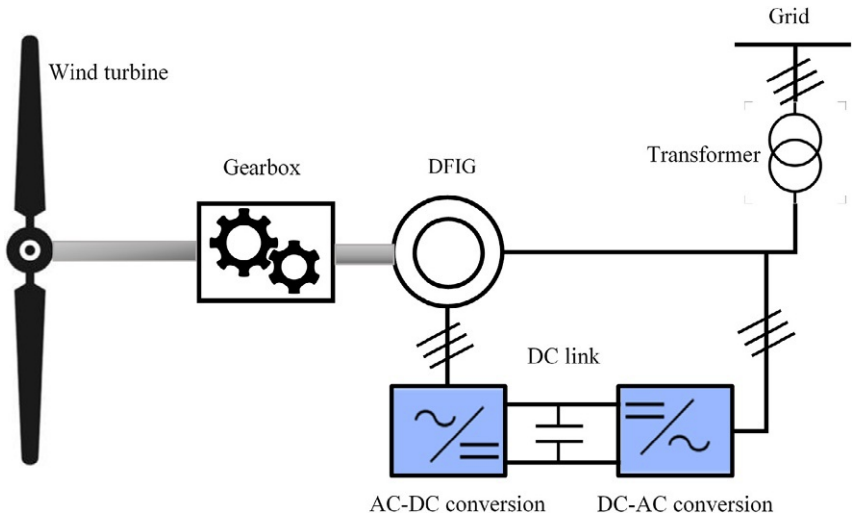

FIG. 6.13 Application of doubly fed induction generator with wind turbine.

voltages in the stator windings. This type of generator in which the excitation is done from an external source through the slip rings and carbon brushes or a separate DC source mounted on the shaft of the rotor is called a wound rotor SG [6]. The above-stated excitation mechanism poses some limitations, since the carbon brushes and the slip rings require continuous maintenance for their proper operation. This mechanism is used for small AC generators [7].

For large SGs, a brushless exciter is used which is a small AC generator whose armature windings are on the rotor and field windings are mounted on the stator. The three-phase output of the brushless exciter is rectified using a three-phase rectifier, which is also mounted on the rotor and is applied to the main rotor windings.

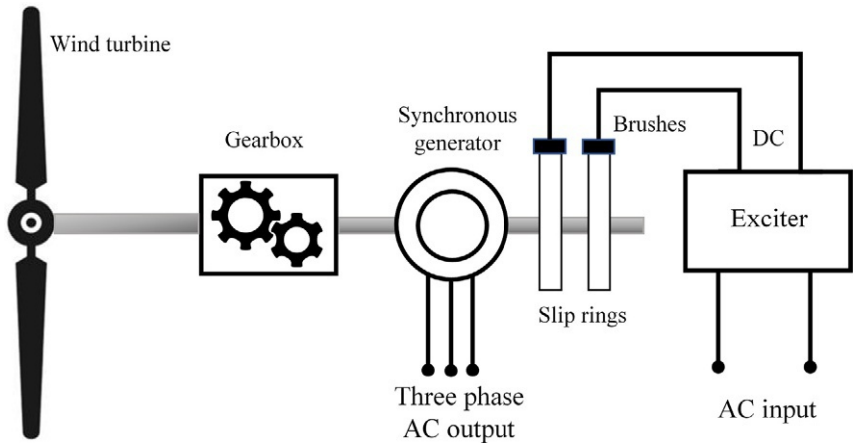

FIG. 6.14 Application of synchronous generators with wind turbines.

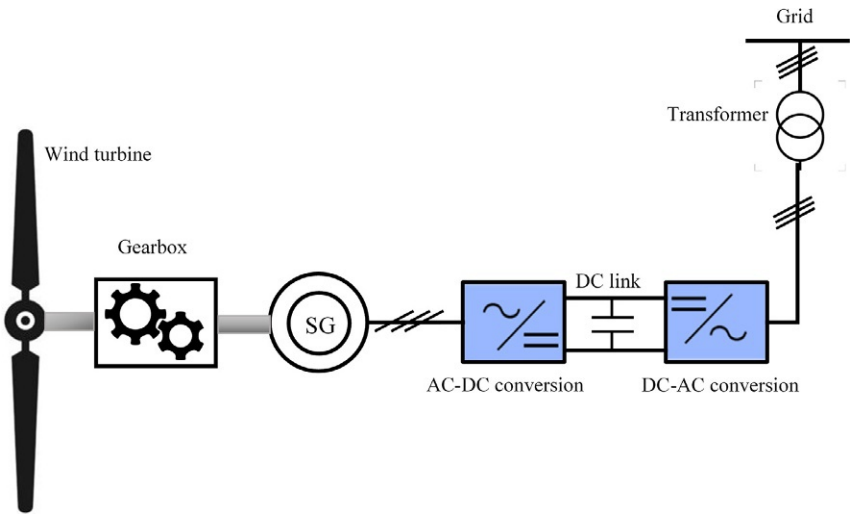

FIG. 6.15 Application of synchronous generator with variable speed wind turbine.

The electrical frequency of the SG is determined using Eq. (6.15).

$$f = \frac{n_s.P}{120} \tag{6.15}$$

where:

f is the electrical frequency in Hz;
n_s is the rotation of the rotor in RPM which is equal to the speed of the rotating magnetic field in a SG also known as synchronous speed; and
P is the number of poles.

SGs are increasingly used in the wind energy system because of their less man and high power density. The operation of the SGs with the wind turbine becomes challenging during varying wind speed. When the wind speed varies, the turbine rotation speed and the rotation speed of the rotor also vary. The variable output is achieved at the terminals of the SG. The schematic diagram of the SG under variable wind speed is shown in Fig. 6.15. The three-phase output of the SG is first passed through the power electronics converters. The converter consists of two back-to-back rectifiers and an inverter in series. The rectifier converts the variable AC into constant DC and the inverter inverts the constant DC into constant AC. Diodes and thyristors in the rectifier and inverter generate harmonic and generate fluctuations through the DC link. A DC link capacitor is used at the output of the rectifier, which acts as a buffer between rectifier and inverter [8].

6.6 Controlling the output frequency for variable speed wind turbines

Classification of the wind frequency control schemes are shown in Fig. 6.16. Frequency control techniques can be categorized as frequency control either with or without battery energy storage systems. Frequency control strategies without battery are further classified into

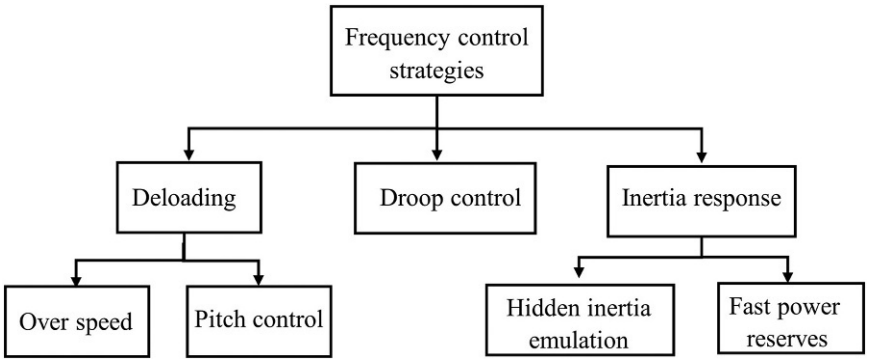

FIG. 6.16 Inertia and frequency control techniques for variable speed wind turbines.

the de-loading method, droop control technique, and inertial response method. Frequency control strategies without batteries are discussed below.

6.6.1 Inertial response

The electrical power system consists of thousands of electrical generators working in synchronism to the grid at a frequency of 60 Hz which is a measure of the health of the grid. Under normal operational conditions, the generation from all the generators is equal to the demand for electricity which keeps the frequency of the system nearly constant. When a power plant for any reason goes out of the system, generation instantly drops but the demand has not changed. All the load connected to the system keeps extracting the same amount of power from the inertia of the spinning generators which are now slowing down. This will decrease the frequency of the system. In conventional generators, the drop in frequency is detected by the governor located at the generator and tells the generator to speed up or slow down to maintain the constant frequency. The levers and valves take several minutes to operate and the grid increases its output. Here the concept of inertia comes in, which gives enough time to the mechanical spinning generators to react to the change while generating the output. The question is: how can we achieve this inertia when more renewables are added to the system? The inertia from the renewables that use conventional generators like, geothermal, solar concentrating, biogas, and hydropower can still be used to maintain the frequency of the grid constant [9,10]. Renewable energy sources having variable outputs like solar photovoltaics and wind do not use conventional generators, and there is less inertia in the grid. They use electronic convertors that do not have an inherent inertial response.

With the advancement in smart grid technologies, the fast inertial response is obtained by the smart sensors that can quickly measure the change in frequency and respond as quickly by disconnecting the noncritical loads in less than 0.5 s. Fast frequency response can also be obtained from the renewables by controlling the output of the wind and solar plants or by extracting the kinetic energy stored in the rotating wind turbines. The inertial controller in wind plants is implemented by one of two methods: hidden inertial emulation and fast power reserve. Both of these methods have a short duration inertial response.

6.6.1.1 Hidden inertia emulation

Hidden inertia emulation is also known as the synthetic inertia controller and its function is to release the kinetic energy from the wind turbine. An active power control signal is obtained

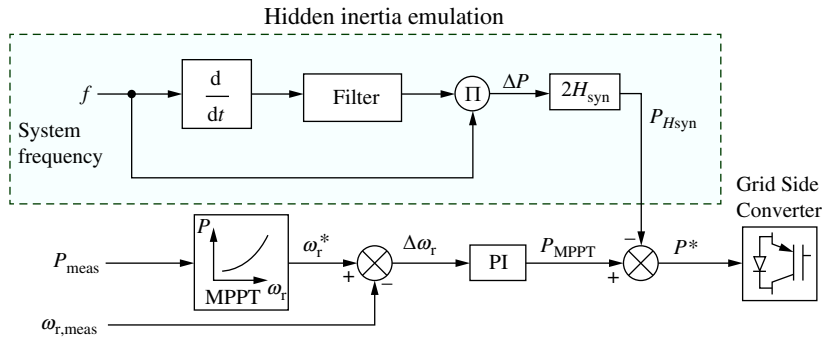

FIG. 6.17 Hidden inertia emulation [11].

by combining the output of the hidden inertia controller with the output of the maximum power point tracker (MPPT), as shown in Fig. 6.17. The hidden inertia emulation controller helps in releasing the large kinetic energy from the wind turbine. The active power of the controller is achieved by Eq. (6.16).

$$P_{HSyn} = 2H_{syn} f \frac{df}{dt} \tag{6.16}$$

where:

P_{HSyn} is the hidden synthetic power;
H_{syn} is the inertia constant; and
$\frac{df}{dt}$ is the rate of change of frequency.

6.6.1.2 Fast power reserves

The fast power reserve is the production of short-term inertial response which is obtained by the kinetic energy stored in the rotating mass of the wind turbine as shown in Eq. (6.17).

$$\begin{aligned} P_{FPR}t &= \frac{1}{2}J\omega^2 \\ P_{FPR}t &= \frac{1}{2}J\left(\omega_i^2 - \omega_f^2\right) \end{aligned} \tag{6.17}$$

Where

t time elapsed during frequency disturbance
ω_i the initial speed of the wind turbine
ω_f the final speed of the wind turbine after time t

6.6.2 Droop control

Power frequency characteristics, as shown in Fig. 6.18, are called droop control. The droop characteristics give a change in active power which is proportional to the deviation in frequency. When the wind turbine operates at the maximum power, the change in power which is an increase in the power is obtained from the kinetic energy of the rotating masses. It becomes possible that the speed of the turbine will slow down, which will take it beyond the stable operating range [12].

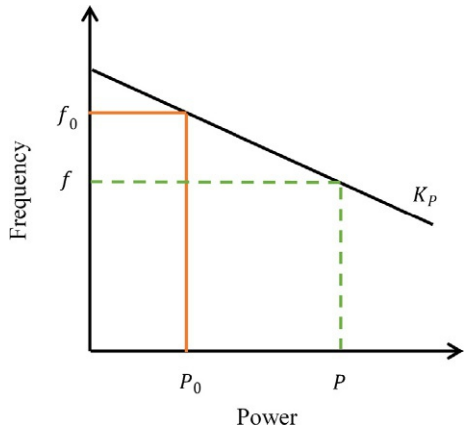

FIG. 6.18 Frequency droop characteristics.

6.6.3 De-loading

Wind power turbines and wind farms must be equipped with the system to maintain the frequency of the generated output by increasing or decreasing the output. Fast power reserve and hidden inertia emulation can control the frequency for a short term. Wind turbines need to be operated in a de-loaded mode. Deloading of the wind turbines can be done in two methods: pitch angle control system and rotor speed control method. The performance of the rotor speed control method is better and the regulation range is narrower than that of the pitch angle controller.

6.6.3.1 Pitch angle control

Based on the pitch angle, wind turbines are classified into a fixed pitch wind turbine and variable pitch wind speed. Fixed pitch wind turbines are unable to change the pitch angle to collect the maximum wind and its kinetic energy. Irrespective of the wind direction, fixed pitch operates on the same fixed angle. Wind turbines with variable pitch angle control can get the maximum kinetic energy of the wind and possibly can achieve maximum efficiency. The use of pitch angle control for the varying wind speed and direction requires a controller to regulate the output power by mechanically controlling the blade angle. In the case of wind speed being lower than or higher than the rated wind speed, the pitch angle or blade angle is controlled. If the wind speed is lower than the rated speed, the pitch angle is adjusted to maximize the output power. In the second case, if the wind speed is greater than the rated speed, the pitch angle is adjusted to get the optimum power and protect the system against the wind pressures. Generally, the pitch angle controller consists of an electromechanical actuator and a motor. The actuator can be installed on each blade individually or collectively for all turbines. Because of the cost, an individual actuator on each blade is installed on large wind turbines. The pitch control system is divided into two: hydraulic pitch control system and electric pitch control system.

(a) Hydraulic pitch control system

In hydraulic pitch controllers, the pitch angle of the blades is controlled by the hydraulic actuators. An accumulator tank along with a hydraulic actuator is placed in the hub of the wind turbine. A hydraulic pump in the nacelle of the turbine is used to perform the rotatory action of the blades. The hydraulic pitch controller has various advantages over the electrical pitch controller. Table 6.3

TABLE 6.3 Characteristics of different pitch control systems.

Techniques	Response speed	Reliability	Complexity	Cost	Performance in rapid changing wind speed
Hydraulic	Slow	High	High	High	Low
PI/PID	Slow	Low	Low	Low	Low
Feed forward/feed backward	Moderate	Medium–low	Medium–high	Medium–low	Low
Sliding mode control	Moderate	Medium	Medium–high	Medium–high	Low
Linear quadratic- Gaussian	Medium–high	Medium–high	Medium–high	Medium–high	Medium–low
H-infinity	Moderate–high	Medium–high	Medium–high	Medium–high	Medium–high
Fuzzy logic	Fast	High	High	Moderate	High
Hybrid	Very fast	High	Medium	Depends	Very high
Neural networks	Fast	High	High	Moderate	Very high

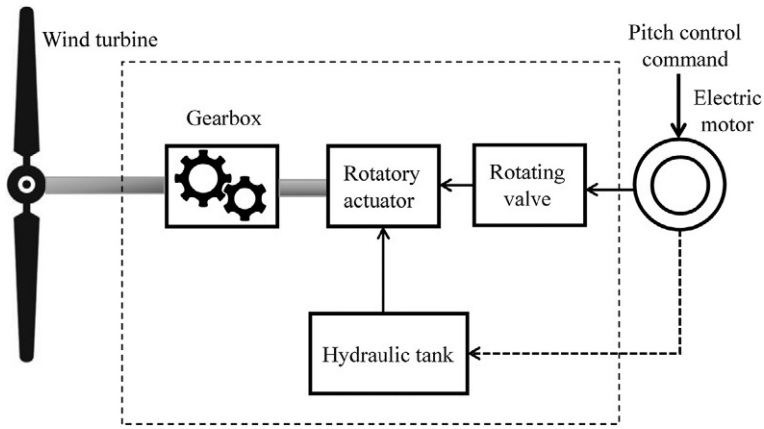

FIG. 6.19 Hydraulic pitch control system

shows a detailed comparison of different pitch controllers. The hydraulic pitch control system is described in Fig. 6.19.

(b) Electric pitch control system

The electric pitch control system consists of both electrical and mechanical systems to alter the pitch angle of the turbine blades. The electrical pitch angle controller consists of an electric motor, an energy storage system to run the electric motor, sensors to measure the direction and speed of the wind, and a gearbox to adjust the motor speed. The electric pitch controller is preferred over the hydraulic pitch controller system since the response time of the electric pitch controller is low. The installation of the electric pitch controller is expensive because

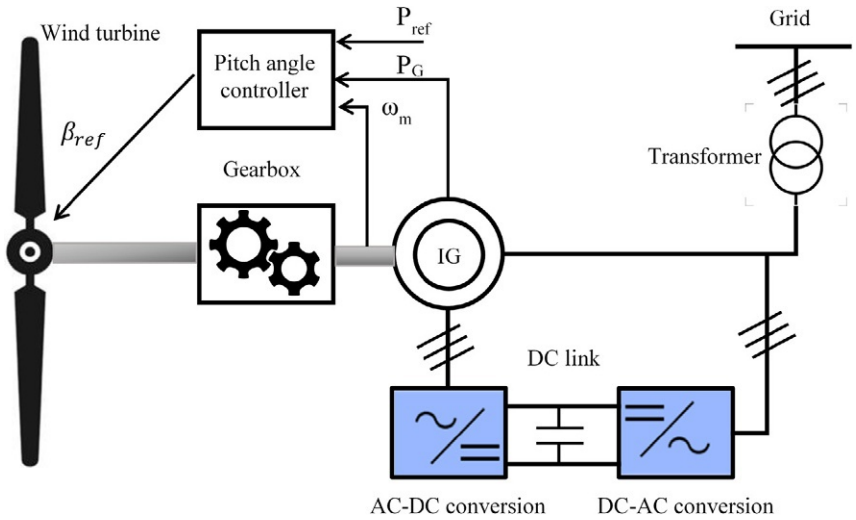

FIG. 6.20 Electric pitch angle control systems.

they need a power backup. Fig. 6.20 shows the application of the pitch angle controller with the induction generator-based wind energy system.

PI and PID controllers are the most suitable controllers for wind turbine control systems. The conventional controllers are derived using wind speed, rotor speed, and generated power. A curve between pitch angle and wind speed is given by the manufacturer. The performance of the conventional controllers is not good because of the delayed response to the variation in the wind speed, so cannot be used in the regions where the variation in the wind speed is occasional. Table 6.3 shows the characteristics of different electric pitch controller techniques in wind energy control systems.

6.7 Advantages of wind energy

6.7.1 Renewable and sustainable

The source of wind energy is the sun. The uneven heating of the air in different areas of a region causes an air density difference. The hot and lower density air moves upward and the nearby air rushes into this vacated area. Thus, whenever there is wind, there is the power to transmit to the grid. This makes wind energy a renewable and sustainable source of energy.

6.7.2 A clean source of energy

As discussed above, the wind is a pollution-free source of energy and have very little health hazards impact on the environment. The production of electricity from the wind carries no CO_2 production. However, the production and transportation of wind turbines and blades involve very little production of greenhouse gas (GHG) emissions. Other pollutants like NO_x, SO_x, and particulates that are generated in coal-, oil-, and gas-fired power plants are absent in wind energy.

6.7.3 Cost-effective

Due to increased demand for electricity, the production scale of wind turbines has been increased and costs have been reduced. Hence the overall cost of the energy from wind turbines has been reduced and they can compete with other renewable energy sources. Wind energy is also about to achieve grid parity. Grid parity is the point in time in a specific region when the cost of electricity per kWh from wind energy is equal to the cost of electricity per kWh from the grid.

6.7.4 Distributed generation

The generation of electricity from a faraway power plant and then transmission to the load-centered area is an expensive one. The transmission of AC power carries power losses and requires more material to transmit. Wind turbines in the distributed generation have no power losses and no transmission cost. Distributed generation in the smart grid makes wind energy more attractive for investors and consumers [3].

6.7.5 Location of wind power plant

There are no specific limitations to the location of wind turbine installation. All windy areas can be used to harness wind energy through wind turbines. These turbines can be installed in the fields with little visibility and noise hindrance to animals and farmers. Installation of wind turbines at the bank of the express highways and motorways presents an arguably beautiful sight.

6.7.6 Miscellaneous energy mix

The production of electricity from large power plants decreases the reliability of the electric power system. In the case of a failure of a power plant, the whole system goes into a blackout. In distributed generation. If a generating unit is failed or shut off for maintenance purposes, the wind turbine will keep the system operational. On the other hand, wind turbines can be shut off for maintenance purposes and the other unit of distributed generation will keep the system live.

6.7.7 Job opportunities

The wind industry is rapidly growing with the innovation in wind turbines. Thousands of jobs are created in the turbine manufacturing industry, the balance of system (BoS), transportation of wind turbines, erection and installation of turbines, and commissioning and daily servicing of the turbines.

6.7.8 National security

Since the utilization of wind energy replaces the imported oil-, coal-, and gas-based power plants, it reduces heavy energy bills paid for the imported oil. A significant part of the national economy is paid for the imported fossil fuel-based energy sources. Locally available wind energy technology is not affected by price hikes in international markets.

6.8 Challenges to wind energy

6.8.1 Intermittent nature of wind

The major challenge that is faced by the wind turbine is the intermittent nature of the source. The wind is an unpredictable source of energy. It is possible that during the peak hours when generation from the wind farm is required, the wind is unavailable and the wind farm is unable to feed the grid. Similarly, when the generation from the wind farm is not required, the production from the wind turbine is maximum. To cope with the intermittent nature of the wind, some energy management systems and energy storage systems like pumped hydro, flywheel, and compressed air energy storage systems are required.

6.8.2 Noise pollution

Any unwanted sound arising from the wind turbine during its operation is termed noise. The severity of the sound depends upon the type of noise, circumstances, and the hearing sensitivity of the individual perceiving the sound. Whether a sound is irritating or not depends largely upon the receptor. The types of noise are broadband noise, which is a swishing sound, and tonal noise, which is called a humming sound at a steady pitch. Broadband noise is produced when the turbine blades encounter turbulence in the air and tonal noise is produced by the working of the mechanical components. This noise pollution could be a challenge for the wind industry if it is beyond the safety levels for animals and humans.

6.8.3 Transmission of wind power

Most of the good windy areas are located in hilly and mountainous regions which are away from the main power consumption areas. To transmit the power that wind farms to the consumers, a transmission line is required, which is much more expensive compared to distributed generation.

6.9 Conclusion

The growing concerns about the environmental impact of the conventional power plants and the increasing global warming have demanded the paradigm shift from the conventional fossil fuels-based power plants to the renewable energy power plants. The concept of distributed generation and the smart grid have increased the demand for energy from wind

turbines. This chapter describes the design of the wind energy system for a specific location. The types of wind turbines that can be used to harness the energy from the wind have been discussed. Energy conversion systems using various types of generators for the variable wind speeds are described. Various control strategies for the variable wind speed and the associated electrical frequency have been discussed in detail. The fundamental equation of the wind turbine and impact of power coefficient given by the Betz limit, wind energy density, capacity factor of the wind turbine, blade tip speed ratio, tip speed of the wind blades, and wind power density are considered in this chapter.

Problems

Problems 1–10 contain four answer options: A, B, C, and D. Choose the correct answer.

1. Which type of energy is carried by wind coming toward the wind turbine?
   A. Electrical energy
   B. Potential energy
   C. Thermal energy
   D. Kinetic energy
2. What is the maximum limit of the power coefficient given by the Betz limit?
   A. 0.60
   B. 0.59
   C. 0.49
   D. 0.40
3. Which of the following gives the capacity factor of a wind turbine?
   A. $capacity\ factor\ (CF) = \frac{E_{actual}}{E_{generated}}$
   B. $capacity\ factor\ (CF) = \frac{E_{actual}}{E_{ideal}}$
   C. $capacity\ factor\ (CF) = \frac{f_{actual}}{E_{ideal}}$
   D. $capacity\ factor\ (CF) = \frac{E_{actual}}{f_{ideal}}$
4. Which of the following gives the blade tip speed ratio?
   A. $\lambda = \frac{blade\ tip\ speed}{wind\ speed}$
   B. $\lambda = \frac{blade\ rotational\ speed}{wind\ speed}$
   C. $\lambda = \frac{blade\ tip\ speed}{RPM}$
   D. $\lambda = \frac{RPM}{wind\ speed}$
5. How is the blade tip speed calculated?
   A. $blade\ tip\ speed = \frac{rotational\ speed \times \pi \times r}{60}$
   B. $blade\ tip\ speed = \frac{rotational\ speed \times \pi \times D}{50}$
   C. $blade\ tip\ speed = \frac{rotational\ speed \times D}{60}$
   D. $blade\ tip\ speed = \frac{rotational\ speed \times \pi \times D}{60}$

6. Among the following types, which is the turbine tower?
   A. Lattice type
   B. Guyed type
   C. Monopole tower
   D. All of the above
7. Which of the following is a type of horizontal axis wind turbine?
   A. Dutch type wind turbine
   B. Savonius wind turbine
   C. Darrieus wind turbine
   D. All of the above
8. Which of the following is a type of vertical axis wind turbine?
   A. Dutch type wind turbine
   B. Savonius wind turbine
   C. Propeller wind turbine
   D. All of the above
9. What of the following is a challenge to wind energy?
   A. Intermittent nature of wind
   B. Noise pollution
   C. Transmission of wind power
   D. All of the above
10. Which of the following is a method of frequency control of the wind energy system?
    A. Droop control method
    B. Pitch control method
    C. Inertial response
    D. All of the above

Give brief answers to the following short questions

1. What is the significance of the power coefficient of the wind turbine?
2. Define the Betz limit.
3. Define the capacity factor of a wind turbine.
4. How is the blade tip speed ratio of a wind turbine measured?
5. How is the power coefficient of a wind turbine for a specific wind speed calculated?
6. What are the advantages of wind energy?
7. List the challenges that wind energy is facing in its deployment.
8. What are the key components of a wind turbine?
9. List the advantages and disadvantages of different types of wind turbine towers.
10. What are the three types of horizontal axis wind turbines?
11. What are the two types of vertical axis wind turbines?
12. Compare horizontal axis and vertical axis wind turbines.
13. Describe the applications of induction generators and doubly fed induction generators with the wind turbine.
14. Draw a diagram of the application of a synchronous generator with a variable speed wind turbine.
15. Differentiate between a Darrieus wind turbine and a Savonius wind turbine.

16. Vertical axis wind turbines are used more in cities than horizontal axis wind turbines. Why?
17. Give the classification of the frequency control strategies of wind turbines.
18. How is hidden inertia emulation used to control the frequency of wind turbines?
19. Which techniques are used to control the pitch angle of the turbine blades?
20. Draw a diagram of the electric pitch angle control system.
21. Explain the hydraulic pitch angle control system.
22. A wind power plant is to be installed on a location having wind speed of 5 m/s. The turbine is rotating at 20 RPM and the blade length is 10 m. Calculate the power coefficient for this wind turbine.

References

[1] Z. Chen, Wind power: an important source in energy systems, Wind 1 (1) (2021) 90–91, https://doi.org/10.3390/WIND1010006.
[2] IEA, Wind Power—Analysis, IEA, 2022. [Online]. Available https://www.iea.org/reports/wind-power. (Accessed 5 June 2022).
[3] M. Sawant, S. Thakare, A.P. Rao, A.E. Feijóo-Lorenzo, N.D. Bokde, A review on state-of-the-art reviews in wind-turbine- and wind-farm-related topics, Energies 14 (8) (2021) 2041, https://doi.org/10.3390/EN14082041.
[4] S. Pfaffel, S. Faulstich, K. Rohrig, Performance and reliability of wind turbines: a review, Energies 10 (11) (2017) 1904, https://doi.org/10.3390/EN10111904.
[5] M. Rayyan Fazal, M. Kamran, Wind energy, in: Renewable Energy Conversion Systems, first ed., Academic Press, 2021, pp. 153–192.
[6] W. Cao, N. Xing, Y. Wen, X. Chen, D. Wang, New adaptive control strategy for a wind turbine permanent magnet synchronous generator (PMSG), Inventions 6 (1) (2020) 3, https://doi.org/10.3390/INVENTIONS6010003.
[7] S.A. Vargas, G.R.T. Esteves, P.M. Maçaira, B.Q. Bastos, F.L. Cyrino Oliveira, R.C. Souza, Wind power generation: a review and a research agenda, J. Clean. Prod. 218 (2019) 850–870, https://doi.org/10.1016/J.JCLEPRO.2019.02.015.
[8] G.M. Joselin Herbert, S. Iniyan, E. Sreevalsan, S. Rajapandian, A review of wind energy technologies, Renew. Sustain. Energy Rev. 11 (6) (2007) 1117–1145, https://doi.org/10.1016/J.RSER.2005.08.004.
[9] T. Ma, H. Yang, L. Lu, A feasibility study of a stand-alone hybrid solar–wind–battery system for a remote island, Appl. Energy 121 (2014) 149–158, https://doi.org/10.1016/J.APENERGY.2014.01.090.
[10] U. Datta, A. Kalam, J. Shi, The relevance of large-scale battery energy storage (BES) application in providing primary frequency control with increased wind energy penetration, J. Energy Storage 23 (2019) 9–18, https://doi.org/10.1016/J.EST.2019.02.013.
[11] P. Fernández-Bustamante, O. Barambones, I. Calvo, C. Napole, M. Derbeli, Provision of frequency response from wind farms: a review, Energies 14 (20) (2021) 6689, https://doi.org/10.3390/EN14206689.
[12] M.R. Aghamohammadi, H. Abdolahinia, A new approach for optimal sizing of battery energy storage system for primary frequency control of islanded Microgrid, Int. J. Electr. Power Energy Syst. 54 (2014) 325–333, https://doi.org/10.1016/J.IJEPES.2013.07.005.

CHAPTER

7

Microgrid and hybrid energy systems

7.1 Introduction

The environmental hazards of conventional fossil fuels (oil, gas, coal) have urged energy investors and energy consumers to shift the energy dynamics from conventional to environmentally friendly renewable energy sources (solar, wind, biomass, biogas, geothermal, micro-hydro, hydrogen, etc.). Renewable energy systems (RESs) help in mitigating greenhouse gas (GHG) emissions. In hybrid energy systems (HESs), some of the renewable energy sources along with the conventional energy sources manage the local load. A microgrid is a decentralized group of electricity generators (distributed generation or DG), loads, energy storage systems, and controlling mechanisms that may either be connected to and synchronized with the national central grid or may operate independently in autonomous mode. Fig. 7.1 shows the basic structure of the HES with conventional and renewable energy sources as the power generating units. The power conditioning units transform the voltage from one form to another. In a grid-connected mode, power from the solar PV is inverted from DC to AC using inverters. Similarly for DC loads and battery storage systems, voltage is either increased or decreased using boost and buck converters, respectively. The next stage in the HESs is the energy storage systems. Energy storage system technologies are electrical, mechanical, and chemical. Electrical energy storage systems include supercapacitors and superconductors. Mechanical energy storage systems are compressed air energy storage systems, flywheel energy storage systems, and pumped hydro energy storage systems. Chemical energy storage systems are batteries, flow batteries, and regenerative fuel cells.

Despite depending upon a single energy source, HES based on conventional and renewable energy sources, energy storage elements, and the load consumption in a single system offer promising advantages over a conventional power system. An HES is usually an off-grid system consisting of renewable energy technologies like solar, wind, micro-hydro, fuel cells, a biogas power plant, or a geothermal power plant, conventional energy sources like oil, gas, and coal power plants, energy storage technology, and load. Depending upon the availability of the renewable energy sources at the specific site, one or more renewable energy sources can be hybridized to manage the load demanded. The general schematic diagram of the HES is shown in Fig. 7.1.

https://doi.org/10.1016/B978-0-323-99560-3.00006-5

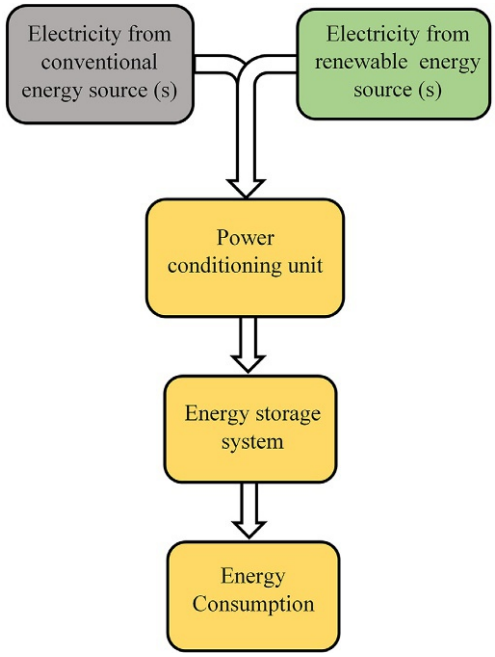

FIG. 7.1 The basic structure of a hybrid energy system.

7.2 Literature review

HESs have been studied extensively in distributed generation, microgrid, smart grid, and RESs. Baghdadi et al. [1] optimized the fossil fuel and renewable energy-based HES. The objective function was to maximize renewable electricity and minimize fuel consumption. Enevoldsen and Sovacool [2] designed an isolated microgrid integrated with an energy storage system. The objective function was to increase the reliability of the microgrid. Biswas and Kumar [3] designed a hybrid RES consisting of solar PV, battery energy storage system, and pumped hydro energy storage system for an academic institution building. Türkay and Telli [4] studied the grid-connected hybrid RES consisting of solar PV, wind turbine, and fuel cell. They also researched the impact of solar PV and fuel cells on the grid and found that the average solar irradiance and the wind speed are feasible for Istanbul. Nafeh [5] developed a microgrid for a home consisting of solar PV, a wind turbine, and a battery storage system. Kamran et al. [6,7] designed a micro-hydro energy system and performed optimization and sensitivity analysis on the Hybrid Optimization Model for Electric Renewables (HOMER). Spyrou and Anagnostopoulos [8] designed an off-grid HES consisting of solar PV and wind turbines. A pumped hydro energy storage system was also integrated with the HES. The project was to power up a desalination plant. Heydari and Askarzadeh [9] used a harmony search algorithm on a HES consisting of PV, WT, DG, and battery storage system, and minimized the sizing of the sources. Abdelhamid and Rachid [10] proposed an isolated HES and performed techno economic optimization.

Abdul Wahab et al. [11]. conducted a study on the battery connected solar PV system for Oman in HOMER and found the minimum emissions, minimum net present value (NPV), and cost of energy (COE) after performing optimization and sensitivity analysis. Shaahid et al. [12]. proposed a 15 MW battery connected wind turbine system for Saudi Arabia and performed techno-economic analysis to study the reduction in COE. Karmaker et al. [13] proposed a HES consisting of electric vehicle and biogas for Bangladesh and found the lowest COE and NPV. Ma and Javed [14] studied a HES consisting of solar PV, WT, and battery in MATLAB for China and mitigated the disharmony between generation balance, load, and cost optimization.

7.3 Distributed generation

Distributed generation cannot be defined by a single definition, as it is a vast concept ranging from the locally available conventional and renewable energy sources connected to a distribution network that further may or may not be connected to the transmission network. However, upon going through the literature, it can be defined as the generation of electricity using conventional or renewable energy sources to manage the load connected to the distribution network. If the distribution network is connected to the transmission network, it may sell and purchase the electricity to the grid. Depending upon the location of the DG, the range is defined as a few kilowatts to 400 MW. Though the renewable energy sources are abundant but intermittent which are available only for a specific time. The availability of the energy sources and the efficiency of the related energy harnessing technology derive the efficiency of the DG. The various energy technologies that are considered a part of the DG are detailed in the table with their power plant size. The concept of the distributed generation interconnected to the grid is shown in Fig. 7.2.

DG technologies are categorized as follows based on the energy source:

(1) DG resources based on conventional fossil fuel-based power plants (microturbine, reciprocating engine, Stirling engine, combined cycle gas turbine, combustion gas turbine (CGT), etc.);
(2) DG resources based on renewable energy sources like solar PV, wind, biogas, geothermal, micro-hydro, and fuel cell; and
(3) mixed DG energy resources where conventional and renewable energy sources are combined to form a microgrid [15].

7.3.1 Why distributed generation?

- Rather than managing the load of the remote localities through a transmission and distribution network, the local load can be fed through the indigenously available energy sources in an efficient way.
- If the DG system is close to the transmission network, its surplus electricity may be sold to the grid and electricity may also be purchased from the grid during peak hours or when the energy sources are not available.

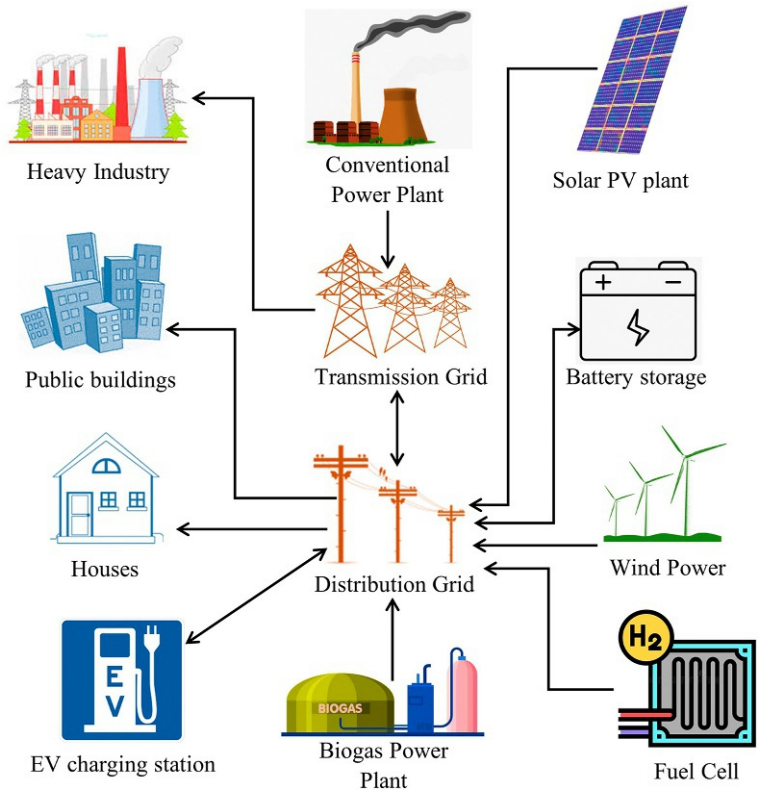

FIG. 7.2 Distributed generation in a microgrid.

- DG is cost-effective as locally available energy sources are used and no cost is incurred on the transmission and distribution line.
- DG ensures energy security as the microgrid based on the DG is more resilient and robust than the transmission and distribution network.
- Generating electricity from biomass/biogas, only 40% of the calorific value is converted into electricity while the other 60% is wasted as heat. In DG, the generation of electricity from biomass/biogas adjacent to the load makes heat recovery possible.
- Being close to the consumer, there are no transmission losses that make the performance better and increase reliability.
- During a natural disaster, the national grid will not go into a blackout. Instead, the DG system will provide electricity to the local areas.
- For maintenance purposes, a feeder does not need to be shut down; instead, the relevant DG system could be turned off.
- DG is environmentally friendly, as most of the energy comes from renewable energy sources.

7.3.2 Distributed generation technologies

The technologies that are considered for the DG are given in Fig. 7.3. DG technologies like solar PV arrays, wind turbines, solar thermal, micro-hydro, diesel engines, fuel cells, and

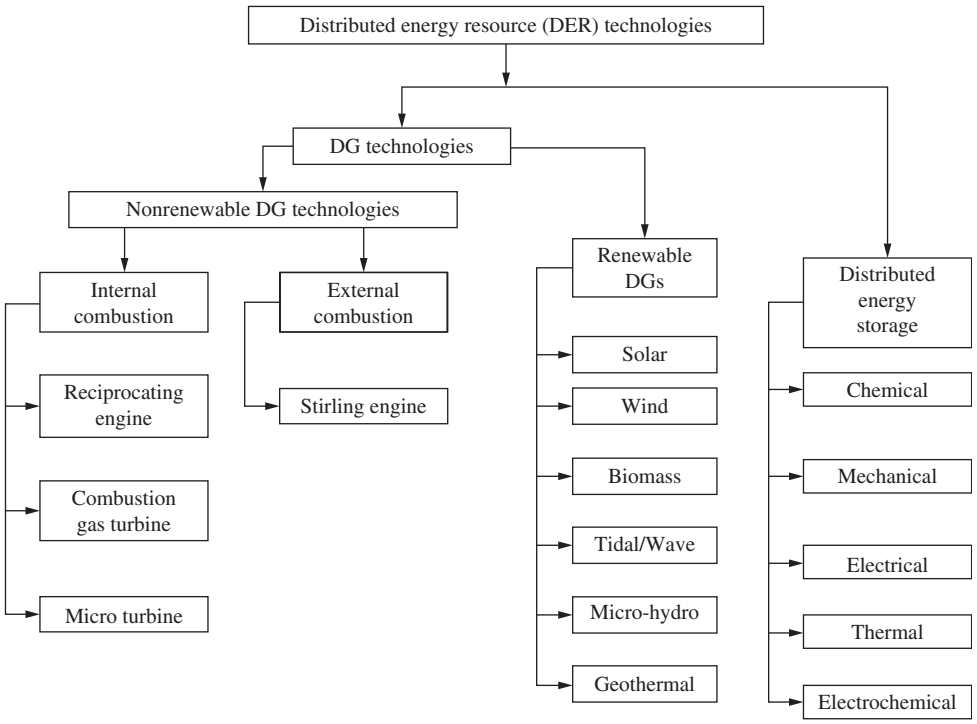

FIG. 7.3 Distributed generation technologies.

storage systems are modular and available in smaller units that can be installed to the system and removed from the system in a very short time. All the distributed generation technologies are shown in Fig. 7.3.

7.3.2.1 Combined cycle gas turbine

In an open cycle gas turbine, the air from the atmosphere is compressed in a compressor where its temperature and pressure are raised. The highly compressed air is then heated in the combustion chamber. The hot gases from the combustion chamber drive the turbine and the coupled generator. The exhaust gases are wasted in the atmosphere without recirculating. A diagram of an open cycle gas turbine is shown in Fig. 7.4.

The term "combine cycle" refers to the combination of thermodynamic cycles. An open cycle gas turbine is incorporated with a heat recovery steam generator (HRSG). The waste heat of the gas turbine working on the Bryton cycles is recovered and is used to drive a steam turbine working on the Rankine cycle. Combined cycle power plants are highly efficient in converting 50%–60% of the input into electricity. These power plants may be single shaft, where both the steam and gas turbines are coupled to the same shaft driving the same generator, or they may be connected to the different shafts driving different generators. A diagram of the flow process of a combined cycle is shown in Fig. 7.5.

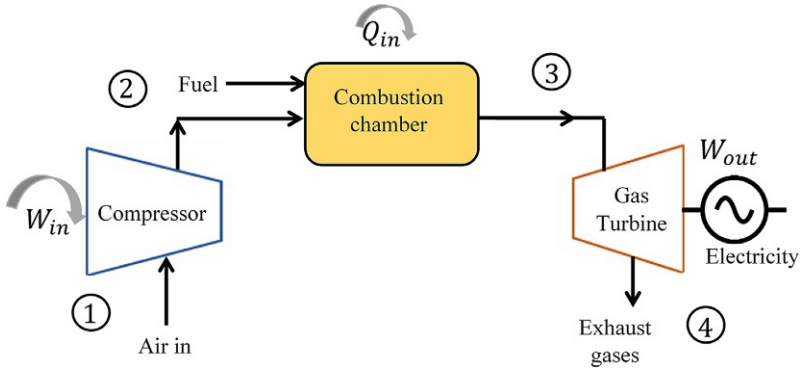

FIG. 7.4 Open cycle gas turbine.

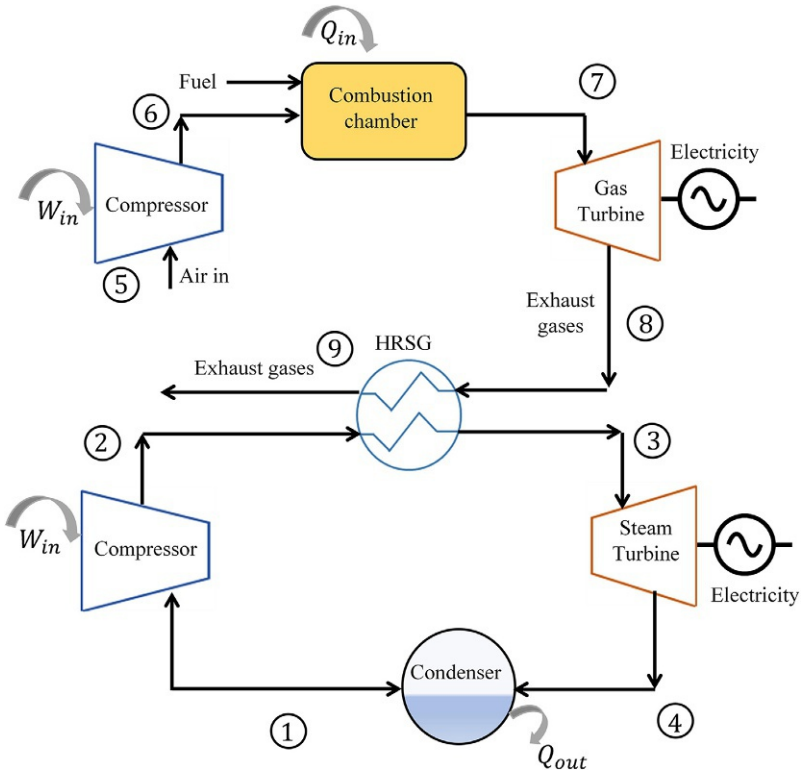

FIG. 7.5 Combined cycle.

7.3.2.2 *Reciprocating engine*

Reciprocating engines were developed more than 100 years ago using fossil fuels as a source and are well-acknowledged DG technologies. Today they are available from different manufacturers in all DG sizes. A reciprocating engine, also known as a piston engine, is a type of internal combustion engine. From the ignition point of view, reciprocating engines are either:

(1) spark ignition (SI) engines, which are generally gas engines working on the principle of the Otto cycle; or
(2) compression ignition (CI) engines, which are diesel engines working a on diesel cycle.

Reciprocating engines consist of one or more pistons working on the four-stroke principle. The piston of the reciprocating engine performs the following four jobs in a single-cylinder, as shown in Fig. 7.6:

1. intake
2. compression
3. ignition
4. exhaust.

The cycle starts with the intake of the fuel from the injector to the combustion chamber, where it reacts with the air coming through the air intake. The subsequent exothermic reaction creates gases at high temperatures and pressure that expand and drive the piston from the top dead center (TDC) to the bottom dead center (BDC). After moving the piston downward, the exhaust gases move upward and drive the piston from the BDC to the TDC. The exhaust hot gases are used for generating low-pressure and high-pressure steam for combined heat and power (CHP) purposes.

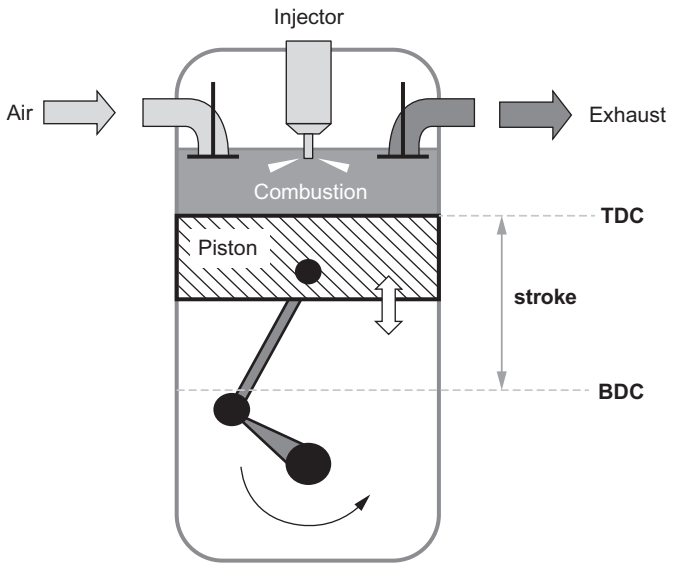

FIG. 7.6 Working of a reciprocating engine.

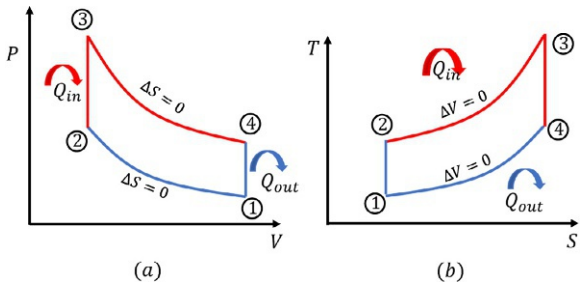

FIG. 7.7 (A) P-V diagram of the Otto cycle and (B) T-S diagram of the Otto cycle.

The Otto cycle: The spark ignition reciprocating engine works on the concept of the ideal Otto cycle. This cycle consists of four processes: two isentropic processes and two isochoric processes, as described in Fig. 7.7. A pressure-volume and temperature-entropy diagram of the ideal Otto cycle is shown in Fig. 7.7A and B.

1. 1→2 process: compression at constant entropy

During this process, the piston moves from the BDC to the TDC, slightly increasing the pressure and temperature of the air-fuel mixture. However, the entropy of the system remains constant as no heat is exchanged until point 2. In thermodynamics, this process is termed the adiabatic process. At point 2, the spark plug meets the fuel for ignition.

2. 2→3 process: heat absorption at constant volume

When the fuel is ignited at point 2, combustion starts, and the exothermic reaction increases the temperature and the pressure of the combustion chamber at constant volume. During this process, the piston does not move and keeps its position at the TDC. This process is called the combustion and isochoric process.

3. 3→4 process: expansion at constant entropy

After the combustion process is completed, the hot gases expand and move the piston from the TDC to the BDC, which increases the volume of the chamber. This is known as the power stoke, as it converts the thermal energy into the mechanical energy of the shaft that rotates the machine. The entropy of the system remains constant as no heat is exchanged until point 4.

4. 4→1 process: heat rejection at constant volume

After doing useful work at the piston and the couples shaft, the heat is expelled from the chamber of the engine. As the heat exchange takes place in this process, the entropy and the temperature of the system are decreased. The piston keeps its position at the BDC, so no change in volume is observed. The process repeats itself and continues in the same direction.

During the execution of the Otto cycle in a closed-loop, the net change in energy is zero and the system returns to its initial state where it started as depicted in Eq. (7.1).

$$\Delta E = E_{in} - E_{out} \tag{7.1}$$

In Fig. 7.7, it can be seen that heat exchange takes place during processes 2→3, and 4→1, and work is done during processes 1→2 and 3→4. Energy balance of this process can be expressed as Eq. (7.1).

7.3.2.3 *Microturbines*

Microturbines are small gas turbines coupled to their generators. They are used to produce both electricity and heat and are available in a range of 25–500 kW and efficiency ranges between 20% and 30%. The technology of microturbines is based on the technology of diesel engine turbochargers, automotive designs, and aircraft auxiliary power systems. In the past, microturbines were designed for small commercial and large domestic applications. With the advancement in the distributed generation technology, they are designed for distributed generation since they feed their electricity to the distribution network.

The construction of microturbines is identical to that of gas turbines, consisting of a compressor, combustor, turbine, and generator. Apart from the size of the turbine, they differ in the shaft. The compressor and the turbine are mounted to the same shaft of the electrical generator. The air is mixed with the fuel in the combustion chamber and the resultant hot gases are used to derive the turbine. The turbine, as a result, rotates both the generator and the compressor. The compressor sends the intake air to the combustion chamber at high pressure. Microturbines are mostly packaged with a coupled high-speed permanent magnet generator to be easily installed in the DG application. Despite being small in size, the rotational speed of the microturbine and the couples generators are very high, normally between 40,000 and 120,000 RPM, which needs to be reduced to get an output of 50–60 Hz for the synchronization purpose. To get the required frequency and voltage, a power electronics inverter and rectifiers are used.

Microturbines can be with or without a recuperator. Microturbines without recuperators are less efficient since the exhaust heat is wasted into the atmosphere without reuse. A recuperator is a cross-flow heat exchanger placed at the exhaust position of the system to recover the heat from the exhaust gases and is used to preheat the discharge of the compressor as shown in Fig. 7.8. Microturbines are also used for CHP applications, which make them more efficient.

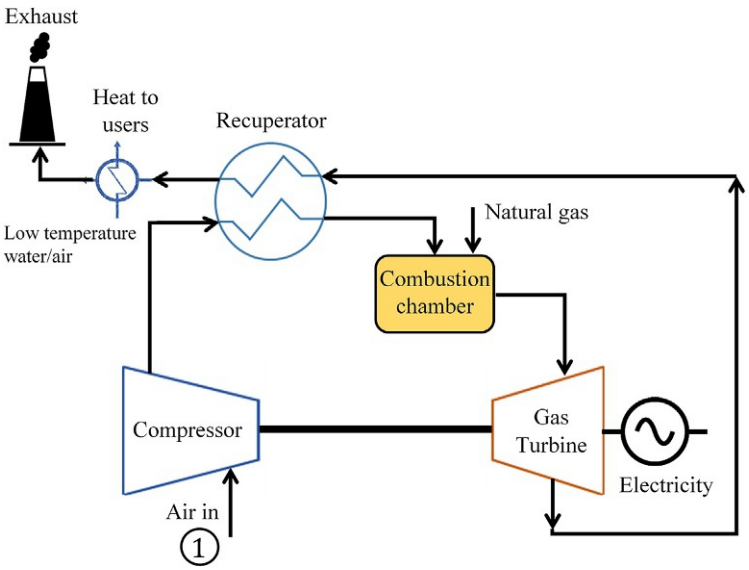

FIG. 7.8 Flow diagram of the microturbine.

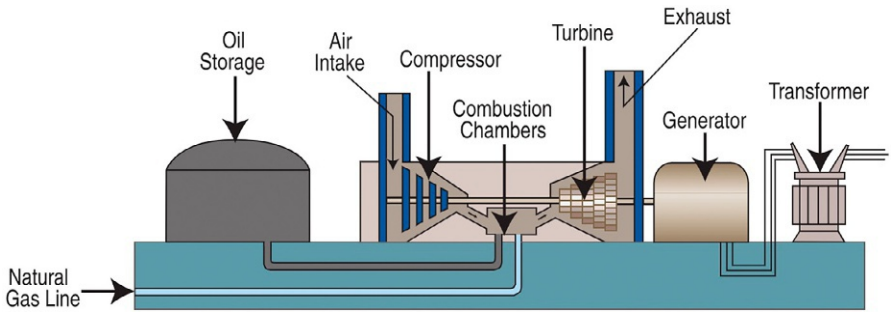

FIG. 7.9 Combustion gas turbine [16].

7.3.2.4 Combustion gas turbine

CGTs are used to derive the large compressors and generators in the range of 1–100 MW. They are used where quick operation of the generation action is required. They work on the principle of jet engines taking air from the atmosphere, compressing and mixing it with the fuel (gas) and igniting it. The immediate combustion and expansion of the gas through the generator coupled to the blades of the turbine make it favorable to be used in DG. A diagram of a CGT is shown in Fig. 7.9.

7.3.2.5 Stirling engine

Stirling engine is a type of external combustion engine that works on the principle of compression and expansion using thermal energy and doing some mechanical useful work. The engine itself is enclosed in an environment and the heat is supplied from the outside from various sources like waste heat, combustion fuels, bioenergy, geothermal energy, nuclear energy, and solar thermal energy. A Stirling engine uses the temperature gradient between the cooling part and the hot part making a complete cycle consisting of heat addition, expansion, cooling, or heat rejection and compression. As the fuels do not come in contact with the internal parts of the engine, the fuels that may contaminate the other types of engines can be used in Stirling engines as a source of heat. Fig. 7.10 shows the solar dish as a source of heat energy to the center-mounted Stirling engine.

7.3.2.6 Solar

The sun is an immense source of free energy. Energy harnessing technologies from the sun are categorized into solar thermal, solar photovoltaics, and solar indoor lighting.

Solar thermal energy is harnessed through the concentration of solar irradiance. Solar thermal technologies are given in Table 7.1. The sunlight is concentrated using mirrors or the shining surfaces and focused on the receiver where it heats the water, generating steam. This concentrated heat is either used to generate electricity, heat for space heating, process heating, or water heating. Solar cookers and solar dryers are used to cook food and to dry fruits and vegetables, respectively.

In solar photovoltaics, semiconductor materials are used. The solar irradiance falls on the solar materials named solar cells and transfers its energy to the electrons in the valence band.

FIG. 7.10 Solar dish with center-mounted Stirling engine [17].

TABLE 7.1 Solar technologies.

Sr. no.	Solar thermal	Solar photovoltaics	Solar indoor lighting system
1	Parabolic trough	Poly-crystalline	Heliobus
2	Solar tower	Mono-crystalline	Arthelio
3	Solar cooker	Amorphous silicon	SLP
4	Solar dryer	Tandem/microcrystalline	HSL
5	Parabolic dish	Copper indium gallium selenide (CIGS)	Parans
6	Solar water heater	Cadmium telluride (CdTe)	SCIS
7		Dye-sensitized (TiO_2)	UFO
8		Compound semiconductor (GaAs based)	

If the energy of the photon is larger than the bandgap energy of the semiconductor material, the valence electrons jump the forbidden gap and reach the conduction band where they flow out of the solar cell, forming DC. In cases where the energy of the solar irradiance is lower than the bandgap energy of the solar material, the electrons stay in the valence band and hence no production of current. The semiconductor materials are detailed in Table 7.1. In DG, solar photovoltaic is an ideal source of energy as it is capable of achieving grid parity. The installation, operation, and maintenance of the solar photovoltaic system make it the best DG source. The balance of the system (BoS) of the solar PV system includes a DC-DC converter, inverter, and battery storage. For the battery efficiency of the system, solar trackers and MPPT are also incorporated into the system. The construction of a solar PV system from a solar cell with its BoS is shown in Fig. 7.11.

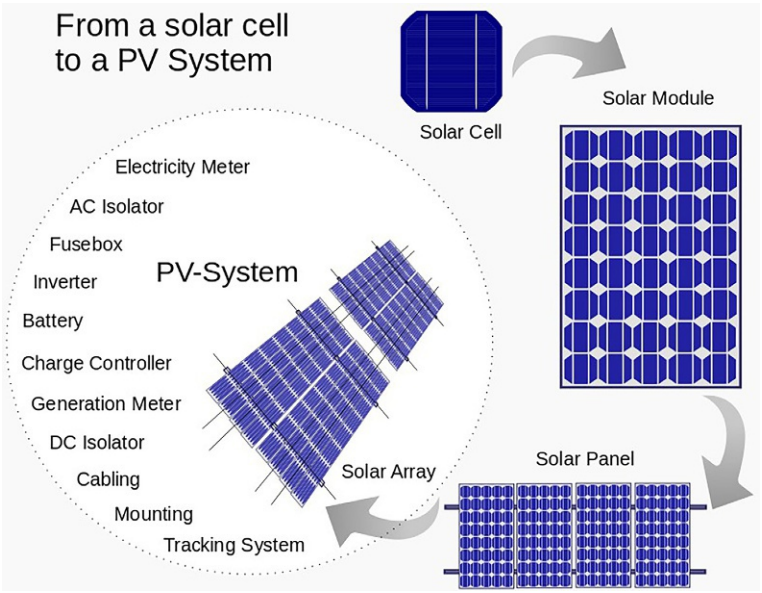

FIG. 7.11 From a PV solar cell to a PV solar system [18].

In solar indoor lighting systems, the system consists of two parts: an indoor unit and an outdoor unit. In the outdoor unit, sunlight is concentrated at the inlet of the optical fibers through Fresnel lenses. The optical fibers lead the sunlight to the indoor unit where each optical fiber works as a separate source of light. Various indoor lighting systems are given in Table 7.1.

7.3.2.7 Wind

Wind energy is another renewable source of energy in which wind turbine is used to harness the energy from the wind. The major source behind wind energy is also solar energy. The physics behind the wind blow is the temperature gradient. When the air is hot in a specific region, its density is decreased and the air is lifted upward. To fill the gap, cold air from the nearby region rushes to this place, generating the wind blow. The kinetic energy in the wind can be harnessed by the use of wind turbines. These turbines are of two types:

(i) horizontal axis wind turbines; and
(ii) vertical axis wind turbines.

Most of the wind turbines used in the electrical power systems in the world are horizontal wind turbines, in which the blades are mounted on the top of the tower. The other components of the turbine are the main rotor shaft coupled to the electrical generator. Horizontal axis wind turbines are seen all over large wind farms, whereas in small and residential wind applications, vertical wind turbines are employed. A horizontal wind turbine is shown in Fig. 7.12. A vertical wind turbine is divided further into two types: Darrieus and Savonius, as shown in Fig. 7.13A and B.

FIG. 7.12 Wind turbine [19].

7.3.2.8 Biomass

Biomass is another source of free and clean energy. The technologies associated with biomass to electricity conversion can be used as a DG. Wet biomass through anaerobic digestion can be converted into biogas. Natural gas (methane) being a major constituent of biogas can operate a gas generator in a DG in areas where biomass is easily and abundantly available. The anaerobic digestion process is the decomposition of complex biodegradable materials into simple molecules soluble in water. The complex molecules are fats, carbohydrates, and proteins found in energy crops, slurry, corn silage, crop residues, slaughterhouse waste, food processing waste, industrial waste, and livestock residues. The anaerobic digestion process consists of four subprocesses: hydrolysis, acidogenesis, acetogenesis, and methanogenesis. Fig. 7.14 shows the anaerobic digestion processes in a flow. Other

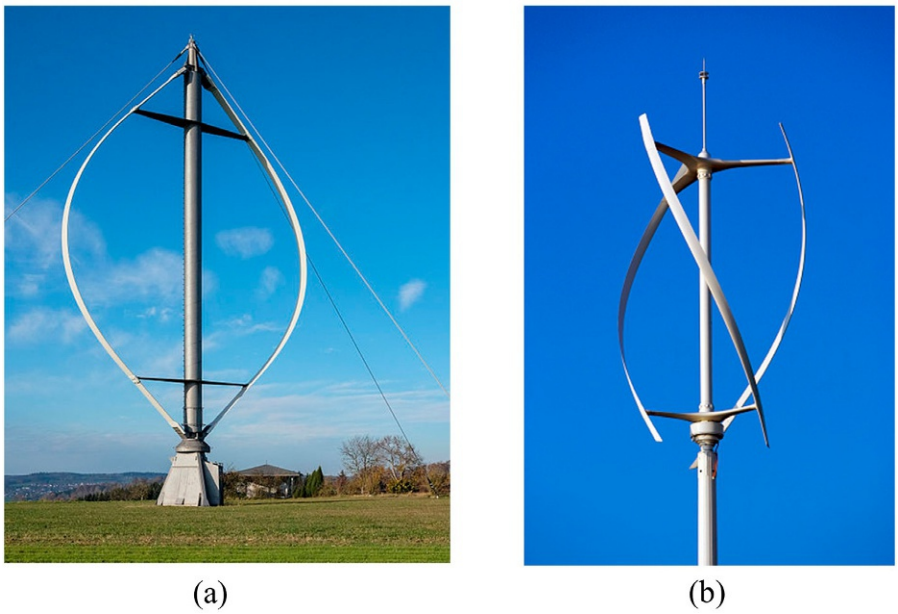

FIG. 7.13 (A) Darrius vertical-axis wind turbine and (B) helix type vertical axis wind turbine [20].

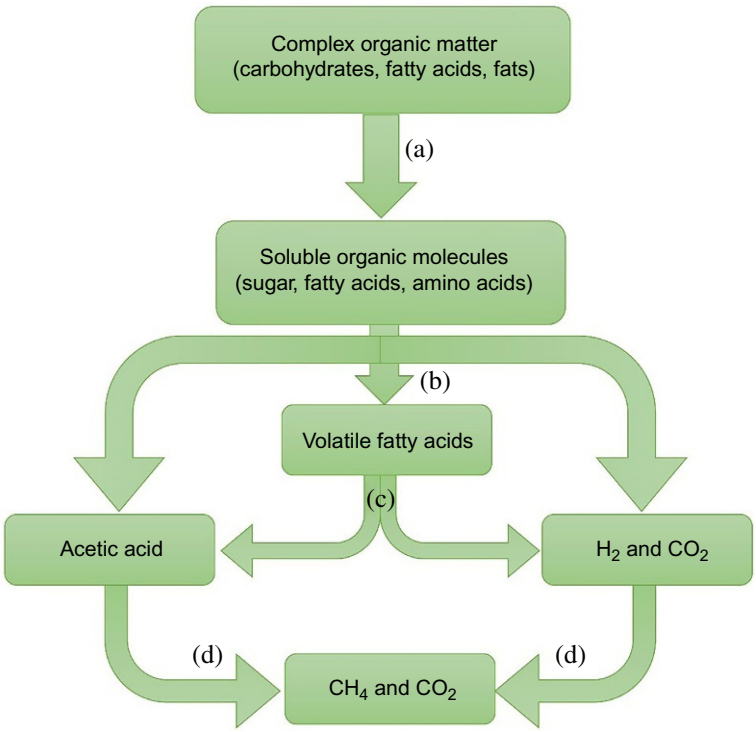

FIG. 7.14 Anaerobic digestion process for biogas production [21].

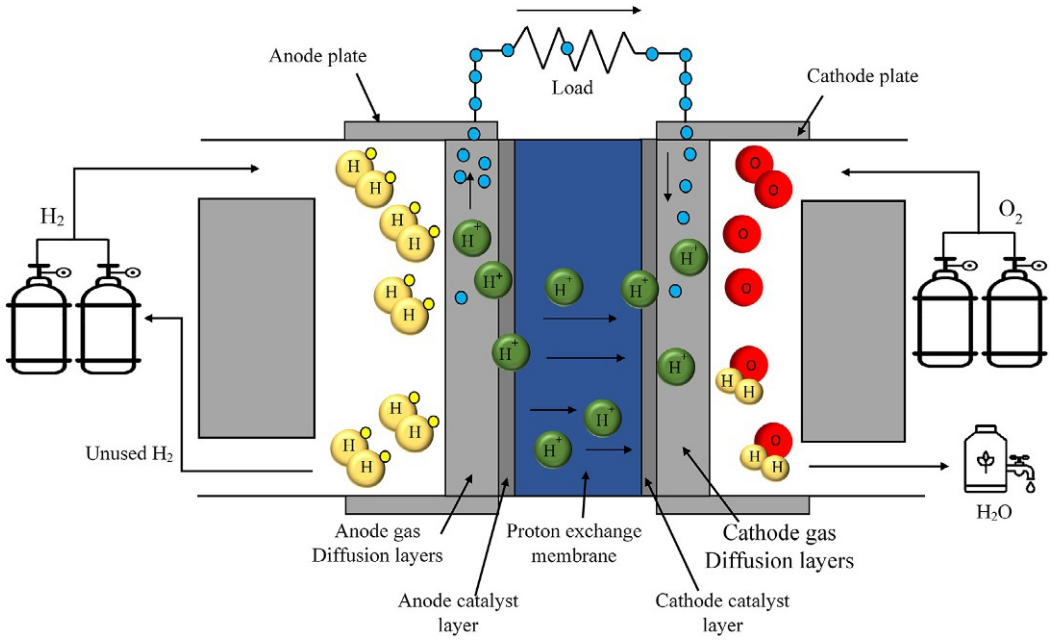

FIG. 7.15 Working and construction of proton exchange membrane fuel cell.

technologies are available that are used to convert biomass into fuel. Transesterification is the process of converting vegetable oils into biodiesel. Sugar and starch are converted into ethanol through the processes of hydrolysis-fermentation-distillation. Gasification of lignocellulosic materials generates producer gas, which is used to generate electricity.

7.3.2.9 Fuel cell

Fuel cells are considered as a source of GHG emission reduction since they are a neat and clean source of energy. Fuel cells take fuel as input mostly hydrogen and DC is an output along with clean water. The working process of the fuel cell can be understood by the simplest proton exchange membrane fuel cell (PEMFC) shown in Fig. 7.15. The fuel cell consists of two electrodes named an anode and cathode, and an electrolyte working as a proton exchange membrane that allows only protons to pass from anode to cathode. A catalyst layer is mounted at anode and cathode to expedite the reactions. Hydrogen is oxidized at the anode as shown in Eq. (7.2), whereas the reduction of oxygen occurs at the cathode shown in Eq. (7.3). As the hydrogen enters the anode side, it liberates electrons leaving behind the protons. The electrons move through the external circuit from the anode to the cathode making a DC. The protons move toward the cathode through the proton exchange membrane where they take electrons coming from the external circuit and the oxygen from the air forming clean water as a by-product. The overall reaction of the PEMFC is shown in Eq. (7.4).

$$\text{Anode} : 2H_2 \longrightarrow 4H^+ + 4e^- \tag{7.2}$$

$$\text{Cathode} : O_2 + 4H^+ + 4e^- \longrightarrow 2H_2O \tag{7.3}$$

$$\text{Overall} : 2H_2 + O_2 \longrightarrow 2H_2O \tag{7.4}$$

When the fuel cell is integrated with a DG or a microgrid, some BoS is required, like the power electronics components. As a power conditioning unit, a DC-DC converter is used that either boosts up or bucks down the fuel cell voltages to the system voltage. A control circuit for the DC-DC converter is required based on the MPPT. To connect the fuel cell system to the utility grid or the microgrid, an inverter and a P, Q controller are also required.

Some positive aspects of fuel cells are as follow:

- The efficiency of the fuel cell is almost 30% higher than the other DG sources.
- Hydrogen fuel cells have almost zero GHG emissions.
- As no moving parts are involved in the operation of the fuel cell, hence no wear and tear occurs and no maintenance is required. Fuel cells have low maintenance and longer life compared to other conventional DG sources.
- When used in DG, CHP is the best application of fuel cell generating both electricity and low-temperature heat for various purposes.
- Being modular and compact in standard sizes, fuel cells can easily be installed and removed from the microgrid without affecting the infrastructure.

7.3.2.10 Micro-hydro

The conversion of hydro potential energy into useful mechanical and electrical energy is the oldest technology among renewable energy resources. Large hydropower plants are older technology compared to micro-hydro. The latter is another source of DG, since the available potential can be harnessed to meet the local electricity demand. Micro-hydro can be integrated with a fuel cell unit, solar photovoltaic, wind, biogas power plants, and geothermal power plants. Depending upon the location and the availability of other renewable energy sources make micro-hydro is a preferred DG source. It can also serve the load independent of other energy sources.

Where the flow of a stream, canal or the river is at high potential from the ground, the main path of the flow is tapped and the path is diverted for the controlled flow of water. The water is passed through a trash rack, which ensures that the trees, leaves, debris, and other unwanted material do not reach the turbine. The clear water is then passed through the weir that controls the flow of water and then enters the penstock where the potential energy of the water is converted into the kinetic energy that at the end of the penstock enters the turbine coupled to the electrical generator. The water, after generating electricity, enters the mainstream of the river or is sent to the fields for irrigation. The concept of micro-hydro along with the constituent components is shown in Fig. 7.16.

7.3.2.11 Geothermal

Geothermal energy is the heat that is produced and preserved beneath the earth. At some specific terrains below the earth, the earth is so hot that heat energy can be extracted in the

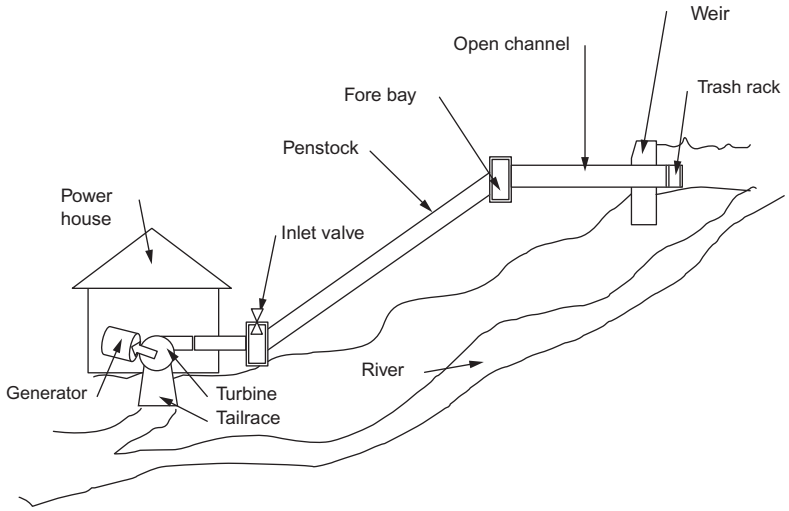

FIG. 7.16 Micro-hydro energy system [22].

form of hot water, steam, or a mixture of both. The term geothermal comes from two Greek words meaning earth (geo) and heat (thermal). There are three types of energy conversion technologies: dry steam power plant, flash steam power plant, and binary cycle power plant. Cold water is sent below the earth through an injection well. The heat from the earth is transferred to the water and is converted into steam. A mixture of steam and hot water is drained out of the earth through a production well. In a separator, steam is separated from the hot water. Steam is sent to the steam turbine coupled to the electrical generator; the hot water is reinjected to the earth to absorb more heat to generate steam. Fig. 7.17 shows the concept of a geothermal power plant.

7.3.3 Advantages of distributed generation

- **Renewable energy sources**: Existing cost-effective DG technologies can be used to manage the load of homes and businesses. For example, solar, wind, and micro-hydro are cheap compared to conventional energy harnessing technologies and sources. In most countries, solar has achieved grid parity, where the electricity from the solar is cheaper than the grid electricity.
- **Transmission line losses**: Since the DG reduces the load on the transmission grid reducing the line losses and as a result reducing the cost of electricity production.
- **Increased efficiency**: Through CHP, the waste energy can be reused for space heating, process heating, and other applications. This increases the overall efficiency of the system, as shown in Eq. (7.5).

$$\eta = \frac{P_e - P_{th}}{P_{in}} \tag{7.5}$$

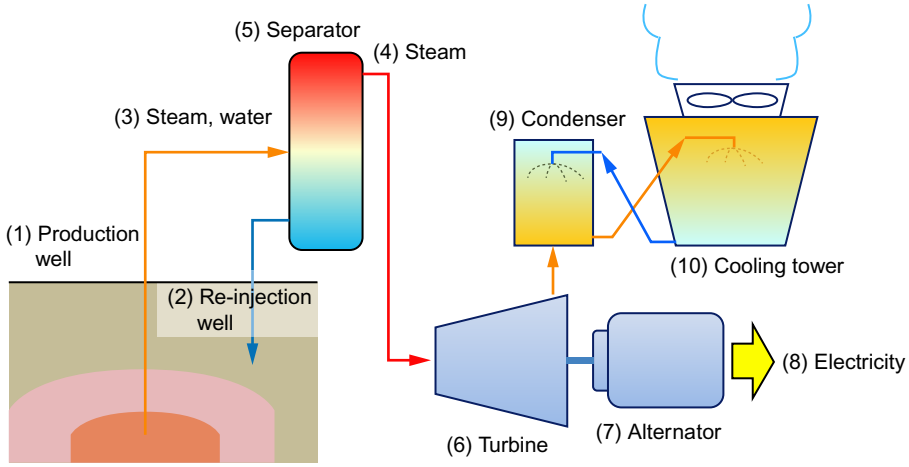

FIG. 7.17 Geothermal power production [23].

where P_e is the electrical power produced, P_{th} is the power produced from heat, and P_{in} is the input power.

- **Spinning reserve**: Spinning reserve is a type of operating reserve and is defined as the extra power generating capacity of the generator that is already synchronized to the system. This extra power is achieved by increasing the torque of the turbine rotor. In the case of steam and gas turbines, spinning is controlled by the combustion in the combustion chamber, and in micro-hydro, it is controlled by the flow rate of the falling water through the turbine. Spinning reserve is considered more reliable in DG since, during a blackout, startup issues are not faced. Spinning reserve is availed for battery efficiency during the peak load demand.
- **Nonspinning reserve**: This is the power generating capacity that is currently not connected/synchronized to the system. Nonspinning reserve requires more time to be online since the generators are started from offline mode to online mode and they may face startup and synchronizing issues. The nonspinning reserve is not used to meet the peak load demand, but instead is operated during a blackout.
- **Peak shaving**: The installed capacity of the power plants in DG must be such that the peak load demand could be satisfied. In DG, spinning reserves and nonspinning reserves plays a role in peak shaving since the new incoming generator is synchronized to the system quickly. Peak shaving can be obtained by controlling both generation side management and load side management. On the load side, the unnecessary load can be avoided in peak hours, e.g., air conditioner can be operated at a relatively high temperature. In generation side management, the spinning and nonspinning reserves may be brought into the system immediately.
- **Reliability**: Some of the loads are considered sensitive and must never be off. DG increases the reliability for sensitive loads since the operating reserves are always ready to start quickly.

- **Environmentally friendly**: The DG technologies, though some of them use conventional sources, have very little emissions compared to the centralized large conventional power plants. Therefore, DG adjacent to the load is considered to be environmentally friendly.
- **Installation and operation**: In the centralized grid, the rapid increase in load demand is unpredictable with accuracy and offhand construction of new fossil fuel-based power plants is a time-consuming and cost-effective project. In DG, distributed technologies are modular and can be installed at a short notice.

7.3.4 Disadvantages of distributed generation

- Since the distributed energy sources are adjacent to the end-users, land acquisition and the health risks from the energy technologies may cause concern among local residents.
- DG technologies based on the conventional technologies, though on a smaller scale, may produce emissions very close to the residents.
- DG technologies like biomass combustion, steam generation, and CHP water are required in abundance that must be available close to the DG system. If not, then arrangements would incur extra cost.

7.4 Renewable energy-based hybrid energy systems

7.4.1 Series hybrid energy system

A series HES is also termed a DC microgrid with the exception that the load is DC, whereas in a series HES, the output or the electricity from the DC bus is inverted to manage the AC load. The configuration of a series HES is shown in Fig. 7.18. Electricity from the sources of the distributed generation sources, either renewable or conventional energy sources, are first converted into DC through power conditioning units comprising of the rectifier and the DC-DC converters. All the DC electricity is dumped on the DC bus. AC sources of energy like a wind turbine, biogas power plant, and the generator set are rectified using rectifiers, whereas the output of the solar photovoltaic, fuel cell and the batteries are either step up or step down using DC-DC boost converter or DC-DC buck converter, respectively, to the voltage level of the DC bus. To manage the AC load, an inverter is connected to the DC bus that converts the DC electricity into AC as shown in Fig. 7.18. Series HESs increase the flexibility of the system for installation of solar PV systems that reduce the cost and losses of the inversion. If the series HES is to deal as a DC microgrid, the DC load can be managed through the DC bus and the power conditioning unit without any conversion of electricity.

7.4.2 Parallel hybrid energy system

A parallel HES consists of both AC and DC buses. Electricity from all the AC sources like wind turbine, biogas power plant and the diesel generator is connected to the AC bus whereas the electricity from solar PV, fuel cell and the battery storage is connected directly to the DC bus through power conditioning units comprising of DC-DC converters. A bidirectional inverter is connected between the AC and DC bus. If the AC bus is unable to meet the load, the

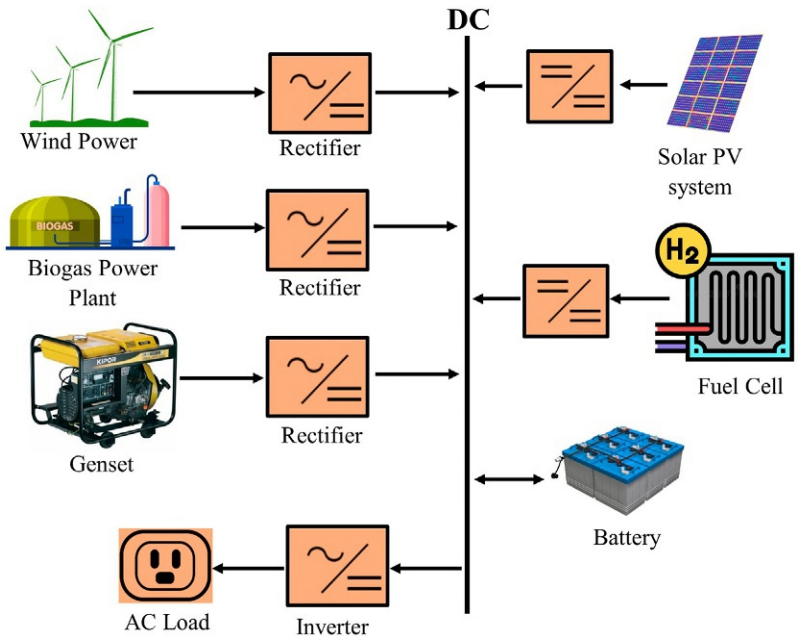

FIG. 7.18 Series hybrid energy system.

DC bus will manage the AC load through the bidirectional inverter. Similarly, if the generation from the DC sources (solar PV and fuel cell) is not enough to charge the battery and the SOC of the batteries is lower, the AC bus charges the batteries through the bidirectional inverter. The configuration of a parallel HES is shown in Fig. 7.19.

7.4.3 Switched hybrid energy system

Switched HES comprises both AC and DC buses with a switching mechanism. When the load is managed by the AC bus, a bidirectional inverter is used to convert the DC power into AC. When there is abundant energy from the solar PV, and the SOC of the battery is greater than the constraints, the DC bus is connected to the load through the inverter. The switching mechanism acts according to the availability of the energy, and the COE. Fig. 7.20 shows the configuration of a switched HES.

7.5 Design parameters of a microgrid and hybrid energy systems

7.5.1 Technical parameters

Loss of power supply probability: Solar parameters like solar irradiance, solar position, and solar cell temperature and wind parameters like wind speed are intermittent and vulnerable to variation, deteriorating the performance. LPSP is a term used to measure the reliability

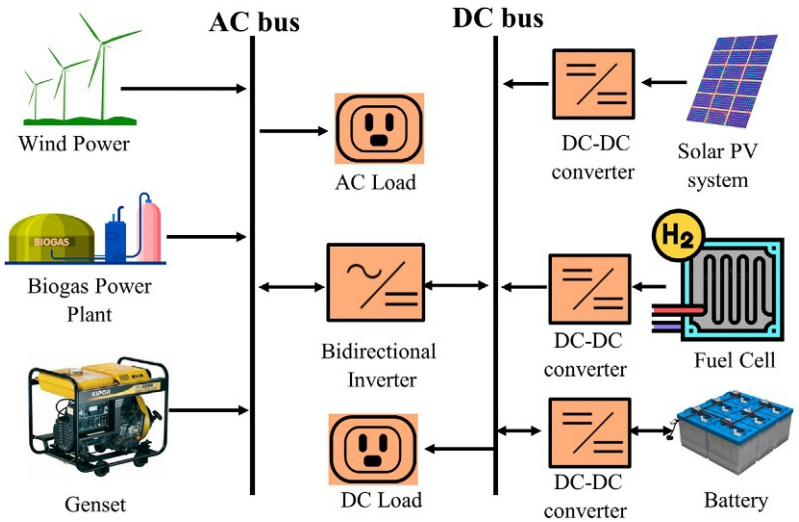

FIG. 7.19 Parallel hybrid energy system.

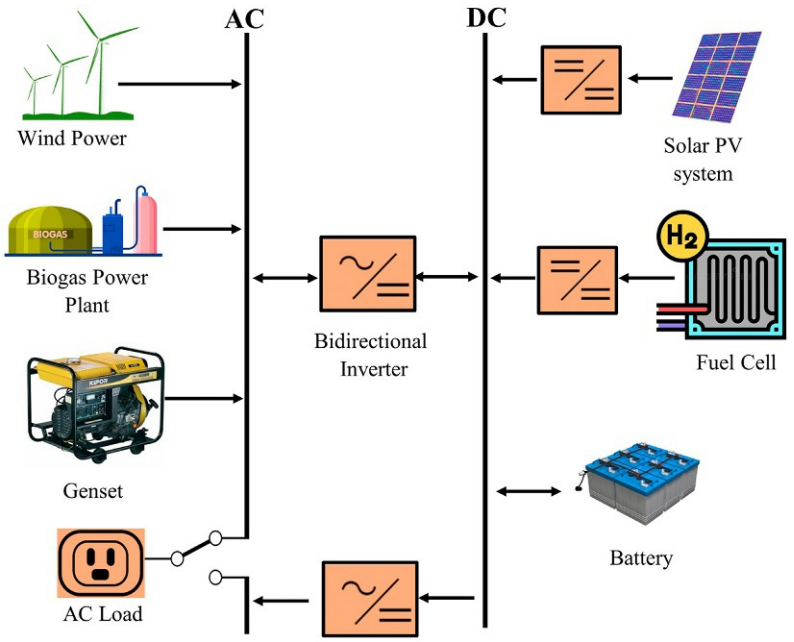

FIG. 7.20 Switched hybrid energy system.

of the system and is defined as the ratio of the discrepancy of the energy to the total energy demand for a specific period. LPSP is determined using Eq. (7.6).

$$\mathrm{LPSP} = \frac{\sum_{t=1}^{T} P_{DE}(t)}{\sum_{t=1}^{T} P_{load}(t)} \tag{7.6}$$

Loss of load expected: When the load is larger than the generation of electricity, a specific load remains unmet, originating the term loss of load expected (LOLE); this is defined as the undeliverable energy under specific conditions due to lower generation.

Equivalent loss factor: Equivalent loss factor is defined as the ratio of the average loss of energy in kW for a specific period to the maximum loss of energy for that specific period.

Total energy loss: Total energy loss (TEL) is defined as the excess generated energy from the HES that is when the generation is more than the load demand. In a grid-connected HES, this excess surplus energy is sold to the grid through the net metering technique. In the case of a stand-alone HES, some constraints to the objective function of generation of the DG sources are imposed. The objective function of the TEL with its constraints is given in Eq. (7.7).

$$\mathrm{TEL}(t) = \begin{cases} \sum_{t=1}^{T}[E(t) - LD(t)], & LD(t) < E(t) \\ 0, & else \end{cases} \tag{7.7}$$

where $E(t)$ is the energy generated by hybrid energy sources at time t and $LD(t)$ is the load demand at time t.

Based on the energy management policy, total energy lost is sold to the grid, or in off-grid cases, generation is imposed with specific constraints.

Level of autonomy: Level of autonomy (LOA) is defined as the fraction of the time for which a specified load can be managed. Mathematically it can be expressed as Eq. (7.8).

$$LA = 1 - \frac{h_{LOL}}{h_{total}} \tag{7.8}$$

where h_{LOL} is the number of hours during which loss of load occurred and h_{total} is the total working hours of the system.

State of charge (SOC) of the battery: This is defined as the amount of charge in the battery relative to the rated capacity and is measured as the percentage of the rated capacity. The SOC of the battery is ranged from 0% to 100%. A SOC of 0% indicates an empty battery depleted of charge while 100% indicates a battery full of charge. The SOC of the battery at any time "t" can be calculated by Eq. (7.9).

$$\mathrm{SOC}(t) = \mathrm{SOC}(t_0) - \frac{\int_0^t I(t) \cdot dt}{\int_0^{total} I(t) \cdot dt} \tag{7.9}$$

where

SOC(t) is the SOC at the given time t;

SOC(t_0) is the initial value of SOC; and

$I(t)$ is the instantaneous load current, positive for charging and negative for discharging.

7.5.2 Economic parameters

Levelized cost of energy: Levelized cost of energy (LCOE) is defined as the average cost of the unit (kWh) generated by a system and is calculated by the ratio of the total annualized cost of the system to the total electrical load served. LCOE is calculated by Eq. (7.10).

$$\text{LCOE} = \frac{C_{ann,tot}}{E_{served}} \tag{7.10}$$

where $C_{ann,tot}$ is the total annualized COE and E_{served} is the total electrical load served.

In a HES or DG system where thermal energy is involved for space heating, water heating, and industrial process, LCOE is calculated by Eq. (7.11). The surplus energy of the system, heat recovery from the generator, can be used to serve the thermal load.

$$\text{LCOE} = \frac{C_{ann,tot} - C_{boiler}H_{served}}{E_{served}} \tag{7.11}$$

where C_{boiler} is the marginal cost of the boiler and H_{served} is the total thermal load served.

Net present cost (NPC): Also known as the life cycle cost of the system or the component, NPC is defined as the present cost of the installation and operation of the system over the lifetime of the project, minus the present value of all the revenues over the lifetime of the project.

7.5.3 Socio-political parameters

Social acceptance: This measures the introduction of new technology into the HES. It measures the willingness of the people to adopt that technology. It is measured by the surveys, and unstructured interviews. Social acceptance may be affected by the resistance toward land acquisition, noise pollution, electromagnetic interference, and environmental concerns.

Portfolio risk: This is defined as the failure of a DG source to meet financial objectives. The investment of each component within a DG source carries its own risk, e.g., in a solar PV system, solar PV cells, converter, battery, and wiring carries its own risk that causes the failure of the system to meet the financial objectives. It must also be noticed that the failure of one DG source may affect the success of another DG source. Portfolio risk depends upon the:

- risk on individual DG source;
- weight of each DG source; and
- correlation between DG sources.

7.5.4 Environmental parameters

Emissions: In cases where a nonrenewable energy source is integrated into the HES, the emissions from that fuel must be considered since in some countries emission penalties are imposed. While calculating the COE, emission penalties are also added to the cost.

7.6 Control strategies for microgrid and hybrid energy systems

In the past, the operation of the islanded and grid-connected DG system was considered two separate entities. However, with the advancement in the DG and microgrid research, flexibility in acting as islanded and grid-connected DG system is required. The control strategies of microgrids, HESs, and distributed generation are classified into three layers: primary level control, secondary level control, and tertiary level control. Primary and secondary level controls are for the islanded operation of the microgrid, and the tertiary level control acts when the microgrid is grid-connected. Fig. 7.21 shows the control strategies of a microgrid.

7.6.1 Primary level control in microgrids

In a microgrid, multiples DG sources like wind, solar, tidal, and geothermal need to be connected in parallel to achieve high-power necessities, improved heat dissipation, and system redundancy and reliability of the DG sources. The problem that arises from the parallel operation of the inverters is power-sharing. How much power will be delivered by each of the inverters? Since in DG most of the sources are intermittent renewables, a minute change at the output voltage of the inverter causes changes in the currents of both inverters generating circulating currents. The circulating current is expressed as Eq. (7.12).

$$I_c = V_1 - \frac{V_2}{2(R + j\omega L)} = \frac{i_1 - i_2}{2} \tag{7.12}$$

It can be seen from Eq. (7.12) that a slight variation in the output voltage of the inverter causes a substantial circulating current in the system that can disturb the power-sharing of

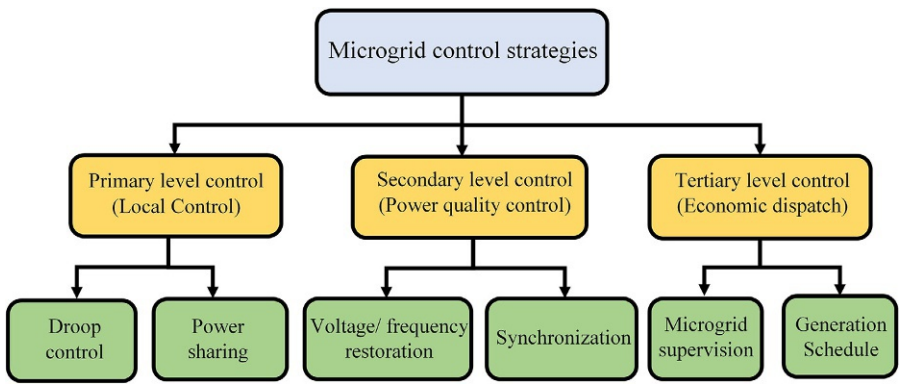

FIG. 7.21 Control strategies of a microgrid.

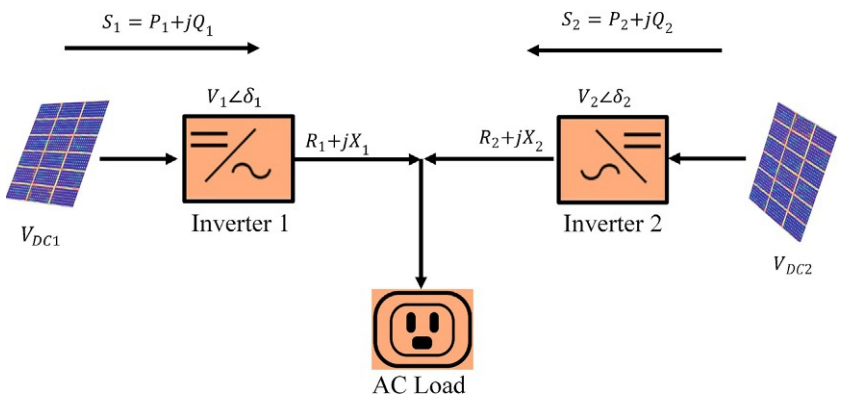

FIG. 7.22 Power flow in two parallel-connected DG sources in a hybrid energy system.

the inverters. The presence of the circulating current in the system demands a control strategy for the microgrid operation.

In conventional power generation systems, power-sharing is controlled by the droop technique. Since the inverter generates both active and reactive powers, the droop technique can be implemented to control the power-sharing in DG. The droop technique is preferred as it is a wireless technique requiring no communication between the inverters. The term "droop" is associated with the synchronous generator power balance. The rotor and the frequency are always vulnerable to variation because of the imbalance between input and output power. Similarly, a change in reactive power causes a change in voltage. Fig. 7.22 shows a simplified diagram of two DG sources operating in parallel in an MG.

The relation between active power and frequency, and reactive power and voltage is expressed by Eqs. (7.13), (7.14), respectively. The characteristics of droop control are expressed in Fig. 7.23 and a comparison of different droop control techniques is given in

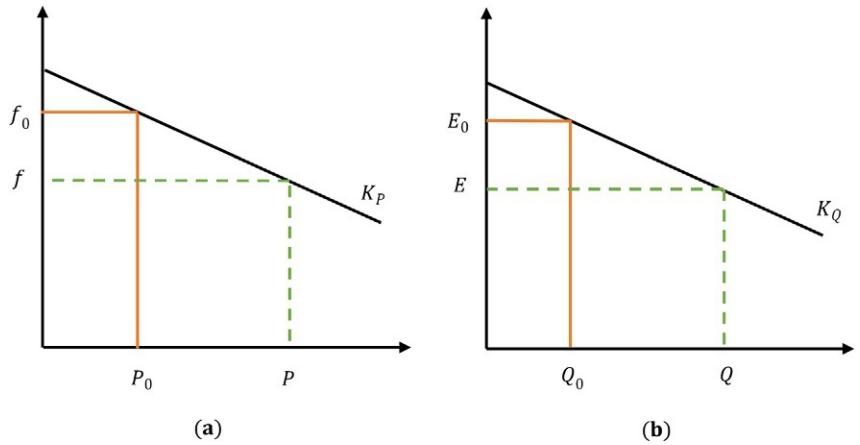

FIG. 7.23 Droop characteristics curves: (A) frequency and active power curve and (B) voltage and reactive power curve.

Table 7.2. Droop coefficients of active and reactive powers are given by Eqs. (7.15), (7.16), respectively.

$$f = f_0 + K_P(P_0 - P) \tag{7.13}$$

$$E = E_0 + K_Q(Q_0 - Q) \tag{7.14}$$

TABLE 7.2 Comparison of various droop control techniques.

	Droop control (DC) methods		Advantage	Disadvantage
Conventional methods	1	Voltage and frequency control	Easy implementation, architecture is modular and flexible	Poor power-sharing, poor reactive power control, unproductive with nonlinear loads
	2	Angle droop control	Improved stability and improved output voltage quality	Poor power-sharing, slow response, and low dynamics
	3	VBD	VBD can be used for microgrids in islanded mode and grid-connected mode	For transition between islanded mode and grid-connected mode, synchronization equipment is necessary
Droop controller with changing output impedance	1	Conventional virtual impedance method	Power transfer is accurate in on-grid and off-grid mode	Power-sharing is not accurate
	2	Adaptive virtual impedance method	Proficient in inevitably adjusting the virtual impedance	Power-sharing is not good because of errors in gain and offset
	3	Enhanced virtual impedance method	Diminishes the voltage harmonics at point of common coupling (PCC), efficient for linear and nonlinear loads	Designing virtual impedance is complex, power-sharing is not accurate
Droop controller to improve transient response	1	Improved DC	Keep the droop properties static in nature. Works well in transient conditions	While designing, approximations are made like, the effect of inductor and capacitors are neglected
	2	Adaptive DC	Works well in transient conditions, microgrid works well in islanded and grid-connected mode by automatically adjusting the grid impedance	Controller is very expensive and complex
	3	Autonomous DC	Reduces transient for large step loads, power-sharing is effective	Grid specifications are required for flexible operation in microgrid mode

TABLE 7.2 Comparison of various droop control techniques—Cont'd

	Droop control (DC) methods		Advantage	Disadvantage
Harmonic current sharing method	1	Harmonic DC	Harmonics can completely be removed by adding harmonic components to the reference inverter	Badly affect the system stability
	2	Harmonic DC for nonlinear loads	The THD in the output current is equally shared among the inverters	Badly affect the system stability
Hybrid DC	1	Conventional hybrid DC method	Contains features of wireless and wired control, best for both linear and nonlinear loads	Power quality is low, voltage regulation is asymmetrical

$$K_P = \frac{\Delta f}{P_{max}} \tag{7.15}$$

$$K_Q = \frac{\Delta E}{Q} \tag{7.16}$$

where

f_0 is the rated frequency of DG source;
K_P is the droop coefficient of active power;
P_0, Q_0 is the active and reactive power set points of the inverter;
E_0 is the rated voltages of DG source; and.
K_Q is the droop coefficient of reactive power.

7.6.2 Secondary level control in microgrids

Secondary level control of the microgrid is to ensure the reliable operation of the microgrid and HESs in both off-grid and on-grid modes. The control system monitors both the variation in voltage amplitude and the frequency deviations and makes necessary adjustments. It ensures the adjustment in frequency and voltage variation within the permissible limits as they are changed because of the changes in load and the generation plant. A secondary level control system also governs the energy management system by regulating and controlling the power flow and the power quality of the microgrid. The energy management system observes the unpredictable load variations and the intermittent renewable energy sources. If the second level control is disconnected from the primary control, the islanded operation of the microgrid, the response of the secondary control becomes slower in dynamic responses of the system parameters since a communication gap occurs. To solve this problem, a centralized control system is required that restores the voltage and frequency deviations produced by the primary control.

7.6.3 Tertiary level control in microgrids

The tertiary level control in the microgrid is to regulate the power flow at the point of common coupling (PCC), or we can say it observes the connection of the microgrid to the main

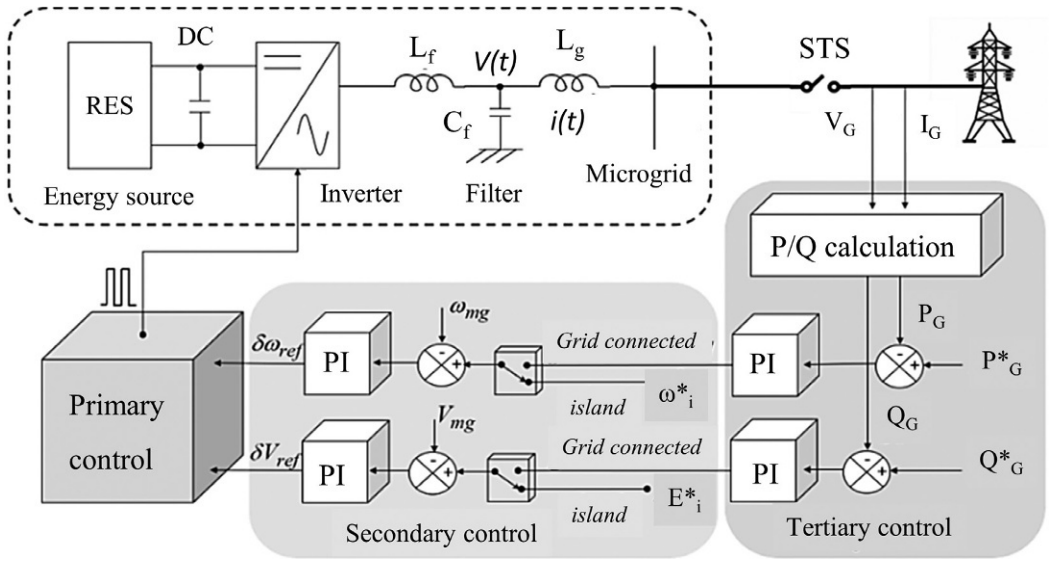

FIG. 7.24 Block diagram of secondary and tertiary level control of a grid-connected renewable energy system [24].

grid. It observes multiple microgrids connected to the system by controlling the active and reactive power, and by comparing the active and reactive powers of the grid with the reference set points. The hierarchy of a microgrid control system is shown in Fig. 7.21. At the PCC, active and reactive powers (P_G/Q_G) are measured and compared to the desired values (P^*/Q^*) to know the desired reference values (P_{ref}/Q_{ref}). A block diagram of the secondary and tertiary level control of a grid-connected RES is shown in Fig. 7.24.

7.7 Case study: Parallel connected VSCs with DG sources in islanded and grid-connected mode

A microgrid based on two DG sources, both solar photovoltaics, in this case, connected to voltage source inverters (VSIs) is shown in Fig. 7.25 that is a MATLAB simulation diagram. Two solar photovoltaic systems are connected in parallel through the inverters that feed the load as well as the grid. Each solar PV system of 255.65 kW connected as DG source in the microgrid is shown in Fig. 7.25.

Active and reactive powers are controlled by the current mode control. The active and reactive powers generated by the VSIs are expressed as Eqs. (7.17), (7.18), respectively.

$$P = \frac{3}{2}\left(V_{sd} \times i_d + V_{sq} \times i_q\right) \tag{7.17}$$

$$Q = \frac{3}{2}\left(V_{sd} \times i_d - V_{sq} \times i_q\right) \tag{7.18}$$

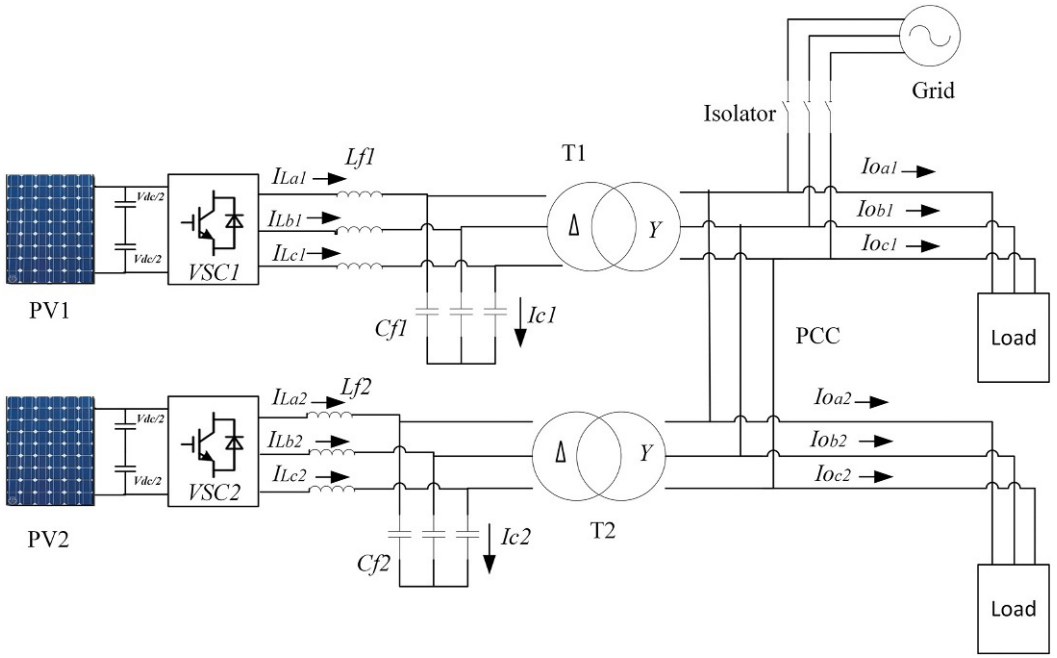

FIG. 7.25 Parallel connection of two voltage source converters.

where V_{sd} and V_{sq} are the *dq*-coordinates of the AC voltage system and i_d and i_q are the *dq*-coordinates of the AC current system.

The control diagram of the proposed VSC is shown in Fig. 7.26. Both DG sources (PV systems in this case) are connected to the input of the inverter through the DC link. The three-phase voltage and the current of the system after the inverter are converted from *abc*-AC coordinates to *dq*-AC coordinates, which is the conversion of the three-phase quantities to the synchronous rotating frame. The ABC-*dq* component takes the three phases A, B, C, and the angle as the input giving d, and q signals at the output. The active and reactive powers given in Eqs. (7.17), (7.18) are regulated by the current controller that takes the V_d, V_q, i_d, i_q and gives its output to the pulse width modulation (PWM) of the inverter. The details of each building block are discussed in the following subsections.

7.7.1 Deep neural network-based MPPT controller

A deep neural network (DNN) is proposed as a maximum power point tracker (MPPT) with a solar photovoltaic system. Voltage and current are the two inputs to the input layer. The DNN controller extracts the maximum power from the solar panel and provides the most efficient V_{dc}*. DNN controller is analogous to the conventional MPPT algorithms in which the algorithm takes the voltage and current from the solar panel as inputs and provides a duty cycle to the DC-DC converter. The proposed DNN layers are shown in Fig. 7.27.

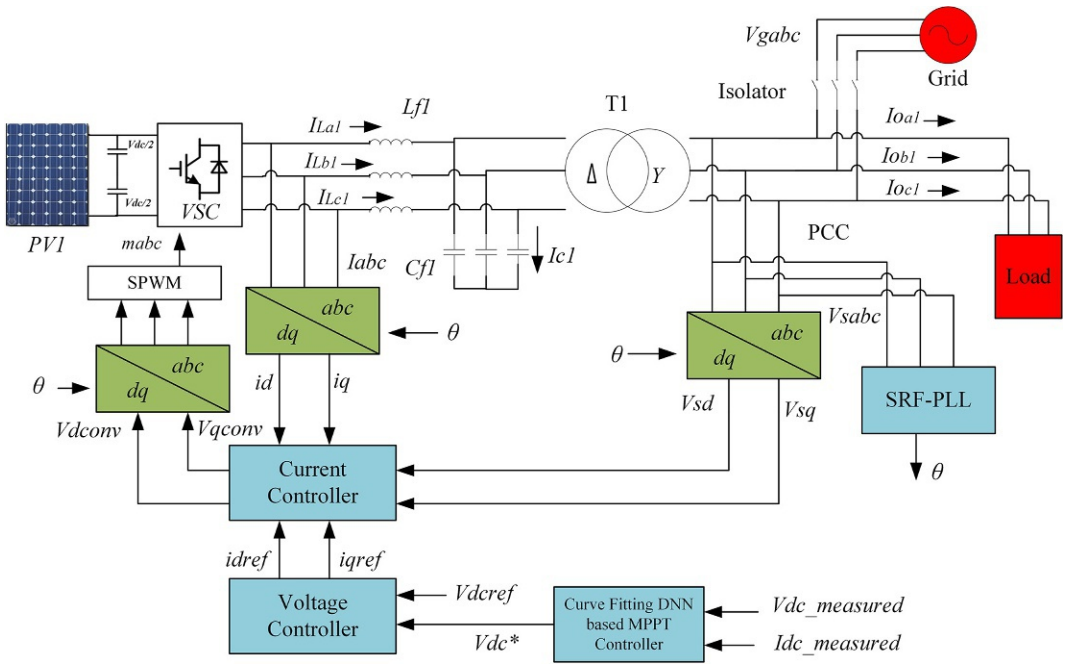

FIG. 7.26 Proposed control technique of a grid-connected photovoltaic system.

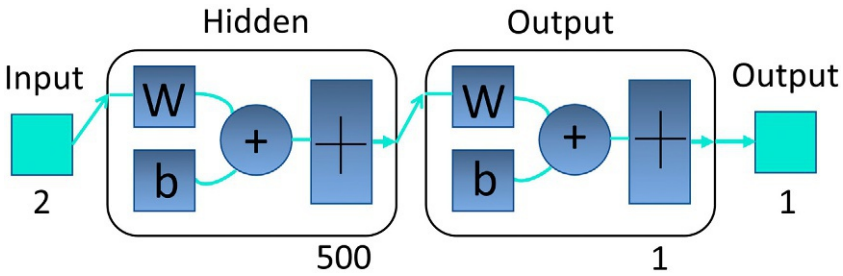

FIG. 7.27 Proposed deep neural network layers.

7.7.2 Voltage controller

A block diagram of the proposed voltage controller is shown in Fig. 7.28, and mathematically can be written as Eq. (7.19).

$$i_{d,ref} = \frac{1}{V_{nom\_dc}}\left[k_{p-Vdc} + k_{i-Vdc}\int\left(V_{dc,ref} - V_{dc^*}\right)dt\right] \tag{7.19}$$

where $k_{p-Vdc} = L/\tau_i$ is the proportional coefficient of PI controller and $k_{i-Vdc} = R/\tau_i$ is the integral coefficient of PI controller.

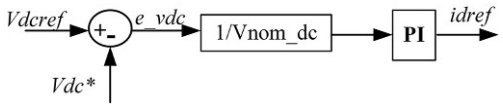

FIG. 7.28 Proposed voltage controller.

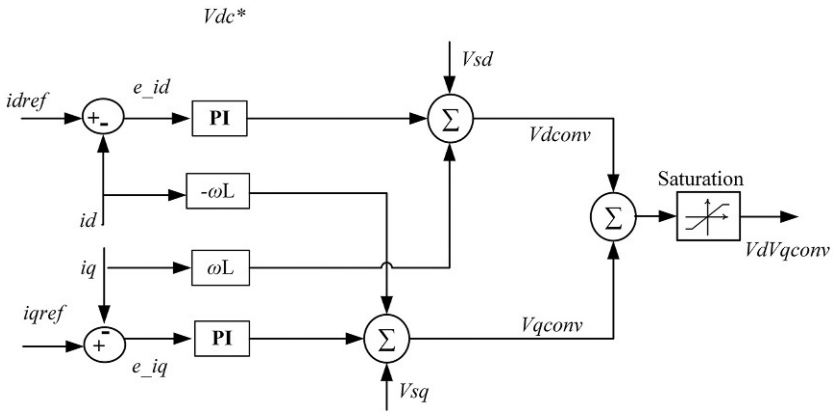

FIG. 7.29 Proposed current controller.

7.7.3 Current controller

A block diagram of the proposed current controller is shown in Fig. 7.29. The output of the voltage controller ($i_{d,\ ref}$) is given as the input to the current controller and the output of the current controller is determined by Eqs. (7.20), (7.21).

$$V_{d,conv} = k_p\left(i_{dref} - i_d\right) + ki\int\left(i_{dref} - id\right)dt \cdot -\omega LfIq + V_{sd} \tag{7.20}$$

$$V_{q,conv} = k_p\left(i_{qref} - i_q\right) + ki\int\left(i_{qref} - iq\right)dt \cdot -\omega LfIq + V_{sq} \tag{7.21}$$

where

V_{sd}, V_{sq} is the dq-coordinate of the AC voltage system;
k_p is the proportional coefficient of PI controller;
ki is the integral coefficient of PI controller;
i_{dref}, i_{qref} is the reference inputs to the current controller in dq-coordinate system; and
i_d, i_q is the dq-coordinate of the AC current system.

7.7.4 Synchronous reference frame-phase locked loop (SRF-PLL)

A phase-locked loop is used to calculate the phase angle of the grid voltage. The calculation of the phase angle contains two voltage transformations. First, the three-phase voltages V_a, V_b, and V_c are transformed into two-phase stationary systems V_α, and V_β using the Clarke transformation. A two-phase stationary system is converted into a rotating reference frame using the Park transformation. The proposed SRF-PLL is shown in Fig. 7.30.

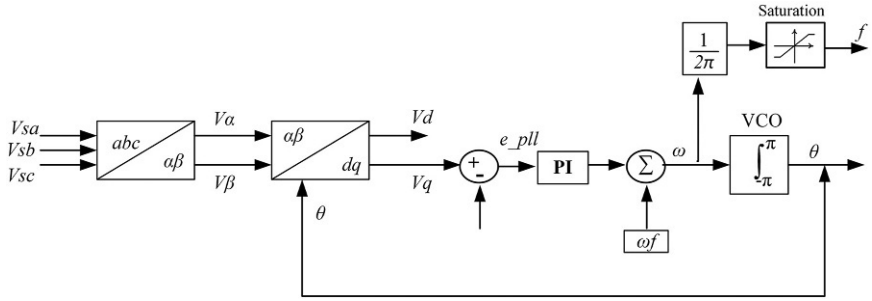

FIG. 7.30 Proposed synchronous reference frame-phase locked loop.

Eqs. (7.22), (7.23) are the transformation matrix for the Clarke transformation.

$$[V_{\alpha\beta}] = [T_{\alpha\beta}][V_{sabc}] \tag{7.22}$$

$$\begin{bmatrix} V_\alpha \\ V_\beta \end{bmatrix} = \frac{2}{3}\begin{bmatrix} 1 & \frac{-1}{2} & \frac{-1}{2} \\ 0 & \frac{-\sqrt{3}}{2} & \frac{\sqrt{3}}{2} \end{bmatrix}\begin{bmatrix} V_{sa} \\ V_{sb} \\ V_{sc} \end{bmatrix} \tag{7.23}$$

Similarly, for the second transformation, Eqs. (7.24), (7.25) are used for the Park transformation.

$$[V_{dq}] = [T_{dq}][V_{\alpha\beta}] \tag{7.24}$$

$$\begin{bmatrix} V_d \\ V_q \end{bmatrix} = \begin{bmatrix} \cos\theta & -\sin\theta \\ \sin\theta & \sin\theta \end{bmatrix}\begin{bmatrix} V_\alpha \\ V_\beta \end{bmatrix} \tag{7.25}$$

The above-proposed HES consisting of two DG sources forming a grid-connected microgrid is simulated in MATLAB, shown in Fig. 7.31. In this simulation, both DG sources are solar PV systems with their separate control systems and connected to the grid. Solar PV systems require two inputs, irradiance, and solar temperature. Solar PV systems generate DC power that is fed to the inverter. Both the inverters are connected in parallel feeding the islanded load and the grid through the PCC.

Figs. 7.32A and B and 7.33A and B show the voltages and current of inverter 1 and inverter 2, respectively, operating in parallel. The proposed microgrid works in a grid-connected mode until 0.33 s. Both the DG sources are providing smooth three-phase voltage and current. After 0.33 s, the microgrid goes into islanded mode working independently of the grid. At 0.33 s, a smooth transition from on-grid mode to off-grid mode can be seen in Figs. 7.32 and 7.33.

Similarly, as the parallel-connected DG resources through the inverter are connected to the grid at PCC, voltage and current waveforms during the transition from on-grid to off-grid mode at 0.33 s can also be seen at the PCC shown in Fig. 7.34. During the on-grid mode, the current at the PCC is shared by both inverters and the grid, whereas in off-grid mode only

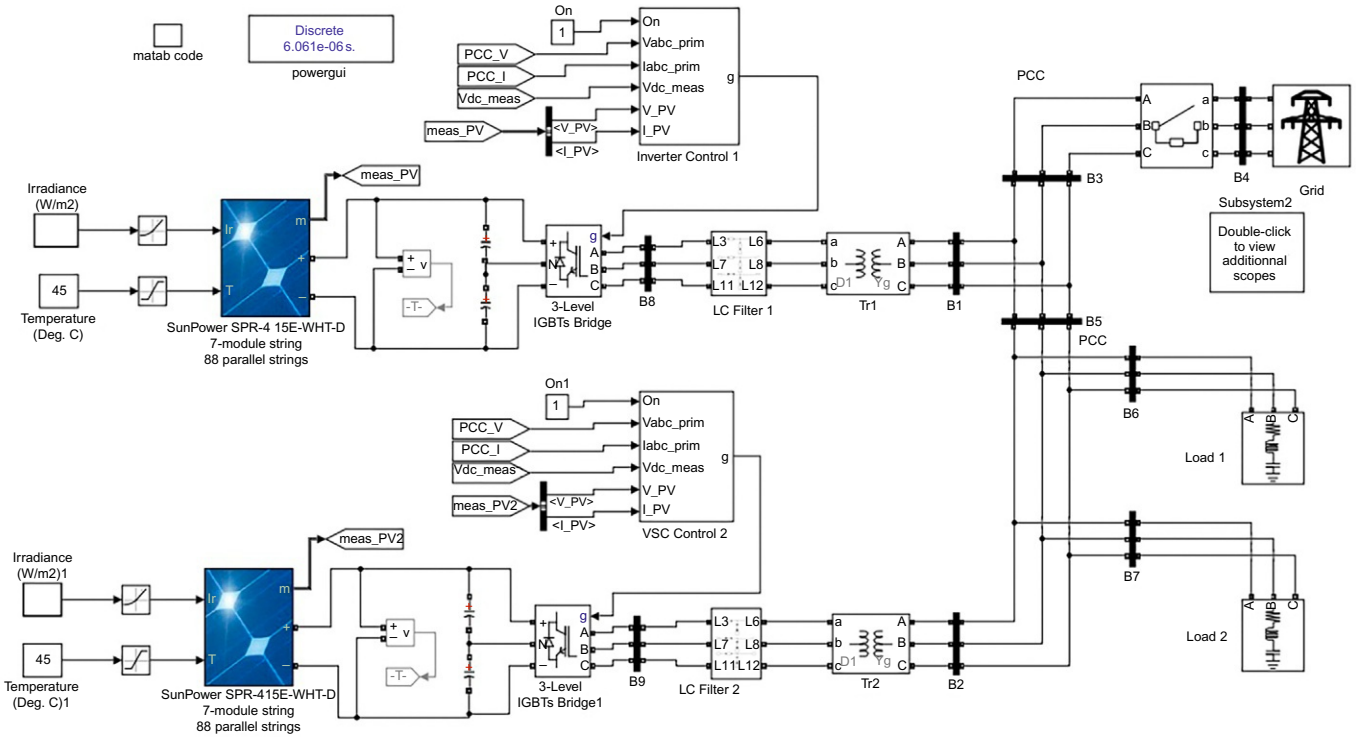

FIG. 7.31 MATLAB simulation of two grid-connected solar photovoltaics in a microgrid.

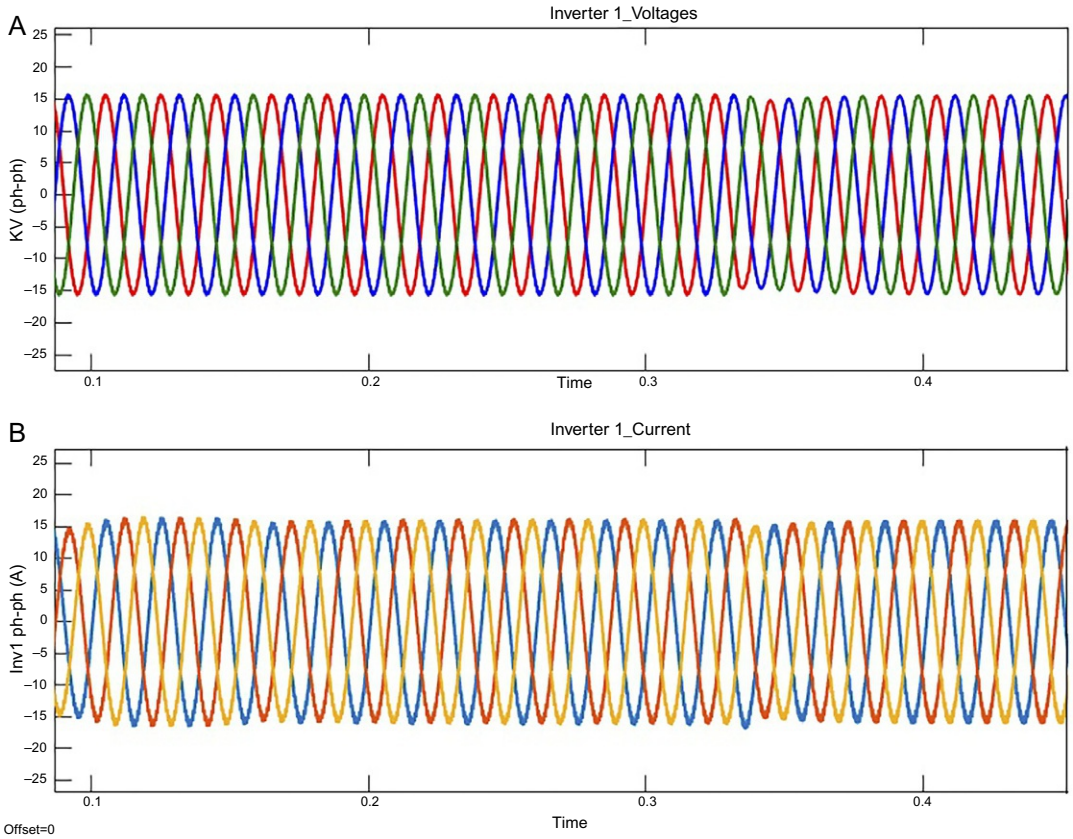

FIG. 7.32 (A) Voltage at inverter 1 and (B) current at inverter 1.

inverters share the current equally at the PCC. That is why in on-grid mode, the current at the PCC is higher than the off-grid mode as shown in Fig. 7.34B.

Figs. 7.35–7.37 show the active and reactive powers at inverter 1, inverter 2, and point of common coupling (PCC) respectively.

7.8 Grid parity

Grid parity also termed as the socket parity may be defined as a situation when the cost of electricity per kWh from the microgrid or the HES is less than the cost of the same kWh of electricity from the grid. Grid parity is not a static situation since it depends upon various factors that are always vulnerable to variation. If one factor is static for a microgrid situated at one location, it may not necessarily be static for another microgrid located at another location. Distributed generation resources, environmental cost and benefits, cost of electricity from the grid, cost of DG components and technology, and grid-related costs are the key driving factors of grid parity. All these factors are shown in Fig. 7.38.

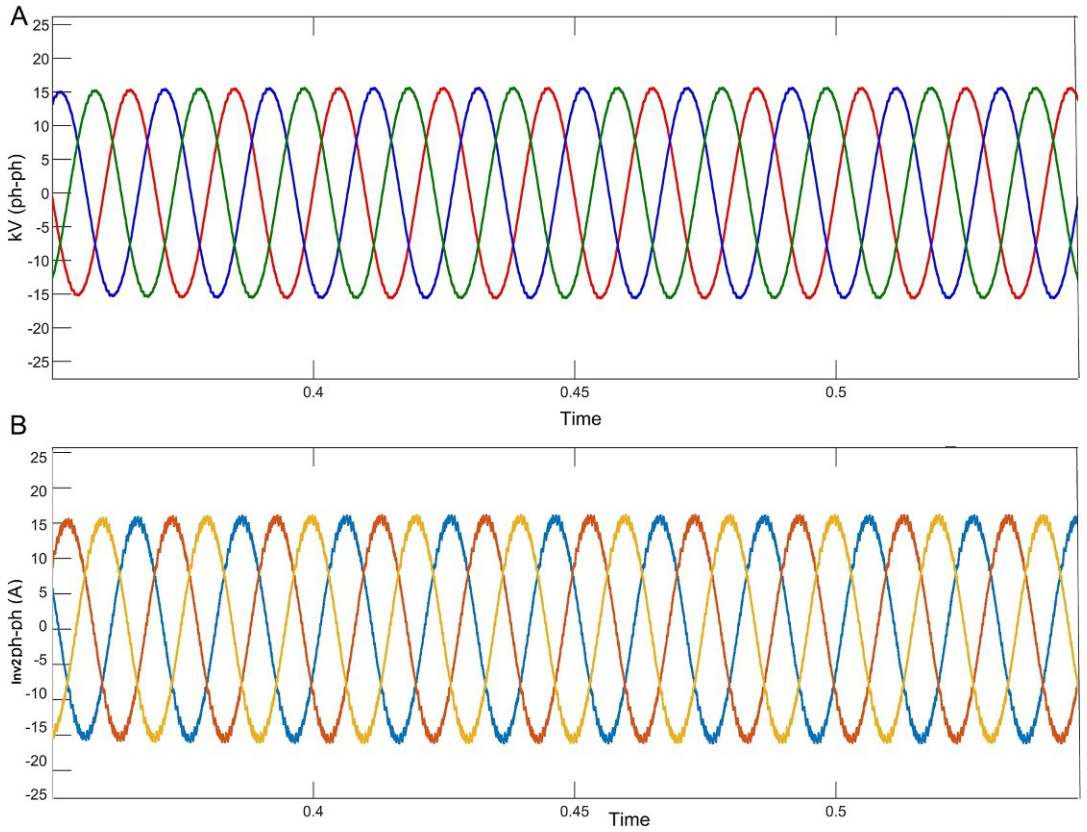

FIG. 7.33 (A) Voltage at inverter 2 and (B) current at inverter 2.

7.8.1 Resources of DG

The availability of the DG resources, either renewable or conventional, depends upon various factors. Energy from the sun varies with the variation in solar irradiance as the sun changes its position in the sky. Similarly, the increased temperature of the solar cell also degrades the performance of the cell. The availability of other renewable energy sources like wind, biomass, biogas, geothermal, and hydrogen decides the achievement of grid parity. A microgrid cannot work in a region with less availability of energy sources, and as a result grid parity for that microgrid cannot be achieved. On the other hand, a microgrid located in a region where renewable energy sources are abundantly available may achieve grid parity earlier. No resources mean no electricity to sell even at the grid price.

7.8.2 DG technologies and components

The inexpensive fuel from renewable energy sources is not enough to get cheap electricity from the microgrid and the DG. The related technology and the BoS also play a vital role in

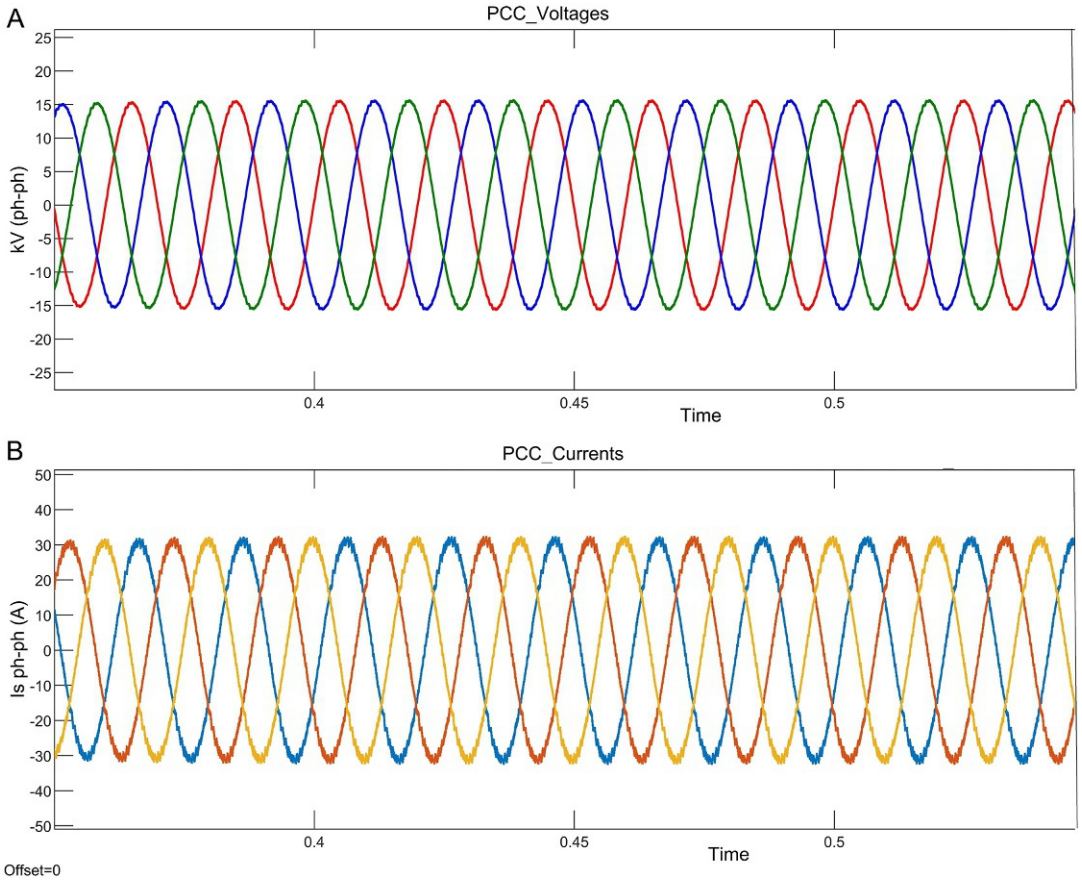

FIG. 7.34 (A) Voltage at point of common coupling and (B) current at point of common coupling.

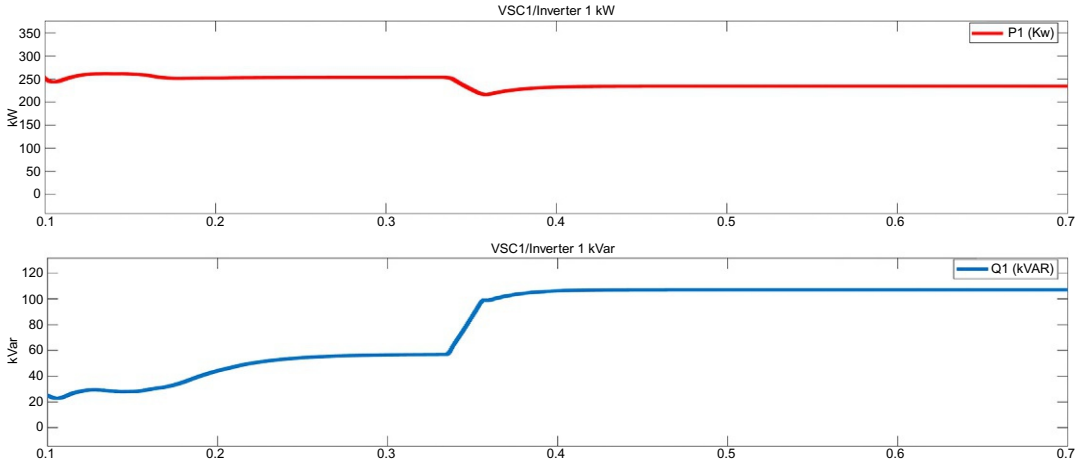

FIG. 7.35 Active and reactive powers at inverter 1.

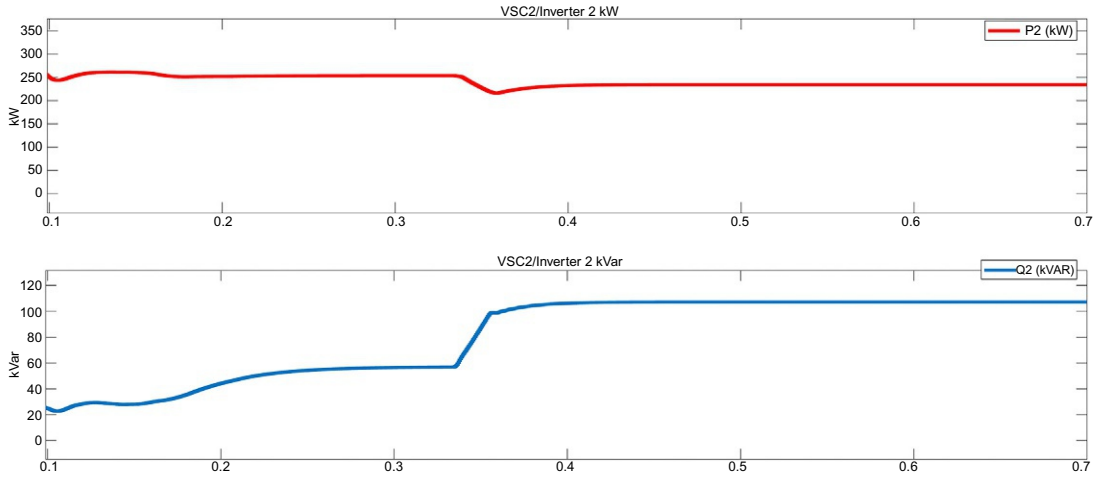

FIG. 7.36 Active and reactive powers at inverter 2.

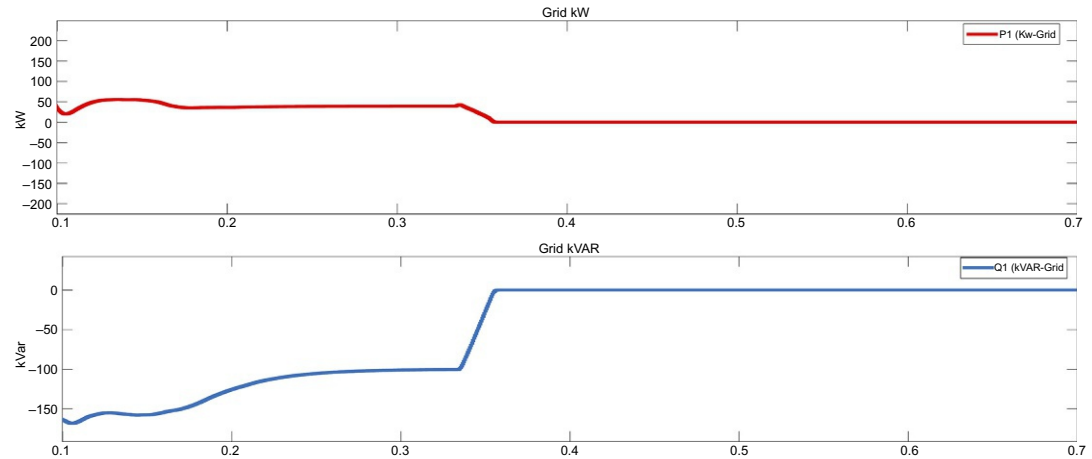

FIG. 7.37 Active and reactive powers of the grid.

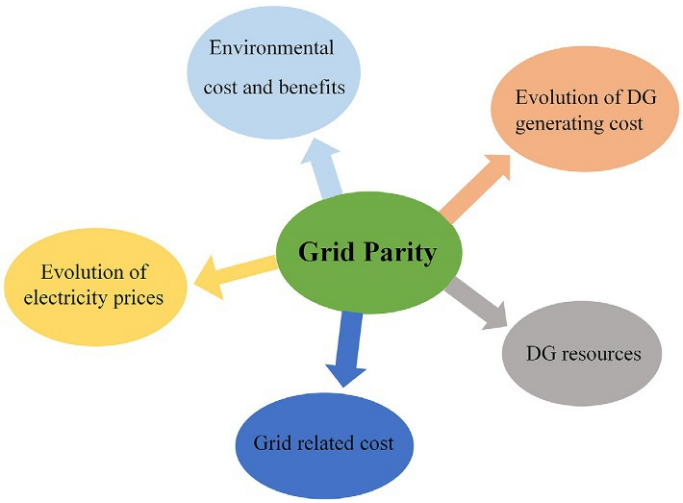

FIG. 7.38 Factors affecting the grid parity occurrence [25].

determining the cost of electricity from the microgrid. When talking about solar energy, we include the cost of solar panels of different materials, cost of the wiring, frame structure, charge controller, MPPT, solar tracker, DC-DC converters, inverters, and land acquisition. If the BoS is inefficient and expensive, grid parity will not be achieved. For biomass to biogas conversion, biomass and residues of the crops are freely available in agricultural areas, but the technology-related biogas digester, biogas collector, and other BoS must also be cheap to bring the cost of electricity down. It is also possible for the technology and BoS to be cheap in a country while in another country they are very expensive, so grid parity will occur at different times in both countries. The availability of energy sources and the availability of inexpensive technology lead to the earlier achievement of grid parity.

7.8.3 Environmental cost and benefits

Another factor that influences the occurrence of grid parity is the tax on the emissions from electricity generation. Renewable energy sources release less or no emissions compared to conventional sources of energy. Many countries are imposing carbon taxes to promote renewable energy sources and discourage fossil fuel technology. Similarly, to promote carbon-free energy sources, feed-in tariff (FiT), and renewable portfolio standards (RPS) are introduced. FiT is the extra amount per kWh paid by the government to the owner for producing electricity from renewable energy sources. RPS ensures that a specific percentage of the electricity in a utility must be generated from renewable energy sources.

7.8.4 Grid related cost

Most villages are still far away from their national grid. Connecting these areas to the grid will incur heavy transmission and distribution costs. Transmission losses will further play a role in increasing the cost of electricity. For such villages, islanded microgrids based on even a single source of energy like solar PV are the best ones to provide electricity cheaper than the grid.

7.8.5 Evolution of electricity prices

Today, electricity from the grid is generated by conventional fossil fuels (oil, gas, and coal). These nonrenewable energy sources are almost extinct. Their growing prices and the carbon taxes increase the cost of electricity. The cost of electricity from the grid is the sum of the COE, tax levies, and other charges, and transmission and distribution costs. The cost breakdown of grid electricity is shown in Fig. 7.39. To compete with the grid electricity, smart microgrids and distributed generation play a role because they avoid heavy taxes, transmission cost, and expensive fuel cost.

7.9 Optimization of hybrid energy systems in RETScreen

In the earlier sections of this chapter, all the renewable energy technologies, renewable energy sources, DG technologies and sources, HESs in a microgrid have been discussed. The

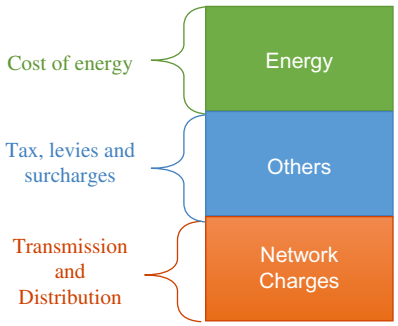

FIG. 7.39 Cost distribution of electricity prices [25].

next step is to perform the optimization analysis on the proposed system. The economic optimization of the proposed HES is done in RETScreen Expert software or the HOMER software. We perform optimization analysis on a proposed HES in both RETScreen Expert and HOMER. RETScreen presents a comparison between a base case and the proposed case. The base case is considered a conventional power plant whereas the proposed case is the clean energy project. For example, in a base case, a conventional fossil fuel-based grid-connected project is generating 1000 MWh in a year. RETScreen compares this to the on-grid wind energy farm generating 1000 MWh in a year. The COE will not be the same from both the sources; however, the initial capital cost of the wind farm will be higher than the conventional one. RETScreen performs the cost analysis and results that whether the balance of cost and savings will be viable for the complete life of the project. In emission analysis, RETScreen also determines the reduction in GHG as we move from the base case to the proposed system.

7.9.1 Step 1—Location and facility

RETScreen adopts a six-step standard project analysis. The first step is the location and facility of the project. RETScreen seeks the coordinates of the location where the project is intended. We provided the coordinates of Riphah International University (31.4°N, 73.1° E), Faisalabad campus. RETScreen showed the location on the map and imported the weather data (air temperature, relative humidity, precipitation, daily horizontal solar irradiance, atmospheric pressure, wind speed, earth temperature, heating degree days, and cooling degree days) for this location from the NASA website shown in Fig. 7.40. The wind speed was measured at the 10 m anemometer height. In this step, RETScreen also shows the benchmarking of energy production costs of other energy sources and grid-connected technologies. Fig. 7.41 shows the benchmarking of other energy sources and related technologies:

- Gas turbine-natural gas
- Gas turbine-combine cycle-natural gas
- Hydro turbine
- Solar photovoltaics
- Solar photovoltaics-tracking system
- Reciprocating engine-diesel
- Reciprocating engine-natural gas

	Unit	Climate data location	Facility location	Source
Latitude		31.4	31.4	
Longitude		73.1	73.1	
Climate zone		0B - Extremely hot - Dry		NASA
Elevation	m	181	187	NASA – Map
Heating design temperature	°C	5.2		NASA
Cooling design temperature	°C	38.6		NASA
Earth temperature amplitude	°C	25.8		NASA

Month	Air temperature	Relative humidity	Precipitation	Daily solar radiation - horizontal	Atmospheric pressure	Wind speed	Earth temperature	Heating degree-days 18 °C	Cooling degree-days 18 °C
	°C	%	mm	kWh/m²/d	kPa	m/s	°C	°C-d	°C-d
January	13.0	37.5%	1085	3.25	99.6	2.2	11.7	155	96
February	15.9	37.3%	22.40	4.19	99.4	2.4	15.2	59	165
March	22.2	31.0%	19.22	5.10	99.0	2.5	22.1	0	378
April	28.8	23.7%	14.70	6.01	98.6	2.6	29.5	0	564
May	35.0	17.2%	12.09	6.71	98.0	2.8	36.7	0	775
June	38.0	23.6%	34.80	6.65	97.6	2.9	40.5	0	840
July	36.4	39.8%	86.80	5.99	97.6	2.8	38.7	0	818
August	34.7	45.0%	70.68	5.60	97.8	2.5	36.5	0	766
September	32.2	38.5%	37.50	5.37	98.3	2.2	33.4	0	666
October	26.9	26.2%	7.13	4.65	98.9	2.0	26.6	0	524
November	20.6	24.5%	3.90	3.73	99.4	2.1	19.3	0	318
December	15.1	31.3%	9.92	3.14	99.6	2.1	13.5	90	158
Annual	**26.6**	**31.3%**	**329.99**	**5.03**	**98.6**	**2.4**	**27.0**	**304**	**6,066**
Source	NASA	NASA	NASA	NASA	NASA	NASA	NASA	NASA	NASA
Measured at					m	10	0		

FIG. 7.40 Weather data of the proposed location in RETScreen imported from NASA.

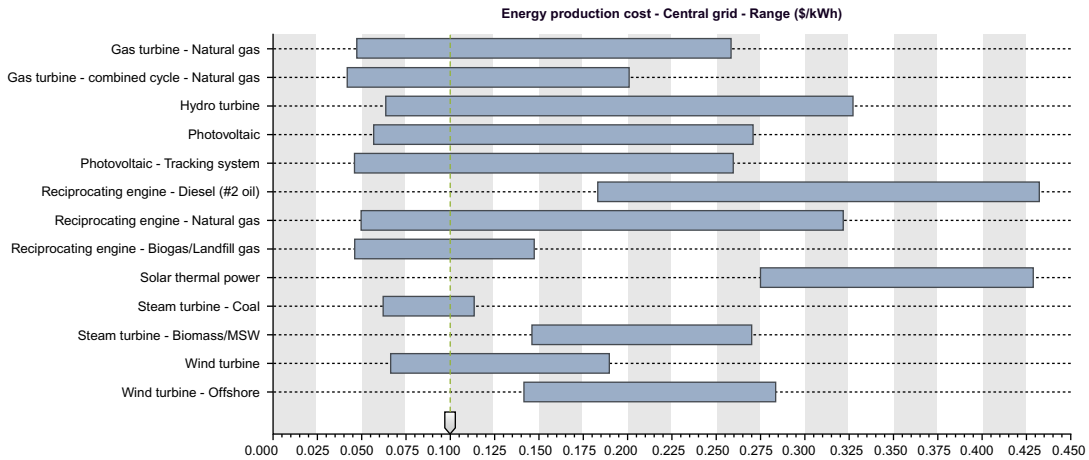

FIG. 7.41 Energy production cost from various energy sources.

- Reciprocating engine-biogas/landfill gas
- Solar thermal power
- Steam turbine-coal
- Steam turbine-biomass/MSW
- Wind turbine
- Wind turbine-offshore

7.9.2 Step 2—Energy model

In this tab, the energy sources and the related technology for the base case and the proposed case are selected. Technologies in the power system subsystem are gas turbine-natural gas, gas turbine-combine cycle-natural gas, hydro turbine, solar photovoltaics, solar photovoltaics-tracking system, reciprocating engine-diesel, reciprocating engine-natural gas, reciprocating engine-biogas/landfill gas, solar thermal power, steam turbine-coal, steam turbine-biomass/MSW, wind turbine, wind turbine-offshore, fuel cell, geothermal power, tidal power, wave power, and ocean current power. Corn silage and beef cattle were selected as the biogas sources. RETScreen has other biomass sources for biogas production like algae, apple pomace, bakery waste, brewer's grains, cow-paunch manure, dairy cattle, dissolved air flotation sludge, distiller's grain, fodder beet, forage leaves, fruit and vegetable waste, fruit wash water, grape pomace, grass silage, lawn clippings, meat trimmings, molasses, municipal solid waste, and pig manure. Figs. 7.42 and 7.43 show the properties of the biogas and landfill gas, respectively. RETScreen also gives the ultimate analysis of each of the biomass sources.

7.9.2.1 Wind energy model

Wind speed distribution: RETScreen in the energy model presents the technologies and their resources. Fig. 7.44 shows the wind resource assessment, wind turbine specifications, losses, and the cost summary. The figure shows that annual wind speed is 4.4 m/s at 10 m hub height; it also shows the number of turbines used, swept area of the turbine, diameter of the rotor of the wind turbine, and the hub height. Fig. 7.45 shows the power and energy curve of the wind turbine concerning wind speed. While determining the wind energy potential at the specific site and time, it is key to calculate the wind speed distribution first. RETScreen uses the Weibull distribution function to calculate the wind power density. The Weibull probability density function is given by Eq. (7.26).

Biogas

Unit	Average weight per unit (kg)	Quantity	Dry matter %	Dry matter-volatile solids %	Biogas production factor m^3/kg	Biogas production - annual m^3	Methane content % Volume
Corn silage	1,000	900,000	27.5%	90.0%	0.58	128,081,250	53%
Beef cattle	400	300,000	9.3%	100.0%	0.86	292,751,553	58%
Total		1,200,000				420,832,803	56.3%

FIG. 7.42 Biogas characteristics in RETScreen.

- Landfill gas

Landfill								
Year landfill opened	yr	1970						
Final year landfill used	yr	2030						
Waste disposal benchmark years	yr	1970	1980	1990	2000	2005	2030	+
Waste disposal rate	t/yr	250,000	1,000,000	2,250,000	2,500,000	2,500,000	2,500,000	
Total waste in landfill (61 yrs)	t	110,362,500	−	−	−	−		

FIG. 7.43 Landfill gas characteristics in RETScreen.

Wind - Level 2

Resource assessment

Resource method		Wind speed
Wind speed - annual	m/s	4.4175
Measured at	m	10
Wind shear exponent		0.14
Air temperature - annual	°C	26.6178
Atmospheric pressure - annual	kPa	98.6429

Wind turbine

Power capacity per turbine	kW	10
Manufacturer		
Model		
Number of turbines		1
Power capacity	kW	10
Hub height	m	25
Rotor diameter per turbine	m	8
Swept area per turbine	m²	50
Energy curve data		Standard
Shape factor		2

Losses

Array losses	%	0%
Airfoil losses	%	2%
Miscellaneous losses	%	6%
Availability	%	98%

Summary

Capacity factor	%	11.3%
Initial costs	$/kW	6,800
	$	68,000
O&M costs (savings)	$/kW-year	70
	$	700
Electricity export rate		Electricity export rate - annual
	$/kWh	0.10
Electricity exported to grid	MWh	9.9
Electricity export revenue	$	992

Other information

		Per turbine
Unadjusted energy production	MWh	11.7
Pressure coefficient		0.974
Temperature coefficient		0.961
Gross energy production	MWh	11
Losses coefficient		0.9
Specific yield	kWh/m²	198

FIG. 7.44 Various parameters of wind energy model.

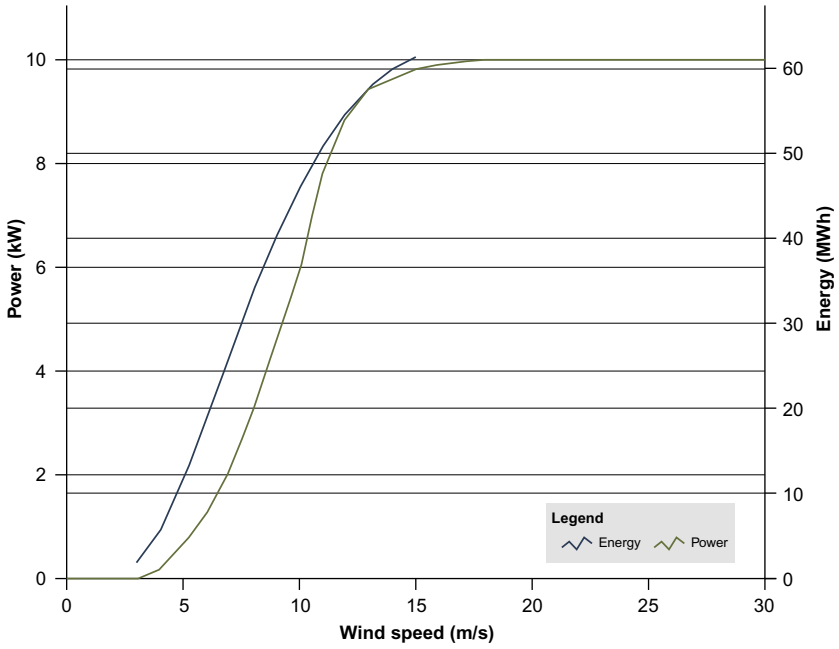

FIG. 7.45 Wind energy and wind power curve with regard to wind speed.

$$\rho(x) = \left(\frac{k}{C}\right)\left(\frac{x}{C}\right)^{k-1} \exp\left[-\left(\frac{x}{C}\right)^{k}\right] \tag{7.26}$$

where "k" is the shape factor which is given by the user, x is the wind speed, and C is the scale factor which is calculated by Eq. (7.27). The shape factor and the wind speed distribution are inversely proportional. The lower shape factor indicates a high energy production at a given wind speed.

$$C = \frac{\overline{x}}{\Gamma\left(1 + \frac{1}{k}\right)} \tag{7.27}$$

where Γ is the gamma function and $\overline{x}$ is the average wind speed. In some cases, wind distribution density is calculated by the wind power density rather than the wind speed by Eq. (7.28).

$$\text{WPD} = \sum_{x=0}^{25} \frac{1}{2}\rho x^3 P(x) \tag{7.28}$$

where ρ is the density of the air, and $P(x)$ is the probability of wind speed x.

Unadjusted energy production: Energy produced by the turbines at standard test conditions (STCs) of temperature and pressure is called unadjusted energy production. Wind speed at the hub height and the anemometer height are different because of the wind shear. The wind energy model uses Eq. (7.29) to adjust the height factor. The wind energy model used in RETScreen is shown in Fig. 7.46.

$$\frac{\overline{V}}{\overline{V}_o} = \left(\frac{H}{H_o}\right)^{\alpha} \tag{7.29}$$

where

H is the hub height;
H_o is the anemometer height;
$\overline{V}$ is the average wind speed at hub height H;
$\overline{V}_o$ is the average wind speed at the anemometer height H_o; and
α is the wind shear exponent.

Wind plant capacity factor: The plant capacity factor (PCF) of wind is defined as the ratio of the plant's average power produced to its rated power capacity over a year given in Eq. (7.30).

$$\text{PCF} = \left(\frac{E_c}{WPC \times h_Y}\right) \tag{7.30}$$

where

E_c is the renewable energy collected, expressed in kWh;
WPC is the wind plant capacity, expressed in kW; and
h_Y is the number of hours in a year.

7.9.2.2 The solar photovoltaic energy model

The solar photovoltaic energy model is shown in Fig. 7.47. The end of the model is the calculation of the total energy production. The energy model starts from the calculation of the

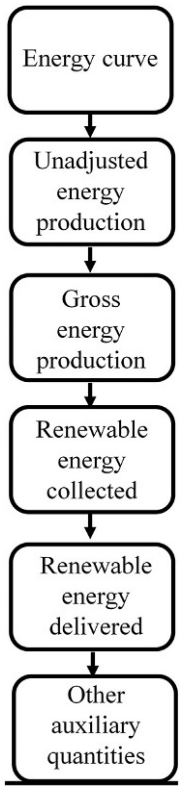

FIG. 7.46 Wind energy model in RETScreen.

solar irradiance on the PV array. Hourly global and diffused irradiance are calculated. The irradiance calculated for each hour is summed up to take the daily solar irradiance. After calculating solar irradiance on the PV array, PV modeling is used to measure the energy delivered by the PV array. In the on-grid energy model, the energy that is available to the grid is the energy delivered by the PV array minus the energy lost in the inverter, whereas in the off-grid model of energy, the energy demand that is being met by the PV array is measured, then the rest of the demand that is being met by the battery is determined. At last, if the energy demand is not completely met by the PV array and the battery, a hybrid system comes into play using the Genset to meet the load demand. In both cases, the efficiency of the charge controller, battery efficiency, Genset efficiency, and charger efficiency are also considered to measure the correct energy delivered by the HES.

7.9.2.3 Hydro energy model

A flowchart of the hydro energy model is shown in Fig. 7.48 that starts from the estimation of the flow rate at the specific location where the project is to be intended. For this purpose, a flow duration curve is drawn that gives the percentage exceedance of the flow rate. Depending upon the type of turbine used its efficiency curve is drawn. The available power at the potential head is determined by Eq. (7.31).

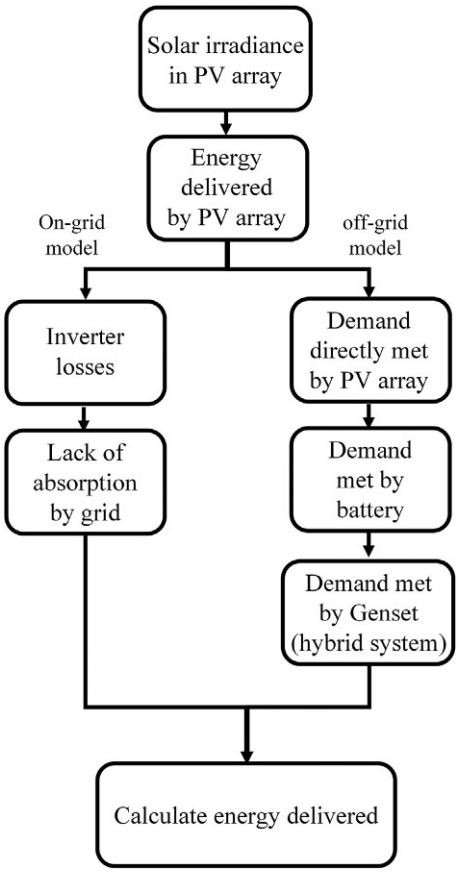

FIG. 7.47 PV energy model in RETScreen.

$$P_{t,hyd} = \rho\, g\, Q\, H_g \tag{7.31}$$

Using Eq. (7.32), plant capacity is determined at the designed flow rate, net heat and incorporating the efficiency of the generator coupled turbine.

$$P_{electrical} = \rho\, g\, Q_{desgned}\, H_n\, \eta \tag{7.32}$$

where

$P_{elect.}$ is the electrical power generated;
$P_{t,\ hyd}$ is the theoretically available hydropower;
ρ is the water density;
g is the gravitational acceleration;
Q is the flow rate;
H_g is the gross head without deducting head losses;
H_n is the net head after deducting head losses from the gross head; and
η is the efficiency of the turbine and electrical generator.

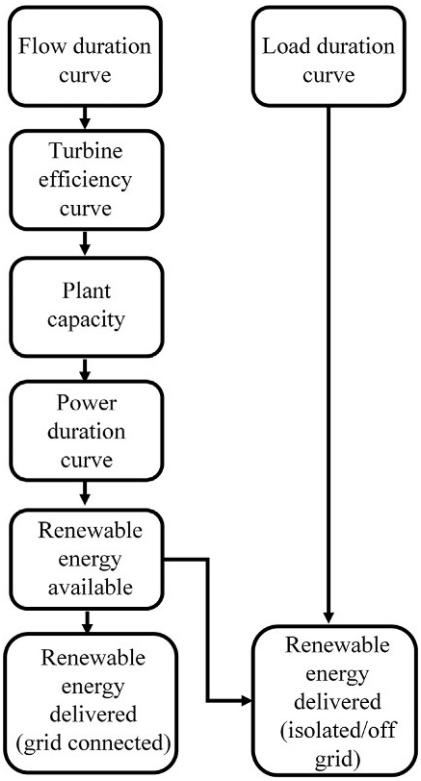

FIG. 7.48 Hydro energy model in RETScreen.

The availability of the designed flow rate throughout the year is determined from the flow duration curve. The power curve is drawn by calculating the power at different flow rates using Eq. (7.32). After calculating the flow duration curve and the power curve for a specific location, renewable energy produced is found in both the off-grid mode and the grid-connected mode.

7.9.3 Step 3—Cost analysis

The cost analysis tab contains annual, initial, and periodic costs of the proposed HES. It also contains any cost reduction credits from the base case such as carbon credits, etc. The costs depend upon the user. For a prefeasibility analysis, less accurate and less detailed costs are enough whereas, for feasibility analysis, accurate and detailed figures are required. Figs. 7.49 and 7.50 show the initial cost and annual cost of the DG technologies, respectively, used in the proposed HES.

RETScreen - Cost Analysis

Initial costs (credits)	Unit	Quantity	Unit cost	Amount
Initial cost			$	301,000
Show data				
Power system				
Gas turbine - 10 kW			$ 35,000	Update cost
Photovoltaic - 10 kW			$ 27,000	Update cost
Photovoltaic - 10 kW - Tracking system			$ 35,000	Update cost
Reciprocating engine - 10 kW - Biogas			$ 68,000	Update cost
Reciprocating engine - 10 kW - Landfill gas			$ 68,000	Update cost
Wind turbine - 10 kW (4.4m/s @10m)			$ 68,000	Update cost
User-defined	cost			$ -
Total initial costs				**$ 301,000**

FIG. 7.49 Initial cost summary of the proposed hybrid energy project.

Annual costs (credits)	Unit	Quantity	Unit cost	Amount
O&M costs (savings)	project		$	12,500
Show data				
Power system				
Gas turbine - 10 kW			$ 2,660	Update cost
Photovoltaic - 10 kW			$ 330	Update cost
Photovoltaic - 10 kW - Tracking system			$ 410	Update cost
Reciprocating engine - 10 kW - Biogas			$ 4,200	Update cost
Reciprocating engine - 10 kW - Landfill gas			$ 4,200	Update cost
Wind turbine - 10 kW (4.4m/s @10m)			$ 700	Update cost
Fuel cost - proposed case			$	10,880
User-defined	cost		$	-
Total annual costs			**$**	**23,380**

FIG. 7.50 Annual cost summary of the proposed hybrid energy project.

7.9.4 Step 4—Greenhouse gas emissions analysis

The emission tab performs the GHG emission reduction analysis by comparing the emissions from the proposed energy model to the base case system. In the proposed energy model, GHG emissions from the base case are 4,550,028.7 tCO_2 whereas from the proposed energy model it is merely 6348 tCO_2, which is a 100% reduction in GHG emissions. Fig. 7.51 shows the base case emissions in black bar whereas green bar indicates the GHG emission reduction by the proposed energy model. RETScreen uses Eq. (7.33) to calculate the reduction in GHG emissions.

$$\Delta_{GHG} = \left(e_{base} - e_{prop}\right) E_{prop} \left(1 - \lambda_{prop}\right) \left(1 - e_{cr}\right) \tag{7.33}$$

where

e_{base} is the base-case GHG emission factor;
e_{prop} is the proposed-case GHG emission factor;
E_{prop} is the electricity produced from the proposed case annually;
λ_{prop} is the transmission and distribution losses; and

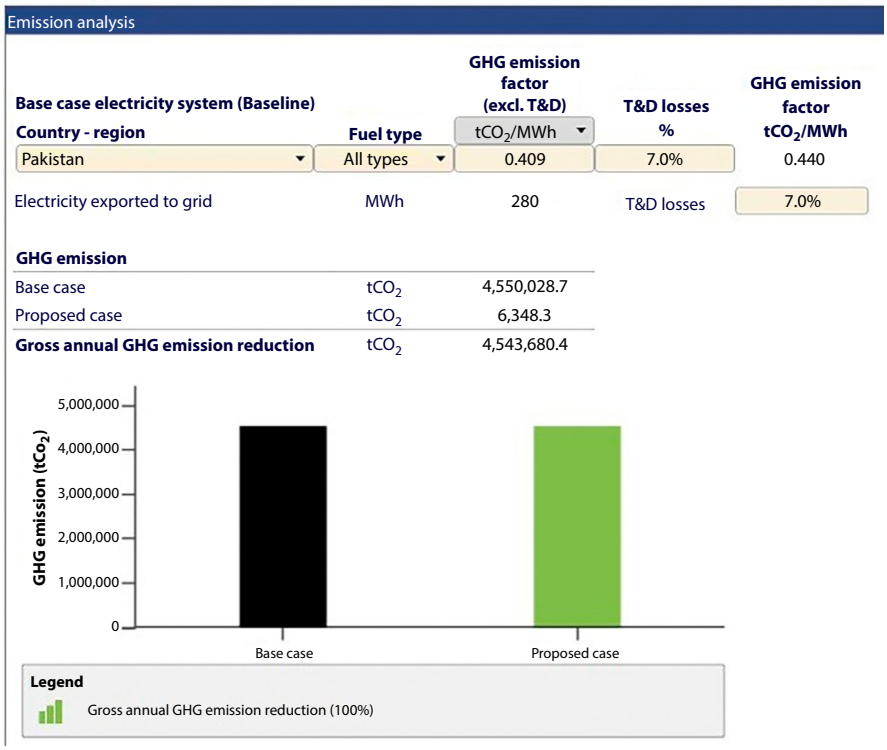

FIG. 7.51 Emission analysis of the proposed hybrid energy project.

e_{cr} is the GHG emission reduction transaction fee.

In the case of a distributed generation or the on-site generation system, transmission and distribution losses are zero.

The GHG emission factor from the base case (e_{base}) present in Eq. (7.33) is determined by using Eq. (7.34), and this equation is used for a single energy source. For a DG or a HES consisting of multiple sources, e_{base} is calculated for each source using Eq. (7.34).

$$e_{base} = (e_{CH_4} \times GWP_{CH_4} + e_{CO_2} \times GWP_{CO_2} + e_{N_2o} \times GWP_{N_2o}) \frac{1}{\eta} \times \frac{1}{1-\lambda} \tag{7.34}$$

where

e_{CH_4} is the CH_4 emission factor for the source used;
GWP_{CH_4} is the global warming potential for CH_4;
e_{CO_2} is the CO_2 emission factor for the source used;
GWP_{CO_2} is the global warming potential for CO_2;
e_{N_2o} is the N_2o emission factor for the source used;
GWP_{N_2o} is the global warming potential for N_2o;
η is the fuel conversion efficiency; and
λ is the transmission and distribution losses.

7.9.5 Step 5—Financial analysis model

The finance tab of the RETScreen consists of multiple input parameters such as fuel escalation rate, inflation rate, discount rate, reinvestment rate, and the project lifetime. After performing various calculations detailed below, it shows various financial indicators such as revenue from electricity sale to grid, GHG reduction revenue, annual cost, sales, and revenues. It also calculates some viability of the project measuring parameters such as internal rate of return (IRR), marginal internal rate of return, simple payback, equity payback, NPV, annual life cycle savings, GHG reduction cost, and energy production cost.

Debt payment is a constant and regular payment until a fixed number of years and is calculated by the formula given in Eq. (7.35).

$$D = Cf_d\left(\frac{i_d}{1-(1+i_d)^{-N}}\right) \tag{7.35}$$

where

C is the initial cost of the project;

f_d is the debt ratio;

i_d is the annual effective debt interest rate; and.

N is the number of payment periods in years.

NPV is the difference between the cash inflows and the cash outflows over a while and is calculated by Eq. (7.36), it is the discounted value of net cash inflows and outflows. Fig. 7.52 shows the cumulative cash flows over the lifetime of the project.

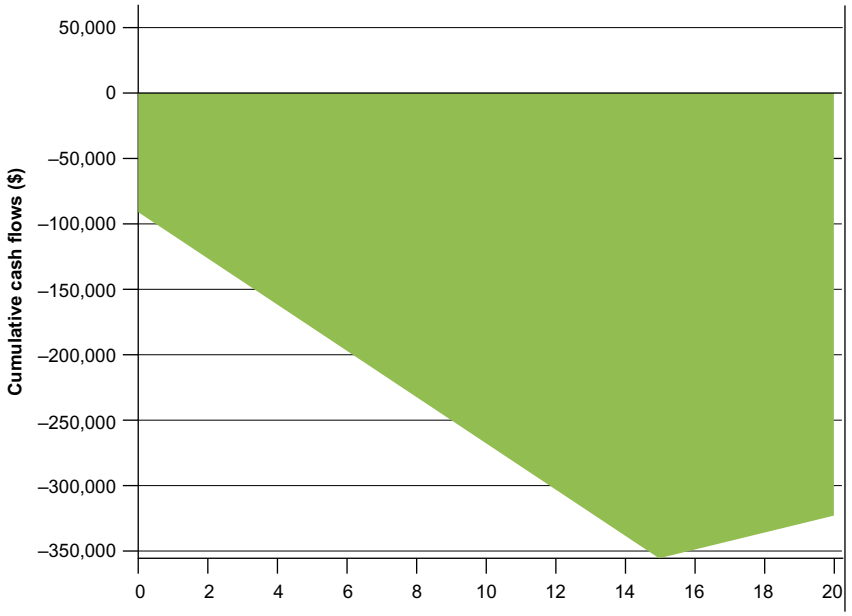

FIG. 7.52 Cumulative cash flow for the lifetime of the project.

$$NPV = \frac{R_t}{(1+i)^t} \tag{7.36}$$

where

R_t is the net cash flows over a time;

i is the discount rate; and

t is the cash flow time period.

Internal rate of return (IRR) is the discount rate because of which the NPV of the project becomes zero. IRR is calculated by Eq. (7.37).

$$0 = NPV = \frac{R_t}{(1+IRR)^t} \tag{7.37}$$

7.9.6 Step 6—Sensitivity and risk analysis

This tab of the RETScreen software consists of two functions: sensitivity analysis and risk analysis. These give information about the relation between input parameters (financial and technical parameters) and output indicators (financial indicators). Financial and technical parameters include avoided COE, fuel cost-proposed case, fuel cost-base case, renewable energy delivered, initial cost, annual operation and maintenance cost, debt ratio, debt interest rate, debt term, GHG reduction credits, renewable energy production credit, and electricity export rate. Financial indicators are IRR and return on investment (ROI), IRR-equity, IRR-assets, equity payback, and NPV. Sensitivity analysis assesses how the variation in the project model alters the output of the project. Sensitivity analysis of the proposed HES is shown in Fig. 7.53.

The impact of each input financial and technical parameter on the output financial indicator is studied by the standardized multiple linear regression. The input parameters are represented by X, an independent parameter, whereas the output financial indicators are represented by the dependent variable Y.

X_1 avoided cost of energy
X_2 renewable energy delivered
X_3 initial cost
X_4 annual operation and maintenance cost
X_5 debt ratio
X_6 debt interest rate
X_7 debt term
X_8 GHG reduction credits
X_9 renewable energy production credit

The multiple linear regression model can be written as Eq. (7.38).

$$Y = \sum_{K=1}^{n} \beta_K X_K + \varepsilon \tag{7.38}$$

where β_K is the coefficient of each value of X which is determined by Eq. (7.39). For 100 values of X, there will be 100 values of Y.

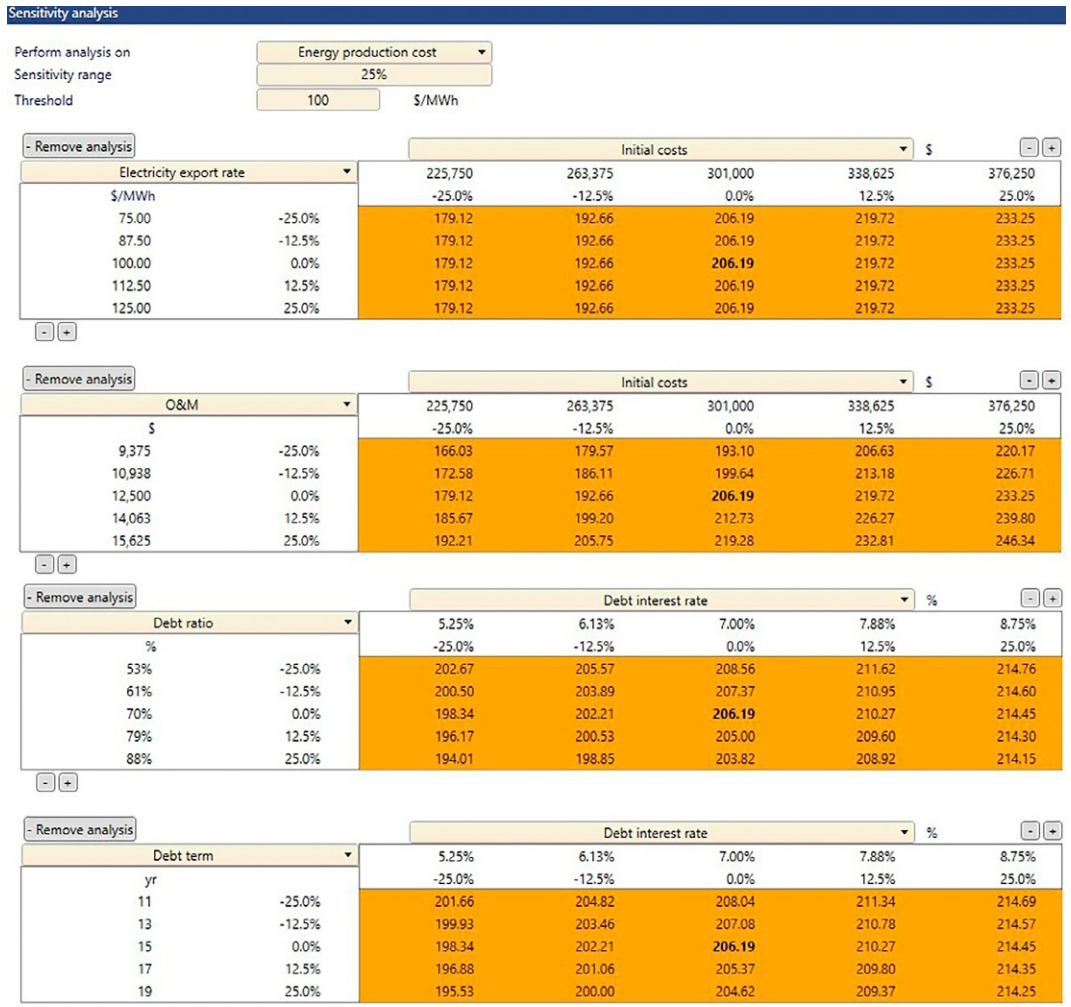

Sensitivity analysis

Perform analysis on: Energy production cost
Sensitivity range: 25%
Threshold: 100 $/MWh

- Remove analysis | Initial costs | $

Electricity export rate		225,750	263,375	301,000	338,625	376,250
$/MWh		-25.0%	-12.5%	0.0%	12.5%	25.0%
75.00	-25.0%	179.12	192.66	206.19	219.72	233.25
87.50	-12.5%	179.12	192.66	206.19	219.72	233.25
100.00	0.0%	179.12	192.66	**206.19**	219.72	233.25
112.50	12.5%	179.12	192.66	206.19	219.72	233.25
125.00	25.0%	179.12	192.66	206.19	219.72	233.25

- Remove analysis | Initial costs | $

O&M		225,750	263,375	301,000	338,625	376,250
$		-25.0%	-12.5%	0.0%	12.5%	25.0%
9,375	-25.0%	166.03	179.57	193.10	206.63	220.17
10,938	-12.5%	172.58	186.11	199.64	213.18	226.71
12,500	0.0%	179.12	192.66	**206.19**	219.72	233.25
14,063	12.5%	185.67	199.20	212.73	226.27	239.80
15,625	25.0%	192.21	205.75	219.28	232.81	246.34

- Remove analysis | Debt interest rate | %

Debt ratio		5.25%	6.13%	7.00%	7.88%	8.75%
%		-25.0%	-12.5%	0.0%	12.5%	25.0%
53%	-25.0%	202.67	205.57	208.56	211.62	214.76
61%	-12.5%	200.50	203.89	207.37	210.95	214.60
70%	0.0%	198.34	202.21	**206.19**	210.27	214.45
79%	12.5%	196.17	200.53	205.00	209.60	214.30
88%	25.0%	194.01	198.85	203.82	208.92	214.15

- Remove analysis | Debt interest rate | %

Debt term		5.25%	6.13%	7.00%	7.88%	8.75%
yr		-25.0%	-12.5%	0.0%	12.5%	25.0%
11	-25.0%	201.66	204.82	208.04	211.34	214.69
13	-12.5%	199.93	203.46	207.08	210.78	214.57
15	0.0%	198.34	202.21	**206.19**	210.27	214.45
17	12.5%	196.88	201.06	205.37	209.80	214.35
19	25.0%	195.53	200.00	204.62	209.37	214.25

FIG. 7.53 Sensitivity analysis of the proposed hybrid energy project.

$$\beta_K = b_K . \frac{S_Y}{S_K} \tag{7.39}$$

where S_K is the standard deviation of 100 values of X, and S_Y is the standard deviation of 100 values of Y.

7.10 Optimization of microgrid and hybrid energy systems in HOMER

The HOMER was developed by the National Renewable Energy Laboratory (NREL). HOMER optimizes the renewable energy-based microgrids or HESs based on the COE

TABLE 7.3 Power sources, energy storage technologies, and loads available in HOMER.

Power sources in HOMER	Storage in HOMER	Loads in HOMER
• Wind turbine • Solar PV • Run-of-river hydro • Hydropower • Fuel cell • Biomass power • Microturbine • Diesel generator • Electric utility grid	• Flywheels • Flow batteries • Hydrogen • Customizable batteries	• Daily profiles with seasonal variation (primary load) • Thermal (space heating, crop drying) • Deferrable (water pumping, refrigeration) • Efficiency measures

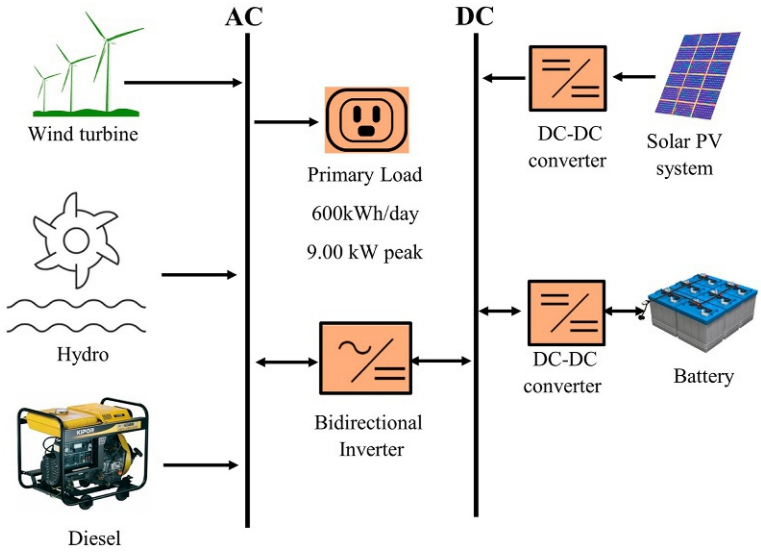

FIG. 7.54 Schematic diagram of the proposed hybrid energy system in HOMER.

and the NPV. For optimization analysis, HOMER asks about the renewable energy sources and imports the weather data from the NASA database, renewable energy technology, its cost and technical parameters, and the load data. Types of sources, storage technologies, and the loads that are available in HOMER are detailed in Table 7.3. A schematic diagram of the proposed HES consisting of AC and DC buses, renewable energy sources, storage technologies, and the load is shown in Fig. 7.54.

7.10.1 Power sources in HOMER

7.10.1.1 Solar resources

For solar photovoltaic system modeling in the HOMER, the user needs to give the solar irradiance data for the location of the project. Solar data includes the direct solar irradiance,

diffused solar irradiance, and the clearness index. The data can be the hourly average global irradiance, monthly average global irradiance, and clearness index. The clearness index is a value between zero and one and is defined as the ratio of the solar irradiance reaching the earth to the solar irradiance reaching the top of the atmosphere. If a user provides monthly average solar irradiance data, HOMER calculates the hourly solar irradiance data using Graham's and Holland's algorithm.

HOMER considers the solar PV as a dc source of electricity whose input solar irradiance is directly proportional to the solar irradiance and independent of the atmosphere temperature. HOMER calculates the output power of the solar panels using Eq. (7.40).

$$P_{pv} = f_{pv} \times Y_{pv} \times \frac{G_T}{G_S} \tag{7.40}$$

where

f_{pv} is the derating factor of the solar PV pane;

Y_{pv} is the rated capacity of the solar array;

G_T is the total global irradiance (direct and diffused); and

G_S is the global irradiance at STC ($1000\,W/m^2$).

The rated capacity of a solar PV is the output power of the solar panel at STCs, i.e., solar irradiance of $1000\,W/m^2$, and solar panel temperature 25°C. The rated capacity of a PV panel accounts for both the area of the panel and the panel efficiency. However, HOMER performs the calculation independent of these two characteristics. The efficiency of the amorphous silicon is greater than the polycrystalline silicon panel, but the efficiency and the area of the solar panel are of no consideration to HOMER. The derating factor is defined as the scaling of the output power of the solar panel to consider the wire losses, losses due to dust particles, increased temperature, or any other thing that deviates the output power of the solar panel from the expected value. HOMER does not account for the effect of the increased temperature on the output power of the solar panel. The solar PV is not directly connected to the load or the battery, since the varying irradiance and the panel temperature expose the load to the varying voltage that is not the same as the voltage at the maximum power point. A MPPT is incorporated between the solar PV and the load. An MPPT is connected to the DC-DC converter whose duty cycle is controlled by the MPPT algorithm. HOMER assumes MPPT in the solar PV system to increase the efficiency of the system. The solar irradiance and the clearness index at the proposed location are shown in Fig. 7.55.

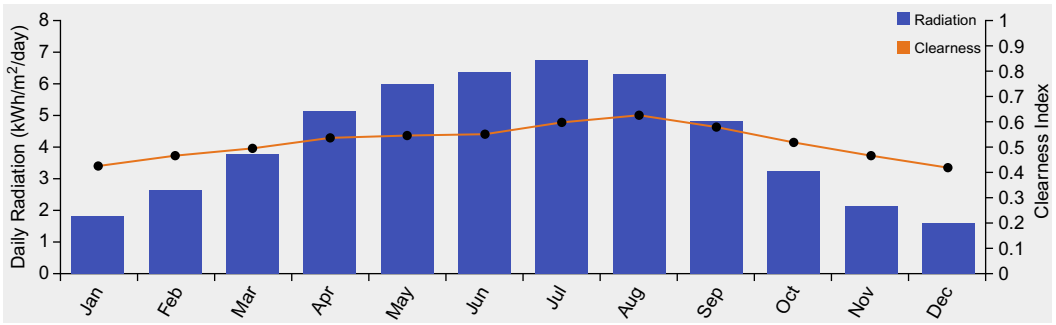

FIG. 7.55 Solar irradiance and clearness index throughout the year.

To determine the total cost analysis of the solar PV system, used puts the initial capital cost, operating and maintenance cost, and replacement cost. The replacement cost is the cost of replacing the complete system after the lifetime of the project, which is specified in years.

7.10.1.2 Wind resources

For a wind energy system modeling in the HOMER, the user needs to give the wind speed data for every year. The average monthly wind speed for the complete year is shown in Fig. 7.56. HOMER takes the wind speed at the anemometer height measured above the ground and calculates the wind speed at the hub height of the wind turbine. HOMER uses the power-law profile or the logarithmic profile to model the wind shear.

Power law profile: Eq. (7.41) is used to measure the ratio of the wind speed at the hub height to the wind speed at anemometer height.

$$\frac{V_{hub}}{V_{anem}} = \left(\frac{Z_{hub}}{Z_{anem}}\right)^{\alpha} \tag{7.41}$$

Logarithmic profile: Eq. (7.42) is used to measure the ratio of the wind speed at the hub height to the wind speed at anemometer height.

$$\frac{V_{hub}}{V_{anem}} = \frac{\ln\left(\frac{Z_{hub}}{Z_0}\right)}{\ln\left(\frac{Z_{anem}}{Z_0}\right)} \tag{7.42}$$

where

V_{hub} is the wind speed at the hub height of wind turbine;

V_{anem} is the wind speed at anemometer height;

Z_{hub} is the hub height of the wind turbine;

Z_{anem} is the anemometer height;

Z_0 is the surface roughness length which depends upon the surface on which wind turbine is installed; and

α is the power-law exponent.

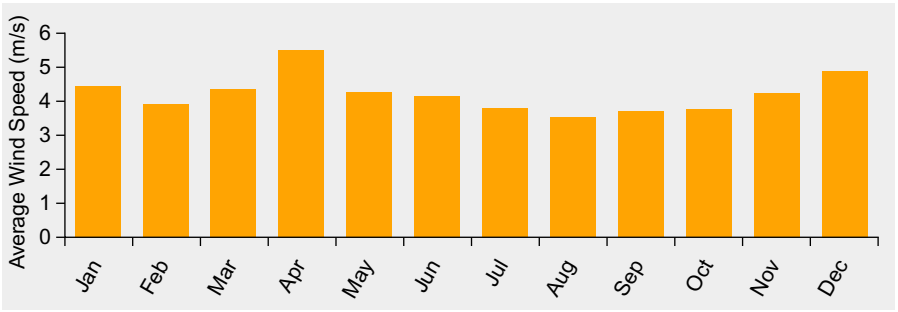

FIG. 7.56 Wind speed distribution throughout the year.

7.10.2 Storage in HOMER

7.10.2.1 Batteries

The battery bank is used to store the energy from the renewable energy sources and to use it during the low generation from the renewable energy sources. HOMER considers the following characteristics of the battery while selecting the battery for the proposed project: capacity curve, nominal voltages, minimum state of charge, lifetime curve, and round trip efficiency.

7.10.2.2 Flywheel

A flywheel is another energy storage technology that is connected to the AC bus as an operating reserve. It absorbs the energy when the generation from the renewable energy is greater than the energy demand and releases it during the peak hours or when the production from the renewable is lower than the requirement. The flywheel is connected to the AC bus through an AC-AC cycloconverter that converts the variable frequency from the flywheel rotor to the constant frequency of the grid.

7.10.3 Loads in HOMER

The reason behind the designing and installation of a microgrid is to manage the load. HOMER provides primary load, deferrable load, and thermal loads as discussed in the following subsections.

7.10.3.1 Primary load

The primary load is the load that is managed by the power system under each circumstance. Common household equipment like lights, fans, computers, TVs, and some necessary industrial processes. This equipment cannot be deferred and the power system must keep them on. If the supply is lower than the energy demand, HOMER considers this load as an unmet load. The user specifies the primary load in kW in HOMER modeling. If the supply is not enough to meet the primary load, battery storage or the operating reserves are used to meet the primary load.

7.10.3.2 Deferrable load

The deferrable load is the load that is not required to be managed at a specific time but it can be deferred until later when the generation is higher than the demand within a specific time range. For example, a water pump is not required all the time because of the storage capacity of the water. Similarly, battery charging stations, ice-makers, laundry machines, and dishwashers can be deferred until later.

7.10.3.3 Thermal load

In HOMER, the thermal load is modeled in the same way as the primary electric load but the concept of operating reserves or the battery storage system does not apply for the thermal loads. The user defines the requirement of the thermal load for each hour of the year and HOMER manage the thermal load from the boiler or the waste heat recovery from the turbine.

7.10.4 Optimization and sensitivity analysis

After simulating the power system with the prescribed equipment, resources, load, and cost, HOMER performs the optimization analysis by making different configurations of the given equipment. HOMER optimizes each configuration within the given constraints. The optimized solution might contain the mixture of components with the best combination and best size and quantity of each component.

Based on the given technical and economical parameters of the system, HOMER performs simulation, optimization, and sensitivity analysis. HOMER simulates all the possible combinations for the provided search space of each parameter. After simulation, HOMER performs optimization for the best feasible combination based on the COE, NPV, and capital investment. The third optional function of the HOMER analysis is the sensitivity analysis, which checks the impact of variation of one parameter on the result. For example, solar irradiance and wind speed are intermittent. Their variation changes the output power of the HES as well as the cost of the system.

After performing simulation for the proposed HES and the optimization analysis, HOMER gives the cost analysis of the system as shown in Fig. 7.57. The cost summary contains the NPV, the LCOE, initial capital investment, and the operation and maintenance cost (O&M).

7.11 Comparison of RETScreen and HOMER analysis

As discussed in the previous section, HOMER uses hourly data to determine the optimal design of the proposed HES. In HOMER, we put the coordinates of the location to determine the monthly average wind speed data from the NREL website and estimate the hourly wind speed data from the monthly wind speed data. RETScreen needs only the average wind speed on annual basis. While comparing the HOMER and RETScreen, we need some adjustment in input parameters, since both do not take the same inputs. In some cases, HOMER asks the user some specific scaling factor and RETScreen automatically determines the adjustment coefficients. For this reason, RETScreen gives unadjusted energy production and HOMER gives

Cost Summary

	Base Case	Lowest Cost System
NPC	$148,565	$104,853
Initial Capital	$6,000	$32,600
O&M	$11,028/yr	$5,589/yr
LCOE	$0.525/kWh	$0.370/kWh

FIG. 7.57 Cost summary.

TABLE 7.4 Comparison between unadjusted energy production by RETScreen and total energy production by HOMER for a small wind farm.

RETScreen Unadjusted energy production MWh	HOMER Total energy production MWh	Difference
1532	1515	+ 1.12%

TABLE 7.5 Comparison between unadjusted energy production by RETScreen and total energy production by HOMER for a large wind farm.

RETScreen Unadjusted energy production GWh	HOMER Total energy production GWh	Difference
258.2	265.2	−2.64%

total renewable energy production. Table 7.4 gives a comparison between unadjusted energy production by RETScreen and total energy production by HOMER for the small wind farm. There is only a 1.12% difference in both results. Similarly, for a large wind farm, the difference is 2.64%, as shown in Table 7.5.

Fig. 7.58 shows the comparison between RETScreen and HOMER regarding the incident solar irradiance. It can be seen that in RETScreen, the solar irradiance is less than the HOMER estimated. Similarly, Figs. 7.59 and 7.60 give a comparison regarding PV energy production and the fuel consumed by the Genset in a HES.

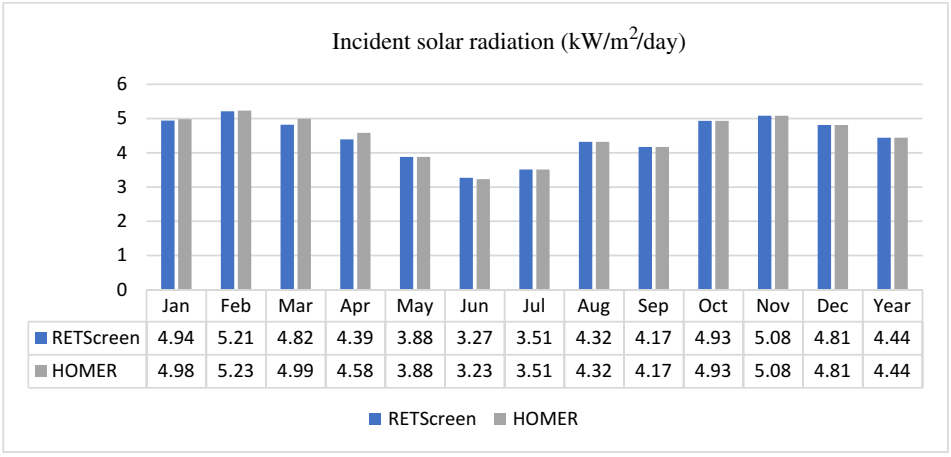

FIG. 7.58 RETScreen and HOMER comparison for incident solar radiation.

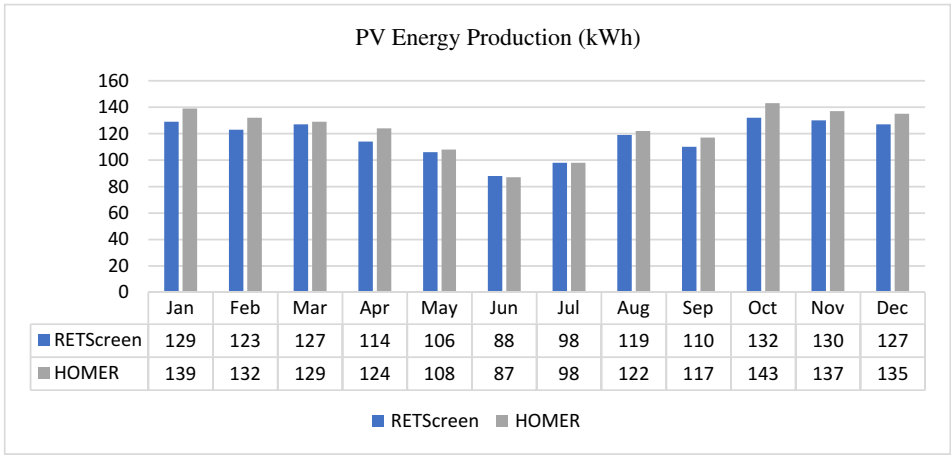

FIG. 7.59 RETScreen and HOMER comparison for PV energy production.

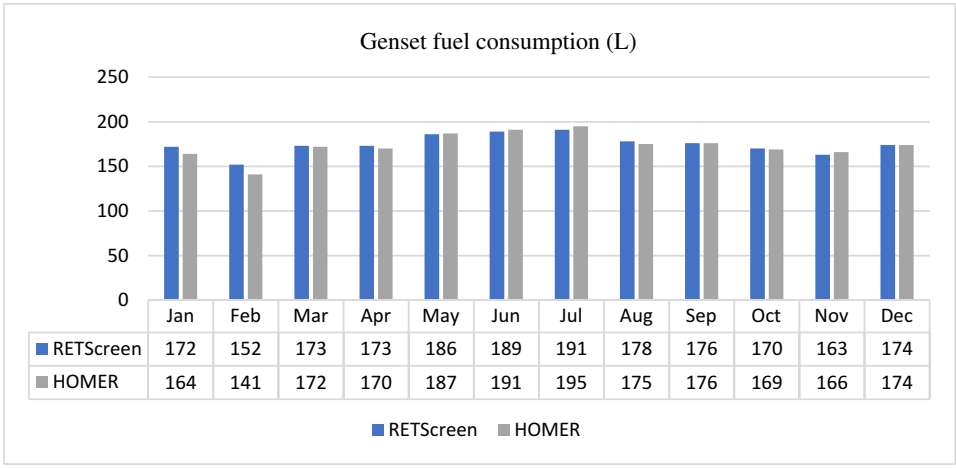

FIG. 7.60 RETScreen and HOMER comparison for Genset fuel consumption.

7.12 Microgrid policy

The growing cost of eradicating fossil fuels has urged power-producing companies to adopt renewable energy sources to mitigate the per-unit cost of electricity. The development of the microgrid in various countries is under development stages because of the lack of microgrid policies. In the following subsection, we discuss the key drivers of the microgrid policies and microgrid policies of some of the countries.

Microgrids provide an opportunity to increase the income resources and further distribute to develop renewable energy resources. In the case of energy from the biomass, the farmers can grow energy crops, sell the crop residues in the field and the industrial processing, and

install their technologies to convert the biomass into electricity or biogas. Similarly, wind turbines, solar photovoltaics, geothermal energy, power producers, operators, maintenance staff, equipment manufacturers, and suppliers of the microgrid constituent equipment can increase their source of income. Conventional energy sources produce emissions to a large extent and renewable energy sources do so to some extent. Many international agencies are playing a role in mitigating the environmental hazardous gases in the production of electricity. Distributed generation in the microgrid is the best way to control the contents of the CO_2 and other particulates in the atmosphere.

7.12.1 Microgrid design policy in Europe

PD IEC TS 62898-2

The operational guidelines given by the policy PD IEC TS 62898-2 include:

- grid-connected/nonisolated and off-grid/isolated operational modes;
- control of the grid-connected/nonisolated and off-grid/isolated operational modes;
- communication between the microgrid and the utility grid, communication inside the microgrid;
- energy storage systems and energy management systems for both grid-connected microgrid and the islanded microgrid;
- protection principles for the microgrid in both on-grid and off-grid operating modes;
- power quality in on-grid and off-grid mode; and
- maintenance and test of microgrids.

IEC TS 62257-9-2

The operational guidelines given by the policy IEC TS 62257-9-2 include:

- limits of the microgrid;
- voltage drops in the microgrid;
- composition of the microgrid;
- protection against electric shocks;
- protection against over currents;
- installation of different types of equipment like cables, poles, cable anchorage, isolation, and switching;
- operational conditions and external influences; and
- verification and acceptance before commissioning.

IEC TS 62898-1

The operational guidelines given by the policy IEC TS 62898-1,2,3 include:

- preliminary study and designing and planning process of the microgrid;
- applications and purposes of nonisolated and isolated microgrids;
- dispatchable and nondispatchable energy sources and generation and load forecasting;
- resource planning of distributed energy resources and energy storage systems;
- topologies of isolated and nonisolated microgrids; and
- commissioning, maintenance, and testing.

7.12.2 Microgrid design policy in the United States of America

- **IEEE Standard 1547 (2003)**: In the series of IEEE standard 1547, IEEE Standard 1547 (2003) is the foundational document related to the integration of the distributed energy generators and energy storage devices to the grid. IEEE 1547 is a distributed energy technology-neutral and it focuses on the interconnection of the DER. It also specifies the operation, testing and performance requirements, and maintenance and safety considerations.
- **IEEE Standard 1547.1 Family (2005)**: 1547.1 specifies the types of the interconnections, generation from the DER, commissioning, and testing of the interconnections of the equipment and distributed energy resources with the electric power system.
- **IEEE Standard 1547.2 (2008)**: 1547.2 specifies the background to the IEEE Standard 1547 (2003). Guidelines for the IEEE 1547 standard for the interconnection of the distributed energy resources with electric power systems.
- **IEEE Standard 1547.3 (2007)**: Guidelines for the monitoring of the interconnection of the distributed energy resources with the electric power system.
- **IEEE Standard 1547.4 (2011)**: Guidelines for the designing, integration, and operation of the distributed generation to the electric power system.
- **IEEE Standard 1547.6 (2011)**: Guidelines for the integration of the distributed generation units to the secondary distribution system.
- The **IEEE Standard 1547.7 (2013)**: Guidelines for studying the impact of the integration of renewable energy resources with the electric power system.

7.12.3 Microgrid design policy in China

The ever-growing energy demands of China are fulfilled by renewable energy sources and distributed generation. To promote the microgrid in China, exploitation of renewable energy and the development of the distributed generation technologies are at the advanced stage of development under the National Development and Reform Commission (NDRC), China's Centre for Renewable Energy Development (CRED), China National Renewable Energy Centre (CNREC), and the National Energy Agency (NEA). The following are the microgrid, renewable energy, and distributed generation policies in China.

- Preferential Tax Policies for Renewable Energy (2003)
- Renewable Energy Law (2006)
- National Climate Change Program (2007)
- Renewable Energy Law Amendments (2009)
- Renewable Electricity Surcharge (2009)
- 12th Five-Year Plan for Renewable Energy (2012)
- 12th Five Year Plan for National Strategic Emerging Industries (2012)
- 2012 Renewable Energy Electricity Feed-in Tariff (2012)
- Energy-Saving and New Energy Automotive Industry Development Plan 2012–20 (2012)
- Renewable Energy Tariff Surcharge Grant Funds Management Approach (2012)
- Notice on New Energy Demonstration City and Industrial Park (2012)
- China Energy White Paper 2012 (2012)
- Notice of Further Improvement of New Energy Demonstration Implementation (2013)

- Renewable Electricity Generation Bonus (2013)

Renewable Energy Law (REL-2006): China's first attempt to improve the renewable energy structure was to formulate the Renewable Energy Law in 2005 implemented in 2006. The REL focused on the five major components of the microgrid including price mechanism, cost mechanism, funding mechanism, connection to the grid, and volume target. In 2010, for the rapid growth in wind and solar energy, REL was amended by the National People's Congress (NPC). The amendment was as follows:

(1) Renewable energy policy was further explained and elaborated in terms of the planning and coordination between the electric power sector and transmission. The coordination between national and local governments for the planning was also elaborated. The role of the electric power utilities in the integration of renewable energy was elaborated and distributed generators were also redefined. The policy overall revised the definition and role of different entities in smart grid and energy storage.
(2) In the previous renewable energy law, the utility was asked to purchase from the renewable energy generators only in peak hours when the demand is high. In the revised policy, a provision to purchase electricity from all the renewable energy generators was made. The concept of smart grid, distributed generation, and HESs was established in its true sense.
(3) To generate the renewable energy funds, the government received a surcharge of 0.4 fen/kWh throughout the country. The amount collected was used to give the FiT and to support the renewable energy projects.

China's 12th Five-Year Plan for Renewable Energy: The National People's Congress of China approved a five-year plan for the promotion of renewable energy in 2011. The energy plan focused mainly on the maximum utilization of the renewable energy technologies and applications, maximum integration of the distributed generation and renewable energy in the national energy mix, and the improvement in the renewable energy technologies. To achieve the overall goal of increasing the renewable energy share in the energy mix, the following measures were taken:

- establishing sustainable and stable market demand;
- renewable power tariff and cost-sharing policies;
- improving the market environment;
- industry development and technology acceleration; and
- increasing fiscal input and tax incentives.

7.13 Conclusion

A microgrid is a more advanced and assured way of electricity connection to the off-grid areas that are far away from the grid. A HES or a microgrid near the national grid can also be connected to the grid for the sale and purchase of electricity in peak and off-peak hours. Renewable energy sources in the form of HESs, microgrid, smart grid, and distributed generation is competing and replacing the conventional fossil fuel power plants. Different control strategies are used to control the HESs or the microgrid in off-grid and on-grid mode. HOMER and RETScreen are the two most reliable examples of energy optimization software. Various countries have developed microgrid policies to promote the renewable energy adoption.

Problems

Problems 1–15 contain four answer options: A, B, C, and D. Choose the correct answer.

1. Which factors affect the achievement of the grid parity?
   A. Grid-related costs
   B. DG resources
   C. Electricity prices
   D. All of the above
2. What are the elements of the power conditioning unit in a hybrid energy system?
   A. Rectifiers
   B. Inverters
   C. Converters
   D. All of the above
3. Which of the following is a nonrenewable DG technology?
   A. Internal combustion engine
   B. Reciprocating engine
   C. Combustion gas turbine
   D. All of the above
4. Which of the following is a renewable DG technology?
   A. Solar
   B. Wind
   C. Geothermal
   D. All of the above
5. Which of the following are DG energy storage technologies?
   A. Mechanical
   B. Electrical
   C. Chemical
   D. All of the above
6. Which of the following is a mechanical energy storage technology?
   A. Pumped hydro energy storage system
   B. Compressed air energy storage system
   C. Flywheel energy storage system
   D. All of the above
7. Which of the following is an electrical energy storage technology?
   A. Capacitor
   B. Supercapacitor
   C. Superconductor
   D. All of the above
8. Which of the following is a chemical energy storage technology?
   A. Battery
   B. Flow battery
   C. Regenerative fuel cell
   D. All of the above

9. What does a combine cycle consist of?
   A. Steam turbine + gas turbine
   B. Steam turbine + biogas
   C. Steam turbine
   D. Gas turbine
10. What are the advantages of distributed generation?
   A. Spinning reserves
   B. Peak shaving
   C. Reliability
   D. Environmentally friendly
   E. All of the above
11. Which of the following is a type of hybrid energy system?
   A. Series hybrid energy system
   B. Parallel hybrid energy system
   C. Switched hybrid energy system
   D. All of the above
12. What technical parameter should be considered while designing a microgrid?
   A. Loss of power supply probability
   B. Loss of load expected
   C. Equivalent loss factor
   D. All of the above
13. Which of the following is a type of energy optimization software?
   A. RETScreen
   B. HOMER
   C. Hybrid2
   D. All of the above
14. What does portfolio risk in distributed generation depend on?
   A. Risk on individual DG source
   B. Weight of each DG source
   C. Correlation between DG sources
   D. All of the above
15. What IEEE Standard sets out microgrid policy in the USA?
   A. IEEE Standard 1547
   B. IEEE Standard 1548
   C. IEEE Standard 1549
   D. IEEE Standard 1550

Answer the following short questions

1. Define microgrid and list the key components of a microgrid.
2. Differentiate between a microgrid and a smart grid.
3. What is grid parity? List the factors influencing the grid parity achievement.
4. What is distributed generation and why do we need to adopt it?
5. List some of the distributed generation technologies.

6. Which energy storage technologies are used in distributed generation?
7. Explain the working principle of the reciprocating engine.
8. What are the thermodynamics processes involved in the Otto cycle?
9. List the applications of microturbines.
10. How is the Stirling engine used in renewable energy systems?
11. What is the difference between a hybrid energy system and distributed generation?
12. Outline the advantages and disadvantages of distributed generation.
13. Differentiate between series and parallel hybrid energy systems.
14. Describe the working of switched hybrid energy systems.
15. Which parameters are involved in the designing of a microgrid?
16. What is the primary level control of a microgrid?
17. Explain the secondary level control of a microgrid.
18. What is the tertiary level control of a microgrid?
19. Express the relation between the frequency and active power.
20. Express the relation between reactive power and voltage.
21. Sketch the droop control characteristics of a microgrid.
22. Define the following parameters:
    - **(i)** Loss of power supply probability
    - **(ii)** Loss of load expected
    - **(iii)** Equivalent loss factor
    - **(iv)** Total energy loss
    - **(v)** Level of autonomy
    - **(vi)** State of charge of the battery
    - **(vii)** Levelized cost of energy
    - **(viii)** Net present cost
    - **(ix)** Social acceptance
    - **(x)** Portfolio risk
    - **(xi)** Internal rate of return
    - **(xii)** Debt payment
    - **(xiii)** Wind speed distribution
    - **(xiv)** Wind plant capacity factor
    - **(xv)** Unadjusted energy production
23. Which steps does RETScreen follow in the optimization of the hybrid energy systems?
24. Define the levelized cost of energy (LCOE) and net present value (NPV) of a hybrid energy system.

References

[1] F. Baghdadi, K. Mohammedi, S. Diaf, O. Behar, Feasibility study and energy conversion analysis of stand-alone hybrid renewable energy system, Energy Convers. Manag. 105 (2015) 471–479, https://doi.org/10.1016/J.ENCONMAN.2015.07.051.

[2] P. Enevoldsen, B.K. Sovacool, Integrating power systems for remote island energy supply: lessons from Mykines, Faroe Islands, Renew. Energy 85 (2016) 642–648, https://doi.org/10.1016/J.RENENE.2015.06.065.

[3] A. Biswas, A. Kumar, Techno-Economic Optimization of a Stand-alone PV/PHS/Battery systems for very low load situation, Int. J. Renew. Energy Res. 7 (2) (2017).

[4] B.E. Türkay, A.Y. Telli, Economic analysis of standalone and grid connected hybrid energy systems, Renew. Energy 36 (7) (2011) 1931–1943, https://doi.org/10.1016/J.RENENE.2010.12.007.
[5] A.E.S.A. Nafeh, Optimal economical sizing of a PV-wind hybrid energy system using genetic algorithm, Int. J. Green Energy 8 (1) (2011) 25–43, https://doi.org/10.1080/15435075.2010.529407.
[6] M. Kamran, R. Asghar, M. Mudassar, M.I. Abid, Designing and optimization of stand-alone hybrid renewable energy system for rural areas of Punjab, Pakistan, Int. J. Renew. Energy Res. 8 (4) (2018), https://doi.org/10.20508/IJRER.V8I4.8696.G7539.
[7] M. Kamran, R. Asghar, M. Mudassar, M.I. Abid, Designing and economic aspects of run-of-canal based micro-hydro system on Balloki-Sulaimanki link canal-I for remote villages in Punjab, Pakistan, Renew. Energy 141 (2019) 76–87, https://doi.org/10.1016/J.RENENE.2019.03.126.
[8] I.D. Spyrou, J.S. Anagnostopoulos, Design study of a stand-alone desalination system powered by renewable energy sources and a pumped storage unit, Desalination 257 (1–3) (2010) 137–149, https://doi.org/10.1016/J.DESAL.2010.02.033.
[9] A. Heydari, A. Askarzadeh, Optimization of a biomass-based photovoltaic power plant for an off-grid application subject to loss of power supply probability concept, Appl. Energy 165 (2016) 601–611, https://doi.org/10.1016/J.APENERGY.2015.12.095.
[10] A. Kaabeche, R. Ibtiouen, Techno-economic optimization of hybrid photovoltaic/wind/diesel/battery generation in a stand-alone power system, Sol. Energy 103 (2014) 171–182, https://doi.org/10.1016/j.solener.2014.02.017.
[11] S. Abdul-Wahab, Y. Charabi, A.M. Al-Mahruqi, I. Osman, S. Osman, Selection of the best solar photovoltaic (PV) for Oman, Sol. Energy 188 (2019) 1156–1168, https://doi.org/10.1016/J.SOLENER.2019.07.018.
[12] S.M. Shaahid, L.M. Alhems, M.K. Rahman, Techno-economic assessment of establishment of wind farms in different provinces of Saudi Arabia to mitigate future energy challenges, Therm. Sci. 2018 (2019) 2909–2918, https://doi.org/10.2298/TSCI171025109S.
[13] A.K. Karmaker, M.A. Hossain, N.M. Kumar, V. Jagadeesan, A. Jayakumar, B. Ray, Analysis of using biogas resources for electric vehicle charging in Bangladesh: a techno-economic-environmental perspective, Sustainability 12 (7) (2020) 2579, https://doi.org/10.3390/SU12072579.
[14] T. Ma, M.S. Javed, Integrated sizing of hybrid PV-wind-battery system for remote island considering the saturation of each renewable energy resource, Energy Convers. Manag. 182 (2019) 178–190, https://doi.org/10.1016/J.ENCONMAN.2018.12.059.
[15] H. Shayeghi, M. Alilou, Distributed generation and microgrids, in: Hybrid Renewable Energy Systems and Microgrids, Academic Press, 2021, pp. 73–102.
[16] File: Combustion Turbine diagram.svg—Wikimedia Commons, Available from: https://commons.wikimedia.org/wiki/File:Combustion_turbine_diagram.svg. (Accessed 3 April 2022).
[17] File:EuroDishSBP front.jpg—Wikimedia Commons, Available from: https://commons.wikimedia.org/wiki/File:EuroDishSBP_front.jpg. (Accessed 3 April 2022).
[18] Rfassbind, File: From a Solar Cell to a PV system.svg—Wikimedia Commons, Available from: https://commons.wikimedia.org/wiki/File:From_a_solar_cell_to_a_PV_system.svg. (Accessed 3 April 2022).
[19] Patrickmak, File: Lamma wind turbine.jpg—Wikimedia Commons, 2008, Available from: https://commons.wikimedia.org/wiki/File:Lamma_wind_turbine.jpg. (Accessed 3 April 2022).
[20] Quietrevolution_Bristol_3513051949.jpg (451 × 581), Available from: https://upload.wikimedia.org/wikipedia/commons/b/b6/Quietrevolution_Bristol_3513051949.jpg. (Accessed 3 April 2022).
[21] M. Kamran, Bioenergy, Renew. Energy Convers. Syst. (2021) 243–264, https://doi.org/10.1016/B978-0-12-823538-6.00002-6.
[22] E.S.N. Raju, T. Jain, Distributed energy resources and control, in: Distributed Energy Resources in Microgrids: Integration, Challenges and Optimization, Academic Press, 2019, pp. 33–56.
[23] S-kei, File: Schematic-Condensing-Geothermal-PowerPlant-Eng.PNG—Wikimedia Commons, Available from: https://commons.wikimedia.org/wiki/File:Schematic-Condensing-Geothermal-PowerPlant-Eng.PNG. (Accessed 3 April 2022).
[24] R. Jackson, et al., A comprehensive motivation of multilayer control levels for microgrids: synchronization, voltage and frequency restoration perspective, Appl. Sci. 10 (23) (2020) 8355, https://doi.org/10.3390/APP10238355.
[25] M. Kamran, et al., Solar photovoltaic grid parity: a review of issues and challenges and status of different PV markets, Int. J. Renew. Energy Res. 9 (1) (2019).

This page intentionally left blank

CHAPTER

8

Energy statistics and forecasting for smart grids

8.1 Introduction

The demand and supply gap of electricity in the smart grid leads to the introduction of energy forecasting and an energy management system. Energy forecasting is a key participant in the planning and management of the smart grid system [1]. Data in a smart grid is collected with the help of an advanced metering infrastructure (AMI), which measures the bidirectional power flow. This data is used by the data analysis applications for forecasting. These forecasting applications can be used for scheduling generation, generation forecasts from renewable energy-based power plants, and demand-side management. In the management of the smart grid, various statistical and machine learning forecasting methods have been used for forecasting power demand and power generation [2,3]. Time series power generation and power demand have been forecasted using statistical forecasting methods that include, autoregressive moving average (ARMA), autoregressive integrated moving average (ARIMA), and vector autoregression (VAR) [4]. Because of the recent advancements in smart grid technologies, bulk generation and demand data cannot be dealt with by the statistical methods of forecasting. Statistical methods cannot be used for complex and nonlinear data points [5].

Accurate and precise forecasting is now possible with the advancements in machine learning and artificial intelligence forecasting methods. Nonlinear time-series data is forecasted using a recurrent neural network (RNN), and long short-term memory (LSTM) forecasting methods [6]. The integration of renewable energy sources in the smart grid has raised the issues of uncertainty and the variation in the energy consumption pattern. These uncertainty issues are solved by probabilistic methods, since they generate prediction intervals as compared to point forecasting [7–9].

Forecasting accuracy is improved by combining multiple forecasting methods into a single approach known as hybrid forecasting methods [10]. The integration of multiple forecasting methods makes the hybrid model more complex. Thus, a trade-off between the

https://doi.org/10.1016/B978-0-323-99560-3.00007-7

computational complexity and the forecasting accuracy is maintained [11–13]. To reduce the complexity of the forecasting model, some pre forecasting methods are used for dimensionality reduction. Singular value decomposition (SVD), and principal component analysis (PCA) are the key techniques that are used for dimensionality reduction and reducing the complexity of the forecasting method [14–16].

8.2 Numerical weather prediction

Numerical weather prediction (NWP) is the implementation of the classical physical laws governing the flow of the atmosphere in the mathematical equation. These mathematical equations are solved using supercomputers. Various regional and global forecasting models are used for weather forecasting. They use weather observations taken from weather satellites, weather cameras, and other observing systems. To perform NWP, the following steps should be carried out.

8.2.1 Governing equations

The following are partial differential equations that describe the dynamics and thermodynamics of the atmosphere:

(i) conservation of momentum (Newton's second law);
(ii) conservation of mass (equation of continuity);
(iii) ideal gas equation;
(iv) conservation of energy (first law of thermodynamics); and
(v) conservation of water mass (moisture equation).

8.2.2 Numerical methods or numerical approximations

Numerical methods are created because computer algorithms cannot understand calculus equations. They can perform arithmetic only. These methods are used to transform temporal and spatial derivatives into equations that computers can solve.

8.2.3 Parameterization

Each of the physical processes and parameters that cannot directly be predicted requires a parameterization scheme based on reasonable physical and statistical representation. Parameterization within the context of NWP is the way of replacing complex or small-scale processes with simplified processes. Some of the parameters and physical processes that require parameterization are:

- incoming solar radiations;
- radiations scattering by aerosols and molecules;
- radiations absorbed by the atmosphere;
- reflection and absorption of radiations by clouds;

- emission of longwave radiation from the earth's surface;
- condensation;
- snow ice;
- sensible heat flux;
- turbulence;
- reflection and absorption of radiations by the earth's surface;
- snow;
- soil water;
- surface roughness;
- emission of longwave radiations from clouds;
- deep convection;
- rain;
- evaporation;
- vegetation;
- topography; and
- soil properties.

8.2.4 Initial and boundary conditions

Initial conditions define the starting point or the current status of the atmosphere. Boundary conditions define the state of the atmosphere or the limits of the domain. In this context, a domain refers to a specific region on the globe or the whole globe.

8.3 Wind energy forecasting

The forecasting of wind power is a complex one with multiple input parameters integrated in a complex way as described in Fig. 8.1. The power that will be generated from a wind farm mainly depends upon the weather forecasting especially wind speed at that location. The weather forecast model depends upon the multiple inputs from numerical weather prediction (NWP), private weather data, public weather data, and the data from public sensors.

As a result, the weather forecast model gives you the wind speed, relative humidity, and air pressure for wind energy forecasting. The outputs from the weather forecast model like wind speed, wind direction, humidity, air pressure, the characteristics of the wind farm, and plant availability are given as input to the statistical wind energy forecasting model. Plant availability is the amount of time for which the output from the power plant is available in a specific period divided by the total amount of time in that period. The plant availability factor is determined by Eq. (8.1). Eqs. (8.2), (8.3) gives the definition of running period and generation period. A wind energy forecasting model is shown in Fig. 8.1.

$$\text{plant availability} = \frac{\text{running period}}{\text{generation period}} \times 100 \tag{8.1}$$

$$\text{running period} = \text{generation period} - \text{trippings} \tag{8.2}$$

$$\text{generation period} = \text{end time} - \text{start time} \tag{8.3}$$

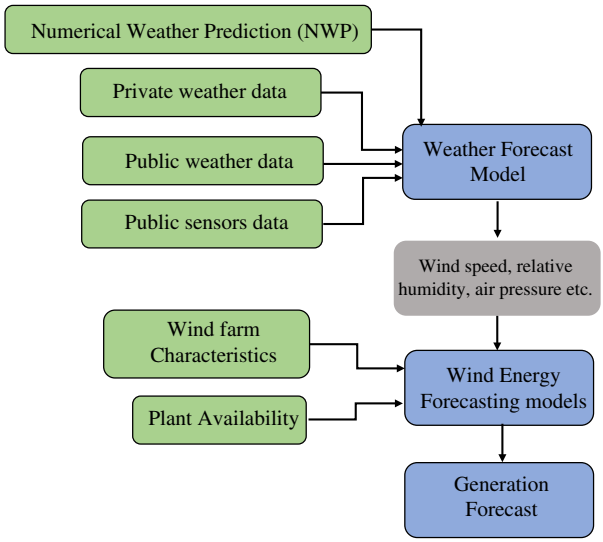

FIG. 8.1 Wind energy forecasting model.

8.4 Solar energy forecasting

The procedure and the components that are required for solar energy forecasting are similar to those for wind energy forecasting, as shown in Fig. 8.2. The major difference between wind energy forecasting and solar photovoltaic forecasting is the output of the weather forecasting model. Solar irradiance and temperature are the key parameters that influence the production of solar photovoltaics. For irradiance forecasting, forecasting the clouds' pattern is required for accurate solar irradiance forecasting. For short-term forecasting of solar PV power, satellite and sky cameras play their role in forecasting solar irradiance. For long-term forecasting, NWP is used for solar irradiance forecasting. In the final step, characteristics of the solar photovoltaic system and the plant availability are used along with the outputs of the weather forecasting model to forecast the generation from the solar photovoltaics. A solar energy forecasting model is shown in Fig. 8.2.

8.5 Energy forecasting time horizons

The period in the future for which prediction is to prepare is called the time horizon. This parameter is considered while forecasting in the smart grid system. Based on the time horizon, forecasting is categorized in the following categories.

8.5.1 Very short-term forecasting (VSTF)

In the literature, very short-term forecasting is less than a few hours with a 4 h upper limit. VSTF can deal with the sudden variations in renewable energy production only for a short

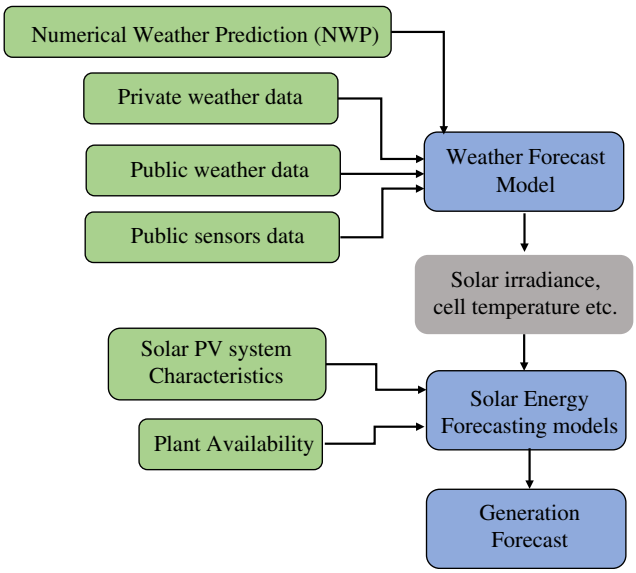

FIG. 8.2 Solar energy forecasting model.

period. VSTF is widely used in the prediction of renewable energy production specifically from solar and wind energy systems. Guan et al. [17] used a hybrid approach consisting of fuzzy logic and an artificial neural network and predicted forecasting of 2.5 min ahead in a wind farm.

8.5.2 Short-term forecasting (STF)

Short-term forecasting (STF) consists of a time horizon ranging from a few minutes to a few days ahead. This type of forecasting is very useful in the prediction of the grid operation like optimal power dispatch and reliability analysis. STF increases the reliability of the grid operation by eliminating the chances of underestimation and overestimation of the load demand [18].

8.5.3 Medium-term forecasting (MTF)

Forecasting in the time horizon ranging from a few days to a few months is called medium-term forecasting (MTF). MTF is used in the smart grid for fuel supply scheduling and maintenance. It is also useful in predicting the economic aspects of the smart grid by forecasting the price and evaluating risk management [19].

8.5.4 Long-term forecasting (LTF)

Long-term forecasting (LTF) ranges from months to quarters to years. LTF is useful in forecasting the load demand and power generation for a long period. The fluctuations in the load

demand and generation in the short-term forecasting can be removed in the long-term forecasting. Xu et al. [20] forecasted the wind speed in the two meteorological stations in Malaysia for a 1-year time horizon to cope with the intermittency of the wind speed.

8.6 Emerging forecasting techniques

Because of the high environmental concerns regarding energy sources, renewable energy sources are penetrating the existing system with advancements in energy harnessing techniques. The economic and environmental benefits of solar and wind energy have attracted energy policymakers, energy investors, and researchers. Wind and solar PV are the key energy sources of a smart grid and the most discussed topics in the research. The output power from wind and solar is intermittent since both depend upon the continuously changing meteorological conditions. Security issues in the power system, optimal dispatch, surplus generation, power curtailment, and the increased cost of energy are some of the issues caused by the intermittency of wind speed and solar irradiance. These issues are addressed by conducting short-term forecasting of the generation from renewable energy sources. Based on the forecasting timescale, it is classified into the following four categories (Fig. 8.3).

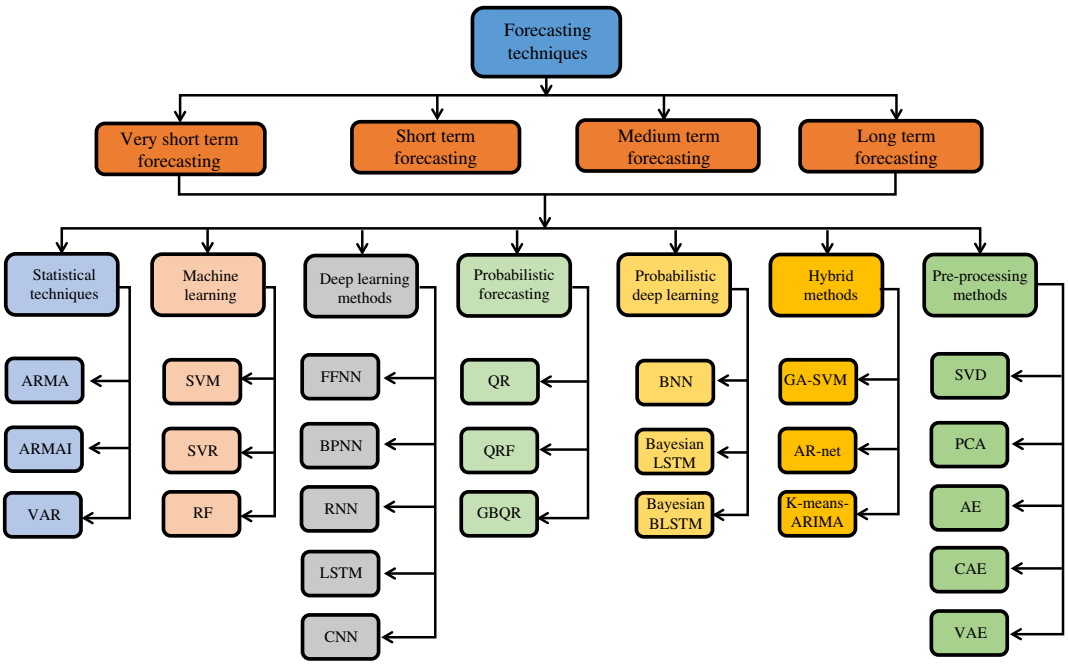

FIG. 8.3 Energy forecasting techniques.

8.6.1 Statistical forecasting techniques

8.6.1.1 Autoregressive moving average (ARMA)

The autoregressive average model (ARMA) is a statistical tool for time series analysis of the stationary variables. ARMA is the combination of two statistical tools: the autoregressive method and the moving average method. An autoregressive model is a model in which the independent variable is the lag of the dependent variable, as shown in Eq. (8.4). The ARMA model is represented as ARMA (p, q), P is the number of lags in AR and q is the number of lags in the MA.

$$Y_t = \alpha + \beta_1 Y_{t-1} + \beta_2 Y_{t-2} \ldots + \beta_p Y_{t-p} \tag{8.4}$$

The moving average model dependent variable depends upon the previous values of the errors, as shown in Eq. (8.5).

$$Y_t = \alpha + \beta_1 e_{t-1} + \beta_2 e_{t-2} \ldots + \beta_p e_{t-p} \tag{8.5}$$

The model is called moving average because the moving averages of the errors in the recursive form with the mean of the dependent variable try to find the moving average of the dependent variable.

The overall ARMA model is expressed by Eq. (8.6).

$$Y_t = \alpha + \beta_1 Y_{t-1} + \beta_2 Y_{t-2} \ldots + \beta_p Y_{t-p} + \beta_1 e_{t-1} + \beta_2 e_{t-2} \ldots + \beta_p e_{t-p} \tag{8.6}$$

8.6.1.2 Autoregressive integrated moving average (ARIMA)

The statistical analysis model autoregressive integrated moving average is used to understand the pattern of a data set and to predict it for the future. An autoregressive model is a model that uses past data values to predict the future trend. The difference between ARMA and ARIMA models is the nonstationary nature of the variable in the ARIMA model. The term integrated with the ARIMA refers to the concept that if the variable is not stationary, it has to be made stationary by taking the first and second-order difference according to the nature of the variable. The ARMA model is represented as ARMA (p, d, q), P is the number of lags in AR, d is the order of the difference after which the variable become stationary, and q is the number of lags in the MA [21–24].

8.6.1.3 Vector autoregression (VAR)

Vector autoregression is another statistical model that is used to forecast the relationship between multiple variables as they change with time. The structure of the VAR is that each variable depends upon the past lag itself and the past lags of the other variables. As an example, we consider solar irradiance and atmospheric temperature as two variables [25]. The vector autoregressive model relating the solar irradiance and the temperature can be shown by Eqs. (8.7), (8.8), respectively.

$$G_t = \alpha_{11} G_{t-1} + \alpha_{12} T_{t-1} + \epsilon_{G,t} \tag{8.7}$$

$$T_t = \alpha_{21} G_{t-1} + \alpha_{22} T_{t-1} + \epsilon_{T,t} \tag{8.8}$$

where G is the solar irradiance and the T is the atmospheric temperature. Eq. (8.7) shows the dependency of the current month solar irradiance on the previous month solar irradiance, and the previous month atmospheric temperature. Similarly, Eq. (8.8) indicates the dependency of the current month atmospheric temperature on the previous month solar irradiance and the previous month atmospheric temperature. $\epsilon_{G,\,t}$ and $\epsilon_{T,\,t}$ are the irradiance and temperature errors in the current month, respectively [26,27]. The above-stated model can be represented as VAR(1) because only one lag of the solar irradiance and temperature are used in the future prediction. Eqs. (8.7), (8.8) can be represented in a vector form, as shown in Eqs. (8.9), (8.10).

$$\begin{bmatrix} G_t \\ T_t \end{bmatrix} = \begin{bmatrix} \alpha_{11} & \alpha_{12} \\ \alpha_{21} & \alpha_{22} \end{bmatrix} \begin{bmatrix} G_{t-1} \\ T_{t-1} \end{bmatrix} + \begin{bmatrix} \epsilon_{G,t} \\ \epsilon_{T,t} \end{bmatrix} \tag{8.9}$$

$$f(t) = Cf(t-1) + \epsilon_t \tag{8.10}$$

8.6.2 Machine learning forecasting techniques

8.6.2.1 Support vector machine (SVM)

A support vector machine (SVM) is a type of machine learning forecasting technique. There could be many hyperplanes between the data points. This technique aims to maximize the marginal distance between the data set points of a variable. The maximization of the marginal distance is to increase the accuracy of the data classification. The marginal distance is maximized by selecting a hyperplane on a position such that the marginal planes parallel to the hyperplane and passing through one of the points of the data sets must be at the highest distance [28]. The points through which the hyperplane is passing are called the support vectors. Fig. 8.4 shows two models of a support vector machine mechanism. In Fig. 8.4A, the marginal distance is maximum, whereas the marginal distance is minimum in Fig. 8.4B. Thus, to increase the higher accuracy of forecasting, Fig. 8.4A is preferred. The given example is of the linear separable data points. If the data points are not linearly separable, SVM kernels are used to convert the lower dimension to the higher dimension [29].

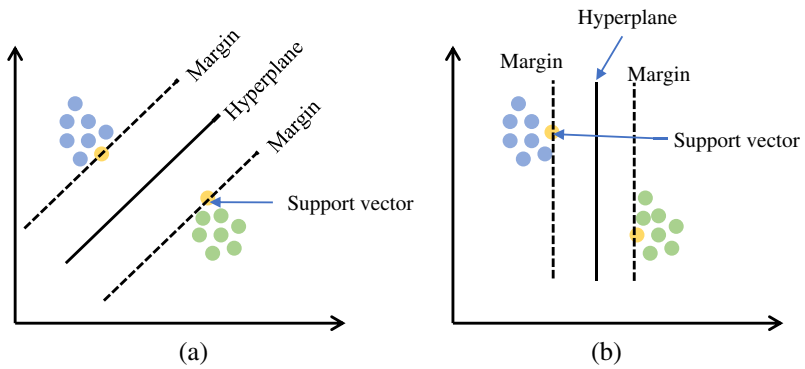

FIG. 8.4 Support vector machine (A) SVM with maximum marginal distance and (B) SVM with minimum marginal distance.

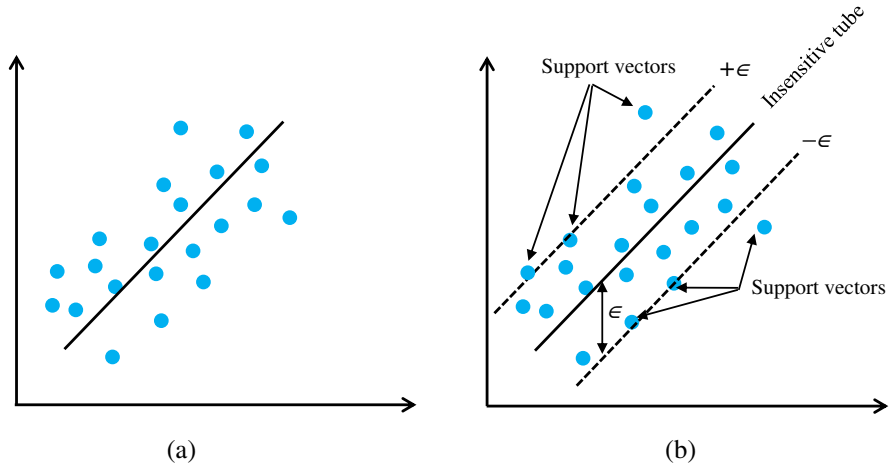

FIG. 8.5 (A) Simple regression and (B) support vector regression.

8.6.2.2 Support vector regression (SVR)

Support vector regression (SVR) is the combination of the regression and the support vector machine. To understand better support vector regression, we first go through the linear regression that will help in understanding SVR. Fig. 8.5A shows a scatter plot of the data values and the best-fitted regression line. The best-fitted regression line is drawn by the mathematics called ordinal least square. The distance between the actual data points and the predicted regression line is termed an error and we try to minimize the error for an accurate prediction [30–33].

In SVR, instead of drawing the regression line, we draw a tube consisting of a hyperplane and two marginal lines. SVR allows some flexibility in error margins which is acceptable for the model. The tube is called an ϵ insensitive tube, and consists of data points that are not considered while calculating the error because these points are not sensitive to the error calculation. Fig. 8.5B shows the SVR in which the upper marginal line is called the positive marginal line and the lower line is called the negative marginal line. The distance between the positive marginal line and the hyperplane and the distance between the negative marginal line and the hyperplane are called maximum allowed marginal error. The data points that are out of the insensitive tube are called slack variables and these are very helpful in calculating the error [34,35]. The data points that are on the marginal lines and out of the insensitive tube are called support vectors.

8.6.2.3 Random forest

Random forest is another type of machine learning algorithm. It is an ensemble classifier that randomly uses decision tree algorithms. Ensemble learning is a process of combining multiple classifiers to solve a complex problem. Thus, random forest can be defined simply as a classifier that has numerous decision trees on various subsets of the given data set and takes the average of them to increase the prediction accuracy [36,37]. A higher number of

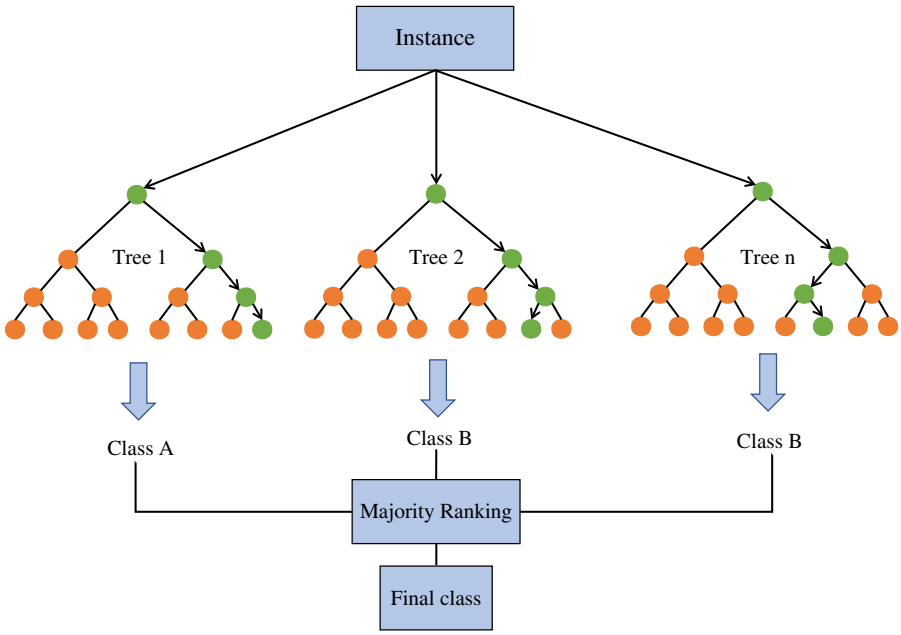

FIG. 8.6 Simplified diagram of random forest.

decision trees leads to higher accuracy and diminishes the overfitting problem [38]. The following steps are involved in predicting the data using the random forest method.

- **Step 1**: In a random forest, select n number of random records from the data set having k number of records using the bootstrapping method.
- **Step 2**: Build decision trees for each sample recorded.
- **Step 3**: Each decision tree will generate an output.
- **Step 4**: The output of each decision tree is averaged to select the output.

The concept of the random forest is shown in Fig. 8.6. It is considered as something like a decision tree, but it is a better method of prediction based on the points discussed in Table 8.1.

TABLE 8.1 A comparison between decision tree and random forest.

	Decision tree	Random forest
1	If a decision tree is allowed to grow without any control, it may overfit the data	The problem of overfitting is solved in the random forest since the random forest is generated from the random subsets of the data and the output is taken by the majority ranking or the average of classes
2	The computation process of a single decision tree is slower	Since multiple subsets and trees are involved in computation, it is a slower method
3	The decision tree takes some featured data sets as input and forms some set of rules for the prediction	Random forest randomly selects some data subsets, builds decision trees, and takes the majority ranking as the output. It does not involve any formulas

Saeedi et al. [39] implemented machine learning methods to predict the output of the PV generation in Hawaii. They claimed that the performance of the random forest is high among all other machine learning methods, with the highest *R*-square value of 98%.

8.6.3 Deep learning forecasting methods

8.6.3.1 Feedforward neural networks (FFNNs)

A feedforward neural network (FFNN) consists of an input layer, hidden layer, and output layer (Fig. 8.7). There is no feedback or cyclic process in FFNN. The higher the number of hidden layers, the more accurate the model will be. The architecture of the neural network is shown in Fig. 8.8. The number 3 indicates the number of independent variables in the input layer, 2 indicates the number of neurons in the hidden layer, and 1 indicates the output neuron [40]. The operation of the FFNN can be summarized as:

1. initializing the weights with some random value between 0 and 1;
2. calculating the output by taking the weighted sum at the output and hence calculating the error; and
3. minimizing the error by adjusting the weights.

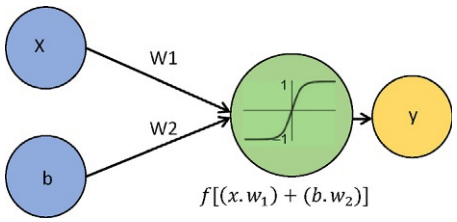

FIG. 8.7 Implementation of activation function in FFNN.

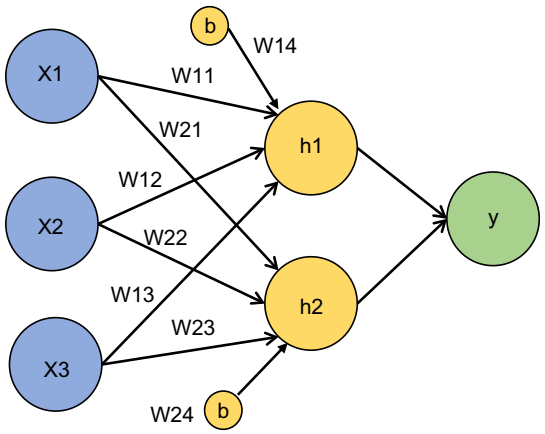

FIG. 8.8 Feedforward neural network.

The activation function is also termed the transfer function. The activation function decides the activation of the neurons. Whether an input is important for the neuron or not, it is also decided by the activation function [41]. In neural networks, various activation functions are used as discussed below.

Sigmoid function: Sigmoid function is a nonlinear s-shaped logistic function. Since the sigmoid function lies between 0 and 1, it is useful where the probability prediction is required. The sigmoid function is nonlinear and differentiable and slope at any point can be found. The sigmoid function is represented by Eq. (8.11).

$$f(x) = \frac{1}{1 + e^{-x}} \tag{8.11}$$

Hyperbolic tangent function: The hyperbolic tangent function is an updated version of the sigmoid function with a range from -1 to $+1$. The graph of the hyperbolic tangent function is also s-shaped and nonlinear. The tan hyperbolic function is given by Eq. (8.12).

$$f(x) = \frac{e^{x} - e^{-x}}{e^{x} + e^{-x}} \tag{8.12}$$

Rectified linear unit function (ReLU): the impression of the ReLU function is that it is a linear function, but it is actually a derivative function. The main advantage of the ReLU is that it does not activate all the neurons at the same time only those neurons are activated whose output of the linear transformation is greater than zero. If the output is less than zero, the neuron will be deactivated. Since a limited number of neurons are activated, ReLU is computationally more efficient than the sigmoid and the tan hyperbolic functions. Mathematically it is represented by Eq. (8.13).

$$f(x) = \max(0, x) \tag{8.13}$$

Soft plus function: The soft plus activation function is the approximation of the ReLU function and is closely related to the sigmoid function. The mathematical representation of the soft plus function is the integral of the sigmoid function, as shown in Eq. (8.14).

$$f(x) = \ln(1 + e^{x}) \tag{8.14}$$

For a deep understanding of the FFNN, we deal with mathematical modeling. The input matrix of the input layer is $[x_1 \ x_2 \ x_3 \ b]$. The input matrix is multiplied by the matrix of averages, as shown in Eq. (8.15).

$$[x_1 \ x_2 \ x_3 \ b].\begin{bmatrix} W_{11} & W_{21} \\ W_{12} & W_{22} \\ W_{13} & W_{23} \\ W_{14} & W_{24} \end{bmatrix} = \begin{bmatrix} x_1.W_{11} + x_2.W_{12} + x_3.W_{13} + b.W_{14} \\ x_1.W_{21} + x_2.W_{22} + x_3.W_{23} + b.W_{24} \end{bmatrix} \tag{8.15}$$

In a feedforward neural network, the sigmoid function is used to find the probability of the point is in the positive region, as shown in Eq. (8.16).

$$\frac{1}{1 + e^{-x}} \begin{bmatrix} x_1.W_{11} + x_2.W_{12} + x_3.W_{13} + b.W_{14} \\ x_1.W_{21} + x_2.W_{22} + x_3.W_{23} + b.W_{24} \end{bmatrix} = probability \tag{8.16}$$

8.6.3.2 *Back-propagation neural networks (BPNNs)*

A back-propagation neural network (BPNN) is the advanced form of the feedforward neural network in which using the FFNN approach, the output is compared with the target values and the error in the outputs is forecasted, and then based on the error, the weights of the previous inputs are calculated and updated. A flowchart of the training algorithm of the BPNN is shown in Fig. 8.9. The BPNN consists of two phases [42,43], forward pass and backward pass, as shown in Fig. 8.10. Both the forward pass and backward pass consists of the propagation phase and weight updating phase as described below.

(1) The propagation phase consists of forwarding propagation and the backpropagation phases.
(2) The weight updating phase is based on the difference between the output and the target values.

The algorithm starts by taking inputs and setting target values. The forward process starts by computing the output of each layer and then comparing the output to the target values to measure the error. The accuracy is measured, if the model is accurate it stops otherwise the back-propagation process starts. In the back-propagation process, the weight change is computed for each output layer, and for each hidden layer, and the weight for all layers is updated. After updating weights for each layer, the forward process starts again by training the inputs [44,45].

8.6.3.3 *Recurrent neural networks (RNNs)*

A recurrent neural network (RNN) is a type of neural network that uses sequential data to proceed. Contrary to the FFNN, the RNN has memory and can receive and process variable-length data. In conventional neural networks, all the input and output variables are independent of each other. In cases where the next value of the variable is to predict, it must require the previous value of the variable. The RNN uses its hidden layer to store the previous value

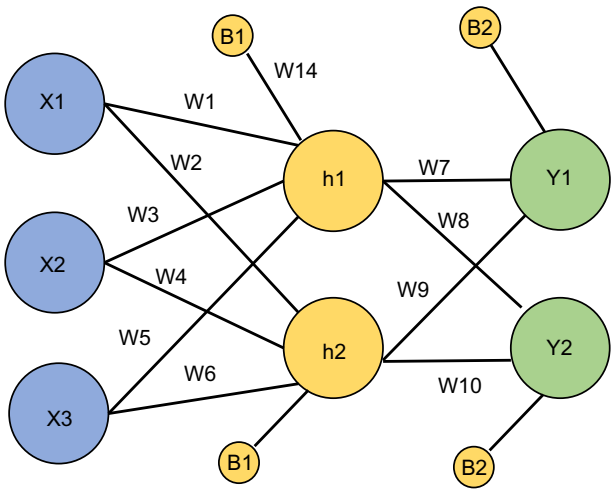

FIG. 8.9 Back-propagation neural network.

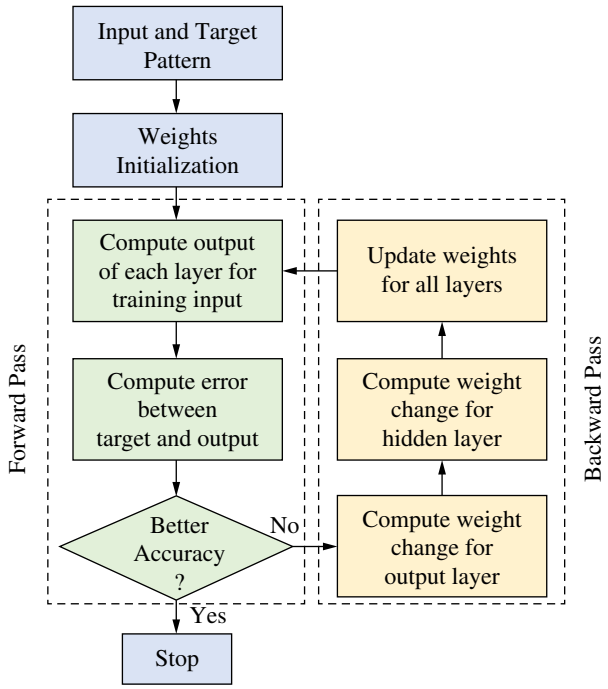

FIG. 8.10 The flow of a back-propagation neural network.

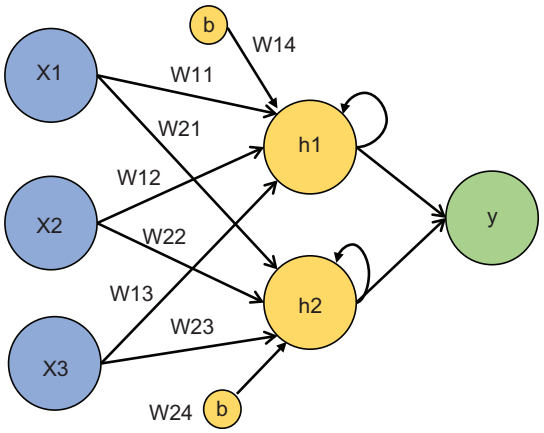

FIG. 8.11 Recurrent neural network.

of the variable. Graphically it is represented as in Fig. 8.11. It was developed because the FFNN is not able to handle the sequential data, it considers only the current input to proceed, and it cannot memorize the previous values.

8.6.3.4 Long short-term memory (LSTM)

Long short-term memory (LSTM) is a special version of the RNN which is capable of handling long-term dependencies and persists the memory. The vanishing gradient problems

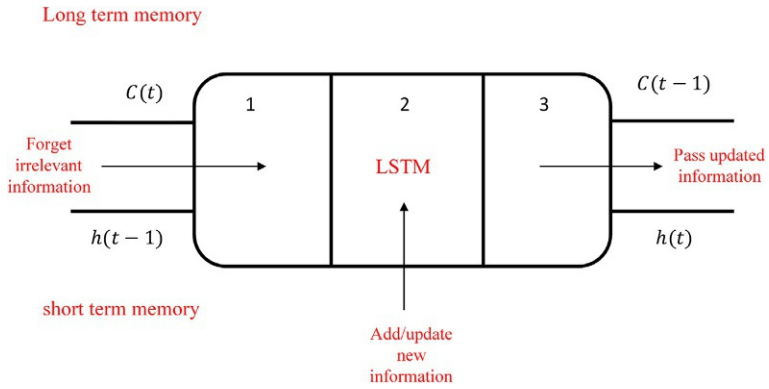

FIG. 8.12 Long short-term memory.

that occurred in the RNN are handled by LSTM. The RNN recalls the previous information to predict future data, but it cannot persist with long-term dependencies. LSTM holds the information in the timesteps. It consists of three parts and each part performs its function as shown in Fig. 8.12. The first step decides about the information coming from the previous timestep. If the information is of importance it is held otherwise it is forgotten in the forget gate. In the second part, the cell trains the information coming from the inputs. The third part is to pass the updated information from the one timestep to the next timestep. The three parts are termed gates: the forget gate, input gate, and output gate.

Like a simple RNN, LSTM also has a hidden layer with different states; $h(t-1)$ is the previous hidden state and $h(t)$ is the current state of the hidden layer. The hidden state is known as short-term memory. There is another state in LSTM termed a cell state with $c(t-1)$ as the cell state at the previous timestep and $c(t)$ as the cell state at the current timestep. The cell state is known as long-term memory. In the forget cell of the LSTM, it is decided which information from the previous timestep should be stored and which should be forgotten. The equation for the forget gate can be written as Eq. (8.17).

$$f_t = \sigma\left(X_t \times U_f + h_{t-1} \times W_f\right) \tag{8.17}$$

where:

X_t is the input to the current timestep;
U_f is the weight associated with the current input;
h_{t-1} is the hidden state of the previous timestep;
W_f is the weight associated with the hidden state; and
f_t is multiplied by the previous time step of the cell state, as shown below.

$$f_t \times C_{t-1} = 0 \text{ if } f_t = 0, \text{ forget all input information}$$

$$f_t \times C_{t-1} = C_{t-1} \text{ if } f_t = 1, \text{ persist input information}$$

The input gate is used to calculate the new information carried by the input. Information carried by the input gate at the current timestep is calculated by Eq. (8.18).

$$i_t = \sigma(X_t \times U_i + h_{t-1} \times W_i) \tag{8.18}$$

To get the new information from the input information, we multiply the sigmoid activation function.

$$N_t = \tanh(X_t \times U_c + h_{t-1} \times W_c)$$

Now the new information that is passed to the cell state will be between −1 and 1 because of the activation function. Based on the new information from the input gate, the updated information is determined using Eq. (8.19).

$$C_t = f_t \times C_{t-1} + i_t \times N_t \tag{8.19}$$

The equations for the output information are shown in Eq. (8.20).

$$O_t = \sigma(X_t \times U_o + h_{t-1} \times W_o) \tag{8.20}$$

The information which is updated is passed to the output.

Kong et al. [46] performed short-term load forecasting by proposing an RNN-based LSTM technique for residential consumers. They performed the load forecasting at aggregate and granular levels, and claimed an improved accuracy in the forecast. Zhang et al. [47] forecasted sunny weather and used the forecasted information to predict the output from the solar PV using LSTM in conjunction with the autoencoders. Shao et al. [48] used customers' energy consumption data and extracted the feature using the K-means algorithm combined with the convolution autoencoders. They integrated the results with the LSTM for customer energy consumption forecasting.

8.6.3.5 Convolutional neural networks (CNNs)

A convolutional neural network (CNN) is a type of deep learning and is used for filtering applications and feature extraction. Various filters are used for various feature extraction. A CNN is mainly used in an image, video, and audio recognition. Before an image is given to the neural network, it is first passed through the CNN, which reduces the dimensionality of the image without losing any important features or information. A CNN consists of two parts: feature learning in which all the important features are extracted, and the classification in artificial neural network (ANN).

Wang et al. [49] forecasted the PV generation by extracting the feature from the PV generation data set using CNN with the wavelength transform method. They compared the results with the real-time data set from the PV generation and claimed that the efficiency of the forecasting is improved compared to other conventional forecasting methods. Zhang et al. [50] have studied a detailed comparison of various forecasting techniques by conducting a case study and determined the forecasting accuracy based on root mean square error (RMSE) and mean absolute error (MAE). Lee et al. [51] forecasted solar PV generation by integrating LSTM with the CNN filter and considering local weather conditions. They claimed that the preprocessing of the input data before applying the forecasting technique increases the forecasting performance. They compared different machine learning for different times of the day and observed little mean absolute percentage error (MAPE), and RMSE. A comparison of different forecasting techniques is shown in Table 8.2.

TABLE 8.2 Pros and cons of different forecasting techniques.

Sr. no.	Forecasting technique	Advantages	Disadvantages
1	Statistical methods	Less complex and less computation cost	Less reliability for complex and nonlinear data sets
2	Deep learning methods	Efficient for long and nonlinear data patterns	Give point forecasting, overfitting, require hyper-parameter tuning
3	Probabilistic methods	Provides prediction intervals	Computational complexity is high
4	Machine learning methods	Highly efficient and capable of handling big data sets	No reliable for long and heterogeneous data sets generated point forecasting
5	Probabilistic deep learning methods	Efficient, reliable, and provides prediction intervals	Computational cost is high
6	Hybrid methods	Scalable and highly accurate	Application-oriented and high computational complexity
7	Preprocessing methods	Forecasting performance is batter	Application-oriented

8.6.4 Probabilistic forecasting methods

With the integration of renewable energy sources with the power system and with the advanced research in a microgrid, distributed generation, and the hybrid energy system, probabilistic forecasting has replaced point forecasting to a large extent. Point forecasting is related to the single value forecasting of the future event, whereas the probabilistic forecasting method finds the probability of happening an event in the future. Hong et al. reviewed probabilistic forecasting methods and claimed that for the rapidly changing energy demands of the power industry, probabilistic forecasting is more important than point forecasting.

8.6.5 Probabilistic deep learning forecasting methods

8.6.5.1 Bayesian neural networks (BNNs)

The integration of the Bayesian probability with the neural network is termed a Bayesian neural network (BNN). This illustrates the uncertainties from the model and gives the distribution over the weight and outputs. In a BNN, weights and outputs are considered as the variables and find out the marginal distribution of the data that best fits the data. It is the extension of the standard neural network (SNN). an SNN focuses on the optimization of the data point and finding the optimal value of the weight whereas a BNN focuses on the marginalization by considering the weight as a variable and finding the distribution of the weights. Yang et al. took the uncertainties of the group of the customers and forecasted the energy demands of the individual households.

8.6.6 Hybrid forecasting methods

Statistical forecasting methods are unable to process big data and the artificial intelligence algorithms depend upon large training data sets and many more complex models than the statistical methods. Deep neural networks require more data to forecast. The models are too complex to train the data and require more machines, which increases the cost. The abovementioned forecasting limitation and shortcomings can be overcome by adopting a hybrid forecasting technique consisting of two or more forecasting techniques. Different deep learning methods and statistical methods can be integrated for a holistic approach. Akhtar et al. [52] integrated different machine learning methods with the optimization algorithm and compared hybrid forecasting models for PV generation forecasting.

8.6.6.1 Genetic algorithm-support vector machine (GA-SVM)

A genetic algorithm-support vector machine (GA-SVM) is the integration of the genetic algorithm with the support vector machine. Wu et al. [53] forecasted 1h PV generation by integrating genetic algorithm with the four best forecasting methods, ARIMA, ANN, SVM, and adaptive neuro fuzzy inference system (ANFIS), and claimed that the hybrid algorithms have more precision and minimum error compared to the abovementioned algorithms separately.

8.6.6.2 Auto regression-neural network (AR-net)

An auto regression-neural network (AR-net) is the integration of autoregression with a neural network. The autoregression lacks long-range data dependencies and neural networks are the complex algorithms. Triebe et al. [54] presented an autoregression model using a neural network and introduced a hybrid model named AR-net.

8.6.6.3 K-means-ARIMA

Benmouiza et al. [55] performed a hybrid energy forecasting method K-means with a neural network for hourly solar forecasting. Similarly, Liu et al. [56] used wavelet packet transform with a neural network for wind energy forecasting.

The limitation faced by the abovementioned hybrid forecasting methods is the enhanced computational complexity. In a hybrid method, if one method gives poor performance, it will affect the performance of the complete forecasting. However, the performance and efficiency of the proposed hybrid method can be increased by integrating an optimization algorithm. There is a trade-off between performance and the computational complexity of the hybrid forecasting method.

8.6.7 Preforecasting methods

Before analyzing the data for forecasting purposes, data preprocessing and data representation are required. Before actual use of data, it is necessary to clean the data by using some of the following data cleaning techniques: dimension reduction, feature extraction, identifying the missing values, and finding the inconsistencies in the data. Data must be according to the algorithm for which it is being prepared. If a data is labeled with the same name, it must be replaced with “0” and “1.” By applying various statistical techniques like data cleaning, data

normalizing, transformation, etc., raw data is converted into a training data set, which can be used for applying the forecasting technique.

8.6.7.1 Singular value decomposition (SVD)

Decomposition or dimension reduction and pattern recognition are highly recommended techniques for the preprocessing of raw data. Kaur et al. in performed the energy forecasting but before that, they reduced the dimension of the data using singular value decomposition (SVD). The dimensionality reduction was done by the tensor and the matrix decomposition method. Kaur et al. [6] forecasted the user load profile by first decomposing and compressing the data using clustering and SVD techniques. The sparsity between the data values was covered by compressing the load profile data using the sparse coding technique. They claimed that the proposed data compression method was better than the existing data compressing techniques like standalone K-means clustering and discrete wavelet transform. Some of the applications of SVD are:

- pseudo inverse;
- solving homogeneous linear equations;
- total least-square minimization;
- range, null space, and rank;
- low rank matrix approximation;
- separable models;
- nearest orthogonal matrix;
- the Kabsch algorithm; and
- signal processing.

8.6.7.2 Principal component analysis (PCA)

Principal component analysis (PCA) is another method of dimensionality reduction used to reduce the high dimensional data into lower dimensions. In renewable energy forecasting, the data variables that are of no concern in the forecasting are eliminated from the data set. Huang et al. [13] proposed the PCA for the forecasting of the power generation from solar photovoltaics. They eliminated the data set from the solar PV generation that has little or no effect on the forecasting of PV generation output. They compared the results with particle swarm optimization (PSO) and differential evolution, and claimed that the proposed method is more precise and contains less root mean square error (RMSE).

8.6.7.3 Autoencoders (AEs)

Autoencoders (AEs) are a type of neural network that reduces the high dimension to the lower representation. An AE consists of three parts: an encoder that converts the high dimensional data into low data representation, the code, and the decoder that reconstructs the original data. Architecture is created with a bottleneck that ensures the low-dimensional representation of the original data. A bottleneck is like a hidden layer in the neural network and it has less dimensionality than the input data, as shown in Fig. 8.13. The output layer again has the same dimension as the input layer. The autoencoder consists of two parts: encoders and decoders. The encoders compress the data into low-dimensional representation.

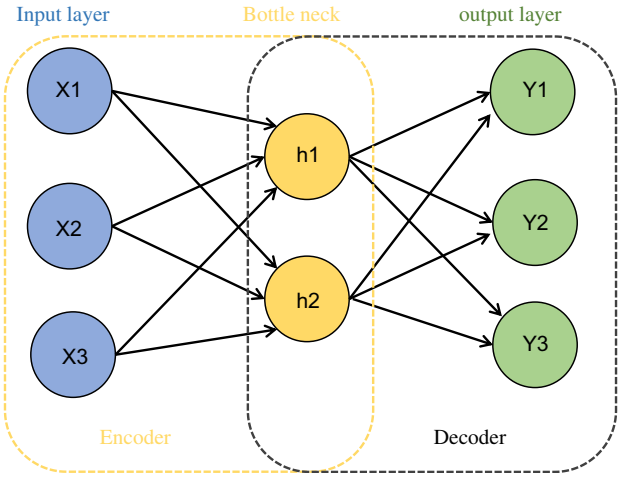

FIG. 8.13 Neural diagram of the autoencoder.

The condition for low dimensional representation is that the dimensions must have a dependence on other dimensions.

If we compare an AE with PCA, we can see from Fig. 8.14 that PCA draws a straight line or relate a linear function between the data points whereas the AE gives a nonlinear relation between the data points. It means that by using PCA we can draw a relation only for data that has a relatively less complex structure. By using an AE, we can have more relations between data having a more complex structure. An AE can be compared with PCA as follows:

- Both PCA and AE perform dimensionality reduction.
- PCA learns linear relationships.
- Encoders can learn nonlinear relationships.
- Encoder and PCA are the same if the encoder's activation function is linear.

8.6.7.4 Convolutional autoencoders (CAEs)

The incorporation of an autoencoder with a convolutional neural network (CNN) is termed a convolutional autoencoder (CAE). Ryu et al. [15] performed data compression and

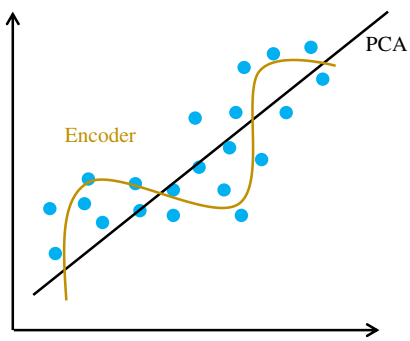

FIG. 8.14 A comparison between an autoencoder and PCA.

dimensionality reduction for the energy storage data and transmission data using CAE. They proposed feature extraction using CAE for the seasonal variation in data. They extracted 100-dimensional vectors from 8640-dimensional spaces. They also compared the proposed method with the standard method and reported a 19%–40% reduction in the reconstruction error and a 130% rise in the compression ratio.

8.7 Energy management in smart grids

The integration of highly intermittent and fluctuating renewable energy-based DG sources like wind energy, solar energy, energy storage systems, and electric vehicles disturbs the stability of the electric power and the power distribution system. The major reason behind this is the imbalance between power generation and power demand, which may cause voltage swings and blackouts in severe conditions. To balance the power supply and power demand and to avoid the peak hours in certain durations, an energy management system (EMS) is introduced. This is divided into two parts. First is the EMS on the supply side, where some power generators are turned ON and OFF to follow the load demand. The second is the EMS on the load or consumer side, which is known as demand-side management. In demand-side management, consumers manage the pattern of their energy consumption following the available power from the generation side.

8.7.1 The importance of the energy management system

The energy demand is continuously rising and the pattern of the energy consumption is unpredictable which may cause serious problems for the power producers. High energy demand during peak hours may reduce the reliability of the system. This issue can be resolved by two options: increasing the dimensions and size of the network, and introducing an EMS to avoid peak demands during peak hours. The first option is not applicable in a normal situation since it is expensive and requires a long period. The second option seems appealing and is essential for smart grid systems because it:

- increases the overall efficiency of the system;
- conserves energy;
- is an automated system and does not require direct human intervention;
- helps power producers to optimize power generation and minimize the cost of energy;
- reduces distribution losses and again minimizes the cost of energy;
- helps end-users to manage their load during the peak hours and minimize their electricity bills;
- helps in forecasting energy sources and load demand with high accuracy; and
- protects the environment.

8.7.2 Application of the energy management system

As discussed earlier, EMS can be applied to two major parts of the smart grid: the generation side and the consumer side.

- Power suppliers including the power generation units, power plant operators, and the electric utility can use the EMS to generate electricity efficiently. For example, during off-peak hours, some of the generators with high operational costs can be shut off and the demand can be fulfilled by operating power generators having the lowest operational costs. Such power generators are used only during peak hours.
- Power consumers can efficiently manage the consumption pattern to reduce their electricity bills. During peak hours, the only necessary load must be operated by using an EMS.

8.7.3 Tools for the energy management system

Conventionally, the power generation units and the power-consuming appliances were controlled manually, which was inefficient for an EMS. In modern control systems, computer-based algorithms are used to control power generation and power-consuming appliances. Some control systems of the EMS in the smart grid are:

- programmable logic controller (PLC);
- supervisory control and data acquisition (SCADA);
- building management system (BMS);
- energy management system (EMS); and
- automation system.

8.7.4 Challenges to the energy management system

An EMS is a part of the smart grid system which is a novel idea and is at the development stage. Moving from the conventional technology to the new technology is a time taking process. There are some limitations and challenges that might be faced in integrating the EMS into the smart grid system:

- The investment in the implementation of EMS is high compared to the return on investment.
- To implement the EMS, the existing system needs to be upgraded which is an expensive process.
- The tariff must be different during peak hours and off-peak hours. The transition from conventional to advanced tariffs is not easy for the power utilities.
- Moving from the conventional grid to the smart grid requires public awareness.
- Bidirectional power flow, which is an important aspect of the EMS, is still in the research phase.

8.8 Conclusion

Energy forecasting plays a vital role in the energy management system of the smart grid. This chapter presents the numerical weather prediction for the weather forecasting which is used in solar and wind forecasting. Further, all the energy forecasting techniques that are

used for different time horizon forecasting are described in detail along with their literature review. Statistical forecasting techniques are used for linear data sets which are less computationally complex, whereas advanced techniques like machine learning, neural networks, and hybrid forecasting methods can be used on nonlinear data sets and dimensionality reduction of the data. The high complexity increases the computation process that requires supercomputers for fast forecasting. Before using the raw energy data in the forecasting model, it is passed through a preprocessing process which applies functions like feature extraction, dimensionality reduction, identifying the missing values, and finding inconsistencies in the data.

Problems

Problems 1–12 contain four answer options A, B, C, and D. Choose the correct answer.

1. Which of the following is a governing conservation law of numerical weather prediction?
   A. Conservation of momentum
   B. Conservation of energy
   C. Conservation of mass
   D. All of the above
2. What steps are involved in numerical weather prediction?
   A. Governing equations
   B. Numerical approximation
   C. Parameterization and boundary conditions
   D. All of the above
3. What time horizon is used for energy forecasting?
   A. Short-term forecasting
   B. Medium-term forecasting
   C. Long-term forecasting
   D. All of the above
4. Which of the following is a statistical forecasting technique?
   A. Autoregressive moving average
   B. Autoregressive integrated moving average
   C. Vector autoregression
   D. All of the above
5. Which of the following is a type of machine learning forecasting method?
   A. Support vector machine
   B. Vector autoregression
   C. Autoregressive moving average
   D. Feedforward neural network
6. What is the aim of the support vector machine method?
   A. Maximize the marginal distance between data points of a variable
   B. Minimize the marginal distance between data points of a variable
   C. All of the above
   D. None of the above

7. Support vectors are the data points that are:
   A. Inside the margin
   B. Outside the margin
   C. At the margin
   D. On the marginal line and outside the marginal line
8. What is the major difference between a decision tree and a random forest?
   A. Majority ranking or the average
   B. Control over the process growth
   C. Computation speed
   D. All of the above
9. Which of the following is a type of deep learning forecasting method?
   A. Feedforward neural network
   B. Back-propagation neural network
   C. Recurrent neural network
   D. All of the above
10. Which of the following is a type of probabilistic deep learning forecasting method?
   A. Bayesian neural network
   B. Bayesian long short-term memory
   C. Bayesian BLSTM
   D. All of the above
11. Which of the following is a type of hybrid forecasting method?
   A. GA-SVM
   B. AR-net
   C. K-means ARIMA
   D. All of the above
12. Which of the following is a type of preprocessing method?
   A. Singular value decomposition (SVD)
   B. Principal component analysis (PCA)
   C. Autoencoders
   D. All of the above

Answer the following short questions

1. Define numerical weather prediction and list the four parts of NWP.
2. Which governing equations are used for the weather forecasting model?
3. Define parameterization and give some processes and parameters that require parameterization.
4. Draw a wind energy forecasting model of a wind farm.
5. Draw a solar energy forecasting model for a solar photovoltaic plant.
6. What are the time horizons of energy forecasting and what are its types?
7. Illustrate very short-term and short-term forecasting.
8. Explain medium-term forecasting and long-term forecasting.
9. Differentiate between the moving average and the autoregressive moving average.
10. What is the significance of p, d, and q in the ARIMA model?
11. Write down the mathematical equations of the solar irradiance and temperature in vector autoregression.

12. How would you represent the solar irradiance and temperature equations in vector form in vector autoregression?
13. Define hyperplane, support vectors, and margins in the support vector machine.
14. SVM is used for linear separable data points. If the data points are not linearly separable, how would you achieve dimensionality reduction?
15. Explain the working process of the support vector regression, using a diagram.
16. Which four steps are involved in the random forest?
17. Give a brief comparison between the decision tree and random forest forecasting methods.
18. Summarize the functioning of a FFNN.
19. Which activation functions are involved in an FFNN? Give mathematical equations of each activation function.
20. Which phases are involved in a BPNN?
21. How is a RNN is different from a BPNN and an FFNN?
22. Briefly discuss the working process of the LSTM forecasting method.
23. How is dimensionality reduction achieved in a CNN?
24. Discuss the advantages and disadvantages of energy forecasting techniques.
25. What are the advantages of the hybrid energy forecasting methods over the conventional forecasting methods?
26. Why are preforecasting methods necessary before applying a forecasting method?
27. Compare principal component analysis (PCA) and autoencoders (AEs).
28. List some of the applications of singular value decomposition (SVD).
29. What is the importance of an energy management system in the smart grid?
30. Identify the areas of the smart grid where an energy management system is applied.
31. Which tools are used for an energy management system?
32. Which challenges are faced by an energy management system?

References

[1] V.C. Güngör, et al., Smart grid technologies: communication technologies and standards, IEEE Trans. Ind. Inf. 7 (4) (2011) 529–539, https://doi.org/10.1109/TII.2011.2166794.
[2] H. Çimen, N. Çetinkaya, J.C. Vasquez, J.M. Guerrero, A microgrid energy management system based on non-intrusive load monitoring via multitask learning, IEEE Trans. Smart Grid 12 (2) (2021) 977–987, https://doi.org/10.1109/TSG.2020.3027491.
[3] S.N. Islam, Z. Baig, S. Zeadally, Physical layer security for the smart grid: vulnerabilities, threats, and countermeasures, IEEE Trans. Ind. Inf. 15 (12) (2019) 6522–6530, https://doi.org/10.1109/TII.2019.2931436.
[4] Y. Wang, Q. Chen, T. Hong, C. Kang, Review of smart meter data analytics: applications, methodologies, and challenges, IEEE Trans. Smart Grid 10 (3) (2019) 3125–3148, https://doi.org/10.1109/TSG.2018.2818167.
[5] X.G. Agoua, R. Girard, G. Kariniotakis, Short-term spatio-temporal forecasting of photovoltaic power production, IEEE Trans. Sustain. Energy 9 (2) (2018) 538–546, https://doi.org/10.1109/TSTE.2017.2747765.
[6] D. Kaur, R. Kumar, N. Kumar, M. Guizani, Smart grid energy management using RNN-LSTM: a deep learning-based approach, in: 2019 IEEE Global Communications Conference GLOBECOM 2019—Proceedings, 2019, https://doi.org/10.1109/GLOBECOM38437.2019.9013850.
[7] Y. Zhang, J. Wang, X. Wang, Review on probabilistic forecasting of wind power generation, Renew. Sustain. Energy Rev. 32 (2014) 255–270, https://doi.org/10.1016/J.RSER.2014.01.033.
[8] T. Gneiting, M. Katzfuss, Probabilistic forecasting, Annu. Rev. Stat. Appl. 1 (2014) 125–151, https://doi.org/10.1146/ANNUREV-STATISTICS-062713-085831.

[9] B. Liu, J. Nowotarski, T. Hong, R. Weron, Probabilistic load forecasting via quantile regression averaging on sister forecasts, IEEE Trans. Smart Grid 8 (2) (2017) 730–737, https://doi.org/10.1109/TSG.2015.2437877.
[10] M. Ali, K. Prakash, H. Pota, A bayesian approach based on acquisition function for optimal selection of deep learning hyperparameters: a case study with energy management data, Sci. Proc. Ser. 2 (1) (2020) 22–27, https://doi.org/10.31580/sps.v2i1.1232.
[11] Y. Yang, W. Li, T.A. Gulliver, S. Li, Bayesian deep learning-based probabilistic load forecasting in smart grids, IEEE Trans. Ind. Inf. 16 (7) (2020) 4703–4713, https://doi.org/10.1109/TII.2019.2942353.
[12] Y. Gal, Z. Ghahramani, Dropout as a bayesian approximation: representing model uncertainty in deep learning, in: 33rd International Conference on Machine Learning. ICML 2016, 3, 2015, pp. 1651–1660, https://doi.org/10.48550/arxiv.1506.02142.
[13] Y.C. Huang, C.M. Huang, S.J. Chen, S.P. Yang, Optimization of module parameters for PV power estimation using a hybrid algorithm, IEEE Trans. Sustain. Energy 11 (4) (2020) 2210–2219, https://doi.org/10.1109/TSTE.2019.2952444.
[14] J.C.S. De Souza, T.M. Lessa Assis, B.C. Pal, Data compression in smart distribution systems via singular value decomposition, IEEE Trans. Smart Grid 8 (1) (2017) 275–284, https://doi.org/10.1109/TSG.2015.2456979.
[15] S. Ryu, H. Choi, H. Lee, H. Kim, Convolutional autoencoder based feature extraction and clustering for customer load analysis, IEEE Trans. Power Syst. 35 (2) (2020) 1048–1060, https://doi.org/10.1109/TPWRS.2019.2936293.
[16] Y.S. Manjili, R. Vega, M.M. Jamshidi, Data-analytic-based adaptive solar energy forecasting framework, IEEE Syst. J. 12 (1) (2018) 285–296, https://doi.org/10.1109/JSYST.2017.2769483.
[17] C. Guan, P.B. Luh, L.D. Michel, Y. Wang, P.B. Friedland, Very short-term load forecasting: Wavelet neural networks with data pre-filtering, IEEE Trans. Power Syst. 28 (1) (2013) 30–41, https://doi.org/10.1109/TPWRS.2012.2197639.
[18] J.C. Lopez, M.J. Rider, Q. Wu, Parsimonious short-term load forecasting for optimal operation planning of electrical distribution systems, IEEE Trans. Power Syst. 34 (2) (2019) 1427–1437, https://doi.org/10.1109/TPWRS.2018.2872388.
[19] N. Amjady, A. Daraeepour, Midterm demand prediction of electrical power systems using a new hybrid forecast technique, IEEE Trans. Power Syst. 26 (2) (2011) 755–765, https://doi.org/10.1109/TPWRS.2010.2055902.
[20] W.T. Xu, et al., Long term intelligent load forecasting method considering the expectation of power market transaction, in: Proceedings of 29th Chinese Control Decision Conference. CCDC 2017, 2017, pp. 2310–2315, https://doi.org/10.1109/CCDC.2017.7978900.
[21] R. Kedrowski, J. Nelson, A.S. Nair, P. Ranganathan, Short-term seasonal energy forecasting, in: IEEE International Conference on Electro/Information Technology, vol. 2018, 2018, pp. 696–700, https://doi.org/10.1109/EIT.2018.8500215.
[22] A. Elmouatamid, R. Ouladsine, M. Bakhouya, N. El Kamoun, K. Zine-Dine, M. Khaidar, A control strategy based on power forecasting for micro-grid systems, in: 5th IEEE International Smart Cities Conference. ISC2 2019, 2019, pp. 735–740, https://doi.org/10.1109/ISC246665.2019.9071722.
[23] D.Z. Amirhosseini, R. Sabzehaar, M. Rasouli, Power management and optimization for a residential smart microgrid using stochastic methods, in: 2018 9th IEEE International Symposium on Power Electronics Distributed Generation Systems. PEDG 2018, 2018, https://doi.org/10.1109/PEDG.2018.8447834.
[24] M.H. Amini, O. Karabasoglu, M.D. Ilić, K.G. Boroojeni, S.S. Iyengar, ARIMA-based demand forecasting method considering probabilistic model of electric vehicles' parking lots, in: IEEE Power and Energy Society General Meeting, vol. 2015, 2015, https://doi.org/10.1109/PESGM.2015.7286050.
[25] S.R. Twanabasu, B.A. Bremdal, Load forecasting in a smart grid oriented building, in: IET Conference Publications, vol. 2013, 2013, https://doi.org/10.1049/CP.2013.0997. no. 615 CP.
[26] J.W. Messner, P. Pinson, Online adaptive lasso estimation in vector autoregressive models for high dimensional wind power forecasting, Int. J. Forecast. 35 (4) (2019) 1485–1498, https://doi.org/10.1016/J.IJFORECAST.2018.02.001.
[27] Y. Liu, M.C. Roberts, R. Sioshansi, A vector autoregression weather model for electricity supply and demand modeling, J. Mod. Power Syst. Clean Energy 6 (4) (2018) 763–776, https://doi.org/10.1007/S40565-017-0365-1/TABLES/13.
[28] Y. Wang, Q. Chen, D. Gan, J. Yang, D.S. Kirschen, C. Kang, Deep learning-based socio-demographic information identification from smart meter data, IEEE Trans. Smart Grid 10 (3) (2019) 2593–2602, https://doi.org/10.1109/TSG.2018.2805723.

[29] J. Shi, W.J. Lee, Y. Liu, Y. Yang, P. Wang, Forecasting power output of photovoltaic system based on weather classification and support vector machine, in: Conference Record—IAS Annual Meeting. (IEEE Industry Application Society, 2011, https://doi.org/10.1109/IAS.2011.6074294.
[30] L. Ghelardoni, A. Ghio, D. Anguita, Energy load forecasting using empirical mode decomposition and support vector regression, IEEE Trans. Smart Grid 4 (1) (2013) 549–556, https://doi.org/10.1109/TSG.2012.2235089.
[31] A. Kavousi-Fard, H. Samet, F. Marzbani, A new hybrid modified firefly algorithm and support vector regression model for accurate short term load forecasting, Expert Syst. Appl. 41 (13) (2014) 6047–6056, https://doi.org/10.1016/J.ESWA.2014.03.053.
[32] Y. Ren, P.N. Suganthan, N. Srikanth, A novel empirical mode decomposition with support vector regression for wind speed forecasting, IEEE Trans. Neural Netw. Learn. Syst. 27 (8) (2016) 1793–1798, https://doi.org/10.1109/TNNLS.2014.2351391.
[33] H. Jiang, Y. Zhang, E. Muljadi, J.J. Zhang, D.W. Gao, A short-term and high-resolution distribution system load forecasting approach using support vector regression with hybrid parameters optimization, IEEE Trans. Smart Grid 9 (4) (2018) 3331–3350, https://doi.org/10.1109/TSG.2016.2628061.
[34] H.T. Yang, C.M. Huang, Y.C. Huang, Y.S. Pai, A weather-based hybrid method for 1-day ahead hourly forecasting of PV power output, IEEE Trans. Sustain. Energy 5 (3) (2014) 917–926, https://doi.org/10.1109/TSTE.2014.2313600.
[35] Q. Hu, S. Zhang, M. Yu, Z. Xie, Short-term wind speed or power forecasting with heteroscedastic support vector regression, IEEE Trans. Sustain. Energy 7 (1) (2016) 241–249, https://doi.org/10.1109/TSTE.2015.2480245.
[36] H. Shi, M. Xu, R. Li, Deep learning for household load forecasting—a novel pooling deep RNN, IEEE Trans. Smart Grid 9 (5) (2018) 5271–5280, https://doi.org/10.1109/TSG.2017.2686012.
[37] M. Sun, T. Zhang, Y. Wang, G. Strbac, C. Kang, Using bayesian deep learning to capture uncertainty for residential net load forecasting, IEEE Trans. Power Syst. 35 (1) (2020) 188–201, https://doi.org/10.1109/TPWRS.2019.2924294.
[38] F. Liu, T. Dong, T. Hou, Y. Liu, A hybrid short-term load forecasting model based on improved fuzzy c-means clustering, random forest and deep neural networks, IEEE Access 9 (2021) 59754–59765, https://doi.org/10.1109/ACCESS.2021.3063123.
[39] R. Saeedi, S.K. Sadanandan, A.K. Srivastava, K.L. Davies, A.H. Gebremedhin, An adaptive machine learning framework for behind-the-meter load/PV disaggregation, IEEE Trans. Ind. Inf. 17 (10) (2021) 7060–7069, https://doi.org/10.1109/TII.2021.3060898.
[40] K. Bhaskar, S.N. Singh, AWNN-Assisted wind power forecasting using feed-forward neural network, IEEE Trans. Sustain. Energy 3 (2) (2012) 306–315, https://doi.org/10.1109/TSTE.2011.2182215.
[41] N.M. Pindoriya, S.N. Singh, S.K. Singh, An adaptive wavelet neural network-based energy price forecasting in electricity markets, IEEE Trans. Power Syst. 23 (3) (2008) 1423–1432, https://doi.org/10.1109/TPWRS.2008.922251.
[42] R. Jiao, X. Huang, X. Ma, L. Han, W. Tian, A model combining stacked auto encoder and back propagation algorithm for short-term wind power forecasting, IEEE Access 6 (2018) 17851–17858, https://doi.org/10.1109/ACCESS.2018.2818108.
[43] Y. Zhang, B. Chen, Y. Zhao, G. Pan, Wind speed prediction of IPSO-BP neural network based on lorenz disturbance, IEEE Access 6 (2018) 53168–53179, https://doi.org/10.1109/ACCESS.2018.2869981.
[44] Z. Qu, W. Mao, K. Zhang, W. Zhang, Z. Li, Multi-step wind speed forecasting based on a hybrid decomposition technique and an improved back-propagation neural network, Renew. Energy 133 (2019) 919–929, https://doi.org/10.1016/J.RENENE.2018.10.043.
[45] Y.R. Zeng, Y. Zeng, B. Choi, L. Wang, Multifactor-influenced energy consumption forecasting using enhanced back-propagation neural network, Energy 127 (2017) 381–396, https://doi.org/10.1016/J.ENERGY.2017.03.094.
[46] W. Kong, Z.Y. Dong, Y. Jia, D.J. Hill, Y. Xu, Y. Zhang, Short-term residential load forecasting based on LSTM recurrent neural network, IEEE Trans. Smart Grid 10 (1) (2019) 841–851, https://doi.org/10.1109/TSG.2017.2753802.
[47] Y. Zhang, C. Qin, A.K. Srivastava, C. Jin, R.K. Sharma, Data-driven day-ahead PV estimation using autoencoder-LSTM and persistence model, IEEE Trans. Ind. Appl. 56 (6) (2020) 7185–7192, https://doi.org/10.1109/TIA.2020.3025742.
[48] X. Shao, C.S. Kim, Multi-step short-term power consumption forecasting using multi-channel LSTM with time location considering customer behavior, IEEE Access 8 (2020) 125263–125273, https://doi.org/10.1109/ACCESS.2020.3007163.

[49] H. Wang, et al., Deterministic and probabilistic forecasting of photovoltaic power based on deep convolutional neural network, Energ. Conver. Manage. 153 (2017) 409–422, https://doi.org/10.1016/J.ENCONMAN.2017.10.008.
[50] D. Zhang, X. Han, C. Deng, Review on the research and practice of deep learning and reinforcement learning in smart grids, CSEE J. Power Energy Syst. 4 (3) (2018) 362–370, https://doi.org/10.17775/CSEEJPES.2018.00520.
[51] W. Lee, K. Kim, J. Park, J. Kim, Y. Kim, Forecasting solar power using long-short term memory and convolutional neural networks, IEEE Access 6 (2018) 73068–73080, https://doi.org/10.1109/ACCESS.2018.2883330.
[52] M.N. Akhter, S. Mekhilef, H. Mokhlis, N.M. Shah, Review on forecasting of photovoltaic power generation based on machine learning and metaheuristic techniques, IET Renew. Power Gener. 13 (7) (2019) 1009–1023, https://doi.org/10.1049/IET-RPG.2018.5649.
[53] Y.K. Wu, C.R. Chen, H. Abdul Rahman, A novel hybrid model for short-term forecasting in PV power generation, Int. J. Photoenergy 2014 (2014), https://doi.org/10.1155/2014/569249.
[54] O.J. Triebe, N. Laptev, R. Rajagopal, AR-Net: a simple auto-regressive neural network for time-series, arXiv (2019), https://doi.org/10.48550/arxiv.1911.12436.
[55] K. Benmouiza, A. Cheknane, Forecasting hourly global solar radiation using hybrid k-means and nonlinear autoregressive neural network models, Energ. Conver. Manage. 75 (2013) 561–569, https://doi.org/10.1016/J.ENCONMAN.2013.07.003.
[56] H. Liu, H.Q. Tian, D.F. Pan, Y.F. Li, Forecasting models for wind speed using wavelet, wavelet packet, time series and artificial neural networks, Appl. Energy 107 (2013) 191–208, https://doi.org/10.1016/J.APENERGY.2013.02.002.

CHAPTER

9

Energy storage in smart grids

9.1 Introduction

Conventional power plants generate electricity using fossil fuels (oil, coal, and gas). These power plants are far away from the load area, and transmission and distribution systems are required to manage the load from the conventional power plant. In conventional power plants, most of the issues with grid ancillary services are solved by the large generators themselves. With the advancements and innovations in renewable energy sources and their harnessing techniques, distributed generation has become a novel concept, and the energy storage system (ESS) is an essential component of the hybrid energy system and the smart grid. The ESS helps in mitigating the intermittency of renewable energy sources; it also helps in bridging the gap between energy production and energy demand. With the intermittent and unpredictable nature of renewable energy sources like solar and wind, grid ancillary services are not easy to obtain. The ESS is the best solution to incorporate these services. The ancillary services include grid stabilization, renewable energy integration, power quality, frequency regulation, load following, peak shaving, spinning reserve, time shifting, and transient stability. Energy is stored in mechanical, chemical, and electrical forms. In mechanical form, energy storing technologies are pumped hydro ESSs, compressed air ESSs, and, flywheel ESSs. In chemical form, energy is stored in batteries, flow batteries, and regenerative fuel cells. In electromagnetic form, energy is saved in capacitors, supercapacitors, and superconductors [1,2]. All these energy storage technologies are detailed in this chapter and a SWOT analysis of each is conducted. The classification of the energy storage technologies is given in Fig. 9.1.

9.2 Compressed air energy storage

Compressed air energy storage (CAES) works on the principle of the gas turbine. The working of the CAES consists of two subprocesses: charging and discharging. In the charging process, when the energy demand is less than the energy production, surplus energy is used to compress the air and store it in underground gas storage known as a gas storage cavern. Underground air

https://doi.org/10.1016/B978-0-323-99560-3.00001-6

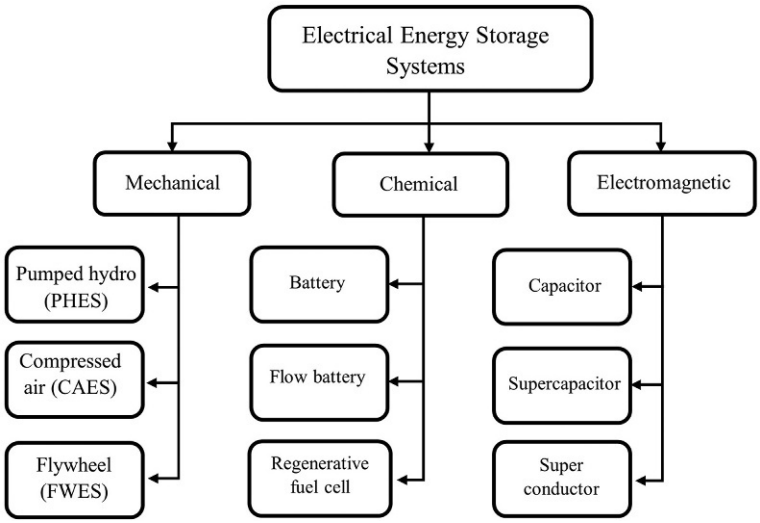

FIG. 9.1 Classification of electrical energy storage systems.

storage could be a hard rock, salt, porous rock, or aquifer. For small-scale CAES, over ground air tanks are used for storing compressed air. In CAES discharging process, the stored compressed air is used to operate the gas turbine. To increase the output of the CAES, compressed air is passed through the combustion chamber operated on natural gas. The motor/generator set works as the motor in the charging process and as a generator in the discharging process.

9.2.1 Types of compressed air energy storage

When a gas is compressed, its pressure and the temperature rise, and the gas after compression becomes warmer. On contrary to this, on expanding a gas, its pressure and temperature go down and the gas after expansion becomes cooler. The storage efficiency of the CAES can be improved by storing the heat generated during the compression process and consuming it during the expansion process. Fig. 9.2 shows the working process of the CAESS.

9.2.1.1 Adiabatic CAES method

In the adiabatic process, no heat is exchanged between the system and the surroundings, and all the heat is retained by the system. Practically, the heat produced during the compression process of the CAES, most of the heat is lost, which decreases efficiency. Adiabatic CAES proposes storing the heat energy produced during the charging process and using this heat energy in the discharging process to reheat the gas withdrawn from the storage cavern to drive the generator coupled gas turbine. The proposed approach of the adiabatic CAES with perfect insulation is anticipated to attain a theoretical efficiency of 70%. Adiabatic CAES reduces the cost of energy by eliminating the use of natural gas for reheating. Heat exchangers are used to extracting the energy from the compressed air and use it to reheat the compressed air [3].

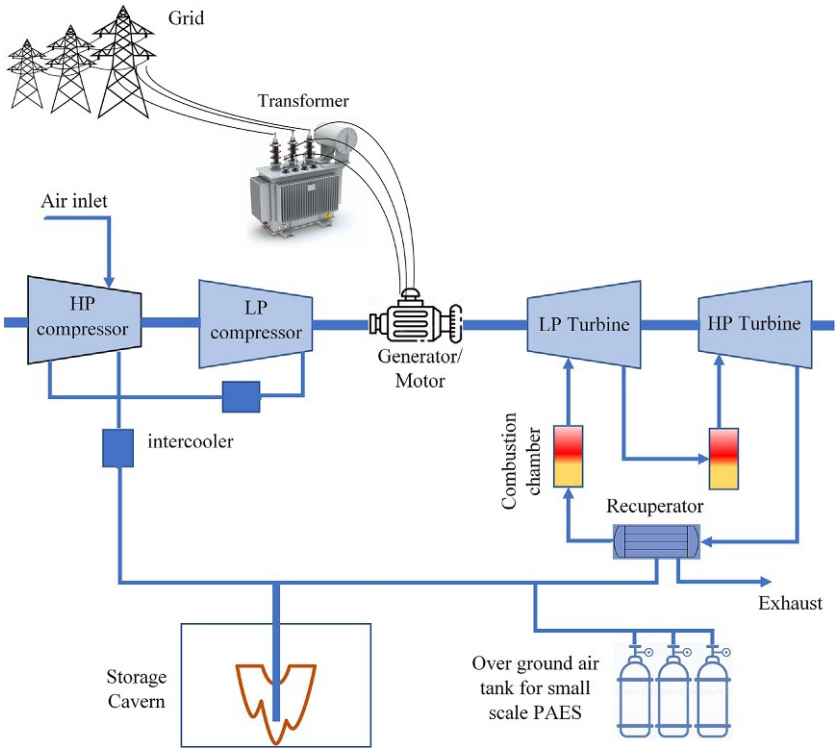

FIG. 9.2 Compressed air energy storage system.

9.2.1.2 Diabatic CAES method

Diabatic CAES is the oldest technology of CAES in which the heat energy generated during the air compression (charging process) is wasted in the atmosphere using intercoolers. During discharging process, the compressed air is reheated using natural gas. The cooling of the compressed air decreases the temperature that increases the storage capacity of the cavern by reducing the volume. It also decreases the thermal stress on the walls of the carven. Fig. 9.2 shows the diabatic CAES process. Today, two diabatic CAES projects are operational; the Huntorf CAES plant in Germany is 42% efficient with salt dome, and the Alabama CAES plant is 54% efficient.

9.2.1.3 Isothermal CAES method

An isothermal process is a process in which the temperature is maintained. In isothermal CAES, gas is compressed and expanded extremely slowly. Isothermal CAES is advantageous over the conventional adiabatic and diabatic CAES methods. The expansion and the compression are done slowly in a controlled way that the temperature remains the same. The heat is removed from the system as it is generated and is transferred to the compressed air in the discharging process to maintain the isothermal process, which makes it more efficient. It allows double compression than the adiabatic CAES and reduces the cost of the conventional adiabatic CAES by one-seventh.

9.2.2 Advantages of compressed air energy storage

- **Load shifting**: CAES is the best solution to load shifting. During high demand, the compressed gas is released to generate electricity and during low demand, the air is compressed and stored.
- **Peak shaving**: CAES can control peak shaving as when the load demand is much higher than the average load, CAES can be used to shift the load.
- **Integration of renewable energy**: CAES gives flexibility to the system by incorporating intermittent renewable energy sources into the conventional sources. When renewable energy sources like solar irradiance and wind are abundant, they can be used to compress and store the air. When these sources are limited, CAES may be activated in the discharging mode.
- **Capacity**: CAES has an advantage over battery storage regarding the chemistry of the battery. Over time, the capacity of the battery decreases because of the irreversibility of the battery reactions.

Example 9.1

The air is compressed from 2 to 40 bar in a CAES that raised the temperature of the system to 645°C. What was the initial temperature of the air before compression? The $\gamma = {}^{C_p}/_{C_v}$ of air is 1.4.

Solution

Given data

$$P_1 = 2 \text{ bar}$$

$$P_2 = 40 \text{ bar}$$

$$T_2 = 645^{\circ}\text{C} = 918 \text{ K}$$

$$T_1 = ?$$

$$\gamma = {}^{C_p}/_{C_v} = 1.4$$

The initial temperature of the air before compression can be determined by the following relation.

$$\frac{T_2}{T_1} = \left(\frac{P_2}{P_1}\right)^{\frac{\gamma-1}{\gamma}}$$

$$\frac{918}{T_1} = \left(\frac{40}{2}\right)^{\frac{1.4-1}{1.4}}$$

$$T_1 = 390 \text{ K} = 117^{\circ}\text{C}$$

9.3 Flywheel energy storage

Flywheel energy storage (FES) is a very interesting technology. Fig. 9.3 shows the working principle of FES. During the off-peak hours or when the electricity production is larger than the energy demand, surplus energy is used to drive the motor connected to the flywheel. This flywheel converts the electrical energy into rotational kinetic energy. During the peak hours when grid electricity is expensive or when the energy demand is greater than the production, the motor is rotated as a generator. The major key components of the flywheel energy storage are as follows.

- **Flywheel rotor**: The most important part of the FES is the flywheel rotor. The efficiency of the FES depends upon the design and shape of the flywheel rotor. The flywheel rotor works at a very high speed, making thousands of rotations per minute and storing energy in kinetic form. The design of the rotor must enhance the energy density without degrading the thermal and mechanical stress-bearing capability. The rotational kinetic energy in the mass of the flywheel rotor is determined by Eq. (9.1).

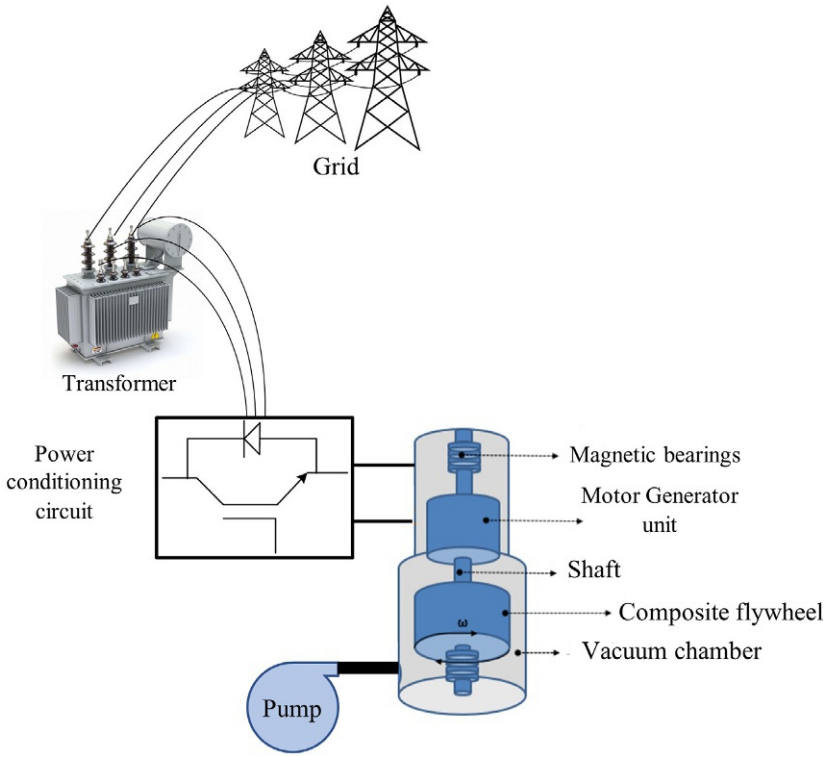

FIG. 9.3 Flywheel energy storage system [4].

$$K.E. = \frac{1}{2} I\omega^2 \tag{9.1}$$

where I is the moment of inertia and ω is the angular velocity.

The moment of inertia (I) depends upon the shape and structure of the body. In the flywheel case, the wheel is solid and its moment of inertia can be determined by Eq. (9.2).

$$I = \frac{1}{2} mr^2 \tag{9.2}$$

where m is the mass of the wheel and r is the radius of the wheel.

The angular velocity (ω) is determined by Eq. (9.3).

$$\omega = \frac{2\pi N}{60} \tag{9.3}$$

- **Containment**: The flywheel rotor is encased in a strong casing since strong forces are involved whose failure can be catastrophic. It is also used to provide a vacuum to the flywheel rotor to protect against air friction.
- **Supporting bearings**: The flywheel rotor is supported in the vacuum chamber using bearings. The proper design of the bearings reduces the air frictional losses. Conventionally, mechanical bearings were used that are inexpensive and reliable but they also need continuous maintenance and replacement because of the wear and tear. For high-speed applications, the flywheel is supported by magnetic levitation to reduce mechanical losses. Magnetic bearings at high speed are reliable, and have a quick response and longer lifetime.
- **Energy conversion system**: In a microgrid application, various power electronics converters (AC-AC, AC-DC, DC-AC, DC-DC) can be employed to integrate the FES into the microgrid. The basic function of the flywheel is to convert the mechanical energy for the end-use application, which is electrical energy. For this conversion, an electromechanical machine is required which could be a motor/generator set.
- **Generator and motor**: When the kinetic energy is being stored, the motor is used to drive the flywheel. When the stored kinetic energy is recovered and converted to electricity, the motor is used as a generator.
- **Vacuum chamber**: Since the flywheel is the rotating part, it is enclosed in a vacuum chamber to avoid air frictional losses and protect it from the outside, which increases the conversion efficiency.
- **Renewable energy integration**: A flywheel can be used with renewable energy systems in hybrid energy mode. Fig. 9.4A shows the integration of the wind turbine with the flywheel. When the wind speed is enough to generate the electricity, the load is managed and the surplus energy is stored in the flywheel. When wind energy is not available, the load is managed with the energy stored in the flywheel. Similarly, when wind energy is not available, the load is managed with the energy stored in the flywheel. As shown in Fig. 9.4B, solar energy is stored in the flywheel. Solar energy is first converted into AC using a power electronic inverter [5].

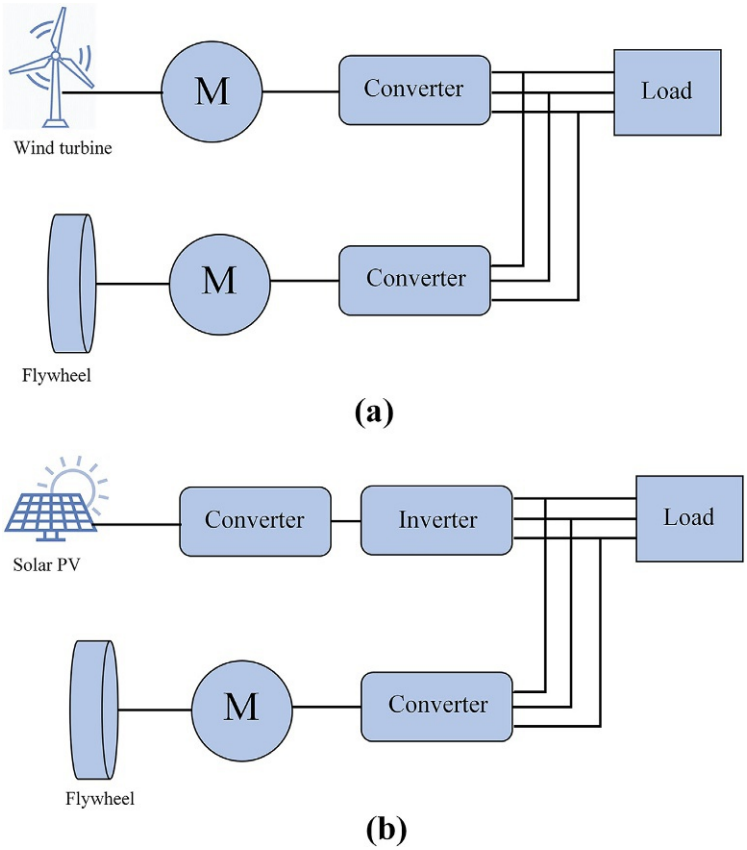

FIG. 9.4 (A) Flywheel energy storage system integrated with wind turbine and (B) flywheel energy storage system integrated with solar PV.

Example 9.2

The disk of a flywheel is rotating at 2000 rpm. On the flywheel, the diameter of the wheel is 15 m and the thickness is 6 m. The disk of the flywheel is made up of material with a uniform density of $1500\,\text{kg/m}^3$.

How much energy is stored in the flywheel?
If the flywheel slows down to 1200 rpm, how much energy can be recovered from the flywheel?

Solution
Given data

$$d = 15\text{ m} \Longrightarrow r = 7.5\text{ m}$$

$$N = 2000\text{ rpm}$$

$$thickness = h = 6\text{ m}$$

$$\rho = 1500 \text{ kg/m}^3$$

Solution

(a)

The energy that is stored in the flywheel can be determined using Eq. (9.1).

$$E = \frac{1}{2} I \cdot \omega^2$$

The moment of inertia of the solid disk (flywheel) is determined by the following relation:

$$I = \frac{1}{2} m r^2$$

The mass of the flywheel can be determined using the density given in the question as follows:

$$\rho = \frac{m}{V}$$

The volume of the flywheel is determined by the method as shown in the following figure:

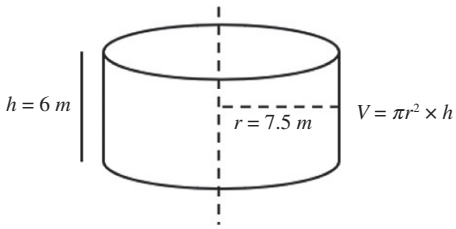

$$1500 = \frac{m}{\pi r^2 \times h}$$

$$m = 1,589,625 \text{ kg}$$

We put the values of m and r in Eq. (9.2) to calculate the moment of inertia:

$$I = \frac{1}{2}(1,589,625)(7.5)^2$$

$$I = 44,708,203 \text{ kg m}^2$$

The angular frequency of the flywheel is determined by Eq. (9.3).

$$\omega = \frac{2\pi N}{60}$$

$$\omega = 209.3 \text{ rad/s}$$

$$E = \frac{1}{2}(44,708,203) \cdot (209)^2$$

$$E = 976 \text{ GJ}$$

(b)

If the rpm of the flywheel changes, it will change the angular frequency of the wheel. We determine the energy in the flywheel at 1200 rpm, then we shall take the difference of both energies to determine the recovered energy from the flywheel.

At $N = 1200$ rpm ω is 125.6 rad/s

$$E = \frac{1}{2}(44, 708, 203) \cdot (125.6)^2$$

$$E = 352 \text{ GJ}$$

Hence the energy recovered from the flywheel is

$$E = \frac{1}{2}I\omega_f^2 - \frac{1}{2}I\omega_i^2$$

$$E = (352 - 976) \text{ GJ}$$

$$E = 624\ GJ$$

9.4 Pumped hydro energy storage

Pumped hydro energy storage (PHES), also known as pumped-storage hydroelectricity, is the storage of energy in the form of potential energy in the water. During off-peak times, low-cost surplus electricity is used to pump the water from low altitudes to higher altitudes. The mechanism of PHES is shown in Fig. 9.5. The reservoir for PHES is smaller than the conventional hydro dams. In off-peak hours, surplus energy from conventional sources (coal or nuclear) or intermittent sources (wind, solar, etc.) is used to lift the water from the lower water

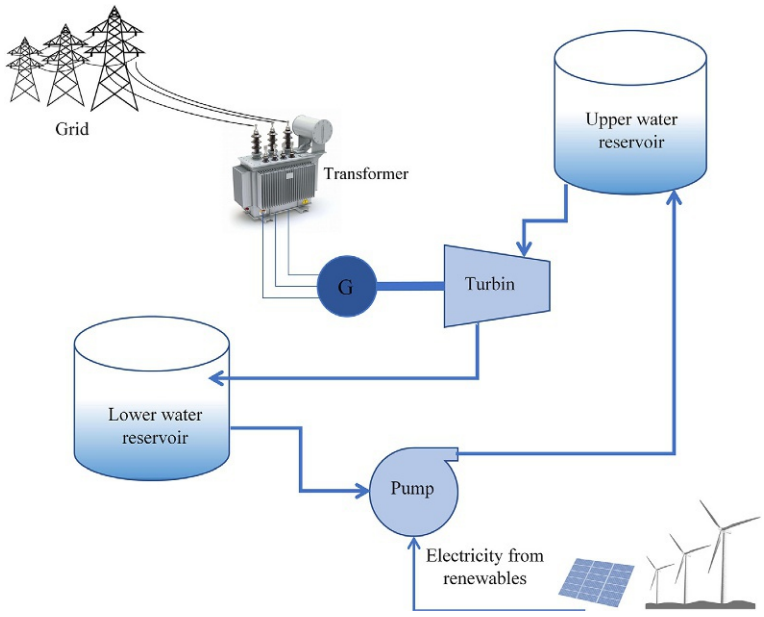

FIG. 9.5 Pumped hydro energy storage system.

reservoir to the upper water reservoir. The water is retained in the upper water reservoir until electricity is required. During the peak hours when there is a shortfall of electricity, the water from the upper water reservoir is used to rotate the hydro turbine coupled to the generator. The cost incurred on the extra consumption of energy by the pump is recovered by selling the electricity during the peak hours at the highest rates [6,7]. Table 9.1 shows the five largest PHES plants. Table 9.2 gives a detailed comparison between the mechanical ESSs.

The potential energy contained by the water at the upper reservoir can be calculated by Eq. (9.4).

$$P.E. = mgh \tag{9.4}$$

The power from this potential energy is determined by incorporating the efficiency of the turbine and coupled generator as given in Eq. (9.5) [8].

$$P = \rho\, g\, h\, Q\, \eta \tag{9.5}$$

where P is the available power; ρ is the water density; g is the gravitational acceleration; Q is the flow rate; h is the gross head without deducting head losses; and η is the combined efficiency of the turbine and generator.

The key advantages of the PHES are as follows.

- **Economically viable**: Having the capability to provide electricity at the highest rates during the peak demand hours makes it cost-effective and economically viable.
- **Reliability and flexibility**: PHES is reliable and flexible in a way that it can respond to sudden fluctuations in the power system by absorbing surplus electricity and generating extra electricity. It is reliable in the sense that even though there is no solar irradiance and no wind, PHES has the capability of generating electricity. PHES also has the longest discharge period compared to other energy storage technologies.
- **Efficiency**: Including the energy consumed by the pump and the head losses, PHES can reach a level of 82% efficiency.
- **Hybrid energy system**: PHES can be hybridized with other renewable energy sources in the distributed generation or can be a part of a hybrid energy system.
- **Lifetime**: The lifetime of the PHES is expected to be more than 80 years.
- **Multifunctional**: PHES is a multifunctional power project. All the following functions can be performed by the PHES: wastewater management, water distribution, and irrigation for agriculture.
- **Matured technology**: Hydropower is the most mature technology since it has the option of power balancing, flexibility, reliability, availability, and more efficiency.

TABLE 9.1 Pumped hydro storage power stations.

Power station	Country	Capacity (MW)
Bath County Pumped Storage Station	USA	3003
Okutataragi Pumped Storage Power Station	China	2400
Guangdong Pumped Storage Power Station	China	2400
Ludington Pumped Storage Power Plant	Japan	1932
Huizhou Pumped Storage Power Station	USA	1872

TABLE 9.2 Comparison of mechanical energy storage systems.

Technology	Advantages	Disadvantages
Compressed air energy storage (CAES)	• High energy storing capacity • Longer lifetime • Matured technology • Efficiency of 80% • High energy density • Comparatively lower cost	• Variable efficiency • Leakage concerns
Pumped hydro energy storage (PHES)	• Reliable and flexible • Advanced technology • Longer lifetime • High storage capacity • Efficiency of almost 82% • Moat matured technology • Less cost/kWh	• Land acquisition cost • Lower energy density • High capital investment
Flywheel energy storage (FES)	• Response time is low • Short discharging time • Highest depth of discharge, more than 100,000 cycles • Efficiency of 90% • Lower maintenance • Negligible environmental effects • Excellent load following characteristics	• High mechanical stress • High mechanical bearings losses • Short discharge time • Potentially harmful catastrophe

- **Renewable and sustainable**: A PHES that is not located at the river or near the natural channel of water is called a closed PHES in which water is recaptured and pumped up after generating electricity. Hence, no environmental hazards are there in closed PHES. This closed PHES can be installed at any location to give a storage backup to the grid.

Example 9.3

500 kg water is at the potential of 50 m in a pumped hydro ESS. Calculate the energy stored in this water if the density of the water is 1000 kg/m^3.

Given data

$$m = 500 \text{ kg}$$

$$h = 50 \text{ m}$$

Solution

The potential energy stored in the water at a height can be calculated by using Eq. (9.4) as follows.

$$E = mgh = 500 \times 9.8 \times 50$$

$$E = 245 \text{ kJ}$$

9.5 Lithium-ion batteries

Batteries are characterized as primary batteries and secondary batteries. Primary batteries are those which cannot be recharged once used or discharged, whereas secondary batteries are those which can be recharged after being used or discharged. In secondary batteries, cells termed anode and cathode are immersed in an electrolyte. The energy is generated and stored by reversible electrochemical reactions. The oxidation takes place at the anode and the reduction takes place at the cathode. In oxidation, electrons are generated at the anode traveling to the external circuit where the load is connected. In reduction, these generated electrons at the cathode and traveling through the external circuit are collected by the cathode. Secondary batteries are of different types (Li-ion, led acid) depending upon the material of the electrodes, and the type of the electrolyte. The construction and charging-discharging process of the Li-ion battery is shown in Fig. 9.6.

Li-ion batteries are those in which Li-atoms are ionized at the anode separating electrons from the Li-atom. The electrons move from the anode to the cathode through the external circuit. Li-ions move from the anode to the cathode through the nonaqueous electrolyte during the discharging process where they recombine the electrons coming from the external circuit. Li-ions are so small that can be passed through the separator between anode and cathode. The anode is made up of metal oxide and the cathode is of graphite.

A Li-ion battery starts its life from fully discharged and its chemicals are not able to provide any electricity.

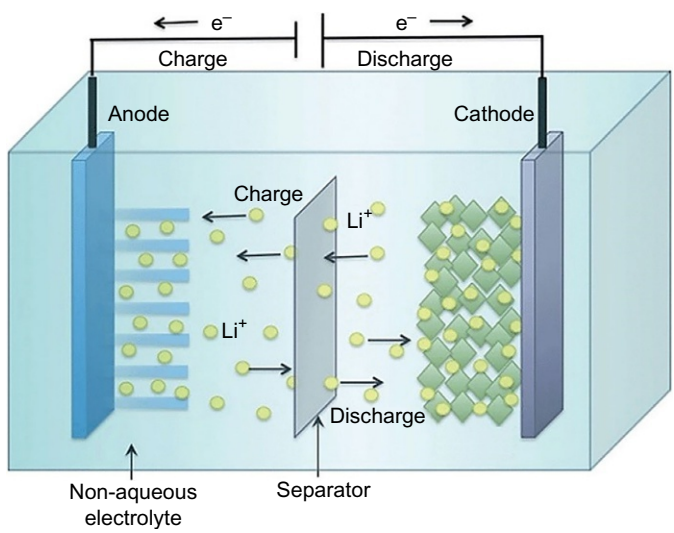

FIG. 9.6 Construction and working of lithium-ion battery [9].

9.6 Lead-acid batteries

The lead-acid battery (La-battery) is the oldest storage technology invented by Gaston Plante, a French physicist, in 1859. The La-battery was the first storage technology that is a rechargeable battery. Although the LA batteries are of low energy density, they have wide applications in solar photovoltaic systems. Their cost is lower than for other batteries and they have a longer lifetime.

An La-battery is constructed by two electrodes named an anode and cathode. The cathode is made up of porous lead (Pb) for easy dissolution of lead. The anode is made up of lead oxide (PbO_2). Both electrodes are immersed in sulfuric acid (H_2SO_4) electrolyte. The reactions occurring at anode and cathode are shown in Eqs. (9.6), (9.7), respectively.

$$Pb + SO_4^{-2} \xleftrightarrow{Charge, Discharge} PbSO_4 + 2e^{-1} \tag{9.6}$$

$$PbO_2 + SO_4^{-2} + 4H^+ + 2e^{-1} \xleftrightarrow{Charge, Discharge} PbSO_4 + H_2O \tag{9.7}$$

The overall reaction of the LA battery is shown in Eq. (9.8).

$$PbO_2 + Pb + 2H_2SO_4 \xleftrightarrow{Charge, Discharge} 2PbSO_4 + 2H_2O \tag{9.8}$$

During the discharging process, both anode and cathode take the sulfate ions (SO_4^{-2}) from the sulfuric acid (H_2SO_4) electrolyte. The separation of sulfate ions from sulfuric acid makes the electrolyte less concentrated. As a result of the complete discharge of the battery, both the electrodes are fully covered by lead sulfate ($PbSO_4$) surrounded by water instead of sulfuric acid. At this stage, there is no potential between the electrodes. In practical applications, the battery is not allowed to discharge fully if the state of charge (SOC) of the battery is kept below the minimum allowed state of charge (SOC_{min}) for an extended period, the $PbSO_4$ crystals grow up on both electrodes, reduce the battery potential, and permanently reduce the battery capacity. When the battery is completely recharged, the anode is PbO_2, the cathode is Pb, and the energy is stored in an aqueous solution of H_2SO_4. In the batteries in which electrolytes are involved, the SOC can easily be found by determining the specific gravity of the electrolyte. The SOC of the battery diminishes with the decrease in specific gravity. Fig. 9.7 illustrates the charging and discharging process of a lead acid battery.

Some key features of the LA batteries are as follows.

9.6.1 Battery capacity and depth of discharge

The energy that a battery can deliver is calculated by multiplying the depth of discharge (DOD) of the battery by its capacity, hence, DOD is an important parameter in the design process of the solar photovoltaic integrated battery bank. Other than the DOD of the battery, battery temperature and the battery discharge rate also affect the capacity of the battery. High temperatures of the battery are not suitable for its life since it increases the aging process, electrolyte usage, and self-discharging. Every degree rise in the temperature of the battery decreases the capacity by 1%.

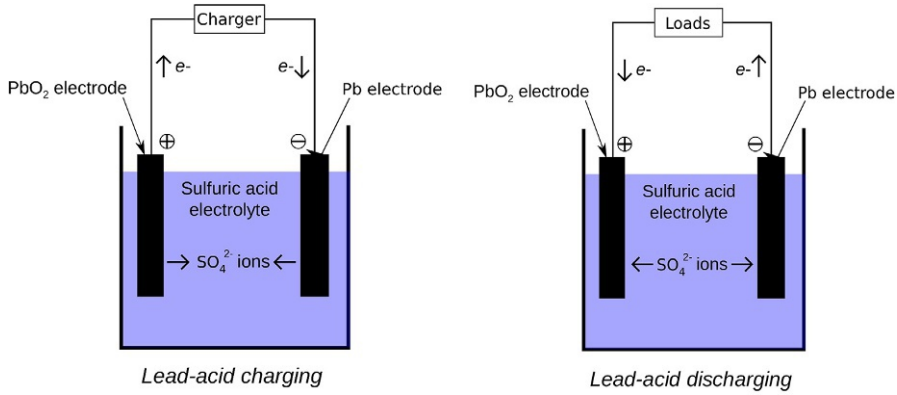

FIG. 9.7 (A) Charging process of lead-acid battery and (B) discharging process of lead-acid battery [10].

9.6.2 Specific energy

Specific energy is also termed the gravimetric energy density of a battery and is defined as the amount of electrical energy that is stored for every kilogram of battery mass. The specific energy of the Li-ion battery is better than that of the nickel-cadmium (Ni-Cd) one. The higher specific energy of Li-ion makes it perfect for lighter-weight applications such as laptops and cell phones. Specific energy is measured in Wh/kg.

9.6.3 Energy density

Energy density is also termed the volumetric density of a battery and is defined as the amount of electrical energy stored per cubic meter of the battery volume. Energy density is measured in Wh/m^3. Energy density is a function of the weight of the battery and the volumetric energy density is the function of the volume of the battery. A battery with a higher energy density means that the battery would be lighter than the battery with a lower energy density. For the same capacity, the battery with high energy density will occupy less volume, whereas the battery with lower energy density will occupy a large volume. The energy density of Li-ion batteries is higher than that of Ni-Cd batteries.

9.6.4 The lifetime of the battery

With the passage of time and the increase in charging/discharging cycles, crystals of lead sulfate are formed on the battery electrode which reduces the effectiveness of the active materials and reduces the capacity of the battery. The reduction in battery capacity is because of the following parameters:

- charging and discharging cycles that the battery has experienced;
- the DOD of the battery over its lifetime;
- the average battery temperature over its lifetime; and
- discharge of the battery below the minimum allowed the state of charge (SOC_{min}) for a protracted time period.

9.6.5 The efficiency of the battery

Energy efficiency is defined as the ability of the battery to convert one form of energy to another, like electrical to mechanical and mechanical to electrical energy. The energy efficiency of the LA battery is about 70% and the Coulombic efficiency (CE) is 85%. CE is the discharge capacity to charge capacity ratio, as shown in Eq. (9.9).

$$\mathrm{CE} = \frac{Q_{discharge}}{Q_{charge}} \tag{9.9}$$

Energy efficiency (EE) is determined by Eq. (9.10).

$$\mathrm{EE} = \mathrm{CE} \times \mathrm{VE} \tag{9.10}$$

where voltage efficiency (VE) is the difference between voltages at the charging and discharging process.

9.6.6 Maintenance

Maintaining the water level of the battery is necessary since the production of oxygen and hydrogen reduces the water level of the battery.

9.7 Nickel-based batteries

Nickel-based batteries are used in electric vehicles, hybrid electric vehicles, and other standby applications. Nickel-cadmium (Ni-Cd) batteries are considered the most mature battery technology and were invented 100 years ago. An Ni-Cd battery is a type of rechargeable battery consisting of nickel oxide hydroxide anode, metallic cadmium as cathode, and an alkaline electrolyte of potassium hydroxide (KOH). The two electrodes are separated by a nylon divider, which prevents the direct charge exchange between the anode and cathode. The operation of the battery depends upon the reduction and oxidation reactions at the electrodes. The equivalent circuit diagram of the Ni-Cd battery in the discharging and charging modes is shown in Figs. 9.8 and 9.9. The gradient of the battery voltage during discharging and charging is shown in Eqs. (9.11), (9.12), respectively.

$$\left(\frac{dv}{dt}\right)_d = -V_{oc}\frac{R_{ex}}{(R + R_{ex})^2 C_1} \tag{9.11}$$

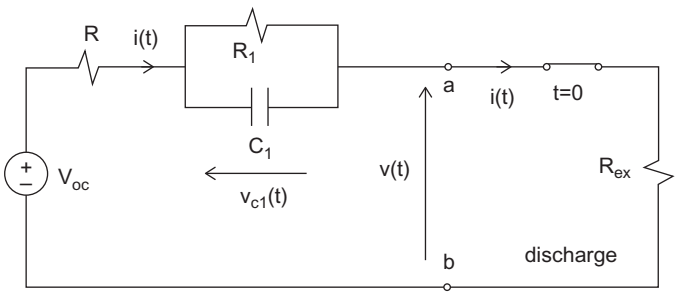

FIG. 9.8 Equivalent circuit of a Ni-Cd battery during the discharging process [11].

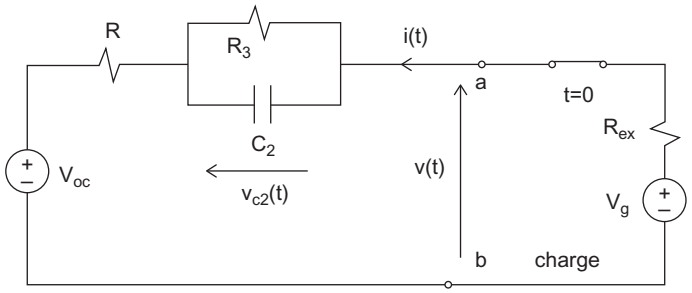

FIG. 9.9 Equivalent circuit of a Ni-Cd battery during charging process [12].

TABLE 9.3 Technical parameters of Ni-based batteries [13].

Battery	Cell voltage (V)	Specific power (W/kg)	Specific energy (Wh/kg)	Energy efficiency (%)
Nickel cadmium	1.2	200	50–60	70–75
Nickel iron	1.2	100	30–60	60–70
Nickel zinc	1.65	170–1000	80–100	70–80
Nickel hydrogen	1.55	220	55–75	85
Nickel-metal hydride	1.2	170–1000	60–70	70–80

$$\left(\frac{dv}{dt}\right)_c = \left(V_g - V_{oc}\right)\frac{-R_{ex}}{\left(R + R_{ex}\right)^2 C_2} \tag{9.12}$$

The other types of Ni-based batteries are nickel-iron, nickel-zinc, nickel-metal hydride, and nickel-hydrogen. The technical properties of these Ni-based batteries are shown in Table 9.3.

9.8 Capacitors and electrochemical capacitors/supercapacitors

The electrochemical capacitor, also known as the supercapacitor, consists of two electrodes named an anode and cathode separated by a dielectric insulator. A dielectric could be made up of plastic film, glass, or ceramic. When a voltage is applied across the electrodes, an electric field is developed between the electrodes. A capacitor stores energy in its electric field. Comparing the capacitors to other energy storage technologies, the charging of the capacitor is very fast, but the energy density is very low, and the self-discharging of the capacitor is very fast.

A supercapacitor is also known as an ultrafast capacitor or electrochemical capacitor. Supercapacitors have very high capacitance, having characteristics between those of a capacitor and battery. An electrochemical capacitor consists of carbon electrodes separated by a porous membrane immersed in an electrolyte. The membrane allows the ions to pass through and blocks electrons. The capacitance and the energy are determined by Eqs. (9.13), (9.14), respectively.

$$C = \frac{A\varepsilon_0}{d} \tag{9.13}$$

$$E = \frac{1}{2}CV^2 \tag{9.14}$$

where A is the effective area of the electrode plates; ε_0 is the dielectric constant of the insulating medium; and d is the distance between the electrodes plates.

Eqs. (9.13), (9.14) indicate that the capacitance is directly proportional to the area of the electrode plates and inversely proportional to the distance between the plates. The energy stored in the electric field of the capacitor is directly proportional to both capacitance and the voltage. Table 9.4 shows a detailed comparison of capacitors and supercapacitors. The working process and the construction of a supercapacitor are shown in Fig. 9.10.

9.9 Superconducting magnetic energy storage

Superconducting magnetic energy storage (SMES) consists of a superconducting coil that stores energy in its magnetic field when DC is passed through that coil. The coil is cooled below the superconducting critical temperature. A SMES consists of two circuits. The primary circuit consists of a superconducting coil and power conditioning unit and the secondary circuit is the cryogenically cooled refrigerator as shown in Fig. 9.11. The energy stored in the magnetic field of the magnetic coil is directly proportional to the inductance of the coil and the current passing through it as shown in Eq. (9.15). The stored energy can be retrieved from the magnetic coil by discharging during peak hours or when demand is higher than the supply. The block diagram and the working of the superconducting magnetic ESS are shown in Fig. 9.11.

$$E = \frac{1}{2}LI^2 \tag{9.15}$$

TABLE 9.4 A comparison between capacitors and supercapacitors.

	Capacitor	Supercapacitor
Definition	Energy is stored in electric field	Energy is stored in electrolyte
Energy density	Low energy density	High energy density
Dielectric material	Electrodes separated by dielectrics: polymer films, ceramic, or aluminum oxide	Double electric field is established between the electrodes using carbon for separation
Applications	Coupling and suppression, oscillators, power conditioning, power factor correction	RAM, microcomputer, CMOS RAM, IC for clocks, the power source for LEDs, buzzer, and toys
Advantages	Avoids excessive power drawing and protects car batteries from deep draining or complete depletion	Supercapacitors can be charged and discharged without damaging the equipment; low internal resistance and low equivalent resistance provide high power density
Charging time	Take longer to charge and discharge than supercapacitor	Energy charging and discharging of a supercapacitor is very fast
Power consumption	Draws less power than supercapacitor	Draw more power and the devices attached will also draw more power
Cost	Comparatively low cost	Comparatively high cost

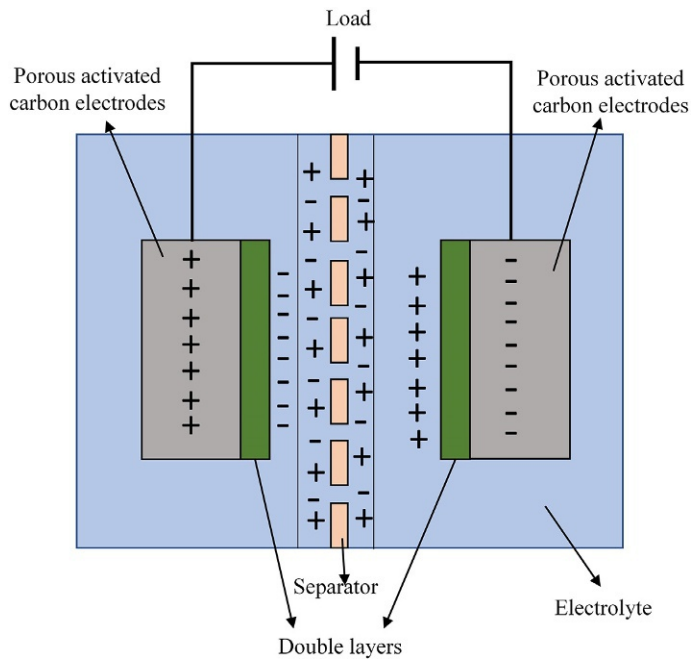

FIG. 9.10 Working process diagram of supercapacitors.

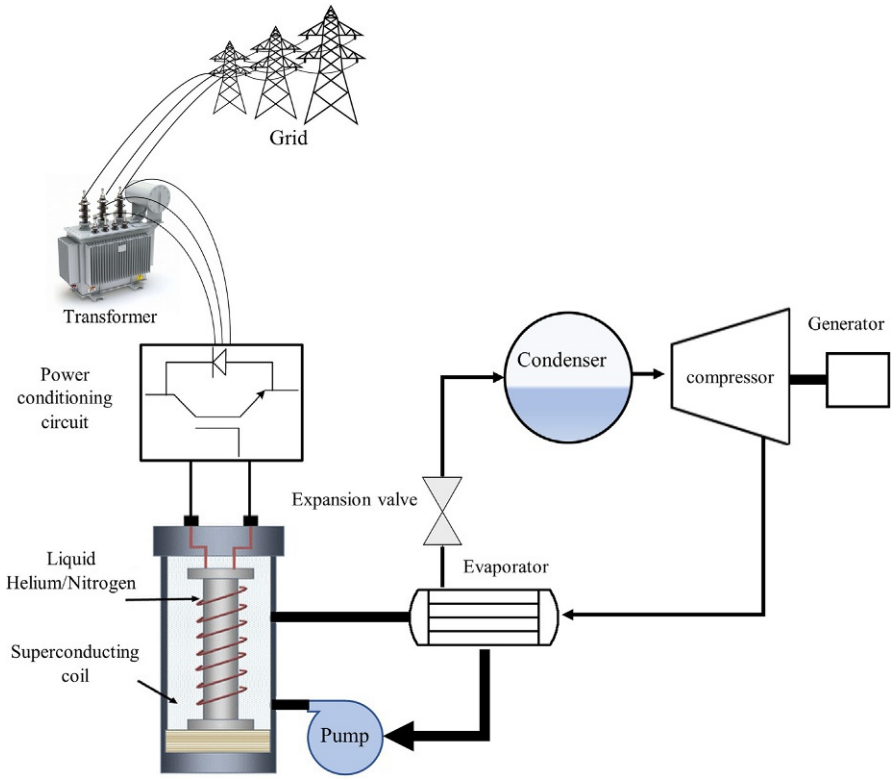

FIG. 9.11 superconducting magnetic energy storage system [4].

The power conditioning unit consists of a rectifier and an inverter. During the charging process, AC is converted into DC to pass it through the magnetic coil. During discharging process, the stored DC energy is converted back into AC using an inverter. Because of the high cost of the magnetic coil and the cooling refrigerator, the system becomes expensive and is used for short-term energy storage and high power applications.

9.10 Flow batteries

A flow battery is a type of electrochemical rechargeable battery in which chemical energy in the form of two electrolytes is pumped through the system separated by the ion exchange membrane. The ion exchange membrane keeps the electrolytes separate in their own space and permit the ions to exchange through the membrane. The electrolyte enclosed in the cathode tank is termed a catholyte and the electrolyte that is filled in the anode tank is called an anolyte. The construction of the flow battery is illustrated in Fig. 9.12. The production of power is dependent on the area of the electrodes and the time of storage of electricity depends upon the volume of the electrolyte. Flow batteries are preferred over other standard batteries since they have a quick response time, a longer lifetime, and capacity can be increased just by

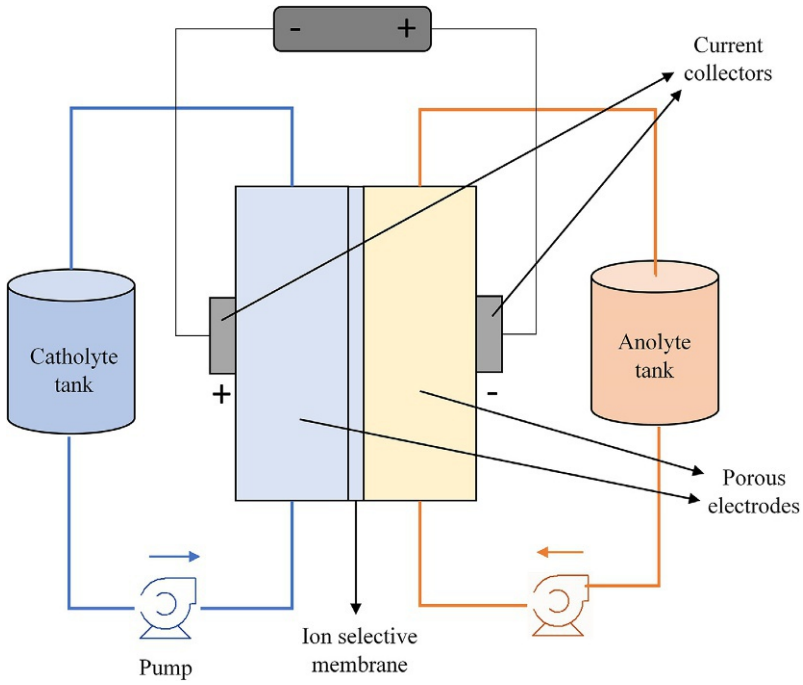

FIG. 9.12 Working process diagram of a flow battery.

increasing the tank size of the electrolytes. At present the main types of flow batteries are zinc bromine, vanadium redox, and polysulfide bromide [14].

Among the three flow batteries, vanadium redox is the most mature technology of flow battery. Both the sections and tanks contain vanadium in sulfuric acid, but at different charge states. The state of the vanadium in the catholyte tank is V^{5+} in the charging mode and V^{4+} in the discharging mode. The state of the vanadium in the anolyte tank is V^{2+} in the charging mode and V^{3+} in the discharging mode.

The ion-selective membrane allows only the protons (H^{+}) to pass through the membrane to balance the charge in the cell, and the completion of the reactions is given in Eqs. (9.16), (9.17). Voltage is applied across the battery terminals during the charging process, which releases an electron on the positive side. The released electrons move through the external circuit and reach the negative side. During the discharge process, the accumulated electrons are released and move through the external circuit (load) to the positive side [15].

$$V^{3+} + e^{-1} \rightleftharpoons V^{2+} \tag{9.16}$$

$$V^{4+} \rightleftharpoons V^{5+} + e^{-1} \tag{9.17}$$

Another type of flow battery is the zinc bromine (ZnBr) battery, which is a hybrid flow battery. Two different electrolytes are kept in two separate tanks separated by an ion-selective membrane. The anolyte tank contains water-based zinc and the catholyte tank contains an organic amine compound-based bromine solution. One pump is used to circulate the electrolyte in the anolyte tank and the other circulates the electrolyte in the catholyte tank. The

electrodes are of carbon. During the charging process, zinc metal is plated on the negative electrode and the electrons travel from the negative electrode to the positive electrode through the load, as shown in Eq. (9.18). At the positive electrode, bromide ions are oxidized to bromine, as shown in Eq. (9.19).

$$Zn^{2+} + 2e^{-1} \rightleftharpoons Zn \tag{9.18}$$

$$2Br^{-} \rightleftharpoons Br_2 + 2e^{-1} \tag{9.19}$$

9.10.1 Advantages of flow batteries

- Flow batteries are scalable and modular. They can be scaled from a few watts to megawatts that can be implemented for a wide range of applications. They can store energy for many days.
- Almost all the parts of the battery can be recovered to reconstruct from the scratch. The electrolyte can also be drained out. This will reduce the cost of the system.
- The electrodes and electrolytes are not permanently damaged if the battery is overcharged or deeply discharged.
- The lifecycle of the battery is long and the response time is quick.
- The balancing of the cell and the operation of the battery are quite simple since the electrolyte is associated with all the cells and the SOC of the battery is the same for each cell.
- When the batteries are in shutdown mode, no self-discharging occurs.

9.10.2 Disadvantages of flow batteries

- The energy density of the flow battery is very low. To increase the energy density, the volume of the electrolyte tanks needs to be increased.
- Charging and discharging rates of the flow batteries are very slow; these can be improved by increasing the area of the electrodes and the separator, which will increase the cost of the system.

9.11 Thermodynamics of battery storage

The first law of thermodynamics, also stated as the law of conservation of energy, is defined as the total energy of the system conserved. It is also stated as the difference between the energies coming into the system and all the energies going out of the system is equal to the change of energy in the system, as shown in Eq. (9.20). Another statement of the first law of thermodynamics is that energy cannot be created or destroyed, but it can be transformed from one type of energy to another. For example, in hydropower, water cannot be transformed into electrical energy. However, the potential energy of the water that is at a high altitude can be transformed into kinetic energy that will rotate the turbine. The generator coupled to the turbine will convert this kinetic energy into electrical energy.

$$\Delta E_{system} = E_{in} - E_{out} \tag{9.20}$$

The thermodynamic definition of the first law of thermodynamics is that when a specific amount of heat is transferred to a system, the energy is used to do some internal work and the rest of the heat is used to raise the internal energy of the system, which can mathematically be written as Eq. (9.21).

$$Q = \Delta U + W \tag{9.21}$$

A battery is a device that converts chemical energy into electrical energy, or if it is rechargeable, it also converts electrical energy into chemical energy. As discussed in the above sections, a battery consists of two electrodes. One electrode is called an anode, where oxidation takes place, and the other is a cathode, where reduction occurs. Both electrodes are immersed in an electrolyte. As a result of the oxidation reaction at the anode, electrons are generated which move from the anode to the external circuit, generating electricity. Another conversion of energy can take place if a motor is connected to the external circuit; this will be a conversion of chemical to electrical and electrical to mechanical conversion. This strengthens the first law of thermodynamics, that energy cannot be created nor destroyed but can be transformed from one form to another. It should be noted here that all the energy is not converted into the required form of energy; some of the energy is also converted into heat energy.

The spontaneity of a reaction that the reaction will continue on its own is determined by the sign of the Gibbs free energy, which is given by Eq. (9.22).

$$\Delta G = \Delta H - T \cdot \Delta S \tag{9.22}$$

If the change in Gibbs free energy is negative, it means the reaction will occur spontaneously. If the change in Gibbs free energy is positive, it means the reaction is not spontaneous. Gibbs free energy is related to the electrical parameters of the battery by Eq. (9.23).

$$E = -\frac{\Delta G}{nF} \tag{9.23}$$

From Eqs. (9.22), (9.23), the value of ΔG can be made equal as follows:

$$-EnF = \Delta H - T \cdot \Delta S$$

$$E = \left(\frac{\Delta S}{nF}\right) T - \left(\frac{\Delta H}{nF}\right) \tag{9.24}$$

$$\Delta \mathrm{H} = \sum \left(h_f\right)_{\text{products}} - \sum \left(h_f\right)_{\text{reactants}} \tag{9.25}$$

$$\Delta \mathrm{S} = \sum \left(S_f\right)_{\text{products}} - \sum \left(S_f\right)_{\text{reactants}} \tag{9.26}$$

Eq. (9.24) is helpful and easy to implement in determining the voltage of the battery since the values of ΔH and ΔS can be measured by Eqs. (9.25), (9.26). The above equation incorporates only the impact of temperature variation on the battery voltage. To incorporate the impact of both temperature change and concentration variation, the Nernst equation can be written as Eqs. (9.27), (9.28).

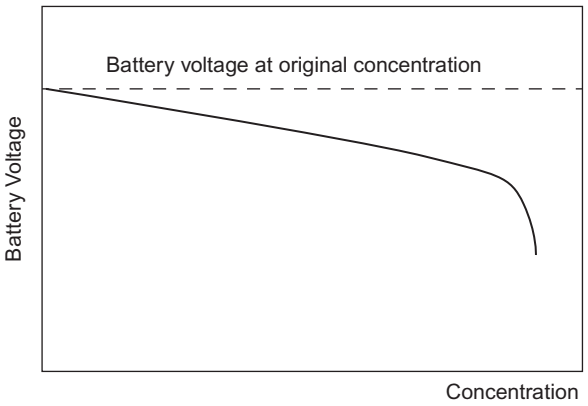

FIG. 9.13 Graph between the concentration of electrolyte and the battery voltages.

$$E = \dot{E} + \left(\frac{RT}{nF}\right) \ln(Q) \tag{9.27}$$

$$E = \dot{E} + \left(\frac{RT}{nF}\right) \ln\left(\frac{(P_{reactants})^x}{(P_{products})^y}\right) \tag{9.28}$$

where E is the open-circuit voltage of the fuel cell at temperature T; $\dot{E}$ is the standard potential of the reaction; T is the operating temperature; R is the general gas constant; $F$is the Faraday's constant, 96,487 C/mol; n is the number of electrons involved; x, y is the coefficient of reactant, and products respectively from the balanced chemical equation; $P_{react.}$ is the partial pressure of the reactant; and $P_{prod.}$ is the partial pressure of the products.

Fig. 9.13 shows the relation between the concentration of the electrolyte in the battery and the battery voltages. Graphs show an inverse relation between them. At the original concentration, the battery voltages are constant. With regular charging and discharging, the concentration of the electrolyte varies, in turn causing the battery voltages to vary.

9.12 Energy storage applications

9.12.1 Grid stabilization

Renewable energy sources are the main energy sources in the smart grid but these energy sources are intermittent. The energy from renewable energy sources may vary unpredictably. It is a significant challenge for power grid operators to manage the sudden variations in the generation and consumption of electricity. The conventional approach to managing the power is to increase or decrease the power generation. For example, in peak hours when there is an increase in demand, quick response and flexible energy sources like a natural gas turbine and hydro turbine are brought into the system. Similarly, when solar irradiance is at its peak or the wind velocity is at its maximum value, generation from other sources is cut down.

Instead of adjusting the output power of the power generation system, an alternative solution is now adopted, provided by the ESSs. ESSs provide the possibility of absorbing the surplus energy generated by the energy sources and providing absorbed energy when the energy sources are not able to generate enough electricity.

9.12.2 Renewable energy integration

Almost all renewable energy resources are intermittent and vulnerable to variation depending upon the time of the day and the weather. These variations can badly degrade the performance of the power electronics equipment, communication, and information systems in the grid. ESSs can overcome this problem. Energy is first stored in the ESS and smoothly gives energy to the load.

9.12.3 Power quality

When comes to renewable energy sources, like wind energy and solar energy are intermittent because of their dependence on environmental conditions. The power quality of the grid is affected when a variation in wind speed or solar irradiance occurs. The variable energy sources cause a variation in active and reactive power, harmonics, voltage, and switching mechanisms. The solution to these variations in the quality of the power injected into the grid is the use of ESS. The wind turbine and the solar PV are connected to the batteries. The batteries maintain the constant power from the varying energy sources.

9.12.4 Frequency regulation

For electrical grids, the frequency of the power generators and the system must be within the set tolerance, known as the frequency regulation. The misalliance between the electricity generation and the required demand leads the system toward varying frequency, which needs control to maintain the frequency within an acceptable range. Frequency regulation is done by adding and removing the power generator governor response, generator inertia, and the ESS. Each method of frequency regulation has advantages and disadvantages, and their execution takes between a millisecond and 20 min. Among ancillary services, frequency regulation has the highest value. Ancillary services are the functions performed by the grid actors to ensure the electricity flows smoothly in the grid.

Because of the fast ramping characteristics, ESSs are exploited to perform frequency regulation. Intermittent renewable energy sources like wind and solar energy will provide frequency regulation if integrated with an ESS, active power controls, and demand response.

9.12.5 Load following

A load following power plant or a load-following strategy adjusts the output power according to the fluctuations in the power demand during the day. In the load-following strategy, the power generators are either completely shut down or their output power is curtailed at night when demand is lower. For intermittent renewable energy resources, as the load

suddenly changes, the ESSs are best for load following as they can manage the load for minutes or hours. The ESS will manage a balance between power production and consumption. It acts in both ways: in the case of excess production, an ESS acts as an energy absorber, and when the energy production is less than the demand, an ESS acts as an energy provider.

9.12.6 Peak shaving

The installed capacity of the power plants in DG must be such that the peak load demand could be satisfied. In DG, spinning reserves and nonspinning reserves plays a role in peak shaving, since the new incoming generator is synchronized to the system quickly. Peak shaving can be obtained by controlling both generation-side management and load-side management. On the load side, the unnecessary load can be avoided during peak hours, e.g., air conditioners can be operated at relatively high temperatures. On generation-side management, spinning and nonspinning reserves may be brought into the system very quickly.

9.12.7 Spinning reserve

Spinning reserve is a type of operating reserve and is defined as the extra power generating capacity of the generator that is already synchronized to the system. This extra power is achieved by increasing the torque of the turbine rotor. In the case of steam and gas turbines, spinning is controlled by the combustion in the combustion chamber, and in micro-hydro, it is controlled by the flow rate of the falling water through the turbine. Spinning reserve is considered more reliable in DG since, during a blackout, start-up issues are not faced. Spinning reserve is used for battery efficiency during peak load demand.

9.12.8 Time shifting

Time-shifting or the arbitrage in the ESS is defined as the purchase of electricity for storage purposes during the off-peak hours when the electricity is cheap and this stored electricity is sold during peak hours when electricity is expensive. Alternatively, we can say that the excess production from renewable energy sources is stored and used when required. The number of transactions in time-shifting depends upon the cost of the energy storage in the battery, efficiency of the storage system, and discharging cost. If the efficiency is reduced or the cost of energy is increased, the number of transactions will be decreased.

9.12.9 Transient stability

The stability of a system is defined as the ability of the power generator to remain in synchronism after a disturbance occurs. The disturbance may occur because of sudden load changes, switching operation, or loss of a generator. In conventional power generators, synchronous generators have the capability of providing enough inertia to compensate the impact of disturbance. In most renewable energy power generators, there is either no inertia or very low inertia. Solar PV does not have any massy rotary part and no inertia is involved. Thus, in case of disturbance, the whole inertia of the system during disturbance will be

decreased, which leads to the loss of synchronism. The solution is to maintain transient stability.

9.13 SWOT analysis of battery energy storage systems in smart grids

9.13.1 Strengths

- **Avoid network reinforcement**: An ESS is used in integration with the generating sources to absorb the surplus energy in the ESS instead of saturating the transmission and distribution. This stored energy can be regained during peak hours or when generation is lower than demand. ESS connected to the distributed generation help to cope with the extra energy demand that cannot be filled by the network.
- **Optimized source utilization**: The integration of an ESS with renewable energy sources makes it beneficial by optimized use of the sources. In cases where a source is producing more than required, the surplus production is stored in the ESS that will be available to consumers when the renewable energy sources are limited and not sufficient to fulfill the electricity demand.
- **Diminish constraints**: When the energy production is greater than the energy demand, such as when solar irradiance is maximum at midday and the time when wind speed is at its maximum, the wind facility and solar field operators are paid to shut down the production because of the absence of energy storage. By incorporating the ESS, surplus energy can be saved and released when required, reducing the cost constraints.
- **Balance the system**: ESS keeps the system balanced when energy production is greater than or lower than the energy demand.
- **Diversity of technologies**: There are various types of ESSs, and advanced research is being carried out on reducing energy irreversibility.
- **Competent intermittent renewables**: By using an ESS with intermittent renewable energy sources like solar and wind, the ESS becomes the same as that of conventional energy sources with the advantage of fewer greenhouse gas (GHG) emissions.
- **Cost reduction**: With the rapid increase in the installation of renewable energy power plants, the use of ESS is also being increased, which in the future will decrease its cost.
- **Ancillary services**: The use of ESS provides various ancillary services like grid stabilization, backup energy reserves, transient stability, enhanced frequency response, stability and reliability, spinning reserves, peak shaving, power quality, and frequency regulation.

9.13.2 Weakness

- **Cost***:* The cost of the batteries and the balance of the system is very high compared to other power-generating technologies and grid services. The capital investment and the replacement cost of the batteries are also very high.
- **Aging***:* Battery ESS suffers from aging of batteries. The performance of the batteries depends upon the number of charging and discharging cycles. After achieving its number of charging cycles, the capacity of the battery is lost and the battery needs to be replaced.

9.13.3 Opportunities

- **Materials**: Technically advanced and innovative materials for the batteries and their balance of systems (BOS) reduce the cost of energy storage, increase the durability and the service life, and increase the power density of the battery.
- **Power technologies**: ESSs can be designed using variant storage technologies for off-grid and on-grid applications. Each storage technology has different efficiency, energy density, and performance characteristics. The established technologies of pumped hydro ESSs and compressed air ESSs are ESSs of large scale having a high duration of discharge. In contrast, batteries, flow batteries, flywheels, and fuel cells are best used on a small scale with a short discharge period.
- **Power electronics**: The advancement in an ESS can be brought by innovation in the power electronics components. Solid-state switches, DC-DC converters, inverters, and rectifiers are the auxiliary parts of an ESS. Power electronics control the power to and from the ESS, and serve as a power conditioning unit.
- **Reliability and safety testing**: Public acceptance of the ESS can be obtained by making it reliable and safe. The demonstration projects and the advanced simulation for different ESS can make it attractive for the public to invest in on a small and large scale.
- **Time of use tariff**: ESS can be improved by introducing the tariff on the time of use of energy from the ESS. Giving tariffs to the electricity purchased from the ESS during peak hours will attract investors investing in the renewable energy systems and the ESS. The investors will charge the batteries during off-peak hours from renewable energy sources.

9.13.4 Threats

- **Electric vehicles**: Electric vehicles can compete in the market of ESS at least behind the meter. This would be a threat to the small-scale ESS as the cars will charge the batteries from the grid during off-peak hours and sell it again to the grid during peak hours at a relatively high price.
- **Technology risk**: Diverse technologies of batteries are at different stages of development. It might be a threat to that technology if testing does not perform as estimated.

Table 9.5 presents a SWOT analysis of pumped hydro ESSs, Table 9.6 gives a SWOT analysis of compressed air ESSs, and Table 9.7 sets out a SWOT analysis of flywheel ESSs. All these systems are types of mechanical ESSs.

9.14 Current market trends and future outlook

With the advancement in renewable energy harnessing technologies, the installed capacity of renewable energy sources is increasing exponentially. To tackle the surplus energy production from these intermittent renewable energy sources, integration of the ESSs is required. ESSs do not only mitigate the intermittency effects of the RES but also act as a source of energy during peak demand. Fig. 9.14 shows the installed capacities of the ESS in different energy markets, which shows a gradual increase in the energy storage capacity in 2018 compared to 2017. Table 9.8 illustrates the current status of the ESSs in the USA. These ESS are of different capacities located in the USA and are used for various applications.

TABLE 9.5 SWOT analysis of pumped hydro energy storage (PHES) systems.

Strengths	• Low operating cost • Flexible and reliable • Longer lifetime • Fast response time • Almost 82% efficient
Weaknesses	• Dependence on the geological formation for construction • High capital investment • Might cause problems for the ecosystem • Land acquisition • Lower energy density
Opportunities	• Keeping the size mall, environmental damages may be diminished. • Using variable speed drives and variable frequency drives can increase the efficiency even under varying flow rates • Wind pumped hydro energy storage
Threats	• Environmental damage • Threatening to aquatic species

TABLE 9.6 SWOT analysis of compressed air energy storage (CAES) systems.

Strengths	• Plant capacity of CAES can be as large as 2700 MW, as was built in Ohio • Fewer storage losses • Large storage period • High response time compared to conventional power plants • Longer lifetime
Weaknesses	• Requires a suitable topographical erection • Minute geographical restrictions compared to PHES • High cost of constructing caverns
Opportunities	• Advanced research on adiabatic CAES has shown the opportunity of storing the heat energy generated during the compression process in charging mode and using this heat to reheat the compressed air during expansion in discharging mode
Threats	• Reheating the compressed air during discharging mode is expensive since it uses conventional energy sources like natural gas • Conventional energy sources will be obsolete in the future

9.15 Environmental impact of energy storage systems

ESSs are considered environmentally friendly since they encourage the integration of the renewable energy system into the existing conventional grid. Hence they increase the harnessing of renewable energy sources minimizing GHG emissions and limiting the usage of conventional energy sources. Whether the ESS is environmentally friendly or not depends upon the storage technology. The environmental impact of compressed air ESSs and pumped

TABLE 9.7 SWOT analysis of flywheel energy storage (FES) systems.

Strengths	• Longer lifetime • High energy density • Electromechanical conversion is very efficient • Magnetic bearing reduces the losses • Environmentally friendly compared to battery energy storage • Numerous charging and discharging cycles are possible in a few minutes
Weaknesses	• Since FES contains rotary parts, regular maintenance is required for wear and tear • High cost to compete with the BES • Power electronics is required for high-speed applications
Opportunities	• Advanced and productive research on the material of the flywheel rotor regarding the tensile strength to endure the rotational and mechanical stresses can also reduce the cost
Threats	• A containment vessel and a vacuum chamber are required to avoid the flywheel explosion for large-scale systems, which increases the cost of the system

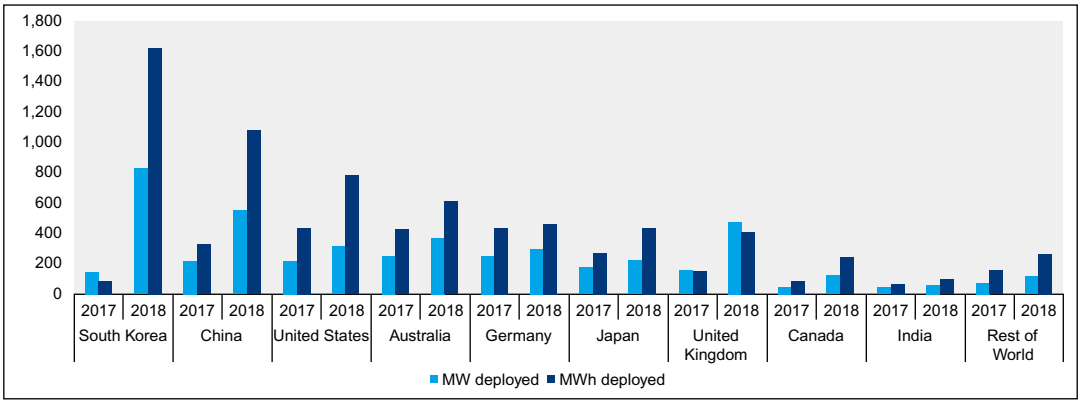

FIG. 9.14 Energy storage capacity of different countries in 2017–2018.

TABLE 9.8 The current status of operational energy storage systems in the USA [11,13,16].

Project name	Location	Technology	Rated capacity	Applications
UCI Microgrid	Irvine, California, USA	Chilled water thermal storage	6.59 MW	• Electric bill management
Riverside Public Utilities	Riverside, California, USA	Ice thermal storage	5 MW	• Electrical energy and renewable energy time shift • System upgradation

Continued

TABLE 9.8 The current status of operational energy storage systems in the USA [11,13,16]—Cont'd

Project name	Location	Technology	Rated capacity	Applications
Raccoon Mountain	Chattanooga, Tennessee, USA	Open loop pumped hydro storage	1652 MW	• Electrical supply capacity • Electrical time shift
Castaic	Pyramid Lake, California, USA	Open loop pumped hydro storage	1247 MW	• Electrical reserve capacity • Electrical energy time shift
Bath County Pumped Storage Station	Bath County, Virginia, USA	Open-loop pumped hydro storage	2772 MW	• Load leveling • Peak shaving
Texas Instruments Manufacturing Plant	Dallas, Texas, USA	Chilled water thermal storage	6.4 MW	• Electric bill management • Electrical energy time shift
Ludington Pumped Storage	Ludington, Michigan, USA	Open-loop pumped hydro storage	1872 MW	• Electric energy time shift • Electric supply capacity • Electric supply reserve capacity—spinning • Load following
Los Angeles Community College District	Los Angeles, California, USA	Ice thermal storage	4.62 MW	• Electric bill management • Electric energy time shift • Electric supply reserve capacity—nonspinning
STMicroelectronics UPS System—S&C Electric	Phoenix, Arizona, USA	Lead-acid battery	10 MW	• Grid-connected commercial (reliability and quality)
Kaheawa Wind Power Project II—Younicos	Maalaea, Hawaii, USA	Advanced lead-acid battery	10 MW	• Electric supply reserve capacity—spinning • Frequency regulation • Ramping • Renewables capacity firming
Green Mountain Energy Storage—NextEra	Somerset County, Pennsylvania, USA	Lithium-ion battery	10.4 MW	• Frequency regulation • Renewables energy time shift
Tucson Electric Power (TEP)—NextEra	Tucson, Arizona, USA	Lithium nickel manganese cobalt battery	10 MW	• Demand response • Electric bill management • Electric bill management with renewables • Ramping

TABLE 9.8 The current status of operational energy storage systems in the USA [11,13,16]—Cont'd

Project name	Location	Technology	Rated capacity	Applications
				• Renewables capacity firming • Resiliency • Transmission upgrades due to solar
Auwahi Wind Farm	Kula, Hawaii, USA	Lithium-ion battery	11 MW	• Ramping
Kings County Energy Storage—PG&E Henrietta Substation	Kings County, California, USA	Zinc air battery	10 MW	• Distribution upgrade due to solar electric energy time shift • Ramping • Renewables capacity • Firming • Renewables energy time shift
Golden Valley Electric Association	Fairbanks, Alaska, USA	Ni-Cd battery	27 MW	• Reserve and power system VAR support • Spinning stabilization
20 MW Flywheel Energy Storage Plant	Stephentown, New York, USA	Flywheel	20 MW	• Frequency regulations • Voltage regulation
McIntosh CAES Plant	Alabama, USA	CAES	110 MW	• Load management • Spinning reserve • Load following • Intermediate power generation
Wallace Dam Pumped Storage	Milledgeville, Georgia, USA	Open-loop pumped hydro storage	208 MW	• Electric energy time shift • Electric supply capacity

hydro ESSs is severe among all other energy storage technologies. During normal operation, the flywheel has little impact on the environment. The following subsections discuss the impact of each energy storage technology.

9.15.1 Mechanical energy storage systems

- **PHES**: The construction of water channels, pipes, tunnels, roads, the switchyard, powerhouse, and the high voltage transmission lines have an impact on the environment. This impact can be mitigated by constructing PHESS at a location far away from the river. The impact of PHES on the environment is greater than that of FES.

- **CAES**: CAES is considered less effective against the environment than PHES. CAES is more flexible and reliable and carries lower operation and maintenance costs, and less discharge rate.
- **FES**: Among mechanical ESSs, FES has less impact on the environment since due to the moving parts in the system, extra security and safety measures are taken to save the premises of the storage system.

9.15.2 The electrical energy storage system

- The SMES system has the limitation of temperature, which is a serious issue to be resolved. SMES requires extra protection against radiation within the premises of the storage system.

9.15.3 The chemical energy storage system

- Hydrogen is produced by the following processes: pyrolysis, gasification, dark fermentation, photofermentation, biophotolysis, photosynthesis, electrolysis, and thermolysis, which are the clean technologies of hydrogen production.
- Synthetic natural gas (SNG) contains less nitrogen and sulfur contents compared to hydrocarbons and coal, and hence has a less negative impact on the environment.

9.15.4 The electrochemical energy storage system

- **Batteries**: Batteries are the most common technology for energy storing since they have no moving parts and require very less maintenance. The scope of large-scale implementation for batteries is limited by weather change, global warming, air pollution, soil water, and the effect on health. Lithium oxide and salts in lithium-ion batteries can easily be recycled and have very little impact on the environment. The toxic materials in lead-acid batteries may have a serious impact on the environment. When a lead acid battery is overcharged, sulfuric acid generates hydrogen, which may explode [17].
- **Fuel cells**: These are a clean source of electricity since only hydrogen and oxygen are involved, as fuel and clean water are generated as by-products. The environmental friendliness of fuel cells depends upon the purity of the hydrogen [18].
- **Supercapacitor**: The environmental impact of the supercapacitors depends upon the material used.

9.16 Conclusion

The concept of smart grids cannot be implemented without the implementation of ESS. With the rapid increase in the installation of renewable energy projects in distributed generation and smart grids, integration of the ESS has become necessary because of the intermittency of renewable energy sources. During the peak production from renewable energy sources, surplus energy is stored in the ESS, and this stored energy is recaptured to meet

the load during peak hours or when the production of electricity from renewables is small. This chapter discussed the technologies of ESSs. These systems not only serve as storage; they also provide ancillary services like energy shift, energy time management, spinning reserves, peak shaving, grid stability, integration of renewable energy sources, power quality, load following, and transient stability. Apart from the technicalities, this chapter also explored the current status of the ESSs in the USA and the rest of the world. The impacts of each ESS on the environment were discussed.

Problems

Problems 1–20 contain four answer options: A, B, C, and D. Choose the correct answer

1. What is the main objective of the energy storage system?
- **A.** To meet the peak energy demand at short notice
- **B.** To balance the adverse effects of fluctuating demand
- **C.** To ensure steady output from power plants
- **D.** All of the above

2. Which of the following is a technology of mechanical energy storage systems?
- **A.** Pumped hydro energy storage system
- **B.** Compressed air energy storage system
- **C.** Flywheel energy storage system
- **D.** All of the above

3. What is the energy density of a battery?
- **A.** The amount of electrical energy stored for every kilogram of battery mass
- **B.** The amount of electrical energy stored per cubic meter of the battery volume
- **C.** The amount of power obtained per kilogram of battery
- **D.** All of the above

4. What does the energy stored in a battery depend on?
- **A.** Voltage
- **B.** Charge
- **C.** Power
- **D.** Voltage and charge
- **E.** All of the above

5. Which of the following is a technology of chemical energy storage systems?
- **A.** Battery
- **B.** Flow battery
- **C.** Regenerative fuel cell
- **D.** All of the above

6. Which of the following is a technology of electromagnetic energy storage systems?
- **A.** Capacitor
- **B.** Supercapacitor
- **C.** Superinductor
- **D.** All of the above

7. Which of the following is a type of compressed air energy storage system?
   A. Adiabatic CAES
   B. Diabatic CAES
   C. Isothermal CAES
   D. All of the above
8. Which of the following is an advantage of compressed air energy storage?
   A. Load shifting
   B. Peak shaving
   C. Renewable energy integration
   D. All of the above
9. Why is the compressed air energy storage system installed at Alabama more efficient than the Huntorf?
   A. Because of the use of the latest technology
   B. Because of the use of a hybrid energy storage system
   C. Because the waste heat from the turbine is captured by the recuperators for reheating
   D. Because of the use of an intercooler between the compression stages
10. How can energy stored by the flywheel be increased?
   A. By minimizing frictional losses
   B. By selecting material of high tensile strength
   C. By locating more mass at the circumference
   D. All of the above
11. In a superconducting magnetic energy storage:
   A. Magnetic energy can be stored indefinitely
   B. Magnetic energy is converted into electrical energy
   C. The electrical resistance of the magnetic coil drops to zero
   D. All of the above
12. In a compressed air energy storage system, the air is cooled before compression for storage. Why?
   A. More air can be stored in a given volume
   B. The turned around efficiency is improved
   C. It helps in the hybrid energy system
   D. All of the above
13. What does the first law of thermodynamics state?
   A. $Q = \Delta U + W$
   B. The heat added to a system is used for some useful work and to raise the internal energy of the system
   C. Energy cannot be created and cannot be destroyed, but can be transformed from one form of energy to another
   D. All of the above
14. Which of the following does not cause losses in a pumped hydro energy storage system?
   A. Losses at the turbine
   B. Head losses
   C. Evaporation
   D. Addition of water due to rain

15. Which of the following is a by-product of a fuel cell?
    A. Hydrogen
    B. Water
    C. Carbon dioxide
    D. All of the above
16. How is the efficiency of a fuel cell determined?
    A. $\eta = \frac{\Delta G}{\Delta H}$
    B. $\eta = \frac{RT}{4F} \ln\left(\frac{P_2}{P_1}\right)$
    C. None of the above
    D. Both A and B
17. How is Gibbs free energy defined?
    A. $\Delta G = \Delta H - T\Delta S$
    B. $\Delta G = \Delta H + T\Delta S$
    C. $\Delta G = \Delta S - T\Delta H$
    D. $\Delta G = \Delta S + T\Delta H$
18. What is the application of the pumped hydro energy system?
    A. Source of energy
    B. Frequency regulation in both pumping and generating modes
    C. Frequency regulation in generating mode
    D. Frequency regulation in pumping mode
19. Fig. 9.2 shows a diagram of the compressed air energy storage system. Which of the following shows the correct flow of energy in CAES?
    A. Storage → LPT → HPT → Generator
    B. LPT → HPT → Storage → Generator
    C. Generator → LPT → HPT → Storage
    D. Storage → HPT → LPT → Generator
20. Which of the following is a technology of thermal energy storage?
    A. Latent heat storage
    B. Sensible heat storage
    C. Reaction heat storage
    D. All of the above

Give brief answers to the following short questions.

1. In how many ways energy can be stored? Briefly illustrate the technologies.
2. How is the compressed air energy storage system helpful for electric power systems?
3. Briefly explain the working principle of a flywheel.
4. In a pumped hydro energy storage system, how and in which form energy is stored?
5. Define the depth of discharge and the state of charge of the battery.
6. What is the difference between Coulomb efficiency and the energy efficiency of a battery?
7. Give a brief SWOT analysis of the mechanical energy storage technologies.
8. Define spinning reserves.
9. How do energy storage systems help in stabilizing the grid?

10. List the applications of energy storage systems in the electric power system.
11. Write down the pros and cons of flow batteries.
12. What is the role of recuperators in compressed air energy storage systems?
13. Write down the chemical reactions of lead-acid batteries.
14. How do the transients in a power system occur and how do energy storage systems help maintain the transient stability?
15. What is Gibbs free energy and how is the spontaneity of a reaction determined by it?
16. Give a brief comparison between capacitors and supercapacitors.
17. Is energy storage technology safe and environmentally friendly?
18. Water weighing 1000 kg is at the potential of 50 m in a pumped hydro energy storage system. Calculate the energy stored in this water if the density of the water is 1000 kg/m^3.
19. Air is compressed from 10 to 50 bar in a compressed air energy storage at 35°C. The $\gamma = {}^{C_p}/_{C_v}$ of air is 1.4. What would be the temperature of the compressed air?
20. The disk of a flywheel is rotating at 5000 rpm. The diameter of the flywheel is 10 m and its thickness is 5 m. How much energy is stored in the flywheel?

References

[1] X. Luo, J. Wang, M. Dooner, J. Clarke, Overview of current development in electrical energy storage technologies and the application potential in power system operation, Appl. Energy 137 (2015) 511–536, https://doi.org/10.1016/J.APENERGY.2014.09.081.

[2] World Energy Outlook 2021—Analysis—IEA, Available from: https://www.iea.org/reports/world-energy-outlook-2021. (Accessed 5 April 2022).

[3] H. Guo, Y. Xu, H. Chen, X. Zhou, Thermodynamic characteristics of a novel supercritical compressed air energy storage system, Energ. Conver. Manage. 115 (2016) 167–177, https://doi.org/10.1016/J.ENCONMAN.2016.01.051.

[4] P. Nikolaidis, A. Poullikkas, A comparative review of electrical energy storage systems for better sustainability, J. Power Technol. 97 (3) (2017) 220–245.

[5] D.R. Brown, W.D. Chvala, Flywheel energy storage: an alternative to batteries for UPS systems, 102 (5) (2009) 7–26, https://doi.org/10.1080/01998590509509440.

[6] U.S. Department of Energy Office of Electricity Delivery and Energy Reliability. Energy Storage Program Planning Document, 2011, 2011.

[7] K. Ohno, Tracking clean energy progress, J. At. Energy Soc. Jpn. 63 (3) (2021) 283–286, https://doi.org/10.3327/jaesjb.63.3_283.

[8] P. Breeze, Power Generation Technologies, third ed., Elsevier, 2019.

[9] M. Ghiji, et al., A review of lithium-ion battery fire suppression, Energies 13 (2020) 5117, https://doi.org/10.3390/EN13195117.

[10] File:Lead-Acid discharging.svg - Wikipedia, Available from: https://en.wikipedia.org/wiki/File:Lead-acid_discharging.svg. (Accessed 5 April 2022).

[11] N. Omar, et al., Analysis of nickel-based battery technologies for hybrid and electric vehicles, in: Reference Module in Chemistry, Molecular Sciences and Chemical Engineering, 2014, https://doi.org/10.1016/B978-0-12-409547-2.10740-1.

[12] K.H. Norian, Equivalent circuit components of nickel-cadmium battery at different states of charge, J. Power Sources 196 (11) (2011) 5205–5208, https://doi.org/10.1016/J.JPOWSOUR.2011.01.074.

[13] E. Hossain, H.M.R. Faruque, M.S.H. Sunny, N. Mohammad, N. Nawar, A comprehensive review on energy storage systems: types, comparison, current scenario, applications, barriers, and potential solutions, policies, and future prospects, Energies 13 (14) (2020) 3651, https://doi.org/10.3390/EN13143651.

[14] S. Mubeen, Y.S. Jun, J. Lee, E.W. McFarland, Solid suspension flow batteries using earth abundant materials, ACS Appl. Mater. Interfaces 8 (3) (2016) 1759–1765, https://doi.org/10.1021/ACSAMI.5B09515/SUPPL_FILE/AM5B09515_SI_001.PDF.

[15] M.R. Mohamed, H. Ahmad, M.N.A. Seman, S. Razali, M.S. Najib, Electrical circuit model of a vanadium redox flow battery using extended Kalman filter, J. Power Sources 239 (2013) 284–293, https://doi.org/10.1016/J.JPOWSOUR.2013.03.127.
[16] M.Z. Daud, A. Mohamed, M.A. Hannan, A review of the integration of energy storage systems (ESS) for utility grid support, Prz. Elektrotech. 88 (10A) (2012) 185–191.
[17] R. Georgious, R. Refaat, J. Garcia, A.A. Daoud, Review on energy storage systems in microgrids, Electronics 10 (2021) 2134, https://doi.org/10.3390/ELECTRONICS10172134.
[18] A. Kirubakaran, S. Jain, R.K. Nema, A review on fuel cell technologies and power electronic interface, Renew. Sustain. Energy Rev. 13 (9) (2009) 2430–2440, https://doi.org/10.1016/J.RSER.2009.04.004.

This page intentionally left blank

CHAPTER

10

Electric vehicles and smart grids

10.1 Introduction

The growing cost of fossil fuels and the increasing environmental health hazard impacts of the fossil fuels in the conventional vehicles have drawn the attention of the researchers, investors, and the governments to electric vehicles (EVs). For the last few decades, the automotive industry of any country is important not only for the economy but also for research and development. Due to modernity, a large number of vehicles have appeared on the roads. However, the increase in the number of vehicles has increased air pollution around the world. According to the European Union, 28% of carbon dioxide emissions come from the transport sector, while 70% come from road transport. Therefore, the world is looking for ways to make the environment greener by reducing carbon dioxide (CO_2) emissions. Developed countries are trying to encourage people to use EVs to reduce air pollution. Meanwhile, people are showing interest in EVs because they are environmentally friendly, improve performance, are reliable, and have low electricity costs. The role of EVs, distributed generation, and renewable energy sources in the electric power system is shown in Fig. 10.1.

Various researchers performed optimization analysis with different software using different objective functions and constraints. Ioakimidis et al. [1] performed linear programming in MATLAB® with peak shaving and valley filling as objective functions. They found that the proposed algorithm is effective for the higher number of parking slots. Van Der Meer et al. [2] used mixed-integer linear programming with maximizing profit and PV utilization as an objective function in GMSA. They concluded that the V2G is not economically feasible because of the battery degradation. V2G is feasible only when the production from the PV is higher. Ivanova et al. [3] also used mixed-integer linear programming in CPLEX with minimizing system cost as an objective function and determined that smart charging and using PV can save the operational cost for the owner of the parking lot. Mohamed et al. [4] implemented fuzzy logic in MATLAB to minimize the charging cost. The implemented algorithm is optimization-based and several objectives can be achieved

https://doi.org/10.1016/B978-0-323-99560-3.00002-8

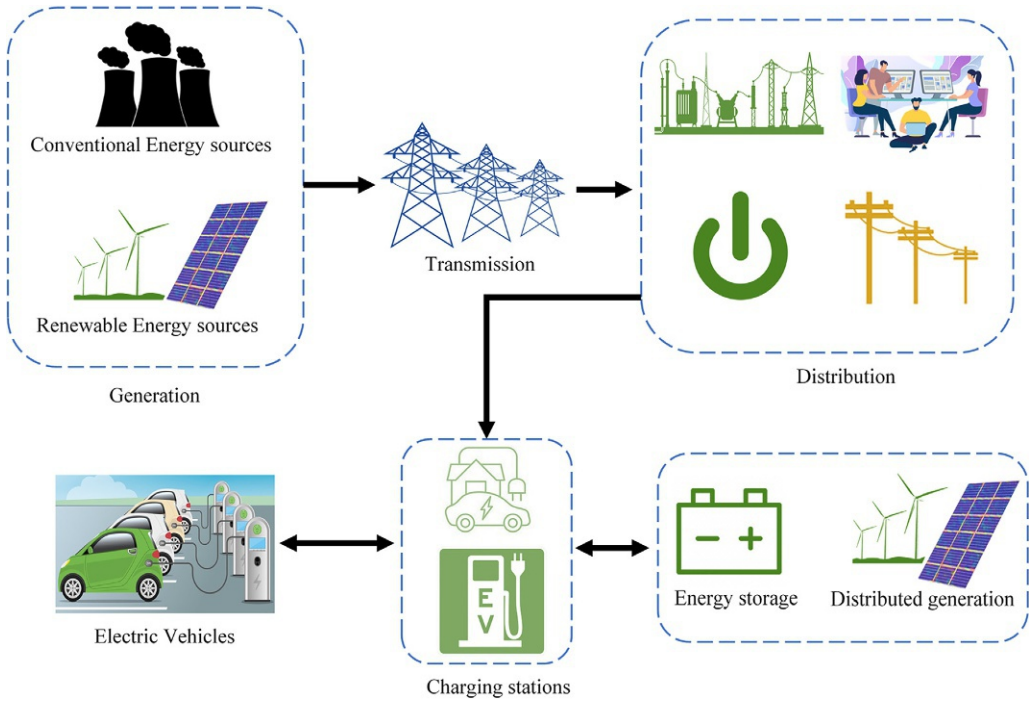

FIG. 10.1 Charging and discharging of EVs in the distribution system.

like reducing system losses and charging costs, and improving voltage profile. Liu et al. [5] optimized the PV utilization by implementing the metaheuristic model in MATLAB. The proposed algorithm optimized the objective function with less computational cost and without forecasting the unpredictable variables. The authors [6–9] implemented different models in MATLAB with different objective functions like minimizing charging cost, maximizing PV utilization, minimizing peak demand, and peak shaving and valley filling.

The evolution of EVs can be categorized into five eras. The first era is called the beginning of EVs, in which the EVs were invented in the USA and Scotland from 1800 to 1850. The second era is called the first age in which the EVs appeared in the market from 1851 to 1900. The production of EVs increased historically when internal combustion engines (ICEs) were displaced by EVs. This era is called the booming age, from 1901 to 1950. The era from 1951 to 2000 is called the second age of the EVs in which the interest of investors, manufacturers, and the public in EVs increased because of the high prices of the oils and the related high emissions. The current era from 2001 to onward is the third age in which the public and private sectors are fully interested in EVs. The evolution of EVs from the beginning to the current situation is shown in Fig. 10.2 (Table 10.1).

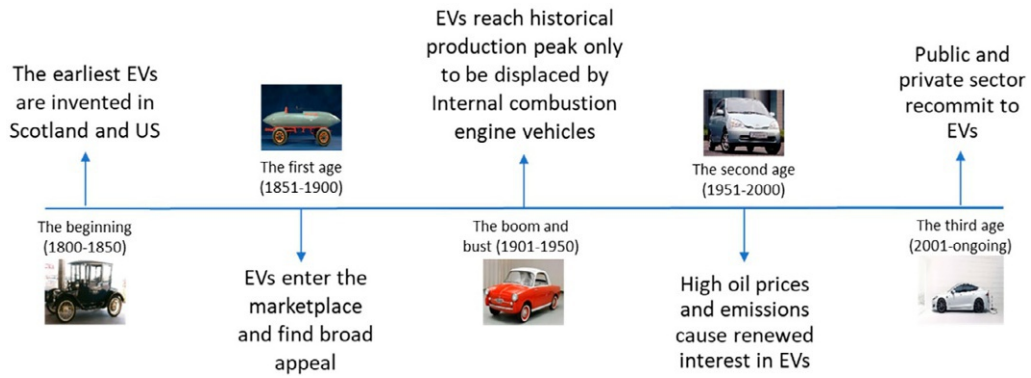

FIG. 10.2 The evolution of electric vehicles [10].

10.2 Electric vehicle modeling

10.2.1 Tractive effort

Tractive effort is the force that thrusts the vehicle frontward and it is the total traction that the vehicle exerts on the surface. The total tractive effort is defined as the sum of the aerodynamic drag, rolling resistance force, hill climbing force, force to give linear acceleration, and force to give angular acceleration to the rotating motor. We consider a vehicle of mass m moving up a slope of angle ψ with velocity v, as shown in Fig. 10.4.

10.2.1.1 Rolling resistance force

Rolling resistance force also called rolling drag force and rolling friction force and is defined as the resistive force in the motion of the vehicle. This resistive force is because of the hysteresis losses in the tires, and friction in bearings and gearing systems. Rolling friction force is represented by Eq. (10.1).

$$Frr = \mu_{rr} F_{rr} = \mu_{rr} mg \tag{10.1}$$

μ_{rr} is the rolling resistance coefficient and it depends upon the type of the tire and the tire pressure. μ_{rr} is defined by Eq. (10.2).

$$\mu_{rr} = \frac{F}{G} \tag{10.2}$$

F is the force required to pull the tire axle horizontally in the direction of motion of the vehicle and G is the vertical load on the tire on the flat horizontal surface.

10.2.1.2 Aerodynamic drag

Aerodynamic drag force is defined as the force which is faced by the vehicle as it moves through the air. This drag force depends mainly on the front area of the vehicle, side mirrors, ducts, and many other factors. Aerodynamic drag force can be calculated by Eq. (10.3).

TABLE 10.1 Literature review of evolution of electric vehicles.

Year	Description	Reference
1832–1839	The first prototype of electric powered carriage was powered by nonrechargeable primary cells was invented by Robert Anderson. After this, various electric power-based vehicles were introduced but because of inefficient electric motors and losses in the rechargeable batteries, they could not keep pace with technology advancements	[11]
1856–1881	With the advancement in the technology and enhancement in the research and development, rechargeable batteries were improved in terms of losses and charging discharging cycles, and DC electric motors were developed for electric vehicles. The increase in efficiency in DC motors made them suitable for electric vehicles	[11]
1859–1881	The first lead acid battery was developed by Gaston Plante in 1859; it was rechargeable and able to be used in electric vehicles. Research continued and the first battery was introduced to the market in 1881 by Camile Alphonse Faure	[12]
1897–1905	The development in DC motors technologies and rechargeable batteries reached the electric vehicle industry in the late 19th century. In 1897, the first electric vehicle was introduced in the market in New York. In the next 3 years, the electric vehicle industry boomed and the electric vehicle reached 28% in 3 years	[13]
1908–1935	After a successful start in 1897, the electric vehicle industry faced a threat from other technology advancements. Gasoline-based vehicles boomed after a decade in 1908 when Henry Ford introduced a T-model vehicle powered by gasoline. Further advancements in gasoline technology were introduced by removing the necessity of a hand crank. Further, the lower costs of petrol compared to electricity and the shorter traveling distance of electric vehicles kept EV technology behind. The limited charging stations further slowed down the progress of EVs. Due to all these factors, gasoline-powered vehicles received great acceptance and EVs distressed out of acceptance. Around 1935, there was not a single EV on the road	[13]
1990–2003	When gasoline technology and the consumption of gasoline-powered vehicles were at their peaks, the emissions from gasoline became a hurdle since it caused various health problems. Furthermore, oil prices reached their highest point, which encouraged researchers and investors to return to electric vehicles. Governments implemented regulatory policies to discourage emissions and promote electric vehicles. In the USA, regulatory action was taken with a mission to make it mandatory to use 2% emission-free electric vehicles by 1998 and 10% emission-free vehicles by 2003. In 2004, the world's first commercial hybrid electric vehicle was introduced by Toyota (Prius model) in Japan. In the first production year, 18,000 hybrid electric vehicles were sold	[14]
2010–2012	After 2010, plug-in hybrid electric vehicles and battery electric vehicles like Chevrolet Volt, Mitsubishi i-MiEV, Nissan Leaf, and Tesla Model S appeared in the industry. By the end of 2012, there were 180,000 electric vehicles on the road	[4]
2020-onward	Sales of electric vehicles reached a record of 3 million in 2020 despite the fact that the overall sale of cars decreased by 16% because of COVID-19. The sales of different types of EVs in different markets from 2010 to 2020 are shown in Fig. 10.3	[14]

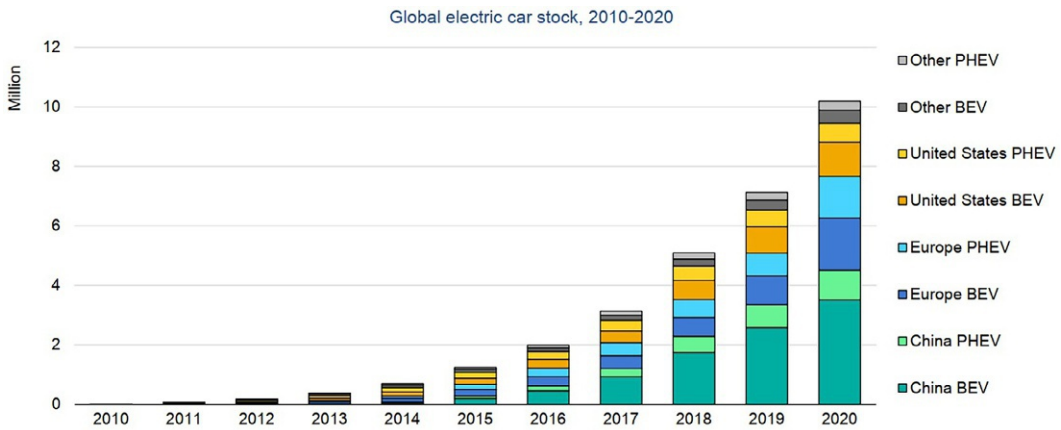

FIG. 10.3 Global electric car stock by region and mode, 2010–2020. *Source: Global EV outlook 2021.*

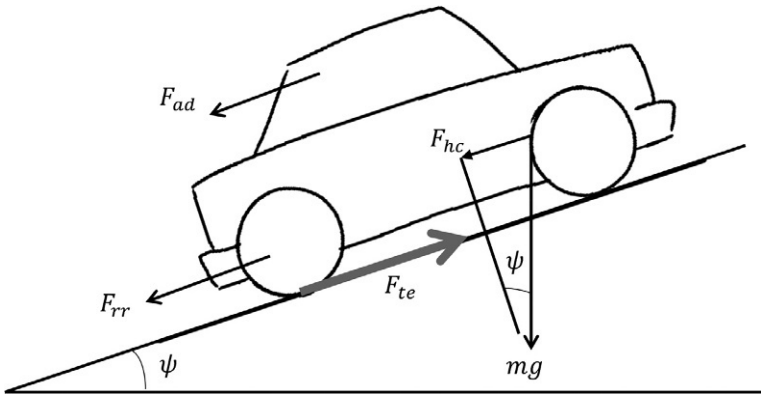

FIG. 10.4 The forces acting upon a vehicle as it moves up the slope.

$$F_{ad} = \frac{1}{2}\rho A C_d v^2 \tag{10.3}$$

where ρ is the density of the air, A is the front area of the vehicle, C_d is the drag coefficient constant, and v is the wind velocity crossing the vehicle. The drag coefficient depends upon the shape of the object and is always associated with the surface area. A lower value of drag coefficient indicated low aerodynamics of the object.

10.2.1.3 Hill climbing force

Hill climbing force is the force required to move the vehicle up the slope; it is the component of the weight of the car that acts along the direction of motion of the vehicle. It can be calculated using Eq. (10.4).

$$F_{hc} = mg\sin\psi \tag{10.4}$$

The value of the hill climbing force will be negative if the vehicle is moving down the slope.

10.2.1.4 Acceleration force

If the velocity of the vehicle is changing, a new force will be developed known as the acceleration force. By the third law of Newton, this linear acceleration force is given by Eq. (10.5).

$$F_{la} = ma \tag{10.5}$$

For a clear picture, we will consider both linear and rotational acceleration. The force required for the angular acceleration is given by Eq. (10.6).

$$F_{\omega a} = I\frac{G^2}{\eta_g r^2}a \tag{10.6}$$

where G is the gear ratio of the system that connects motor to the axle; r is the radius of the tire; I is the moment of inertia of the rotor of the motor; and a is the linear acceleration.

10.2.1.5 Total tractive effort

The total tractive effort is the sum of the rolling resistance force, hill climbing force, aerodynamic drag force, and forces required to give linear and angular acceleration. Total interactive force is given by Eq. (10.7).

$$F_{te} = F_{rr} + F_{ad} + F_{hc} + F_{la} + F_{\omega a} \tag{10.7}$$

Example 10.1

A vehicle of weight 1550 kg accelerates up a hill with a slope of 15° and a final speed 23 m/s. The density of air is 1.32 kg/m^3, aerodynamic drag coefficient is 0.109, rolling resistance coefficient is 0.03, frontal area of the vehicle is 1.67 m^2. The following need to be calculated:

(1) Aerodynamic force
(2) Rolling resistance
(3) Hill climbing force
(4) Total tractive effort

Given data

$$m = 1550\ \text{kg}$$

$$\psi = 15^{\circ}$$

$$v = 23\ \text{m/s}$$

$$\rho = 1.32\ \text{kg/m}^3$$

$$C_d = 0.109$$

$$A = 1.67\ \text{m}^2$$

$$\mu_{rr} = 0.03$$

$$F_{ad} = ?$$

$$F_{hc} = ?$$

$$F_{rr} = ?$$

Solution

(1) Aerodynamic force

$$F_{ad} = \frac{1}{2}\rho A C_d v^2$$

$$= \frac{1}{2}\left(1.32\ \text{kg/m}^3\right)\left(1.67\ \text{m}^2\right)(0.109\ )(23\ \text{m/s})^2$$

$$F_{ad} = 63.5\ N$$

(2) Rolling resistance

$$Frr = \mu_{rr}\, mg$$

$$= 0.03\ (1550)(9.8)$$

$$Frr = 455\ N$$

(3) Hill climbing force

$$F_{hc} = mg \sin \psi$$

$$= (1550)(9.8) \sin (15)$$

$$F_{hc} = 3931\ N$$

(4) Total tractive effort

$$F_{te} = F_{rr} + F_{ad} + F_{hc}$$

$$= 455\ N + 63.5\ N + 3931\ N$$

$$F_{te} = 4449.96\ N$$

10.3 Technologies of electric vehicles

Electric vehicles are configured in different ways base on the available resources, cost, and the components. The configurations are shown in Fig. 10.5.

10.3.1 Battery electric vehicles (BEVs)

A battery electric vehicle (BEV) is a type of EV that uses the energy from the battery to drive the electric motor and no other source of energy is used like an ICE or hydrogen fuel cell. The technologies that are involved in BEVs are electric motors, motor controllers, and the battery pack. The battery pack can be charged either by the external charging station or by the regenerative braking. The simplest diagram of a BEV is shown in Fig. 10.6. The main technologies involved in the battery EV are discussed below.

10.3.2 Hybrid electric vehicles (HEVs)

Hybrid electric vehicles (HEVs) are EVs that use a dual propulsion system, an ICE, and an electric motor. These systems can work either together or separately. The electric motor also works as an electric generator that can generate energy during the braking. The efficiency of the ICE is optimized by draining the electricity from the batteries. Moreover, an HEV can also be defined as the EV that can be propelled through either a conventional fuel-based engine or a rechargeable battery. The batteries can be recharged either from the external source of electricity, from the electric motor/generator, or both. Compared with the conventional ICE vehicle, an HEV contains more electrical components like power electronics converters, switching systems, advanced electricity storage systems, and electric motors/generators. Based on the power flow from the source of energy to the point of energy consumption, an HEV is configured in one of the following three ways.

10.3.2.1 Series hybrid electric vehicles (SHEVs)

A series hybrid electric vehicle (SHEV) consists of an ICE, generator, charger, battery, converter, and electric motor. The configuration shows that both propulsion systems feed the transmission as shown in Fig. 10.7. In a SHEV, there is no direct mechanical connection of an ICE with the transmission. When the battery pack is fully charged, the ICE is turned off and the battery alone operates the electric motor. In urban drive, where the braking system

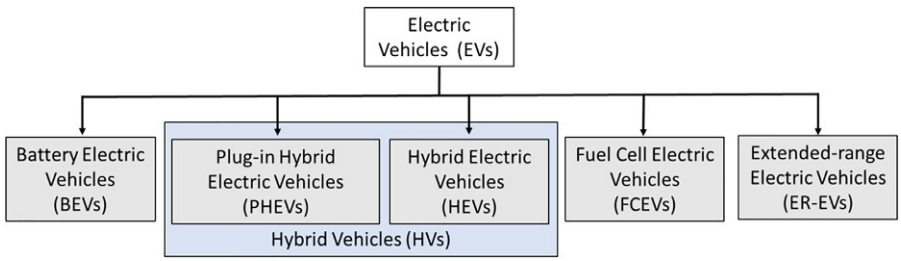

FIG. 10.5 Classification of EVs based on engine technologies.

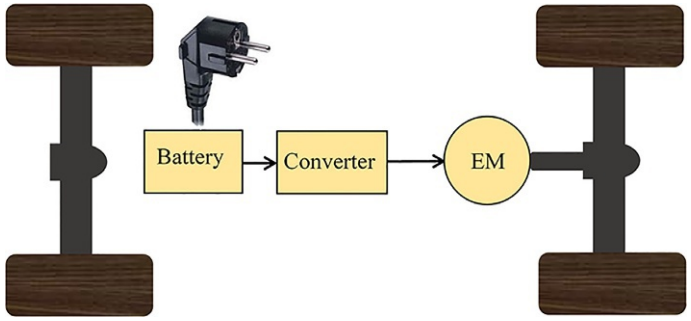

FIG. 10.6 Schematic diagram of battery electric vehicle.

is frequently applied, the regenerative braking recharges the batteries. The regenerative braking system is explained here. To speed up the vehicle, the driver accelerates and gives energy to the vehicle, converting electrical energy into mechanical energy. On the other hand, when the driver applies brakes and decelerates the vehicle, the kinetic energy of the vehicle is used to generate the electricity that would otherwise be lost in the discs of the brakes in the form of heat. This regenerative braking generates electricity to recharge the battery. In this way, the ICE is operated at maximum efficiency, which leads to better fuel efficiency and a reduction in GHG emissions from the fuel. The configuration of a SHEV is shown in Fig. 10.7.

We can conclude that in a SHEV, an electric motor is the primary source of transmission and the ICE is the secondary source of transmission to the drivetrain. This type of configuration is used in heavy vehicles, buses, and military vehicles. The advantage of the SHEV is that the ICE is turned off when the battery pack is fully charged and producing the transmission. The other advantage is that the engine and the electric motor are independent of each other and can be positioned at different locations.

10.3.2.2 Parallel hybrid electric vehicles

In parallel hybrid electric vehicles, the ICE and the electric motors are directly connected to the driveline. The configuration of a PHEV is shown in Fig. 10.8. A good performance is

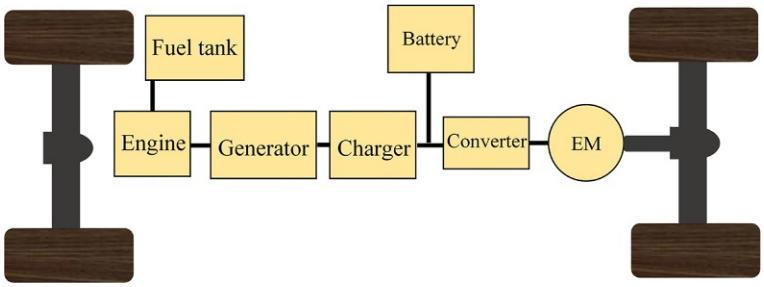

FIG. 10.7 Schematic diagram of a series hybrid electric vehicle.

observed during the acceleration to bring the vehicle to a constant speed since both the engine and the electric motor participate to drive the wheels. Contrary to a SHEV, in a parallel hybrid electric vehicle the engine is mechanically connected to the drivetrain, and the electric motor backs up the engine during startup. It can be seen from the configuration that both engine and the electric motor can independently drive the wheels. If the electric motor is of high power, it can be solely used to drive the wheels while starting or while the vehicle is stopped idle. A bigger or high-power engine and a less powerful electric motor is used in a parallel hybrid electric vehicle than in a SHEV. In a parallel hybrid electric vehicle, the battery pack is kept small and is recharged by the regenerative braking system.

10.3.2.3 Series-parallel hybrid electric vehicles

Two power flow paths can be followed in the series-parallel hybrid electric vehicle, as shown in the configuration in Fig. 10.9: the mechanical energy path and the electrical energy path. The ICE is directly connected to the wheel drive system and to the generator that can charge the battery. In the electrical energy path, a battery is used to drive the electric motor. The efficiency of the series-parallel hybrid electric vehicle is questioned if the conversion from the mechanical to the electrical is considered.

10.3.3 Plug-in hybrid electric vehicles

Plug-in electric vehicles also contain two sources of energy. One is the ICE and the other is the battery pack. During the urban drive, the batteries are charged by the regenerative braking system and the batteries can also be charged by the charging satiations. PHEV is similar to the HEV with other options of a large battery pack and an external source for charging the batteries. Since the electric power is the main propulsion in the PHEV, so a large battery pack is required. PHEV operates in two different modes depending upon the state of charge (SOC) of the battery. If the SOC of the battery is 100%, the PHEV operates in charge-depletion (CD) mode, in which the battery starts discharging from 100% and when the SOC comes to the limits of the CD range, the PHEV is switched to the charge-sustaining (CS) mode. In CS mode, PHEV uses the energy from the other two sources, i.e., regenerative braking and the engine. Once the SOC of the battery reaches the limits of the

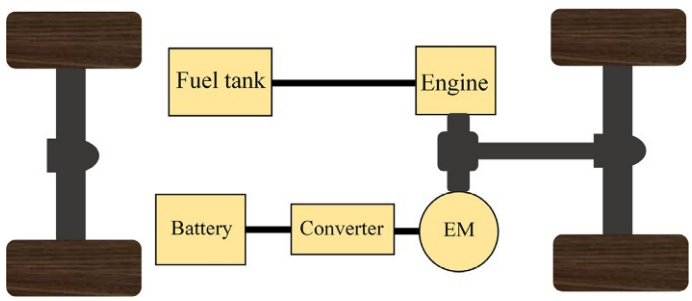

FIG. 10.8 Schematic diagram of a parallel hybrid electric vehicle.

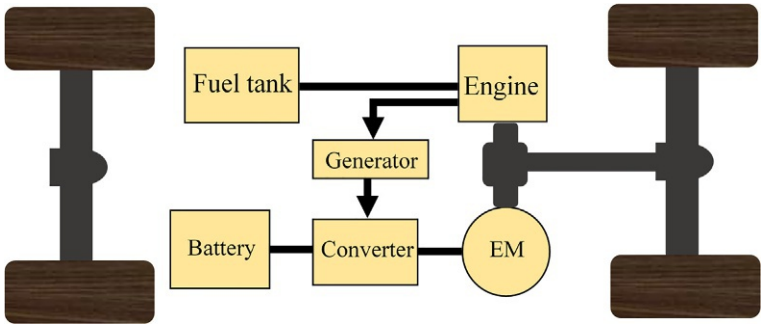

FIG. 10.9 Schematic diagram of a series-parallel hybrid electric vehicle.

CD range, the mode is again switched to the CD mode. Fig. 10.10 shows a schematic diagram of a plug-in EV.

10.3.4 Fuel cell electric vehicles (FCEVs)

Fuel cell electric vehicles (FCEVs) are similar in operation to BEVs except for the source of energy. Hydrogen fuel and the fuel cell replace the battery. The process of conversion is taken place by taking compressed hydrogen from the vehicle-mounted tank and mixing it with the atmospheric air that produces DC electricity to drive the electric motor and the water is produced as a by-product which is exhausted through the tailpipe. The FCEV is environmentally friendly because no carbon is involved in the fuel and hence no carbon dioxide, carbon monoxide, or hydrocarbons are emitted. In addition, there is no combustion is involved in the conversion process, and no high temperatures are involved. A schematic diagram of a FCEV is shown in Fig. 10.11.

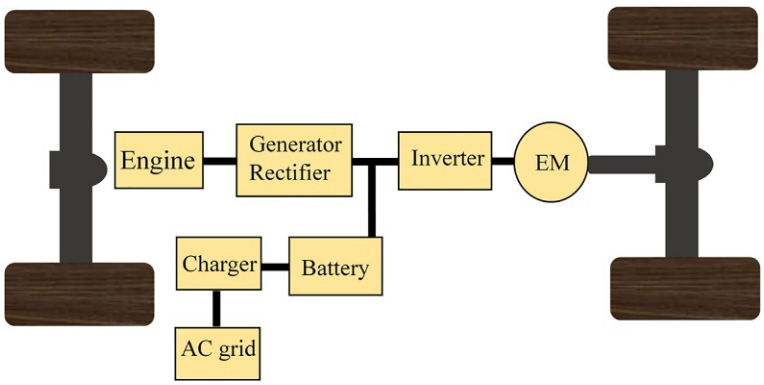

FIG. 10.10 Schematic diagram of a plug-in hybrid electric vehicle.

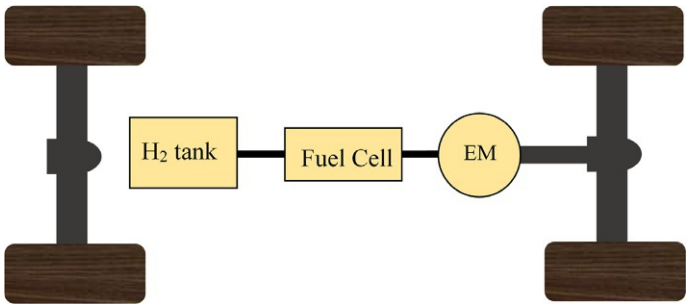

FIG. 10.11 Schematic diagram of a fuel cell electric vehicle.

10.4 Integration of EVs into the electric grid

The charging and discharging of the EV in the electric power grid is a major challenge in terms of technical and economic issues. In literature, many researchers have worked on the impact of EVs on the power distribution system. EVs are considered to be charged either at the home or they can be charged at the public charging stations. The integration of EVs into the grid has some serious impacts on the performance of the grid, as discussed below.

10.4.1 Phase imbalance and voltage instability

As EVs penetrate the electric grid, voltage instability becomes a challenge to the system. This is because of the unexpected increase in the number of EV users that increases the load demand. The changing load significantly affects the reliability of the grid voltage at the points of common coupling of the charging station and the distribution grid.

10.4.2 Electric vehicle charging and grid interaction

Fig. 10.12 shows the EV charging system for AC level 1 and AC level 2. The EV charging system consists of a charging point and an onboard charging system. The onboarding charging system consists of an EMI filter, a rectifier, a DC-DC converter, a protection circuit, and a battery pack. The rectifier takes the AC input from the charging station and converts it into DC. A DC-DC converter takes the voltage to the voltage level of the battery pack. Similarly, Fig. 10.13 indicates the EV charging system for DC level 1 and DC level 2. The EV charging system consists of an off-board charging point and the battery pack of the vehicle. Off-board charging point directly converts the input AC into DC using a rectifier and a DC-DC converter. DC-DC converter levels the voltage up or down according to the voltage level of the battery. Table 10.2 shows the nominal voltage, maximum current capacity, and power ratings of different AC and DC levels of charging stations. Characteristics of different AC and DC charging levels are described in Table 10.2.

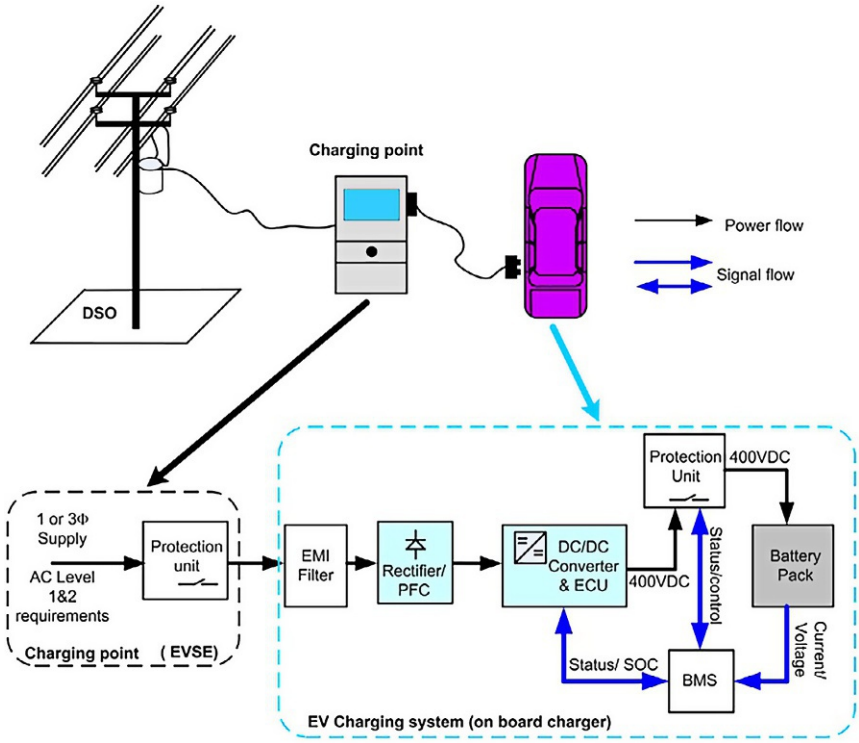

FIG. 10.12 EV charging configuration at AC level 1 and AC level 2 (on board charger) [15].

10.5 Integration of renewable energy sources with EVs

Advancements in renewable energy technologies are replacing conventional energy sources with renewable energy sources. These intermittent renewable energy sources, especially solar energy and wind energy, have made energy production unpredictable. Throughout the day, solar irradiance and wind speed are continuously varying. The energy production from these sources could be larger or lower than the energy demand. Most researchers have revealed in the literature that the integration of the solar photovoltaic system and the wind energy system is technically and economically viable. These renewable energy resources are the backbone of the distributed generation that can be used off-grid and on-grid both. To make renewable energy sources more effective, these are integrated with the energy storage systems. The energy storage systems absorb the energy when the production from renewable energy sources is in excess and release energy when the generation is low. However, energy storage systems increase the cost of the system.

The use of conventional fuels in the transport sector poses serious impacts on the environment. The emission of carbon dioxide from vehicles has not only affected public health but the temperature of the earth has also risen. The solution to the above-stated problems of the conventional vehicles and the intermittency of the renewable energy sources is the integration of

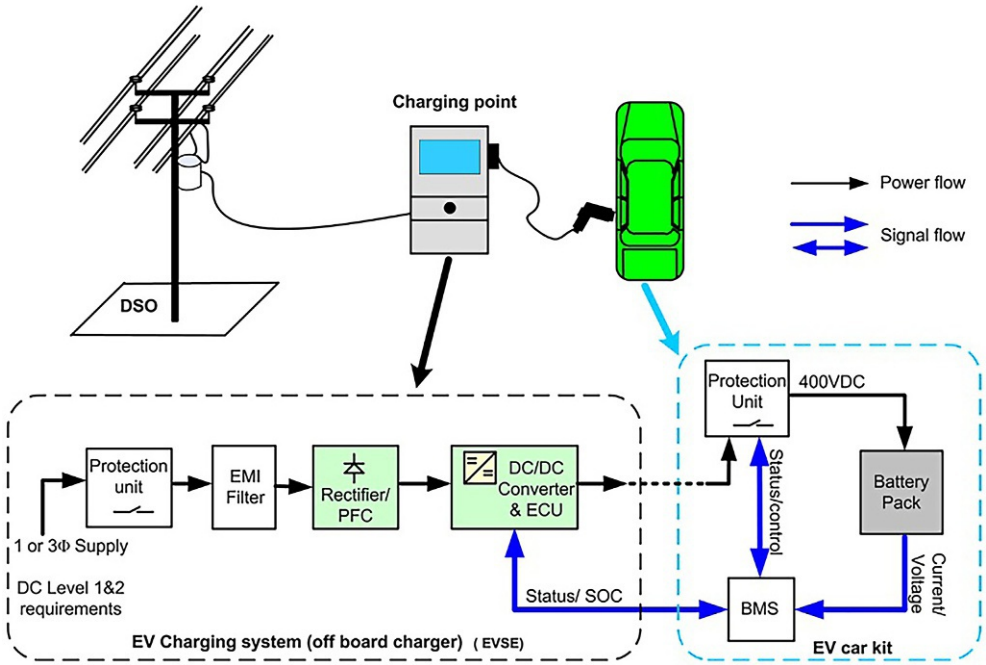

FIG. 10.13 EV charging configuration at DC level 1 and DC level 2 (off-board charger) [15].

TABLE 10.2 Characteristics of different charging levels.

Power levels	Charging type	Nominal voltage (V)	Max. current (A)	Power (kW)
AC Level 1	Slow	120	Up to 16	1.9
AC Level 2	Slow	240	Up to 80	19.2
AC Level 3	Slow	400	More than 80	≤130
DC Level 1	Slow	200–500	≤80	≤36
DC Level 2	Medium	200–500	≤200	≤90
DC Level 3	Fast	200–600	≤400	≤240

the renewable energy sources with EVs and the power grid. The concept of the integration of the solar PV system and the wind turbines into the grid with EVs is shown in Fig. 10.14. All the EVs are aggregated at EV charging stations where their batteries can be charged during off-peak hours and discharged in peak hours. A fleet of EVs can act as a backup source of energy when the renewable energy sources are limited or during peak hours. On the other hand, this fleet of EVs will absorb all the excess generation of electricity from renewable energy sources.

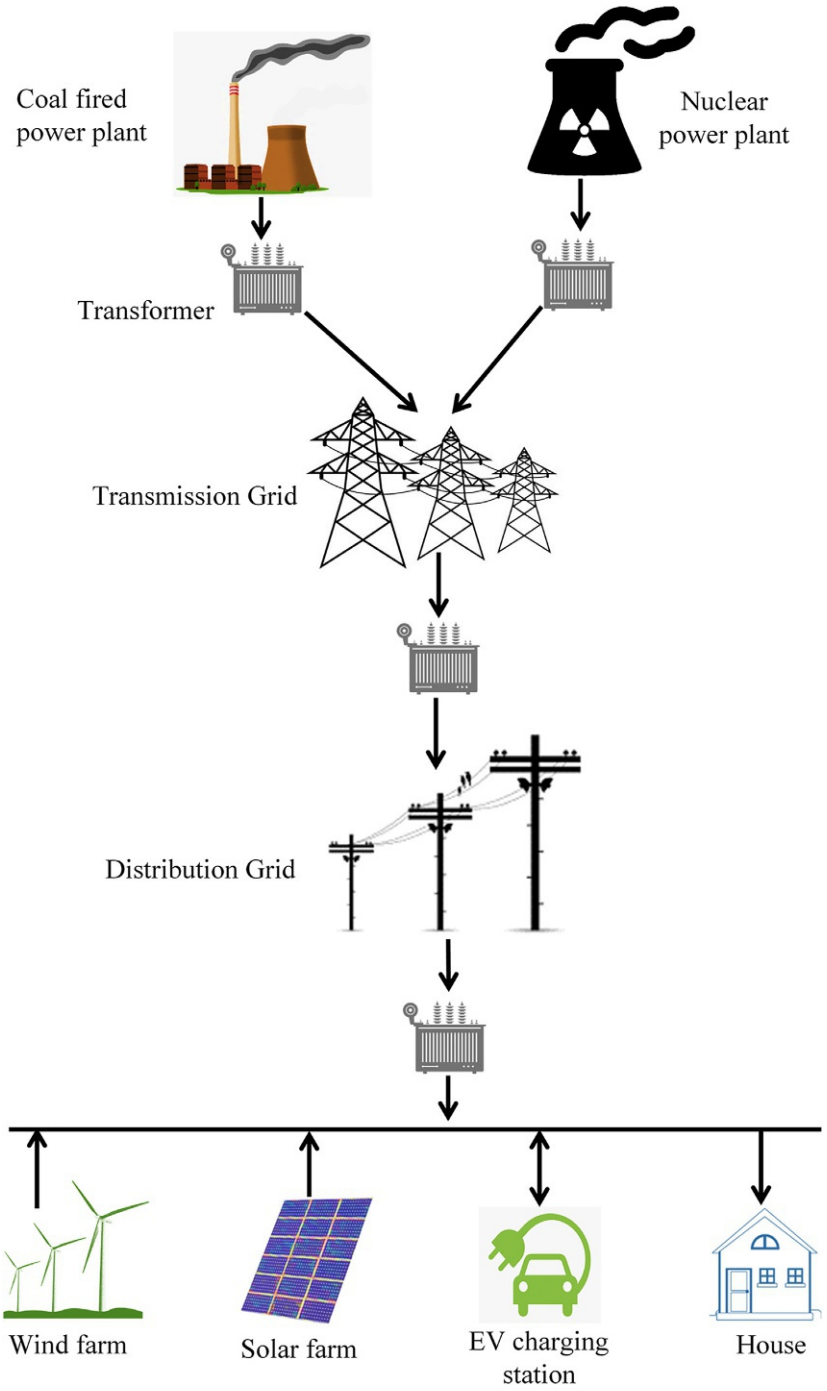

FIG. 10.14 Integration of renewable energy sources and EV in the electric power system.

If a compact energy management system is adopted, EVs have the capability of becoming an energy storage system for renewable energy sources.

10.5.1 Integration of solar energy with electric vehicles

EVs have made their way into the smart grid. The increasing demand for the charging of EVs creates an opportunity for individual solar charging stations. The sustainability of electric charging stations and EVs depends upon the source of energy. PV power plants are already working efficiently and feeding the grid and with the increased penetration of the EVs, the solar PVs are likely to be deployed for the EVs. Emissions from the EVs are low if the source of the energy to the electric charging station is environmentally friendly, clean, renewable energy. Because of the following reasons, solar photovoltaics is considered best for electric charging stations.

- The cost of the solar PV panels and the balance of systems (BoS) is decreasing such that the cost of 1 kWh has reached grid parity.
- No wear and tear occur and no maintenance is required in solar PV, because of the absence of the moving parts.
- Solar PV is easily accessible and can be installed close to the charging station, rooftop, charging station rooftop, or roof of the vehicle.
- The surplus energy generated by the solar PV can be stored in the EVs, eliminating the requirement of a battery for the PV system.

Fig. 10.15 shows a simplified diagram of the integration of the solar PV into the grid for the EV. In the conventional PV system, the battery is replaced by the EV through the charge controller. Keeping in view the SOC of the battery of the EV, the charge controller decides

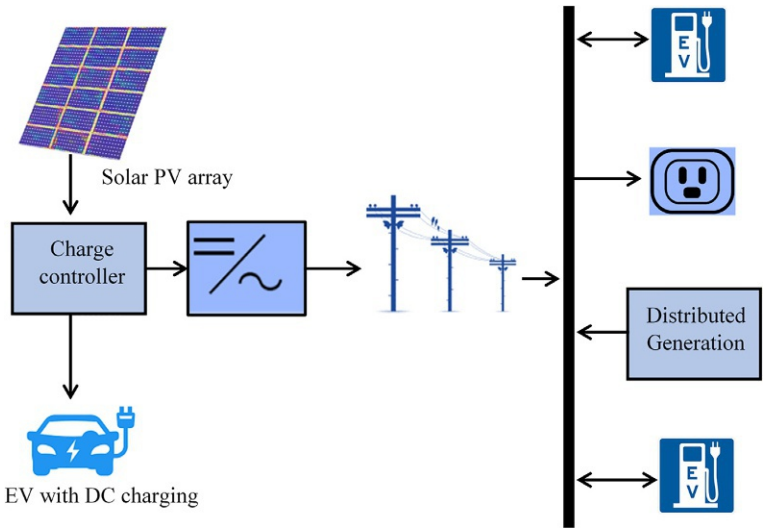

FIG. 10.15 Integration of solar photovoltaic system into the distribution system.

whether to charge the EV or to feed the grid through the distribution system. To the distribution system, distributed generation sources, loads, and the EV charging stations are connected that can charge the EVs and drain out the EV to the grid. In the energy management system, the charging of the EVs is preferred during off-peak hours and the draining of the EV into the grid during peak hours.

10.6 Concept and framework of V2G

Vehicle to grid (V2G) is a concept in which EVs like BEVs, HEVs, plug-in hybrid electric vehicles (PHEVs), and FCEVs communicate to the grid for the sale of electricity. During peak hours, the energy can be drawn from EVs to the grid to meet the energy demand at this time. On the other hand, if a home runs on renewable energy sources like solar and wind, it may get electricity from an EV during bad weather conditions. Power flow between EVs and grid is shown in Fig. 10.16.

The concept of V2G or the smart grid has made the communication protocols necessary for the integration of EVs into the smart grid. The communication protocols are beyond the safety measures. Communication protocols are required to incorporate the following features:

- identification of the peak hours and cost of electricity sold to the grid and the tariff for peak hours and off-peak hours and
- identification and information related to the vehicle (SOC of the vehicle, duration of the charging session), its billing, and payment made against the vehicle charging at any public charging station.

EV batteries can store limited energy up to 56 kWh because of the capacity of the battery; an individual EV cannot provide various ancillary services to the grid and cannot maintain the demand and generation balance. To cope with the above problems, an aggregator is used, which acts as a middleman between charging stations and plug-in EVs. Depending upon the charging and discharging perspective, aggregative is seen as the power generation source and the load, respectively. The aggregator is responsible for gathering the EVs and communicating with them and the grid. The owners of EVs that reach the charging station with a sufficient SOC of the battery discharge this energy to the grid. The charging and discharging of the EVs in the smart grid are shown in Fig. 10.17.

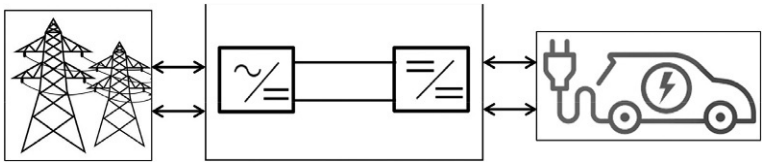

FIG. 10.16 Power flow between an electric vehicle and the power grid.

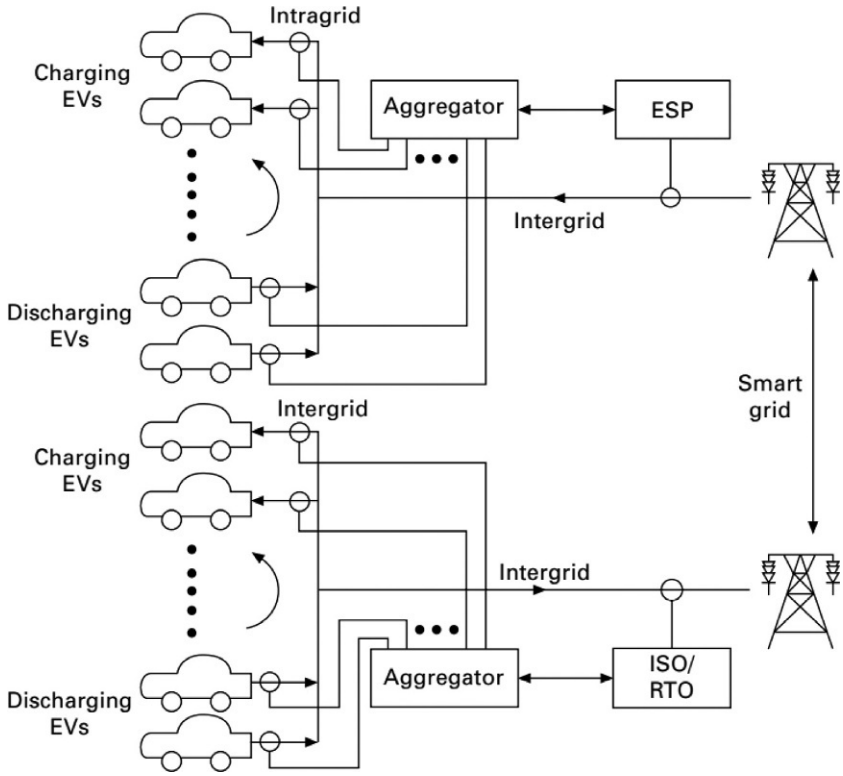

FIG. 10.17 Aggregated dual grid V2G framework.

10.6.1 Unidirectional V2G

Unidirectional V2G is also termed the smart charging or the V1G technology in which the charging rate is controlled between an EV and the power grid. Unidirectional V2G is less expensive than bidirectional V2G, since it only involves a controller that will determine and control the peak hour-based charging rates. Ancillary services like spinning reserves and the power grid regulation can also be provided to the smart grid by the unidirectional V2G. An energy-trading policy between the EV owner and the power utility is required to implement the unidirectional V2G technology. The energy trading policy must ensure differing charging rates for off-peak and peak hours. If a vehicle owner charges the vehicle in off-peak hours, they must be charged less than for charging in peak hours.

10.6.2 Bidirectional V2G

In bidirectional V2G technology, the power flows in two ways. EVs are charged from the charging stations, i.e., power flows from grid to vehicle. Owners of EVs also sell their surplus energy to the grid in which energy flows from V2G. During peak hours, vehicle owners can drain out their charged batteries to the grid in return for significant revenue and can again

charge their batteries in off-peak hours at cheaper rates. The battery charger of the bidirectional V2G technology contains a DC/DC converter and a bidirectional AC/DC converter. During the charging process, the power from the grid is first rectified using an AC-DC rectifier, and then the DC voltages are bucked or boosted using a DC-DC converter to maintain the EV battery voltage level. During the discharging process, the battery voltage from the EV is first converted to the input voltage level of the inverter. The inverter converts the DC voltage into AC to feed the grid. A comparison between unidirectional and bidirectional V2G is presented in Table 10.3.

10.6.3 Ancillary services

Ancillary services of the grid are used to balance the demand and supply, maintaining the grid reliability, and supporting the power flow from the generating point to the consumer. The novel concept V2G can provide the following ancillary services to the grid: voltage and frequency regulation, load leveling and peak shaving, spinning reserves, and integration of energy storage systems to mitigate the intermittency of renewable energy sources.

10.6.3.1 Frequency regulation

For electrical grids, the frequency of the power generators and the system must be within the set tolerance known as the frequency regulation. The misalliance between the electricity generation and the required demand leads the system toward varying frequency, which needs control to maintain the frequency within an acceptable range. Frequency regulation is done by adding and removing the power generator governor response, generator inertia, and the energy storage system. Each of the methods of frequency regulation has its advantages and disadvantages, and their execution takes from a millisecond to 20 min. Among ancillary services, frequency regulation has the highest value. Ancillary services are the function performed by the grid actors to ensure the smooth flow of electricity in the grid.

The frequency regulation of the grid requires a balance between power generation and demand. The grid frequency is disturbed when the balance between generation and demand occurs. Grid frequency regulation is a service provided by the power plants. The power plants increase or decrease their generation during a frequency disturbance in the system. EVs allow the correction of frequency variations and maintain grid stability and quality. Conventionally frequency regulation is achieved with the help of generators that put extra cost because of the consumption of fuel. In V2G systems, EVs can respond quickly to frequency variation through the charging and discharging of EV batteries. Generally, when the grid frequency is low, EV batteries are discharged and when the grid frequency is high, EV batteries are charged through the grid. Frequency regulation using EVs present in the V2G system is economically beneficial.

10.6.3.2 Voltage regulation

Voltage regulation service helps in compensating for the variations in the grid because of the mismatch between the power generation and power demand; it also facilitates the integration of the distributed energy sources into the grid. Like frequency regulation, in voltage regulation service, EVs are charged when there is increased production and less demand, and they are discharged when the demand is higher than the power generation [16].

TABLE 10.3 Comparison between unidirectional and bidirectional V2G.

Sr. no.	Key features	Unidirectional V2G	Bidirectional V2G
1	Power flow	• Grid to vehicle (G2V)	• Grid to vehicle (G2V) • Vehicle to grid (V2G)
2	Hardware infrastructure	• Communication system	• Communication system • Bidirectional battery charger
3	Complexity	• Low	• High
4	Cost	• Low	• High
5	Services	• Frequency regulation • Power grid regulation • Spinning reserves • Voltage regulation • Load shifting • Load profile management	• Frequency regulation • Load peak shaving • Load leveling • Spinning reserves • Active power support • Reactive power support • Harmonic filter • Voltage regulation • Backup power support • Improve power system stability • Power factor correction
6	Optimization objective	• Maximize profit • Minimize losses • Minimize operating cost • Minimize emissions	• Maximize profit • Minimize losses • Minimize operating cost • Minimize emissions • Maximize the renewable energy fraction • Minimize load curve error

7	Constraints	• SOC limits of the battery • Battery capacity • Electric vehicle availability • Energy prices • Energy exchange rate limits of the battery	• SOC limits of the battery • Battery capacity • Electric vehicle availability • Energy prices • Energy exchange rate limits of the battery • Efficiency of the system
8	Optimization method	• Genetic algorithm • Linear programming • Convex optimization	• Genetic algorithm • Linear programming • Quadratic programming • Particle swarm optimization • Ant colony optimization
9	Advantages	• Grid overloading prevention • Profit maximization • Emission minimization • Load leveling	• Grid overloading prevention • Integration of RES • Profit maximization • Emission minimization • Load leveling • Improve voltage profile • Failure recovery
10	Disadvantages	• Limited service	• Complexity in infrastructure • Battery system degradation • Social barriers • High investment cost

10.6.3.3 Peak shaving and load leveling

The installed capacity of the power plants in DG must be such that the peak load demand could be satisfied. In DG, spinning reserves and nonspinning reserves plays a role in peak shaving since the new incoming generator is synchronized to the system quickly. Peak shaving can be obtained by controlling both generation-side management and load-side management. On the load side, the unnecessary load can be avoided during peak hours, e.g., air conditioners can be operated at relatively high temperatures. On generation-side management, the spinning and nonspinning reserves may be brought into the system within no time.

A load following power plant or a load-following strategy adjusts the output power according to the fluctuations in the power demand all over the day. In the load-following strategy, the power generators are either completely shut down or their output power is curtailed at night when demand is low. In this regard, EVs in the V2G system can play a role in peak shaving by discharging their batteries to the grid during peak hours and charging their batteries during off-peak hours.

10.6.3.4 Spinning reserve

Spinning reserve is another ancillary service provided by EVs in the V2G system. Spinning reserve is a type of operating reserve and is defined as the extra power generating capacity of the generator that is already synchronized to the system. This extra power is achieved by increasing the torque of the turbine rotor. In the case of steam and gas turbines, spinning is controlled by the combustion in the combustion chamber, and in micro-hydro, it is controlled by the flow rate of the falling water through the turbine. In the case of EVs, the spinning reserve is offered by the energy storage systems of the EV. One challenge that might be faced is the presence of sufficient EVs during the high-demand periods with a high SOC of the batteries to serve as a spinning reserve.

10.6.3.5 Renewable energy storage and reduction of intermittence

Almost all renewable energy resources are intermittent and vulnerable to variation depending upon the time of the day and the weather. These variations can badly degrade the performance of the power electronics equipment, communication, and information systems in the grid. Energy storage systems of EVs can overcome this problem. Intermittency of renewable energy sources can be mitigated with the help of the V2G system. The surplus energy produced by the solar power plants and wind farms can be used to charge the ESS of the EVs during the off-peak hours and this stored energy is used for journeys. During peak hours, EVs can discharge their energy to the grid. The integration of renewable energy systems (RES) and the EVs into the grid increases the reliability and flexibility of the grid.

10.6.4 Applications of V2G

10.6.4.1 Load shifting

Renewable energy sources like wind and solar energy are intermittent. Having backup generators for these sources during the peak demands is not cost-effective. The use of battery storage systems with renewable energy sources is also a bulky and expensive solution. The batteries of the EVs can be used as a backup to the intermittent sources. During off-peak hours

and when the sources are fully available, the generated electricity can be used to charge the batteries of EVs. During peak hours, when the demand is much higher than the generation and the intermittent sources are not fully available, demand can be fulfilled by the batteries of EVs.

10.6.4.2 Load leveling and peak shaving

For a balanced system, the generation capacity of the system must be enough to manage the load. If the load demand is suddenly increased, the cost will be increased by managing the increased load. EV batteries can be used to absorb the excessive generation during off-peak hours, which is called load leveling. During peak periods, the absorbed energy in the EVs can be used for load shaving. The concept of load leveling and load shifting is shown in Fig. 10.18.

10.7 Energy storage systems for electric vehicles

10.7.1 Batteries

Batteries store energy in the form of chemical energy and when required this chemical energy is converted into electrical energy. Various types of batteries have been proposed for EVs. The most viable batteries for EVs are lead-acid batteries and lithium-ion batteries. Some key features that are observed while choosing electrical vehicles are battery capacity and depth of discharge (DOD), specific energy, energy density, the lifetime of the battery, efficiency of the battery, and maintenance. Characteristics of different batteries that are used in EVs are given in Table 10.4.

The following are important characteristics of lead-acid batteries which affect their use for EVs.

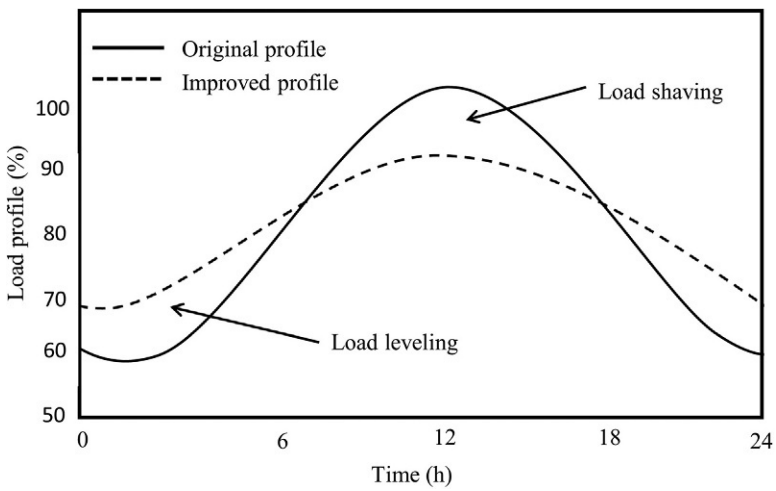

FIG. 10.18 Load leveling and load shaving in a V2G framework.

TABLE 10.4 Characteristics of EV batteries.

Characteristics	Li-ion	Ni-Cd	Ni-MH	Na-S	Pb-PbO_2	Na-NiCl	Zn-Br_2
Working temperature (°C)	−20–60	0–50	0–50	300–350	−20–45	300–350	20–40
Energy density (Wh/L)	200–735	60–150	100–300	120–130	60–100	110–120	60–70
Specific energy (Wh/kg)	100–275	60–80	60–120	130	30–60	160	75–140
Specific power (W/kg)	350–3000	120–150	250–1000	150–290	75–100	150–200	80–100
Cycle durability	400–3000	2000	500	2500–4500	500–800	1500–2000	>2000
Cell voltage (V)	3.6	1.35	1.35	2.08	2.1	2.58	1.79

- *Battery capacity and depth of discharge*

The energy that a battery can deliver is calculated by multiplying the *DOD* of the battery by its capacity, hence, *DOD* is an important parameter in the design process of the solar photovoltaic integrated battery bank. Other than the *DOD* of the battery, battery temperature and the battery discharge rate also affect the capacity of the battery. High battery temperatures are not suitable since they increase the aging process, electrolyte usage, and self-discharging. Every degree rise in temperature of a battery decreases the capacity by 1%.

- *Specific energy*

Specific energy is also termed gravimetric energy density of a battery, and is defined as the amount of electrical energy that is stored for every kilogram of battery mass. The specific energy of the Li-ion battery is better than that of the Ni-Cd battery. The higher specific energy of Li-ion makes it perfect for lighter-weight applications such as laptops and cell phones. Specific energy is measured in Wh/kg.

- *Energy density*

Energy density is also termed the volumetric density of a battery and is defined as the amount of electrical energy stored per cubic meter of the battery volume. Energy density is measured in Wh/m^3. Energy density is a function of the weight of the battery and the volumetric energy density is the function of the volume of the battery. A battery with a higher energy density means that the battery would be lighter than the battery with a lower energy density. For the same capacity, the battery with high energy density will occupy less volume whereas the battery with lower energy density will occupy a large volume. The energy density of Li-ion batteries is higher than that of Ni-Cd batteries.

- *Lifetime of the battery*

With the passage of time and the increase in charging/discharging cycles, crystals of lead sulfate are formed on the battery electrode, which reduces the effectiveness of the active materials and the capacity of the battery. Reduction in battery capacity is because of the following parameters: charging and discharging cycles that the battery has experienced, the DOD of the battery over its lifetime, the average battery temperature over its lifetime, and discharge of the battery below the minimum allowed state of charge (SOC_{min}) for an extended period of time.

- *Efficiency of the battery*

Energy efficiency is defined as the ability of the battery to convert one form of energy to another electrical to mechanical and mechanical to electrical energy. The energy efficiency of the LA battery is about 70% and the Coulomb efficiency (CE) is 85%. CE is the discharge capacity to charge capacity ratio, as shown in Eq. (10.8).

$$\mathrm{CE} = \frac{Q_{discharge}}{Q_{charge}} \tag{10.8}$$

Energy efficiency (EE) is determined by Eq. (10.9).

$$\mathrm{EE} = \mathrm{CE} \times \mathrm{VE} \tag{10.9}$$

where voltage efficiency (VE) is the difference between voltages at the charging and discharging process.

- *Maintenance*

Maintaining the water level of the battery is necessary since the production of oxygen and hydrogen reduces the water level of the battery.

10.7.2 Ultracapacitors

The electrochemical capacitor, also known as the supercapacitor, consists of two electrodes named an anode and cathode separated by a dielectric insulator. A dielectric could be made up of plastic film, glass, or ceramic. When a voltage is applied across the electrodes, an electric field is developed between the electrodes. A capacitor stores energy in the form of an electric field. Comparing the capacitors to other energy storage technologies, the charging of the capacitor is very fast, but the energy density is very low, and the self-discharging of the capacitor is very fast.

A supercapacitor is also known as an ultrafast capacitor or electrochemical capacitor. Supercapacitors have very high capacitance having characteristics between a capacitor and battery. An electrochemical capacitor consists of carbon electrodes separated by a porous membrane immersed in an electrolyte. The membrane allows the ions to pass through and blocks electrons. The capacitance and the energy are determined by Eqs. (10.10), (10.11), respectively.

$$C = \frac{A\varepsilon_0}{d} \tag{10.10}$$

$$E = \frac{1}{2}CV^2 \tag{10.11}$$

where A is the effective area of the electrode plates; ε_0 is the dielectric constant of the insulating medium; and d is the distance between the electrodes plates.

Eq. (10.10) indicates that the capacitance is directly proportional to the area of the electrode plates and inversely proportional to the distance between the plates. The energy stored in the

electric field of the capacitor is directly proportional to both capacitance and the voltage as given in Eq. (10.11).

Since the supercapacitors are of low voltages, to obtain the required voltage levels, supercapacitors are connected in series.

10.7.3 Flywheels

The flywheel is one of the favored energy storage systems for EVs because it has:

- an easily estimated SOC;
- a long life cycle;
- no degradation over a lifetime; and
- high power density.

These properties make the flywheel useful in a high and frequent flow of energy whenever needed. In grid fluctuations and intermittent sources of energy, the flywheel can be used to overcome the fluctuations. Flywheels can be used as an energy storage system in buses, EVs, container cranes, construction machines, garbage trucks, charging stations, cable ferries, and train stations; they are used for frequency regulation, microgrid stabilization, and improving power quality.

10.8 SWOT analysis of electric vehicles

10.8.1 Strengths

- EVs and electric grids both are additives to the smart grid and microgrid concept.
- Since batteries and electric motors are involved in EVs, they are environmentally and eco-friendly.
- Instead of increasing the power generation capacity during peak hours, EVs are best to serve as a grid (V2G).
- Solar energy-based charging stations can be installed and the other renewable energy sources can also be integrated into the grid.
- A regenerative braking system can increase the efficiency of the EV.
- Silent operation since less working of the engine is required.
- Simpler mechanism.

10.8.2 Weaknesses

- A longer time is required for the charging process.
- Expensive energy storage systems since different charging and discharging cycles reduce the lifecycle of the whole system.
- Unavailability of charging stations.
- Since the technology is not mature and is relatively new in the market, its deployment and social acceptance are based on the reputation and credibility of the EV providers.

10.8.3 Opportunities

- Subsidies for the EV owners and the charging station owners.
- Lower taxes.
- Feed-in tariff for energy sold to the grid.
- Depletion of the fossil fuels and their rising cost.
- Solar PV grid parity.
- Development of new control techniques for charging processes of EVs.

10.8.4 Threats

- Conventional matured technologies.
- The continuous charging and discharging of the batteries decreases the lifecycle which reduces the energy storage capacity and as a result, the owner earns less profit by selling electricity to the grid.
- Since the EVs and smart grid depend upon the communication systems, like other systems they may face cyber attacks degrading the grid and vehicle security.
- Competition with other technologies like hydrogen-powered fuels, alternative fuels.
- Rise in electricity prices from the grid.

10.9 Conclusion

Advancements in smart grid technologies have brought a revolution in EV deployment. The smart grid allows EVs to be charged by the smart charging stations powered by renewable energy sources like wind and solar photovoltaics. EVs are classified as BEVs, plug-in hybrid electric vehicles, and FCEVs. EVs provide various ancillary services to the grid like voltage and frequency regulation, peak shaving, load leveling, spinning reserve, and integration of renewable and intermittent sources to the grid. Batteries, ultracapacitors, and flywheels can be used as an energy storage system in EVs. Finally, a SWOT analysis of the EVs was presented.

Problems

Problems 1–10 contain four answer options: A, B, C, and D. Choose the correct answer

1. What is tractive effort?
   A. Aerodynamic drag force
   B. Hill climbing force
   C. Rolling resistance force
   D. Acceleration force
   E. All of the above

2. What is the mathematical representation of aerodynamic drag force?
   A. $F_{ad} = \mu_{rr}\, mg$
   B. $F_{ad} = \frac{1}{2}\rho A C_d v^2$
   C. $F_{ad} = mg\sin\psi$
   D. $F_{ad} = I\frac{G^2}{\eta_g r^2}a$
3. What is the mathematical representation of rolling resistance force?
   A. $F_{rr} = \mu_{rr}\, mg$
   B. $F_{rr} = \frac{1}{2}\rho A C_d v^2$
   C. $F_{rr} = mg\sin\psi$
   D. $F_{rr} = I\frac{G^2}{\eta_g r^2}a$
4. What is the mathematical representation of hill climbing force?
   A. $F_{hc} = \mu_{rr}\, mg$
   B. $F_{hc} = \frac{1}{2}\rho A C_d v^2$
   C. $F_{hc} = mg\sin\psi$
   D. $F_{hc} = I\frac{G^2}{\eta_g r^2}a$
5. What is the mathematical representation of the force required for angular acceleration?
   A. $F_{\omega a} = \mu_{rr}\, mg$
   B. $F_{\omega a} = \frac{1}{2}\rho A C_d v^2$
   C. $F_{\omega a} = mg\sin\psi$
   D. $F_{\omega a} = I\frac{G^2}{\eta_g r^2}a$
6. Which of the following are types of electric vehicles?
   A. Battery electric vehicles
   B. Hybrid electric vehicles
   C. Plug-in electric vehicles
   D. Fuel cell electric vehicles
   E. All of the above
7. What is the AC charging level of electric vehicles?
   A. AC level 1
   B. AC level 2
   C. AC level 3
   D. All of the above
8. What is the DC charging level for electric vehicles?
   A. DC level 1
   B. DC level 2
   C. DC level 3
   D. All of the above
9. Which of the following is an application of V2G?
   A. Load shifting
   B. Load leveling
   C. Peak shaving
   D. All of the above

10. Which of the following is a general energy storage system for electric vehicles?
    A. Batteries
    B. Ultracapacitors
    C. Flywheel
    D. All of the above

Give brief answers to the following short questions

1. Define tractive effort and explain the role of various forces acting on the vehicle as it moves up a hill.
2. Illustrate the working of a battery electric vehicle with the help of a schematic diagram.
3. Illustrate the working of a hybrid electric vehicle with the help of a schematic diagram.
4. Illustrate the working of a plug-in hybrid electric vehicle with the help of a schematic diagram.
5. Illustrate the working of a fuel cell electric vehicle with the help of a schematic diagram.
6. Discuss the impact of the integration of electric vehicles into the grid.
7. Differentiate between an on-board charger and an off-board charger.
8. Discuss the characteristics of different AC and DC charging levels.
9. Why is solar photovoltaics considered best for an electric vehicle charging station?
10. Explain the concept and framework of V2G.
11. Give a brief comparison between unidirectional and bidirectional V2G.
12. Discuss the role of an aggregator in a framework of electric vehicles and the smart grid.
13. Which ancillary services are provided by electric vehicles to the grid?
14. How is frequency regulation achieved in a grid with the help of electric vehicles?
15. How is voltage regulation achieved in a grid with the help of electric vehicles?
16. How are peak shaving and load leveling achieved in a grid with the help of electric vehicles?
17. Spinning reserve is an ancillary service of the electric vehicle to the grid. How does it act in a conventional power plant and electric vehicles?
18. How is the intermittency of renewable energy sources overcome with the help of electric vehicles?
19. How are electric vehicles applied in load shifting, load leveling, and peak shaving?
20. List the characteristics of lead-acid batteries based on which they are used in electric vehicles.
21. Which energy storage system can be used in electric vehicles?
22. Present a brief SWOT analysis of electric vehicles.

References

[1] C.S. Ioakimidis, D. Thomas, P. Rycerski, K.N. Genikomsakis, Peak shaving and valley filling of power consumption profile in non-residential buildings using an electric vehicle parking lot, Energy 148 (2018) 148–158, https://doi.org/10.1016/J.ENERGY.2018.01.128.

[2] D. Van Der Meer, G.R.C. Mouli, G. Morales-España, L.R. Elizondo, P. Bauer, Erratum to: Energy management system with PV power forecast to optimally charge EVs at the workplace (IEEE Transactions on Industrial

Informatics (2018) 14:1 (311 – 320) DOI: 10.1109/TII.2016.2634624), IEEE Trans. Ind. Inf. 14 (7) (2018) 3298, https://doi.org/10.1109/TII.2018.2848538.
[3] A. Ivanova, J.A. Fernandez, C. Crawford, N. Djilali, Coordinated charging of electric vehicles connected to a net-metered PV parking lot, in: 2017 IEEE PES Innov. Smart Grid Technol. Conf. Eur. ISGT-Europe 2017—Proc., Vol. 2018-January, 2017, pp. 1–6, https://doi.org/10.1109/ISGTEUROPE.2017.8260291.
[4] A. Mohamed, V. Salehi, T. Ma, O. Mohammed, Real-time energy management algorithm for plug-in hybrid electric vehicle charging parks involving sustainable energy, IEEE Trans. Sustain. Energy 5 (2) (2014) 577–586, https://doi.org/10.1109/TSTE.2013.2278544.
[5] N. Liu, et al., A heuristic operation strategy for commercial building microgrids containing EVs and PV system, IEEE Trans. Ind. Electron. 62 (4) (2015) 2560–2570, https://doi.org/10.1109/TIE.2014.2364553.
[6] R. Fachrizal, J. Munkhammar, Improved photovoltaic self-consumption in residential buildings with distributed and centralized smart charging of electric vehicles, Energies 13 (5) (2020) 1153, https://doi.org/10.3390/EN13051153.
[7] X. Wu, X. Hu, Y. Teng, S. Qian, R. Cheng, Optimal integration of a hybrid solar-battery power source into smart home nanogrid with plug-in electric vehicle, J. Power Sources 363 (2017) 277–283, https://doi.org/10.1016/J.JPOWSOUR.2017.07.086.
[8] A.R. Bhatti, Z. Salam, A rule-based energy management scheme for uninterrupted electric vehicles charging at constant price using photovoltaic-grid system, Renew. Energy 125 (2018) 384–400, https://doi.org/10.1016/J.RENENE.2018.02.126.
[9] G. Barone, A. Buonomano, F. Calise, C. Forzano, A. Palombo, Building to vehicle to building concept toward a novel zero energy paradigm: modelling and case studies, Renew. Sust. Energ. Rev. 101 (2019) 625–648, https://doi.org/10.1016/J.RSER.2018.11.003.
[10] A. Mohammad, R. Zamora, T.T. Lie, Integration of electric vehicles in the distribution network: a review of PV based electric vehicle modelling, Energies 13 (17) (2020) 4541, https://doi.org/10.3390/EN13174541.
[11] M. Guarnieri, When cars went electric, part 1, IEEE Ind. Electron. Mag. 5 (1) (2011) 61–62, https://doi.org/10.1109/MIE.2011.940248.
[12] M. Guarnieri, When cars went electric, Part 2, IEEE Ind. Electron. Mag. 5 (2) (2011), https://doi.org/10.1109/MIE.2011.941122.
[13] Global EV Outlook 2020—Analysis—IEA, Available from: https://www.iea.org/reports/global-ev-outlook-2020. (Accessed 26 May 2022).
[14] Electric Vehicles—Analysis—IEA, Available from: https://www.iea.org/reports/electric-vehicles. (Accessed 27 May 2022).
[15] F. Mwasilu, J.J. Justo, E.K. Kim, T.D. Do, J.W. Jung, Electric vehicles and smart grid interaction: a review on vehicle to grid and renewable energy sources integration, Renew. Sust. Energ. Rev. 34 (2014) 501–516, https://doi.org/10.1016/J.RSER.2014.03.031.
[16] M. Yilmaz, P.T. Krein, Review of benefits and challenges of vehicle-to-grid technology, in: 2012 IEEE Energy Convers. Congr. Expo. ECCE 2012, 2012, pp. 3082–3089, https://doi.org/10.1109/ECCE.2012.6342356.

CHAPTER

11

Global status of smart grids

11.1 Introduction

The monitoring and controlling of grid-related activities using advanced digital communication and advanced metering infrastructure (AMI) for distributed generation systems is termed the smart grid. This chapter considers all the parts of the smart grid, like power generation, transmission, distribution, energy storage systems, integration of renewable energy sources, integration of electric vehicles, and AMI. Since the conventional grid has been obsolete and does not give an insight into the energy consumption pattern, no integration of the distributed generation to the grid is involved. Each component of the smart grid system is getting more popular every year. Governments around the world are investing and funding smart grid projects at the initiative level and advanced level. Various countries are developing smart cities and smart grids with the representation of the feature of the smart grid. This chapter gives an insight into the status of the smart grid in different countries of the world. The status of the components of the smart grid from 2010 to 2020 is also given in this chapter.

11.2 Global smart grid market—Global forecast to 2026

The major growth factor of the smart grid market is the modernization of the obsolete grid. The global market for smart grids is estimated at USD 43.1 billion in 2021 and it is estimated that it will reach USD 103.4 billion in 2026. To promote the smart grid, governments are encouraging the public to invest in the smart grid by giving different incentives. The dynamics of the smart grid market are as follows [1].

11.2.1 Driver

The governments of the world have adopted the smart grid driving policies and opportunities and created awareness among the people for energy conservation in industrial, residential, and commercial applications. The US government initiated a smart grid investment

https://doi.org/10.1016/B978-0-323-99560-3.00011-9

program to drive the modernization of the electric power transmission and distribution. Canada invested in driving the smart grid implementation by integrating renewable energy sources into the grid without compromising the stability and also implemented digital and IoT-based communication technologies in the grid. China, South Korea, Australia, and Japan are expected to enhance the smart grid market. ECHONET Lite, a new communication standard, was developed by Japan to interface smart meters with the home energy management system.

11.2.2 Restraints: High capital investment and operation and maintenance costs

The first step in implementing the smart grid is the capital investment to change the transmission infrastructure of the grid. The transmission in the smart grid must be supportive of two-way communication. The deployment of the smart grid requires huge capital investment and high operation and maintenance costs, which incur a heavy load on governments.

11.2.3 Opportunities: Existing smart city projects in developing countries

Smart cities are economically and technically developed urban areas demonstrating high living standards with easy mobility, a clean and healthy environment, advanced technologies, and government rules and regulations. Smart cities exhibit the proper utilization of resources like smart metering, transportation, health care, and safety. These segments are managed more efficiently and intelligently using digital and Internet of Things (IoT) communication. Smart cities depend upon the smart grid platform in which the infrastructure is centrally planned connecting different components of the smart grid.

11.2.4 Challenges: Managing smart grid-related complex information

Implementation of the smart grid generates huge data. This data concerns consumer information, load demand pattern, power generation pattern, availability of the energy sources, time of use, peak hours and off-peak hours, state of the charge of energy storage systems, and the electric vehicles. The data is unmanaged and unstructured, and needs to be processed further using statistical tools to ensure a good understanding of any patterns. A major challenge faced by the utility is not knowing the importance of smart grid-related environmental data, transmission and distribution data, and distributed generation data. This data can be used as a sample for future predictions. A small utility receives huge data from smart meters, control devices, smart sensors, and other connected networks. Generating and gathering such huge data for intelligent decision-making is another challenge to the small utilities.

11.3 Key characteristics of the smart grid

The key characteristics of a smart grid system are detailed in Table 11.1. Among these are the ability of the distributed generation sources to be integrated into the energy storage

TABLE 11.1 Key characteristics of the smart grid.

Characteristics	Description
Integrates all energy storage systems into the power generation units	The smart grid does not restrict itself to large and medium power plants. It accommodates all the distributed generation sources from small scale to the combined heat and power generations, renewable energy sources, energy storage systems, and electric vehicles. Integration of all the components will increase the flexibility of the smart grid
Maintains the power quality	A smart grid does not provide the same power quality and same electricity prices. The services contract of premium quality power may include the cost of the high quality and other services like monitoring and control methods of some essential loads and components. It provides a diagnosis of the events like surges, harmonics, lighting, and switching harmonics affecting the power quality. The protection of the components causes extra cost
Provides resiliency to instabilities, attacks and natural disasters	Resilience is defined as the ability of a system to isolate a particular part of the smart grid from the rest of the grid in case of a sudden fault in keeping the healthy grid operational. The self-healing ability of the smart grid reduces the interruption of the service to consumers
Enables new technologies, services, and new markets	If the smart grid market is efficiently designed and operated, it gives opportunities to consumers to choose from the competitive smart grid markets. The operators, owners, and consumers need the facility to modify the business rules to suit different time and market conditions
Optimum utilization of assets	Smart grid uses the latest and most efficient technologies to utilize its assets efficiently. The system control senses the requirement of the load and the generation and can send signals to the power generating units to optimize their functioning, keeping in mind the peak hours and different price slots

systems, maintaining the power quality in the grid since there is a complex flow of energy from sources to the load in a complex integrated system, ability of the grid network to provide resilience in case of natural disasters and instability in the grid, ability of the grid to enable and accept new communication, storage, and generation technologies, related services, and balance of the system. The major characteristic of the smart grid is optimum utilization of the sources.

11.4 Smart grid road maps from different electric utilities

Different countries of the world are working toward smart grids by investing and funding smart grid-related technologies and equipment. Table 11.2 describes the status of different smart grid markets and their future roadmap toward the implementation of the smart grid.

TABLE 11.2 Status of smart grids in different countries of the world.

Country	Description
China	The government of China has developed a long-term plan to invest in the smart grid, power grids, water systems, and rural infrastructure. Smart grids are intended to increase the penetration of the renewable energy source in the power generation, enhance the power system efficiency, develop energy management systems, and optimize the energy consumption
United States	Under the American Recovery Reinvestment Act of 2009, USD 4.5 billion for the smart grid system. Among these USD 4.5 billion, USD 3.48 billion are for the integration of well-established renewable energy technologies into the existing smart grid, USD 435 million for the general demonstration of the smart grid system, and USD 185 million for the integration of energy storage systems to the smart grid. In 2020, 102,933,903 smart meters were installed cumulatively in residential, commercial, industry, and transportation sectors. The details of these smart meters are given in Table 11.3
Italy	The Italian regulator 2011, has given tariffs to eight funded projects of active medium voltage distribution systems. The purpose of these projects was to find the energy management systems, and energy automation solutions while integrating the distributed generation sources into the existing grids. A grant of EUR 200 million was also granted by the Ministry of Economic Development of Italy to demonstrate the different characteristics of the smart grid and to modernize the features of the network
Japan	The Electric Power Companies Federation of Japan is investing USD 100 million in developing a smart grid integrating the solar photovoltaic systems in 2020. An initiative of smart metering has also been announced by the government and large utilities have started demonstrating features of the smart grid. In Japan, the smart grid is limited to smart communities with specific geographical areas. No separate legislation regarding smart grid exists in Japan rather it is covered under the Renewable Energy Act, Electricity Business Act, and the Basic Energy Act. In 2018, Japan stood second with 7600 fast-charging stations, and 22,000 publicly available slow-charging stations
Spain	In 2008, the Spanish government gave a mandate to power distribution companies to replace conventional energy meters with smart meters with no extra replacement cost. Different power utilities replaced the energy meters from 2010 to 2015
Germany	In Germany, Baden-Württemberg and North Rhine-Westphalia are the two major smart grid communities equipped with key features of the smart grid-like smart grid technology, smart meters, electric vehicles and charging infrastructure, smart buildings and smart cities, and energy storage systems. The Climate Protection Act for both the smart grid communities has led them to set a target to reduce GHG emissions by 43% by 2030 and 90% by 2050 in Baden-Württemberg, and in North Rhine-Westphalia to reduce GHG emissions by 55% by 2030 and achieve climate neutrality by 2050
Australia	In July 2021, the Energy Security Board of Australia announced that most of its conventional power plants were outdated and that renewable energy-based latest technology power plants would be installed. The Australian government also initiated a demonstration of key features of the smart grid. It is estimated that an investment of USD 6.1 billion will be there in the infrastructure of the smart grid in Australia
United Kingdom	In 2014, the UK government published its vision for the smart grid. The government decided to implement 53 million smart meters in domestic households in the UK. The vision divided the development into three stages: the development stage from 2014 to 2020, the rollout stage from 2020 to 2030, and the developed phase from 2030 onward. In the development phase, regulatory authority, standards, and a commercial framework will be developed and the rollout of smart meters across the UK. In the rollout phase, smart meters, distributed energy sources, energy storage systems, and smart appliances will be developed. In the developed phase, energy systems will be integrated that will constitute the smart grid
France	France initiated smart grid projects in Corsica, Guadeloupe, and La Reunion in 2012. The projects were completed in 2016. The project was comprised of advanced metering infrastructure, battery energy storage system, smart homes and smart cities, and the integration of renewable energy sources into the grid [2]
Brazil	To promote smart grid systems, the Brazilian government has initiated the following key features of the smart grid: tariff flag system, white hourly tariff, electricity prepayment, smart meters, distributed generation, demand-side management, energy storage technologies, and electric vehicles. The deployment of the distributed generation projects is shown in Fig. 11.1

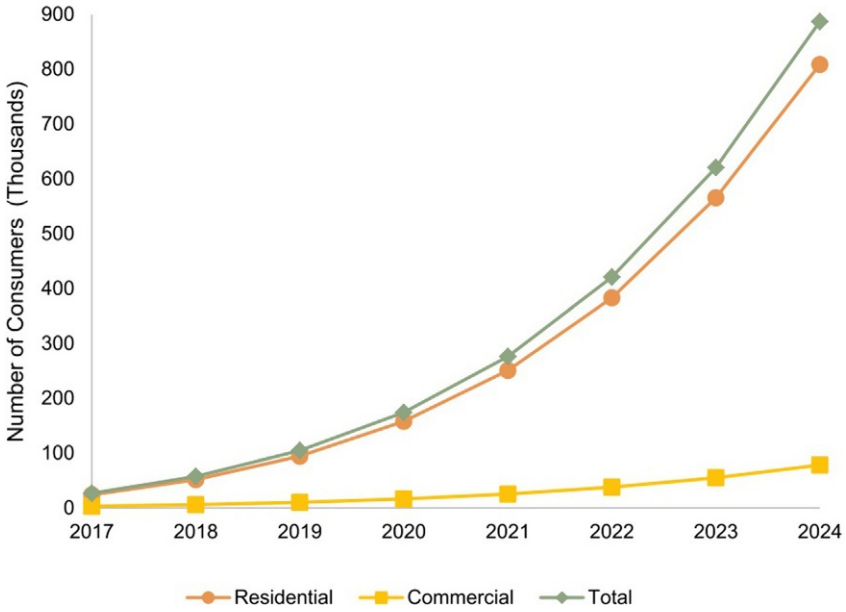

FIG. 11.1 Number of customers attached to the distributed generation in Brazil. *Source: EIA.*

11.5 Components-based status of the smart grid

The current status of the smart grid can be completely comprehended by understanding the current status of the components of the smart grid-like electric vehicles, energy storage, energy metering, solar energy, and wind energy. The following subsections discuss the global status of each of these, to contribute to an understanding of the status of the smart grid.

11.5.1 Electric vehicles

Fig. 11.2 shows the sale of electric vehicles from 2012 to 2021. The graph shows the sale of plug-in hybrid EVs, sales of battery EVs, and the market share of electric vehicles. It can be seen that there was a record sale of EVs in 2021. There was a 108% increase in sales in 2021 compared to 2020. In 2020, 324 million units of EVs were sold and in 2021, 675 million units were sold. The global market share in 2020 was 4.2%, which increased to 8.3% in 2021.

Fig. 11.3 shows the stock of electric vehicles on the road in 2021. In 2012, 125,000 units were sold while the same number of units were sold in 2021 in just a week. Fig. 11.3 shows the stock of electric vehicles in China, the USA, Europe, and other members of the International Energy Agency (IEA). The other members include Australia, Brazil, Canada, Chile, India, Japan, Korea, Malaysia, Mexico, New Zealand, South Africa, and Thailand.

The progress in the sales and stock of electric vehicles is useless if there are no charging stations available. The consumers of electric vehicles would demand the same fuel facility from the EV and grid-related services as they would for conventional vehicles. China is

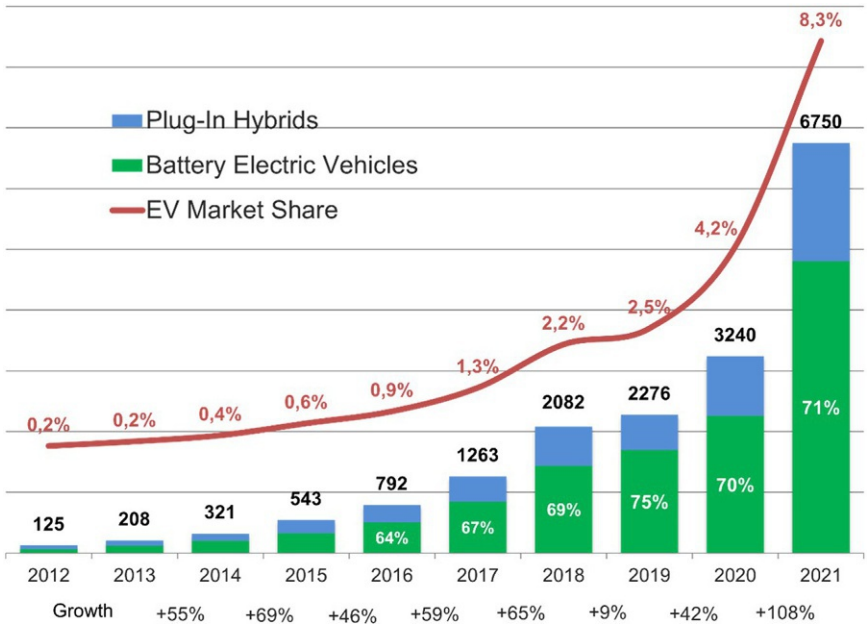

FIG. 11.2 Global sales of battery electric vehicles and plug-in hybrid electric vehicles (000s).

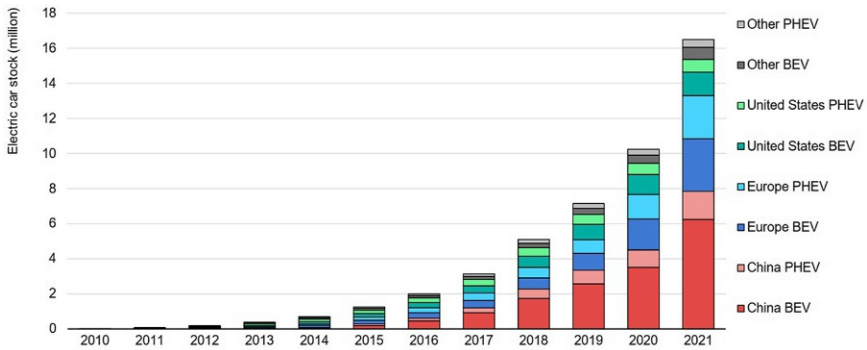

FIG. 11.3 Number of electric vehicles stock on the road from 2010 to 2021 in different markets of the world. *Source: IEA.*

leading in providing the highest number of charging points to the public, having installed 85% of the world's fast charging points and 55% of slow charging points. In 2021, China installed 650,000 slow chargers that were publicly accessible nits and this was an increase of 35% which is four times the slow chargers that were available in 2018. Europe stands second in installing slow chargers, with 300,000 slow chargers in 2021. For a long journey, fast charging points are adopted. The stock of fast charging is also shown in Fig. 11.4. In 2021, 470,000 fast chargers were installed in China, which is 50% of the installed fast chargers globally (Fig. 11.5).

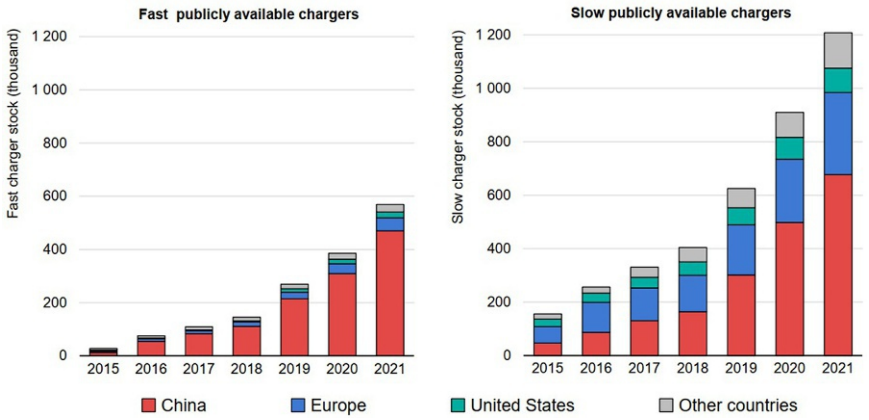

FIG. 11.4 Number of fast publicly available chargers and slow publicly available chargers from 2015 to 2021 in China, the USA, Europe and other EV markets. *Source: IEA.*

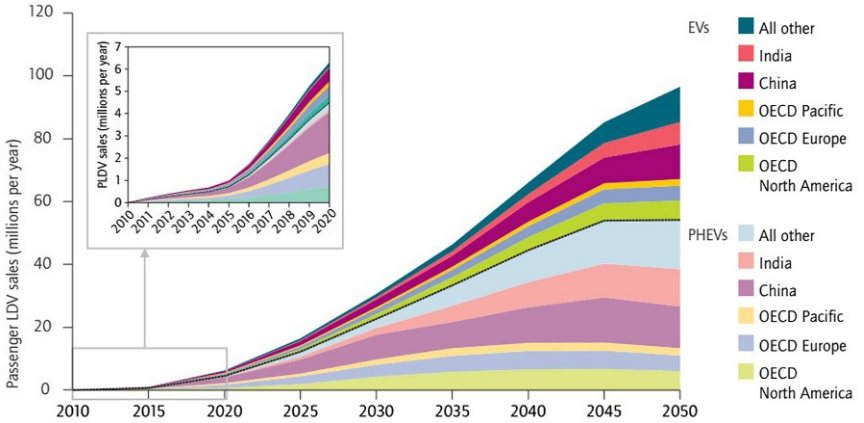

FIG. 11.5 Current status and future forecasting of EVs and PHEVs in different EV markets. *Source: IEA.*

11.5.2 Energy storage

Various energy storage systems are used in smart grid systems: mechanical, electrical, and chemical. Energy storage systems provide various services to the smart grid-like electrical energy time-shift, electrical supply shift, frequency regulation, voltage regulation, spinning reserve, etc. The total installed capacity of the battery energy storage in 2020 was 17 GW, which was twice that of 2019. The installed capacity was increased by 50% from 2019 to 2020. Fig. 11.6 shows the capacity addition by different regions from 2015 to 2020. The capacity addition by China from 2019 to 2020 was from 0.6 to 1.6 GW, while 0% was added from 2018 to 2019. Capacity addition by the USA in the same period was from 0.5 GW in 2019 to 1.5 GW in 2020. Fig. 11.6 shows the installation capacity of energy storage systems in different countries from 2016 to 2020.

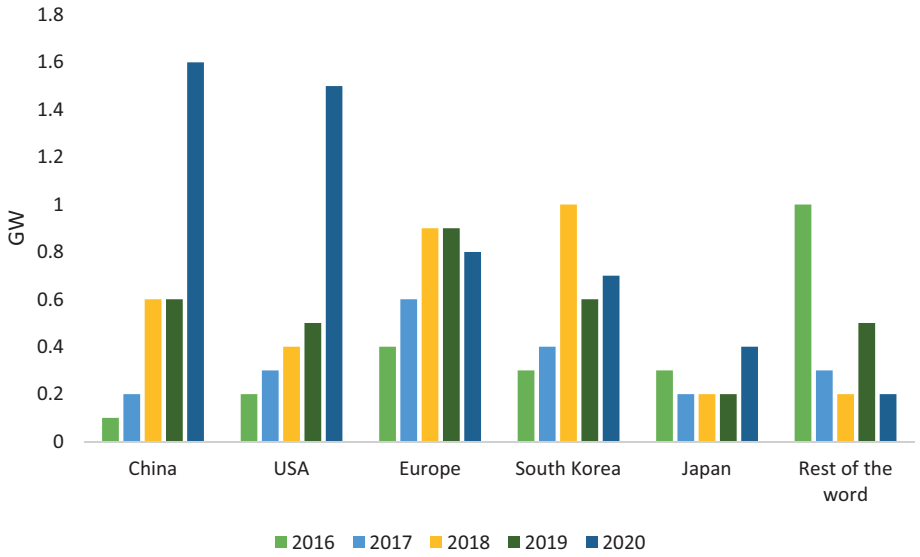

FIG. 11.6 Installed capacity of energy storage systems in different smart grid markets of the world from 2016 to 2020. *Source: International Renewable Energy Agency (IRENA).*

11.5.3 Smart metering

In 2020, the market for AMI was valued at USD 10.47 billion, and it is expected that the market will reach USD 22.98 billion by 2026. This AMI presents key characteristics of the smart grid and without which, the smartness of the grid and the modernization of the grid cannot be achieved. Smart meters give an insight into the energy consumption pattern and forecast the future energy demands for different time horizons. Smart meters are equipped with a communication system that is either one-way or two-way. The adoption of smart meters has increased since consumers can observe their energy consumption patterns easily. Smart meters enable real-time monitoring of the grid, which is helpful for a home or building energy management system. Fig. 11.7 shows the number of units of smart electric meters in million as of 31 December 2020. The detail of the smart meters installed in the USA from 2011 to 2020 is given in Table 11.3 [3].

11.5.4 Solar energy

The sun is a giant source of energy that can be harnessed in different ways. Two mostly adopted methods are solar photovoltaics and the solar concentrated which are used for electric power generation and thermal applications. Fig. 11.8 shows the global installed capacity of solar photovoltaics and solar thermal power from 2010 to 2021. In 2020, the total installed capacity of solar photovoltaics was 710,281 MW, which rose to 843,086 MW in 2021; this is an increase of 18.7%. The installed capacity of solar thermal power in 2020 was 6507 MW, which decreased to 6387 MW in 2021 [4,5]. Because of policy relaxations and cost reductions, the cost of solar PV is expected to decrease after 2022. The cost of solar PV is being reduced because of the maturity of the technology, innovation in the PV materials, and market competition.

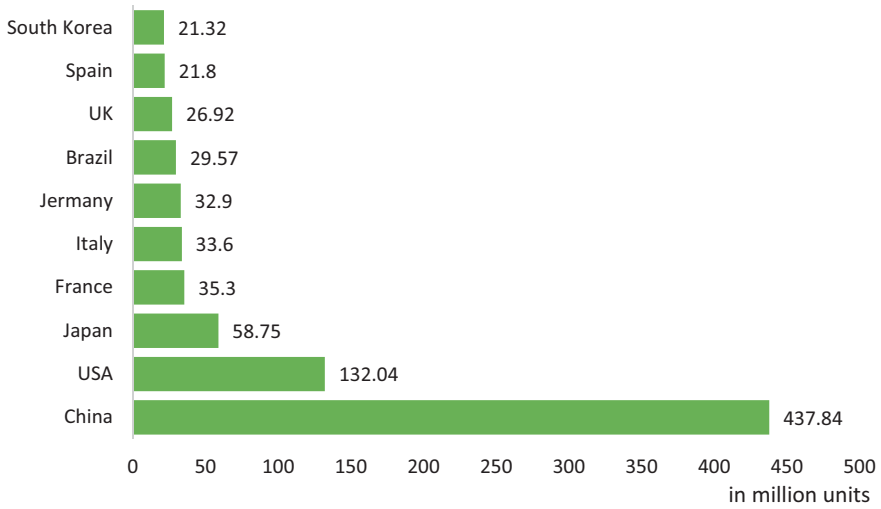

FIG. 11.7 Installed capacity of advanced metering infrastructure in different smart grid markets of the world as of December 31, 2020.

TABLE 11.3 Deployment of advanced metering infrastructure in different energy sectors of USA from 2011 to 2020.

Year	Residential	Commercial	Industrial	Transportation	Total
2011	33,453,548	3,682,159	154,659	7	37,290,373
2012	38,524,639	4,461,350	179,159	35	43,165,183
2013	47,321,995	5,770,067	248,515	845	53,341,422
2014	51,710,725	6,563,614	270,683	916	58,545,938
2015	57,107,785	7,324,345	310,889	813	64,743,832
2016	62,360,132	8,119,223	342,766	1345	70,823,466
2017	69,474,626	9,060,128	365,447	1389	78,901,590
2018	76,498,388	9,932,993	411,287	1489	86,844,157
2019	83,539,594	10,850,886	446,871	1504	94,838,855
2020	90,692,768	11,771,565	468,071	1499	102,933,903

11.5.5 Wind energy

Wind energy is one of the growing sources of electricity and its cost is being reduced because of the reduction in wind turbine prices. The cost of the wind energy from the onshore new wind power plant in 2019 was USD 0.053/kWh. Depending upon the region, the cost may vary between USD 0.051 and USD 0.099/kWh. The cost of energy from most of the competitive projects is as low as USD 0.030/kWh. The installed capacity of the offshore wind turbines was 34 GW, which increased by 64% with a total installed capacity of 56 GW. Similarly,

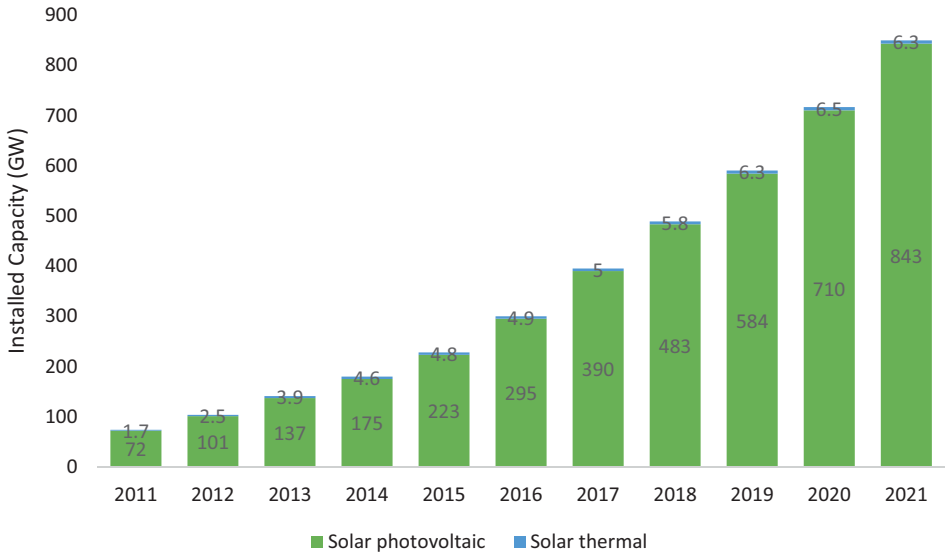

FIG. 11.8 Global installed capacity (GW) of solar photovoltaics and solar thermal power from 2011 to 2021. *Source: IRENA.*

the installed capacity of the onshore wind turbines in 2020 was 697 GW, which in 2021 increased by 10% with a total installed capacity of 769 GW. Because of the maturity of the technology and the increased competition in the market, the cost of wind energy is gradually reducing. Fig. 11.9 shows the global installed capacity of onshore and offshore wind turbines from 2011 to 2021 [6].

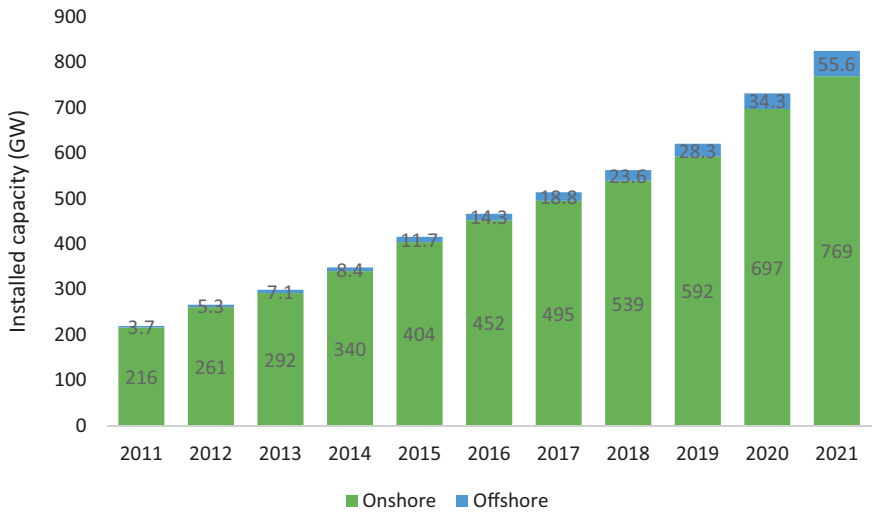

FIG. 11.9 Global installed capacity (GW) of onshore and offshore wind energy from 2011 to 2021. *Source: IRENA.*

11.6 Future research and development in smart grids

11.6.1 Power electronics

Power electronics is the fundamental research subject of the smart grid, since it involves the control and conversion of the current from one form to another and from one level to another. Power electronics materials, switching, and components are involved in electric vehicles, energy storage systems, and the integration of distributed generation sources. The research need in the power electronics can be in the solid-state semiconductor materials, components inverters, converters, and rectifiers. DOE identified the following research gaps in power electronics that can be filled by further research and development.

- Technical help must be available to the power utilities and regulators in applying power electronics technologies in the smart grid.
- Common circuit topologies must be developed that must be used in the integration of customers' solar PV systems, energy storage systems, and electric vehicles to the existing power electric grid.
- Advanced solid-state materials must be developed for different applications with high power density, low switching losses, and fast switching speed.
- Advanced fundamental materials must be developed for the transformer, active and passive switches, and filters.
- Development of a thermal management system for the fast solid state switching devices and modules.
- Development of the components like DC circuit breakers for the huge power handling operations.

11.6.2 Sensing

In conventional power grids, observability was the main problem faced by the grid operators even though they have to observe the voltages and power flow at specific nodes of the transmission and distribution system. In the advanced and modern grids, the number of nodes in the distribution system and at the distributed generation sources has been increased. Because of the integration of the renewable energy sources and the AMI, energy storage system, the frequency, voltage, power flow, state of charge of the batteries, and the demand and supply at each DG source need to be observed for the reliability of the smart grid.

An integrated sensor is an advanced mechanism for measuring the parameters and it consists of a physical transducer that converts the physical quantity measured into an electrical signal for further processing. A computational device is used to convert the electrical signal from the transducer into digital information to be used in microprocessors or microcontrollers. A communication device is used to communicate the sensed data over wired or wireless communication for further analysis of the data and decision making. A power supply unit provides power to all the sensing equipment. Since, the data from the sensors like the irradiance from the pyranometer, solar temperature from the LM35, and the wind speed from the anemometer, etc. are necessary for the future prediction. There are still various gaps in sensing the data and storing it for further actions. The following gaps must be covered for a healthy smart grid system.

- A low-cost and robust multiparameter sensor must be developed that continuously observes the performance and health of the grid and other assets of the grid and the environment.
- The range and functionality of the power electronics devices must be improved by inventing new advanced materials.
- A mechanism must be developed that ensures the use of different types of sensors and integrate them for multiple applications.
- New sensing technologies must be adopted to invent power electronics-based solid-state devices.

11.6.3 Grid control

The advancement in the smart grid and its technologies, integration of renewable energy resources into the existing grid, and the energy management system require a robust control that maintains the voltage, current, and frequency of the grid. The following areas require further research and development for the modernization of the grid.

The integration of distributed energy sources to the grid requires additional research on solid-state inverters that can coordinate the energy management system and energy dispatching system under various conditions.

11.6.4 Communication network

The communication network is the fundamental feature of the smart grid without which no coordination between the operators, and distributors, generating units, meters, and energy storage devices will be possible. The energy management system requires data from all the components of the smart grid, which is done through the communication network. There are various gaps in the reliable operation of the communication network. The following gaps must be filled for reliable communication between all the entities of the smart grid.

- A more reliable communication network must be developed for distributed generation which is a flexible, reliable, and managed system.
- A data handling system must be developed that can collect and store the unstructured data from all the communicating devices that can further be used for future trend prediction.

11.6.5 Energy storage system

Every microgrid or a distributed generation system is incorporated with an energy storage system. For the normal operation of the grid, the energy storage system acts as a buffer. If no storage system is present, there must be a balance between demand and supply. Energy storage systems must be developed that carry very little conversion losses [7].

11.7 Conclusion

This chapter gave an insight into the current status of the smart grid and the future trend of the smart grid was also forecasted based on the smart grid reports. As discussed earlier, the smart grid involves the integration of communication technologies, AMI, energy storage systems, electric vehicles, and distributed generation. The status of these components of the smart grid in terms of the installed capacity and the investments was discussed in this chapter.

Problems

Answer the following short questions

1. Describe the status of solar photovoltaic energy from 2015 to 2021.
2. What was the wind energy status from 2015 to 2021?
3. How many units of advanced metering infrastructure were installed in the USA by 2020?
4. Describe some of the areas that require research and development for the future advancement in smart grids.
5. List the research gaps in the field of power electronics for smart grids.
6. Which research gaps of smart sensors and smart meters must be covered for the advancement of the smart grid?
7. Write down the key characteristics of a smart grid.
8. What was the status of electric vehicles in 2021?
9. Describe the status of energy storage systems in the smart grid in 2021.
10. What are the dynamics of the smart grid in smart grid forecasting for up to the year 2026?

References

[1] Smart Grid Market Size, Share, Industry Analysis to 2026, Available from: https://www.marketsandmarkets.com/Market-Reports/smart-grid-market-208777577.html. (Accessed 23 June 2022).
[2] France Smart Grid Project, France, Available from: https://www.power-technology.com/marketdata/france-smart-grid-project-france/. (Accessed 21 June 2022).
[3] Advanced Metering Infrastructure Market Size, Share, Analysis (2022–27), Available from: https://www.mordorintelligence.com/industry-reports/advanced-metering-infrastructure-market. (Accessed 23 June 2022).
[4] Solar PV—Analysis—IEA, Available from: https://www.iea.org/reports/solar-pv. (Accessed 25 June 2022).
[5] Solar Energy, Available from: https://www.irena.org/solar. (Accessed 25 June 2022).
[6] Wind Energy, Available from: https://www.irena.org/wind. (Accessed 25 June 2022).
[7] Energy Storage—Analysis—IEA, Available from: https://www.iea.org/reports/energy-storage. (Accessed 23 June 2022).

This page intentionally left blank

Index

Note: Page numbers followed by *f* indicate figures and *t* indicate tables.

P

R

S

This page intentionally left blank

FUNDAMENTALS OF SMART GRID SYSTEMS

MUHAMMAD KAMRAN

Fundamentals of Smart Grid Systems is an expansive introduction to the core principles and applications relating to the operationalization, integration, and management of smart grids - the distributed, renewable, responsive, and highly efficient power grid on the verge of radically transforming our energy system. Reviewing the design of smart grid systems, their associated technologies, and operations, the work helps users to synthesize a modern foundational understanding of smart grid systems and to comprehend many of their advanced implementations, where sophisticated technologies are employed. It serves as a guidebook and primer for early career researchers, offering rich integration of current science, modern applications, and future implementations.

This book is of interest to engineering graduates, researchers, professors, and industry professionals involved in advanced engineering courses, renewable energy systems, and smart grid systems.

Key Features

- Presents critical enabling technologies of smart grid systems alongside relevant aspects of their design, modeling, control, and operations, accompanied by numerical examples
- Discusses how to approach the integration and management of renewable energy sources in smart grid environments
- Features didactic pedagogical elements including end-of-chapter problems, supplementing slideshows, and explicative figurative elements to clarify and explain complex concepts
- Focuses on modern applications and current implementations in the industry such as power electronics for smart grids, artificial intelligence and machine learning-driven modeling, advanced control strategies, and electric vehicles

About the Author

Dr. Muhammad Kamran is a lecturer in the department of Electrical Engineering and Technology, Riphah International University, Faisalabad campus, Pakistan. He has published 20 research articles in international journals and authored the book *Renewable Energy Conversion Systems*, which was published by Elsevier Science, Academic Press in 2021. He is interested in smart grid power systems, grid integration, renewable energy technologies, power electronics, and solar photovoltaic systems.

ELSEVIER

ACADEMIC PRESS
An imprint of Elsevier
elsevier.com/books-and-journals

ISBN 978-0-323-99560-3